Investigating the cellular response to mitochondrial dysfunction in Drosophila

Duncan, Olivia

Awarding institution:
King's College London

Investigating the cellular response to mitochondrial dysfunction in *Drosophila*

Thesis submitted to King's College London for the degree of Doctor of Philosophy

Olivia F. Duncan

Wolfson Centre for Age-Related Diseases
The Institute of Psychiatry, Psychology and Neuroscience
King's College London
2012-2016

Declaration

I declare that the research presented in this thesis is my own work, unless otherwise stated in the text.

Olivia Duncan

August 2016

Acknowledgements

I would firstly like to thank my supervisor Dr Joe Bateman, for his support, help and enthusiasm throughout my PhD. His supervisory excellence was well deserved. I would also like to thanks Prof. Clive Ballard, my second supervisor, for his guidance particularly with regards to the human tissue work. Many thanks also to Dr Dave Chambers for performing the microarrays and always being there for a chat, and to Sean Sweeney for taking the time to teach me how to prepare TEM samples.

I must also thank David Mazaud and Manolis Fanto for selecting the RNAi lines I used in the genetic modifier screen. Thanks to all of the students who assisted me over the past 4 years giving me an opportunity to further my teaching and people management skills and were (mostly) a pleasure to have around. Those who helped with the modifier screen Marisol Zuniga, Danielle Joseph, Tom Gardener, Fatima Chowdhury, Sharon Yuk Chan, Daniel Potter and Fernando Avila. As well as Dr Vandana Singh, who performed the climbing assay with *yan* overexpressing flies described in this thesis. I would also like to thank Rachel Finlay for her voluntary lab help during her gap year.

Many thanks go to previous and current members of the lab for help at work and fun outside of work. Thanks to Amelie Avet-Rochex, Nancy Carvajal, Umut Cagin, Elin Vinsland for her sense of humour and dancing skillz, Rachel Hunt for the cricket and crossword lessons, Katja Maierbrugger for all the heart-to-hearts and silliness, and of course Ariana Gatt my ‘mitochondrial partner in crime’ who’s side I didn’t leave for at least the first year in the lab. I have many happy memories of singing and dancing in the flyroom with you on a Friday night. Thank you, Bateman ladies for making the last four years so wonderful!

I would also like to thank the other members of the Wolfson CARD, who have made this a lovely place to work, especially Fiona, Katalin, Elisa, Lorenzo, Joao, Merrick, Ed, Emily, Natalie, Holly, Christina, Leanne, Andrea, Rachel, Rie, Prav and many more. Particular thanks to John Chesson for always being there to help and for all the great chats. Thank you also to Simon for the all de-stressing and support at home, and of course my parents and sisters for their continued love and support.

Publications produced during this thesis

1. **Mitochondrial retrograde signalling regulates neuronal function.**

Cagin U[1], Duncan OF[1], Gatt AP[1], Dionne MS, Sweeney ST, Bateman JM.
Proceedings of the National Academy of Science U S A, 2015 Nov 3, volume 112 (44), pages E6000-9

2. **Dementia in Parkinson's disease is associated with enhanced mitochondrial complex I deficiency.**

Gatt AP[1], Duncan OF[1], Attems J, Francis PT, Ballard CG, Bateman JM.
Movement Disorders, 2016 March, volume 31 (3), pages 352-9.

3. **Mitochondrial retrograde signalling in the *Drosophila* nervous system and beyond.**

Duncan OF, Bateman JM.
Fly (Austin), 2016 Jan 2, volume 10 (1), pages 19-24

[1]Indicates co-first authors

Abstract

Neurons are particularly susceptible to mitochondrial dysfunction, due to their high energy demand, resulting in a strong association between mitochondrial dysfunction and neurodegenerative disease. Cellular changes in response to mitochondrial dysfunction are currently poorly understood and appear to change depending on the cause of the mitochondrial dysfunction. However, manipulation of pathways known to be involved in this response have reversed the effects of mitochondrial dysfunction in *Drosophila* and mouse models. In this thesis, I aim to further investigate the cellular response to mitochondrial dysfunction in different models of mitochondrial dysfunction and to identifying novel genes that may be useful therapeutic targets in the future.

To investigate neuronal responses to different mitochondrial insults, I developed and characterised five different *in vivo* models of mitochondrial dysfunction in *Drosophila* neurons. I then evaluated transcriptional changes in these models to look for common pathways. Loss of synaptic mitochondria and overlapping transcriptional changes were observed in all five models of neuronal mitochondrial dysfunction. However, differences in ROS production and response to HIF-1α knockdown highlighted differences between the models. Manipulation of HIF-1α was beneficial in four of the models, identifying HIF signalling as a possible avenue for future translational research.

To identify novel genes involved in the cellular response to mitochondrial dysfunction, I also carried out a genetic modifier screen in the *Drosophila* wing. A library of 650 RNAi lines were screened and 80 genes were identified that modify the mitochondrial dysfunction phenotype. Hits were then tested in neuronal assays, to determine if they also modify mitochondrial dysfunction in neurons. I identified two components of the Ras/MAPK pathway, Yan and Pointed, as genetic modifiers of mitochondrial dysfunction. The Ras/MAPK pathway may therefore be a potential therapeutic target for diseases associated with mitochondrial dysfunction.

Contents

Declaration 2

Acknowledgements 3

Publications produced during this thesis 4

Abstract 5

Contents 6

List of Figures 12

List of Tables 15

Abbreviations 16

1 Introduction 19

1.1 Cellular energy production 19

1.1.1 Beta oxidation of fatty acids 19

1.1.2 Glycolysis 19

1.1.3 Kreb's Tricarboxylic Acid (TCA) cycle 21

1.1.4 Oxidative Phosphorylation (OXPHOS) 22

1.1.4.1 Supercomplexes 25

1.1.4.2 Assembly of Complexes 26

1.2 Mitochondrial structure and function 28

1.2.1 Mitochondrial origins 28

1.2.2 Mitochondrial Structure 29

1.2.3 Mitochondrial DNA 31

1.2.3.1 Transcription of mtDNA 32

1.2.3.2 MtDNA Replication 34

1.2.3.3 mtDNA inheritance 37

1.2.4 Reactive Oxygen Species 38

1.2.4.1 ROS induced damage and signalling 39

1.2.5 Additional mitochondrial functions 40

1.2.5.1 Iron sulphur cluster synthesis 40

1.2.5.2 Calcium Sequestering 41

1.2.5.3 Apoptosis 42
1.2.6 Mitochondrial Dynamics 43
1.2.6.1 Fusion and fission 43
1.2.6.2 Transport 45
1.2.7 Mitochondrial Turnover 45
1.2.7.1 Mitophagy 45
1.2.7.2 Biogenesis 46
1.3 Mitochondrial damage in disease 49
1.3.1 mtDNA diseases 49
1.3.2 Mitochondrial disease caused by nuclear mutations 50
1.3.3 Neurodegenerative disease and mitochondrial dysfunction 51
1.3.3.1 Current treatments for AD and PD 53
1.3.4 Animal models of mitochondrial dysfunction 54
1.3.4.1 Animal models of mtDNA loss and damage 56
1.3.4.2 Animal models targeting individual OXPHOS complex subunits 58
1.4 Mitochondrial retrograde signalling 60
1.4.1 Discovery of retrograde signalling in yeast 60
1.4.2 Retrograde signalling in multicellular organisms 61
1.4.2.1 Calcium mediated mitochondrial retrograde signalling 62
1.4.2.2 ROS mediated mitochondrial retrograde signalling 63
1.4.2.3 The mitochondrial unfolded protein response (UPR^{mt}) 64
1.4.3 The mitochondrial retrograde response in neurons 66
1.5 Premise of this thesis 67
2 Materials and Methods 68
2.1 Materials 68
2.1.1 Kits: 68
2.1.2 Antibodies and dyes: 68
2.1.3 Fly stocks 68
2.2 Methods 72
2.2.1 Fly maintenance and breeding 72
2.2.2 Behavioural and wing inflation assays 72
2.2.2.1 Negative geotaxis (climbing assay) 72
2.2.2.2 Wing inflation assay 73
2.2.3 Quantitative reverse transcription-polymerase chain reaction (qRT-PCR) 73
2.2.4 Dissections and immunofluorescence 74

2.2.4.1 Neuromuscular junctions (NMJ) 75
2.2.4.2 Central nervous system & eye disc dissections 76
2.2.4.3 Wing discs 76
2.2.5 Microscopy and image quantification 76
2.2.5.1 Neuromuscular junctions (NMJ) 77
2.2.5.2 Redox potential 77
2.2.5.3 MitoTimer 77
2.2.5.4 Perceval ATP: ADP ratio 78
2.2.5.5 Wing discs 78
2.2.5.6 Phosphorylated MAPK 78
2.2.5.7 Eye discs 78
2.2.6 Generating transgenic flies 78
2.2.7 Microarray 79
2.2.8 Lifespan assays 80
2.2.9 Genetic modifier screen 80
2.2.10 Statistical analysis and graphs 81
3 Modelling mitochondrial respiratory dysfunction in the *Drosophila* nervous system 83
3.1 Introduction 83
3.1.1 Chapter Aims 85
3.2 Results 86
3.2.1 Identifying OXPHOS models of mitochondrial dysfunction which impair neuronal function. 86
3.2.2 Validation of RNAi knockdown and *TFAM* overexpression 93
3.2.3 Loss of synaptic mitochondria in all ETC models 96
3.2.4 Changes in Reactive Oxygen Species (ROS) in the mitochondrial dysfunction models 99
3.2.5 MitoTimer oxidation changes in mitochondrial dysfunction models 102
3.2.6 ATP to ADP ratio in flies with neuronal complex V and complex I knockdown and *TFAM* overexpression. 105
3.3 Summary 108
4 Investigating the transcriptional response to OXPHOS subunit knockdown and *TFAM* overexpression models of mitochondrial dysfunction in neurons. 110
4.1 Introduction 110
4.1.1 Chapter aims 112
4.2 Results 113

4.2.1 Characterisation of the transcriptional response to mitochondrial dysfunction in *TFAM* overexpression and OXPHOS complex knockdown models. 113

4.2.2 Validation of the microarrays *in vivo*: *Ilp3* and *Thor* expression in neurons with *ATPsynCf6* RNAi..... 123

4.2.3 Neuronal *TFAM* overexpression phenotypes are partially rescued by *sima* knockdown..... 125

4.2.4 *Sima* knockdown partially rescues neuronal phenotypes in complex III, IV and V knockdown models. 128

4.2.5 Pan- neuronal *sima* knockdown rescues lethality of *nSyb-Gal4* driven complex III, IV and V knockdown and *TFAM* overexpression..... 132

4.2.6 Identifying HIF-1α responsive genes that are regulated differently in *ND-75* RNAi CNS 133

4.3 Summary..... 140

5 A Genetic screen to identify genes involved in the cellular response to mitochondrial dysfunction 142

5.1 Introduction..... 142

5.1.1 Chapter aims 143

5.2 Results..... 143

5.2.1 Mitochondrial dysfunction in the wing results in a scorable phenotype 143

5.2.2 Modifier screen assay 147

5.2.3 Validation of the genetic modifier screen 149

5.2.4 Genes identified by the genetic modifier screen..... 151

5.2.5 *Sima* knockdown enhances the wing phenotype 162

5.2.6 Modification of cell death by genes identified in the screen 163

5.3 Summary..... 165

6 Investigating the role of genes identified in the modifier screen, in neuronal mitochondrial dysfunction. 166

6.1 Introduction..... 166

6.1.1 Chapter aims 167

6.2 Results..... 168

6.2.1 Evaluation of genes identified in the modifier screen in neurons..... 168

6.2.2 Knockdown of *Hr39* enhances neuronal mitochondrial dysfunction 170

6.2.3 Knockdown of *yan* suppresses neuronal mitochondrial dysfunction..... 171

6.2.4 Knockdown of *yan* suppresses mitochondrial dysfunction in a *Drosophila* model of Leigh syndrome, but not in a Parkinson's disease model. 175

6.2.5 Pointed mutant suppresses neuronal mitochondrial dysfunction. 177

6.2.6 MAP kinase signalling pathway activity is altered by mitochondrial dysfunction 178
6.3 Summary 180
7 Discussion 182
7.1 Characterising different mitochondrial insults in the *Drosophila* nervous system 182
7.1.1 Functions of the OXPHOS subunits targeted by the selected RNAi lines 182
7.1.2 Validation of OXPHOS subunit RNAi knockdown 184
7.1.3 Reduced synaptic mitochondria caused by mitochondrial dysfunction 186
7.1.4 Measuring reactive oxygen species in models of mitochondrial dysfunction 188
7.1.5 Analysis of ATP:ADP ratios 190
7.1.6 Summary 193
7.2 Evaluating the transcriptional changes in different models of mitochondrial dysfunction. 195
7.2.1 Pathways affected in all mitochondrial dysfunction models 196
7.2.2 HIF signalling in neuronal mitochondrial dysfunction 199
7.2.3 Inhibition of retrograde signalling can provide salutatory effects 200
7.2.4 Mechanisms of HIF-1α regulation 201
7.2.5 Interactions between complex I and HIF-1α 203
7.2.6 Summary 205
7.3 Identifying genes involved in the cellular response to mitochondrial dysfunction, in a modifier screen. 206
7.3.1 *TFAM* knockdown and *TFAM* overexpression as models of mitochondrial dysfunction 206
7.3.2 Mitochondrial dysfunction driven in the dorsal wing compartments causes a curved wing phenotype 207
7.3.3 Genes that affect the mitochondrial dysfunction phenotype in the *Drosophila* wing 208
7.3.4 Advantages and limitations of the genetic wing screen 210
7.3.5 Summary 212
7.4 Evaluating genes identified in the modifier screen, in neurons. 213
7.4.1 Tissue or model specific effects of RNAi lines on mitochondrial dysfunction phenotypes 213
7.4.2 Neuronal mitochondrial dysfunction phenotypes suppressed by *yan* RNAi 214
7.4.3 The interplay between Yan and Pointed 215

7.4.4 Ras/MAPK pathway activation in disease 216
7.4.5 Regulation of the Ras/MAPK pathway 218
7.5 Conclusions and future directions 220
7.5.1 Future Experiments 221
8 References 225
9 Appendix 256
9.1 Microarray appendices 256
9.1.1 The number of genes changed in each microarray condition, compared to control, p < 0.05 with fold change cut-offs of >1.5 and >2. 256
9.1.2 Correlation genes significantly changed in common *ND-75* RNAi and *UQCR-14* RNAi and *ND-75* RNAi and *COX5B* RNAi, without outlier removed. 257
9.1.3 Enriched functional annotation clusters for genes significantly changed in *ND-75* RNAi, compared to control. 258
9.1.4 Enriched functional annotation clusters for genes significantly changed in *UQCR-14* RNAi, compared to control. 266
9.1.5 Enriched functional annotation clusters for genes significantly changed in *COX5B* RNAi, compared to control. 285
9.1.6 Enriched functional annotation clusters for genes significantly changed in *ATPsynCf6* RNAi, compared to control. 292
9.1.7 Enriched functional annotation clusters for genes significantly changed in *TFAM* overexpression compared to control. 298
9.1.8 Significant gene expression changes of the OXPHOS knockdown and *TFAM* overexpression models in HIF responsive genes, identified by Li et al., 2013 306
9.2 Modifier screen appendices 314
9.2.1 RNAi lines screened in the modifier wing screen. 314
9.2.2 Enhancers classified as pathway components in Panther 347
9.2.3 Suppressors classified as pathway components in Panther 347
9.2.4 Independent RNAi lines for screen enhancers 348
9.2.5 Climbing and wing inflation assays of RNAi lines identified in screen. 352

List of Figures

Figure 1.1 Glycolysis, in the cytoplasm. 20
Figure 1.2 Kreb's TCA cycle in the mitochondrial matrix 21
Figure 1.3 Oxidative phosphorylation at the inner mitochondrial membrane 25
Figure 1.4 TFAM bends mtDNA 180^{o} 34
Figure 1.5 Models of mtDNA replication 36
Figure 1.6 Cellular ROS pathways. 40
Figure 1.7 Apoptotic mechanisms in Drosophila and vertebrates 42
Figure 1.8 The roles of mitochondrial fission and fusion 43
Figure 1.9 PGC-1α signalling cascade 47
Figure 1.10 The mitochondrial retrograde response in yeast 61
Figure 1.11. Retrograde response pathways identified in multicellular organisms 62
Figure 1.12 The role of ATFS-1 in UPR^{mt} 65
Figure 3.1 Neuronal models of mitochondrial dysfunction cause behavioural defects 91
Figure 3.2 Neuronal knockdown of *ATPsynCf6* and overexpression of *TFAM* disrupt wing inflation 93
Figure 3.3 Level of knockdown of ubiquitously expressed RNAi lines 94
Figure 3.4 Level of knockdown of pan-neuronally expressed complex I and complex III RNAi in the CNS 95
Figure 3.5 Reduced mitochondrial gene expression with *TFAM* overexpression 96
Figure 3.6 Neuronal specific knockdown of OXPHOS complex subunits causes loss of synaptic mitochondria 98
Figure 3.7 Neuronal specific knockdown of ETC complex subunits causes altered glutathione redox potential in the mitochondrial matrix 101
Figure 3.8 Neuronal specific knockdown of *ND-75* causes mitochondrial oxidation at the cell body 103
Figure 3.9 Oxidation of mitoTimer in synaptic mitochondria in complex I, IV and V RNAi and *TFAM* overexpression 104
Figure 3.10 Neuronal specific knockdown of complex I reduces the ATP:ADP 107
Figure 4.1 Volcano plots of gene expression changes in OXPHOS knockdown models and *TFAM* overexpression 114
Figure 4.2 Heat maps showing genes with the most significant p-values in each condition of mitochondrial dysfunction 115

Figure 4.3 Correlations between genes significantly changed in the OXPHOS knockdown and *TFAM* overexpression models 117
Figure 4.4 Heat maps of genes in glutathione transferase activity and oxidoreductase activity clusters and glycolysis cluster 121
Figure 4.5 GO enrichment of common genes between each OXPHOS model and *TFAM* overexpression model, pairwise 122
Figure 4.6 Neuronal Ilp3 expression is reduced by complex V subunit knockdown in vivo 124
Figure 4.7 Neuronal Thor expression is increased by *ATPsynCf6* knockdown in vivo 125
Figure 4.8 Knockdown of sima improves function of neurons overexpressing *TFAM* 127
Figure 4.9 D42-Gal4 driven sima knockdown rescues the climbing phenotype of complex IV knockdown and wing inflation phenotype of complex V knockdown 129
Figure 4.10 OK371-Gal4 driven sima knockdown partially rescues the climbing phenotype of complex IV and complex V knockdown 131
Figure 4.11 GO enrichment analysis on HIF responsive genes that are differentially regulated in complex I knockdown 139
Figure 5.1 Reduced mitochondrial gene expression with *TFAM* RNAi 144
Figure 5.2 Wing phenotype induced by mitochondrial dysfunction 146
Figure 5.3 Modifier screen assay 148
Figure 5.4 Validation of the modifier screen assay with disease associated genes 150
Figure 5.5 Enhancers identified in the modifier screen 153
Figure 5.6 Suppressors identified in the modifier screen 155
Figure 5.7 Sima knockdown enhances the wing phenotype 162
Figure 5.8 Screen suppressors, Ino80 and yan RNAi, reduced mitochondrial dysfunction mediated cell death in the wing disc 164
Figure 6.1 *TFAM* RNAi, $TFAM^{c01716}$ knockdown in motor neurons causes a weak climbing phenotype and no wing inflation phenotype 168
Figure 6.2 Enhanced neuronal mitochondrial dysfunction due to *Hr39* RNAi 171
Figure 6.3 Suppressed neuronal mitochondrial dysfunction due to *yan* RNAi NIGR-1 172
Figure 6.4 A non-overlapping yan RNAi also suppressed mitochondrial dysfunction 172
Figure 6.5 Validation of *yan* RNAi lines in the eye disc 174

Figure 6.6 Motor neuron overexpression of *yan* is in lethal in the *TFAM* overexpression model of mitochondrial dysfunction 175
Figure 6.7 Knockdown of *yan* restores neuronal function in a Drosophila model of Leigh syndrome 176
Figure 6.8 Knockdown of *yan* does not restore climbing ability in a *Drosophila* model of Parkinson's disease 177
Figure 6.9 *Pointed* mutant restores neuronal function in *TFAM* overexpressing and parkin mutant flies 178
Figure 6.10 Increased activation of MAPK in neurons overexpressing *TFAM* 179
Figure 7.1 Complex I deficiency can inhibit HIF-1α stabilisation 204

List of Tables

Table 1. Causes and symptoms of the most common mtDNA diseases. 49
Table 2. Drosophila and mouse models of mtDNA loss and OXPHOS complex dysfunction 54
Table 3. RNAi, used in this study, for subunits of OXPHOS complexes. 70
Table 4. Primer sequences used for qRT-PCR 74
Table 5. Primers used to clone Perceval 79
Table 6. Climbing result and p-values for OXPHOS RNAi lines 88
Table 7. The number of genes changed in the microarray, in each condition compared to control, $p < 0.05$. 116
Table 8. Genes significantly changed in all microarrays, compared to control 118
Table 9. GO molecular function and biological processes for genes significantly changed in all microarrays 119
Table 10. Statistical analysis of lifespan assays in female flies. 128
Table 11. Number of flies and median age of female flies in lifespan assay. 128
Table 12. Viability of pan-neuronally driven OXPHOS knockdown models when sima is knocked down with heterozygous $sima^{KG07607}$. 133
Table 13. HIF-1α responsive genes that respond differently in ND-75 RNAi compared to other OXPHOS knockdown and TFAM overexpression microarrays. 134
Table 14. Validation of screen. 151
Table 15. Enhancers identified in the screen with GO Molecular Function 156
Table 16. Suppressors identified in the screen with GO Molecular Function. 159
Table 17. Comparison of modifier screen enhancers with genes significantly altered in OXPHOS and TFAM overexpression arrays. 161
Table 18. Results of neuronal assay for selected hits identified in the modifier screen. 170

Abbreviations

2D-AGE	two-dimensional agarose gel electrophoresis
2-DG	2-deoxyglucose
4E-BP	initiation factor 4E binding protein
AD	Alzheimer's disease
ADP	adenine diphosphate
AMP	adenine monophosphate
AMPK	AMP-activated protein kinase
ANOVA	analysis of variance
AOX	alternative oxidase
ATFS-1	activating transcription factor associated with stress-1
ATP	adenine triphosphate
ATPsynCf6	ATPsynthase coupling factor 6
BDNF	brain-derived neurotrophic factor
CI	complex I
CII	complex II
CIII	complex III
CIT	citrate synthase
CIV	complex IV
CNS	central nervous system
CoA	coenzyme A
COX5B	cytochrome c oxidase 5B
cpYFP	circularly permuted yellow fluorescent protein
CV	complex V
Cybrid	cytoplasmic hybrid
DA	diamide
DAVID	Database for Annotation, Visualisation and Integrated Discovery
D-loop	displacement loop
Drp1	dynamin related Protein 1
DTT	dithiothreitol
duox	dual oxidase
E_{GSH}	glutathione redox potential
ER	endoplasmic reticulum
ERIOLS	extensive RNA incorporation on the lagging strand
ERK	extracellular signal–regulated kinases
EtBr	ethidium bromide
ETC	electron transport chain
ETS	E-twenty six
F_0	ATPsynthase transmembrane domain
F_1	ATPsynthase enzymatic domain
$FADH_2$	flavine adenine dinucleotide
FCCP	carbonyl cyanide trifluoro-methoxyphenyl hydrazone
Fe-S	iron sulphur clusters

Fis1	mitochondrial fission 1
FMN	flavin mononucleotide
GO	gene ontology
Grx	glutaredoxin
GSH	glutathione
GSSG	glutathione disulphide
HD	Huntington's disease
HIF	hypoxia inducible factor
HMG	high mobility group
HRP	horseradish peroxidase
HSP	heavy strand promoter
Ilp3	insulin-like peptide 3
IMM	inner mitochondrial membrane
IMS	intermembrane space
IκBβ	inhibitor of the nuclear factor-κβ
JNK	c-Jun N-terminal kinase
L-Dopa	L-3,4-Dihydroxyphenylalanine
LHON	Leber's hereditary optic neuropathy
LRRK2	Leucine- Rich Repeat Kinase 2
LSP	light strand promoter
Mae	modulator of the activity of ETS
MAO-B	monoamine oxidase-B
MAPK	mitogen activated phosphokinase
Mdv1	mitochondrial division protein 1
MELAS	Mitochondrial encephalopathy lactic acidosis, and stroke-like episodes syndrome
MERRF	Myoclonus epilepsy and ragged-red fibres
MIM	mitochondrial import machinery
Miro	mitochondrial Rho
mitoGFP	Mitochondrially targeted green fluorescent protein
MOM	mitochondrial outer membrane
MPTP	1-methyl-4-phenyl-1,2,3,6-tetrahydropyridine
mtDNA	mitochondrial DNA
MTS	mitochondrial target sequence
NADH	nicotinamide adenine dinucleotide
ND-75	NADH-ubiquinone oxidoreductase 75 kDa
Nf-κB	nuclear factor-κ
NMJ	neuromuscular junction
NRF	nuclear respiratory factors
OH	origin of heavy strand synthesis
OL	origin of light strand synthesis
OPA1	optic atrophy protein 1
ORP	oxidant receptor peroxidase
OXA	oxidase assembly machinery
OXPHOS	oxidative phosphorylation
PBS	Phosphate buffered saline

PBST	Phosphate buffered saline/0.1% triton X100
PD	Parkinson's disease
PEO	Progressive external ophthalmoplegia
pERK	phosphorylated ERK
PGC-1α	peroxisome proliferator activated receptor γ co-activator 1α
PHD	prolyl hydroxylase
PINK1	Pten-Induced Putative Kinase 1
Pnt	pointed
POLRMT	human mtRNA polymerase
qRT-PCR	Quantitative reverse transcription-polymerase chain reaction
RFeSP	Rieske iron-sulfur protein
roGFP	redox sensitive green fluorescent protein
ROS	reactive oxygen species
RP041	yeast mtRNA polymerase
RpL4	ribosomal protein L4
RTK	protein tyrosine kinase receptor
SA	succinate
SDM	strand displacement model
SEM	standard eror of the mean
sima	similar
SIRT1	sirtuin 1
SOD	superoxide dismutase
TCA	tricarboxylic Acid
TFAM	mitochondrial transcription factor A
TFB1M	mitochondrial transcription factor B1
TFB2M	mitochondrial transcription factor B2
TGFβ	transforming growth factor beta
TIM	translocase of the inner mitochondrial membrane
tko	technical knock-out
TMRM	tetramethylrhodamine methyl ester
TOM	translocase of the outer mitochondrial membrane
UPR^{mt}	mitochondrial unfolded protein response
UQCR-14	ubiquinol-cytochrome c reductase 14 kDa
UQH_2	ubiquinol
VNS	ventral nervous system
Yan^{ACT}	constitutively active Yan
α-KG	α-ketoglutarate

1 INTRODUCTION

1.1 Cellular energy production

Chemical energy is transiently stored in our cells in the form of adenine triphosphate (ATP). The universal use of ATP to directly, or indirectly to provide energy for cellular reactions makes this molecule essential for life. ATP was discovered by Karl Lohmann in 1929, when he isolated it from muscle and liver tissue. In 1935 the structure of ATP was proposed by Katashi Makino, but it wasn't for another 10 years that this was confirmed (Khakh and Burnstock 2009). Enzymatic hydrolysis of ATP releases energy, from the high energy phosphate bond. This energy is required for cellular work. ATP is produced in eukaryotic cells via four main processes β-oxidation of fatty acids, glycolysis, the tricarboxylic acid cycle (TCA) and oxidative phosphorylation (OXPHOS).

1.1.1 Beta oxidation of fatty acids

Muscle tissues, particularly cardiac muscle, produce ATP through β-oxidation of fatty acids. Other tissues, such as the liver and kidneys can use the products of this process, ketone bodies, to create ATP. The enzymes required for β-oxidation are located in the mitochondria and peroxisomes. Fatty acids from adipose tissue are transported into the cell via plasma membrane transport proteins, which simultaneously add coenzyme A (CoA) to the fatty acid creating acyl CoA. The acyl CoA is transported into the mitochondria via the carnitine transporter system, where it is shortened in a series of oxidation steps, to produce acetyl CoA and NADH (Houten and Wanders 2010). Acetyl CoA can enter the TCA cycle and NADH donates an electron to complex I in OXPHOS (see 1.1.3 & 1.1.4).

1.1.2 Glycolysis

Glycolysis uses glucose to create ATP, and can do so in aerobic and anaerobic conditions. In this reaction the six-carbon molecule glucose is split into two molecules of pyruvate, each containing three carbons, in a ten stage process (Figure 1.1). The early

stages of glycolysis require energy from two molecules of ATP, however, later stages generate four ATP molecules, resulting in a net gain of two ATP molecules. In aerobic conditions, pyruvate is converted into acetyl CoA in mitochondria. In anaerobic conditions however, pyruvate is converted to lactate or fermented to ethanol and CO_2 in yeast.

Glycolysis is a less efficient process than oxidative phosphorylation at producing ATP. However, yeast growing on glucose will rely on glycolytic fermentation of glucose for ATP production rather than oxidative phosphorylation, this is termed the Crabtree effect (Crabtree 1929). A similar phenomenon is observed in highly proliferative tumour cells. Cancerous cell are observed to switch from OXPHOS to mainly glycolytic metabolism even though conditions are still aerobic, this was first observed by Warburg in the 1920s and so is called the 'Warburg effect' (Gatenby and Gillies 2004).

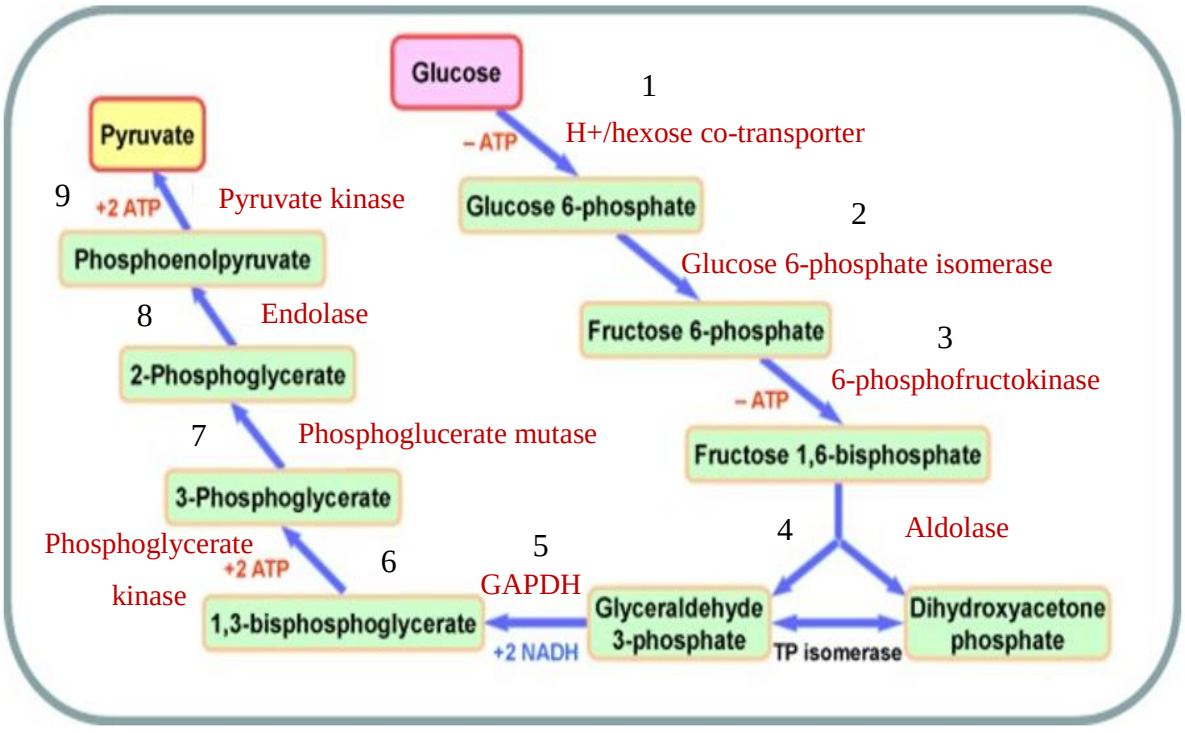

Figure 1.1 Glycolysis, in the cytoplasm.
In reactions 1-4 two phosphorylation events occur requiring input of ATP, converting glucose into two molecules of glyceraldehyde 3-phosphate. The aldehyde group on each glyceraldehyde 3-phosphate is oxidised in reactions 5 and 6, producing two molecules of ATP and NADH. In reactions 7-9, the phosphate groups are removed to create two more molecules of ATP. Figure adapted from Li et al., 2015 (Li, Gu et al. 2015).

1.1.3 Kreb's Tricarboxylic Acid (TCA) cycle

In 1937 Krebs proposed the TCA cycle as a mechanism cells use to convert food into cellular energy (Akram 2014). The TCA cycle takes place in mitochondrial matrix, using acetyl-CoA created from fatty acids or from the pyruvate created during glycolysis (Akram 2014). In this process acetyl-CoA is combined with oxaloacetate to produce citrate. A series of eight, enzyme catalysed oxidative steps convert citrate back into oxaloacetate. Electrons released in this process are donated to NAD^+ and FAD to create NADH or $FADH_2$ (Figure 1.2). Two CO_2 molecules and one molecule of ATP/GTP are also created in a single cycle.

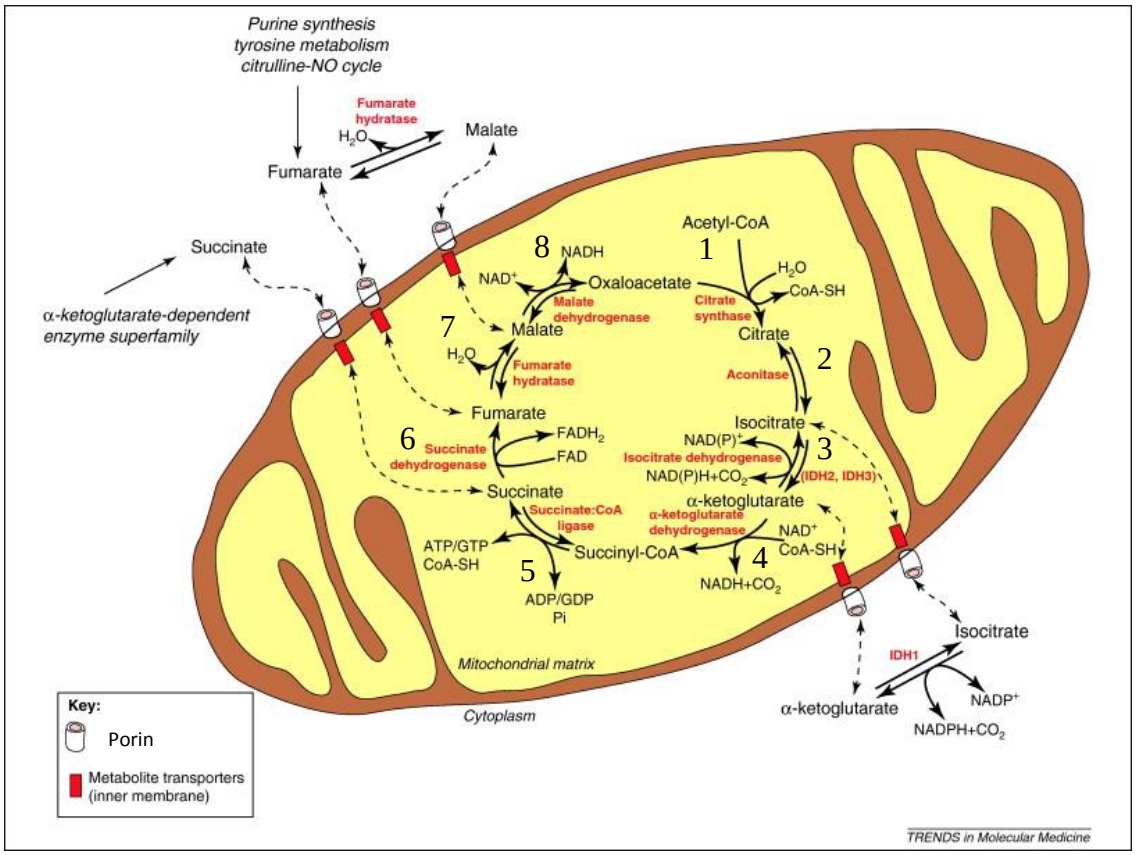

Figure 1.2 Kreb's TCA cycle in the mitochondrial matrix.
(1) Citrate synthase converts Acetyl-CoA and oxaloacetate into a six- carbon citrate molecule. (2) Citrate is isomerised by aconitase, by dehydration followed by rehydration, to form isocitrate. (3) Decarboxylation of isocitrate results in the production of α-ketogluterate and by-products CO_2 and NADH. (4) The multi-enzyme complex, α-ketogluterate dehydrogenase, decarboxylates α-ketogluterate into succinyl-CoA, also producing CO_2 and NADH. (5) Succinyl-CoA is converted to Succinate and one molecule of GDP is phosphorylated. (6) Transmembrane Succinate dehydrogenase (also complex II in the Electron Transport Chain) converts succinate to fumarate, converting FAD to $FADH_2$ in the process. (7) Fumarate hydratase hydrates the double bond C=C bond in fumarate to produce malate. (8) Dehydrogenation of malate results in

the reformation of oxaloacetate which can re-enter the cycle, and conversion of a further NAD molecule into $NADH_2$ (Akram 2014). Figure adapted from Raimundo et al., 2011 (Raimundo, Baysal et al.)

NADH or $FADH_2$ are required for the process of OXPHOS, which produces 95% of cellular ATP. However, the TCA cycle also plays an integral role in producing intermediates for biosynthesis. Oxaloacetate can be converted to the amino acid alanine with the addition of an amino group (Berg JM 2002). Succinyl CoA can be converted into heme and citrate is a precursor of fatty acids and sterols (Berg JM 2002). These metabolites diffuse through the mitochondrial membrane or are transported via active carriers to take part in these biosynthetic pathways in the cytosol (Raimundo, Baysal et al.) (Figure 1.2).

TCA metabolites are also known to regulate the cells response to hypoxia. Hypoxia inducible factor HIF-1α is normally targeted for degradation by α-ketagluterate dependant prolyl hydroxylases (PHDs) (Majmundar, Wong et al. 2010). Levels of α-ketoglutarate therefore have a key role in HIF regulation. Other TCA metabolites, succinate, oxaloacetate, isocitrate and fumarate, have also been shown to inhibit the activity of PHDs (Raimundo, Baysal et al. , Isaacs, Jung et al. 2005, Selak, Armour et al. 2005).

1.1.4 Oxidative Phosphorylation (OXPHOS)

OXPHOS is the transfer of electrons from NADH or $FADH_2$ to O_2, along the electron transport chain (ETC) coupled to ATP production through ATP synthase (Complex V) (Figure 1.3A) (Mitchell 1961). Electrons donated by NADH and $FADH_2$ enter the chain at either NADH dehydrogenase-ubiquinone oxidoreductase (complex I), made up of 44 subunits, or succinate dehydrogenase-ubiquinone oxidoreductase (complex II), made up of 4 subunits. Electrons are passed from one electron carrier to another, each carrier having a greater affinity for electrons than the last. As it is passed along the chain the electron releases energy, which is used to pump H^+ ions (protons) across the inner mitochondrial membrane (IMM) into the intermembrane space (IMS), through all ETC complexes apart from complex II.

Complex I accepts two electrons from NADH through its co-factor, flavin mononucleotide (FMN). The electrons are then passed one by one through seven iron sulphur clusters (Fe-S) in the hydrophilic domain of the complex, until they reach the Coenzyme Q reduction site, in the hydrophobic domain. From this site two electrons are donated to Coenzyme Q (also known as ubiquinone) reducing it to UQH_2 (ubiquinol). For every two electrons donated to Coenzyme Q by complex I, four H^+ ions are translocated though the hydrophobic domain of complex I into the IMS. Coenzyme Q is also reduced by electrons from the hydrophobic domain of complex II. Complex II acts in the TCA cycle oxidising succinate to fumarate, in this process FAD is reduced to $FADH_2$. The flavoprotein subunit of complex II, covalently binds FAD, when FAD is reduced, the electrons are then passed one by one from this subunit to the Fe-S clusters in the second hydrophilic subunit, and then to the Fe-S clusters in the two hydrophobic subunits. Finally, the electron is donated to heme b, which reduces Coenzyme Q. Coenzyme Q freely moves in the IMM, carrying electrons from complex I and II to coenzyme Q reductase (complex III).

Complex III consists of 11 subunits, and it passes electrons from reduced Coenzyme Q (UQH_2) to cytochrome c via the Q-cycle. In the first half of this cycle, one electron is donated from UQH_2 to the Rieske iron-sulphur subunit and a second electron is donated to cytochrome b_L heme. As UQH_2 donates two electrons, two H^+ ions are released into the IMS. The Rieske iron-sulphur subunit donates its electron to the cytochrome c_1 subunit, whereas the electron donated to cytochrome b_L heme is passed onto a Coenzyme Q molecule that also binds to complex III. In the second stage of the Q-cycle, a second molecule of UQH_2 binds and the process is repeated. However, when the second electron is donated to Coenzyme Q, two protons are also taken up from the mitochondrial matrix to created UQH_2, which diffuses back into the IMM. The two electrons donated to cytochrome c_1 in this cycle proceed along the ETC as they are donated to the soluble electron carrier cytochrome c. Cytochrome c diffuses through the intermembrane space shuttling electrons from complex III to the 14 subunit cytochrome c oxidase complex (complex IV). Complex IV accepts an electron from cytochrome c with the copper bound protein (Cu_A), the electron is then passed to a cytochrome c subunit and on to a tightly associated copper (Cu_B) and cytochrome b subunit. A second electron from another cytochrome c electron carrier passes along this pathway to the Cu_B site. These two electrons are donated to O_2, the final electron acceptor of the ETC and two H^+ ions are transferred from the matrix into the IMS.

Accumulation of H^+ ions inside the IMS results in an electrochemical gradient, as it gives the IMS an overall positive charge and acidic pH compared to the negatively charged, neutral matrix. This creates a proton motive force, however, because the IMM is impermeable to protons, protons cannot freely pass back through the IMM. Therefore, this acts like a battery to store the energy released from the electrons. Protons can pass through the membrane via the 19 subunit complex ATPsynthase (complex V). The transmembrane domain, (F_0), of complex V forms a narrow hydrophilic channel. As protons move through this channel, the large enzymatic domain, (F_1), which is located in the matrix, rotates (Abrahams, Leslie et al. 1994). ADP and inorganic phosphate can enter the active site of F_1 when it is in its 'open' state. As the motor rotates the enzyme moves into a 'closed' and then 'tight' confirmation, pushing the ADP and phosphate closer together until they are forced to form a covalent bond, forming ATP (Kayalar, Rosing et al. 1977). Further rotations allow for the release of the newly produced ATP and the enzyme returns to its open state (Abrahams, Leslie et al. 1994).

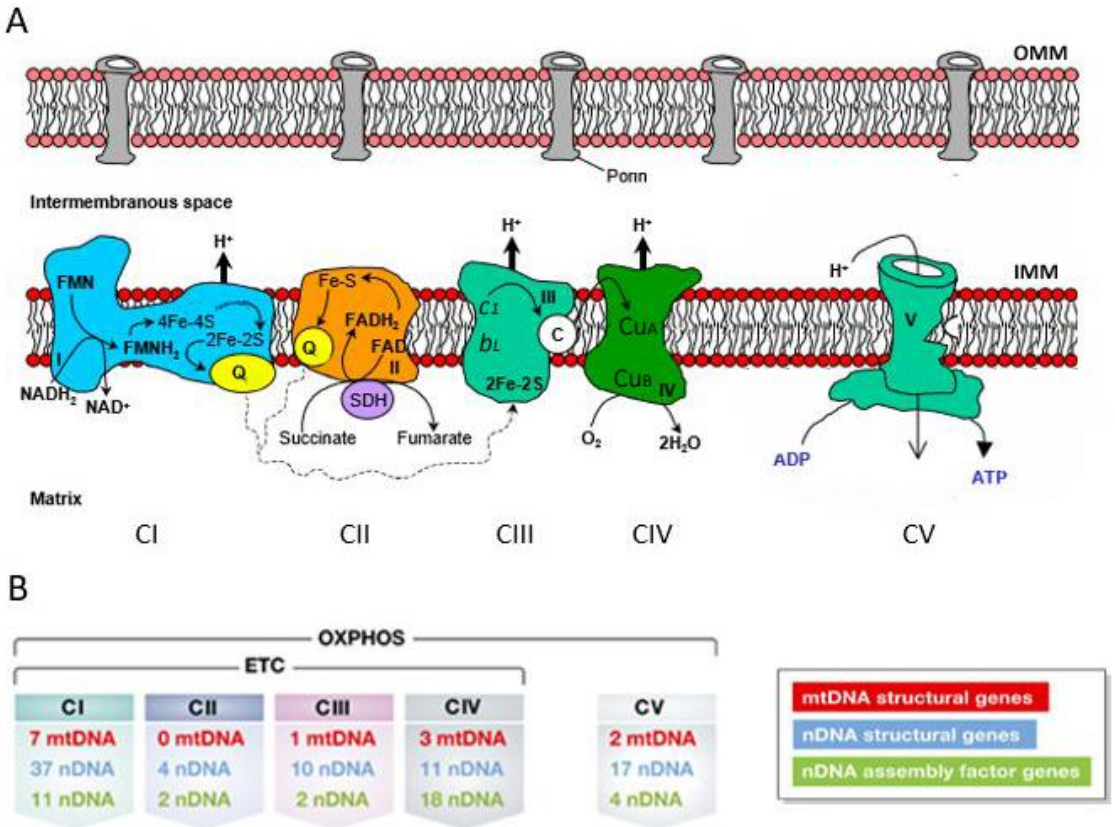

Figure 1.3 Oxidative phosphorylation at the inner mitochondrial membrane. **(A)** Oxidation of NADH occurs at complex I (CI) and $FADH_2$ at complex II (CII). Electrons are then passed to complex III (CIII) by Coenzyme Q (Q), then via cytochrome c (c) to complex IV (CIV). This makes up the electron transport chain. The energy produced is used to pump hydrogen into the IMS, creating an electrochemical gradient. This proton motive force pushes H^+ through complex V (CV), driving ATP synthesis. ROS are produced at CI, CII and CIII. **(B)** The number of OXPHOS complex subunits that are encoded in the nuclear and mitochondrial genome. All assembly factors are nuclear encoded. Figure adapted from Koopman et al., (Koopman, Distelmaier et al. 2013) and Baker et al. (Baker and Tarnopolsky 2003)

1.1.4.1 Supercomplexes

Evidence that the five OXHPOS complexes can be isolated and still remain functional lead to the 'fluid state' hypothesis, in which electrons are thought to pass from complexes that collide randomly, as the complexes diffuse freely in the IMM (Dudkina, Kouril et al. 2010). As predicted by this model, OXPHOS complexes diffuse laterally within the IMM and activity of the electron transport chain is coupled to diffusion (Hackenbrock, Chazotte et al. 1986). However, blue native gel electrophoresis revealed the presence of unexpected bands from solubilised mitochondria. When resolved in a second dimension the presence of subunits from multiple complexes were revealed, in

plant, yeast and mammalian mitochondria (Schagger and Pfeiffer 2000, Eubel, Heinemeyer et al. 2004). This suggests that stable interactions are formed between certain OXPHOS complexes, creating higher-ordered oligomers, named supercomplexes (Dudkina, Kouril et al. 2010). Existence of these supercomplexes has been confirmed by electron microscopy (Dudkina, Eubel et al. 2005), and they have been shown to act as a functional unit (Bianchi, Genova et al. 2004). Supercomplexes of two or more individual OXPHOS complexes have been observed, that can also contain Coenzyme Q and cytochrome c (Acin-Perez, Fernandez-Silva et al. 2008). The formation of supercomplexes poses a challenge to the 'fluid state' hypothesis, replacing it with a 'solid-state' model. Further evidence of interaction between OXPHOS subunits from genetic studies shows that point mutations in one complex can impair the assembly and stability of other complexes (Acin-Perez, Bayona-Bafaluy et al. 2004, Diaz, Fukui et al. 2006).

It is thought that OXPHOS complexes co-exist in the IMM as supercomplexes and singular complexes, although complex I is not found independent of a supercomplex (Acin-Perez, Fernandez-Silva et al. 2008). Evidence from potato mitochondria suggests that there are also even larger structures of OXPHOS complexes (Bultema, Braun et al. 2009). Single particle electron microscopy has revealed the presence of 'megacomplexes' made up of at least five supercomplexes (Bultema, Braun et al. 2009). These structures were not previously observed on blue native gels as they are disrupted by detergent treatment. Higher complex strings of ATPsynthase have also been reported, these oligomeric structures bend the IMM membrane and are often found at the base of IMM cristae (Allen, Schroeder et al. 1989, Krause, Reifschneider et al. 2005, Dudkina, Sunderhaus et al. 2006).

1.1.4.2 Assembly of Complexes

For OXPHOS to work properly subunits have to be assembled into complexes, which need to correctly incorporate redox cofactors (metals) and then assemble into supercomplexes (Vartak, Porras et al. 2013, Hildenbeutel, Hegg et al. 2014). To complicate matters some OXPHOS subunits are encoded by mitochondrial DNA, however most are encoded by nuclear DNA (Figure 1.3B). Accessory proteins have been identified that are required for the assembly of individual subunits into the

complexes, but are not present in the assembled complex (Fernandez-Vizarra, Tiranti et al. 2009). For example, the chaperone NDUFAF1 is required for complex I assembly (Vogel, Janssen et al. 2005), BCS1L is an ATP dependant chaperone that is needed for the incorporation of the Rieske iron sulphur subunit into complex III (Cruciat, Hell et al. 1999) and Surf1 is required for complex IV assembly, although the mechanism of its function is unknown (Stiburek, Vesela et al. 2005). Complete complexes are formed in stages with the production of sub-assemblies of subunits which are sequentially incorporated in the IMM (Fernandez-Vizarra, Tiranti et al. 2009).

Maintenance of supercomplexes is mediated by the mitochondrial lipid cardiolipin. Patients with Barth syndrome have destabilised supercomplex which more readily dissociate when treated with mild detergents (McKenzie, Lazarou et al. 2006). The disorder is caused by a mutation in *Tafazzin*, which is known to remodel cardiolipin (McKenzie, Lazarou et al. 2006). Evidence *in vitro*, suggests that cardiolipin is required for supercomplex assembly in yeast, as purified complex III and IV subunits only formed supercomplexes in the presence of cardiolipin (Bazan, Mileykovskaya et al. 2013). Knockdown experiments in yeast also demonstrate a role for respiratory supercomplex factors (Rcf-1, Rcf-2) and ADP/ATP carrier proteins (ACC-1, ACC-2) in supercomplex assembly (Dienhart and Stuart 2008, Chen, Taylor et al. 2012, Strogolova, Furness et al. 2012).

1.2 Mitochondrial structure and function

Recordings of intracellular structures that were most likely mitochondria were first made in the 1840s. However, in was Altmann in 1890 who realised that they were ubiquitous features in many cell types. Altmann, postulated that they were living organisms that had been endocytosed into the cell and carried out essential processes (Ernster and Schatz 1981): a theory not too dissimilar to what is thought today. Development of the electron microscope allowed greater resolution imaging of mitochondria and in 1953, the first pictures of the mitochondrial ultrastructure were published. From these Palade described a double membrane structure with internal folds of the inner membrane that protrude into the mitochondria approximately perpendicular to the long axis (Palade 1953). The mechanisms of mitochondrial respiratory function were more elusive. In 1961, Mitchell proposed the theory of chemiosmotic coupling although this theory was dismissed at the time (Mitchell 1961).

1.2.1 Mitochondrial origins

Without mitochondria, eukaryotic life may never have evolved. There are eukaryotes without mitochondria, however, mitochondrial DNA fragments can still be found in their nuclei, presumably relics from mitochondria in their ancestors (Clark and Roger 1995, Hampl, Silberman et al. 2008). It is argued, that the evolution of complex eukaryotic cells was dependant on the increased capacity of the cell to produce energy, via the mitochondria, to support a vast increase in gene expression (Lane and Martin 2010). Although whether mitochondria actually confer a net gain in energy production to eukaryotes compared to prokaryotes is still debated (Lynch and Marinov 2016). Numerous similarities between mitochondria and bacteria gave rise to the theory that mitochondria were once free living α-proteobacteria which came to live in endosymbiosis within another cell (Yang, Oyaizu et al. 1985). Genetic evidence suggests that this host cell was a methanogen (Rivera and Lake 1992). According to the hydrogen hypothesis, a symbiotic relationship was driven by the methanogens metabolic requirement for hydrogen and the proteobacterium's ability to produce hydrogen as a waste metabolic waste product (Martin and Muller 1998). However, this hypothesis is unable to explain why all eukaryotes have a complex endomembrane system (Baum and Baum 2014). The inside-out model builds on the ideas behind the

hydrogen hypothesis, but postulates that the host cell becomes the nucleus of eukaryotes and protrusions of the membrane engulf the α-proteobacteria, producing endomembrane structures in the process (Baum and Baum 2014). Recently, the closest relative to eukaryotes, the archaea Lokiarchaeota, was identified in a deep sea vent, via comparative genomic analysis (Spang, Saw et al. 2015). Lokiarchaeota contains genes that were previously thought to be exclusively eukaryotic, e.g. for actin and small GTPases, however, there is no evidence of mitochondria (Spang, Saw et al. 2015). Future studies of this archaea may throw further light on the evolution of eukaryotic organisms.

1.2.2 Mitochondrial Structure

Mitochondria are double membrane organelles, and are therefore comprised of four individual compartments each with distinct functions: the mitochondrial outer membrane (MOM), the inner mitochondrial membrane (IMM), the intermembrane space (IMS) between these two membranes and the matrix within the IMM.

The outer mitochondrial membrane provides a barrier between the cytosol and the mitochondria, regulating what can pass in and out, therefore controlling communication between the mitochondria and the rest of the cell (Gellerich, Trumbeckaite et al. 2000). Abundant voltage-gated, 'β-barrel' porin channels (also known as VDAC) (Forte, Guy et al. 1987) within the phospholipid bilayer, allow passage of small molecules, up to 8 kDa through the membrane (Zalman, Nikaido et al. 1980). It is estimated that there are approximately 1500 proteins in the mitochondrial proteome (Taylor, Fahy et al. 2003), 99% of which are encoded in the nucleus. So far 615 individual proteins have been identified in human heart mitochondria (Taylor, Fahy et al. 2003). Proteins targeted to the mitochondria that are larger than 8 kDa enter via the outer membrane translocase (TOM). The TOM complex has a receptor, which can recognise the mitochondrial target sequence (MTS) of nuclear encoded pre-proteins (Ahting, Thun et al. 1999). Critical regions of many MTS form amphiphilic α-helices, with hydrophobic residues on one side and hydrophilic residues on the other (von Heijne 1986). Recognised pre-proteins can then translocate through the MOM via TOM's cation selective, high-conductance channel (Kunkele, Heins et al. 1998). TOM also mediates integration of MOM proteins into the membrane, in co-ordination with the mitochondrial import machinery (MIM) (Bohnert, Pfanner et al. 2015). A number of mitochondrial proteins do not have an

obvious MTS, but are thought to contain internal targeting sequences (Chacinska, Koehler et al. 2009).

The intermembrane space is the aqueous phase between the two mitochondrial membranes. It is often overlooked, and assumed to be equivalent to the cytosol. However, it can actually be described as a 'logistics hub', coordinating protein, lipid and metal ion exchange between the mitochondrial compartments and the rest of the cell, as well as being important for ATP production, apoptosis and redox control (Herrmann and Riemer 2010). During oxidative phosphorylation protons accumulate in the IMS, creating the essential electrochemical gradient. The electron carrier, cytochrome c, which shuttles electrons between the third and fourth complex in the electron transport chain, is thought to diffuse freely in the IMS and is in fact the most abundant protein in the compartment (Martin, Eckerskorn et al. 1998) (Figure 1.3A). Free diffusion of cytochrome c within the IMS is also imperative for its apoptotic role; when the MOM is permeabilised, rapid release of cytochrome c into the cytosol is required to trigger apoptosis (Gillick and Crompton 2008) (see Introduction 1.2.5.3).

The inner mitochondrial membrane is far less permeable than the outer membrane and has a far higher protein content. This is mainly due to OXPHOS complexes which take up 50% of the IMM. Proteins cross the IMM via two translocase of the inner mitochondrial membrane (TIM) complexes. Proteins with cleavable N-terminal MTSs are transported through the IMM via TIM23 (Bohnert, Pfanner et al. 2015). The domain of TIM23 which forms a pore through the IMM, TIM23/17, is regulated by the IMM membrane potential (Truscott, Kovermann et al. 2001). The membrane potential also provides the driving force that makes the charged pre-sequence (the MTS, which is cleaved in the matrix), translocate through TIM23 (Martin, Mahlke et al. 1991). One subunit of the TIM23 complex has also been implicated in orchestrating insertion of OXPHOS complex subunits both into the IMM and into functional complexes (Mick, Dennerlein et al.). Complex subunits encoded by mitochondrial DNA (mtDNA) are inserted into the IMM from the matrix by the oxidase assembly machinery (OXA) (Bonnefoy, Fiumera et al. 2009). A second translocase, TIM22, recognises proteins with internal targeting sequences and inserts them into the IMM (Rehling, Brandner et al. 2004). Again this process is driven by the membrane potential (Pfanner and Neupert 1985).

The matrix within the IMM is the site of the TCA cycle and ATP production. It also contains the mtDNA.

1.2.3 Mitochondrial DNA

Margit and Sylvan Nass observed threadlike structures within mitochondria on electron micrographs of chick embryos. Discovery that these structures could be digested by DNase, but not RNase, led to the conclusion that mitochondria contain their own DNA (Nass and Nass 1963). Shortly afterwards, DNA was isolated from purified mitochondrial samples from yeast (Schatz, Haslbrunner et al. 1964).

MtDNA is present in multiple copies in the cell, with a copy number that can be thousands of times that of the diploid nuclear genome (Miller, Rosenfeldt et al. 2003). It is packaged into nucleoids with a diameter of about 100nm, often containing a single mitochondrial genome (Kukat and Larsson 2013). Double stranded mtDNA is circular, made up of a heavy and a light strand and encodes a total of 37 genes in humans. The nomenclature heavy and light stems from the relative abundance of G and T bases in each strand. This determines how buoyant each strand is in a caesium chloride gradient (Taanman 1999). In animals, mtDNA ranges from 15 to 20kb (Garesse and Kaguni 2005), human mtDNA is approximately 16.5 kb (Holt and Reyes 2012). These differences in size are due to gene duplications rather than additions. Sequencing of the human mitochondrial genome revealed that it is extremely compact, with hardly any noncoding DNA and that most mitochondrial genes do not contain a stop codon (Anderson, Bankier et al. 1981). It encodes for 13 proteins, which are all subunits of OXPHOS complexes, 2 rRNAs and 22 tRNAs, which are involved in the translation of the OXPHOS proteins. A fourteenth mitochondrially encoded peptide, humanin, has also been identified in brains of Alzheimer's (AD) patients (Hashimoto, Niikura et al. 2001). The open reading frame of humanin is nested within the coding region for the 16s rRNA (Yen, Lee et al. 2013). Humanin has been shown to play a role in stress resistance, providing resistance to oxidative stress in rat renal cultures (Yang, Zhang et al. 2008) and injections of humanin analogues have protective effects in transgenic murine models of Alzheimer's disease (Niikura, Sidahmed et al. 2011, Zhang, Zhang et al. 2012).

The non-coding regions of the genome are mainly found in the displacement loop (D-loop) which contains the control element for mtDNA transcription and replication (Arnberg, van Bruggen et al. 1971, Kasamatsu, Robberson et al. 1971). Large areas, of up to 150bp, in the D-loop appear, however, to be dispensable in humans (Behar, Blue-Smith et al. 2008). The D-loop is so named because it was identified in electron micrographs as containing triple stranded DNA, which was hypothesised to be a stalled replication intermediate (Kasamatsu, Robberson et al. 1971). An R-loop, made up of double stranded DNA hybridized with a single strand of RNA, has also been observed *in vivo* and is thought to also play a role is in the regulation of transcription (Xu and Clayton 1996, Brown, Tkachuk et al. 2008).

Nuclear encoded proteins are necessary for the regulation of mtDNA, its transcription and translation. MtDNA only codes for 13 subunits of the five ETC complexes; the remaining subunits are nuclear encoded and thus co-ordinated gene expression in both the mitochondria and the nucleus is required (Figure 1.3B).

1.2.3.1 Transcription of mtDNA

In 1982, the yeast mtRNA polymerase, *RP041*, was isolated (Greenleaf, Kelly et al. 1986). Unlike multi-subunit bacterial RNA polymerase, *RP041* encoded a single subunit polymerase homologous to T3 and T7 bacteriophage (Masters, Stohl et al. 1987). Human mtRNA polymerase (*POLRMT*), also encodes a single subunit protein, homologous to phage RNA polymerases (Tiranti, Savoia et al. 1997). It is made up of two domains, one is catalytic and the other is proposed to play a role in coupling mtDNA transcription and replication (Shadel 2004).

Genes are located on both strands of mtDNA, although most mRNA and both rRNAs open reading frames are located on the heavy strand (Bonawitz, Clayton et al. 2006). Transcription is initiated from two promoters on the heavy strand (HSP1 and HSP2) and a single promoter on the light strand (LSP). Transcription from both HSP2 and LSP results in a transcript almost the length of the whole genome. Genes encoding tRNA are dispersed between the rRNAs and mRNAs within these polycistronic transcripts. It is removal of these tRNAs that results in individual mRNA and rRNA sequences.

Transcripts from HSP1 are relatively short terminating after the two rRNA genes (Bonawitz, Clayton et al. 2006).

Mitochondrial transcription factor A (TFAM) was first identified as essential for the transcription of mtDNA *in vitro* (Fisher, Topper et al. 1987). When TFAM levels are reduced by 15% in HeLa cells, mtDNA transcription drops by 50% (Kanki, Ohgaki et al. 2004). Mutational analysis and the construction of chimeric TFAM, from human TFAM and the yeast homolog, Abf2, which does not activate transcription, demonstrates that the C-terminal is required for transcription (Dairaghi, Shadel et al. 1995).

TFAM is a nuclear encoded, mitochondrial targeted protein. It is made up of two high mobility group (HMG) domains separated by a linker sequence, and a short C-terminal domain (Fisher and Clayton 1988, Parisi, Xu et al. 1993). The HMG domain is a DNA binding motif, known to bind to the minor groove of the DNA helix in either a specific or nonspecific manner (Stros, Launholt et al. 2007). Crystallography studies of human TFAM have recently shown that TFAM is able to bend mtDNA 180^{o}, in complex with the light strand promoter (LSP) (Ngo, Kaiser et al. 2011). Each HMG domain wedges into the minor groove forcing the DNA to bend. HMG1 has a higher affinity than HMG2, so it is suggested that HMG1 binds first, placing HMG2 closer to the mtDNA and thus increasing its probability of binding (Figure 1.4) (Ngo, Kaiser et al. 2011, Rubio-Cosials, Sidow et al. 2011).

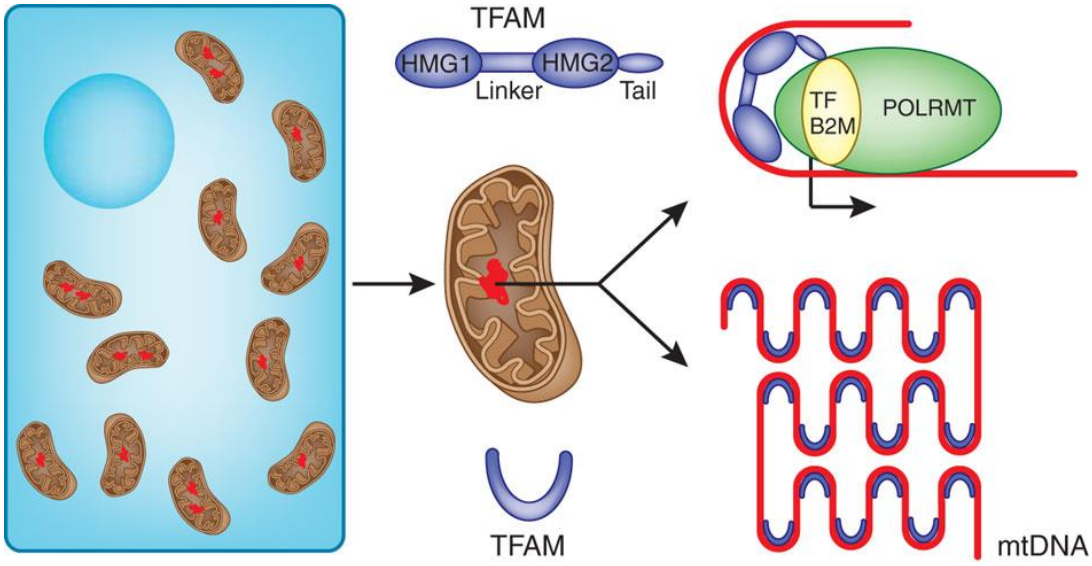

Figure 1.4 TFAM bends mtDNA 180º
TFAM binds upstream of transcription initiation, to recruit promoters. Non-specific binding of TFAM packages the DNA into its nucleoid structure. Figure from Hallberg and Larsson (2011) (Hallberg and Larsson 2011).

It has been disputed whether TFAM is both necessary and sufficient for *in vivo* mtDNA transcription (Goto, Matsushima et al. 2001) and two other mitochondrial transcription factors have been discovered, TFB1M and TFB2M (Bogenhagen 1996). TFAM's C-terminal region binds to TFB1M (McCulloch and Shadel 2003), so it is possible that TFAM binding is required for TFB1M recruitment. In the absence of TFAM *in vitro,* transcription is initiated at the heavy strand promoter 1, by a complex of mtRNA polymerase and TFB2M (McCulloch and Shadel 2003). Adding small amounts of TFAM increases transcription at the light strand promoter and adding large amounts of TFAM returns it to normal (McCulloch and Shadel 2003).

1.2.3.2 MtDNA Replication

Replication of mtDNA is carried out by a multi-protein 'replisome'. This is made up of Twinkle, a helicase that unwinds the DNA, mtDNA single stranded binding proteins which maintain the DNA in an open state and DNA polymerase γ, which synthesises the new strand of DNA. All of these components are encoded in the nucleus.

Electron microscope images of isolated rodent mitochondria led to the development of the strand displacement model (SDM) of mtDNA replication (Figure 1.5) (Kasamatsu and Vinograd 1973). In this model mtDNA replication is initiated at an origin of heavy strand synthesis (OH) at the start of the D-loop. Unidirectional replication of this strand continues for about two thirds of the genome until the origin of light strand synthesis (OL) is revealed. When this happens, replication can initiate in the opposite direction, leading to a delay before the displaced strand is replicated. This model is now disputed as conflicting evidence has been reported. Two-dimensional agarose gel electrophoresis (2D-AGE) of mtDNA restriction fragments shows many replication arcs between OH and OL (Bowmaker, Yang et al. 2003). Thus, another model has been proposed, the symmetric strand-coupled replication model, in which replication occurs both symmetrically and bi-directionally, on the light and heavy strand, from multiple origins from a broad zone within the D-loop (Figure 1.5) (Bowmaker, Yang et al. 2003). 2D-AGE resolves DNA on the basis of shape and mass, addition of particular restriction enzymes to these gels has also revealed the presence of several types of replication intermediates, suggesting several different types of replication may occur simultaneously in the mitochondria. Three classes of mitochondrial replication intermediates, have been identified, one that would be expected by strand displacement replication (single stranded DNA), one that would be expected by symmetric strand-coupled replication (double stranded DNA) and another class with extensive RNA incorporation on the lagging strand (ERIOLS) (Holt, Lorimer et al. 2000, Yang, Bowmaker et al. 2002). A third model of mtDNA replication has been devised to account for these ERIOLS (Figure 1.5), in which RNA is incorporated throughout the lagging strand during the replication of mtDNA (RITOLS model) (Yasukawa, Reyes et al. 2006, Holt and Reyes 2012). This model is very similar to the strand-coupled model of replication; however, in this model RNA is incorporated into the lagging strand and then converted to DNA (Holt and Reyes 2012).

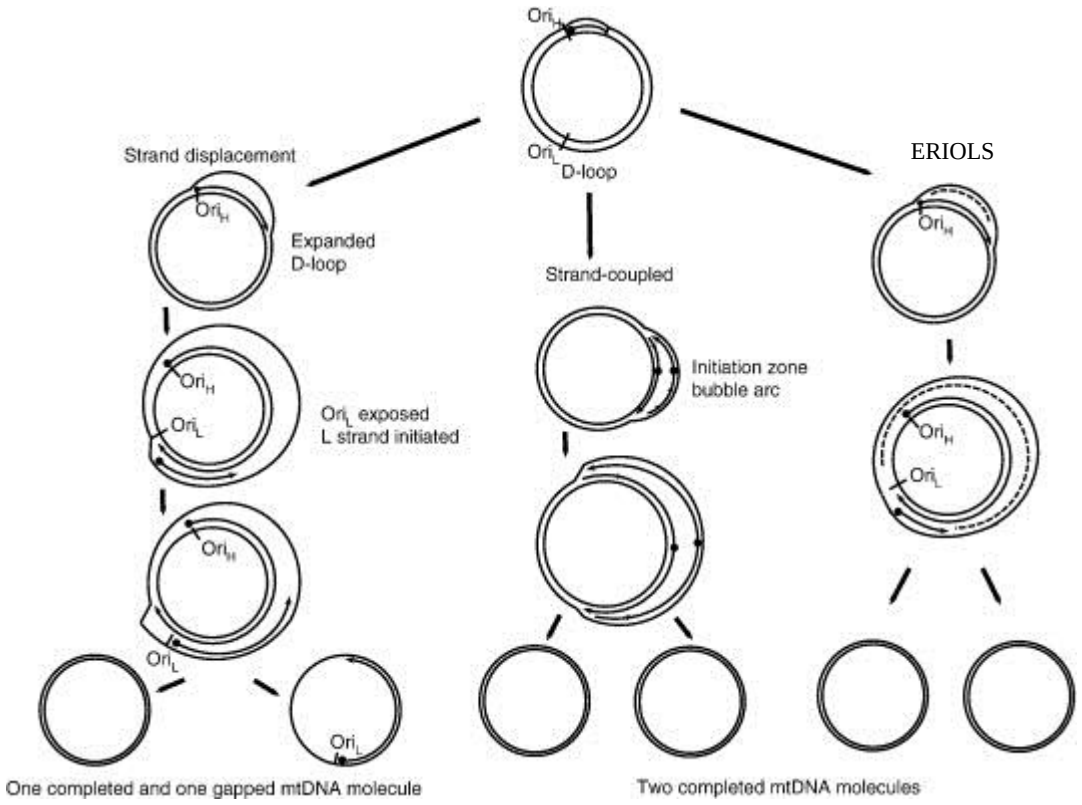

Figure 1.5 Models of mtDNA replication.
In the strand displacement model, replication starts at the OH. Only once the initial strand reaches the OL does replication of the complementary strand begin. This results in single strand intermediates of replication. In the stand-coupled model replication can initiate from multiple origins, which form bubble arcs. Strands proceed in a bidirectional symmetrical manner, creating double stranded intermediates. In the third model, replication is initiated from the OH, but as replication proceeds complementary RNA is also incorporated, which is later replaced with DNA. This results in DNA coupled to RNA intermediates. Figure from Kasiviswanathan et al. (2012) (Kasiviswanathan, Collins et al. 2012).

Overexpression of *TFAM* increases the number of replication intermediates associated with the stand coupled model, with some evidence that this is due to slowing of the replication fork (Pohjoismaki, Wanrooij et al. 2006). This led to the hypothesis that TFAM levels influence the type of DNA replication that occurs (Pohjoismaki, Wanrooij et al. 2006). TFAM's role in replication seems to be mainly due to its non-specific DNA binding, which has been shown to package mtDNA into its nucleoid structure (Figure 1.4) (Kang, Kim et al. 2007, Kaufman, Durisic et al. 2007). This packaging role is also thought to maintain mtDNA stability, as reduction of *TFAM* expression via RNAi in HeLa cells, or tissue specific *TFAM* knockout mice, cause a corresponding decrease in mtDNA levels (Larsson, Wang et al. 1998, Kanki, Ohgaki et al. 2004).

Replication of mtDNA appears to be controlled by mitochondrial - endoplasmic reticulum (ER) contacts. In human cell lines, GFP-tagged mitochondrial polymerase localises to a subset of mitochondrial - ER contacts in which the mitochondria lie perpendicular to the ER. Perturbation of ER morphology, to increased sheet-like structures rather than tubules, reduced levels of EdU-incorporation in mitochondrial nucleoids (Lewis, Uchiyama et al. 2016).

1.2.3.3 mtDNA inheritance

Unlike nuclear DNA, which is propagated via Mendelian inheritance, mtDNA is maternally inherited. Mitochondria from the paternal sperm do enter the oocyte, however, their DNA is degraded (Sato and Sato 2013). MtDNA is therefore solely inherited maternally.

As there are multiple copies of mtDNA per cell, symmetric segregation of mitochondria must occur. In order to achieve symmetric segregation of mitochondria during cell division, mitochondria are tethered to the actin cytoskeleton via Myosin-XIX (Rohn, Patel et al. 2014). If Myosin-XIX levels are reduced, mitochondria move to the edge of the cell and cell division fails (Rohn, Patel et al. 2014). Connections to the actin-myosin cytoskeleton are also important for correct segregation of mtDNA within the mitochondria. OMM proteins that tether to the cytoskeleton, Mmm1, Mdm12 and Mdm10, maintain mtDNA at the membrane (Boldogh, Vojtov et al. 1998).

If all copies of mtDNA are identical in the cell this is called homoplasmy. However, mtDNA is located in the mitochondrial matrix, which due to the production of ROS is a reactive environment (Tuppen, Blakely et al. 2010). In addition, DNA repair mechanisms are less efficient in mitochondria than the nucleus (Akbari, Sykora et al. 2015). Therefore, mutations in mtDNA are common (Tuppen, Blakely et al. 2010). This leads to heteroplasmy of mtDNA, in which different copies of mtDNA contain different mutations within one cell (Taylor and Turnbull 2005). The threshold hypothesis suggests that there is a threshold over which a mutation may cause biochemical and clinical defects. This is particularly important in maternal mitochondrial inheritance, in which a genetic bottleneck can occur, that may lead to an increased load of deleterious mtDNA mutations. During oocyte formation, a restricted number of mitochondria are

segregated into the oocyte. There is then a 50-fold increase in mtDNA as these mitochondria replicate (Chen, Prosser et al. 1995). If mitochondria with deleterious mtDNA mutations were segregated into the oocyte, then their damaged mtDNA will be amplified and increase the load of that mutation (Brown, Samuels et al. 2001). Selection against severe mtDNA mutations has been observed in the murine germline (Fan, Waymire et al. 2008). Similarly, selection against a temperature sensitive COXI mutation was also observed in *Drosophila* (Hill, Chen et al. 2014). Selective proliferation of mtDNA that supports more robust OXPHOS may explain this phenomenon (Ma, Xu et al. 2014).

1.2.4 Reactive Oxygen Species

Mitochondria are the main source of reactive oxygen species (ROS) in the cell, as ROS are produced as a by-product of OXPHOS. When electron carrier complexes prematurely transfer a single electron to molecular oxygen, the free-radical, superoxide is generated in either the IMS or matrix (Shadel and Horvath 2015). The rate of superoxide production is governed by the concentration of O_2 and electron donors within the mitochondria (Murphy 2009). When activity of the electron transport chain is reduced (by mutations or loss of ETC complexes for example), the NADH:NAD^+ ratio is relatively high. The proportion of fully reduced FMN, the complex I cofactor which accepts electrons from NADH, is therefore also high. If the donated electrons cannot pass along the ETC, then fully reduced FMN donates an electron to O_2 instead, creating superoxide (Murphy 2009). Superoxide is also produced when ATP production is impaired, causing a reduced pool of Coenzyme Q (due to increased electron supply) and a high proton motive force. In these conditions electrons flow backwards and are thought to be donated to O_2 from Complex I via FMN or the Coenzyme Q binding site (Murphy 2009). Complex III, which accepts electrons from Coenzyme Q, has also been reported to produce superoxide, although substantial amounts of ROS are only produced when antimycin directly inhibits complex III acceptance of an electron from Coenzyme Q (Andreyev, Kushnareva et al. 2005). Recently, it has been revealed that complex II also has the capacity to generate ROS. Complex II produces ROS at a comparable rate to maximum complex I and III ROS production, in conditions of low succinate concentration and complex I and complex III inhibition (Quinlan, Orr et al. 2012).

Superoxide has lower reactivity than other free radicals (Indo, Yen et al. 2015), however, it forms the extremely reactive peroxynitrite ($ONOO^-$) when it reacts with nitric oxide (NO). Superoxide dismutase (SOD) enzymes scavenge superoxide preventing this reaction from occurring, converting superoxide into hydrogen peroxide (H_2O_2). CuZnSOD (SOD1) acts in the cytoplasm and IMS (Okado-Matsumoto and Fridovich 2001) and has been associated with ageing and neurodegenerative diseases (Indo, Yen et al. 2015). MnSOD (SOD2) is targeted to the mitochondrial matrix and is also found on the IMM (Okado-Matsumoto and Fridovich 2001). There is also an extracellular SOD, ECSOD (SOD3). H_2O_2 is converted into water and oxygen by catalase peroxiredoxins and glutathione peroxidase enzymes (Figure 1.6).

1.2.4.1 ROS induced damage and signalling

Due to their highly reactive nature, ROS can cause damage to lipids, proteins and DNA (Schieber and Chandel 2014). Overproduction of ROS has been associated with numerous diseases, from cancer and diabetes to neurodegeneration. In 1956, Harman proposed the free radical theory of ageing, which hypothesised that ageing was a side effect of the damage caused by ROS (Harman 1956). Indeed, levels of mitochondrial H_2O_2 correlate to ageing in *Drosophila* (Cocheme, Quin et al. 2011). If this theory is correct, then reducing cellular ROS should increase healthy lifespan. Longevity studies in mice and *Drosophila* provide unclear evidence on whether ROS do contribute to ageing. Increased cytosolic SOD and catalase activity was reported to increase *Drosophila* lifespan (Orr and Sohal 1994), although other groups have had difficulty replicating this data (Mockett, Sohal et al. 2010). In mice, ectopic expression of catalase in mitochondria increased lifespan as well as reducing cataracts and cardiac pathology (Schriner, Linford et al. 2005). Overexpression of cytosolic SOD, however, did not increase murine longevity (Huang, Carlson et al. 2000). Loss of three of the five *C. elegans* SODs actually *increases* lifespan, contrary to the free radical theory of ageing (Van Raamsdonk and Hekimi 2009). Moreover, exposure to low concentrations of the oxidant Paraquat also increased longevity in worms (Yang and Hekimi 2010). Proteomic analysis of the oxidative state of cysteine residues in *Drosophila*, revealed no change in the redox state of proteins in aged flies (Menger, James et al. 2015).

The role of ROS in ageing may be difficult to elucidate because as well as causing damage, ROS also play a role in cellular signalling. This redox signalling is thought to be mediated via H_2O_2 oxidation of proteins' cysteine residues (Figure 1.6). ROS act on numerous cellular pathways, including MAPK cascades and HIF. HIF-1α, which is normally degraded in normoxia, can be stabilised in normoxia by ROS signalling (Knowles, Raval et al. 2003). Conversely, in hypoxic conditions ROS can reduce HIFs accumulation and DNA-binding activity (Brune and Zhou 2003).

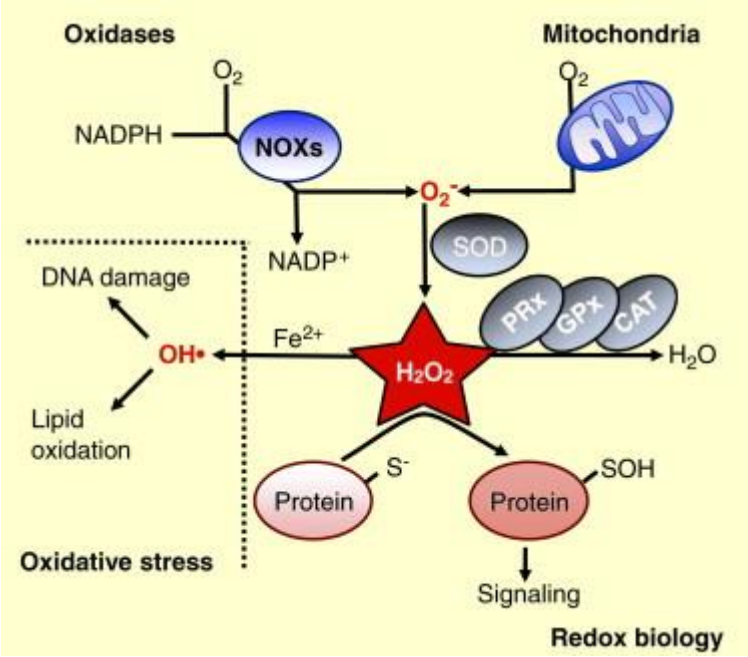

Figure 1.6 Cellular ROS pathways
ROS are produced as a by-product of OXPHOS or NADPH oxidase enzymes (NOXs). Superoxide is converted to H_20_2, which is either converted to water, oxidises cysteine residues for cellular signalling (redox biology), or in high quantities causes cellular damage when converted to hydroxyl radicals, catalysed by iron in the Fenton reaction (oxidative stress). Figure from Schieber and Chandel 2014 (Schieber and Chandel 2014).

1.2.5 Additional mitochondrial functions

1.2.5.1 Iron sulphur cluster synthesis

The membrane potential created by the electron transport chain (ETC) is essential for the proton motive force that produces ATP via ATPsynthase. However, it also creates a driving force for accumulation of positively charged ferrous iron (Fe^{2+}) to accumulate in the mitochondrial matrix. Once inside the mitochondria Fe^{2+} is incorporated into iron

sulphur (Fe-S) clusters in a two stage process. In the first stage, a *de novo* Fe-S cluster is created on a scaffold protein. This requires a donation of electrons to reduce sulphur to sulphide. In the second stage the liable Fe-S cluster is transferred to an apoprotein to create the holoenzyme (Lill 2009).

Fe-S clusters are important co-factors for enzymes that carry out redox reactions. The electronic conformation of the clusters allows them to easily donate and accept electrons. This makes them particularly important in the complexes that make up the ETC. Complex I contains eight Fe-S clusters (Rouault 2015). Fe-S clusters synthesised in the mitochondria are also exported and incorporated into cytosolic and nuclear enzymes, such as DNA polymerases and helicases (Stehling, Vashisht et al. 2012).

1.2.5.2 Calcium Sequestering

Positively charged calcium ions (Ca^{2+}) are also driven into the mitochondrial matrix down the electrochemical gradient. Positioning of mitochondria next to calcium transporters on the endoplasmic reticulum and the plasma membrane of synaptic terminals means that mitochondria are particularly sensitive to influxes of calcium and therefore act a calcium buffers in the cell (Rizzuto, De Stefani et al. 2012).

Accumulation of Ca^{2+} in the matrix signals increased stimulation of the cell and therefore an increase in ATP demand. Influx of Ca^{2+} increases the metabolic activity of the mitochondria as Krebs cycle dehydrogenases, such as isocitrate dehydrogenase and α-ketoglutarate dehydrogenase, are directly regulated by Ca^{2+} (Denton and McCormack 1985, Wan, LaNoue et al. 1989). Increased Ca^{2+} therefore results in increased free NADH able to donate electrons to the ETC. A vicious cycle is therefore created when OXPHOS complexes are damaged; deficits in ETC reduce the membrane potential, which is required for influx of Ca^{2+}, so less NADH is available for ATP production (Visch, Rutter et al. 2004).

1.2.5.3 Apoptosis

Ca^{2+} signalling also plays a key role in mitochondrial initiation of apoptosis. This is the process of programmed cell death which removes damaged or unwanted cells for the benefit of the organism as a whole. Cell intrinsic apoptosis is triggered by the release of proteins from the IMM which activate a family of cysteine proteases, called caspases, which digest the cellular components. The exact mechanisms are, however, not conserved from mammals to invertebrates (Figure 1.7).

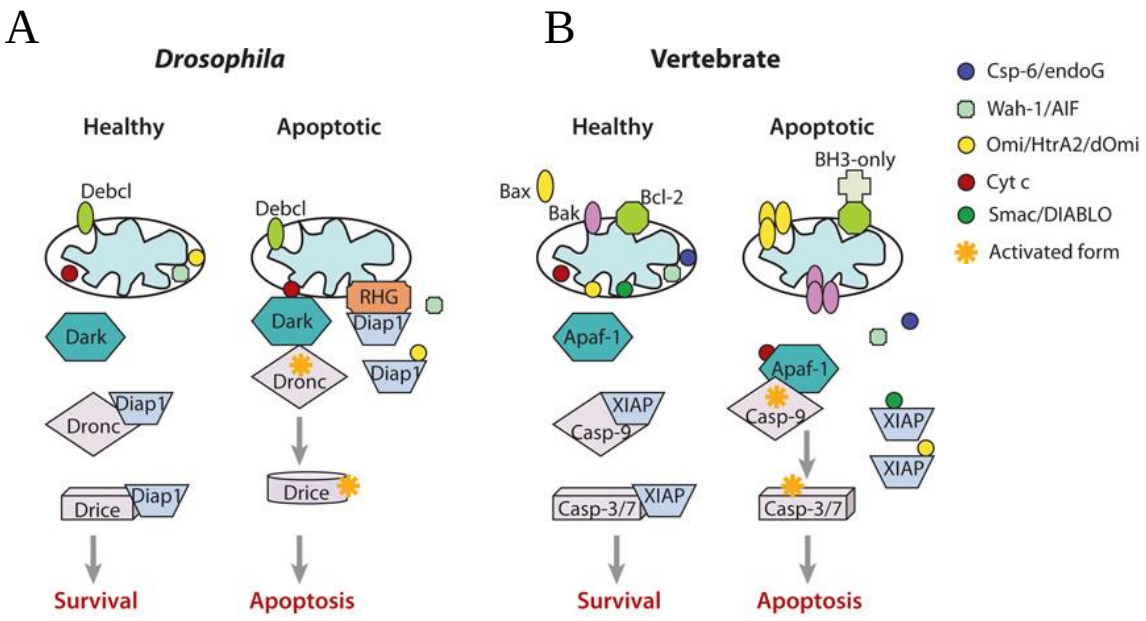

Figure 1.7 Apoptotic mechanisms in *Drosophila* and vertebrates
(A) *Drosophila* caspases, Dronc and Drice, are normally ubiquitinated for degradation by Diap1. Apoptosis is triggered when Diap1 itself is ubiquitinated by Reaper, Hid and Grim (RHG). Omi and AIF are released from the IMM to further interact with Diap1 and trigger caspase independent events, respectively. **(B)** Vertebrate apoptosis is mediated by Bax translocation to the mitochondria triggering the release of cytochrome c (Cyt c). In normal conditions Cyt c shuttles electrons between OXPHOS complex III and IV, however, cytosolic Cyt c binds Apaf1 to initiate formation of the apoptosome. Figure adapted from Wang and Youle 2009 (Wang and Youle 2009).

1.2.6 Mitochondrial Dynamics

1.2.6.1 Fusion and fission

Mitochondria function as a dynamic network that are constantly fusing, dividing and moving around the cell. Fusion allows communication between mitochondria and protects against transient mitochondrial dysfunction, as it allows sharing of mtDNA and its products (Chen, Vermulst et al. 2010, Rolland, Motori et al. 2013). Fission is required for mitochondrial movement, allowing mitochondria to move to the parts of the cell with the highest demand. Fission events are also needed for the removal of damaged mitochondrial components. The interplay of fission and fusion is therefore extremely important in the maintenance of healthy mitochondria (Figure 1.8).

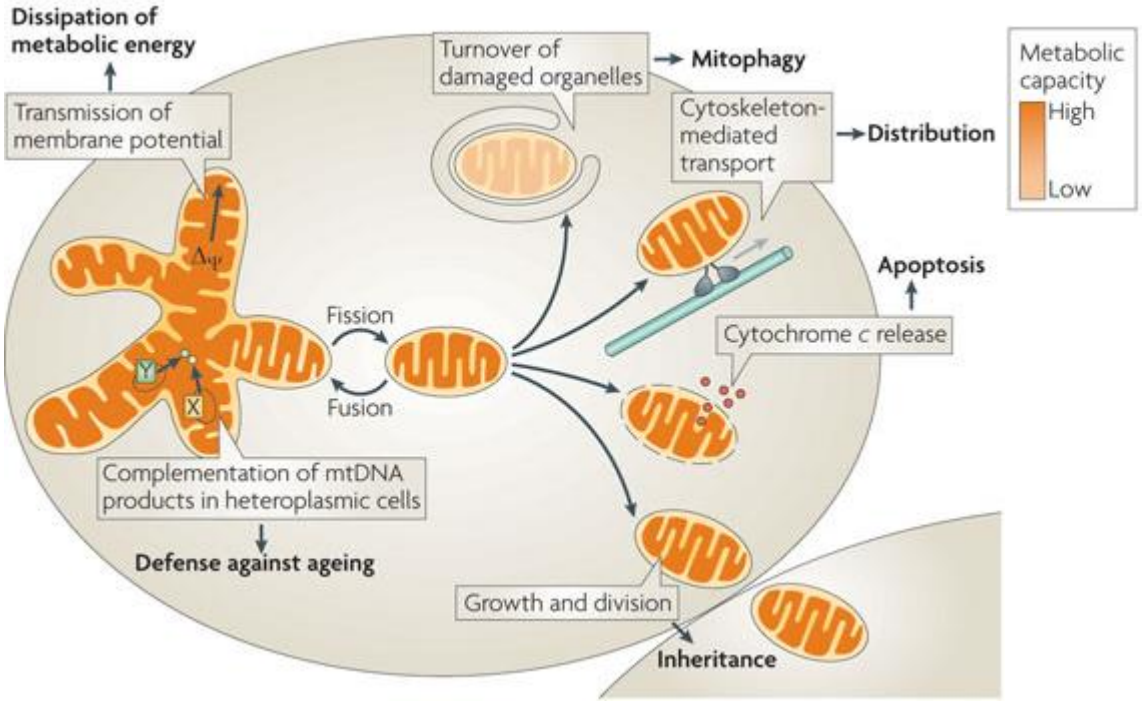

Figure 1.8 The roles of mitochondrial fission and fusion
Fusion of mitochondria occurs in highly active cells allowing mitochondria to act as a network, pooling of mtDNA product and dissipation of ATP. Fission is important for mitochondrial inheritance, transport and the turnover of damaged mitochondrial components. Figure adapted from Westermann 2010 (Westermann 2010).

Fusion of mitochondria is a particularly complex process due to the double membrane structure of the organelle, this means a fusion event requires four membranes to fuse into two. It is hypothesised that membranes due to fuse are tethered together and energy

from GTP is then used to mix the lipid bilayers (Sesaki and Jensen 2001). The first regulator of mitochondrial fusion was identified in *Drosophila* (Hales and Fuller 1997). *Fuzzy onions,* which is required for male fertility, is a large transmembrane, dynamin-related GTPase. Members of the same protein family are conserved in yeast, worms and mammals, and as they also regulate mitochondrial fusion they are called mitofusins (Hales and Fuller 1997, Westermann 2010). Mitofusins regulate fusion of the OMMs, the IMMs are fused by the dynamin-related GTPase optic atrophy protein 1 (OPA1). OPA1 and mitofusins can act independently of each other, as mutations in OPA1 disrupt fusion of the IMM, without inhibiting OMM fusion (Malka, Guillery et al. 2005). However, the outer membrane protein, Ugo1p, is essential for inner membrane fusion, suggesting that normally these to processes are co-regulated (Sesaki and Jensen 2001).

Dynamin related protein 1 (Drp1, known as Dnm1 in yeast) is the master regulator of mitochondrial fission in eukaryotic cells. In yeast, recruitment of Dnm1 depends on two proteins, mitochondrial fission 1 (Fis1) and mitochondrial division protein 1 (Mdv1). Fis1s anchors to the OMM and is necessary for the assembly of Dnm1 puncta on the OMM. Mutants of the WD repeat protein, Mdv1, retain Dnm1 OMM puncta, but are unable to complete mitochondrial division (Tieu and Nunnari 2000). Mdv1 is therefore thought to play role in a later stage of mitochondrial fission (Tieu and Nunnari 2000). It turns out Mdv1 interacts with Fis1 and Dnm1 to catalyse the fission reaction, using the WD repeat domain to interact with Dnm1 (Tieu, Okreglak et al. 2002).

Mutations in genes required for fission result in extended networks of mitochondria that are unable to move adequately around the cell. This is particularly apparent in neurons, due to their elongated shape and high energy demands at dendritic and axonal synapses. Dominant negative mutations in Drp1 lead to microencephaly, optic atrophy and premature death in humans (Waterham, Koster et al. 2007). Drp1 mutant mice are embryonic lethal with undeveloped forebrains (Ishihara, Nomura et al. 2009). Primary neuronal cultures from these mice reveals an accumulation of large mitochondria at the cell body with few mitochondria in neurites and a loss of synapses (Ishihara, Nomura et al. 2009).

1.2.6.2 Transport

Mitochondrial transport occurs along the microtubule cytoskeleton. Kinesin motors drag mitochondria towards the plus end of microtubules, whereas dynein motors move toward the minus pole (in axons this corresponds to anterograde and retrograde respectively). Mutation in Milton and mitochondrial Rho (Miro) in *Drosophila* results in a loss of synaptic mitochondria, identifying these proteins as adapters, required to hold the mitochondria and kinesin motors together (Stowers, Megeath et al. 2002, Guo, Macleod et al. 2005).

Spatial distribution of neuronal mitochondria correlates with synaptic activity, with mitochondria accumulating at active synapses. Live imaging of the murine sensory neurons shows that neuronal stimulation increases the speed of anterograde transport while having no effect of retrograde movement (Sajic, Mastrolia et al. 2014). Calcium concentration can also control the distribution of mitochondria. Nodes of Ranvier which have a high energy demand and accumulate mitochondria also have high concentrations of Ca^{2+}. Removal of Ca^{2+} results in the loss of mitochondria, suggesting that high Ca^{2+} causes stalling of mitochondria (Ohno, Kidd et al. 2011). Miro, which attaches mitochondria to kinesin motor proteins, contains two calcium-binding EF hand motifs (Fransson, Ruusala et al. 2003). Mutations in these EF hand motifs impairs Ca^{2+} dependant dissociation from kinesin motor proteins *in vitro* (MacAskill, Rinholm et al. 2009). Furthermore, transfection of neuronal cultures with EF hand Miro mutants selectively impairs mitochondrial stalling in response to neuronal activation (MacAskill, Rinholm et al. 2009). These data indicate that the EF hand of Miro mediates Ca^{2+} regulation of mitochondrial localisation in neurons by initiating dissociation from kinesin motors.

1.2.7 Mitochondrial Turnover

1.2.7.1 Mitophagy

Autophagy is a self-degradative process that removes misfolded proteins, damaged organelles and pathogens from within the cell. Mitophagy is a form of autophagy which selectively clears mitochondria. PTEN induced putative kinase 1, PINK1, is normally degraded in the mitochondrial matrix, however, when the membrane potential

decreases, PINK1 accumulates on the OMM. PINK1 phosphorylates Parkin, promoting its translocation to mitochondria and its E3 ubiquitin ligase activity (Kim, Park et al. 2008, Narendra, Tanaka et al. 2008, Sha, Chin et al. 2010). Parkin is then able to ubiquinate numerous OMM proteins, such as TOM and Porin targeting mitochondria for degradation. Parkin also ubiquitinates Mitofusins, resulting in fragmentation of dysfunctional mitochondria (Gegg, Cooper et al. 2010) and Miro, reducing transport of dysfunctional mitochondria (Liu, Sawada et al. 2012). These mechanisms were elucidated *in vitro*, however *in vivo* studies suggest that the role of PINK1 and Parkin may not be equivalent *in vitro* and *in vivo* (see Discussion 7.1.3). Mitophagy can also be stimulated in a PINK1/Parkin independent manner. HIF-1α stabilisation and iron chelation have both been implicated in PINK1/Parkin independent mitophagy (Allen, Toth et al. 2013). Increased OXPHOS activity also induces increased mitophagy, which promotes energy efficiency and may protect against damage caused by increased ROS production (Mishra and Chan 2016). This is mediated by recruitment of the small GTPase Rheb, which interacts with regulators of autophagy (Melser, Chatelain et al. 2013).

1.2.7.2 Biogenesis

Mitochondrial biogenesis is not thought to occur *de novo*, but rather by expansion and division of existing mitochondria, in response to environmental factors. Physical activity is observed to correlate with increased OXPHOS activity and accumulation of mitochondria in muscle tissue (Holloszy 1967, Gollnick, Armstrong et al. 1972). Thyroid hormone is also associated with increased mitochondrial mass and enhanced synthesis of cytochrome c (Booth and Holloszy 1975). Adaptive thermogenesis, in which mammals increase their body heat when exposured to cold temperatures by ETC activity uncoupled from ATP production, also results in an increase in mitochondrial mass (Cannon and Nedergaard 2004). Analysis of mice exposed to temperatures of 4°C allowed identification of the master regulator of mitochondrial biogenesis, Peroxisome proliferator activated receptor γ co-activator 1α, (PGC-1α) (Puigserver, Wu et al. 1998).

Biogenesis of mitochondria must co-ordinated environmental signals with expression of mitochondrial proteins encoded in the nucleus and mitochondria themselves. 99.1% of mitochondrial genes are nuclear encoded, so the expression of the mitochondrial

proteome is mainly controlled by the nucleus (Hock and Kralli 2009). However, as mitochondria also respond to environmental stresses, there are also retrograde signals which allow cells to adjust to fluctuating demands on mitochondria (Woodson and Chory 2008). PGC-1α responds to environmental factors and synchronises biogenesis by binding transcription factors such peroxisome proliferator –activated receptors (PPAR), estrogen related receptors (ERR) and nuclear respiratory factors (NRF)
(
Figure **1.9**) (Finck and Kelly 2007).

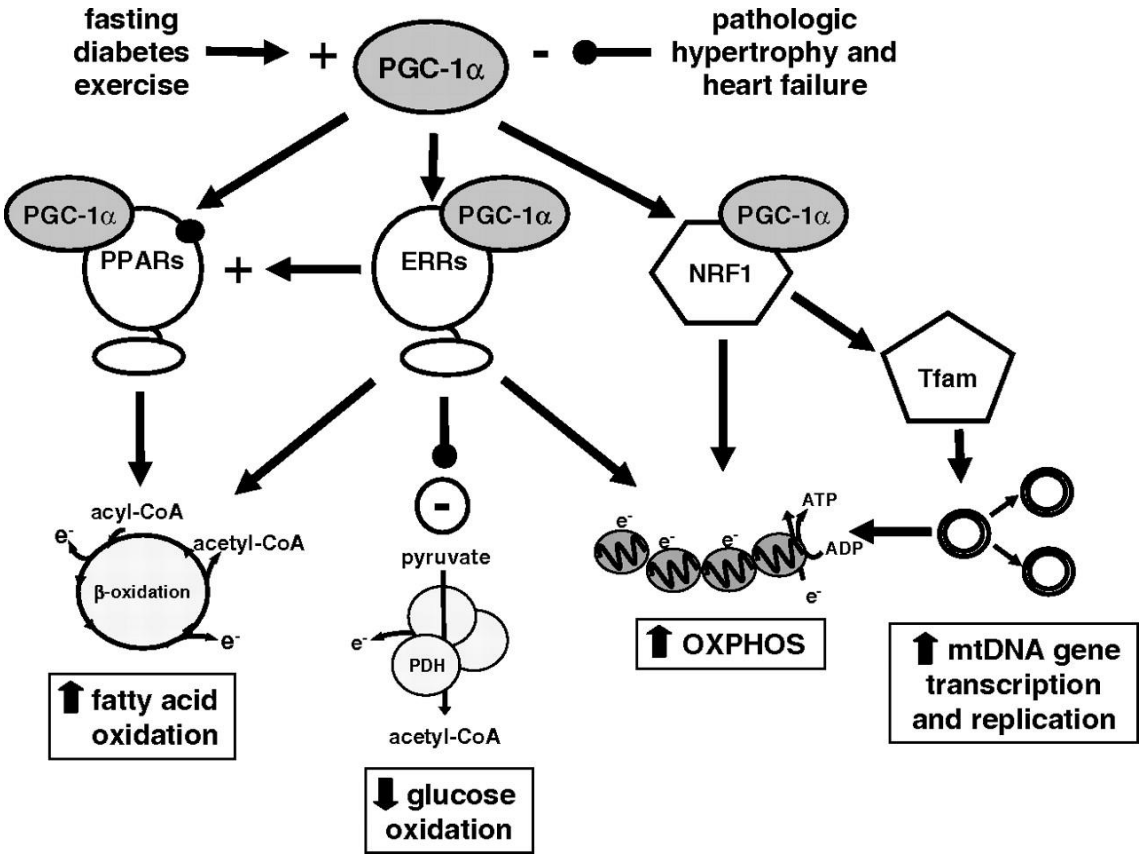

Figure 1.9 PGC-1α signalling cascade
PGC-1α binds transcription factors PPARs, ERRs and NRF1 to increase expression of genes required for fatty acid oxidation and OXPHOS and to inhibit glucose oxidation. Figure from Finck and Kelly 2007 (Finck and Kelly 2007).

Nuclear respiratory factors, NRF1 and NRF2, were the first regulators identified in vertebrates as co-ordinators of nuclear encoded mitochondrial genes. NRF1 and NRF2 regulate gene expression of nuclear encoded OXPHOS complex subunits. They also control expression of nuclear genes involved in mitochondrial import, *TOM22*, and transcription of mtDNA, *TFAM* (Booth and Holloszy 1975). By regulating expression of nuclear encoded OXPHOS subunits and the expression of nuclear genes that regulate

mitochondrial gene expression, these factors are implicated in the co-ordination of the two genomes.

PGC-1α and sirtuin 1 (SIRT1), a NAD^+ dependant protein deacetylase, are known to control mitochondrial biogenesis by regulating expression of mitochondrial genes in the nucleus (Nemoto, Fergusson et al. 2005). However, PGC-1α and SIRT1 have also been detected in mitochondria isolated from HeLa cells and murine organs, where they interact with TFAM. This suggests that they directly regulate levels of mtDNA encoded protein expression as well (Nemoto, Fergusson et al. 2005).

1.3 Mitochondrial damage in disease

Mitochondrial dysfunction is associated with a wide variety of diseases. Primary mitochondrial diseases are caused by mutations in genes within the mitochondrial genome or in nuclear genes that are required for mitochondrial function. Environmental damage to mitochondria can also lead to disease states. Clinical presentation of mitochondrial dysfunction is extremely varied, in the tissues affected and the effects on those tissues. This may reflect the multifunctional nature of mitochondria.

1.3.1 mtDNA diseases

The role of mtDNA in mitochondrial disease was first identified in 1988, when Holt et al., identified two populations of mtDNA in muscles of patients with mitochondrial myopathies (neuromuscular disorders), due to a 7kb deletion in a subset of muscle mtDNA (Holt, Harding et al. 1988).

Due to the nature of mtDNA, any damage, due to deletions or mutations, affects mitochondrial encoded OXPHOS subunits, or the translation of these proteins. However, the outcome of different deletions and mutations are heterogeneous (Table 1).

Table 1. Causes and symptoms of the most common mtDNA diseases.

Disease	Cause	Symptoms	Tissues affected
Pearson's Syndrome	Large mtDNA deletions	Anaemia and pancreatic dysfunction	Haematopoietic cells
Kearns-Sayre Syndrome	Large mtDNA deletions	Cerebellar ataxia, paralysis of muscles that move the eyeballs, droopy eyelids and retinopathy	Multi-system disorder
Progressive external ophthalmoplegia (PEO)	Large mtDNA deletions	Paralysis of muscles that move the eyeballs	Muscle
Mitochondrial encephalopathy lactic acidosis, and stroke-like episodes	Point mutation in mitochondrial $tRNA^{Leu}$, also associated with mutations in other tRNA and	Stroke and paralysis. Death in childhood or adolescence	Multi-system disorder, particularly effecting the nervous system,

Disease	Cause	Symptoms	Tissues affected
syndrome (MELAS)	mitochondrial encoded proteins		muscles and endocrine system
Myoclonus epilepsy and ragged-red fibres (MERRF)	Point mutations in $tRNA^{Lys}$	Epilepsy and excess succinate dehydrogenase in muscle tissue (ragged red fibres)	Multi-system disorder, particularly effecting muscles and the nervous system
Leber's hereditary optic neuropathy (LHON)	Homoplasmic point mutations in complex I subunits *ND1, ND4* and *ND6*	Loss of vision, mostly in males	Retinal ganglion cells
Leigh syndrome	Predominantly caused by nuclear mutations, but also can be caused by mutations in a complex V subunit, *ATP6*	Developmental delay, respiratory problems, lesions in the basal ganglia and brainstem and premature death	Multi-system disorder with particularly strong effects on the nervous system

Pioneering work is currently being carried out in Newcastle, to develop mitochondria replacement therapy. This therapy involves donation of a zygote containing healthy mtDNA from a third party, with nuclear material removed. Pronuclear DNA from the fertilised egg of a woman with mtDNA problems is then fused with the healthy zygote. This aims to eliminate inheritance of mtDNA damage from mother to child. In practice the transfer of mtDNA is reduced to <2%, so the risk of mtDNA disease is greatly reduced although not completely eliminated (Hyslop, Blakeley et al. 2016).

1.3.2 Mitochondrial disease caused by nuclear mutations

Nuclear mutations in mitochondrial proteins can also cause deficits in OXPHOS subunits or assembly of OXPHOS complexes. The single most common cause of Leigh syndrome is mutations in the complex IV assembly factor *Surf1* (Lee, El-Hattab et al. 2012).

Nuclear mutations can also result in damaged maintenance of mtDNA. This can be caused by mutations in the nuclear genes required for the mitochondrial replisome, such as *Pol γ* and *Twinkle*, or mutations in nuclear genes required for the supply of deoxynucleotide triphosphates (dNTPs) for replication of mtDNA (Copeland 2008).

Mitochondrial processes other than OXPHOS can also be affected by nuclear mutations, for example fission and fusion. Dominant *OPA1* mutations, impairing fusion, in patients, leads to reduced mitochondrial mass and mtDNA, caused by increased fragmentation and mitophagy (Dombi, Diot et al. 2016). Nuclear mutations disrupting fission have also been reported to cause mitochondrial disease. Mutations in *STAT2*, an immune response gene that has been shown to activate Drp1, caused severe neurological impairments in patients (Shahni, Cale et al. 2015).

Dysfunction of mitochondrial dynamics has also been implicated in neurodegenerative disorders. Mutations in *KIF1B*, a member of the kinesin motor superfamily, required for mitochondrial transport, is associated with the neurodegenerative disease Charcot-Marie-Tooth (Jani-Acsadi, Krajewski et al. 2008). Clinically, this presents as muscle weakness, sensory loss and atrophy of the hands.

1.3.3 Neurodegenerative disease and mitochondrial dysfunction

Most neurodegenerative diseases are complex disorders with multiple causes influenced by genetic and environmental factors (Ballard, Gauthier et al. 2011, A. Armstrong 2013, Ramanan and Saykin 2013, Kalia and Lang 2015). Discussion of all of these factors is beyond the scope of this thesis, so I will focus on the role of mitochondrial dysfunction in neurodegenerative disorders, which is increasingly investigated and accepted (Lezi and Swerdlow 2012). Mitochondrial dysfunction is considered by some researchers to be a common pathway of several neurodegenerative disorders (Lezi and Swerdlow 2012).

Parkinson's disease (PD) is characterised pathologically by a loss of dopamine releasing neurons in the substantia nigra pars compacta and the formation of intracellular Lewy bodies (aggregates of α-synuclein often coated in ubiquitin). A causative role of mitochondrial dysfunction was first suggested by Langston from the study of 1-methyl-4-phenyl-1,2,3,6-tetrahydropyridine (MPTP), a synthetic drug which gave users Parkinson's disease symptoms (Langston, Ballard et al. 1983). The active form of MPTP (1-methyl-4-phenylpyridinium, MPP+), was found to inhibit complex I activity (Murphy, Krueger et al. 1995) and decrease mtDNA by selectively decreasing mtDNA replication (Miyako, Irie et al. 1999). Complex I deficiencies in PD were first identified

by Shapira et al., in post mortem brain tissue (Schapira, Cooper et al. 1989:Schapira, 1990 #1068) and were also identified in idiopathic PD patients platelets (Parker, Boyson et al. 1989). Inhibiting complex I activity in cell culture also increases aggregates of α-synuclein (Lee, Shin et al. 2002). Cytoplasmic hybrids containing mtDNA from PD patient cells in a human neuroblastoma cell line, show complex I deficiencies and increased ROS production (Swerdlow, Parks et al. 1996). We recently showed that complex I activity is also impaired and mtDNA is lost in the frontal cortex of patients with Parkinson's disease dementia (PDD), compared to aged matched controls and patients with Parkinson's disease who have not developed dementia (Gatt, Duncan et al. 2016). This indicates that dementia in these patients may be linked to a spread of mitochondrial dysfunction throughout the brain.

Most cases of PD arise spontaneously, however, genetic studies of familial forms of PD have linked several genes to the disorder, including *Leucine- Rich Repeat Kinase 2* (*LRRK2*), *Pten-Induced Putative Kinase 1* (*PINK1*), *Parkin* and *DJ-1* (Xiong, Wang et al. 2009). LRRK2 has been shown to modulate mitochondrial vulnerability as it improves viability of *C. elegans* in the presence of a complex I inhibitor (Saha, Guillily et al. 2009), and also may play a role as a negative regulator of mitophagy (Alegre-Abarrategui, Christian et al. 2009). PINK1 and Parkin, initiate mitophagy of depolarised mitochondria (see 1.2.7.1). This evidence suggests a pivotal role of altered mitophagy in the mitochondrial pathology of PD. DJ-1 acts in response to oxidative stress. Mutations in *DJ-1* genes in *Drosophila* causes increased sensitivity to paraquat, motor impairments and reduced lifespan (Park, Kim et al. 2005, Lavara-Culebras and Paricio 2007).

Mitochondrial dysfunction is also a very early sign of Alzheimer's disease (AD) and has been detected even before neurofibrillary tangles develop. Mitochondrial diameter and surface area are reduced and morphology altered in AD patients (Baloyannis, Costa et al. 2004), as well as reduced mitochondrial biogenesis (Sheng, Wang et al. 2012) and loss of mitochondria in dendritic spines (Baloyannis 2006). Deficiencies in complex I, IV and V are also reported in AD patients compared to controls (Maurer, Zierz et al. 2000, Manczak, Park et al. 2004). Complex IV deficits in platelets from AD patients are accompanied by decrease ATP production and increased ROS (Cardoso, Proença et al. 2004). Increased levels of oxidative damage to mitochondrial and nuclear DNA has been reported in brain tissue of AD patients (Wang, Xiong et al. 2005:Mecocci, 1994

#1096). The amyloid-β plaques, characteristic of AD, have been reported to contribute to increased ROS production by impairing mitochondrial dynamics, leading to mitochondrial fragmentation (Wang, Su et al. 2008). ROS have also been reported to contribute to amyloid-β aggregation, as increased ROS exacerbates amyloid-β formation in a mouse model of AD (mutant for the amyloid precursor protein) (Karuppagounder, Xu et al. 2009).

Huntington's disease (HD) is known to be caused by expanded CAG repeats in the *Htt* gene on chromosome 4, encoding the Huntingtin protein. PET scans consistently show HD patients have reduced levels of glucose metabolism and NMR studies revealed increased levels of lactate (Jenkins, Koroshetz et al. 1993). Further evidence linking mitochondrial dysfunction to HD, comes from post mortem tissue, where levels of complex II and III are seen to have dropped in the basal ganglia of HD patients (Browne, Bowling et al. 1997).

1.3.3.1 Current treatments for AD and PD

Currently treatments for AD and PD reduce the symptoms of the diseases, but do not provide neuroprotection or impair disease progression.

Impairments in glutamatergic and cholinergic signalling in the AD brain have led to the development of five FDA approved drugs: four cholinesterase inhibitors, Tacrine, Donepenzil, Rivastigmine, Galantamine and a N-methy-D-aspartate (NMDA) receptor antagonist, Memantine. Combined treatment with Memantine and a cholinesterase inhibitors provides greater benefit than the individual drugs alone (Parsons, Danysz et al. 2013).

PD is characterised by a dramatic loss of dopaminergic neurons in the basal ganglia, which results in the motor symptoms of the disease. Therapeutic strategies have therefore mainly been focussed on dopamine replacement. L-3,4-Dihydroxyphenylalanine (L-Dopa) has been used as an anti-Parkinsonian agent since 1968 (Cotzias 1968). L-dopa is a precursor to dopamine, and is effective at treating PD motor symptoms. However, it results in acute phasic dopamine stimulation, which over time sensitises the dopaminergic system causing motor side-effects of involuntary

movements (dyskinesia). Other pharmaceuticals provide a more tonic release of dopamine, such as pramipexole, ropinirole and pergolide.

In order to limit disease progression, a number of drugs which protect dopaminergic neurons are being investigated. These include monoamine oxidase-B (MAO-B) inhibitors, anti-apoptotic drugs, growth factors, calcium channel blockers, glutamate antagonists and promitochondrial agents (coenzyme Q10, creatine). Trials of the MAO-B inhibitor, selegiline, and the promitochondrial drug, coenzyme Q10, have so far shown positive signs in reducing progression of motor symptoms (Shoulson, Oakes et al. 2002, Storch, Jost et al. 2007).

1.3.4 Animal models of mitochondrial dysfunction

Furthering our understanding of mitochondrial dysfunction and its consequences will allow for the development of more effective treatments for mitochondrial disease and hopefully facilitate therapies that target disease causes rather than just symptoms. To do this it is important to have *in vivo* models of mitochondrial dysfunction, as the activity of mitochondria, redox state, ATP production and membrane potential change with the physiological environment (Murphy 2009). Murine and *Drosophila* models of mtDNA loss and individual OXPHOS complex dysfunction are summarised in Table 2.

Table 2. *Drosophila* and mouse models of mtDNA loss and OXPHOS complex dysfunction

Organism	Gene	Phenotype	Reference
Fly	*Pol γ-α* overexpression	ubiquitous and muscle overexpression -lethality	(Lefai, Calleja et al. 2000)
Fly	*Pol γ-α* RNAi	ubiquitous - lethality neuronal - age-related motor deficits, DA neuron degeneration	(Humphrey, Parsons et al. 2012).
Fly	*Pol γ-β* mutant	loss of mtDNA, impaired cell proliferation in the CNS, pupal lethality	(Iyengar, Luo et al. 2002)
Fly	*mito-XhoI* mtDNA linearisation	ubiquitous- embryonic lethality neuronal- pupal lethal, synaptic mitochondria loss	(Xu, DeLuca et al. 2008) (Cagin, Duncan et al. 2015)
Fly	*ATP6* point mutation	reduced lifespan, neuromuscular degeneration, conditional paralysis	(Celotto, Frank et al. 2006)

Organism	Gene	Phenotype	Reference
Fly	*tko*^{25t} point mutation	developmental delay, hearing impairments, conditional paralysis	(Toivonen, O'Dell et al. 2001)
Fly	*COX6A* point mutation	reduced lifespan, age-related COX activity and ATP reduction, conditional paralysis and neurodegeneration	(Liu, Gnanasambandam et al. 2007)
Fly	*COX7A RNAi* expressed neuronally	conditional paralysis and locomotor impairments	(Kemppainen, Rinne et al. 2014)
Fly	*Surf1* RNAi	ubiquitous- larval lethality neuronal-increased lifespan and locomotor impairments	(Dell'agnello, Leo et al. 2007)
Mouse	*Twinkle* mutation 'deletor mice'	progressive ETC deficits in muscles and neurons	(Tyynismaa, Mjosund et al. 2005)
Mouse	*Pol γ* point mutation 'mutator mice'	ageing phenotypes e.g. hair and weight loss, anaemia, reduced fertility, reduced lifespan	(Trifunovic, Hansson et al. 2005)
Mouse	mtDNA from aged mice ‘mito-mice’	reduced lifespan, increased lactate, kidney failure	(Inoue, Nakada et al. 2000)
Mouse	*TFAM* knockout	ubiquitous- embryonic lethality DA neuron- progressive DA neurodegeneration, mtDNA loss and OXPHOS impairments	(Larsson, Wang et al. 1998) (Ekstrand, Terzioglu et al. 2007)
Mouse	*mito-PstI* induced mtDNA loss	neuronal- motor impairments DA neurons- progressive DA neurodegeneration and motor impairments	(Fukui and Moraes 2009) (Pickrell, Pinto et al. 2011)
Mouse	*ATP5A1* mutant	homozygous- lethal heterozygous- weight loss, abnormal albumin level in serum	(White, Gerdin et al. 2013)
Mouse	*ATPAF2* mutant	homozygous- lethal heterozygous- abnormal vertebrate morphology	(White, Gerdin et al. 2013)
Mouse	*NdufS5* knockout	ubiquitous and neuronal- reduced CI levels, growth and motor impairments, increased lactate and death at 7 weeks	(Kruse, Watt et al. 2008) (Quintana, Kruse et al. 2010)

1.3.4.1 Animal models of mtDNA loss and damage

Models of mtDNA loss and dysfunction have been developed by targeting proteins in the mtDNA replisome, Twinkle and DNA Pol γ. Mice with a mutation in *Twinkle* homologous to patients with PEO, are called 'deletor' mice as they accrue multiple deletions in mtDNA. These mice develop progressive ETC deficits in muscles and specific subsets of neurons (Tyynismaa, Mjosund et al. 2005).

In *Drosophila*, mtDNA loss has been stimulated by overexpression of the catalytic subunit of Pol γ (*Pol γ-α*, also known as *tamas*), as overexpression interrupts the process of replication (Lefai, Calleja et al. 2000). Ubiquitous and muscle specific overexpression is pupal lethal, whereas neuronal overexpression of *Pol γ-α* is not lethal, but does increase adult mortality (Lefai, Calleja et al. 2000). Neuronal expression of *Pol γ-α* RNAi, which results in decreased levels of mtDNA encoded OXPHOS complex subunits, has also been used to study neurodegeneration (Humphrey, Parsons et al. 2012). Expression of *Pol γ-α* RNAi in cholinergic neurons caused impaired climbing ability, without neuronal loss. However, *Pol γ-α* knockdown in dopaminergic neurons caused neurodegeneration as well as climbing impairments. This suggests a particular sensitivity of DA neurons to cell death when mitochondria are dysfunctional (Humphrey, Parsons et al. 2012).

A 'knock-in' point mutation in murine *Pol γ*, which inactivates Pol γ's proof reading ability, causes increased mtDNA mutagenesis. These 'mutator' mice display phenotypes of premature ageing such as hair and weight loss, anaemia and reduced fertility and lifespan, not seen in the deletor mice. This suggests that ageing is caused by accumulation of mtDNA mutations, as the free radical theory of ageing predicted (see 1.2.4.1). Whether these changes are accompanied by increased ROS has been difficult to elucidate. *Ex vivo* analysis of ROS and antioxidant enzyme levels show no change in mutator mice compared to control (Trifunovic, Hansson et al. 2005). Measurements of mitochondrial ROS *in vivo*, using a mitochondrially targeted mass spectrometry probe, reveal that there is an increase of H_2O_2 in aged mutator mice (Logan, Shabalina et al. 2014). The relevance of this model to human ageing has also been questioned, as mutations in these mice occur throughout development, and the levels of mtDNA mutations are much higher than observed in humans (Vermulst, Bielas et al. 2007). These mutator mice have, however, been used to inform on inheritance of mtDNA

mutations. Mutations in protein coding areas (which may have strong phenotypes) are strongly selected against in the oocyte, resulting in many tRNA mutations (which may have milder phenotypes) being passed on to the next generation (Stewart, Freyer et al. 2008). This may explain why tRNA mutations are relatively abundant in human mtDNA disease (Tyynismaa and Suomalainen 2009).

The role of mitochondria in ageing has also been explored with the 'mito-mice' model. This model was created from mitochondria isolated from old mice, fused to a cell line lacking mitochondria. Cybrids were screened for respiratory deficiencies to select a cybrid with a mtDNA deletion, which was then fused with a fertilised egg (Inoue, Nakada et al. 2000). These mice showed increased levels of lactate in their blood, renal failure and shortened lifespans. Kidney failure is not normally associated with mitochondrial disorders, however, this work suggests that human renal failure with unknown cause may be due to mtDNA mutations (Inoue, Nakada et al. 2000).

Loss of mtDNA has been modelled in mice using knockout of *TFAM*. Specific knockout of *TFAM* in the dopaminergic (DA) neurons causes adult onset, progressive, parkinsonian phenotypes: 'mito-park' mice (Ekstrand, Terzioglu et al. 2007). The mid-brain DA neurons have reduced mtDNA levels, OXPHOS deficits and intracellular inclusions, which lead to DA neuronal death (Ekstrand, Terzioglu et al. 2007). mtDNA loss in DA neurons of mice to model PD has also been achieved with a mitochondrially targeted restriction enzyme, *mito-PstI*. This model also results in progressive loss of DA neurons and motor phenotypes, which are reversed by L-Dopa administration (Pickrell, Pinto et al. 2011).

Expression of a mitochondrially targeted restriction enzyme, *mito-XhoI*, has also been used in *Drosophila* to create an *in vivo* model of mitochondrial dysfunction (Xu, DeLuca et al. 2008). *Mito-XhoI* linearises mtDNA by creating a single cut in *COXI*, a mitochondrially encoded subunit of complex IV. Ubiquitous expression of *mito-XhoI* is embryonic lethal and expression solely in motor neurons lead to synaptic loss of mitochondria and late pupal lethality (Cagin, Duncan et al. 2015).

An alternative method of reducing mtDNA gene expression is to target translation, by mutating mitochondrial ribosomes. A viable mutation in the *Drosophila* gene for mitochondrial ribosomal protein S12, *tko*, results in a ≈ 30% decrease in the activity of

complex I, III and IV (Toivonen, O'Dell et al. 2001). The *tko*^{25t} mutation also results in bang sensitivity, developmental delay, male courtship impairments and a severe hearing deficiency. Mutations in mitochondrial rRNAs and tRNAs have also been associated with deafness in humans (Jacobs 1997).

1.3.4.2 Animal models targeting individual OXPHOS complex subunits

As well as models of mtDNA damage, there are also several *Drosophila* and mouse models that target individual OXPHOS subunits. A point mutation in the *ATP6* subunit of complex V causes reduced lifespan, conditional paralysis to mechanical stress and neuromuscular degeneration in *Drosophila* (Celotto, Frank et al. 2006). The mutation induced altered morphology of the IMM and reduced ATPsynthase activity. Conversely, total respiration of these animals was no different from control, which perhaps indicates that respiration is uncoupled in these flies. Mutations in the nuclear encoded *COX6A* (also known as levy) subunit of complex IV in *Drosophila* causes reduced lifespan and age related COX activity impairments, ATP loss, bang sensitivity and neurodegeneration (Liu, Gnanasambandam et al. 2007).

RNAi knockdown of individual mitochondrial subunits has also been used to study mitochondrial dysfunction in *Drosophila.* The Jacobs lab knocked down complex IV subunits (*COX4, COX5A, COX5B, COX6A, COX6B, COX6C, COX7A*) with RNAi, in order to investigate whether OXPHOS dysfunction in these flies could be rescued by alternative oxidase (AOX) (Kemppainen, Rinne et al. 2014). AOX acts as a non-proton-pumping respiratory chain protein in lower eukaryotes. Neuronal knockdown of *COX7A* caused adult locomotion deficits and a seizure-sensitive phenotype (Kemppainen, Rinne et al. 2014). RNAi knockdown of *Surf1*, a complex IV assembly protein, has been used in *Drosophila* to model Leigh syndrome. Ubiquitous knockdown of *Surf1* causes larval lethality. Expression of *Surf1* RNAi with the post-mitotic neuronal driver *elav-Gal4* actually increased the lifespan of the flies, however this was accompanied by locomotor and photobehaviour impairments. Increased longevity is also observed in *Surf1* knockout mice (Dell'agnello, Leo et al. 2007).

Ubiquitous knockout of the complex I subunit *Ndufs4* in mice results in reduced levels of complex I, indicating a role for this subunit in assembly or stabilisation of the

complex. Mice had growth impairments and after 5 weeks developed motor impairments, blindness and elevated lactate levels in the serum, dying prematurely at 7 weeks (Kruse, Watt et al. 2008). Knockout of *Ndufs4* in glia and neurons alone produced the same phenotypes, suggesting that the phenotypes are mainly due to dysfunction in these cell types (Quintana, Kruse et al. 2010). The phenotypes observed were delayed by administration of rapamycin, the mTOR inhibitor (Johnson, Yanos et al. 2013). Exposure to hypoxic conditions also was able to ameliorate the phenotypes, without rescuing complex I activity (Jain, Zazzeron et al. 2016). Two mouse models with complex V mutations (in *ATP5A1*, CV F_1 domain subunit, and *ATPAF2*, CV assembly factor) have also been made and characterised in the genome-wide Sanger Institute mouse genetics project (White, Gerdin et al. 2013). These mice are homozygous lethal, but heterozygous viable.

Microarray analysis of *Drosophila* S2 cells with knock-down of the *COX5A* subunit of complex IV reveals changes in transcriptional activity and a switch to glycolytic processes in these cells compared to control (Freije, Mandal et al. 2012).

1.4 Mitochondrial retrograde signalling

Mitochondrial retrograde signalling is the process by which mitochondria communicate information about their function to the nucleus, inducing transcriptional changes (Liu and Butow 2006).

1.4.1 Discovery of retrograde signalling in yeast

The mitochondrial retrograde response was first identified in yeast, when gene expression between yeast strains with varying levels of mtDNA was compared (mtDNA p^0 petites with no mtDNA and hyper-suppressive p^- petites with only 700bp of mtDNA) (Parikh, Morgan et al. 1987). Transcripts of nuclear encoded genes were altered not only between the two petite strains and the respiratory competent parent, but they were also different between the two petites, which were otherwise phenotypically identical (Parikh, Morgan et al. 1987). This showed that yeast are able to modulate nuclear gene transcription depending on the quality and quantity of mtDNA, even in the absence of oxidative respiration.

Peroxisomal citrate synthase, CIT2, was identified as highly upregulated in yeast lacking mtDNA, or treated with a drug to inhibit respiration (Liao, Small et al. 1991). Analysis of the 5' end of CIT2 revealed an upstream activating sequence (UAS) required for this upregulation, the R-box, which has been used to identify regulators of this pathway (Liu and Butow 2006).

The pathway in yeast is mediated by three Rtg proteins. Rtg2p is a cytoplasmic protein with an ATP binding domain. Rtg2p responds to low levels of glutamate and glutamine by inhibiting two other cytoplasmic proteins, Mks1p and Lst8p. These proteins phosphorylate Rtg3p and inhibit Rtg3p and Rtg1p translocating to the nucleus. When the pathway is activated, and Mks1p and Lst8p activity is inhibited, Rtg1p and Rtg3p are able to translocate to the nucleus and form a heterodimer. Rtg1p and Rtg3p are basic helix-loop-helix leucine zipper proteins (bHLH/Zip) which bind to the R box motif to regulate gene expression (Figure 1.10). This pathway is regulated directly by levels of glutamate and glutamine within the cell, by external levels sensed by the SPS amino acid sensing pathway and by the intracellular nutrient sensing mechanistic target of

rapamycin (mTOR) complexes. Activation of the pathway leads to expression of proteins such as peroxisomal citrate synthase and lactate dehydrogenase, which act to increase levels of glutamine and glutamate, and switch the pathway off (Burns, Grimwade et al. 1994).

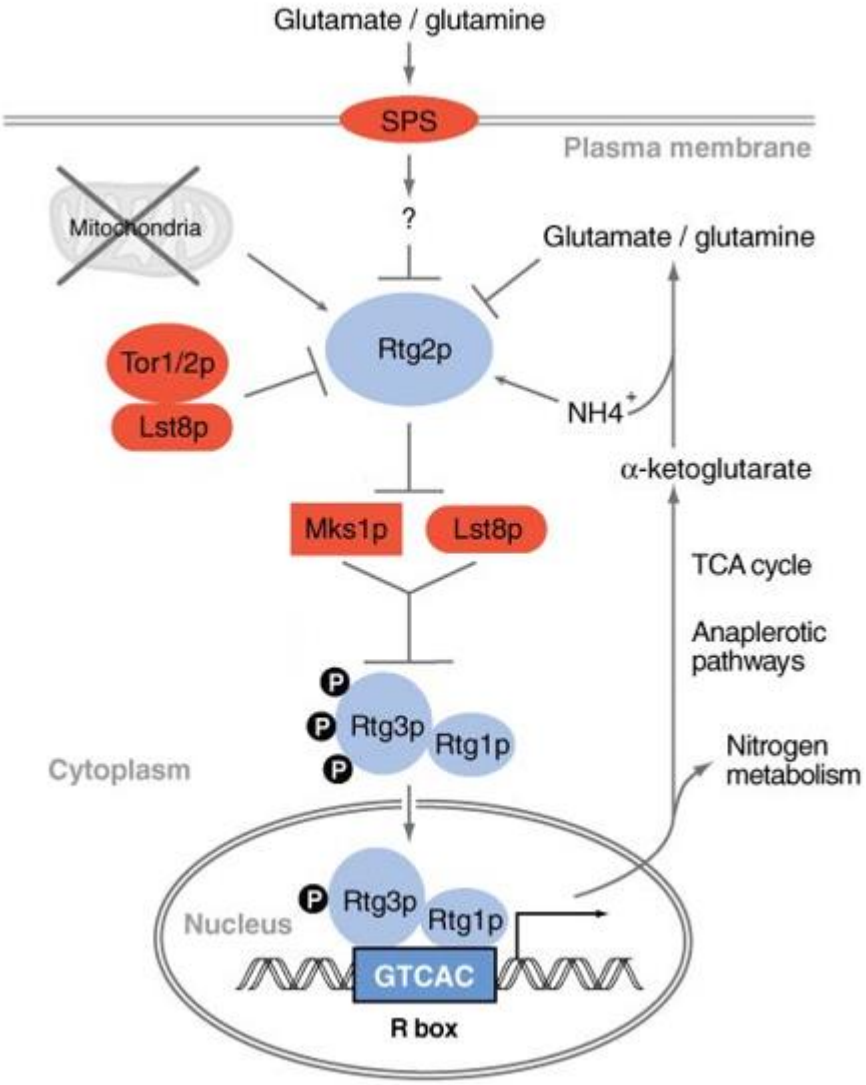

Figure 1.10 The mitochondrial retrograde response in yeast
Positive regulators are shown in blue and negative regulators in red. Adapted from Liu and Butow 2006 (Liu and Butow 2006)

1.4.2 Retrograde signalling in multicellular organisms

Retrograde signalling was first observed in vertebrates when nuclear gene expression in chicken cells was found to be different in cells without mtDNA compared to parent cells that contain mtDNA (Wang and Morais 1997). Although the *process* of retrograde

signalling is conserved from yeast to humans, the molecular mechanisms and proteins involved are not. This is unsurprising given that yeast are single cell organisms that are able to live on non-fermentable and fermentable carbon sources, choosing to use anaerobic respiration when possible (see Introduction 1.1.2). Some regulators of the yeast retrograde response do also play a role in multicellular organisms, such as mTOR. Various signalling pathways have been implicated in multicellular organisms (Figure 1.11), however there is still much we do not know about these processes.

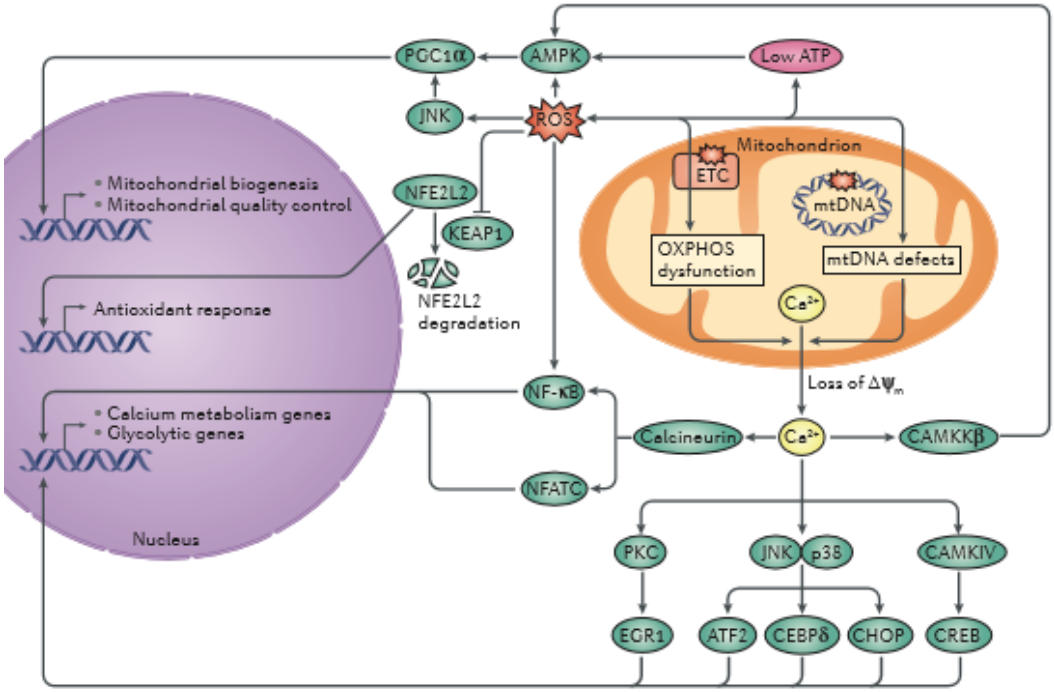

Figure 1.11. Retrograde response pathways identified in multicellular organisms. Changes in metabolites (such decreased ATP), increased ROS production and cytosolic accumulation of Ca^{2+} ions, have all been implicated in the retrograde response in multicellular organisms. These initiate signalling pathways that regulate gene expression. Figure from Quiros et el., 2016 (Quiros, Mottis et al. 2016).

1.4.2.1 Calcium mediated mitochondrial retrograde signalling

As previously discussed (see Introduction 1.2.5.2), Ca^{2+} is sequestered into the mitochondrial matrix by the negative membrane potential. Depolarisation of dysfunctional mitochondria therefore results in accumulation of cytosolic Ca^{2+}. This process was observed in cell culture when treating murine skeletal myocytes cells with ethidium bromide (EtBr, which causes mtDNA loss) and carbonyl cyanide m-chlorophenyl hydrazone (CCCP, a chemical inhibitor and uncoupler of OXPHOS)

(Biswas, Adebanjo et al. 1999) and a human lung carcinoma cell line with EtBr (Amuthan, Biswas et al. 2002).

Build-up of cytosolic Ca^{2+} activates several signalling pathways, which all alter transcriptional regulation, increasing expression of genes involved in Ca^{2+} storage and transport, as well as glycolytic genes (Figure 1.11). Ca^{2+} activates calcineurin which dephosphorylates inhibitor of the nuclear factor-κβ (IκBβ). IκBβ normally inhibits nuclear translocation of nuclear factor-κ (Nf-κB), so inhibition of IκBβ results in activation and nuclear translocation of Nf-κB with its Rel active factor (Biswas, Anandatheerthavarada et al. 2003).

The increased Ca^{2+} concentration also activates several Ca^{2+}-regulated kinases, such as protein kinase C (PKC), c-Jun N-terminal kinase (JNK), p38 mitogen activated kinases (MAPK) and calcium/calmodulin-dependent protein kinase type IV (CAMKIV), which in turn activate transcription factors. Rat PC12 cells treated with carbonyl cyanide trifluoro-methoxyphenyl hydrazone (FCCP, uncoupler of OXPHOS), show an increase in cytosolic Ca^{2+}, decrease in ATP levels and an increased activated of MAPKs, ERK1 and ERK2 (Luo, Bond et al. 1997). Interestingly ERK1 and ERK2 were not activated by comparable Ca^{2+} concentrations released from the ER by caffeine stimulation (Luo, Bond et al. 1997).

1.4.2.2 ROS mediated mitochondrial retrograde signalling

Increased levels of ROS, caused by mitochondrial dysfunction, also regulates the activity of transcription factors (Figure 1.11). A systems biology approach, using data from muscle tissue from people with mtDNA disease, has led to the identification of a retrograde pathway in which ROS activates the biogenesis regulator PGC-1α via JNK (Chae, Ahn et al. 2013). Mice on a high fat diet have increased ROS production that is further increased by knockdown of the protein deglycase, DJ-1. In these mice an upstream regulator of PGC-1α, AMP-activated protein kinase (AMPK) is activated (Shi, Lu et al. 2015). Taken together, this suggests that ROS upregulation promotes mitochondrial biogenesis via retrograde signalling. PGC-1α also regulates antioxidant gene expression to buffer ROS levels, in murine skeletal cells (Baldelli, Aquilano et al. 2014).

AMPK is known to regulate glycolytic processes and was also shown to mediate the increase in glycolysis also observed in DJ1 knockdown mice on a high fat diet (Shi, Lu et al. 2015). Glycolysis has also been shown to be regulated by HIF. HIF-1α is activated by increased ROS resulting from mitochondrial dysfunction in *C. elegans* (Miyadera, Amino et al. 2001). However, glycolysis in the DJ-1 knockdown mice on a high fat diet, was not effected by HIF-1α siRNA, so is presumably is independent of HIF signalling (Shi, Lu et al. 2015).

As well as affecting transcription factor activity, evidence shows that ROS can also regulate epigenetic control of gene expression. In mouse cell lines, treatment with H_2O_2 results in epigenetic changes in DNA methylation, because areas of DNA that are damaged recruit DNA methyltransferase and SIRT1(O'Hagan, Wang et al. 2011). A signalling pathway that senses only mitochondrial ROS has been identified from microarrays of yeast with increased mitochondrial ROS. This pathway inhibits the activity of the histone demethylase Rph1p, enhancing transcriptional silencing, particularly at subtelomeric regions (Schroeder, Raimundo et al. 2013).

Increased ROS has also been associated with activation of the mitochondrial unfolded protein response (UPR^{mt}).

1.4.2.3 The mitochondrial unfolded protein response (UPR^{mt})

Stress that interferes with correct protein folding leads to an unfolded protein response (UPR) in the effected cellular compartment, be it the cytosol, ER or mitochondria. In order to restore protein homeostasis, these pathways initiate upregulation of chaperone gene expression and, in the case of UPR^{ER} and UPR^{mt}, impose a general inhibition of translation (Runkel, Liu et al. 2013).

In normal conditions, proteins targeted to the mitochondrial matrix traverse the mitochondrial membranes through TOM and TIM. On entering the mitochondrial matrix, the mitochondrial targeting sequence is cleaved and the protein folded by mitochondrial chaperones, such as heat shock proteins Hsp60 and mtHsp70 (Haynes, Fiorese et al. 2013). Mitochondrial dysfunction impairs mitochondrial protein import,

due to loss of membrane potential, and mitochondrial chaperone depletion. Impairments in mitochondrial import has therefore been proposed as a trigger for the UPR^{mt}. Import of activating transcription factor associated with stress-1 (ATFS-1) has been identified as key for initiating the UPR^{mt} in *C. elegans* (Figure 1.12) (Nargund, Pellegrino et al. 2012). Deletion of ATFS-1's mitochondrial targeting sequence (MTS) in *C. elegans*, in the absence of mitochondrial dysfunction, was sufficient to activate the UPR^{mt} (Nargund, Pellegrino et al. 2012).

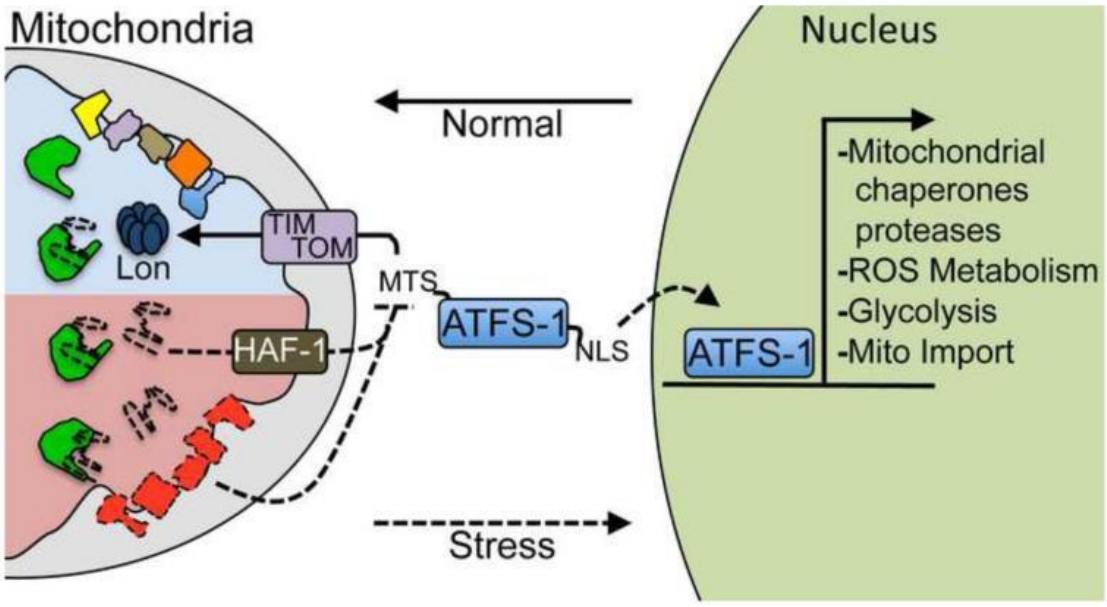

Figure 1.12 The role of ATFS-1 in UPR^{mt}
ATFS-1 is imported into the mitochondrial matrix (blue) due to its MTS, where it is degraded by the protease, Lon. When mitochondria become dysfunctional and depolarised (pink), import is impaired and ATFS-1 can no longer translocate into the mitochondria. If chaperone capacity is exceeded by quantity of unfolded proteins, then import is also impaired due to peptide efflux from the ATP-binding cassette transporter, HAF-1. ATFS-1 also contains a nuclear localisation sequence (NLS), so when mitochondrial import is impaired, ATFS-1 localises to the nucleus where it can activate transcription. Figure from Haynes et al., 2013(Haynes, Fiorese et al. 2013).

UPR^{mt} can also be activated by 'mitonuclear protein imbalance'. This describes an imbalance between levels of nuclear and mitochondrial encoded OXPHOS subunits. Knockdown of mitochondrial ribosomal protein *mrps-5* in *C. elegans*, results in a loss of mtDNA encoded OXPHOS subunits and increased expression of UPR^{mt} upregulated chaperones, *hsp6* and *hsp60* (Houtkooper, Mouchiroud et al. 2013).

One of the major outcomes of the UPR^{ER}, is reduced translation, mediated by phosphorylation of the translation initiator eukaryotic initiation factor 2 (eIF2α) (Harding, Zhang et al. 1999). This reduces the burden of unfolded proteins on the ER chaperones. A similar inhibition of cytosolic translation is observed in *C. elegans* mutant for a mitochondrial protein kinase, *clk-1* (Baker, Nargund et al. 2012). Phosphorylation of eIF2α in conditions of mitochondrial stress is mediated by the kinase general control non-derepressible-2 (Gcn-2) (Baker, Nargund et al. 2012). This results in a general inhibition of translation as well as increased translation of specific mRNAs, with small upstream open reading frames, such as activating transcription factor 4 (ATF4) in mammals and general control non-derepressible-4 (Gcn4) in yeast (Dever, Feng et al. 1992, Vattem and Wek 2004).

C. elegans with combined loss of *GCN-2* and *ATFS-1* are more sensitive to mitochondrial dysfunction than those with loss of only one of these genes (Baker, Nargund et al. 2012). This suggests that these two arms of the UPR^{mt} act in parallel with each other.

1.4.3 The mitochondrial retrograde response in neurons

The retrograde response to mitochondrial dysfunction has been little studied in neurons. The neuronal retrograde response is particularly important when considering neurodegenerative diseases associated with mitochondrial dysfunction (see Introduction 1.3.3). Previously, this has been addressed by the Bateman lab by modelling mitochondrial dysfunction in the nervous system of *Drosophila*. Microarray analysis of two neuronal mitochondrial dysfunction models (overexpressing *TFAM* and knockdown of a complex V subunit, *ATPsynCf6*), suggested an upregulation in glycolytic processes and a downregulation in global protein translation (Cagin, Duncan et al. 2015). These processes have also been identified in studies of other tissue types, however, further study is required to elucidate the mechanisms of these responses in neurons.

1.5 Premise of this thesis

Mitochondrial dysfunction causes human disease. Neurons are often affected due to their high energy demand and so mitochondrial dysfunction is particularly associated with neurodegenerative disease, such as AD and PD. Current treatment for these diseases target the symptoms, but there is limited inhibition of disease pathology. Mitochondria are a good therapeutic target, as mitochondrial dysfunction is a common feature of many neurodegenerative disease, and contributes to the disease mechanism. It is known that cells respond to mitochondrial damage, however, these processes are particularly poorly understood in neurons. I therefore hypothesise that furthering our knowledge of the neuronal response to mitochondrial dysfunction will allow strategies to enhance beneficial responses and to block negative pathways, leading to potential therapeutic use.

In this thesis, I aim to address this hypothesis with two main objectives.

Firstly, we need a greater understanding of the neuronal response to different mitochondrial insults: what responses are common and unique? To do this I will-

1. Characterise the mitochondrial dysfunction and cellular changes in neurons with different mitochondrial insults.
2. Identify molecular pathways that are altered in these conditions.
3. Manipulate these pathways to evaluate the effects in the different mitochondrial dysfunction models.

Secondly, I aim to identify novel regulators of the cellular response to mitochondrial dysfunction. To achieve this, I will utilise the strengths of *Drosophila* as a model organism to-

1. Carry out a genetic screen to identify genes that are able to modulate phenotypes caused by mitochondrial dysfunction.
2. Evaluate hits from this screen in the nervous system.
3. Identify molecular pathways that these genes are part of that may be involved in the neuronal response to mitochondrial dysfunction.

2 MATERIALS AND METHODS

2.1 Materials

2.1.1 Kits:

Absolutely RNA Microprep kit (Agilent Technologies, Strategene)
Nugen Ovation V2 kit (NuGEN Technologies Inc.)
DNaseI Amplification Grade kit (Sigma-Aldrich)
First strand cDNA synthesis kit (Fermentas)

2.1.2 Antibodies and dyes:

Primary antibodies
Dcp1 (rabbit, 1/200, Cell Signalling), Wingless (mouse, 1/200, DSHB), DAPI (in Vectashield mounting medium, Vector Laboratories), Yan 8B12H9 (mouse, 1/200, DSHB), Phospho-Erk1/2 (rabbit, 1/200, Cell Signalling)

Secondary antibodies
AlexaFlour 488, AlexaFlour 594, AlexaFlour 633 (1/1000, Invitrogen)

Conjugated antibodies
HRP-Cy3 (goat, 1/1000, Stratech 123-605-021-JIR), HRP-Alexa Fluor 647 (goat, 1/1000, Jackson ImmunoResearch Laboratories)

2.1.3 Fly stocks

In order to target genetic manipulations to specific tissues, the *UAS-Gal4* system was utilised. Yeast transcriptional activator, *Gal4*, was expressed under different promoters, depending on the tissue or cell type of interest in each assay. The *Gal4* binds to the yeast upstream activator sequence (*UAS*) driving transcription of the gene of interest. In some stocks, the *Gal4* inhibitor, *Gal80*, was also used to inhibit transcription of the specified gene and to maintain a healthy stock. *Gal80* acts by binding to *Gal4* and therefore physically inhibiting it from binding to the *UAS*.

Background strain

w^{1118} (Bloomington, 6326)

Gal4 driver lines

Ok371-Gal4 (Bloomington, 26160) – VGLUT- expressed in glutamatergic neurons

D42-Gal4 (Bloomington, 8816) – Toll-6- expressed in motor neurons and peripheral sensory neurons

tub-Gal80^{ts} (Bloomington, 7018) – Tubulin - expressed ubiquitously (temperature sensitive *Gal80*

tub-Gal4 (Bloomington, 5138) – Tubulin - expressed ubiquitously

nSyb-Gal4 (Sousa-Nunes lab) – synaptobrevin- expressed in post mitotic neurons

MS1096-Gal4 (Sally Leevers lab) – Beadex- expressed in the dorsal compartment of the wing

OK6-Gal4 (Sweeney lab) – Rapgap 1 -expressed in motor neurons

c380-Gal4 (Sweeney lab) – futsch- expressed in motor neurons and peripheral neurons

Da-Gal4 (Perrin, Bloyer et al. 2003) – daughterless- expressed ubiquitously

UAS stocks

UAS-Dcr2 (Bloomington, 24648), *UAS-ATPsynCf6* dsRNA (VDRC, CG4412, 107826/KK), *UAS-ND-75*^{HMS00853} dsRNA (Bloomington, CG2286, 33910), *UAS-UQCR-14* dsRNA (VDRC, CG3560, 109542/KK), *UAS-COX5B* dsRNA (VDRC, CG11015, 105769/KK), *UAS-mitoGFP* (Bloomington, 8442), *UAS-sima*^{HMS00833} shRNA (Bloomington, 33895), *UAS-sima*^{HMS00832} shRNA (Bloomington, 33894), *UAS-TFAM* dsRNA (NIG, 4217R-1), *UAS-SurfI*$^{23.4}$ dsRNA (Zordan, Cisotto et al. 2006), *UAS-yan* (Bloomington, 5790).

See Table 6 below for additional OXPHOS RNAi lines.

See Table 14 and Appendix 9.2.1 for lines used in the modifier screen.

GFP fluorescent probes

Mito-ro-GFP2-Grx1 (Albrecht, Barata et al. 2011), *Mito-ro-GFP2-ORP1* (Albrecht, Barata et al. 2011), *Cyto-ro-GFP2-Grx1* (Albrecht, Barata et al. 2011), *UAS-MitoTimer* (Bloomington, 57323), *UAS-Perceval* (this study).

Table 3. RNAi, used in this study, for subunits of OXPHOS complexes. RNAi lines that were studied in more detail are in bold.

Complex	Gene Name	Gene (CG #)	Stock Number	Source	Type
I	***NADH dehydrogenase (ubiquinone) 75 kDa subunit (ND-75)***	**CG2286**	**33910**	**Bloomington**	**shRNAi**
I	*ND-75*	CG2286	33911	Bloomington	shRNAi
II	*Succinate dehydrogenase, subunit D (SdhD)*	CG10219	26776	VDRC	dsRNAi
II	*SdhD*	CG10219	101739	VDRC	dsRNAi
III	*Ubiquinol-cytochrome c reductase 14 kDa subunit-like (UQCR-14L)*	CG17856	33015	VDRC	dsRNAi
III	*UQCR-14L*	CG17856	33016	VDRC	dsRNAi
III	*UQCR-14L*	CG17856	55631	Bloomington	shRNAi
III	***Ubiquinol-cytochrome c reductase 14 kDa subunit (UQCR-14)***	**CG3560**	**109542**	**VDRC**	**dsRNAi**
III	*Cytochrome c1 (Cyt-c1)*	CG4769	34583	Bloomington	shRNAi
III	*Ubiquinol-cytochrome c reductase ubiquinone-binding protein (UQCR-Q)*	CG7580	51357	Bloomington	shRNAi
III	*oxen (ox)*	CG8764	35828	VDRC	dsRNAi
III	*ox*	CG8764	35829	VDRC	dsRNAi
IV	*Cytochrome c oxidase subunit 5B (COX5B)*	CG11015	30892	VDRC	dsRNAi
IV	***COX5B***	**CG11015**	**105769**	**VDRC**	**dsRNAi**
IV	*Cytochome c oxidase subunit 5A (COX5A)*	CG14724	27548	Bloomington	lhRNAi
IV	*COX5A*	CG14724	58282	Bloomington	shRNAi
IV	*Cytochrome c oxidase subunit 6B (COX6B)*	CG18809	55399	Bloomington	shRNAi
IV	*COX6B*	CG18809	56907	Bloomington	shRNAi
IV	*Cytochrome c oxidase subunit 7A (COX7A)*	CG9603	37496	VDRC	dsRNAi
IV	*COX7A*	CG9603	106661	VDRC	dsRNAi

Complex	Gene Name	Gene (CG #)	Stock Number	Source	Type
V	*ATP synthase, subunit C (ATPsynC)*	CG1746	35464	Bloomington	shRNA
V	*ATPsynC*	CG1746	57705	Bloomington	shRNA
V	*Bellwether (blw)*	CG3612	34664	VDRC	dsRNAi
V	*ATP synthase, oligomycin sensitivity conferring protein (ATPsynO)*	CG4307	12792	VDRC	dsRNAi
V	*ATPsynO*	CG4307	12794	VDRC	dsRNAi
V	*ATP synthase, coupling factor 6 (ATPsynCf6)*	CG4412	35385	VDRC	dsRNAi
V	***ATPsynCf6***	**CG4412**	**107826**	**VDRC**	**dsRNAi**
V	*ATP synthase, subunit F (ATPsynF)*	CG4692	13324	VDRC	dsRNAi
V	*ATPsynF*	CG4692	13325	VDRC	dsRNAi
V	*ATP synthase, γ subunit (ATPsynγ)*	CG7610	28723	Bloomington	lhRNA
V	*ATPsynγ*	CG7610	50543	Bloomington	shRNA
V	*ATP synthase, subunit B (ATPsynB)*	CG8189	14210	VDRC	dsRNAi
V	*ATPsynB*	CG8189	14211	VDRC	dsRNAi
V	*ATPsynB*	CG8189	106758	VDRC	dsRNAi
V	*Stunted (sun)*	CG9032	23685	VDRC	dsRNAi
V	*sun*	CG9032	50958	VDRC	dsRNAi

LacZ reporter lines

Thor-lacZ (Bloomington, 9558), *Ilp3- lacZ* (Ikeya et al., 2002)

Mutants

TFAM ^{c01716} (Bloomington, 10713), *sima*^{KG07607} (Bloomington, 14640), *park*^{25} (Greene, Whitworth et al. 2003), *pointed*^{delta88} (Bloomington, 861)

2.2 Methods

2.2.1 Fly maintenance and breeding

Flies were maintained in temperature controlled incubators at either 18 or 25°C, unless otherwise stated. Incubators were set to a 12 hour light/dark cycle. Virgin female flies were collected in the morning and evening. Two recipes were used for fly food, R1 and the richer R2. R1 was made up of 6.4g Agar (Fisher), 64g glucose (Sigma), 16g ground yellow corn and 40g brewer's yeast (MP Biomed Europe) in 1 litre total volume of distilled water. Ingredients were mixed and cooked in a SystecMediaPrep media steriliser. The mixture was cooled to less than 60^{o}C and the following ingredients were added, 1.8g methyl 4-hydroxybenzoate (Sigma), 3ml propionic acid (Fisher Scientific) and 16ml ethanol. After a further 10 minutes of mixing, food was dispensed into vials and bottles (Regina Industries Ltd). R2 was made in exactly the same manner, apart from it was made with 80g of brewer's yeast, rather than 40g. R1 food was used for virgin fly collection, maintaining stocks and males separated for climbing assays. R2 was used for experimental crosses.

2.2.2 Behavioural and wing inflation assays

2.2.2.1 Negative geotaxis (climbing assay)

Climbing assays were performed on 2-3 day old, male flies. To ensure climbing was not affected by anaesthetising the flies, males were anaesthetised with CO_2 and separated into new vials and left to recover overnight. Climbing ability was tested between 8am (one hour after illumination) and 10am, when the flies are in the most active phase of their sleep/wake cycle. Individual flies were aspirated from the vials with a mouth pipette and tapped gently into a 5ml Falcon pipette, with the end cut off. The cut end of the pipette was placed on the bench and tapped, so that the fly dropped to the bottom. This initiates the innate escape response of the fly, causing it to vertically climb the sides of the pipette. The distance climbed in 10 seconds was measured three times per fly and averaged. Measurements were only recorded if the fly climbed without pausing. At least 10 flies were used per genotype, unless otherwise stated.

2.2.2.2 Wing inflation assay

Flies were transferred into a new vial after eclosion, and left for at least 24 hours. This allowed time for normal wing inflation to occur. Numbers of flies with straight, half inflated and folded wings were then recorded. All flies that eclosed from the vial were counted. Statistical analysis was performed on raw data and data were displayed as a percentage.

2.2.3 Quantitative reverse transcription-polymerase chain reaction (qRT-PCR)

RNA was isolated from five wandering third instar larvae, which had been incubated at 25ºC for three days during egg-laying and then 29ºC for three days. Larvae were homogenised in 0.1ml TRIzol (Life Technologies) and incubated for five minutes at room temperature. RNA was isolated according to the manufacturer's instructions. RNA was measured with the spectrophotometer (Nanodrop Technologies, ND1000, 3.3.1) and diluted to 150ng/µl. DNA was removed from the samples with a DNaseI Amplification grade kit (Sigma-Aldrich) according to the manufacturer's instructions. Reverse transcription of 10µl RNA, to synthesise cDNA, was then performed with random hexamer primers using the First strand cDNA synthesis kit (Fermentas) in a total reaction volume of 20 µl. PCR was performed on 30ng/µl of cDNA with qPCRBIO Sygreen Mix Lo-ROX (PCRBiosystems), in triplicate per genotype, unless otherwise stated. All cDNA for qRT-PCR was prepared in this way apart from for the qRT-PCR performed on brain tissue which was diluted from the cDNA prepared for microarrays (see Methods 2.2.7).

OXPHOS subunit cDNA levels were quantified using the Roche Lightcycler 480 Instrument II, the PCR program was 10 minutes at 95°C, then 35 cycles of 10 seconds at 95 °C, 15 seconds at 53 °C, 20 seconds at 72 °C and finally increasing from 72 °C to 95 °C. The levels of the gene of interest were compared with levels of the housekeeping gene, *ribosomal protein L4* (*RpL4*). Primers used are listed in Table 4. Primers for the OXPHOS RNAi lines did not have equivalent efficiencies, so levels of cDNA were extrapolated from standard curves for each primer. Standard curves, made up of a serial dilution from 100ng/µl to 1.5625 ng/µl, were run with each plate. Levels of the gene of interest were controlled to *RpL4* per sample.

qRT-PCR of tissue from the central nervous system (CNS) cDNA was performed on 20ng/µl of cDNA with qPCRBIO Sygreen Mix Lo-ROX (PCRBiosystems). The same primers were used as previously (Table 4). A standard curve was made for each primer, from which levels of cDNA were extrapolated. Seven-point standard curves were made from a serial dilution of 90ng/µl to 1.4 ng/µl. Levels of the gene of interest were controlled to *RpL4* per sample.

Sima cDNA levels were quantified using the Roche Lightcycler 480 Instrument II, the PCR program was 10 minutes at 95°C, then 35 cycles of 10 seconds at 95 °C, 15 seconds at 60 °C, 20 seconds at 72 °C and finally increasing from 72 °C to 95 °C. CT values were calculated for *sima* and *RpL4*, and used to calculate the ΔCT between these two genes. A serial dilution of cDNA, from 120ng/µl to 0.94 ng/µl, were used to create a standard curve for each primer, to ensure that they had comparable efficiencies.

Table 4. Primer sequences used for qRT-PCR

Gene	**Primer**	**Sequence**
Rpl4	Forward Primer	5'-TCCACCTTGAAGAAGGGCTA-3'
Rpl4	Reverse Primer	5'-TTGCGGATCTCCTCAGACTT-3'
ATPsynCF6	Forward Primer	5' -GGAACAGCTGCTGGATGG- 3'
ATPsynCF6	Reverse Primer	5'-AGCATTTGCAAAGGAAAATAAGA-3'
COX5B	Forward Primer	5'-CCCATCTCCAACGTTCTCAT-3'
COX5B	Reverse Primer	5'-AATGGCCGCACTCACAAC-3'
UQCR-14	Forward Primer	5'-GCATTGTGGGCTGCATCT-3'
UQCR-14	Reverse Primer	5'-GAGATTGTAGGCCCATCTGC-3'
ND-75	Forward Primer	5'-ACATTAACTACACGGGCAAGC-3'
ND-75	Reverse Primer	5'- CAATCTCGGAGGCGAAAC-3'
sima	Forward Primer	5'-CAAACCAAAGGAGAAAAGAAGG-3'
sima	Reverse Primer	5'-CAGCCGAGAGTTCCATGAAT-3'

2.2.4 Dissections and immunofluorescence

Egg laying occurred at 25ºC. Adult flies were then removed and larvae were transferred to 29ºC for three days. Wandering third instar larvae were cleaned in ice cold PBS to remove food residues and then transferred to ice cold PBS on a Sylgard dish.

2.2.4.1 Neuromuscular junctions (NMJ)

To visualise NMJs, larval flat preparations were dissected under the dissection microscope using fine forceps (Agar Scientific). Larvae were pinned dorsal side up, with a micro-pin (Entomoravia, Czech Republic) through the head and tail. Fine iridectomy scissors (Fine Science Tools) were used to pierce the larvae close to the tail and then slice the larvae open along the dorsal midline, from tail to head. Forceps were used to remove fat, guts and trachea, but care was taken not to remove the CNS. Four more pins, at each corner, were used to stretch the cuticle flat against the Sylgard dish. PBS was removed and replaced with 4% formaldehyde (Thermo Scientific)/ PBS to fix the flat prep. After fixing for 25 minutes, the flat preps were washed with PBS and the pins removed. Fixed preps were moved to 1.5ml Eppendorfs and washed for ten minutes, 3 times, in PBS/0.1% triton X100 (PBST) on the platform rocker. Preps were then blocked for 30-60 minutes in PBST with 5% normal goat serum (NGS, Sigma-Aldrich), to reduce nonspecific antibody binding. Flat preps were then incubated overnight with the appropriate primary antibody, in PBST/5% NGS, at 4°C. Preps were then washed three times in PBST at room temperature (RT) for ten minutes, followed by incubation with the relevant secondary antibody, diluted in PBST, for 1.5 hours. Samples were washed a further three times, for ten minutes each, in PBST and finally washed for ten minutes in PBS. The head, tail and brain were removed from the flat preps on a microscope slide (Thermo Scientific). Vectashield mounting media (Vector Laboratories) was used to mount the slides and 22x22mm size 0 coverslips (Academy) were lowered gently on top. Slides were stored in the dark at 4°C. The type 1b neuromuscular junctions, on muscle four, of segment A3 were imaged using the Zeiss LSM710 confocal microscope.

To analyse ROS levels, flat preps were dissected as described, with a few alterations outlined here. Larvae were dissected in 20mM n-ethylmaleimide (NEM), instead of PBS, and left in NEM for 10 minutes, in order to protect against formaldehyde mediated oxidation. In order to obtain control larval preps that were of fully oxidised, dissections were carried out in 2mM diamide (DA) and left to incubate for 10 minutes. The DA was then replaced with 20mM NEM for a 10 minute incubation period. After a single wash with PBS, the preps were fixed in 4% formaldehyde/PBS. Fully reduced larvae were attained following the same procedure using 20mM dithiothreitol (DTT), rather than DA. All the preps were rinsed in PBS and then washed for ten minutes, three times in

PBST. The fixed preps were then incubated for 40 minutes with anti-HRP-Cy3 (1:1000 in PBST/NGS, Stratech). This was followed by another three 10 minute washes in PBST and a final wash in PBS. The preps were then mounted on slides in Vectashield. Larvae were dissected, mounted and imaged on the same day. This protocol was adapted from Albrecht et al. (Albrecht, Barata et al. 2011). The type 1b neuromuscular junctions, on muscle four, of segment A3 were imaged using the Zeiss LSM710 confocal microscope.

2.2.4.2 Central nervous system & eye disc dissections

The ATP: ADP ratio was assessed in flies expressing the *UAS-Perceval* construct. The CNS and eye discs were dissected out in PBS, by inverting the cuticle at the head. Larvae were pulled apart with forceps, one third of the length of the larvae from the head. The head was then gently held with forceps, and the mouth parts pushed through to invert the cuticle. Salivary glands, guts and wing discs were removed, leaving the brain and eye discs attached to the cuticle and mouth parts. This tissue was then moved to a 1.5ml Eppendorf and fixed for 25 minutes in 4% formaldehyde/ PBS. The samples were then washed three times in PBST, for ten minutes per wash, and finally washed in PBS. Mouth parts and cuticle were removed on the slide (Superfrost Plus, Thermo Scientific). Brains or eye discs were mounted in Vectashield and imaged using the Zeiss LSM710 confocal microscope.

2.2.4.3 Wing discs

Wing discs were also dissected by inverting the cuticle, however, when removing the salivary glands and guts, the CNS was also removed and the wing discs left attached. Wing discs were fixed for 25 minutes in 4% formaldehyde/ PBS. They were then washed, blocked and stained in the same manner as the flat preps (see above 2.2.4.1). Wing discs were mounted in Vectashield containing DAPI.

2.2.5 Microscopy and image quantification

All images were taken using the Zeiss LSM710 confocal microscope with Zen software (Version 6, 2010). Resolution was set to 1024 x 1024, unless otherwise stated, at a

speed at of 7. Lenses with magnification 10x, 20x and 40x were used, numerical apertures of these lenses were 0.3, 0.5 and 1.30 respectively. The 40x lens was used with oil immersion. Images were quantified using Volocity (Version 5.5, 2011, PerkinElmer Inc.) using image projections, containing information from all z stacks. Intensity thresholds were set independently for different experiments, but the same threshold was used for the controls and experimental images in each experiment. The area of interest for each image was selected using the freehand tool. The methods used for image quantification were as follows:

2.2.5.1 Neuromuscular junctions (NMJ)

Bouton number and diameter were quantified using the distance measure tool. Mitochondrial volume and number were measured using a measurement protocol. Within the area of interest, the protocol identified areas of fluorescence in the 488nm channel, over an intensity threshold. Objects of 0.05μm^3 were separated and anything less than 0.02μm^3 was excluded. The number of areas identified and the volume of each area were recorded.

2.2.5.2 Redox potential

The same protocol was used to measure the redox potential. The total intensity in the whole area selected by this protocol was recorded for the 488nm channel and for the 405nm channel. The ratio of the 405:488nm intensities were calculated, giving a measure of redox potential per NMJ.

2.2.5.3 MitoTimer

The protocol was adapted to measure mitoTimer fluorescence, anything less than 0.02μm^3 was excluded. In the CNS objects were identified in the 488nm channel and measured in the 488nm and 546nm channel. In the NMJ objects were identified in the 546nm channel and measured in the 488nm and 546nm channel.

2.2.5.4 Perceval ATP: ADP ratio

ATP:ADP ratio was analysed using ImageJ. Images were quantified as maximum intensity projections. The point tool was used to multi-select a point in each motor neuron cell body in the ventral nerve cord (VNC) visible in the image. Care was taken to avoid the auto-fluorescent trachea. A ratio of the intensity in the 405nm to the 488nm channel was calculated.

2.2.5.5 Wing discs

The protocol was adapted to measure caspase signalling in the wing disc. The dorsal compartment was selected as the area between the wingless dorsoventral boundary and the third fold line in the hinge area of the wing disc. The protocol identified areas of fluorescence in the 488 channel, over an intensity threshold. Objects of 15μm^3 were separated and anything less than 5μm^3 was excluded. Intensity of the signal in the area selected by this protocol were measured in the 488 channel.

2.2.5.6 Phosphorylated MAPK

Phosphorylated MAPK was measured in ImageJ. The point tool was used to multi-select a spot of cytoplasm of each GFP positive motor neuron cell body in the VNC possible. The intensity of each point was measured and the average taken per VNC.

2.2.5.7 Eye discs

Posterior to the morphogenetic furrow, an area of 20μm^2 was identified in Volocity. The total intensity in this area was recorded.

2.2.6 Generating transgenic flies

The *UAS-Perceval* construct was cloned from the pRsetB-his7-Perceval plasmid (Addgene) engineered by Berg, Hung, and Yellen (Berg, Hung et al. 2009). The gene was amplified using PCR with primers Perc5.EcoRI.Fw and Perc3.XhoI.Rv (Table 5).

The primers contained the *XhoI* and *EcoRI* restriction sites respectively. The amplicon was then cloned into *pUAST* (DGRC) at *XhoI* and *EcoRI* sites. Transgenic flies were generated by BestGene.

Table 5. Primers used to clone Perceval. Restriction enzyme sites are underlined

Primers	**Sequence**
Perc5.EcoRI.Fw	5'-CATGGAATTCGCATGAAAAAGGTGGAATCCATC-3'
Perc3.XhoI.Rv	5'-TTATCTCGAGTCACAATGCTTCCTTTCCCTC-3'

2.2.7 Microarray

For microarray analysis, the CNS of 20 larvae per genotype were dissected in cold PBS as described above (see Methods 2.2.4). Instead of fixing the brains, they were lysed in 100µl lysis buffer, containing β-Mercaptoethanol (Absolutely RNA Microprep kit, Agilent Technologies, Strategene). Once dissected, each brain was picked up immediately with tweezer, excess PBS was removed from the tweezers with a paper towel and the brain was placed directly into the lysis buffer. The lysis buffer was kept on ice while all the brains were dissected. RNA was prepared following manufacturer's instructions, including DNase treatment. Samples were prepared in triplicate from individual crosses, per genotype. RNA was stored at -80^{o}C.

RNA was measured for quantity and integrity on an RNA Pico Chip (Agilent Technologies). 10ng of RNA, per genotype, was converted into labelled cDNA with the Nugen Ovation V2 protocol (NuGEN Technologies Inc.). 7mg of labelled cDNA was hybridised to Affymetrix *Drosophila* genome v2 GeneChips for 20 hours at 45^{o}C. They were then washed, stained (GeneChip® Fluidics Station 450) and scanned (GeneChip Scanner 3000 7G) according to manufacturer's instructions (Nugen Technologies Inc & Affymetrix). Conversion of RNA to labelled cDNA and the microarray processing was carried out by Dr David Chambers.

Microarray data was processed using the Affymetrix Expression Console (2014) and the Affymetrix Transcriptome Analysis Console (version 3.0.0.466, 2014, Affymetrix Inc.) using gene level differential expression analysis. This software was used to create Volcano plots and carry out statistical analysis. Means were calculated using Tukey's

Bi-weight average algorithm and differential expression between groups was calculated using un-paired one way ANOVA. Fold change cut-offs were not used, unless stated otherwise. Correlations between datasets were analysed using GraphPad Prism (Version 5.02, 2008, GraphPad Software Inc.). Heatmaps were produced using Gitools software (version 2.3.0, Biomedical Genomics Laboratory, Parc de Recerca Biomedica de Barcelona).

Gene Ontology (GO) analysis was performed on Panther (Version 10.0, 2015, Geneontology) and the Database for Annotation, Visualisation and Integrated Discovery (DAVID, version 6.7) (Dennis, Sherman et al. 2003). Panther was used to attribute GO terms to gene lists. DAVID was used to determine enriched GO terms, with the Affymetrix 3' *Drosophila*_ 2 Array as the background dataset, using the functional annotation chart and functional annotation clustering features. Bar charts of these data were created on Microsoft Excel (Microsoft Office 365 ProPlus).

2.2.8 Lifespan assays

Female flies, were separated in vials of ten, according to genotype and kept at 25°. Dead flies were counted three times a week and flipped into fresh food twice a week. Data was analysed on GraphPad Prism. The log-rank test was used to calculate p-values, and the significant threshold was adjusted for multiple comparisons.

2.2.9 Genetic modifier screen

Males from a library of *UAS* lines (mostly RNAi) were crossed to virgin females from a stock containing the *MS1096-Gal4* driver, which drives GAL4 expression in the dorsal compartment of the wing, *UAS-TFAM* RNAi and $TFAM^{c01716}$. This line also contained Gal80, to inhibit the expression of *UAS-TFAM* RNAi in the stock and the TM6B balancer chromosome. Flies were kept at 25ºC, one or two days after the adult males eclosed, their wings were observed and scored. Males with *MS1096> TFAM RNAi,* $TFAM^{c01716}$ have an approximately 45º curve at the tip of their wings. We screened to find RNAis that would modify this phenotype, either by increasing (enhancers) or decreasing (suppressors) the curve (see results chapter 3, Figure 5.3A). (The initial crosses were performed by myself or a number of undergraduate students - see

acknowledgments - any hits were crossed a second time and assessed by myself). A scale was developed to score the phenotype by severity (see results chapter 3, Figure 5.3B).

Colour photographs were taken with a Nikon D70s attached to a dissecting microscope with a MCA Nikon SLR adapter (Nikon). Black and white photographs were taken with NIS- Elements Microscope viewing software (Nikon, F 4.00.00)

To exclude genes which may have a phenotype by themselves, virgin females with the MS1096- Gal4 were crossed to all lines that were screened. If the progeny of this cross have a wing phenotype, then they were omitted from the screen (see results chapter 3, Figure 5.3C).

GO Molecular function of genes identified in the screen were obtained from Panther Classification System (Version 10.0, 2015, Geneontology).

2.2.10 Statistical analysis and graphs

GraphPad Prism (Version 5.02, 2008, GraphPad Software Inc.) was used to create graphs and for statistical analysis. Data with a p-value less than or equal to 0.05 was considered significant ($p \leq 0.05$ *, $p \leq 0.01$**, $p \leq 0.001$***). Panther Classification System (Version 10.0, 2015, Geneontology) was used to make pie charts.

Comparisons of two samples of continuous data were analysed with an unpaired, two-tailed student's t-test, where appropriate. Variance of the samples was assessed with an F test. If the variances of the two samples were significantly different then the Welch's correction was applied to the t-test. Data was analysed for normality, using the D'Agostino & Pearson omnibus normality test. Data that did not pass the normality test were analysed with the Mann Whitney test.

In order to compare more than two samples of continuous data, one way analysis of variance (ANOVA) was used, to control for multiple comparisons. Tukey's post hoc test was used to analyse the data further. If data did not pass the D'Agostino & Pearson omnibus normality test, the Kruskal-Wallis, followed by Dunn's post hoc test were utilised.

Categorical data was analysed using chi-squared. This was always done from raw data rather than percentages.

3 MODELLING MITOCHONDRIAL RESPIRATORY DYSFUNCTION IN THE *DROSOPHILA* NERVOUS SYSTEM

3.1 Introduction

Damage to the OXPHOS complexes, causing mitochondrial dysfunction, has been associated with many diseases (see Introduction 1.3). Some diseases are associated with dysfunction in particular complexes, for example, loss of complex I is reported in tissue for Parkinson's patients, whereas no change in complex II - V is observed (Keeney, Xie et al. 2006). Alzheimer's disease has been associated with a selective deficit in complex IV activity, in platelets and brain tissue (Maurer, Zierz et al. 2000, Cardoso, Proença et al. 2004). However, reduced levels of complex V and complex I subunits have also been reported in brain tissue from AD patients (Manczak, Park et al. 2004, Beck, Guo et al. 2016).

Studies in yeast and human cybrid cells demonstrate that different mitochondrial insults can cause different cellular responses (McCammon, Epstein et al. 2003, Jahangir Tafrechi, Svensson et al. 2005, Picard, Zhang et al. 2014). Similarly, human disease caused by mutations in mtDNA results in a wide range of diverse clinical phenotypes (Schapira). The majority of mtDNA mutations give rise to impairments in oxidative phosphorylation, the process that produces most cellular ATP. Yet the variety of phenotypes produced by different mutations, or even different copy numbers of a single mutation, suggest that there are additional factor other than just ATP depletion (Jahangir Tafrechi, Svensson et al. 2005). This is illustrated by the point mutation in the mitochondrially encoded $tRNA^{Leu}$. This mutation results in misincorporation of one amino acid in two OXPHOS complex IV subunits and one complex V subunit (Sasarman, Antonicka et al. 2008). Low levels (below 30% copy number) of this mutation have been associated with autism and diabetes (van den Ouweland, Lemkes et al. 1992, Pons, Andreu et al. 2004). Higher abundance of the mutation results in the multisystem disorder mitochondrial encephalomyopathy, lactic acidosis, and stroke-like episodes (MELAS) syndrome (Goto, Nonaka et al. 1990).

It is important to understand the similarities and differences between different types of mitochondrial dysfunction, in order to design treatments beneficial for multiple disorders or specific for one. To address this, mitochondrial dysfunction needs to be modelled, caused by deficits in different OXPHOS complexes.

Drosophila RNAi libraries available can be utilised to create tissue specific models of mitochondrial dysfunction *in vivo*. Multiple independent libraries also allow validation of the models with non-overlapping RNAi lines targeting the same gene. This allows for the generation of new tools to further investigate the effects of mitochondrial dysfunction in neurons.

3.1.1 Chapter Aims

In order to further understand how insults of different OXPHOS complexes may affect neurodegenerative disease, models need to be developed of different types of mitochondrial dysfunction *in vivo*.

In this chapter I aim to -

1. Develop *Drosophila* models of neuronal mitochondrial dysfunction for each of the OXPHOS complexes.
2. Characterise the phenotypes of these different models, focussing on behavioural phenotypes, mitochondrial number and size, and production of ATP and ROS.
3. Compare the similarities and differences between the different models of mitochondrial dysfunction.

3.2 Results

3.2.1 Identifying OXPHOS models of mitochondrial dysfunction which impair neuronal function.

In the last ten years, whole genome libraries of transgenic *Drosophila* RNAi lines have been developed, which can be expressed under the control of the *UAS-Gal4* system. These libraries provide the opportunity for reverse genetics, in which the gene of interest can be targeted for knockdown in individual tissues. Two independent libraries, the GD RNAi and NIG RNAi libraries, were created from clones of short gene fragments, which were inserted into P-elements as inverted repeats (Dietzl, Chen et al. 2007). A third library (KK transgenic library) was produced which was designed to have fewer off target effects as its target sequences are more specific to the target gene (Yamamoto-Hino and Goto 2013). This library also has a targeted landing site for the RNAi hairpin, aimed to reduce variability in transgene expression However, it has been revealed that the flies used actually contain two landing sites, inserts in both landing sites are found in approximately 25% of these lines (Vissers, Manning et al. 2016). Transgenic flies in this library may therefore contain a hairpin in either of these landing sites or in some cases two copies, one in each site. A fourth, TRiP library has also been produced, with site specific integration at a single landing site. This library uses either long hairpin or short hairpin RNAi to reduce off target effects (Ni, Markstein et al. 2008).

I used the RNAi libraries to obtain transgenic lines that knocked down nuclear encoded subunits of the OXPHOS complexes. The aim was to identify RNAi lines that cause neuronal mitochondrial dysfunction, which could be used to further investigate neuronal mitochondrial dysfunction *in vivo*. Gene knockdown using RNAi is advantageous, because reduced expression of a gene is potentially physiologically relevant and RNAi can be activated in the tissue of interest alone. First, RNAi lines that induce a significant mitochondrial dysfunction phenotype in neurons were identified. To do this, the motor neuron driver *OK371-Gal4* was used to drive RNAi expression. Climbing ability of these flies, compared to the driver alone, was assessed. The *Gal4*, in the *OK371* line, has been inserted close to the *Drosophila* gene for the vesicular glutamate transporter (Mahr and Aberle 2006). Unlike mammals, *Drosophila* motor neurons are glutamatergic and so this enhancer trap drives expression of *Gal4* specifically in motor

neurons. This driver line also contained *UAS-Dicer2*, which enhances the RNAi knockdown (Kim, Lee et al. 2006). Multiple RNAi lines per OXPHOS complex were used to identify RNAi lines that resulted in a robust effect for each complex. RNAi lines were chosen for complex subunits that had caused lethality when ubiquitously expressed, in *Drosophila* by Copeland et al., (Copeland, Cho et al. 2009), as this lethality indicates that loss of these subunits causes cellular dysfunction. Thirty-six transgenic RNAi lines targeting OXPHOS subunits were tested at 25°C with *OK371-Gal4*. Climbing ability was significantly impaired in 20 of those lines, and 5 lines were not viable under these conditions (Figure 2.1A, Table 6).

Many RNAi lines targeting knockdown of complex V (CV) and complex IV (CIV) subunits caused climbing defects (Figure 3.1A). Eleven RNAis for complex V reduced climbing with a p-value less than 0.001, with seven of those reducing the average distance climbed to less than 25% of control. Four RNAis for complex IV also obtained a p-value of less than 0.001 and reduced climbing below 25%. Knockdown of complex III (CIII) and complex II (CII) did not give such a robust result. Out of 8 RNAi lines targeting complex III subunits two were lethal and only one reduced climbing below 25% of control ($p<0.001$) (Figure 3.1A). The two complex III RNAi that were lethal were also lethal with another motor neuron driver *D42-Gal4* (data not shown). Complex II is composed of only four subunits, as a result there is a more limited selection of RNAi lines to select from for this complex. One of the two RNAi lines targeting complex II did significantly reduce climbing, however, the phenotype was comparatively very weak, only reducing climbing to 75% of control flies ($p<0.05$) (Figure 3.1A). Complex II (also known as succinate dehydrogenase, SDH) is the only complex which also plays a role in the citric acid cycle and OXPHOS (Rutter, Winge et al. 2010). Knockdown of complex II subunits may therefore lead to phenotypes due to reduced OXPHOS and TCA. I therefore did not pursue complex II knockdown for further analysis. The two non-overlapping RNAi lines that knockdown the complex I *ND-75* subunit were not viable with the motor neuron drivers *OK371* and *D42* at 25°C. However, at 21°C, the lines were viable with *OK371-Gal4*, with a significant climbing defect, less than 25% of control ($p<0.001$) (Figure 3.1B). Thus, RNAi lines that produced a strong climbing deficit were identified for all complexes apart from complex II. Non-overlapping RNAi lines, or RNAi lines for independent subunits, for each complex were also significantly impaired in climbing (Table 6). This suggests that the climbing deficits produced were not due to off target effects.

One RNAi line was selected for a subunit of each complex, that induced a strong climbing phenotype (Figure 3.1A, red arrows, Table 6, in bold). The RNAi lines selected target *ND-75* (33910, CI), *UQCR-14* (109542, CIII), *COX5B* (105769, CIV) and *ATPsynCf6* (107826, CV). These RNAi lines were tested with a second motor neuron driver, *D42-Gal4*. *ATPsynCf6* (CV) and *COX5B* (CIV) knockdown significantly impaired climbing (Figure 3.1C). *UQCR-14* (CIII) RNAi, which previously resulted in the weakest phenotype, did not significantly impair climbing at 25°C (data not shown). However, when the flies were grown at 29°C, climbing was significantly impaired in *D42-Gal4* driven *UQCR-14* (CIII) RNAi (Figure 3.1D). *ND-75* (CI) RNAi was lethal at both 25°C and 21°C with *D42-Gal4*.

As a comparison to these models of mitochondrial dysfunction caused by a knockdown of single OXPHOS subunits, a model which targets mtDNA was also investigated. Mitochondrial transcription factor A (TFAM) binds to mtDNA, stabilising the DNA and promoting transcription (see Introduction 1.2.3.1 & Figure 1.4). As previously discussed, altered levels of TFAM can result in mitochondrial dysfunction. When driven in motor neurons, with *D42-Gal4*, *TFAM* overexpression causes a significant impairment in climbing ability (Figure 3.1E).

Table 6. Climbing result and p-values for OXPHOS RNAi lines. RNAi lines that were studied in more detail are in bold. See Methods Table 3 for further stock details.

OXPHOS complex	**Gene Name (gene symbol)**	**Gene (CG #)**	**Stock ID**	**Climbing deficit with *OK371-Gal4* at 25°C**	**Number of flies tested**
I	***NADH dehydrogenase (ubiquinone) 75 kDa subunit (ND-75)***	***CG2286***	**33910**	**lethal**	
I	*ND-75*	*CG2286*	33911	lethal	
II	*Succinate dehydrogenase, subunit D (SdhD)*	*CG10219*	26776	Not significant	6
II	*SdhD*	*CG10219*	101739	* $p \leq 0.05$	12
III	*Ubiquinol-cytochrome c reductase 14 kDa subunit-like (UQCR-14L)*	*CG17856*	33015	Not significant	12

OXPHOS complex	**Gene Name (gene symbol)**	**Gene (CG #)**	**Stock ID**	**Climbing deficit with *OK371-Gal4* at 25°C**	**Number of flies tested**
III	*UQCR-14L*	*CG17856*	33016	Not significant	6
III	*UQCR-14L*	*CG17856*	55631	Not significant	7
III	***Ubiquinol-cytochrome c reductase 14 kDa subunit (UQCR-14)***	***CG3560***	**109542**	***** p≤0.001**	**6**
III	*Cytochrome c1 (Cyt-c1)*	*CG4769*	34583	lethal	
III	*Ubiquinol-cytochrome c reductase ubiquinone-binding protein (UQCR-Q)*	*CG7580*	51357	lethal	
III	*oxen (ox)*	*CG8764*	35828	Not significant	6
III	*ox*	*CG8764*	35829	Not significant	10
IV	*Cytochrome c oxidase subunit 5B (COX5B)*	*CG11015*	30892	*** p≤0.001	10
IV	***COX5B***	***CG11015***	**105769**	***** p≤0.001**	**10**
IV	*Cytochome c oxidase subunit 5A (COX5A)*	*CG14724*	27548	*** p≤0.001	10
IV	*COX5A*	*CG14724*	58282	*** p≤0.001	6
IV	*Cytochrome c oxidase subunit 6B (COX6B)*	*CG18809*	55399	** p≤0.01	9
IV	*COX6B*	*CG18809*	56907	** p≤0.01	10
IV	*Cytochrome c oxidase subunit 7A (COX7A)*	*CG9603*	37496	Not significant	10
IV	*COX7A*	*CG9603*	106661	*** p≤0.001	10
V	*ATP synthase, subunit C (ATPsynC)*	*CG1746*	35464	*** p≤0.001	10
V	*ATPsynC*	*CG1746*	57705	Not significant	7
V	*Bellwether (blw)*	*CG3612*	34664	*** p≤0.001	28
V	*ATP synthase, oligomycin sensitivity conferring protein (ATPsynO)*	*CG4307*	12792	*** p≤0.001	7
V	*ATPsynO*	*CG4307*	12794	*** p≤0.001	6

OXPHOS complex	**Gene Name (gene symbol)**	**Gene (CG #)**	**Stock ID**	**Climbing deficit with *OK371-Gal4* at 25°C**	**Number of flies tested**
V	*ATP synthase, coupling factor 6 (ATPsynCf6)*	*CG4412*	35385	*** p≤0.001	10
V	***ATPsynCf6***	***CG4412***	**107826**	***** **p≤0.001**	**9**
V	*ATP synthase, subunit F (ATPsynF)*	*CG4692*	13324	Not significant	12
V	*ATPsynF*	*CG4692*	13325	*** p≤0.001	6
V	*ATP synthase, γ subunit (ATPsynγ)*	*CG7610*	28723	*** p≤0.001	9
V	*ATPsynγ*	*CG7610*	50543	lethal	
V	*ATP synthase, subunit B (ATPsynB)*	*CG8189*	14210	*** p≤0.001	10
V	*ATPsynB*	*CG8189*	14211	*** p≤0.001	6
V	*ATPsynB*	*CG8189*	106758	*** p≤0.001	10
V	*Stunted (sun)*	*CG9032*	23685	Not significant	12
V	*sun*	*CG9032*	50958	Not significant	5

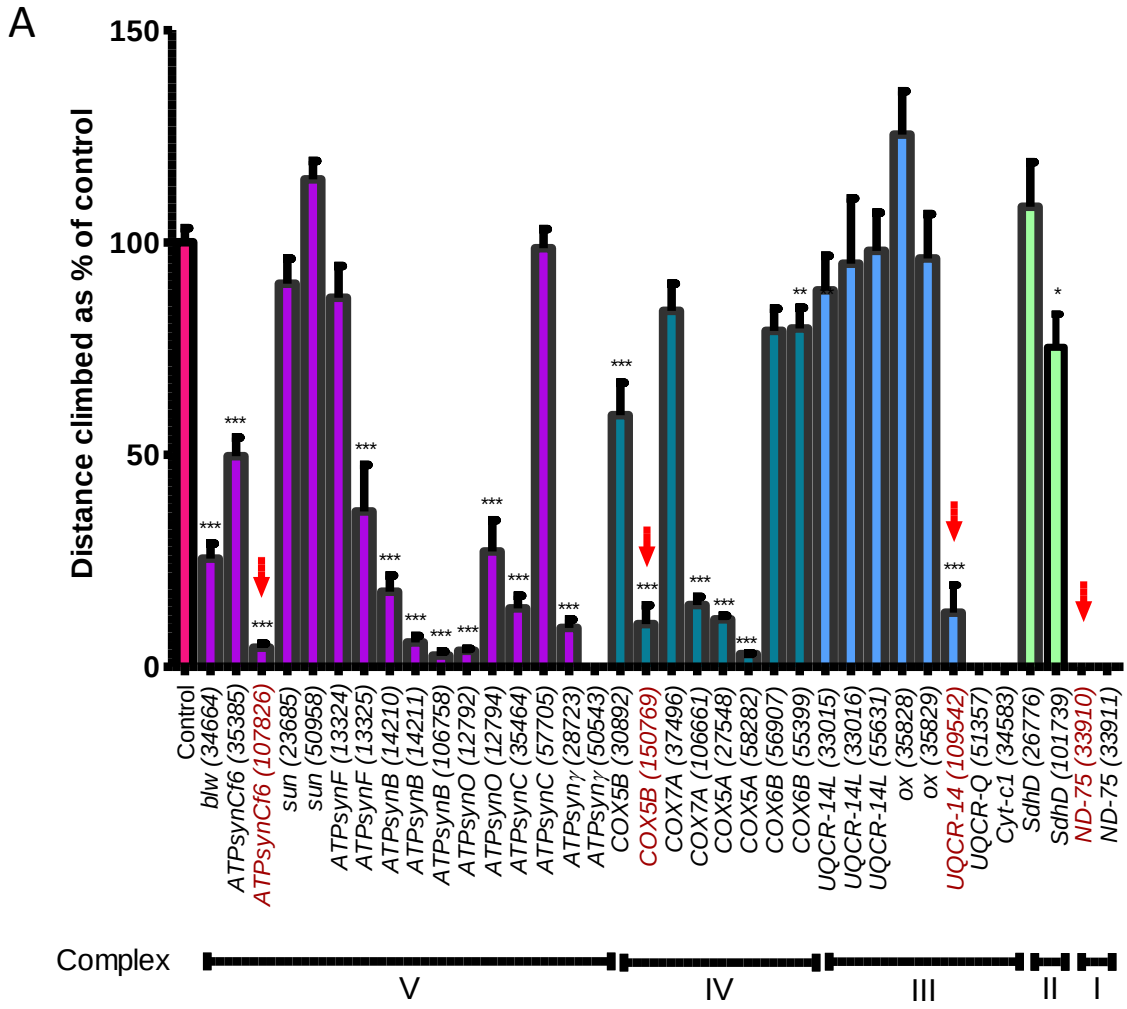
A
Distance climbed as % of control
150
100
50
0
Control
blw (34664)
ATPsynCf6 (35385)
ATPsynCf6 (107826)
sun (23685)
sun (50958)
ATPsynF (13324)
ATPsynF (13325)
ATPsynB (14210)
ATPsynB (14211)
ATPsynB (106758)
ATPsynO (12792)
ATPsynO (12794)
ATPsynC (35464)
ATPsynC (57705)
ATPsynγ (28723)
ATPsynγ (50543)
COX5B (30892)
COX5B (150769)
COX7A (37496)
COX7A (106661)
COX5A (27548)
COX5A (58282)
COX6B (56907)
COX6B (55399)
UQCR-14L (33015)
UQCR-14L (33016)
UQCR-14L (55631)
ox (35828)
ox (35829)
UQCR-14 (109542)
UQCR-Q (51357)
Cyt-c1 (34583)
SdhD (26776)
SdhD (101739)
ND-75 (33910)
ND-75 (33911)
Complex
V
IV
III
II
I

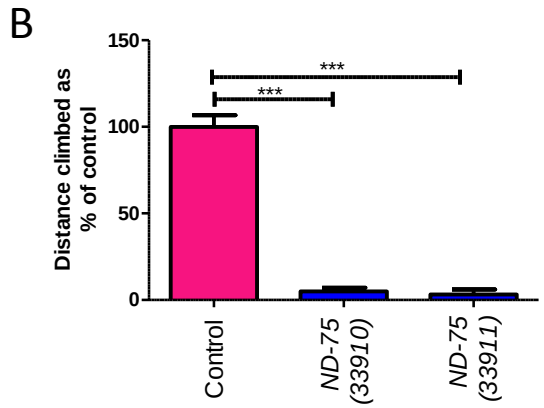
B
Distance climbed as % of control
150
100
50
0
Control
ND-75 (33910)
ND-75 (33911)

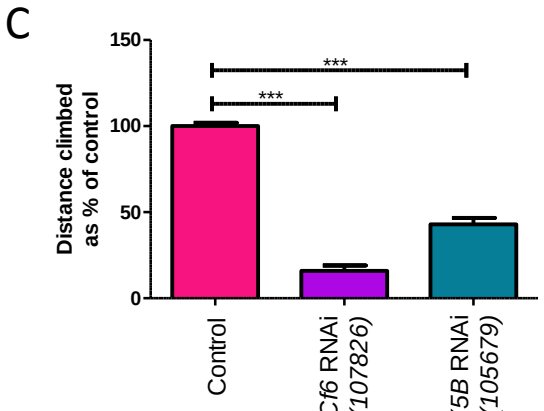
C
Distance climbed as % of control
150
100
50
0
Control
ATPsynCf6 RNAi (107826)
COX5B RNAi (105679)

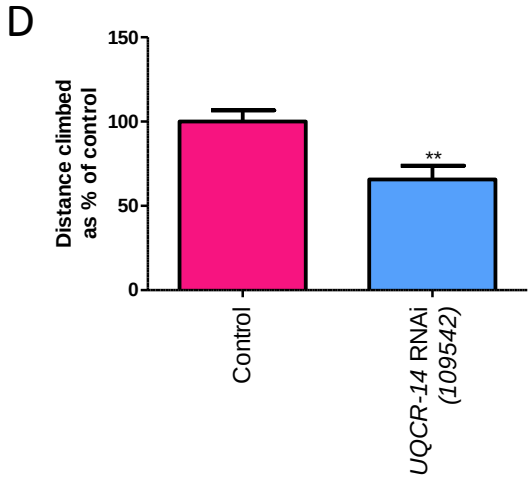
D
Distance climbed as % of control
150
100
50
0
Control
UQCR-14 RNAi (109542)

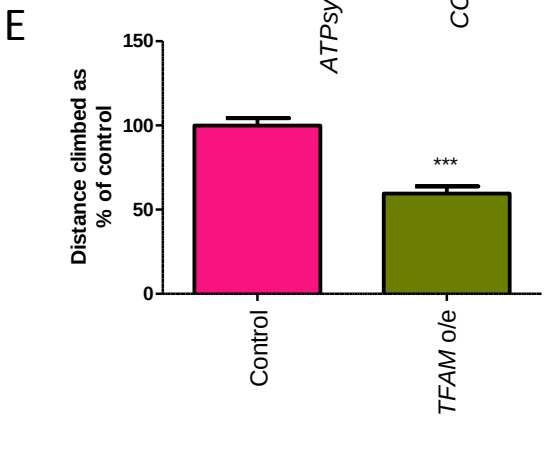
E
Distance climbed as % of control
150
100
50
0
Control
TFAM o/e

Figure 3.1 Neuronal models of mitochondrial dysfunction cause behavioural defects. Climbing assays of **(A)** RNAi for OXHPOS complex subunits driven in motor neurons by *OK371-Gal4,* with *UAS-Dcr2* at 25°C. Red arrows indicate RNAi lines used as models of mitochondrial dysfunction. Data were analysed with ANOVA, using the Dunnett's post hoc test to compare each RNAi to control. Stock IDs shown in brackets, see Table 6 for n numbers and p-values. Control is *w1118* crossed with *OK371-Gal4* with *UAS-Dcr2*. Climbing assay of **(B)** *OK371-Gal4, UAS-Dcr2* driven RNAi for complex I subunit *ND-75* (n = 10 for 33910, 2 for 39911) compared to control (n = 10), flies grown at 21°C, **(C)** *D42-Gal4* driven complex V *ATPsynCf6* (n = 10) and complex IV *COX5B* (n = 12) subunit RNAi at 25°C compared to control (n = 20), **(D)** *D42-Gal4* driven complex III *UQCR-14* (n = 13) subunit RNAi grown at 29°C compared to control (n = 13). **(E)** Climbing assay of *D42-Gal4* driven overexpression of *TFAM* (n = 10) compared to control (n = 10) at 25°C. All controls were the driver line crossed to *w1118.* Data were analysed using ANOVA or the student's t-test. Error bars represent SEM. * $p \leq 0.05$, ** $p \leq 0.01$, *** $p \leq 0.001$.

When driven with *D42-Gal4*, *ATPsynCf6* (CV) RNAi and *TFAM* overexpression also produced a wing inflation phenotype (Figure 3.2). This phenotype is not observed with *UQCR-14* (CIII) or *COX5B* (CIV) RNAi. During normal *Drosophila* development, neuronal activity stimulates inflation of the wing, post eclosion. A subset of 14 crusteacean cardioactive peptide (CCAP) expressing neurons in the ventral nerve cord (VNC) release a neurohormone called bursicon (Luan, Lemon et al. 2006). Bursicon initiates pumping of the haemolymph into the wing, causing inflation which allows the dorsal and ventral layers to straighten (Figure 3.2A). Broeck et al. observed a disruption of this process, leading to a folded wing phenotype, when inducing neuronal damage due to loss of TDP-43, a RNA processing protein associated with amyotrophic lateral sclerosis (ALS) (Vanden Broeck, Naval-Sánchez et al. 2013). When I induced neuronal mitochondrial dysfunction, with *D42-Gal4* driven *ATPsynCf6* (CV) knockdown and *TFAM* overexpression, approximately 80% and 50% of flies are unable to inflate their wings fully respectively (Figure 3.2C, D).

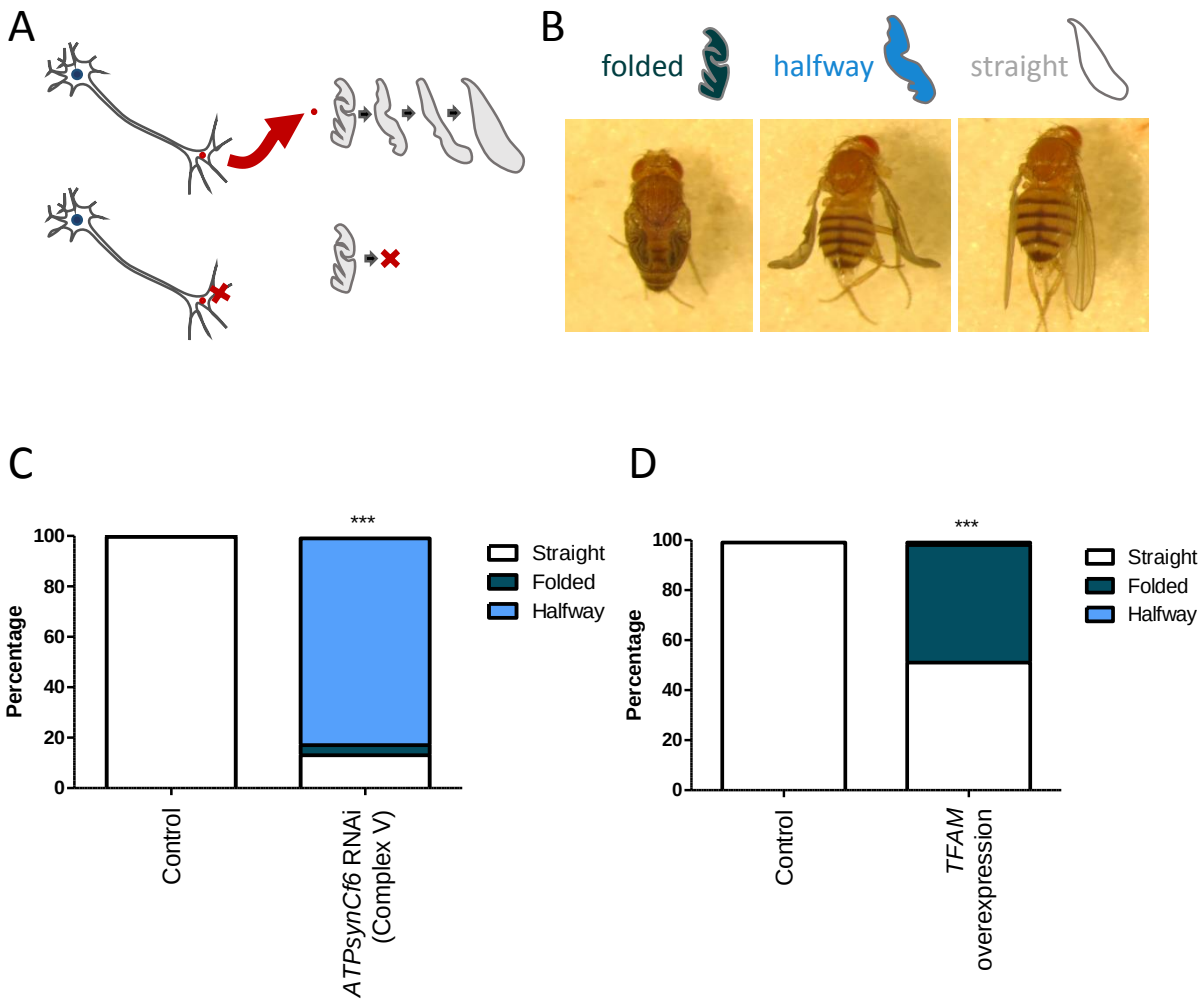

Figure 3.2 Neuronal knockdown of *ATPsynCf6* and overexpression of *TFAM* disrupt wing inflation.) Schematic showing CCAP neurons that release bursicon, triggering wing inflation. Neuronal dysfunction (**x**) can disrupt this processing leading to inhibited wing inflation. **(B)** For the inflation assay, wings are classified as folded, halfway or straight, at least 12 hours after eclosion. **(C)** *D42-Gal4* driven *ATPsynCf6* RNAi (n = 139) compared to control (n = 261) **(D)** *D42-Gal4* driven *TFAM* overexpression (n = 96) compared to control (n = 229). Controls are *D42-Gal4* crossed to *w1118*. Data were analysed with chi-squared test. *** $p \leq 0.001$

3.2.2 Validation of RNAi knockdown and *TFAM* overexpression

To confirm that the RNAi lines selected for each OXPHOS subunit are causing knockdown of the expected gene qRT-PCR was performed. Each RNAi was expressed ubiquitously for three days, from second to late third instar using temperature sensitive *tubulin-Gal80^{ts}; tubulin-Gal4.* Primers for qRT-PCR were designed to avoid the region targeted by the RNAi lines. In each RNAi line, expression of the expected mRNA was reduced, apart from *ND-75* RNAi. *UQCR-14* RNAi reduced *UQCR-14* expression by

95% (p = 0.0019), *COX5B* RNAi reduced *COX5B* expression by 84% (p = 0.0134) and *ATPsynCf6* RNAi reduced *ATPsynCf6* expression by 90% (p < 0.0001) (Figure 3.3).

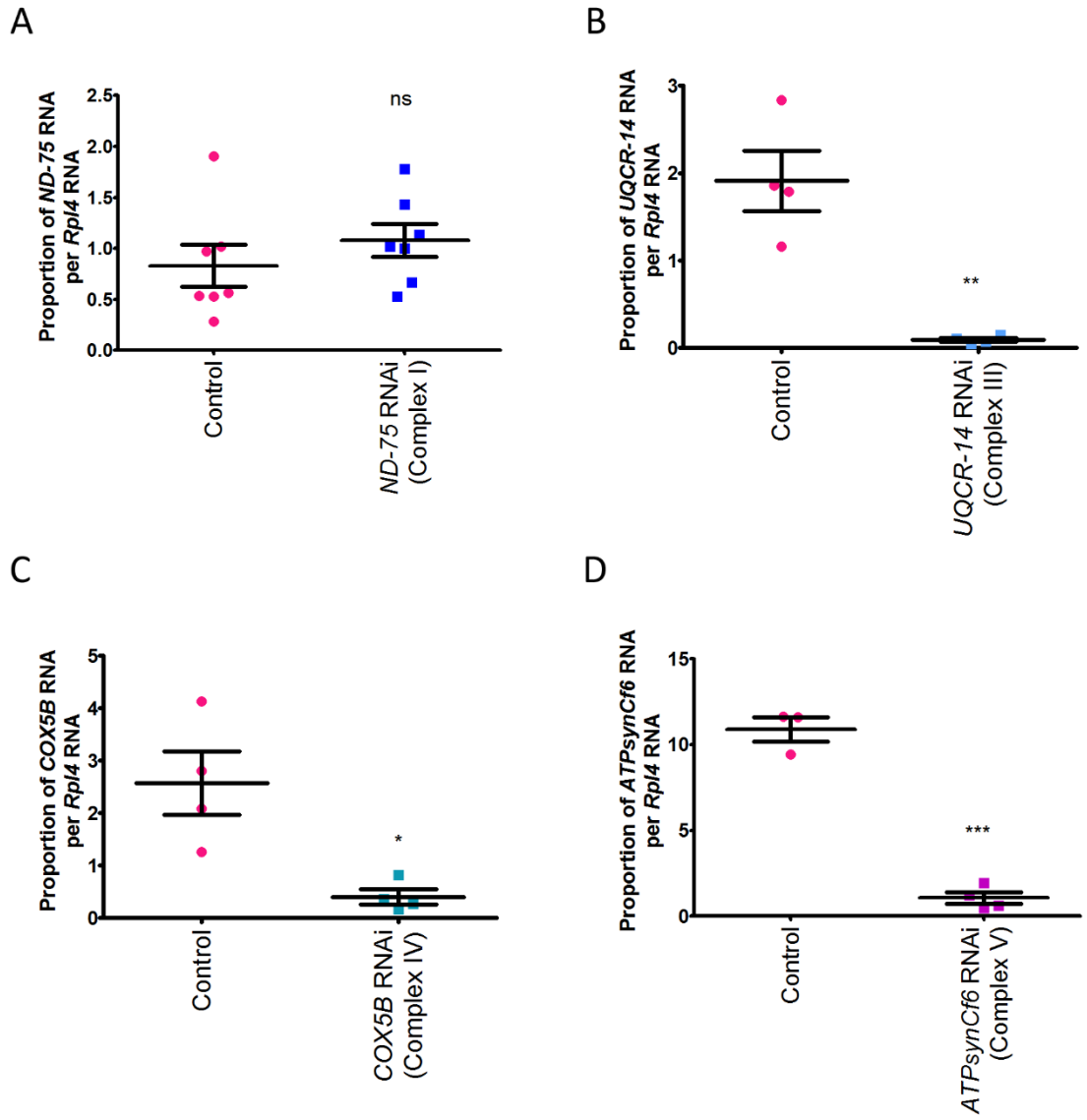

Figure 3.3 Level of knockdown of ubiquitously expressed RNAi lines
RNA was extracted from wandering third instar larvae with *tubulin-Gal4* and *tubulin-Gal80^{ts}* that had been at 29ºC for three days. **(A)** *ND-75* RNAi (CI) (n = 7) **(B)** *UQCR-14* RNAi (CIII) (n = 4) **(C)** *COX5B* RNAi (CIV) (n = 4) **(D)** *ATPsynCf6* RNAi (CV) (n = 4). RNA levels of each gene of interest were controlled to levels of the housekeeping gene *Rpl4*. Controls were *tubulin-Gal4* and *tubulin-Gal80^{ts}* crossed to *w1118*. Data were analysed using the student's t-test. Error bars represent SEM. ns not significant, * p≤0.05, ** p≤0.01, *** p≤0.001.

To further investigate whether *ND-75* RNAi was causing a knockdown of *ND-75* expression in the brain, I drove *ND-75* RNAi pan-neuronally, with *nSyb-Gal4*, and

measured levels of *ND-75* mRNA in the CNS. The *Gal4* in this driver line is expressed with the gene for synaptobrevin. Synaptobrevin is involved in neuronal vesicle release at the synapse and is therefore expressed in all post-mitotic neurons. The caveat with this method is that the CNS also contains non-neuronal cells in which *ND-75* RNAi is not expressed although *ND-75* is expressed in all cells, so I would expect to measure a knockdown that is smaller than is occurring in neurons. With this method, levels of *ND-75* were reduced by 50% ($p = 0.0364$) in the *ND-75* RNAi line (Figure 3.4A). As a comparison, I also measured the level of *UQCR-14* knockdown in *UQCR-14* RNAi under the same conditions. *UQCR-14* was decreased by 74%, although this difference was not statistically significant ($p = 0.0693$), most likely due to large variation in the control (Figure 3.4B). This indicates that, in the brain at least, *ND-75* RNAi is causing *ND-75* mRNA knockdown, and this knockdown is to a similar extent as *UQCR-14* RNAi knockdown.

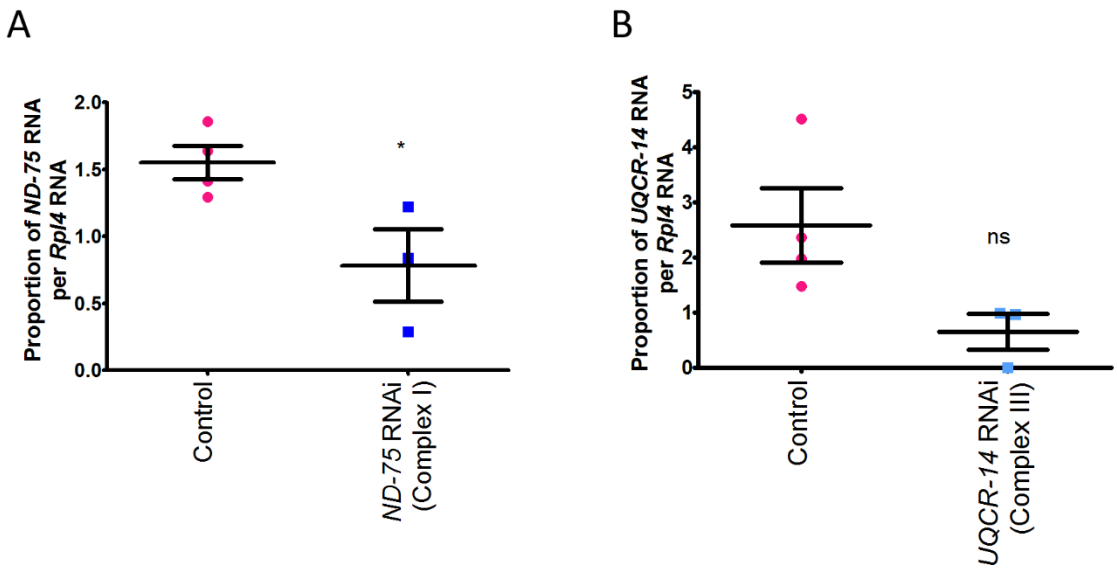

Figure 3.4 Level of knockdown of pan-neuronally expressed complex I and complex III RNAi in the CNS. RNA was extracted from brains of wandering third instar larvae with *nSyb-Gal4*, that had been at 25ºC for three days. **(A)** *ND-75* RNAi CI (n = 3-4) **(B)** *UQCR-14* RNAi CIII (n = 3-4). mRNA levels of each gene was controlled to levels of the housekeeping gene Rpl4. Controls are *nSyb-Gal4* crossed to *w1118.* Data were analysed using the student's t-test. Error bars represent SEM. ns not significant, * $p \leq 0.05$.

Ubiquitous overexpression of *TFAM* in third instar larvae, with *Tubulin-Gal80^{ts}; tubulin-Gal4* does not affect mtDNA levels, measured by qRT-PCR (Cagin, Duncan et al. 2015). Western blot analysis confirmed that TFAM protein levels were increased

when *TFAM* was overexpressed (Figure 3.5A). Ubiquitous overexpression of *TFAM* also results in a reduction of mitochondrially encoded COXI, with no significant change in levels of nuclear encoded ATP synthase α (Figure 3.5). This suggests that overexpression of *TFAM* inhibits the expression of mtDNA encoded genes, as observed in other models (Terskikh, Fradkov et al. 2000, Maniura-Weber, Goffart et al. 2004, Ylikallio, Tyynismaa et al. 2010).

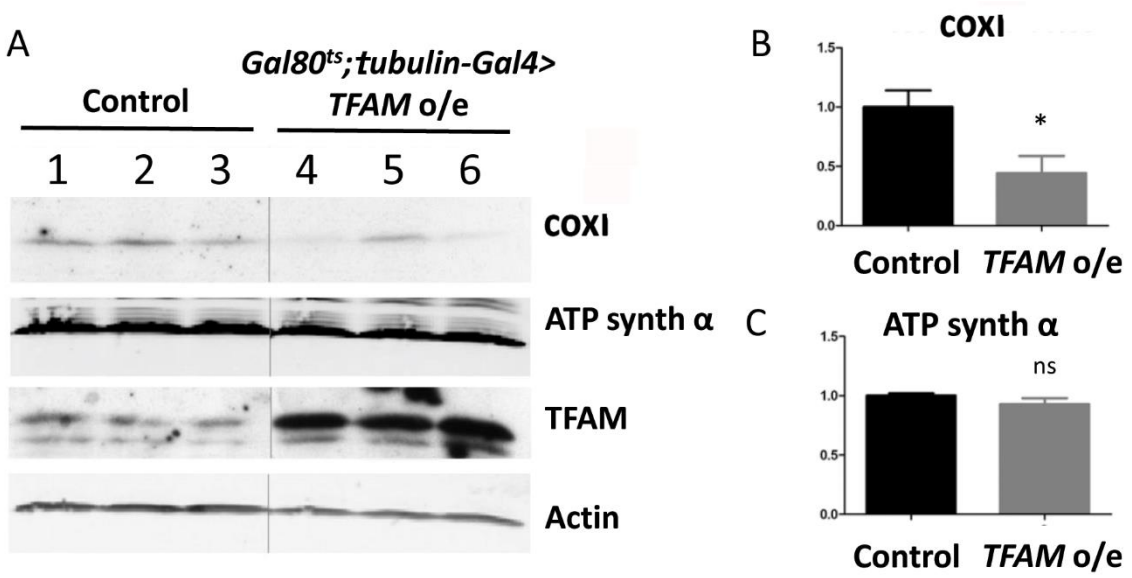

Figure 3.5 Reduced mitochondrial gene expression with *TFAM* overexpression
(A) Representative western blot of third instar larvae with COXI, ATP synthase α, TFAM and Actin antibodies. Controls in lane 1-3 and ubiquitously expressed *UAS-TFAM* in lane 4-6. Actin is used as a loading control, to which other proteins were normalised. **(B)** Quantification of mitochondrially encoded COXI (n = 3) **(C)** Quantification of nuclear encoded ATP synthase α (n=3). Controls are *Gal80ts; tubulin-Gal4* crossed to *w1118*. Data were analysed with a student's t-test. Error bars represent SEM. ns, not significant, * $p \leq 0.05$

3.2.3 Loss of synaptic mitochondria in all ETC models

I have identified and validated RNAi lines, which target knockdown of a single subunit of 4 out of 5 OXPHOS complexes, which may be suitable models of neuronal mitochondrial dysfunction. We have also identified a model of mitochondrial dysfunction which potentially affects all OXPHOS complexes by reducing expression of mtDNA encoded genes- *TFAM* overexpression. Each of these models induces climbing dysfunction, when knockdown or overexpression occurs in motor neurons. However, it is unclear how the mitochondria are effected in these neurons. To investigate this, genetically encoded, mitochondrially targeted GFP (mitoGFP) was used

to visualise mitochondria at the NMJ. I visualised mitochondria at the NMJ for three reasons. Firstly, the synaptic compartment has a large energy demand, due to synaptic transmission. Mitochondria are therefore particularly important here for their role in ATP production (Harris, Jolivet et al.) and are preferentially trafficked from the soma, where the majority of mitochondria are produced, to pre- and postsynaptic terminals (Chang, Honick et al. 2006). Neurons are therefore particularly reliant on the correct trafficking of mitochondria to the synapse (Schwarz 2013). Secondly, motor neurons synapse on muscles at the neuromuscular junction (NMJ). Neuromuscular junctions in *Drosophila* third instar larvae are well characterised and so it is easy to identify the same synapse repeatedly (Figure 3.6A). Finally, Umut Cagin (Bateman lab) has previously imaged mitochondria in the NMJ, proximal axon, distal axon and cell body in the *TFAM* overexpression model. In this model mitochondrial loss was observed at the NMJ, but not at the cell body (Cagin, Duncan et al. 2015).

The number and volume of mitochondria in the NMJ of third instar larvae was significantly reduced when *ND-75* (CI), *UQCR-14* (CIII), *COX5B* (CIV) and *ATPsynCf6* (CV) were knocked down in motor neurons with the *OK371-Gal4* driver (Figure 3.6B-H). The degree of mitochondrial loss mirrors the severity observed in climbing dysfunction.

It is possible that OXPHOS RNAi reduced the mitochondrial volume and number because the NMJs were smaller. Altered ATP and ROS levels have previously been shown to alter NMJ size. *Drosophila* mutants with disrupted glycolysis display a loss in ATP in the brain and an increase in bouton diameter at the NMJ (Wang, Saraswati et al. 2004). Similarly, increased oxidative stress causes bouton overgrowth, quantified by bouton number (Milton, Jarrett et al. 2011). To determine whether the bouton size or number was affected in our models of mitochondrial dysfunction, the number and diameter of boutons at the NMJ were measured. Volume of the entire NMJ would have been a more preferable measure, however, due to the variability of the HRP stain, this could not be measured reliably. A small decrease in bouton number was observed in *ATPsynCf6* (CV) knockdown, whereas *ND-75* (CI) knockdown resulted in a small increase in bouton number (Figure 3.6I). All RNAi lines resulted in a small decrease in bouton diameter (Figure 3.6J). However, these changes are too small to fully explain the decrease in mitochondria. Thus the loss of mitochondria in the NMJ is more likely to be

due to the OXHOPS subunit knockdown directly, rather than a secondary effect on NMJ size.

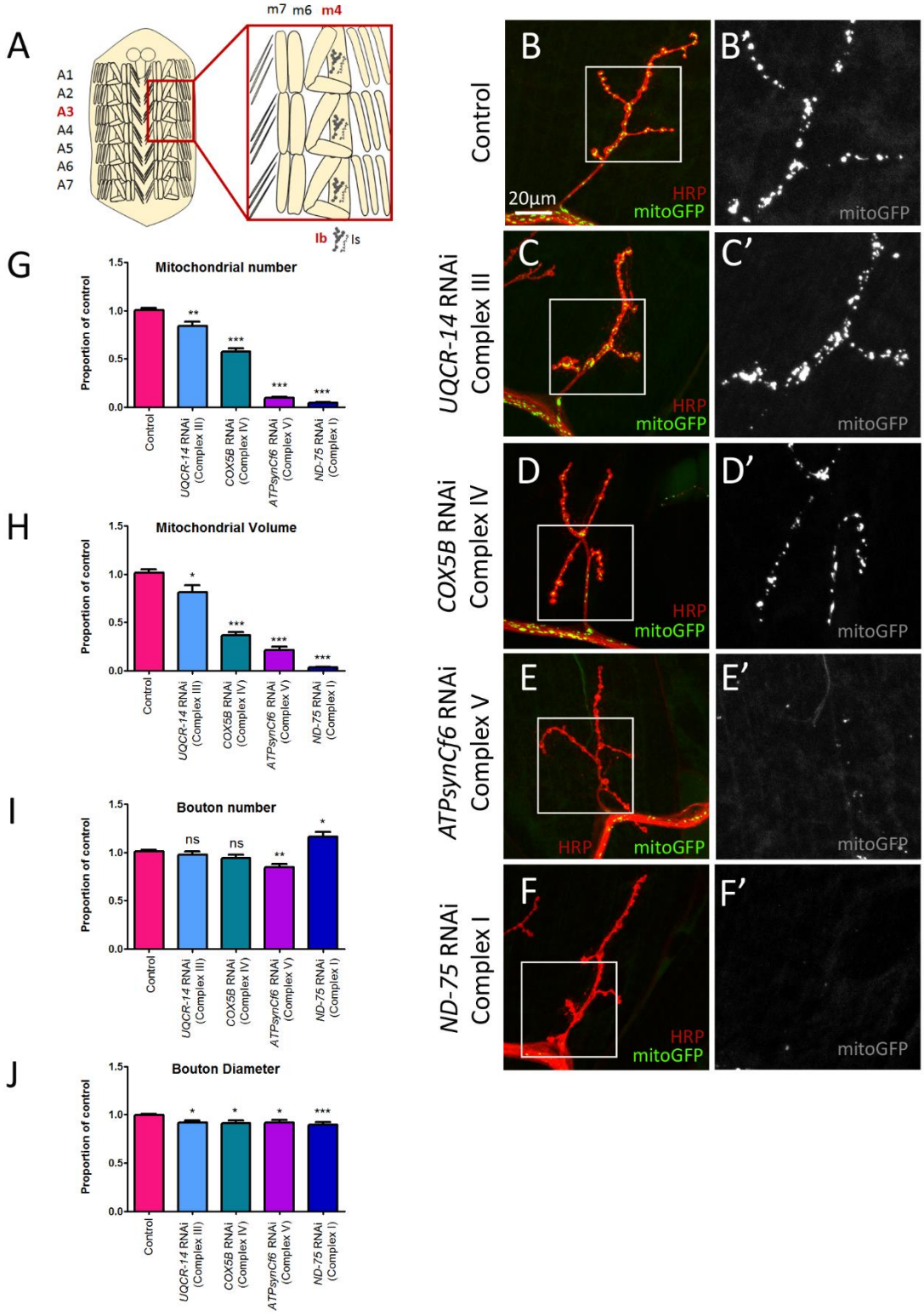

Figure 3.6 Neuronal specific knockdown of OXPHOS complex subunits causes loss of synaptic mitochondria. (A) Schematic to show the position of the Ib NMJ on muscle 4, segment 3 in late third instar larvae. **(B-F)** NMJ stained with HRP (red) of *OK371-Gal4* and *UAS-mitoGFP* (green) with **(B)** *w1118* (control) (n = 19 - 21), **(C)** *UQCR-14* RNAi (n = 21), **(D)** *COX5B* RNAi (n = 20), **(E)** *ATPsynCf6* RNAi (n = 22), **(E)** *ND-75* RNAi (n = 24). **(B'-F')** Close up of mitoGFP expression in the white box.

Quantification of **(G)** mitochondrial number and **(H)** mitochondrial volume, **(I)** bouton number and **(J)** bouton diameter. Each RNAi line was dissected individually together with a control, so statistical analysis compared each RNAi to the relevant control using the student's t-test if data was normally distributed, and Mann-Whitney U if not. Error bars represent SEM. ns not significant, * $p \leq 0.05$, ** $p \leq 0.01$, *** $p \leq 0.001$.

3.2.4 Changes in Reactive Oxygen Species (ROS) in the mitochondrial dysfunction models

ROS are produced as a by-product of OXPHOS produced at complexes I, II and III (see Introduction 1.2.4). Damage to all OXPHOS complexes has been reported to result in increased production of ROS, as if one complex is dysfunctional then the normal flow of electrons down the ETC is disrupted (Reinecke, Smeitink et al. 2009). Increased ROS, due to OXHOS dysfunction, can damage mitochondrial DNA and therefore damage mitochondrial OXPHOS subunits, producing a cycle of increasing dysfunction (Bonawitz, Rodeheffer et al. 2006). It is therefore important to characterise changes in ROS in the models of mitochondrial dysfunction we have developed.

A genetic tool developed by Albrecht et al, measures tissue specific changes in ROS *in vivo*, using reporters fused to redox sensitive GFPs (roGFP) (Hanson, Aggeler et al. 2004, Albrecht, Barata et al. 2011). A pair of redox-sensitive cysteine residues have been added to YFP and GFP close to the chromophore, to create fluorescent probes that respond to oxidation (Ostergaard, Henriksen et al. 2001, Hanson, Aggeler et al. 2004). When reduced, roGFP is excited at 488nm whereas oxidised roGFP is excited at 405nm. The ratio of 488:405nm therefore provides a readout of the redox potential of the roGFP. roGFP fused to glutaredoxin (Grx) was used as a reporter of the glutathione redox potential (E_{GSH}). Glutathione (GSH) is a ROS scavenger that reduces H_2O_2 produced in the cell, becoming oxidised itself and converting into glutathione disulphide (GSSG) and water. This system acts to protect the cell from increased ROS (Albrecht, Barata et al. 2011). Grx is a catalyst for this reaction (Lillig, Berndt et al. 2008). A dithiol/disulphide switch on the fused roGFP responds to oxidation of Grx, producing measurable fluorescent changes, irrespective of physiological changes in pH. When fused to Grx (roGFP2-Grx1), the roGFP is reduced by GSH and oxidised by GSSG, and so the roGFP fluorescence depends on the E_{GSH} (Gutscher, Pauleau et al. 2008). roGFP fused to oxidant receptor peroxidase (ORP), a microbial sensor of H_2O_2, responds to oxidation of ORP and therefore provides a tool to measure levels of H_2O_2,

independent of Grx. Mitochondrial target sequences have also been coupled to these constructs, so that ROS levels can be measured independently in these sub-compartments of the cell.

I used these redox sensors to examine ROS levels in my models of mitochondrial dysfunction, at the NMJ, where mitochondrial levels are reduced. The *OK371-Gal4* driver was used to drive expression of the OXPHOS complex RNAi lines and the ROS reporters in motor neurons. The fluorescence signal for each probe was measured at the NMJ in fully oxidised and fully reduced condition in order to measure the dynamic range of each probe at the NMJ. Cytosolic roGFP2-Grx and mitochondrial roGFP-ORP were tested at the NMJ, however, the fluorescent range at the NMJ was not sufficient for these two probes (data not shown), so they were not pursued further. The dynamic range of fully oxidised and fully reduced mitochondrial roGFP2-Grx controls was adequate and so the mitochondrial E_{gsh} was assessed (Figure 3.7).

In motor neurons with the *UQCR-14* (CIII) RNAi, the redox state of mitochondrial targeted roGFP2-Grx was no different from control (Figure 3.7D-E). *COX5B* (CIV) and *ATPsynCf6* (CV) knockdown in motor neurons resulted significantly reduced roGFP2-Grx, which signifies lower levels of ROS (Figure 3.7F-I). *TFAM* overexpression also results in reduced mitochondrial roGFP-Grx in the NMJ (this experiment was carried out by Dr Ariana Gatt)(Cagin, Duncan et al. 2015). One possible explanation for this reduction of ROS, may be that the dysfunctional mitochondria in these models are not as active and normal, so ETC activity is reduced and less ROS produced.

Complex I dysfunction is strongly associated with increased ROS in the literature (Pitkanen and Robinson , Tretter, Sipos et al. 2004). At the NMJ of flies with *ND-75* (CI) knockdown, mitochondrial roGFP2-Grx was significantly oxidised compared with control (Figure 3.7J-K).

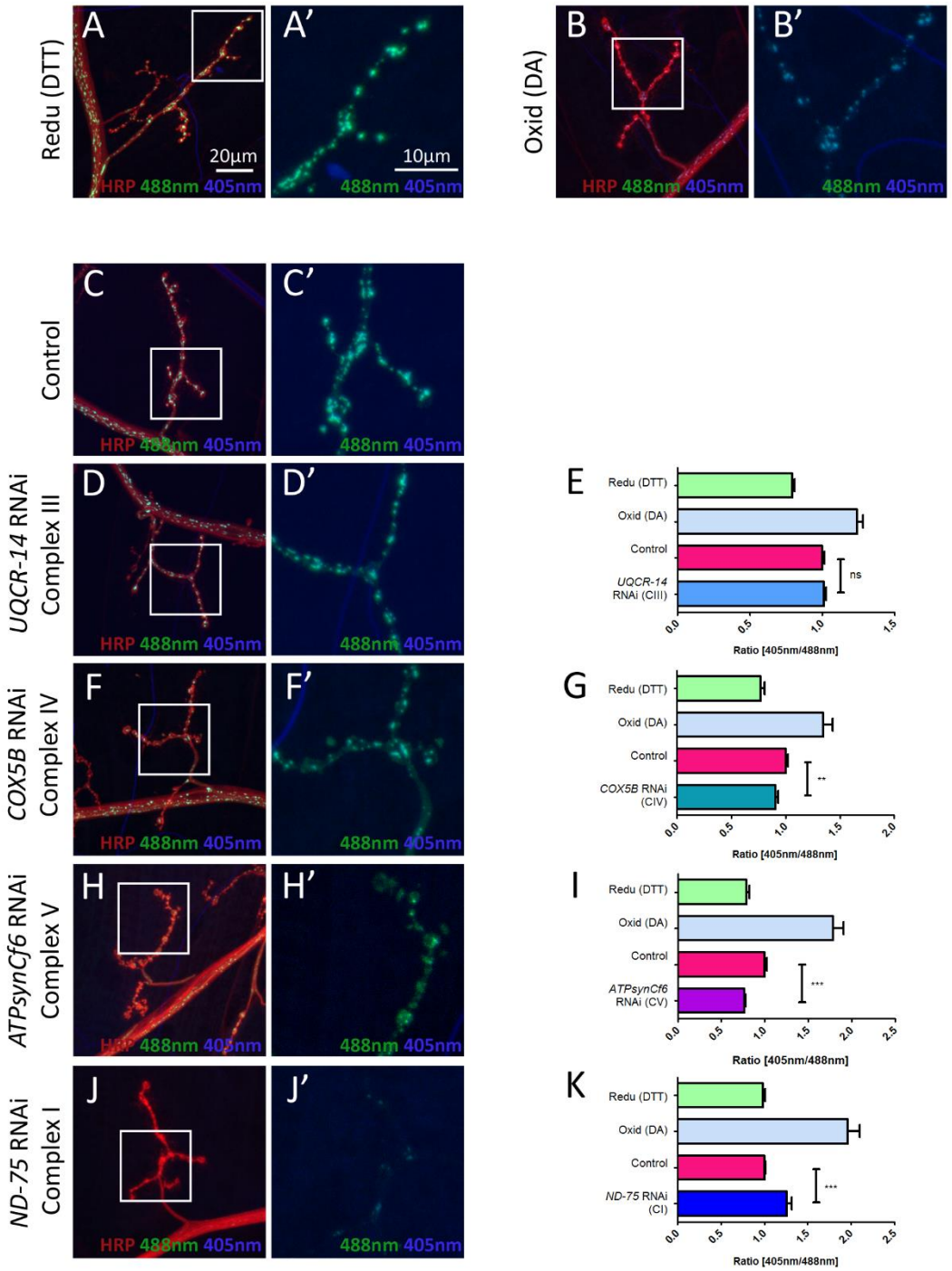

Figure 3.7 Neuronal specific knockdown of ETC complex subunits causes altered glutathione redox potential in the mitochondrial matrix. Representative images of NMJs on muscle 4 segment 3 with *OK371-Gal4* driven *mito-roGFP2-Grx1*. NMJs are stained with HRP (red), ro-GFP was excited with 488nm (green) and 405nm (blue) images show these channels merged. **(A)** Fully reduced (Redu) controls (n = 5-11) and **(B)** fully oxidised (Oxid) controls (n = 5-12) were produced by treatment with DTT and DA respectively. **(C)** Control (*w1118*) NMJ (n = 18-26) **(D)** *UQCR-14* RNAi (n = 20) quantified in **(E)**. **(F)** *COX5B* RNAi (n = 27) quantified in **(G)**. **(H)** *ATPsynCf6* RNAi (n = 19) quantified in **(I)**. **(J)** *ND-75* RNAi (n = 18) quantified in **(K)**. **(A', B', C', D', E', F')** Closer detail of 488nm and 405nm overlay in the white boxed area. Data were analysed using one way ANOVA. Error bars represent SEM. ns not significant, * $p \leq 0.05$, *** $p \leq 0.001$.

3.2.5 MitoTimer oxidation changes in mitochondrial dysfunction models

Glutaredoxin and ORP fused to roGFP are tools to measure instantaneous ROS changes. To understand the health of mitochondria over time another *in vivo* reporter was utilised. A 'fluorescent timer' construct has been developed which irreversibly changes fluorescent emission when oxidised (Terskikh, Fradkov et al. 2000). It encodes a mutant of DsRed which is excited at 488nm (green) until it is oxidised, when it shifts to excition at 546nm (red). Laker et al. fused the mitochondrial targeting sequence from a nuclear encoded subunit of OXPHOS complex IV (cytochrome c oxidase subunit VIII), to target the 'fluorescent timer' construct to mitochondria, creating mitoTimer (Laker, Xu et al. 2014). When driven by a constitutively active driver mitoTimer accumulates in the mitochondria. The ratio of 546nm signal (oxidised) to 488nm signal therefore gives an indication mitochondrial stress and turnover, and is therefore a general indicator of mitochondrial health.

MitoTimer oxidation was measured in the motor neuron cell bodies in the VNC, as well as at the NMJ, for *D42-Gal4* driven *ND-75* (CI), *UQCR-14* (CIII), *COX5B* (CIV) and *ATPsynCf6* (CV) RNAi and *TFAM* overexpression. In the cell bodies, *UQCR-14* (CIII), *COX5B* (CIV), *ATPsynCf6* (CV) knockdown and *TFAM* overexpression had no effect on mitoTimer oxidation (Figure 3.8A-E,G). However, the mitoTimer reporter shows increased oxidation in the motor neuron cell bodies in flies with *ND-75* (CI) RNAi (Figure 3.8F).

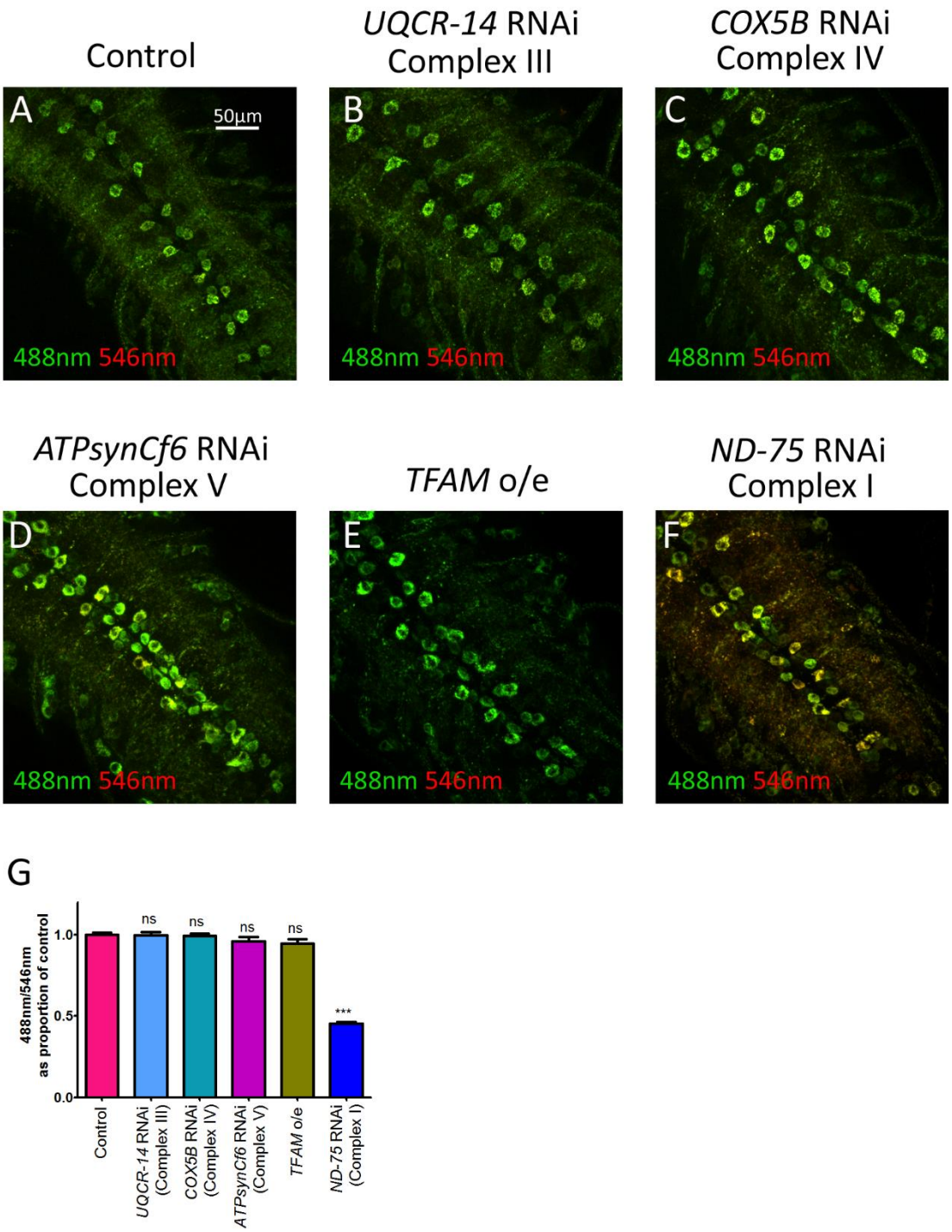

Figure 3.8 Neuronal specific knockdown of *ND-75* causes mitochondrial oxidation at the cell body. Representative images of mitoTimer expressed in motor neuron cell bodies with *D42-Gal4.* MitoTimer fluoresces when excited by 488nm (green), until it is oxidised when it is excited at 546nm (red), these two channels are overlaid. Images of the VNC from **(A)** control (*w1118*) (n = 57), **(B)** complex III RNAi (n = 21), **(C)** complex IV RNAi (n = 23), **(D)** complex V RNAi (n = 21), **(E)** *TFAM* overexpression (n = 21), **(F)** complex I RNAi (n = 21). **(G)** Quantification of all genotypes compared to control using a one way ANOVA. Error bars represent SEM. ns not significant, *** $p \leq 0.01$.

At the NMJ, *UQCR-14* (CIII) knockdown had no effect on the oxidation of mitoTimer (Figure 3.9A-B', G). However, *COX5B* (CIV), *ATPsynCf6* (CV) and *ND-75* (CI) RNAi and *TFAM* overexpression all caused an increase in oxidation of the mitoTimer reporter (Figure 3.9C-G). This could indicate increased ROS production at the NMJ mitochondria, however it may also be due to reduced turnover of damaged synaptic mitochondria.

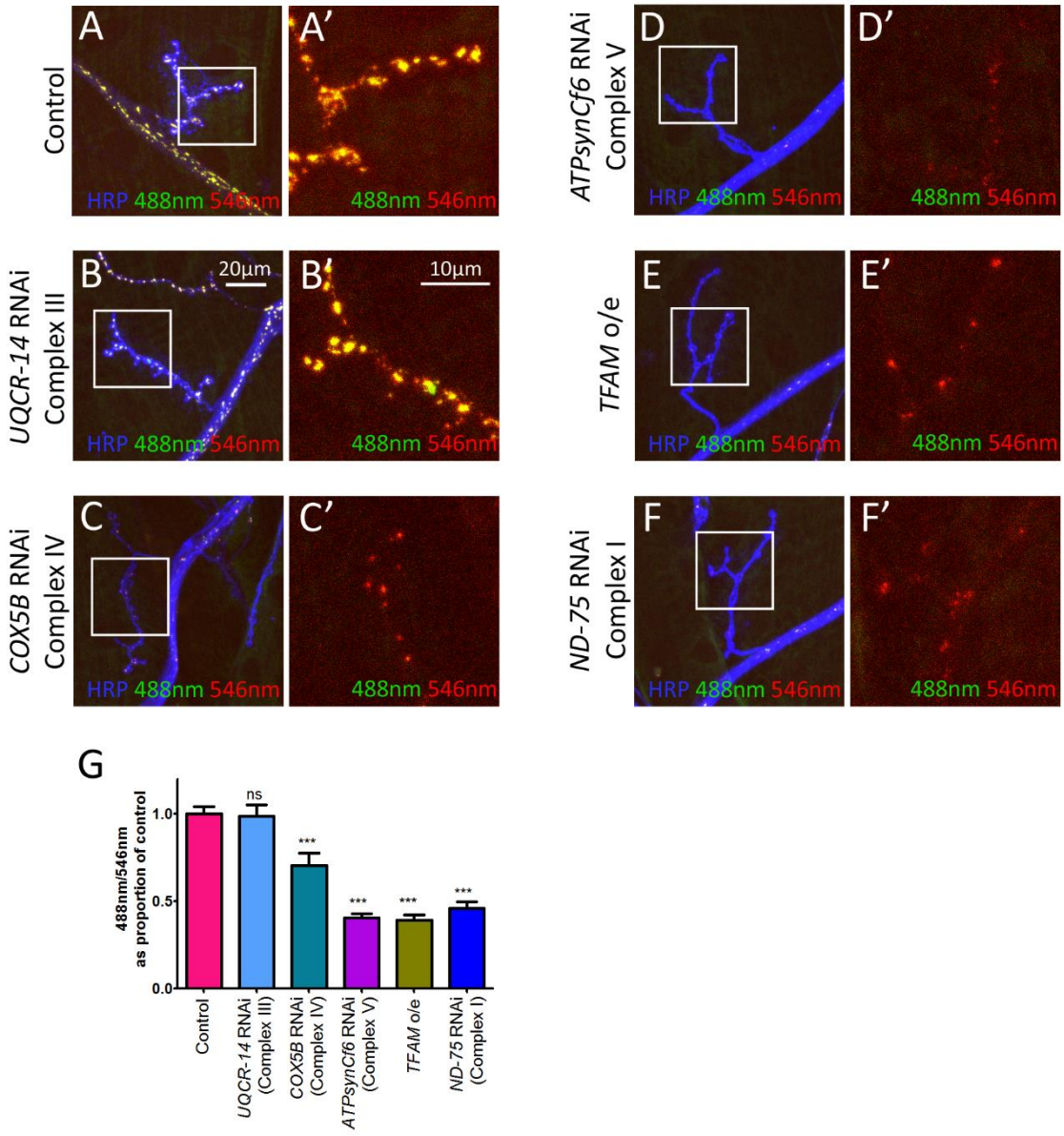

Figure 3.9 Oxidation of mitoTimer in synaptic mitochondria in complex I, IV and V RNAi and *TFAM* overexpression. Representative images of mitoTimer at the NMJ with *D42-Gal4*. The NMJ is stained with HRP (blue). MitoTimer fluoresces when excited by 488nm (green), until it is oxidised when it is excited at 546nm (red), these two channels are overlayed. Images of **(A)** control (n = 22), **(B)** complex III RNAi (n = 18), **(C)** complex IV RNAi (n = 18), **(D)** complex V RNAi (n = 18), **(E)** *TFAM* overexpression (n = 17), **(F)** complex I RNAi (n = 17). **(A', B', C', D', E', F')** 488nm and 546nm signal in the white boxed area. **(G)** Quantification of all genotypes

compared to control using a one way ANOVA. Error bars represent SEM. ns not significant, *** $p \leq 0.01$.

3.2.6 ATP to ADP ratio in flies with neuronal complex V and complex I knockdown and *TFAM* overexpression.

Mitochondria are best known for their role in ATP production, so it is important to characterise changes in ATP levels in our models of mitochondrial dysfunction. Measuring ATP levels in neurons poses a challenge. ATP can be measured from homogenate of the CNS, however, this will also contain a large number of glia, which provide metabolic support for neurons. CNS homogenate will there contain a mix of neurons with mitochondrial dysfunction and healthy glia. These glia may be compensating for changes in neuronal ATP and so affect ATP measurements. To avoid these problems we used a fluorescent reporter, which had been developed in bacteria to measure the neuronal ratio of ATP to ADP *in vivo*. The ratio of ATP to ADP is thought to be more important than the total amount of ATP (Tantama, Martínez-François et al. 2013). Total ATP varies considerably from cell to cell, whereas the ratio of ATP to ADP gives a more accurate measure of metabolism (Veech, Lawson et al. 1979, Berg, Hung et al. 2009).

Berg, Hung and Yellen identified a bacterial protein, GlnK1, which acts as an endogenous energy sensor, which they fused to a fluorescent biosensor to create a tool that visualises ATP:ADP (Berg, Hung et al. 2009). GlnK1 regulates transport of ammonia into the bacterium, depending on cellular energy. It blocks the ammonia transporter unless bound to both ATP and 2-ketaglutarate (Durand and Merrick 2006, Yildiz, Kalthoff et al. 2007). ATP binds to GlnK1 with a very high affinity, approximately 0.04µM (Berg, Hung et al. 2009). This binding results in a conformational change in the disordered 'T-loop' of GlnK1, into a closed loop (Yildiz, Kalthoff et al. 2007). ADP also binds to GlnK1, however, it has a 5 times lower binding affinity and results in a smaller conformational change (Berg, Hung et al. 2009). A circularly permuted yellow fluorescent protein (cpYFP) was fused to GlnK1. To create a circularly permuted YFP, the N and C termini were fused with a peptide linker and new termini were created closer to the chromophore. When the new termini are fused to another protein, the fluorescence of the YFP becomes dependant on conformational changes in the fused protein (Baird, Zacharias et al. 1999). Fluorescence of cpYFP, inserted in the T-loop of GlnK1 between tyrosine 51 and isoleucine 52, is sensitive to

conformational changes in Glnk1. Excitation of Glnk1-cpYFP at 488nm produces a prominent emission peak, with a smaller peak when excited at 405nm. When ATP binds to GlnK1, the conformational change in the T-loop produces a ratiometric change in cYFP excitation. The 405nm peak is reduced and the 488nm peak is enhanced. Binding of ADP to the GlnK1-cpYFP also results in the same ratiometric change, however, ADP does not completely close the T-loop and so the change in fluorescence is smaller.

GlnK1's ability to act as an ATP:ADP sensor depends four of its properties: ADP and ATP have a very high binding affinity with GlnK1, ADP and ATP bind competitively to the protein, ATP has a higher binding affinity than ADP, ATP produces a greater conformational change in GlnK1 and therefore a larger ratiometric change. When ATP:ADP levels are very high ATP will outcompete ADP and produce the maximal ratiometric change in cpYFP fluorescence with a large peak at 488nm and a small peak at 405nm. If ATP:ADP levels are lower, ADP will compete with ATP, therefore reducing the 488nm excitation and increasing the 405nm excitiation. GlnK1 was optimised through mutagenesis, to have a lower sensitivity to 2-ketaglutarate, faster kinetics and a higher affinity for ADP (0.02µM) and this optimised construct fused to cpYFP was called Perceval (Berg, Hung et al. 2009).

In order to use Perceval as a ATP:ADP sensor in *Drosophila*, I cloned the construct into a P-element that was then inserted into the *Drosophila* genome. A single copy of the construct emitted fluorescence when excited with 488nm light, however the 405nm was barely visible above background (data not shown). This was the case for fixed samples, fixed in 4% formaldehyde or using PLP, a fixative protocol aimed to preserve fluorescent signals, and during live imaging. Two copies of the construct also gave a signal that was similar to background levels at the 405nm excitation (data not shown). However, with 3 copies of Perceval, it was possible to measure both wavelengths in motor neuron cell bodies in the VNC (Figure 3.10).

Third instar larvae with *ATPsynCf6* (CV) RNAi or *TFAM* overexpression in motor neurons did not display any change in ATP:ADP ratio in motor neuron cell bodies compared to control (Figure 3.10A-E). *ND-75* (CI) RNAi, however, resulted in a decrease in ATP:ADP by approximately 50% (Figure 3.10F-G). *UQCR-14* (CIII) and *COX5B* (CIV) RNAi have not been tested to date, however the relevant flies for these experiments are currently being made.

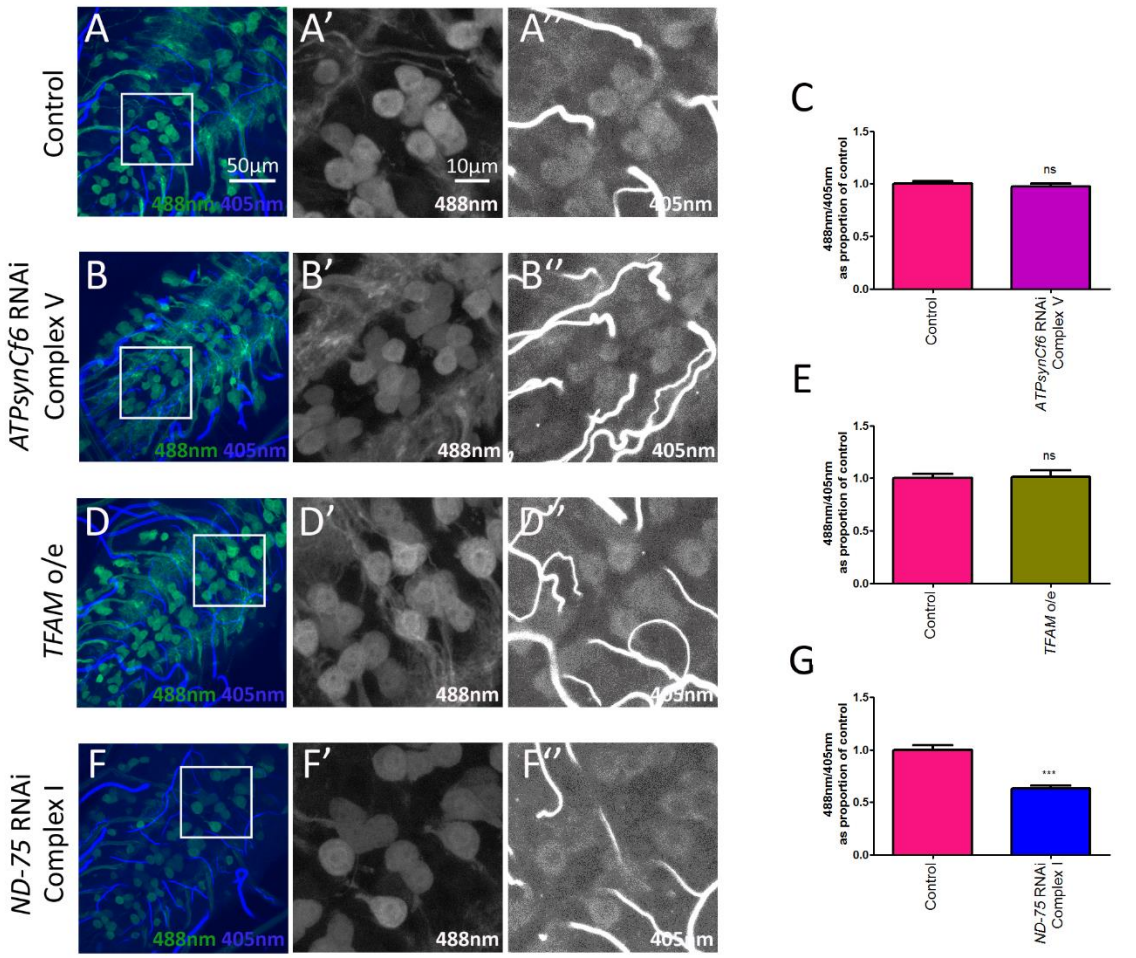

Figure 3.10 Neuronal specific knockdown of complex I reduces the ATP:ADP ratio Motor neuron cell bodies in the VNC with *OK371-Gal4* and three copies of the Perceval construct. Merged images with 488nm (green) and 405nm (blue) in **(A,B,D,F)**. The ratio of 488nm/405nm represents the ATP:ADP ratio in **(A)** Control (*w1118*) larvae (n = 16-17), **(B)** *ATPsynCf6* knockdown (n = 17) quantified in **(C). (D)** Larvae overexpressing *TFAM* (n = 17) quantified in **(E)**. *ND-75* knockdown **(F)** quantified in **(G)**. Signal in the 488nm channel in the white boxed areas are shown in **(A',B',D',F')** and the 405nm signal from the same areas are shown in **(A'',B'',D'',F'')**. Data were analysed using the student's t-test, using Welch's correction when the variance was not equal. Error bars represent SEM. ns not significant, *** $p \leq 0.001$.

3.3 Summary

The aim of this chapter was develop and characterise models of neuronal mitochondrial dysfunction induced by knockdown of the five complexes involved in oxidative phosphorylation and one model inhibiting mtDNA transcription. A library of RNAi lines that targeted neuronally encoded subunits of each complex was screened, to identify knockdowns that caused a climbing phenotype. Suitable RNAi lines were identified for complex I, III, IV and V. There was a scale of phenotype severity, with *ND-75* (CI) RNAi inducing the most extreme phenotype and *UQCR-14* (CIII) knockdown causing the mildest climbing dysfunction. *TFAM* overexpression was used as a model that targets mitochondrial dysfunction via mtDNA, and had a severe effect on climbing ability.

One RNAi for each of these complexes was further characterised. Loss of mitochondria was observed at the synapse of each model. This phenotype was most severe with *ND-75* (CI) knockdown and least penetrant in the *UQCR-14* (CIII) knockdown, as with the climbing phenotype. Similar loss of mitochondria at the synapse had previously been observed in the *TFAM* overexpression model (Cagin, Duncan et al. 2015).

The RNAi knockdown for these models was validated with qRT-PCR, and is similar in all lines. *ND-75* was shown to be significantly knocked down in the brain, however, it was not significantly knocked down when the RNAi was expressed ubiquitously (see Discussion 7.1.2). *TFAM* overexpression was validated by western blot, which showed TFAM levels were increased and that this causes reduced expression of mtDNA encoded protein COXI.

ROS levels were measured using mitochondrially targeted roGFP-Grx, to measure the glutathione redox potential. Mitochondrial roGFP-Grx revealed no change in mitochondrial ROS in synaptic mitochondria with *UQCR-14* (CIII) RNAi and reduced ROS levels in *COX5B* (CIV) and *ATPsynCf6* (CV) RNAi. Our previous work had also shown a reduced ROS level in synaptic mitochondria when *TFAM* is overexpressed (Cagin, Duncan et al. 2015). *ND-75* (CI) RNAi, however, caused oxidation in mitochondria at the synapse using this probe.

The mitoTimer construct reports accumulation of oxidation in the mitochondria. In motor neuron cell bodies, no change in oxidation occurred in *UQCR-14* (CIII), *COX5B* (CIV) or *ATPsynCf6* (CV) knockdown models, or in *TFAM* overexpression. *ND-75* (CI) knockdown, however caused an increase in oxidation in mitochondria at the cell body. At the NMJ all of the mitochondrial dysfunction models led to increased oxidation in mitochondria apart from *UQCR-14* (CIII) RNAi.

To assess possible changes in energy levels, the ATP:ADP ratio was measured in motor neuron cell bodies of *ND-75* (CI) and *ATPsynCf6* (CV) RNAi models and the *TFAM* overexpression model, using the Perceval probe. Knockdown of *ATPsynCf6* (CV) and overexpression of *TFAM* did not alter ATP:ADP, however, there was a reduction in ATP:ADP when *ND-75* (CI) was knocked down in motor neurons.

4 INVESTIGATING THE TRANSCRIPTIONAL RESPONSE TO OXPHOS SUBUNIT KNOCKDOWN AND *TFAM* OVEREXPRESSION MODELS OF MITOCHONDRIAL DYSFUNCTION IN NEURONS.

4.1 Introduction

A retrograde response, from dysfunctional mitochondria back to the nucleus, has been well characterised in budding yeast (see Introduction 1.4.1) (Jia, Rothermel et al. 1997), but the retrograde response in multicellular organisms is less well understood. Analysis of transcriptional changes following different mitochondrial insults has shown how varied the retrograde response in multicellular organism can be.

A study in human cell lines, compared a mtDNA mutation, A3243G, with loss of mtDNA. The A3243G mutation is associated with MELAS disease and is caused by a point mutation in $tRNA^{Leu}$, required for translation of mitochondrial proteins. There were common transcriptional changes in both cases, leading to an upregulation in extracellular matrix genes and a downregulation in genes involved in ribosomal protein synthesis and ubiquitin degradation (Jahangir Tafrechi, Svensson et al. 2005). However, there were also a subset of genes, involved in OXPHOS that were only upregulated in the cell with complete mtDNA loss (Jahangir Tafrechi, Svensson et al. 2005). A further study looked at increasing copy number of the A3243G mutation in mitochondria and found distinct transcriptional and phenotypic changes depending on the A3243G mutation load (Picard, Zhang et al. 2014).

The transcriptional response to loss of individual components of the TCA cycle also varies depending on which component of the TCA cycle is affected. Microarray analysis of yeast cells with mutations in different subunits of TCA cycle enzymes reveals a subset of 23 genes that are altered in an inverse pairwise fashion along the cycle (McCammon, Epstein et al. 2003). These differences may be mediated by the metabolites that are differentially produced depending on which enzyme is affected (McCammon, Epstein et al. 2003).

These studies demonstrate that there are unique transcriptional responses depending upon the specific mitochondrial insult. However, they also show that there are commonly regulated genes and pathways that are modulate by mitochondrial dysfunction. Elucidating these pathways is essential for developing new therapeutic approaches to diseases associated with mitochondrial dysfunction.

Transcriptional changes have been studied in different models of mitochondrial dysfunction in *Drosophila*. Microarrays have been performed on adult flies containing a point mutation in *technical knockout* (*tko*), the gene that encodes mitochondrial ribosomal protein S12 (Fernandez-Ayala, Chen et al. 2010) and adult *pink1* mutants (Tufi, Gandhi et al. 2014). Transcriptional changes due to the knockdown of complex IV subunit *COX5A* in *Drosophila* S2 cells, have also been documented (Freije, Mandal et al. 2012). It is difficult however, to determine if differences between the transcriptional changes in these models are due to the different mitochondrial insults, or differences in the models, tissue type and conditions. To address this issue I aim to perform microarray analysis of the OXPHOS knockdown and *TFAM* overexpression models described in the previous chapter.

Previous microarray analysis of neuronal *ATPsynCf6* RNAi and *TFAM* overexpression in the *Drosophila* CNS showed that approximately 50% of genes differentially regulated in the two conditions are common to both (Cagin, Duncan et al. 2015). I therefore hypothesise that the mitochondrial models I describe in Chapter 3 will also produce unique and overlapping transcriptional responses. Knowledge of the transcriptional changes in these models may allow me to identify pathways that can modulate the phenotypes caused by mitochondrial dysfunction in all of these conditions.

4.1.1 Chapter aims

In this chapter my aims are to –

1. Characterise transcriptional changes in the OXPHOS knockdown and *TFAM* overexpression models I have described in the previous chapter.
2. Validate the microarray data by looking at expression of transcriptional reporters *in vivo*.
3. Identify common pathways between the conditions as well as differences between them.
4. Regulate the transcriptional response, to modulate the functional outcome of mitochondrial dysfunction in the different models.

4.2 Results

4.2.1 Characterisation of the transcriptional response to mitochondrial dysfunction in *TFAM* overexpression and OXPHOS complex knockdown models.

In order to characterise the neuronal transcriptional response to different forms of mitochondrial dysfunction, I carried out microarray analysis on CNS tissue from third instar larvae expressing OXPHOS complex subunit knockdown or *TFAM* overexpression, pan-neuronally with the *nSyb-Gal4* driver. Pan-neuronal knockdown of OXPHOS complex subunits (*ND-75, UQCR-14, COX5B, ATPsynCf6)* and over expression of *TFAM* with this driver is pupal lethal.

The Affymetrix *Drosophila* genome v2 GeneChip array, which contains a set of 18, 880 probes, for over 18 500 transcripts, was used. The microarrays were performed by Dr David Chambers. Data from these arrays were processed using the Affymetrix Expression Console and the Affymetrix Transcriptome Analysis Console, significance was determined using one way ANOVA. In each condition of mitochondrial dysfunction 358-840 genes were differentially expressed ($p < 0.05$) (Table 7, Figure 4.1). Heat maps show gene expression of the 20 genes with the lowest p-value in each condition, and how these genes changed in the other mitochondrial dysfunction models (Figure 4.2). In many cases gene expression changes are similar in all mitochondrial dysfunction models compared to control.

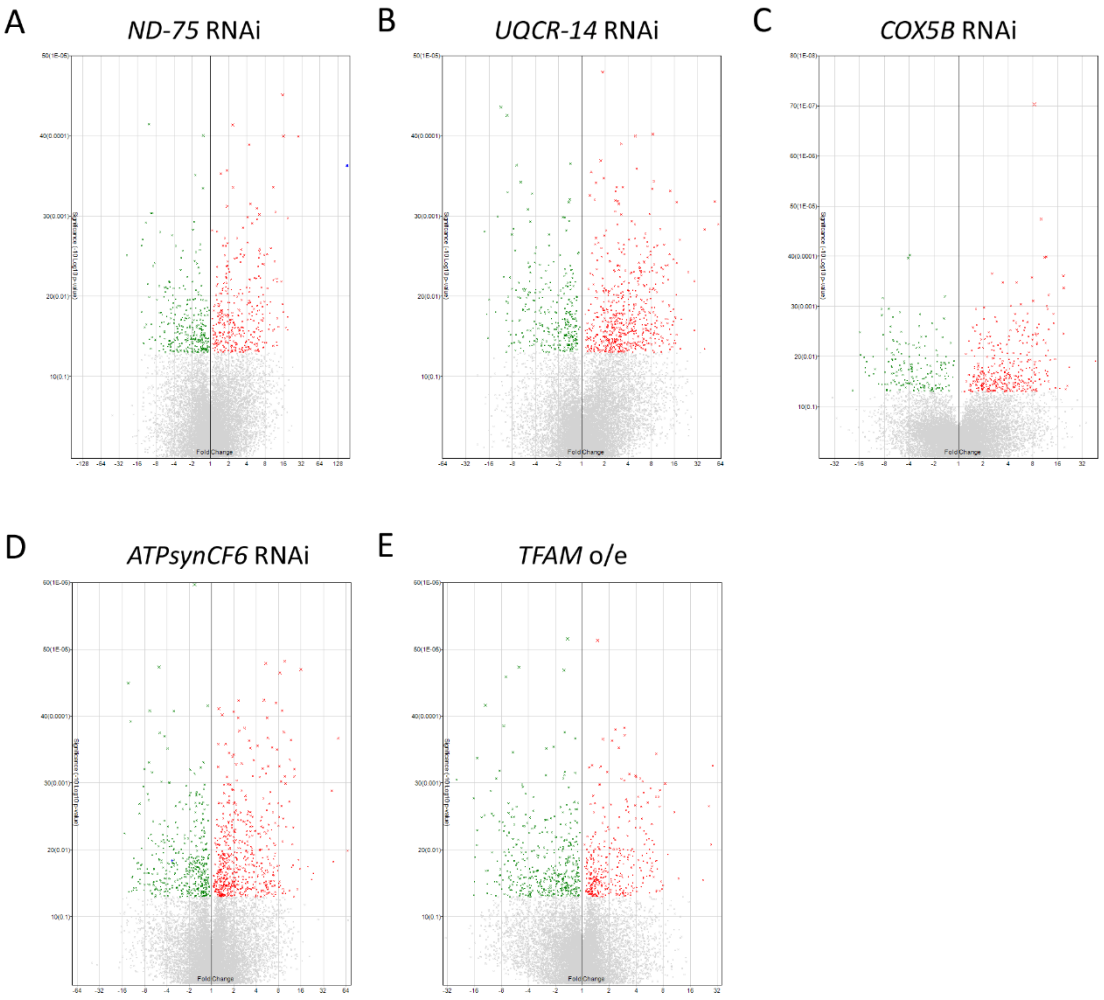

Figure 4.1 Volcano plots of gene expression changes in OXPHOS knockdown models and *TFAM* overexpression. Gene expression levels in *nSyb-Gal4* **(A)** *ND-75* (CI) RNAi, **(B)** *UQCR-14* (CIII) RNAi, **(C)** *COX5B* (CIV) RNAi, **(D)** *ATPsynCf6* (CV) RNAi, **(E)** *TFAM* overexpression, compared to control. Genes that are increased with $p < 0.05$ are highlighted in red. Genes that are decreased with $p < 0.05$ are highlighted in green. Controls are *nSyb-Gal4* crossed to *w1118.* The X axis represents fold change and the Y axis p-value (-10 $\log_{10}$ p-value).

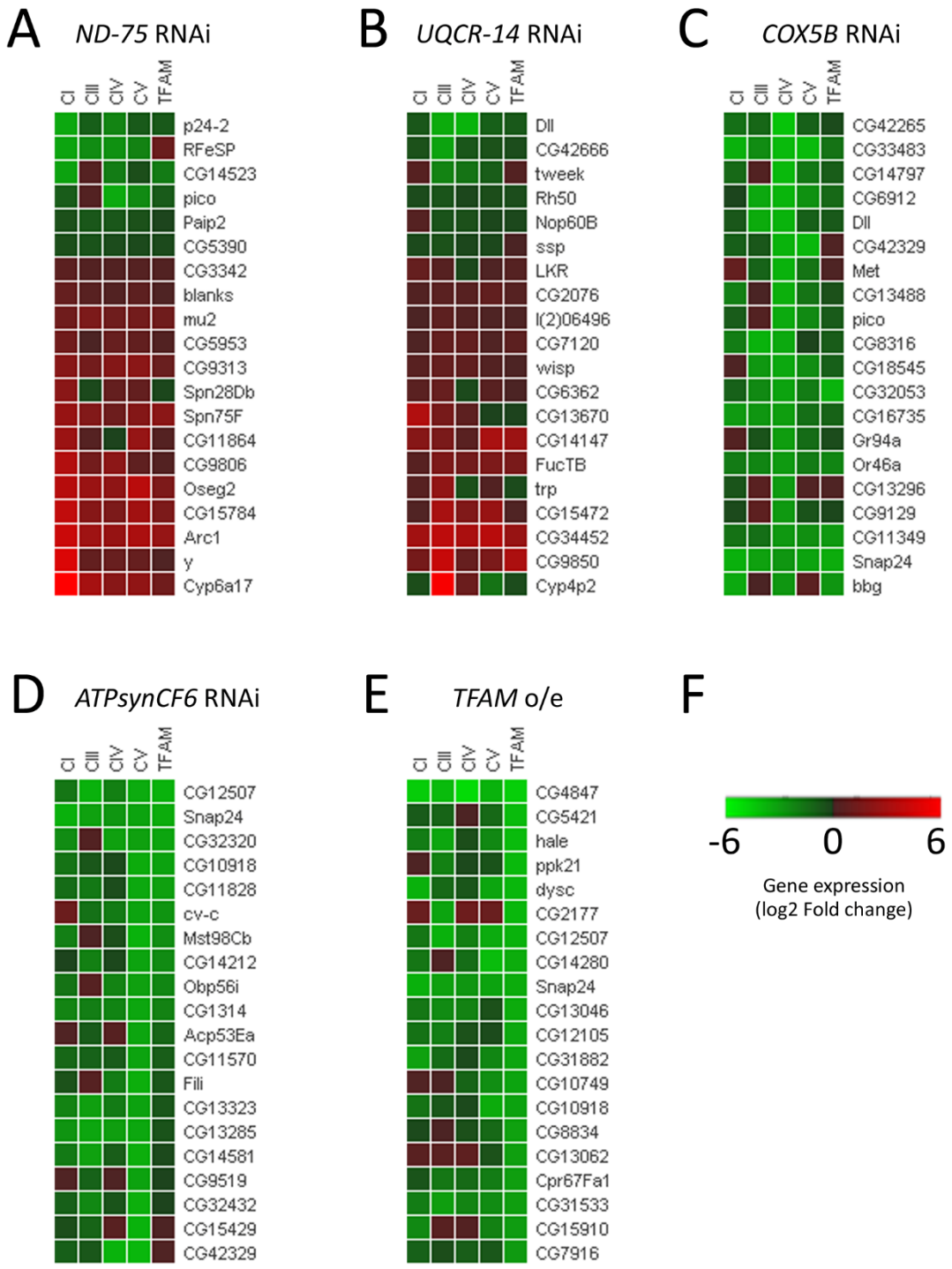

Figure 4.2 Heat maps showing genes with the most significant p-values in each condition of mitochondrial dysfunction. Twenty genes with the lowest p-value in *nSyb-Gal4* driven **(A)** *ND-75* RNAi (CI), **(B)** *UQCR-14* RNAi (CIII), **(C)** *COX5B* RNAi (CIV), **(D)** *ATPsynCf6* RNAi (CV), **(E)** *TFAM* overexpression from the microarray analysis. Fold change of each other condition is shown, whether significant or not. Controls are *nSyb-Gal4* crossed to *w1118*. **(F)** Scale bar showing colour representation of $\log_2$ fold change.

However, the conditions do display individual adaptations to mitochondrial dysfunction. Approximately 50% of the differentially regulated genes in each model were only changed in that model alone (Table 7). The percentage of uniquely altered genes remains at approximately 50% when fold change cut-offs of 1.5 or 2 were applied (see Appendix 9.1.1). This shows that there is a unique transcriptional response to different mitochondrial insults.

However, approximately 50% of the genes changed in each condition were also changed in at least one other model (Table 7, see Appendix 9.1.1 for fold change cut offs 1.5 and 2). When the commonly altered genes are compared pairwise, it is revealed that there is a positive correlation in each comparison (Figure 4.3). This suggests that there are also commonly regulated responses to mitochondrial dysfunction.

Table 7. The number of genes changed in the microarray, in each condition compared to control, $p < 0.05$. Different probes for a single gene that were significantly changed were recorded as one apart from when oppositely regulated, in which case these probes were recorded separately in this table. Controls are *nSyb-Gal4* crossed to *w1118*. Genes with oppositely regulated probes were (CI) *CG43102, mamo, mod(mdg4),* (CIII) *CG42594, CG42755, CG9650,* (CIV) *CG32369, Cyp18a1,* (CV), *Meltrin, tlk,* (*TFAM*) *muscleblind.*

		Increased		Decreased		Only changed in this condition		Number of genes in common			
	number of genes	number of genes	%	number of genes	%	number of genes	%	C III	C IV	C V	*TFAM*
CI	523	270	**52**	253	**48**	266	**51**	102	54	128	121
CIII	669	401	**60**	268	**40**	354	**53**		95	181	125
CIV	358	220	**62**	138	**39**	202	**56**			92	86
CV	840	477	**57**	363	**43**	413	**49**				262
TFAM	632	299	**47**	333	**53**	272	**43**				

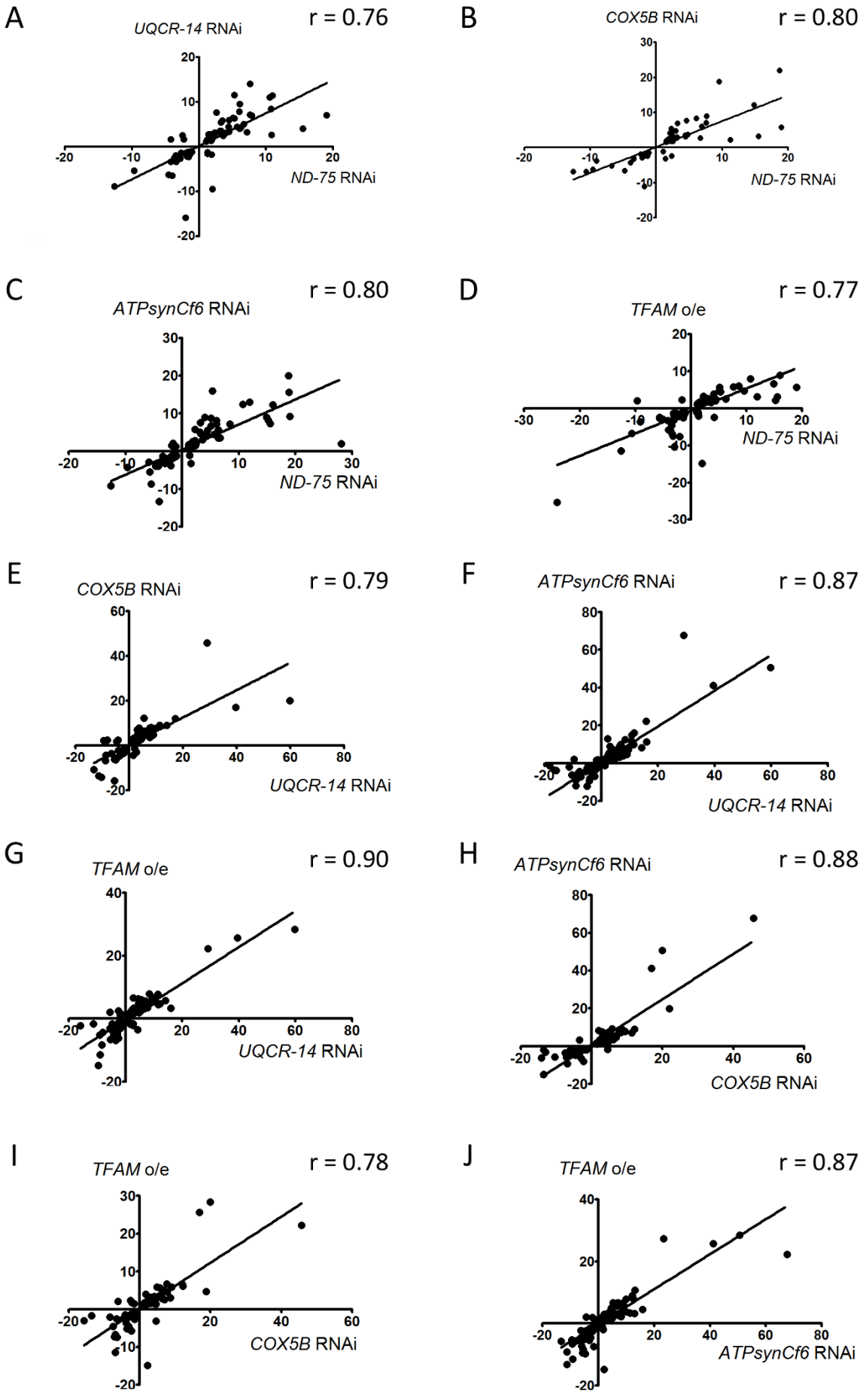
A
UQCR-14 RNAi
r = 0.76
ND-75 RNAi
B
COX5B RNAi
r = 0.80
ND-75 RNAi
C
ATPsynCf6 RNAi
r = 0.80
ND-75 RNAi
D
TFAM o/e
r = 0.77
ND-75 RNAi
E
COX5B RNAi
r = 0.79
UQCR-14 RNAi
F
ATPsynCf6 RNAi
r = 0.87
UQCR-14 RNAi
G
TFAM o/e
r = 0.90
UQCR-14 RNAi
H
ATPsynCf6 RNAi
r = 0.88
COX5B RNAi
I
TFAM o/e
r = 0.78
COX5B RNAi
J
TFAM o/e
r = 0.87
ATPsynCf6 RNAi

Figure 4.3 Correlations between genes significantly changed in the OXPHOS knockdown and *TFAM* overexpression models. (A-J) Graphs showing the correlation between genes that were commonly regulated in each condition pairwise. All correlations were significant with p-value < 0.001 (***). R value corresponds to Pearson r. **(A,B)** One outlier has been removed from these two graphs. Cyp6a17 is upregulated in *ND-75* RNAi, *COX5B* RNAi and *UQCR-14* RNAi. However, it has a fold change of 179 in *ND-75* RNAi, tenfold greater than any other transcript in *ND-75* RNAi. See Appendix 9.1.2 for graphs containing this outlier. Controls are *nSyb-Gal4* crossed to *w1118.* Axes indicate fold change.

Eleven genes are significantly altered in all 5 conditions of mitochondrial dysfunction compared to control (Table 8). Gene ontology (GO) analysis reveals roles for these genes in membrane transport, chromatin remodelling, glycolysis and behaviour regulation suggesting that these are commonly regulated processes in the response to mitochondrial dysfunction (Table 9).

Table 8. Genes significantly changed in all microarrays, compared to control. Cells highlighted in green correspond to significantly ($p < 0.05$) decreased gene expression. Red cells show significantly upregulated genes. Controls are *nSyb-Gal4* crossed to *w1118.*

		Fold change vs control				
Gene	**Symbol**	**CI**	**CIII**	**CIV**	**CV**	***TFAM***
Synapse protein 24	Snap24	-12.59	-8.87	-6.81	-9.2	-11.46
Rieske iron-sulphur protein	RFeSP	-9.63	-5.43	-6.16	-4.32	2.11
CG11324	homer	-1.88	-1.66	-1.84	-1.97	-1.77
CG16753	CG16753	-1.33	-1.67	-2.33	-1.35	-1.36
CG10960	CG10960	1.79	2.1	1.79	1.78	1.48
Zinc/iron regulated transporter-related protein 102B	Zip102B	2.03	-9.51	2.21	2.05	-14.83
mutator 2	mu2	2.34	3.13	2.32	2.54	2.34
CG5079	CG5079	3.19	3.49	3	7.6	2.5
Ecdysone-inducible gene L3	ImpL3	4.49	3.34	3.13	5.51	2.38
CG15784 gene	CG15784	15.54	4	3.19	7.34	3.16
Activity-regulated cytoskeleton associated protein 1	Arc1	19.02	7.02	5.78	9.2	5.68

Table 9. GO molecular function and biological processes for genes significantly changed in all microarrays. GO terms gene identified using Panther. Changes with $p < 0.05$ are considered significant.

Gene	Symbol	Molecular function	Biological Process
Synapse protein 24	Snap24	SNAP receptor activity(GO:0005484); syntaxin binding(GO:0019905)	vesicle-mediated transport(GO:0016192); neurotransmitter secretion(GO:0007269); Golgi to plasma membrane transport(GO:0006893); membrane fusion(GO:0061025)
Rieske iron-sulfur protein	RFeSP	ubiquinol-cytochrome-c reductase activity(GO:0008121); 2 iron, 2 sulfur cluster binding(GO:0051537)	mitochondrial electron transport, ubiquinol to cytochrome c(GO:0006122)
CG11324	homer	protein binding(GO:0005515)	adult behaviour(GO:0030534); regulation of locomotion(GO:0040012); response to ethanol(GO:0045471); behavioural response to ethanol(GO:0048149); positive regulation of circadian sleep/wake cycle, sleep(GO:0045938)
CG16753	CG16753	unknown	unknown
CG10960	CG10960	glucose transmembrane transporter activity(GO:0005355)	transmembrane transport(GO:0055085); positive regulation of JAK-STAT cascade(GO:0046427)
Zinc/iron regulated transporter-related protein 102B	Zip102B	metal ion transmembrane transporter activity(GO:0046873)	metal ion transport(GO:0030001); transmembrane transport(GO:0055085)
mutator 2	mu2	RNA polymerase II transcription coactivator activity(GO:0001105)	double-strand break repair(GO:0006302); regulation of chromatin silencing at centromere(GO:0090052); regulation of chromatin organization(GO:1902275)
CG5079	CG5079	unknown	unknown
Ecdysone-inducible gene L3	ImpL3	L-lactate dehydrogenase activity(GO:0004459)	glycolytic process(GO:0006096); carboxylic acid metabolic process(GO:0019752); carbohydrate metabolic process(GO:0005975); oxidation-reduction process(GO:0055114); myoblast fusion(GO:0007520); somatic muscle development(GO:0007525)
CG15784 gene product from transcript CG15784-RA	CG15784	unknown	unknown
Activity-regulated cytoskeleton associated protein 1	Arc1	nucleic acid binding(GO:0003676); zinc ion binding(GO:0008270)	muscle system process(GO:0003012); behavioural response to starvation(GO:0042595)

To further investigate the transcriptional changes induced by mitochondrial dysfunction, GO enrichment analysis was performed (see appendices 9.1.3, 9.1.4, 9.1.5, 9.1.6, 9.1.7 for the 15 most significant GO enrichment clustering per each genotype). All enrichment analysis was done on DAVID, using the *Drosophila* Genome v2 Array as the background gene list. Among the enriched clusters, there were a number of themes which were reoccurring in all genotypes, particularly secondary metabolic processes, including glycolysis and transport of sugar, as well as response to ROS such as glutathione transferase activity and oxidoreductase activity. Heat maps were made of genes in the glutathione transferase activity and oxidoreductase activity clusters (Figure 4.4A) and glycolysis cluster (Figure 4.4B). These show that although there were some difference between the genotypes, regulation of genes from these clusters were quite similar in all mitochondrial dysfunction models. Other common enriched clusters include amino acid transportation, immune response and response to stimuli.

To look more closely at the common changes between different mitochondrial insults, the genes that were changed in common between pairs of each genotype were analysed for GO enrichment, using DAVID when $p < 0.05$. Figure 4.5 shows bar graphs representing the enriched GO terms of the commonly regulated genes.

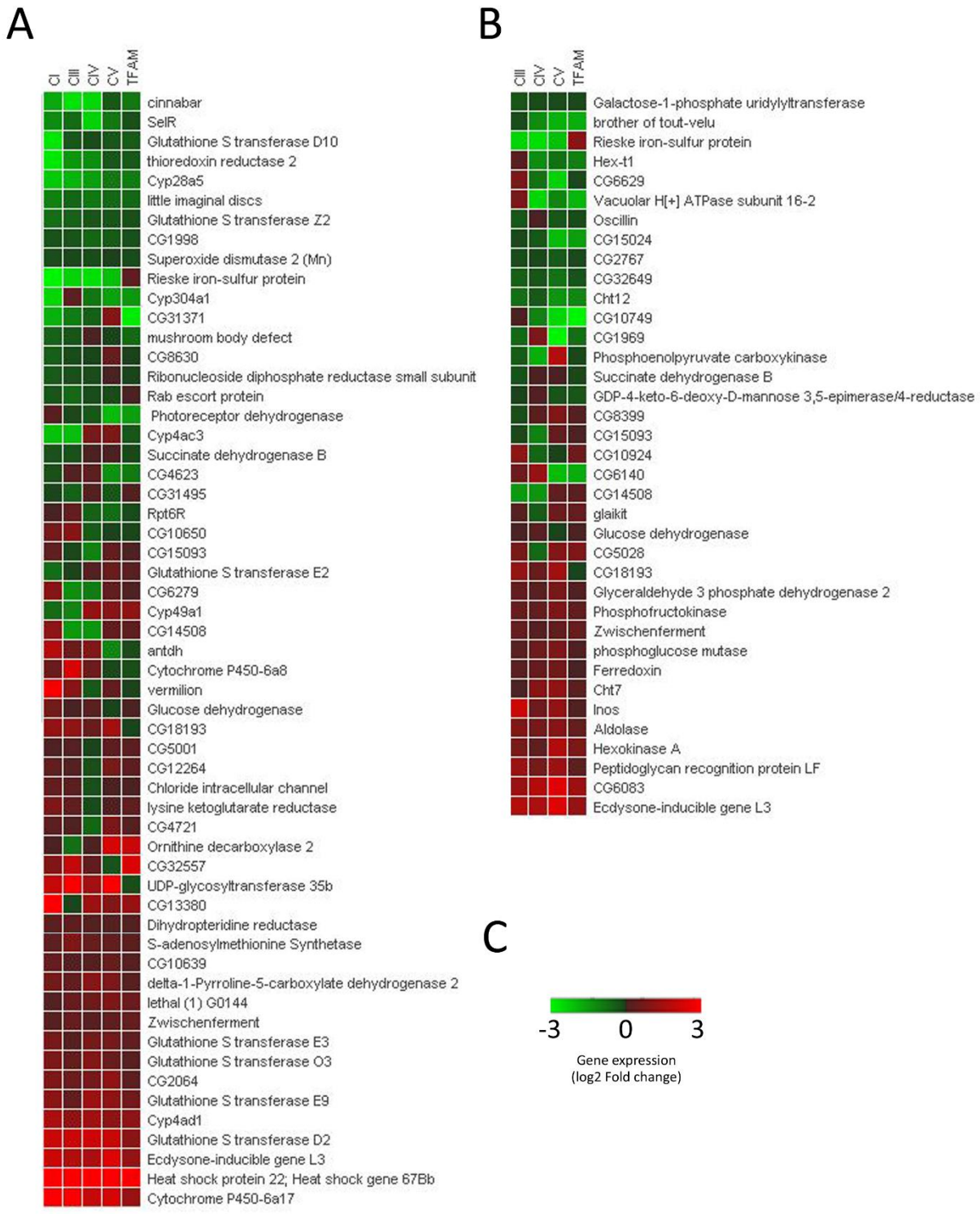

Figure 4.4 Heat maps of genes in glutathione transferase activity and oxidoreductase activity clusters and glycolysis cluster. Heat maps showing fold change in *nSyb-Gal4* driven *ND-75* RNAi (CI), *UQCR-14* RNAi (CIII), *COX5B* RNAi (CIV), *ATPsynCf6* RNAi (CV), *TFAM* overexpression in a subset of genes from **(A)** glutathione transferase activity and oxidoreductase activity functional annotation clusters, and **(B)** glycolysis functional annotation cluster. Controls are *nSyb-Gal4* crossed to *w1118*. **(C)** Scale bar shows the $\log_2$ fold change, green indicates downregulation and red indicates upregulation.

A

ND-75 RNAi & *UQCR-14* RNAi

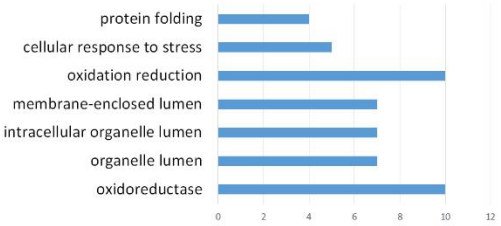

B

ND-75 RNAi & *COX5B* RNAi

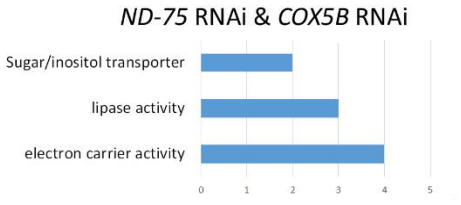

C

ND-75 RNAi & *ATPsynCf6* RNAi

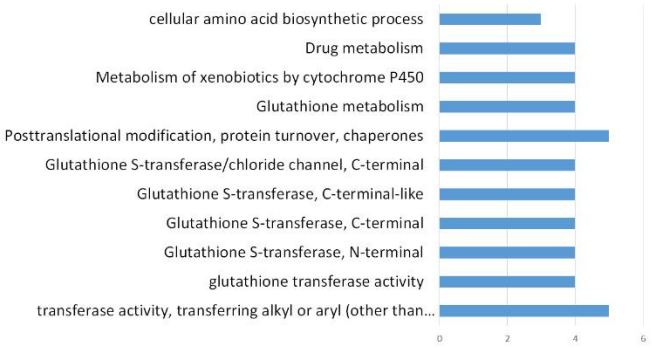

D

ND-75 RNAi & *TFAM* o/e

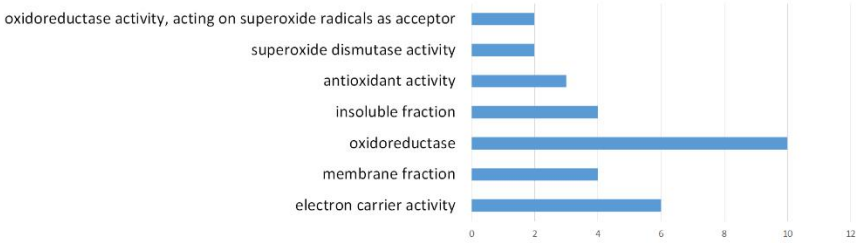

E

UQCR-14 RNAi & *COX5B* RNAi

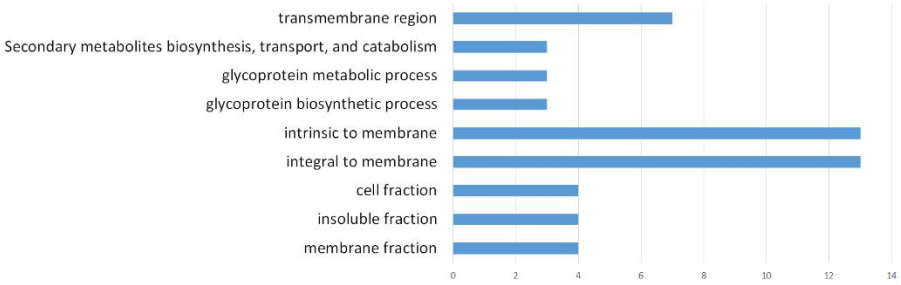

F

UQCR-14 RNAi & *ATPsynCf6* RNAi

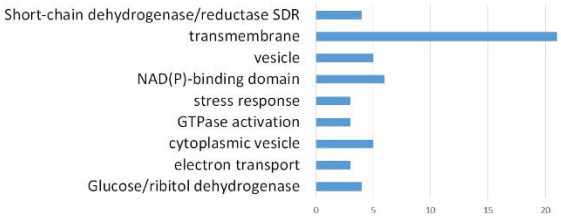

G

UQCR-14 RNAi & *TFAM* o/e

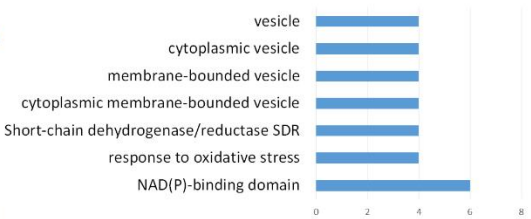

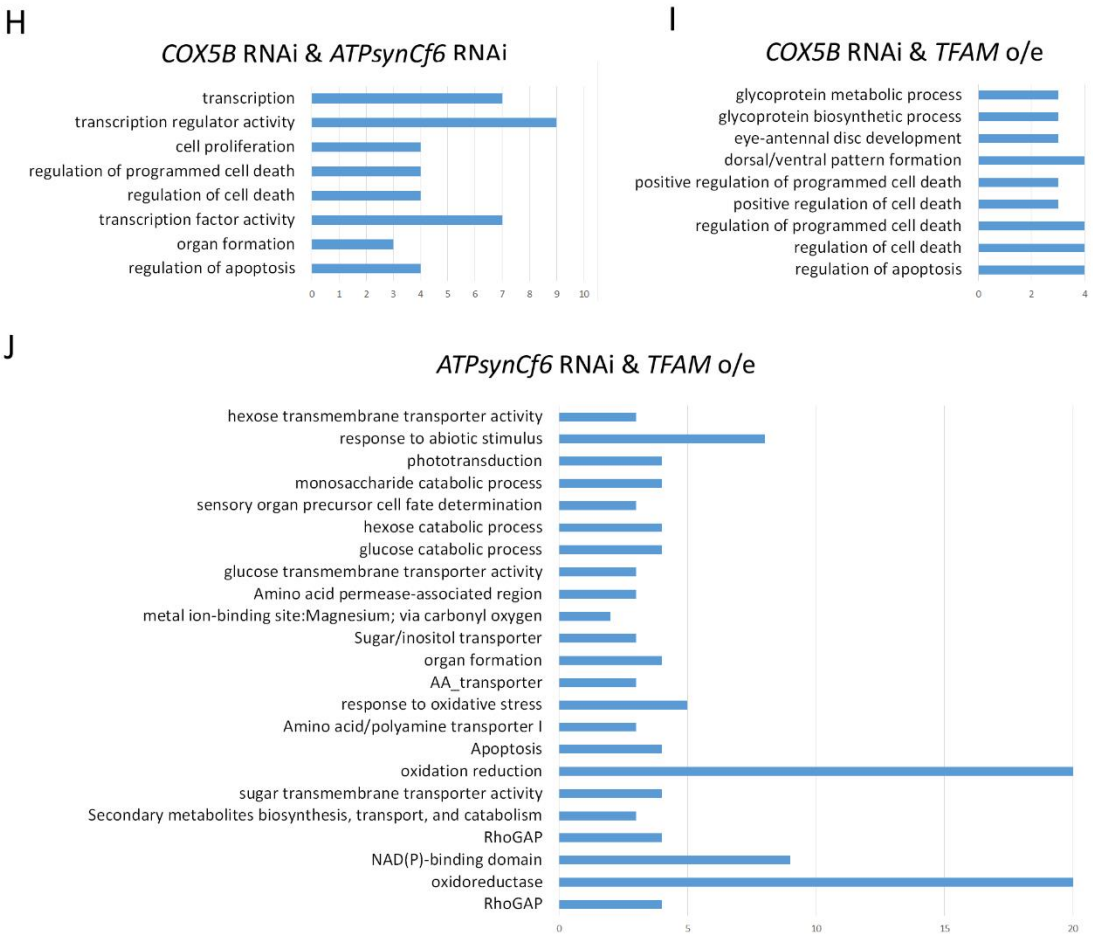

Figure 4.5 GO enrichment of common genes between each OXPHOS model and *TFAM* overexpression model, pairwise. Statistically significant ($p < 0.05$) enriched functional annotation terms for commonly regulated genes ($p<0.05$) between **(A)** *ND-75* RNAi and *UQCR-14* RNAi, **(B)** *ND-75* RNAi and *COX5B* RNAi, **(C)** *ND-75* RNAi and *ATPsynCf6* RNAi, **(D)** *ND-75* RNAi and *TFAM* o/e, **(E)** *UQCR-14* RNAi and *COX5B* RNAi, **(F)** *UQCR-14* RNAi and *ATPsynCf6* RNAi, **(G)** *UQCR-14* RNAi and *TFAM* o/e, **(H)** *COX5B* RNAi and *ATPsynCf6* RNAi, **(I)** *COX5B* RNAi and *TFAM* o/e, **(J)** *ATPsynCf6* RNAi and *TFAM* o/e. The x axis represents the number of genes associated with each term significantly changed in both conditions.

4.2.2 Validation of the microarrays *in vivo*: *Ilp3* and *Thor* expression in neurons with *ATPsynCf6* RNAi

In order to validate the microarrays, genes that were significantly altered in the microarray were assayed *in vivo* in CNS of third instar larvae of *ATPsynCf6* RNAi (CV) compared to control larvae. I focussed on two genes, *Drosophila* insulin-like peptide 3 *(Ilp3)* and *Thor*, the *Drosophila* homolog of human initiation factor 4E binding protein *4E-BP*. The microarray analysis revealed a significant decrease in *Ilp3* transcripts when *TFAM* was overexpressed and *ATPsynCf6* was knocked-down, compared to control (*TFAM* overexpression fold change = -1.88, $p = 0.029$, *ATPsynCf6* RNAi fold change =

-3.4, p = 0.014). Levels of *Ilp3* were also reduced in *COX5B* RNAi, (fold change = -1.58, p = 0.144), *UQCR-14* RNAi (fold change = -1.92, p = 0.084) and *ND-75* RNAi (fold change = -1.2, p = 0.57) although these decreases did not reach significance. Neuronal *Ilp3* expression levels have previously been shown to be decreased *in vivo* when *TFAM* is overexpressed (Cagin, Duncan et al. 2015). I measured *Ilp3* expression levels in the median secretory neurons in the CNS of third instar larvae with pan-neuronal *ATPsynCf6* RNAi (CV) and found reduced levels of *Ilp3* expression compared to control (Figure 4.6).

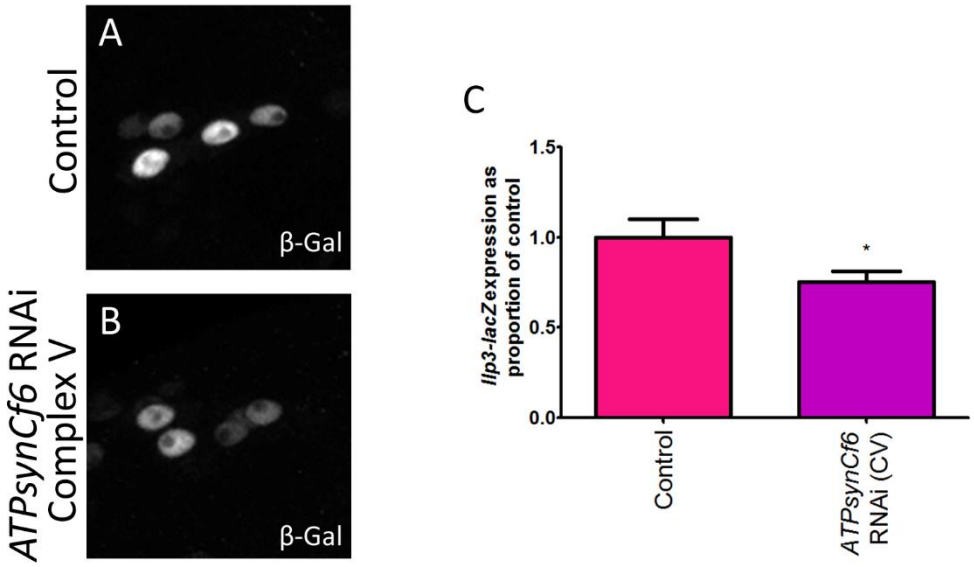

Figure 4.6 Neuronal *Ilp3* expression is reduced by complex V subunit knockdown *in vivo*. Expression of *Ilp3-lacZ* is visualised in the CNS neurosecretory cells by β-galactose immunostaining, in *nSyb-Gal4* driven **(A)** *w1118* (control) (n = 34) and **(B)** *ATPsynCf6* RNAi (n = 33). **(C)** Quantification of *Ilp3-lacZ* expression using student's t-test. Error bars represent SEM. ns, not significant, * p≤0.05.

Thor was significantly upregulated in three of the mitochondrial dysfunction conditions (*TFAM* overexpression fold change = 3.77, p = 0.011, *ATPsynCf6* RNAi fold change = 9.98, p = 0.001, *UQCR-14* RNAi fold change = 6.89, p = 0.012). A non-significant upregulation was also seen in complex IV and I knockdowns (*COX5B* RNAi fold change = 5.67, p = 0.239, *ND-75* RNAi fold change = 2.71, p = 0.074). Thor levels have previously been shown to increase in the CNS when *TFAM* is overexpressed (Cagin, Duncan et al. 2015). Similarly, using *lacZ* enhancer trap insertion in the last exon of Thor, I find increased Thor expression in the motor neuron cell bodies when *ATPsynCf6* is knocked down compared to controls (Figure 4.7). For this experiment the *OK371-*

Gal4 driver and *UAS-mCD8-GFP* were used to allow identification of the motor neuron cell bodies. mCD8 is a mouse lymphocyte marker, which when fused with GFP, labels the membrane of cells expressing *Gal-4*, as mCD8 is a transmembrane protein (Lee and Luo 1999).

These results suggest that the data obtained in the microarrays reflect bona fide expression changes occurring *in vivo*, in response to mitochondrial dysfunction.

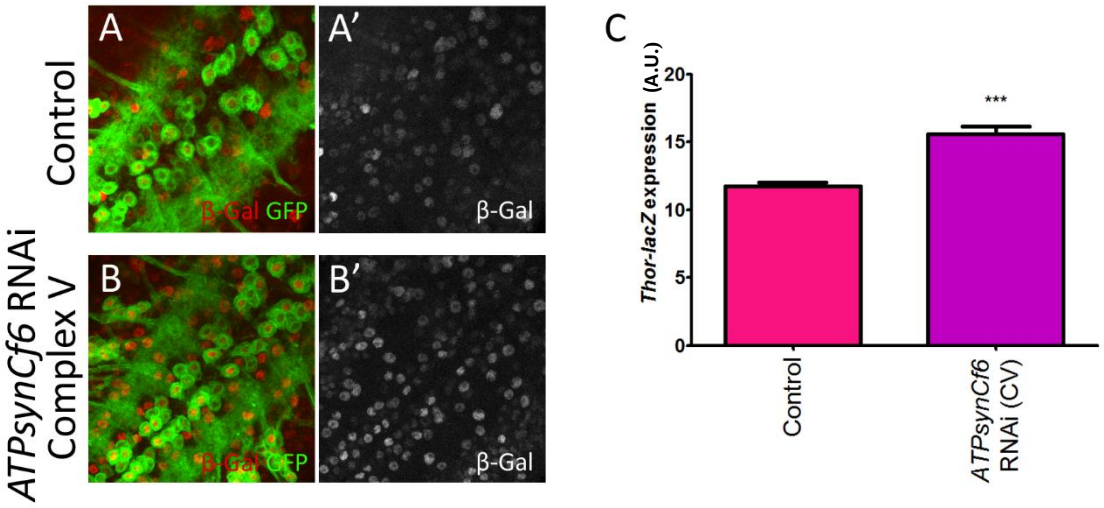

Figure 4.7 Neuronal Thor expression is increased by *ATPsynCf6* knockdown *in vivo*. *OK371-Gal4* driven expression of *Thor-lacZ, UAS-CD8-GFP* (green) and *UAS-Dicer2. Thor-lacZ* expression is visualised in the motor neuron cell bodies by β-galactose immunostaining (red) in *OK371-Gal4* driven **(A)** *w1118* (control) (n = 8) and **(B)** *ATPsynCf6* RNAi (n = 7). **(C)** Quantification of *Thor-lacZ* expression, measured in the nuclei of GFP positive cells, using student's t-test. Error bars represent SEM. *** $p \leq 0.001$.

4.2.3 Neuronal *TFAM* overexpression phenotypes are partially rescued by *sima* knockdown

The transcriptional changes that occur following mitochondrial dysfunction are likely to be co-ordinated by key transcription factors. Glycolytic processes were enriched in all of the mitochondrial dysfunction conditions and so transcription factors known to regulate glycolysis are likely to be involved in the retrograde response from dysfunctional mitochondria back to the nucleus. The basic helix-loop-helix PAS domain transcription factor, HIF-1α, is a cellular oxygen sensor, which plays a well characterised role in the cellular response to hypoxia, mediating a shift towards

glycolytic respiration and reduced protein synthesis (Lavista-Llanos, Centanin et al. 2002, Majmundar, Wong et al. 2010). Several of the genes identified in the microarrays, such as *Thor*, *Ilp3* and *Impl3*, are known to be regulated by hypoxia inducible factor (HIF-1α) (Firth, Ebert et al. 1995, Lavista-Llanos, Centanin et al. 2002, Cagin, Duncan et al. 2015). Moreover, knockdown of the *Drosophila* homolog of *HIF-1α, similar (sima),* has been shown to inhibit the increase of *Thor* expression, when *TFAM* is overexpressed in neurons (Cagin, Duncan et al. 2015).

In conditions of normoxia, HIF-1α is hydroxylated by prolyl hydroxylases (PHDs). Hydroxylated HIF-1α is recognised and ubiquitinated by Von Hippel-Lindau (VHL) and therefore targeted for degradation (Maxwell, Wiesener et al. 1999, Ziello, Jovin et al. 2007). These interactions are oxygen dependant, so in hypoxic conditions HIF-1α is stabilised. When stabilised, HIF-1α is able to bind to its constitutively acting dimerization partner, HIF-1β, and to bind to genomic hypoxia-responsive elements to activate transcription of target genes (Semenza 2010).

There is already evidence that *sima* regulates *Thor* expression levels in *Drosophila* overexpressing *TFAM* in the CNS (Cagin, Duncan et al. 2015). So to investigate whether *sima* (the *Drosophila* homolog of *HIF-1α*) plays a role in regulating transcriptional changes due to mitochondrial dysfunction, I knocked down *sima* in flies overexpressing *TFAM*. *Sima* RNAi was able to rescue the climbing deficit and wing inflation phenotype cause by neuronal *TFAM* overexpression (Figure 4.8A-B). An independent *sima* RNAi was also able to rescue these phenotypes (experiments performed by Dr Ariana Gatt) (Cagin, Duncan et al. 2015). Knockdown of *sima* by two independent RNAi lines was also able to partially rescue lifespan deficits caused by *D42-Gal4* driven *TFAM* overexpression (Figure 4.8C, Table 10, and Table 11), suggesting the benefits of *sima* knockdown are not purely transitory. It is important to note that the flies for these lifespan assays were not backcrossed, so the genetic background may have had an effect on their lifespan. However, the use of two independent RNAi increases the probability that the lifespan rescue observed was due to *sima* knockdown rather than background differences. qRT-PCR from larvae with ubiquitously expressed *sima* RNAi driven by daughterless (*Da-Gal4)* causes a 70% (*sima* HM00832 RNAi) and 65% (*sima* HM00833 RNAi) knockdown in levels of *sima* mRNA (Figure 4.8D). Taken together, these data suggest that *sima* knockdown is able

to reduce the impact of *TFAM* overexpression induced mitochondrial dysfunction on neuronal function.

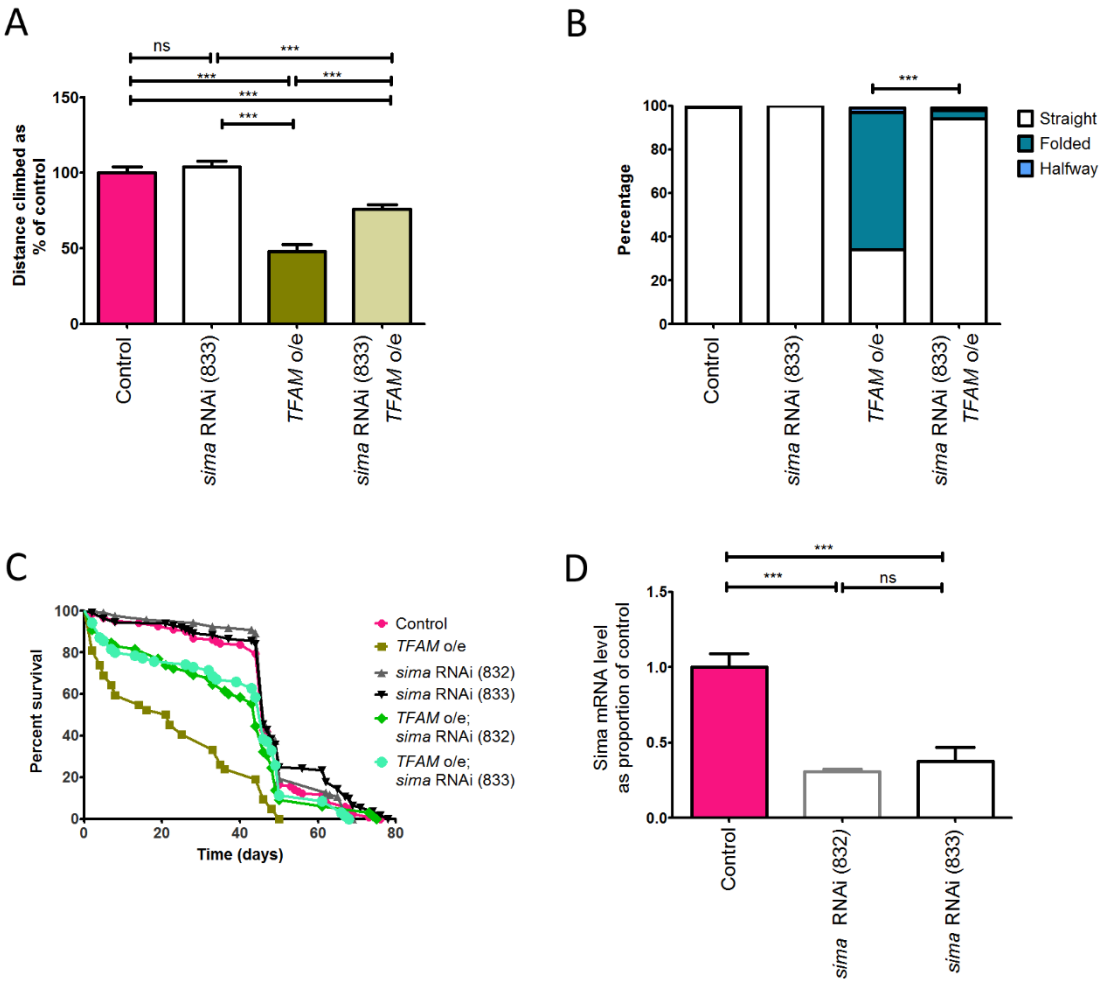

Figure 4.8 Knockdown of *sima* improves function of neurons overexpressing *TFAM*. (A) Climbing at 25°C of *D42-Gal4* driven control (*w1118*) (n = 17), *sima* knockdown (n = 16), *TFAM* overexpression (n = 12) and *sima* RNAi with *TFAM* overexpression (n = 16) analysed by one way ANOVA. **(B)** Wing inflation of *D42-Gal4* driven control (n = 187), *sima* knockdown (n = 97), *TFAM* overexpression (n = 47) and *sima* RNAi with *TFAM* overexpression (n = 95) analysed by chi-squared. **(C)** Lifespan assay of female flies overexpressing *TFAM* in motor neurons compared to two non-overlapping RNAi lines for *sima* with *D42-Gal4.* See Table 10 for statistical analysis and Table 11 for n numbers and median age. (D) RT-qPCR comparing levels of sima mRNA in *Da-Gal4* driven control (n = 8), *sima* RNAi HMS00883 (833) (n = 8), *sima* RNAi HMS00882 (832) (n = 7), analysed with a one way ANOVA. Error bars represent SEM. ns, not significant, *** $p \leq 0.001$.

Table 10. Statistical analysis of lifespan assays in female flies. Log-Rank (Mantel Cox) test was used and the threshold p-value for significance was adjusted to account for 9 comparisons, to $p < 0.0056$. Control is *D42-Gal4* crossed to *w1118*.

			p-value	significance
Control	vs	*TFAM* o/e	<0.0001	*
Control	vs	*sima 832*	0.4122	ns
Control	vs	*sima 833*	0.0711	ns
Control	vs	*TFAM* o/e; *sima 832*	0.0053	*
Control	vs	*TFAM* o/e; *sima 833*	0.0238	ns
TFAM o/e	vs	*TFAM* o/e; *sima 832*	0.0002	*
TFAM o/e	vs	*TFAM* o/e; *sima 833*	<0.0001	*
sima 832	vs	*TFAM* o/e; *sima 832*	0.0007	*
sima 833	vs	*TFAM* o/e; *sima 833*	0.0004	*

Table 11. Number of flies and median age of female flies in lifespan assay.

Genotype	Number of flies	Median age
Control	122	46
sima 832	120	46
sima 833	112	46
TFAM o/e	42	21.5
TFAM o/e; *sima 832*	65	44
TFAM o/e; *sima 833*	70	46

4.2.4 *Sima* knockdown partially rescues neuronal phenotypes in complex III, IV and V knockdown models.

Genes regulated by Sima, such as, *Impl3*, *Ilp3* and *Thor*, were also observed to change in the microarray analysis of OXPHOS models of mitochondrial dysfunction (see Table 8, and data not shown). So I next asked whether *sima* knockdown could also rescue mitochondrial dysfunction caused by complex I, III, IV and V subunit knockdown.

With the motor neuron driver *D42-Gal4* I have previously shown (see Results chapter 3, Figure 3.1) that *ND-75* RNAi (CI) is lethal and *D42-Gal4* driven *ATPsynCf6* (CV) and *COX5B* (CIV) RNAi cause a greater than 50% decrease in climbing ability at 25°C. *Sima* knockdown significantly improves the climbing of *COX5B* (CIV) RNAi flies, but has no effect on *ATPsynCf6* (CV) (Figure 4.9A-B). *ATPsynCf6* RNAi also results in a wing inflation defect, when driven by *D42-Gal4* (see Results chapter 3, Figure 3.1). This defect is rescued by *D42-Gal4* driven *sima* knockdown (Figure 4.9D). *D42-Gal4* driven *UQCR-14* (CIII) RNAi had no climbing deficit at 25°C, however, when grown at

29°C, these flies climb to approximately 75% of the distance climbed by controls (see Results chapter 3, Figure 3.1). This climbing defect was not altered by *sima* RNAi (Figure 4.9C).

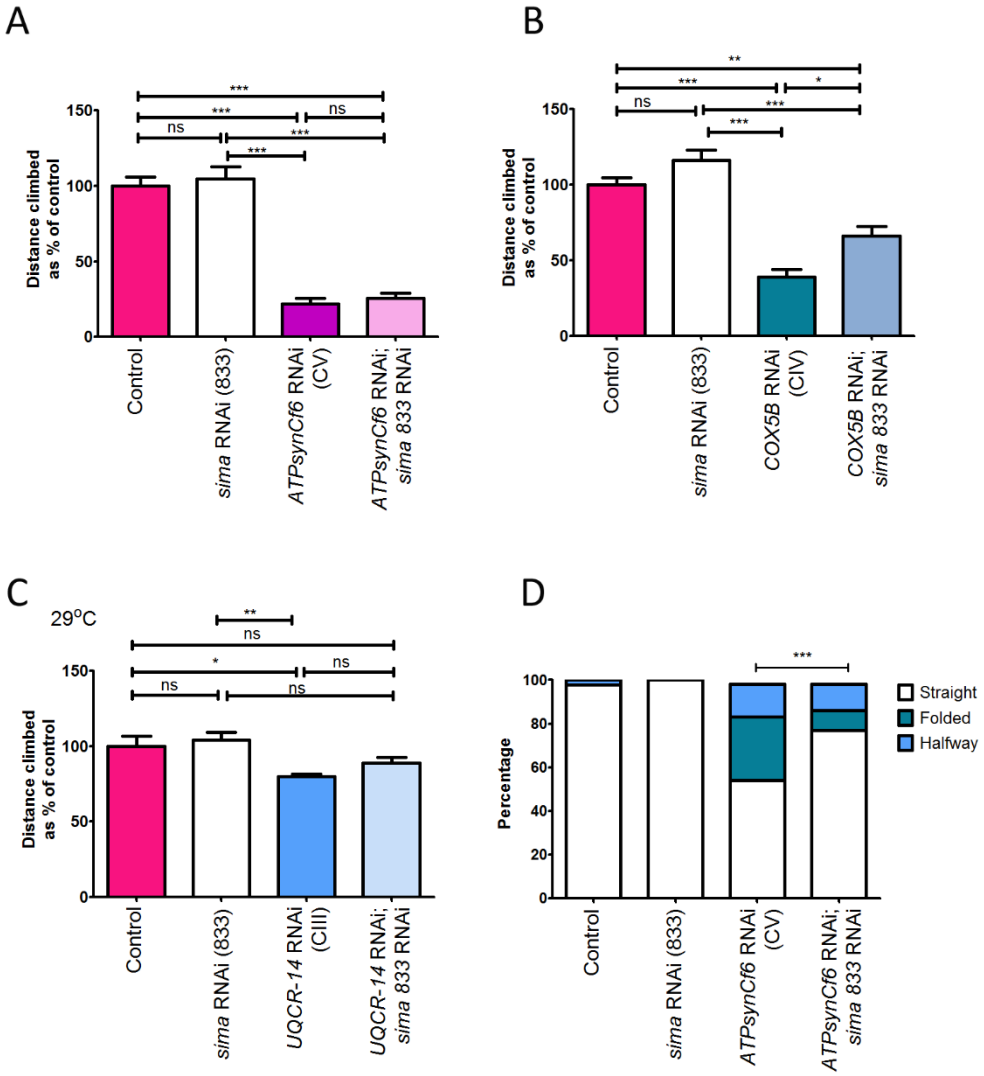

Figure 4.9. *D42-Gal4* driven *sima* knockdown rescues the climbing phenotype of complex IV knockdown and wing inflation phenotype of complex V knockdown. **(A)** Climbing assay of *D42-Gal4* driven *w1118* (control) (n= 10), *sima* RNAi (n = 10), *ATPsynCf6* RNAi (n = 11) and *ATPsynCf6* RNAi; *sima* RNAi (n = 11) at 25°C. **(B)** Climbing assay of control (n= 10), *sima* RNAi (n = 10), *COX5B* RNAi (n = 10) and *COX5B* RNAi; *sima* RNAi (n = 10) driven with *D42-Gal4* at 25°C. **(C)** Climbing assay at 29°C of *D42-Gal4* driven *w1118* (control) (n= 11), *sima* RNAi (n = 11), *UQCR-14* RNAi (n = 11) and *UQCR-14* RNAi; *sima* RNAi (n = 11). Data were analysed with a one way ANOVA. **(D)** Wing inflation assay of *D42-Gal4* driven *w1118* (control) (n = 224), *sima* RNAi (n = 130), *ATPsynCf6* RNAi (n = 58) and *ATPsynCf6* RNAi; *sima* RNAi (n = 143) at 25°C. Error bars represent SEM. ns, not significant, * $p \leq 0.05$, ** $p \leq 0.01$, *** $p \leq 0.001$.

The motor neuron driver *OK371-Gal4,* in combination with *UAS-Dicer2,* gave a severe climbing phenotype with *ATPsynCf6* (CV), *COX5B* (CIV) and *UQCR-14* (CIII) RNAi (see Results chapter 3, Figure 3.1). When tested concurrently with *sima* knockdown, there was no significant change in the distance climbed in any of these three genotypes (Figure 4.10A,C,E). However, *ATPsynCf6* (CV) and *COX5B* (CIV) RNAi flies were visually healthier with *sima* RNAi. Although *ATPsynCf6* (CV) and *COX5B* (CIV) RNAi flies with *sima* knockdown were unable to climb very far up the tube, they were more able to get their whole bodies onto the vertical sides of the tube, than the flies expressing *ATPsynCf6* (CV) and *COX5B* (CIV) RNAi alone. This difference in is not picked up by the climbing assay quantification as it only compares distance climbed by the flies. Therefore, I quantified the climbing ability of these flies more sensitively. Flies were categorised depending on their ability to climb up the tube, get their whole bodies on the tube without climbing further, placing their front legs on the tube, or being unable to get their legs on at all, in a three minute time period. When quantifying the data in this manner, a subtle yet significant improvement of climbing ability was revealed when *sima* was knocked down in *ATPsynCf6* (CV) and *COX5B* (CIV) RNAi flies (Figure 4.10B,D). *UQCR-14* RNAi flies were almost all able to climb up the vertical edge of the tube, apart from one fly (Figure 4.10F).

ND-75 RNAi is lethal with *D42-Gal4,* however it is possible to get adult flies with the *OK371-Gal4* driver with a severe climbing phenotype (see Results chapter 3, Figure 3.1). *ND-75* RNAi is inserted in the same genomic locus as both *sima* HMS00832 and HMS00833 RNAi, so I was unable to generate a stock with these RNAis together. A stock containing the $sima^{KG07607}$ mutant and *OK371-Gal4* was therefore used to determine if reduced Sima levels rescues *ND-75* RNAi induced climbing dysfunction. This stock was not lethal at 25°C, probably because it did not contain *UAS-Dicer2* and so flies were grown at this temperature. $Sima^{KG07607}$ is a loss of function mutant due to a P-element insertion in the second intron of *sima* (Lavista-Llanos, Centanin et al. 2002, Centanin, Ratcliffe et al. 2005). $sima^{KG07607}$ was unable to change the climbing deficit of *OK371-Gal4* driven *ND-75* RNAi (Figure 4.10G). The low number of flies in this assay is due to the fact that many flies that eclosed died overnight (of both *ND-75* RNAi and *ND-75* RNAi, $sima^{KG07607}$ genotypes). Repeats of this experiment are in progress to increase the n number. Categorisation of climbing ability of these flies was also not compared due to the low n number.

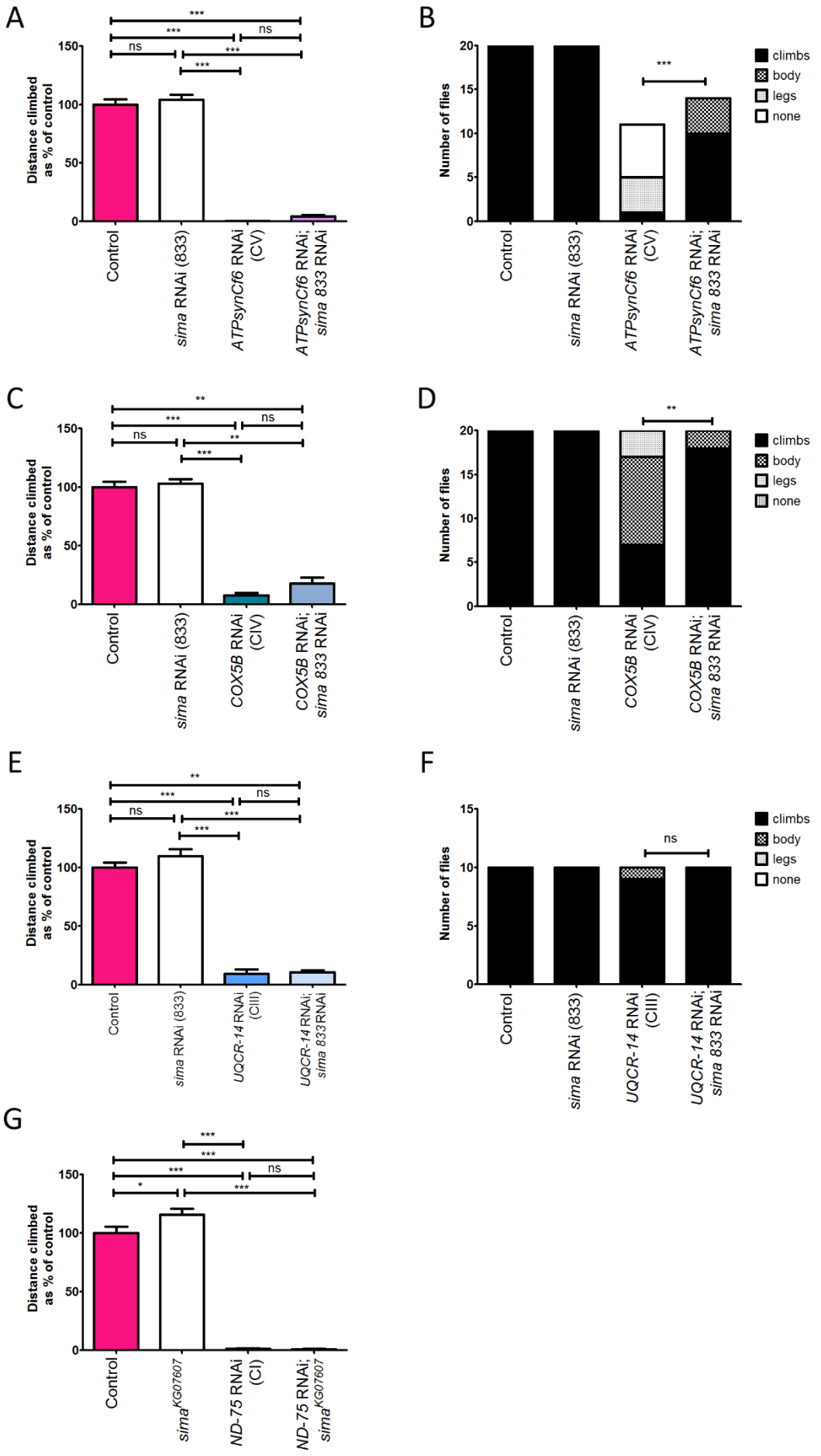
A
B
C
D
E
F
G
Distance climbed as % of control
Number of flies
climbs
body
legs
none
Control
sima RNAi (833)
ATPsynCf6 RNAi (CV)
ATPsynCf6 RNAi; sima 833 RNAi
COX5B RNAi (CIV)
COX5B RNAi; sima 833 RNAi
UQCR-14 RNAi (CIII)
UQCR-14 RNAi; sima 833 RNAi
simaKG07607
ND-75 RNAi (CI)
ND-75 RNAi; simaKG07607
ns

Figure 4.10 *OK371-Gal4* driven *sima* knockdown partially rescues the climbing phenotype of complex IV and complex V knockdown. Climbing assays at 25°C with *OK371-Gal4* and *UAS-Dicer2* **(A)** Climbing assay of control (n= 10), *sima* RNAi (n = 10), *ATPsynCf6* RNAi (n = 8) and *ATPsynCf6* RNAi; *sima* RNAi (n = 10). **(B)** Climbing assay quantification when flies are binned into four groups depending on whether they could climb up the tube (climb), get their whole body on the vertical edge of the tube (body), get their front legs on the tube (legs) or could not get any of their legs onto the tube (none) for control (n= 20), *sima* RNAi (n = 20), *ATPsynCf6* RNAi (n = 11) and *ATPsynCf6* RNAi; *sima* RNAi (n = 14) driven by *OK371-Gal4* with *UAS-Dicer*. **(C)** Climbing assay of control (n= 10), *sima* RNAi (n = 10), *COX5B* RNAi (n = 10) and *COX5B* RNAi; *sima* RNAi (n = 10). **(D)** Climbing assay quantification when flies are binned into the four groups for control (n= 20), *sima* RNAi (n = 20), *COX5B* RNAi (n = 20) and *COX5B* RNAi; *sima* RNAi (n = 20) driven by *OK371-Gal4* with *UAS-Dicer2*. **(E)** Climbing assay of control (n= 10), *sima* RNAi (n = 10), *UQCR-14* RNAi (n = 10) and *UQCR-14* RNAi; *sima* RNAi (n = 10). **(F)** Climbing assay quantification when flies are binned into the four groups for control (n= 10), *sima* RNAi (n = 10), *UQCR-14* RNAi (n = 10) and *UQCR-14* RNAi; *sima* RNAi (n = 10) driven by *OK371-Gal4* with *UAS-Dicer2*. **(G)** *OK371-Gal4* driven climbing assays at 25°C of control (n= 5), heterozygous $sima^{KG07607}$ (n = 5), *ND-75* RNAi (n = 5) and *ND-75* RNAi with heterozygous $sima^{KG07607}$ (n = 5). Continuous data were analysed with one way ANOVA, Categorical data were analysed with chi-squared. Error bars represent SEM. ns, not significant, ** $p \leq 0.01$, *** $p \leq 0.001$.

4.2.5 Pan- neuronal *sima* knockdown rescues lethality of *nSyb-Gal4* driven complex III, IV and V knockdown and *TFAM* overexpression

Climbing assays and wing inflation assays reveal some ability of *sima* knockdown to rescue neuronal function in *ATPsynCf6* (CV) and *COX5B* (CIV) RNAi flies. To investigate further, I tested whether *sima* knockdown was able to rescue the lethality of *nSyb-Gal4* driven OXPHOS knockdown models and *TFAM* overexpression. Heterozygous $sima^{KG07607}$ rescued the lethality of *ATPsynCf6* (CV), *COX5B* (CIV) and *UQCR-14* RNAi (CIII) at 25°C and 29°C. Heterozygous $sima^{KG07607}$ rescued the lethality of *TFAM* overexpression at 25°C (experiment performed by Rachel Hunt). However, $sima^{KG07607}$ was not able to rescue *nSyb-Gal4* driven *ND-75* RNAi lethality at 25°C or 29°C. *Sima* RNAi (833) was unable to rescue the lethality of any of the models of mitochondrial dysfunction at 25°C (Table 12).

Table 12. Viability of pan-neuronally driven OXPHOS knockdown models when *sima* is knocked down with heterozygous *sima*^{KG07607}. Viability of *TFAM* overexpression with heterozygous *sima*^{KG07607} was assessed Rachel Hunt.

	25°C			29°C	
sima^{KG07607}/+	-	+	-	-	+
nSyb-Gal4 > *sima* RNAi (833)	-	-	+	-	-
nSyb-Gal4 > *ND-75* RNAi (CI)	pupal lethal	pupal lethal	N/A	pupal lethal	pupal lethal
nSyb-Gal4 > *UQCR-14* RNAi (CIII)	pupal lethal	**viable**	pupal lethal	pupal lethal	**viable**
nSyb-Gal4 > *COX5B* RNAi (CIV)	pupal lethal	**viable**	pupal lethal	pupal lethal	**viable**
nSyb-Gal4 > *ATPsynCf6* RNAi (CV)	pupal lethal	**viable**	pupal lethal	pupal lethal	**viable**
nSyb-Gal4 > *TFAM* overexpression	pupal lethal	**viable**	pupal lethal	not done	not done

4.2.6 Identifying HIF-1α responsive genes that are regulated differently in *ND-75* RNAi CNS

The experiments above show that mitochondrial dysfunction phenotypes caused by the OXHPOS knockdown models and *TFAM* overexpression can by modified by manipulation of *sima* levels, apart from mitochondrial dysfunction caused by *ND-75* RNAi (CI). To probe further into the difference between *ND-75* RNAi (CI) and the other models, I looked at genes known to be regulated by *sima* in *Drosophila* and identified any genes that were differentially regulated in *ND-75* RNAi (CI) compared to the other conditions (Table 13).

The HIF dependant and independent response to hypoxia has been studied in *Drosophila* third instar larvae (Li, Padmanabha et al. 2013). HIF responsive genes were identified in two ways. Firstly, microarrays from control larvae and *sima* mutant larvae, under hypoxic conditions were compared. This gave a list of gene changes that were HIF independent (common to both conditions) and HIF dependent (only occurred in control larvae) (Li, Padmanabha et al. 2013). A second list of HIF responsive genes was produced by comparisons between *sima* mutant larvae in normoxia and hypoxia (giving genes that must be independent of HIF) and removing these genes from the list of genes that change in control larvae in hypoxia compared to normoxia (Li, Padmanabha et al. 2013). I compiled genes from both of these data sets to create a list of genes known to

be responsive to HIF in *Drosophila.* It is important to note that these genes were identified whole larval extracts, as opposed to just CNS tissue and that these are genes that are modified by HIF in hypoxic conditions. Therefore, this may not be an exhaustive list of HIF responsive genes and these genes may also be regulated by other transcription factors in different conditions. This list may also over-represent genes that are abundantly expressed in larval tissues such as the fat body, and miss genes expressed predominantly in neurons.

I compared the genes known to be responsive to HIF with genes that were significantly changed in the OXPHOS knockdown and *TFAM* overexpression models (see Appendix 9.1.8 for full dataset, $p < 0.05$). HIF responsive genes which were differentially regulated in *ND-75* RNAi were then identified, these included genes that were only significantly altered in *ND-75* RNAi or genes that were significantly changed in a conserved manner in least three of the other models and either not changed in *ND-75* RNAi or oppositely regulated (Table 13). GO analysis was then performed on this set of genes to determine which HIF dependant process are being differentially regulated. Oxidoreductase activity and metal ion binding were the main clusters identified in this analysis (Figure 4.11). The role of these processes in the different mitochondrial dysfunction models may therefore be key to understanding why *ND-75* RNAi is resistant to changes in *sima* levels.

Table 13. HIF-1α responsive genes that respond differently in *ND-75* RNAi compared to other OXPHOS knockdown and *TFAM* overexpression microarrays. Downregulation is highlighted in green, upregulation is highlighted in red. Grey cells indicate no significant change in expression level. Biological Function annotation is from Panther.

		Fold change (p < 0.05)				
Gene Symbol	**Gene's Biological Function**	**CI**	**CIII**	**CIV**	**CV**	**o/e**
CG10178		-13.51				
p24-2	proteolysis(GO:0006508)	-10.43				
Cyp28a5	regulation of multicellular organism growth(GO:0040014); regulation of insulin receptor signalling pathway(GO:0046626); ribosomal large subunit biogenesis(GO:0042273); ribosome biogenesis(GO:0042254);	-4.92				

		Fold change (p < 0.05)				
Gene Symbol	**Gene's Biological Function**	**CI**	**CIII**	**CIV**	**CV**	**o/e**
	mitotic spindle assembly(GO:0090307); cellular response to starvation(GO:0009267); positive regulation of multicellular organism growth(GO:0040018)					
CG42335	oxidation-reduction process(GO:0055114)	-4.66				
CG33468		-3.97				
SCAP	oxidation-reduction process(GO:0055114); lipid metabolic process(GO:0006629)	-3.48				
lectin-28C	phagocytosis(GO:0006909); dephosphorylation(GO:0016311)	-2.67				
CG11652	gastrulation involving germ band extension(GO:0010004)	-2.24				
CG9449	tricarboxylic acid cycle(GO:0006099); mitochondrial electron transport, succinate to ubiquinone(GO:0006121)	-1.38				
CG8630		-1.38				
RnrS	defense response(GO:0006952); antibacterial humoral response(GO:0019731); peptidoglycan catabolic process(GO:0009253); negative regulation of JNK cascade(GO:0046329); peptidoglycan recognition protein signalling pathway(GO:0061057); response to bacterium(GO:0009617); determination of adult lifespan(GO:0008340); defense response to other organism(GO:0098542)	-1.31				
CG1542	one-carbon metabolic process(GO:0006730)	-1.3				
SdhB	positive regulation of transcription from RNA polymerase II promoter(GO:0045944); regulation of transcription, DNA-templated(GO:0006355); salivary gland cell autophagic cell death(GO:0035071); oogenesis(GO:0048477);	-1.19				

		Fold change (p < 0.05)				
Gene Symbol	**Gene's Biological Function**	**CI**	**CIII**	**CIV**	**CV**	**o/e**
	autophagy(GO:0006914);cell death(GO:0008219); regulation of development, heterochronic(GO:0040034)					
CG3940	oxidation-reduction process(GO:0055114); lauric acid metabolic process(GO:0048252); insecticide metabolic process(GO:0017143); response to caffeine(GO:0031000)	-1.19				
CG10623	protein autoubiquitination(GO:0051865); protein ubiquitination involved in ubiquitin-dependent protein catabolic process(GO:0042787)	1.3				
CG11158	antibacterial humoral response(GO:0019731); immune response(GO:0006955); defense response(GO:0006952); regulation of cell growth(GO:0001558); negative regulation of cell size(GO:0045792); negative regulation of translational initiation(GO:0045947); triglyceride metabolic process(GO:0006641); response to starvation(GO:0042594); response to oxidative stress(GO:0006979); determination of adult lifespan(GO:0008340); regulation of mitochondrial translation(GO:0070129); response to bacterium(GO:0009617); myoblast fusion(GO:0007520); somatic muscle development(GO:0007525); regulation of terminal button organization(GO:2000331)	1.38				
Cyp6a8	neurogenesis(GO:0022008); negative regulation of programmed cell death(GO:0043069); oogenesis(GO:0048477)	1.45				
Gld	metabolic process(GO:0008152)	1.61				
Eip74EF		1.67				

		Fold change (p < 0.05)				
Gene Symbol	**Gene's Biological Function**	**CI**	**CIII**	**CIV**	**CV**	**o/e**
MESK2	ribosome biogenesis(GO:0042254); rRNA processing(GO:0006364); pseudouridine synthesis(GO:0001522); germ cell development(GO:0007281); wing disc development(GO:0035220); neurogenesis(GO:0022008); cellular response to starvation(GO:0009267)	1.93				
CG32850	DNA replication(GO:0006260); oxidation-reduction process(GO:0055114); deoxyribonucleoside diphosphate metabolic process(GO:0009186); activation of cysteine-type endopeptidase activity involved in apoptotic process(GO:0006919); neurogenesis(GO:0022008)	1.94				
Aatf	response to X-ray(GO:0010165); defense response to Gram-negative bacterium(GO:0050829); regulation of reactive oxygen species metabolic process(GO:2000377)	2.06				
CG43078	phagocytosis(GO:0006909); peptidyl-diphthamide biosynthetic process from peptidyl-histidine(GO:0017183)	2.38				
Mocs1	rRNA processing(GO:0006364)	2.57				
CG31274	metabolic process(GO:0008152)	2.73				
CG10182	regulation of GTPase activity(GO:0043087); signal transduction(GO:0007165); positive regulation of GTPase activity(GO:0043547); imaginal disc-derived leg morphogenesis(GO:0007480)	2.9				
PGRP-LF	transport(GO:0006810); Golgi vesicle transport(GO:0048193); reproduction(GO:0000003); regulation of post-mating oviposition(GO:0048042)	3.18				
UGP	RNA catabolic process(GO:0006401); multicellular organism reproduction(GO:0032504)	4.4				

		Fold change (p < 0.05)				
Gene Symbol	**Gene's Biological Function**	**CI**	**CIII**	**CIV**	**CV**	**o/e**
Nop60B	positive regulation of Ras protein signal transduction(GO:0046579)	1.3	-1.44		-1.11	-1.13
CG10559	oxidation-reduction process(GO:0055114)		-3.99	-2.29	-8.2	-5.76
RpL28	biological_process(GO:0008150)		-3.04		-2.57	-2.46
Wwox	nucleobase-containing compound metabolic process(GO:0006139); methylation(GO:0032259)		-1.46		-1.47	-1.27
CG14906	glucose metabolic process(GO:0006006); pupal chitin-based cuticle development(GO:0008364); cuticle development(GO:0042335); sperm storage(GO:0046693); oxidation-reduction process(GO:0055114); sensory perception of pain(GO:0019233)		1.43		1.41	1.49
CG2065	Mo-molybdopterin cofactor biosynthetic process(GO:0006777)		1.56		2.36	1.58
RhoGAP15B			2.91	3.23	2.28	2.67
ptr	UDP-glucose metabolic process(GO:0006011)		5.53	6.4		2.81
Thor	protein targeting to Golgi(GO:0000042); sterol regulatory element binding protein cleavage(GO:0035103); protein processing(GO:0016485); cholesterol metabolic process(GO:0008203); SREBP signalling pathway(GO:0032933)		6.89		9.88	3.77
Jon66Cii	translation(GO:0006412); mitotic spindle organization(GO:0007052); mitotic spindle elongation(GO:0000022); centrosome duplication(GO:0051298); neurogenesis(GO:0022008)		9.57		6.92	5.93
ns1					1.12	
DsecGM11932	proteolysis(GO:0006508)			1.74	1.51	1.37
Cyp6v1	regulation of multicellular organism growth(GO:0040014); regulation of insulin receptor signalling pathway(GO:0046626); ribosomal large subunit biogenesis(GO:0042273);			2.89	3.7	2.58

Gene Symbol	Gene's Biological Function	Fold change (p < 0.05)				
		CI	CIII	CIV	CV	o/e
	ribosome biogenesis(GO:0042254); mitotic spindle assembly(GO:0090307); cellular response to starvation(GO:0009267); positive regulation of multicellular organism growth(GO:0040018)					
RNaseX25	oxidation-reduction process(GO:0055114)			1.62	2.21	1.77

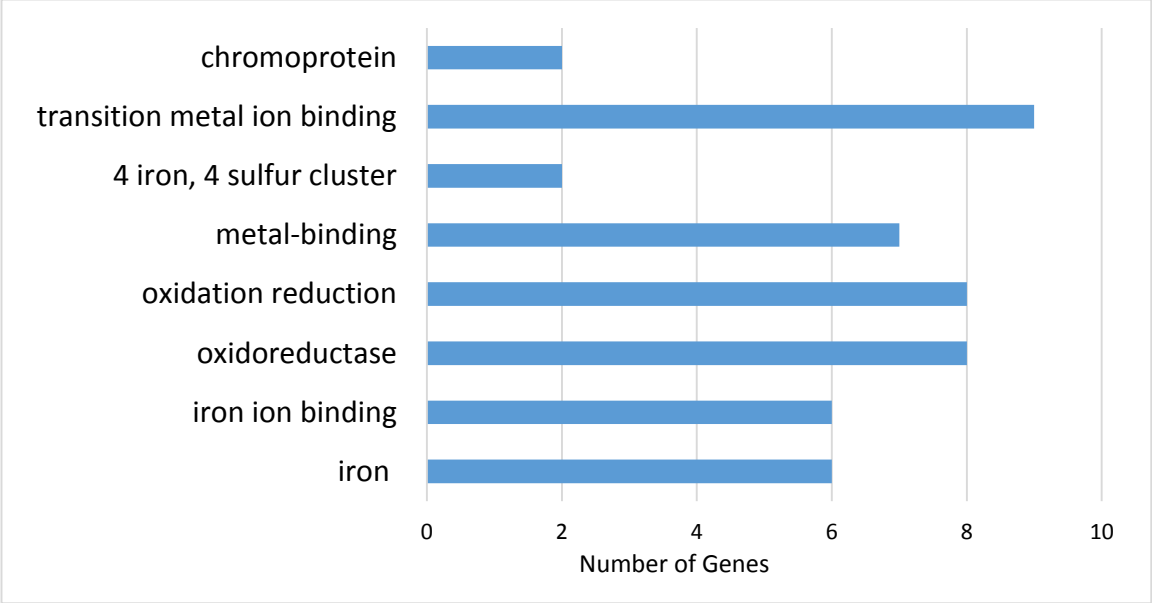

Figure 4.11 GO enrichment analysis on HIF responsive genes that are differentially regulated in complex I knockdown. Enrichment of these terms with p-value < 0.05

4.3 Summary

In this chapter I aimed to investigate the transcriptional response in neurons to mitochondrial dysfunction in the models I characterised in Chapter 3. Microarray analyses were performed on CNS tissue for each genotype and gene expression was compared to control. Each mitochondrial dysfunction model resulted in differential regulation of at least 300 genes compared to control. In each model, approximately 50% of the altered genes were only significantly changed in that model, showing that there are individual transcriptional changes depending on the cause of mitochondrial dysfunction. The other ~50% of genes were also changed in at least one other model, suggesting that there are also common responses to mitochondrial dysfunction, which may be particularly useful as therapeutic targets.

GO analysis identified numerous common functions between the different conditions, highlighting response to ROS and alternative metabolism as two extremely important pathways in all conditions.

HIF-1α (the homolog of *Drosophila* Sima) is a known to instigate a shift toward a glycolytic state and has also previously been shown to regulate levels of *Thor* expression when *TFAM* is overexpressed in motor neurons (Cagin, Duncan et al. 2015). It was therefore considered as a candidate transcription factor that may mediate some of the transcriptional changes observed in the mitochondrial dysfunction models. Knockdown of *sima* was therefore tested in all the models of mitochondrial dysfunction to determine if removal of this transcription factor would affect neuronal function in these models.

Sima knockdown was able to rescue climbing, wing inflation, and lifespan phenotypes caused by *TFAM* overexpression in motor neurons as well as rescuing lethality of pan-neuronally expressed *TFAM* overexpression. Knockdown of *sima* in motor neurons gave some improvement to climbing phenotypes in *ATPsynCf6* (CV) and *COX5B* (CIV) RNAi, however was not able to alter climbing in *UQCR-14* (CIII) or *ND-75* (CI) RNAi. Pan-neuronal lethality of *ATPsynCf6* (CV), *COX5B* (CIV) and *UQCR-14* (CIII) RNAi, was rescued by reduced levels of *sima.* However, *nSyb-Gal4* driven *ND-75* (CI) RNAi lethality was not rescued by *sima* knockdown. The fact that four out of five of my models of mitochondrial dysfunction could in some way be rescued by *sima*

knockdown, suggests that Sima is involved in a common response to mitochondrial dysfunction. The fact that *ND-75* RNAi phenotypes are not rescued by *sima* knockdown highlights the fact that although there may be common responses to mitochondrial dysfunction, there are also individual differences depending on the cause of the mitochondrial deficit.

Analysis of the HIF responsive genes that are altered in each microarray identified a number of HIF related processes that were regulated in a differential manner in *ND-75* RNAi (CI) to the other mitochondrial dysfunction models. These processes are mainly associated with iron binding and oxidoreductase activity. This indicates that these may be interesting processes to investigate further and may be related to *ND-75* RNAi (CI) insensitivity to rescue by *sima* knockdown.

5 A GENETIC SCREEN TO IDENTIFY GENES INVOLVED IN THE CELLULAR RESPONSE TO MITOCHONDRIAL DYSFUNCTION

5.1 Introduction

Mitochondrial dysfunction results in a change in many cellular functions, altering transcription, metabolism and bioenergetics (as seen in chapters 3 & 4). In order to identify genes that are involved in the cellular reprogramming that occurs in response to mitochondrial dysfunction, I developed a genetic modifier screen in *Drosophila*.

Drosophila are a very useful tool for genetic screening. They are cheap, have a short life cycle, only have four chromosomes with a low level of genetic redundancy and roughly 75% of human disease linked genes have a *Drosophila* homologue (Reiter, Potocki et al. 2001). In 1980, Nüsslein-Volhard and Wieschaus carried out a pioneering genetic screen in *Drosophila*, which identified genes involved in developmental patterning in the embryo (Nusslein-Volhard and Wieschaus 1980, St Johnston 2002). Traditional forward genetic screens like this, have some limitations. They only reveal the first, essential role of a gene and do not identify genes that may only be activated in pathological circumstances (St Johnston 2002). Simon et al., came across this problem when trying to identify genes which interact with the tyrosine kinase, Sevenless (Simon, Bowtell et al. 1991). They developed a sensitised screen, in which Sevenless activity was reduced to a level that was only just adequate for normal eye development. Small perturbations in genes downstream of Sevenless could then disrupt eye development (Simon, Bowtell et al. 1991). Modifier screens, such as this, can therefore identify factors that act in a specific pathway or biological process.

Several recent genetic screens have aimed to identify mitochondrially-targeted genes. A genome wide RNAi screen in *Drosophila* cells, identified 152 genes involved in mitochondrial function (Chen, Shi et al. 2008). Among these genes, 22 were involved in transcription regulation (Chen, Shi et al. 2008) and therefore may be involved in the retrograde response. The role of mitochondrial genes in different metabolic environments has also been studied in cell culture (Lanning, Looyenga et al.). An RNAi screen in HeLa cells, of genes known to localise to the mitochondria, was carried out

with four different fuel sources (Lanning, Looyenga et al.). This study reveals how the mitochondria respond to different metabolic, and potentially disease, states.

I aimed to identify genes that are involved in the cellular response to mitochondrial dysfunction *in vivo*. To do this I developed and carried out a modifier screen in which mitochondrial dysfunction was induced and then genes screened in the background of this dysfunction. This should enable the identification of genes that are involved in the response to mitochondrial dysfunction, even if they are not normally involved in mitochondrial function.

5.1.1 Chapter aims

The aims of this chapter are:

1. To develop a genetic modifier assay with an easily scorable phenotype for screening.
2. To ensure the screen identifies genes that regulate mitochondrial dysfunction.
3. To identify novel genes that regulate the cellular response to mitochondrial dysfunction.

5.2 Results

5.2.1 Mitochondrial dysfunction in the wing results in a scorable phenotype

To screen a large number of genes, it is imperative that the phenotype utilised is quick and easy to observe. Therefore, a method of inducing mitochondrial dysfunction, which results in a suitable phenotype, is required. The wing was a good candidate tissue for the screen as it is easily visible and dysfunction in the wing alone has the potential not to affect viability. I used two genetic tools, *TFAM* RNAi and *TFAM* overexpression, which had previously been shown to cause mitochondrial dysfunction in *Drosophila* (Cagin 2012, Cagin, Duncan et al. 2015).Previous work by Umut Cagin, has shown ubiquitous expression of *TFAM* RNAi results in a significant reduction in TFAM levels and a loss of mitochondrial DNA (Cagin 2012). Western blot analysis reveals a significant

decrease in TFAM protein levels, as well as a significant decrease in mitochondrially encoded cytochrome c oxidase subunit I (COXI), when *TFAM* RNAi is ubiquitously expressed with *tubulin-Gal4* (Figure 5.1A-B). Protein levels of the nuclear encoded α subunit of ATP synthase are not significantly different from control (Figure 5.1D-E). These data suggest that mtDNA encoded gene expression is specifically reduced in *TFAM* RNAi flies. This aligns with the data in other studies, which show that reduced *TFAM* expression results in a loss of mtDNA and mtDNA encoded gene expression (Larsson, Wang et al. 1998, Kanki, Ohgaki et al. 2004). In chapter 3 (see Figure 3.5), I have shown that overexpression of *TFAM* also causes a loss of mtDNA encoded protein expression.

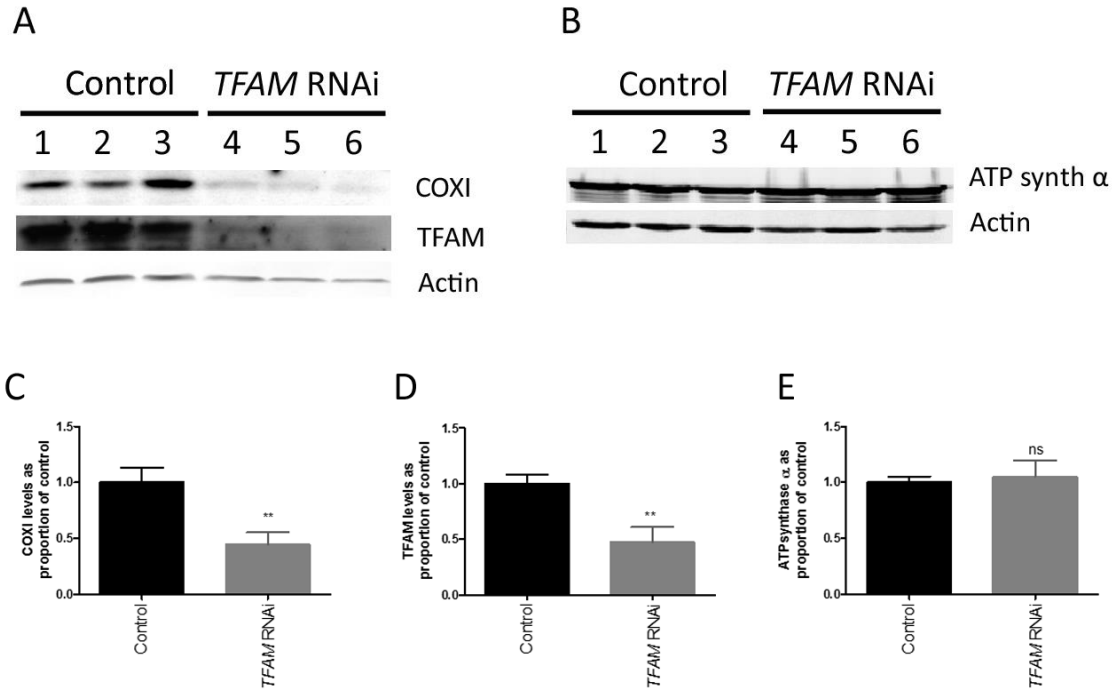

Figure 5.1 Reduced mitochondrial gene expression with *TFAM* RNAi
(A) Representative western blot of third instar larvae with COXI, TFAM and Actin antibodies. *Tubulin-Gal4* driven controls in lane 1-3 and *TFAM* RNAi in lane 4-6. Actin is used as a loading control, to which other proteins were normalised. **(B)** Quantification of *TFAM* RNAi western blot for COXI (n = 6) compared to control (n = 6). **(C)** Quantification of TFAM levels in *TFAM* RNAi (n = 6) compared to control (n = 6). **(D)** Representative western blot with controls in lane 1-3 and *TFAM* RNAi in lane 4-6, with ATP synthase α and Actin antibodies. **(E)** Quantification of nuclear encoded ATP synthase α (n=9) compared to control (n=9) normalised to actin. Data were analysed with a two-tailed t-test. Error bars represent SEM. ns, not significant, ** $p \leq 0.01$

The enhancer trap *MS1096-Gal4* driver can be used to drive UAS controlled gene expression in the dorsal compartment of the wing. In this driver the *Gal4* is inserted in the second intron of *Beadex*, a gene which controls dorsal cell fate in the wing disc

(Milan, Diaz-Benjumea et al. 1998). *MS1096-Gal4* was used to induce mitochondrial dysfunction with *TFAM* overexpression and *TFAM* RNAi. The effects of mitochondrial dysfunction in the wing are observed in adult flies. *MS1096-Gal4* driven knockdown of *TFAM* results in a phenotype of a curve at the tip of the wing (Figure 5.2A-A'). *TFAM* overexpression is pupal lethal, so adult wings could not be observed.

The adult wing phenotype observed in the *MS1096-Gal4 TFAM* RNAi flies, is an appropriate phenotype for the modifier screen: it is easy and quick to score and there is potential to enhance and suppress the phenotype. In order to screen a large number of lines in the background of mitochondrial dysfunction, a stock was made with both the *MS1096-Gal4* and *UAS-TFAM* RNAi in the same fly. To inhibit constitutive *TFAM* knockdown in the wing disc, *Gal80* expression was also required in the fly. For this purpose, the *tub-Gal80* transgene inserted in the TM6B balancer chromosome was used. To maintain a stock with TM6B, *tub-Gal80* and *TFAM* RNAi, the chromosome containing the *TFAM* RNAi must be homozygous lethal. With this in mind, *TFAM* RNAi was recombined with $TFAM^{c01716}$, a lethal piggyBac (pBAC) insertion in the second intron of *TFAM*. Addition of the $TFAM^{c01716}$ enhanced the wing curve phenotype, giving a curve of approximately 45° (Figure 5.2B-B'). This result also demonstrates the *TFAM* RNAi wing phenotype can be modified, and is therefore suitable for the screen assay.

Mitochondria are known to regulate apoptosis (see Introduction 1.2.5.3) and so I hypothesise that mitochondrial dysfunction resulting from *TFAM* RNAi may result in increased apoptosis in the dorsal compartment of the wing, resulting in a curved wing in the adult. Wing discs from third instar larvae were stained with an antibody for cleaved caspase, to assess levels of apoptosis. An antibody for wingless was used to identify the boundary between the ventral and dorsal compartments of the wing pouch. A significant increase in cleaved caspase, indicative of increased apoptosis, was observed in the dorsal compartment of the wing when *TFAM* was both knocked down and overexpressed (Figure 5.2C-F).

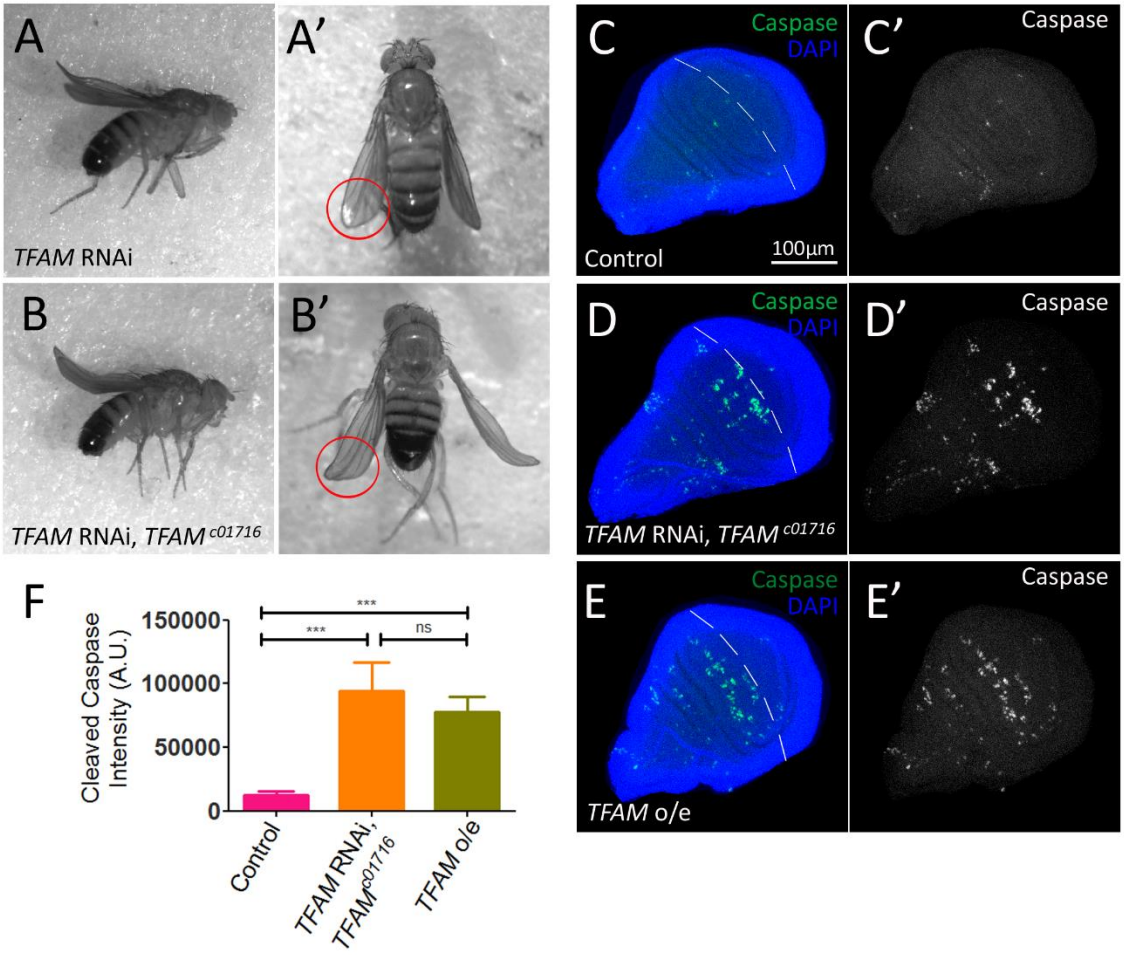

Figure 5.2 Wing phenotype induced by mitochondrial dysfunction
The tip of adult wing is curved (red circle) due to mitochondrial dysfunction. **(A,A')** *MS1096-Gal4* driven *TFAM* RNAi results in a small curve. **(B, B')** The curve is enhanced to approximately 45° in *MS1096-Gal4; TFAM* RNAi, $TFAM^{c01716}$ flies. **(C - E)** Representative wing discs from *MS1096-Gal4* driven **(C,C')** control, **(D,D')** *TFAM* RNAi, $TFAM^{c01716}$ and **(E,E')** *TFAM* overexpression from third instar larvae. **(C,D,E)** Merged images of cleaved caspase antibody (green) indicating apoptotic cells, and DAPI to visualise the wing discs (blue). The boundary between the dorsal (left) and ventral (right) compartments is indicated with a white dashed line. **(C',D',E')** Show caspase staining alone (white) **(F)** Quantification of cleaved caspase antibody intensity, control (n = 26), *TFAM* RNAi, $TFAM^{c01716}$ (n=14) and *TFAM* overexpression (n = 15) driven by *MS1096-Gal4*. Data were analysed using the Kruskal Wallis test. Error bars represent SEM. ns, not significant, *** $p \leq 0.001$.

5.2.2 Modifier screen assay

An assay was developed, to identify genes that modulate the wing phenotype caused by mitochondrial dysfunction induced by *TFAM* knockdown (Figure 5.3). The wing curve in male flies with *TFAM* knockdown and RNAi expression is compared to flies with *TFAM* knockdown alone (Figure 5.3A). Male flies were used because they displayed a stronger phenotype than female flies. The *MS1096-Gal4* driver is on the X chromosome, so the male phenotype may be stronger due to dosage compensation. In preliminary tests it was hard to distinguish weak enhancement of the *TFAM* RNAi $TFAM^{c01716}$ phenotype from the variation in wing curvature that occurred in control crosses. Therefore, a semi-quantitative scoring system was developed, RNAi lines were only considered enhancers if most flies had a $\geq 90^{o}$ wing curve (Figure 5.3B). Suppressors were scored when an RNAi reduced the wing curve in most flies $< 45^{o}$. In a second control cross, RNAi lines were crossed to *MS1096-Gal4* alone: any RNAi that caused a wing phenotype alone was excluded from the screen (Figure 5.3C). Therefore, any of the RNAi lines identified in the screen act synergistically with *TFAM* RNAi $TFAM^{c01716}$ induced mitochondrial dysfunction, rather than causing an additive effect.

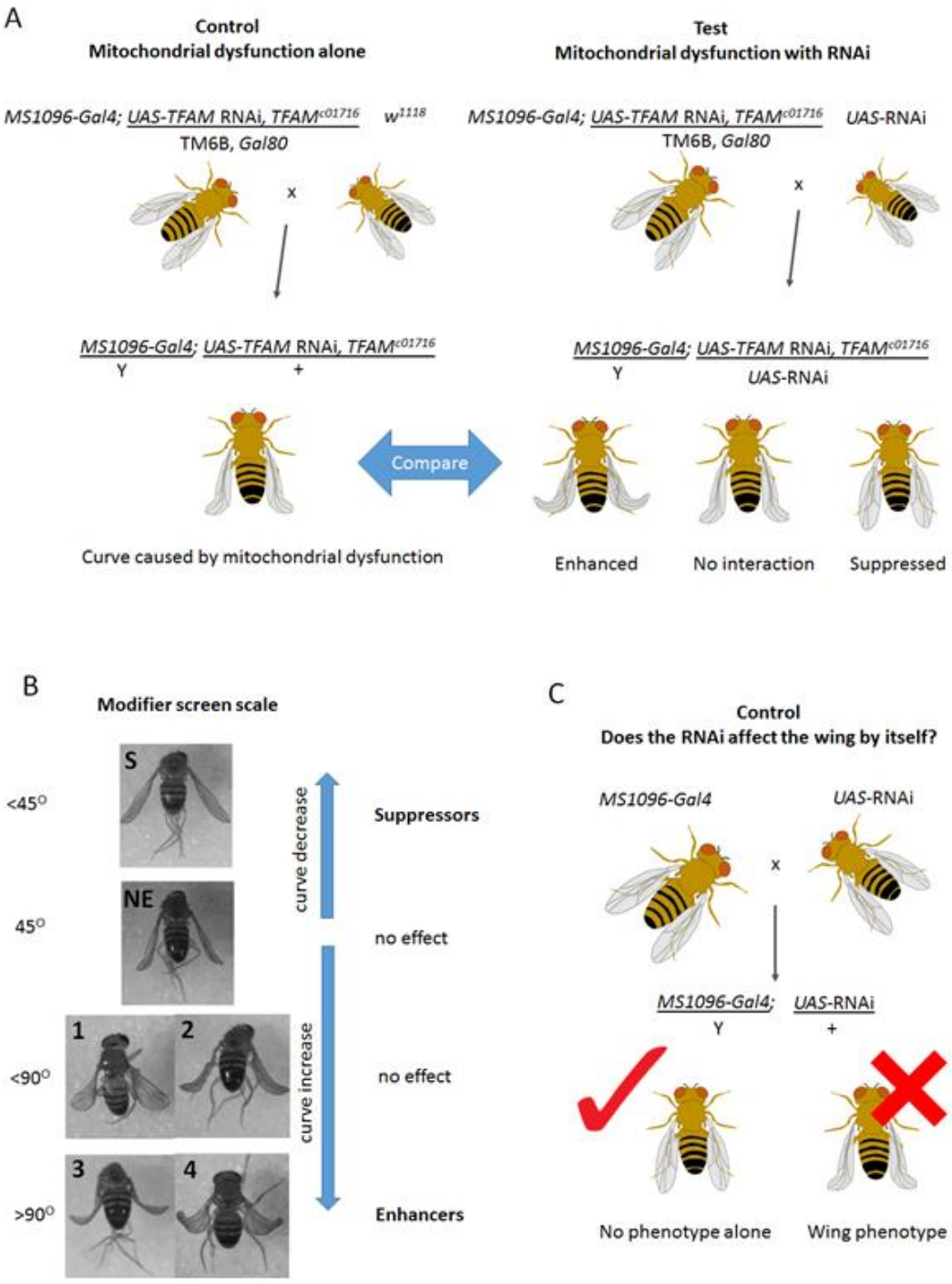

Figure 5.3 Modifier screen assay
(A) A schematic of the crosses performed for the modifier screen. Males of the *UAS* lines to be screened were crossed to virgins containing the *MS1096-Gal4* driver and *UAS TFAM RNAi, TFAM* ^{c01716}. The curvature at the tip of the wing was analysed in flies from the F1 generation. **(B)** Semi quantitive scale, suppressor (S), no effect (NE). 1-4 were scored for increasingly curved wings. Only scores of 3 or 4 were considered enhancers. **(C)** Schematic of the control cross, to identify genes in the screen that have a phenotype on their own when driven by *MS1096-Gal4*. If flies in the F1 generation show a wing phenotype, they are omitted from the screen. The RNAi insertion is shown on the third chromosome for illustration purposes only, RNAis inserted on the second and third chromosomes were screened. Crosses for all lines that were categorised as enhancers or suppressors were repeated both alone and with *TFAM* knockdown.

5.2.3 Validation of the genetic modifier screen

To validate the screen assay, disease associated genes that have a function linked to mitochondria were tested using the devised assay (Figure 5.3). Parkinson's disease is a neurodegenerative disease associated with mitochondrial dysfunction (see Introduction 1.3.3). Linkage analysis has shown an association with familial Parkinson's disease and mutations in genes that encode PTEN-induced putative kinase 1 (PINK1), parkin, leucine rich repeat kinase (LRRK) and DJ-1 (Klein and Westenberger 2012). PINK1 and parkin, play a well-established role in mitochondrial quality control (Pickrell and Youle). The cellular function of LRRK has been less extensively studied, however, it is reported to interact with Drp1 to regulate mitochondrial dynamics (Sandra M Cardoso 2015). DJ-1 is involved in the response to oxidative stress (Menzies, Yenisetti et al. 2005) and although there is only one mammalian gene, there are two *Drosophila* homologues, DJ-1α and DJ-1β (Moore, Dawson et al. 2006). RNAi and overexpression lines for these five PD-linked genes were tested with *MS1096-Gal4* in the background of mitochondrial dysfunction, and on their own (Figure 5.4, Table 14). Lines that resulted in a wing phenotype when driven with *MS1096-Gal4* alone were excluded (Table 14). At least one transgenic line for each gene was scored as an enhancer (Table 14). Interestingly, overexpression and knockdown of the *DJ-1α, DJ-1β* and *Pink1* enhanced the mitochondrial dysfunction wing phenotype (Figure 5.4C-F and H-I). This suggests that the *level of expression* of these genes is important in mitochondrial dysfunction.

All of these disease related, mitochondrial associated genes were identified by the modifier screen assay, suggesting that the screen will identify biologically relevant genes. However, not all lines increased the wing curve enough to be considered enhancers (Table 14). This highlights that the screen is limited by the effectiveness of the transgenic lines screened. If, for example, the RNAi does not reduce the level of gene expression enough, a strong phenotype may not be observed resulting in false negatives. A relevant RNAi may also cause a wing phenotype alone and so be excluded.

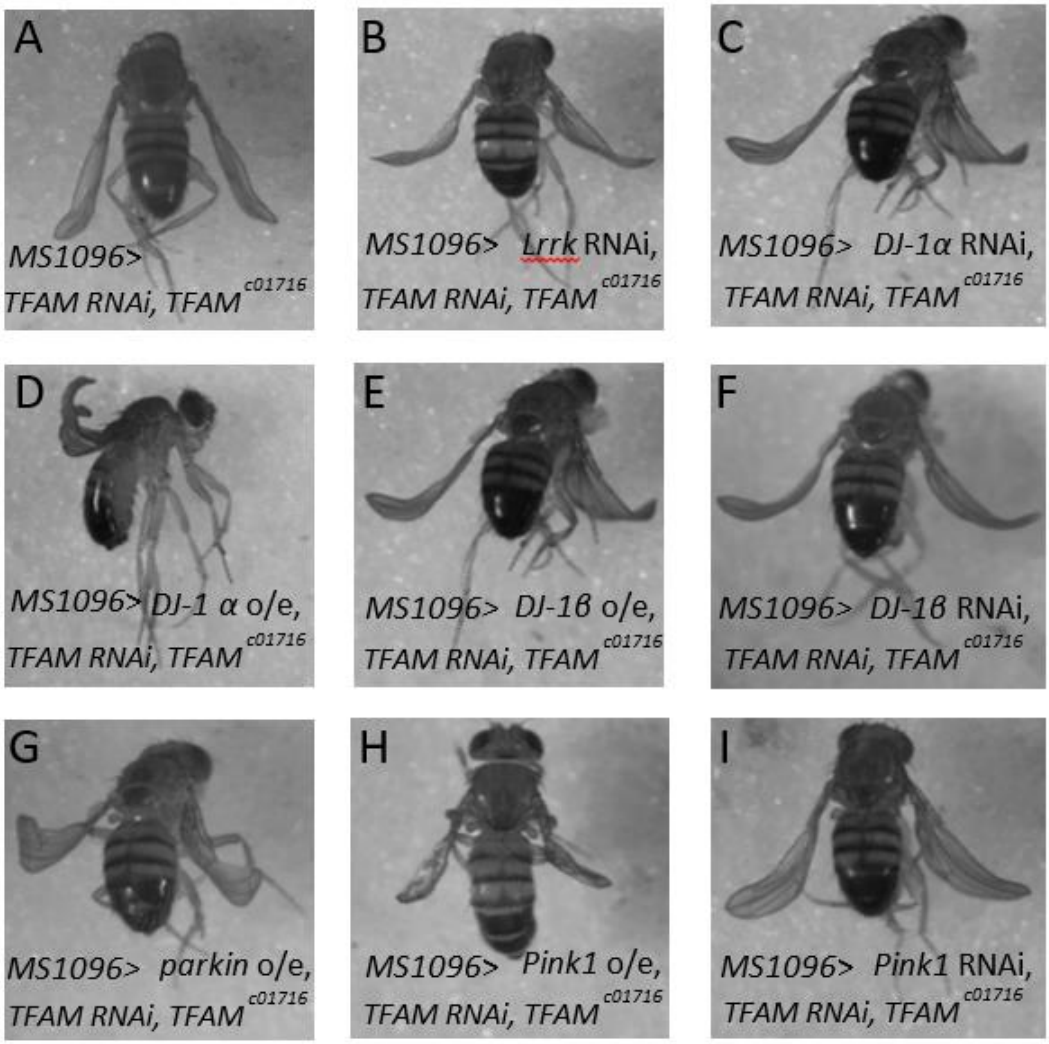

Figure 5.4 Validation of the modifier screen assay with disease associated genes. **(A)** Representative image of the wing curve induced by *MS106-Gal4* driven mitochondrial dysfunction. Representative images of the enhanced wing curve with **(B)** *Lrrk* RNAi (32457), **(C)** *DJ-1α* RNAi (51177) and **(D)** *DJ-1α* overexpression (33603), **(E)** *DJ-1β* overexpression (33604) and **(F)** *DJ-1β* RNAi (38999), **(G)** *parkin* overexpression (51651), **(H)** *Pink1* overexpression (51648) and **(I)** *Pink1* RNAi (31170).

Table 14. Validation of screen. All transgenic lines sourced form Bloomington

Gene	Type	Gene (CG#)	Bloomington Stock number	TRIP ID	Phenotype with *MS1096-GAL4*?	Interaction with *TFAM* knockdown	Screen Score
DJ-1α	Over-expression	*CG6646*	33603		No	**Enhanced**	**3**
DJ-1α	RNAi	*CG6646*	38330	HMS01797	No	No effect	1
DJ-1α	RNAi	*CG6646*	51177	HMJ21180	No	**Enhanced**	**4**
DJ-1α	RNAi	*CG6646*	39055	HMS01975	Yes	Excluded	
DJ-1β	Over-expression	*CG1349*	33604		No	**Enhanced**	**3**
DJ-1β	RNAi	*CG1349*	31261	JF01202	No	No effect	1
DJ-1β	RNAi	*CG1349*	38999	HMS01915	No	**Enhanced**	3
DJ-1β	RNAi	*CG1349*	38378	HMS01847	Yes	Excluded	
Lrrk	Over-expression	*CG5483*	35249		No	No effect	2
Lrrk	RNAi	*CG5483*	39019	HMS01937	No	**Enhanced**	3
Lrrk	RNAi	*CG5483*	32457	HMS00456	No	**Enhanced**	3
parkin	Over-expression	*CG10523*	51651		No	**Enhanced**	**3**
parkin	RNAi	*CG10523*	38333	HMS01800	No	No effect	2
parkin	RNAi	*CG10523*	31259	JF01200	No	No effect	2
parkin	RNAi	*CG10523*	37509	HMS01651	Yes	Excluded	
Pink 1	Over-expression	*CG4523*	51648		No	**Enhanced**	**4**
Pink 1	RNAi	*CG4523*	31262	JF01203	No	No effect	1
Pink 1	RNAi	*CG4523*	31170	JF01672	No	**Enhanced**	**3**
Pink 1	RNAi	*CG4523*	38262	HMS01707	Yes	Excluded	
Pink 1	RNAi	*CG4523*	41671	HMS02204	Yes	Excluded	

5.2.4 Genes identified by the genetic modifier screen

To identify novel genes, which are involved in the cellular response to mitochondrial dysfunction, a library of RNAi lines was screened. As the ultimate goal is to find genes involved in the cellular response to neuronal mitochondrial dysfunction, genes were identified that have a higher expression in the brain compared to the rest of the body. David Mazaud (Fanto lab, Maurice Wohl building, KCL), used gene expression data

available on FlyAtlas, to select genes which are expressed more strongly in the brain than in the whole body (Chintapalli, Wang et al. 2007). Where available, UAS-RNAi lines were selected for these genes (this collection of lines was selected by David Mazaud, Fanto lab). Preliminary results from the screen also indicated a role of chromatin remodelling factors in the response to mitochondrial dysfunction. This is particularly interesting because I am also investigating the retrograde response from the mitochondria back to the nucleus. Therefore, I also added RNAi lines for all known *Drosophila* chromatin remodelling genes, as described in Clapier and Cairns, to the library (Clapier and Cairns 2009).

646 RNAi lines, targeting 579 different genes have been screened (Appendix 9.2.1). Of these lines, 295 were discounted from the screen, because they gave wing phenotypes by themselves with *MS1096-Gal4.* Undergraduate students Marisol Zuniga, Danielle Joseph, Tom Gardener, Fatima Chowdhury, Sharon Yuk Chan, Daniel Potter and Fernando Avila helped with some of the screen crosses, although I repeated the screen crosses for every gene identified as a hit. 71 genes were identified which enhanced the phenotype, giving a greater curl than *TFAM* knockdown alone, with the majority of male flies of that genotype presenting a curve 90° or greater (Figure 5.5A-B, Table 15). Gene ontology (GO) analysis revealed that these genes are involved in a wide range of functions and pathways (Figure 5.5C-D, Table 15, Appendix 9.2.2). A large number are involved in transcription and translation regulation, and so therefore may be involved in the retrograde response from dysfunctional mitochondria to the nucleus.

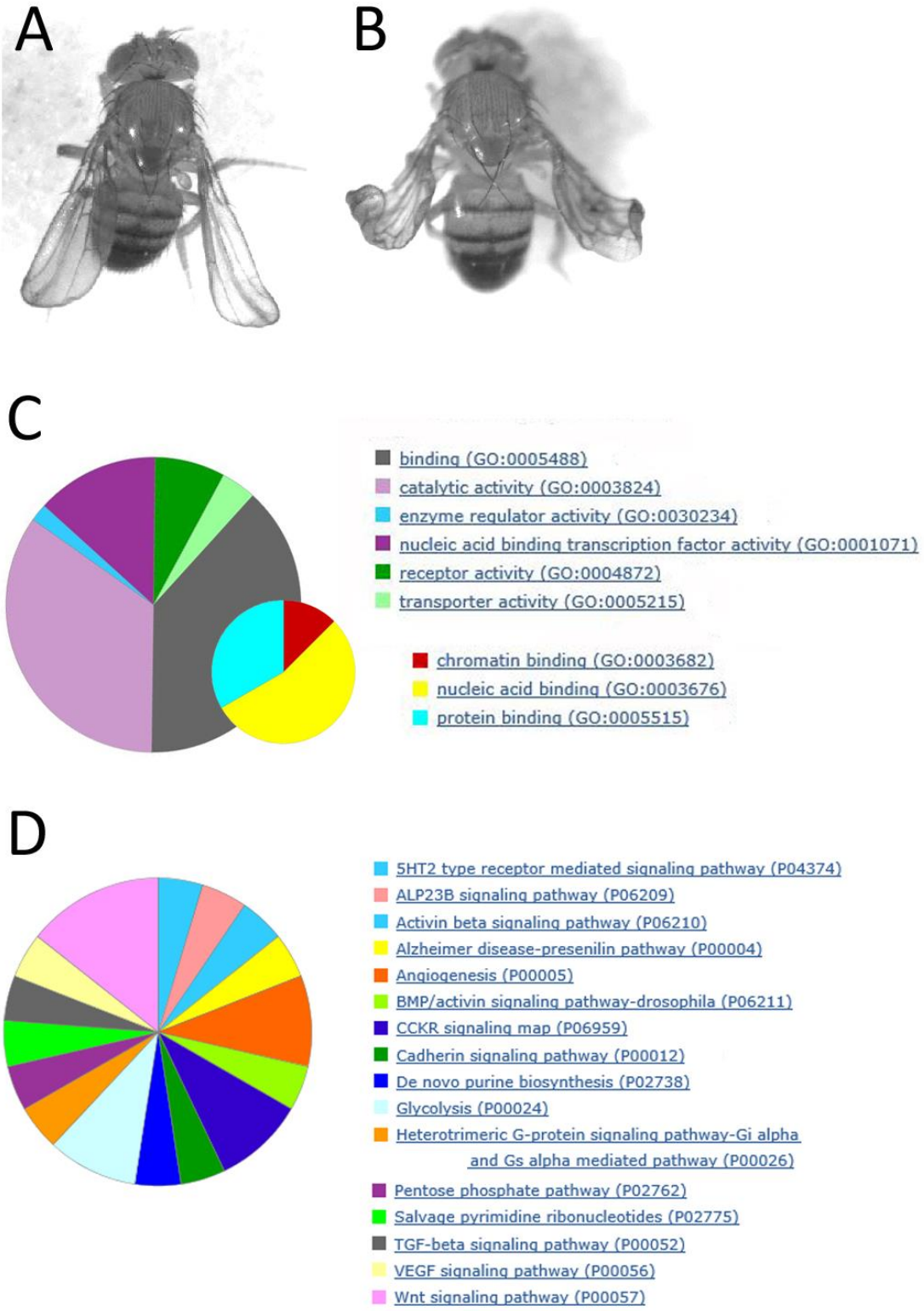

Figure 5.5 Enhancers identified in the modifier screen
Representative images showing wing phenotype of adult flies with *MS1096-Gal4* driven **(A)** *TFAM* RNAi, *TFAM*^{c01716} and **(B)** a validated enhancer, *Phosphoglycerate kinase* RNAi with *TFAM* RNAi, *TFAM*^{c01716}. **(C)** Pie chart showing the GO molecular function of the genes which enhanced the mitochondrial phenotype. The smaller inset pie chart shows the breakdown of molecular functions in the 'binding' category. **(D)** Pie chart showing molecular pathways identified from the enhancer RNAi lines. Pie charts were made using the Geneontology Panther Classification System software.

Nine lines were identified that suppressed the mitochondrial dysfunction phenotype, with a curve of less than 45° (Figure 5.6A-B, Table 16). The majority of these genes regulate DNA in some manner (Figure 5.6C, Table 16, Appendix 9.2.3).

In order to confirm the identified genes are not false positives, crosses with enhancer and suppressor lines were repeated with independent non overlapping RNAi lines. Out of the 82 lines 30 were validated (Table 15, Table 16, Appendix 9.2.4). Knockdown of two genes, *RYamide receptor* and *CG8778*, resulted in an enhanced wing curve with one RNAi line and a suppressed curve when knocked down with an independent RNAi line. This could be due to the level of knockdown or may be due to off target effects. These two genes have therefore not been included in the list of enhancers or suppressors.

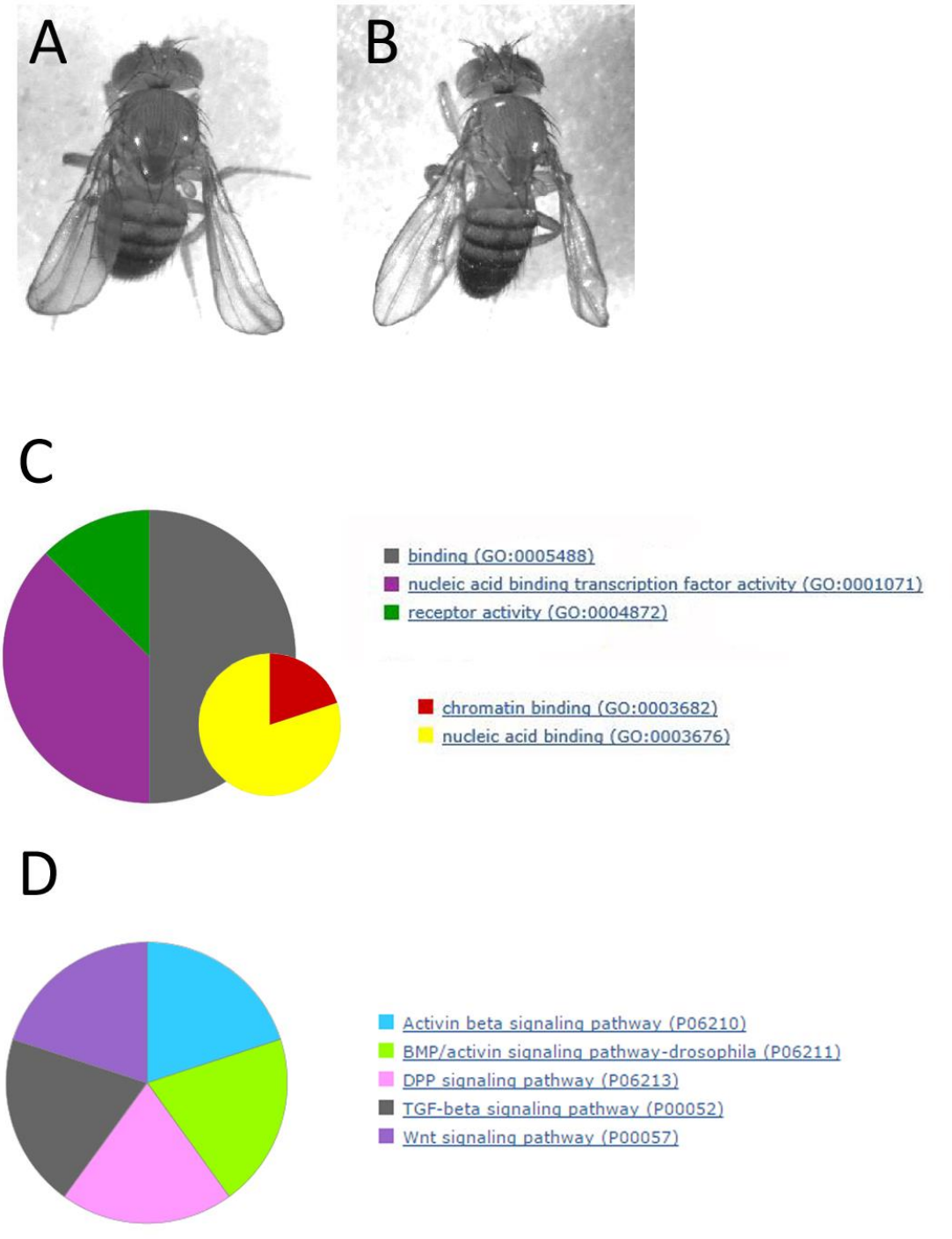

Figure 5.6 Suppressors identified in the modifier screen
Representative images showing wing phenotype of adult flies with *MS1096-Gal4* driven **(A)** *TFAM* RNAi, *TFAM*^{c01716} and **(B)** a validated suppressor, *yan* RNAi with *TFAM* RNAi, *TFAM*^{c01716}. **(C)** Pie chart showing the GO molecular function of the genes which suppressed the mitochondrial phenotype. The smaller inset pie chart shows the breakdown of molecular functions in the 'binding' category. **(D)** Pie chart showing pathways identified from the suppressed RNAi lines. Pie charts were made using the Geneontology Panther Classification System software.

Table 15. Enhancers identified in the screen with GO Molecular Function. Lines validated with a non-overlapping RNAi are in bold. GO Molecular function obtained from the Geneontology Panther Classification System website version 10.

Gene name	GO Molecular Function
Arrow	low-density lipoprotein receptor activity(GO:0005041); Wnt-activated receptor activity(GO:0042813); Wnt-protein binding(GO:0017147)
Disabled	protein binding(GO:0005515); SH2 domain binding(GO:0042169); SH3 domain binding(GO:0017124)

Enhancer of bithorax	zinc ion binding(GO:0008270);
	DNA binding(GO:0003677);
	ligand-dependent nuclear receptor binding(GO:0016922);
	nucleosome-dependent ATPase activity(GO:0070615);
	methylated histone binding(GO:0035064);
	lysine-acetylated histone binding(GO:0070577)

Heat shock gene 67Bc	Unknown function
Phosphoglucose isomerase	phosphogluconate dehydrogenase (decarboxylating) activity(GO:0004616); glucose-6-phosphate isomerase activity(GO:0004347)

sloppy paired 1	transcription factor activity, RNA polymerase II distal enhancer sequence-specific binding(GO:0003705);
	transcription factor activity, sequence-specific DNA binding(GO:0003700);
	enhancer sequence-specific DNA binding(GO:0001158);
	DNA binding, bending(GO:0008301);
	double-stranded DNA binding(GO:0003690);
	transcription factor binding(GO:0008134)

5-hydroxytryptamine (serotonin) receptor 1A	G-protein coupled serotonin receptor activity(GO:0004993); Gi/o-coupled serotonin receptor activity(GO:0001586); G-protein coupled amine receptor activity(GO:0008227)

elbow B	protein binding(GO:0005515);
	nucleic acid binding(GO:0003676);
	metal ion binding(GO:0046872)

breathless	fibroblast growth factor-activated receptor activity(GO:0005007); protein tyrosine kinase activity(GO:0004713); ATP binding(GO:0005524)
Wnt oncogene analog 5	receptor binding(GO:0005102); frizzled-2 binding(GO:0005110)

Imitation SWI	nucleosome-dependent ATPase activity(GO:0070615);
	ATP binding(GO:0005524);
	DNA-dependent ATPase activity(GO:0008094);
	nucleotide binding(GO:0000166);
	ATPase activity(GO:0016887);
	DNA helicase activity(GO:0003678);
	protein binding(GO:0005515);
	DNA binding(GO:0003677);
	nucleosome binding(GO:0031491);

Gene name	GO Molecular Function
	transcription factor binding(GO:0008134)
Cytochrome P450-6a9	electron carrier activity(GO:0009055); oxidoreductase activity, acting on paired donors, with incorporation or reduction of molecular oxygen(GO:0016705); heme binding(GO:0020037);iron ion binding(GO:0005506)
branchless	fibroblast growth factor receptor binding(GO:0005104); growth factor activity(GO:0008083)
late bloomer	Unknown function

Dual-specificity tyrosine phosphorylation-regulated kinase 2	protein kinase activity(GO:0004672);
	protein serine/threonine kinase activity(GO:0004674);
	ATP binding(GO:0005524);
	transferase activity(GO:0016740)

twin of eyeless	transcription factor activity, sequence-specific DNA binding(GO:0003700);
	transcription factor activity, RNA polymerase II distal enhancer sequence-specific binding(GO:0003705);
	RNA polymerase II regulatory region sequence-specific DNA binding(GO:0000977)

Adenylate kinase 1	adenylate kinase activity(GO:0004017); ATP binding(GO:0005524); uridylate kinase activity(GO:0009041)
lipase2	triglyceride lipase activity(GO:0004806)
MORF-related gene 15	methylated histone binding(GO:0035064); protein binding(GO:0005515)

ATP-dependent chromatin assembly factor large subunit	nucleosome-dependent ATPase activity(GO:0070615);
	protein binding(GO:0005515);
	DNA binding(GO:0003677);
	zinc ion binding(GO:0008270)

lethal (1) G0289	Unknown function
phtf	protein dimerization activity(GO:0046983); transcription factor activity, sequence-specific DNA binding(GO:0003700)
CG2124	poly(A) RNA binding(GO:0044822)
Amun	Unknown function
CG4004	Unknown function
CG5599	dihydrolipoamide branched chain acyltransferase activity(GO:0004147)
CG9095	carbohydrate binding(GO:0030246)
CG6847	carboxylic ester hydrolase activity(GO:0052689); lipase activity(GO:0016298)
CG7337	Unknown function
dawdle	transforming growth factor beta receptor binding(GO:0005160); growth factor activity(GO:0008083)
Neuroligin 2	neurexin family protein binding(GO:0042043); receptor activity(GO:0004872)

Gene name	GO Molecular Function
Sodium/solute co-transporter-like 5A11	sodium-dependent multivitamin transmembrane transporter activity(GO:0008523)

GATAd	zinc ion binding(GO:0008270);
	sequence-specific DNA binding(GO:0043565);
	RNA polymerase II transcription factor activity, sequence-specific DNA binding(GO:0000981)

CG2225	Unknown function
caskin	protein phosphatase binding(GO:0019903); signalling adaptor activity(GO:0035591)
pyrexia	calcium channel activity(GO:0005262); cation channel activity(GO:0005261)
gamma-glutamyl carboxylase	gamma-glutamyl carboxylase activity(GO:0008488)
CG11347	ligand-dependent nuclear receptor transcription coactivator activity(GO:0030374); steroid hormone receptor binding(GO:0035258)

Forkhead box K	transcription factor activity, sequence-specific DNA binding(GO:0003700);
	sequence-specific DNA binding(GO:0043565);
	magnesium ion binding(GO:0000287);
	transcription factor binding(GO:0008134);
	double-stranded DNA binding(GO:0003690);
	transcription factor activity, RNA polymerase II distal enhancer sequence-specific binding(GO:0003705);
	DNA binding, bending(GO:0008301)

CG11658	ubiquitin-protein transferase activity(GO:0004842)

roquin	zinc ion binding(GO:0008270);
	poly(A) RNA binding(GO:0044822);
	ubiquitin-protein transferase activity(GO:0004842)

CG5059	
capability receptor	G-protein coupled receptor activity(GO:0004930); neuropeptide receptor activity(GO:0008188); neuromedin U receptor activity(GO:0001607)
CG17734	Unknown function
CG18549	Unknown function
CG5466	Unknown function
distal antenna-related	DNA binding(GO:0003677); protein binding(GO:0005515); transcription factor activity, sequence-specific DNA binding(GO:0003700)
CG6154	dipeptidase activity(GO:0016805)
CG5455	Unknown function
plum	Unknown function
CG6330	uridine phosphorylase activity(GO:0004850)
taranis	Unknown function
defective proboscis extension response 6	Unknown function

Gene name	GO Molecular Function
CG18809	Unknown function
CG31324	Unknown function
CG31436	Unknown function
Keren	epidermal growth factor receptor binding(GO:0005154); growth factor activity(GO:0008083)
CG32521	Unknown function
defective proboscis extension response 8	Unknown function
X11Lβ	beta-amyloid binding(GO:0001540)
CG32685	protein phosphatase 1 binding(GO:0008157)
Reticulon-like1	Unknown function
CG33170	Unknown function
tropomodulin	tropomyosin binding(GO:0005523);actin binding(GO:0003779)
Phosphoglycerate kinase	phosphoglycerate kinase activity(GO:0004618); ATP binding(GO:0005524)
Integrator 6	Unknown function
scribbled	protein binding(GO:0005515)
spoonbill	protein kinase A binding(GO:0051018); RNA binding(GO:0003723)
CG4068	Unknown function
Inositol 1,4,5-triphosphate kinase 2	inositol-1,4,5-trisphosphate 3-kinase activity(GO:0008440); calcium-dependent protein binding(GO:0048306); calmodulin binding(GO:0005516)
stathmin	microtubule binding(GO:0008017); tubulin binding(GO:0015631)

Table 16. Suppressors identified in the screen with GO Molecular Function. Lines validated with a non-overlapping RNAi are in bold. GO Molecular function obtained from the Genontology Panther Classification System website version 10.

Gene name	Molecular Function
yan (anterior open)	transcription factor activity, sequence-specific DNA binding(GO:0003700); protein binding(GO:0005515); transcription factor activity, RNA polymerase II distal enhancer sequence-specific binding(GO:0003705); sequence-specific DNA binding(GO:0043565); protein domain specific binding(GO:0019904)
Daughters against dpp	transforming growth factor beta receptor, inhibitory cytoplasmic mediator activity(GO:0030617); transcription factor activity, sequence-specific DNA binding(GO:0003700); protein binding(GO:0005515)

Gene name	Molecular Function

Metastasis associated 1-like	chromatin binding(GO:0003682);
	zinc ion binding(GO:0008270);
	transcription factor activity, sequence-specific DNA binding(GO:0003700);
	sequence-specific DNA binding(GO:0043565)

Inhibitor of growth family, member 3	zinc ion binding(GO:0008270)

Chromatin accessibility complex 14kD	protein heterodimerization activity(GO:0046982);
	protein binding(GO:0005515);
	nucleosome-dependent ATPase activity(GO:0070615);
	histone acetyltransferase activity(GO:0004402)

CG31125	Unknown function
CG31301	nucleic acid binding(GO:0003676)

Ino80	helicase activity(GO:0004386);
	ATP binding(GO:0005524);
	regulatory region DNA binding(GO:0000975);
	DNA binding(GO:0003677);
	DNA helicase activity(GO:0003678);
	ATPase activity(GO:0016887)

Hormone receptor-like in 39	RNA polymerase II transcription factor activity, ligand-activated sequence-specific DNA binding(GO:0004879);
	RNA polymerase II core promoter proximal region sequence-specific DNA binding(GO:0000978);
	transcription factor activity, sequence-specific DNA binding(GO:0003700);
	transcription cofactor activity(GO:0003712);
	DNA binding(GO:0003677);
	zinc ion binding(GO:0008270);
	steroid hormone receptor activity(GO:0003707)

The genes identified in the screen were compared to genes regulated in the microarray carried out in the previous chapter. None of the genes identified as suppressors in the modifier screen were significantly changed in the microarrays. However, 12 enhancers were also identified in at least one microarray of *ND-75* RNAi (CI), *UQCR-14* RNAi (CIII), *COX5B* RNAi (CIV), *ATPsynCf6* RNAi (CV) and *TFAM* overexpression in the CNS (Table 17).

Table 17. Comparison of modifier screen enhancers with genes significantly altered in OXPHOS and *TFAM* overexpression arrays. Molecular function was obtained from Panther. Significant fold changes of gene expression from *ND-75* RNAi (CI), *UQCR-14* RNAi (CIII), *COX5B* RNAi (CIV), *ATPsynCf6* RNAi (CV) and *TFAM* overexpression are displayed. Green indicated downregulation and red indicated upregulation.

Gene name	**Molecular function**	**CI**	**CIII**	**CIV**	**CV**	***TFAM***
breathless					-2.1	
dawdle						-2.0
Neuroligin 2	transcription factor activity, sequence-specific DNA binding(GO:0003700); transcription factor activity, RNA polymerase II distal enhancer sequence-specific binding(GO:0003705); RNA polymerase II regulatory region sequence-specific DNA binding(GO:0000977)		-8.6	-4.5		
twin of eyeless	transforming growth factor beta receptor binding(GO:0005160); growth factor activity(GO:0008083)		2.5			
taranis					-1.1	
branchless	ligand-dependent nuclear receptor transcription coactivator activity(GO:0030374); steroid hormone receptor binding(GO:0035258)				1.7	
CG4004						-1.1
CG2124	fibroblast growth factor-activated receptor activity(GO:0005007); protein tyrosine kinase activity(GO:0004713); ATP binding(GO:0005524)		-1.4			
CG31436		1.4				
CG17734	poly(A) RNA binding(GO:0044822)				1.4	
defective proboscis extension response 6	neurexin family protein binding(GO:0042043); receptor activity(GO:0004872)		-2.3			
CG11347	fibroblast growth factor receptor binding(GO:0005104); growth factor activity(GO:0008083)					-1.6

5.2.5 *Sima* knockdown enhances the wing phenotype

In Chapter 4, knockdown of *sima* was able to rescue neuronal mitochondrial dysfunction due to overexpression of *TFAM* or knockdown of complex III, IV and V subunits. I therefore looked at *sima* knockdown in the wing modifier assay to determine if it is also able to suppress mitochondrial dysfunction here. Two non-overlapping *sima* RNAi and a heterozygous $sima^{KG07607}$ mutant gave a mild enhancement of the *TFAM* RNAi $TFAM^{c01716}$ wing phenotype (Figure 5.7).

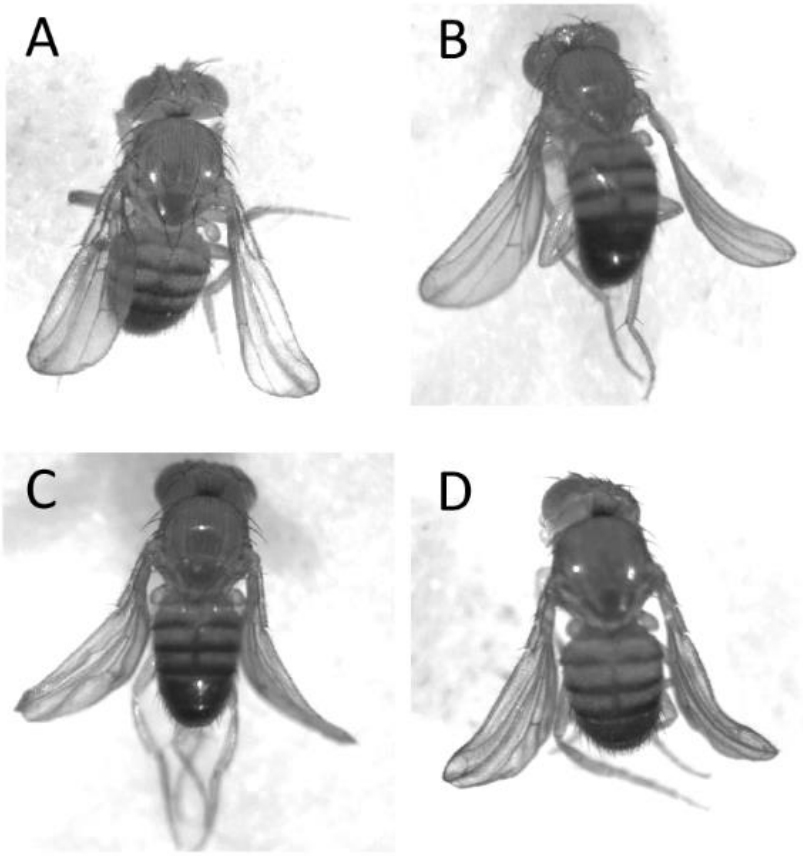

Figure 5.7 *Sima* knockdown enhances the wing phenotype
Representative images showing wing phenotype of adult flies with *MS1096-Gal4* driven **(A)** *TFAM* RNAi, $TFAM^{c01716}$, **(B)** *sima* HMS00833 RNAi with *TFAM* RNAi, $TFAM^{c01716}$, **(C)** *sima* KK102226 RNAi with *TFAM* RNAi, $TFAM^{c01716}$ and **(D)** $sima^{KG07607}$ *with TFAM* RNAi, $TFAM^{c01716}$.

5.2.6 Modification of cell death by genes identified in the screen

Previously (Figure 5.2C-F), I reported that mitochondrial dysfunction, caused by *TFAM* knockdown, increased apoptosis in the dorsal compartment of the wing disc. I therefore asked whether the suppressors identified in the screen, have the same effect respectively on the apoptosis phenotype.

Knockdown of the chromatin remodelling factor, *Ino80*, was identified as causing suppression of the adult wing phenotype. The effect of *Ino80* on apoptosis in the wing disc of third instar larvae was assessed. Knockdown of *Ino80* alone did not alter the level of apoptosis from the control (Figure 5.8A-B', G). However, when *TFAM* was knocked down, *Ino80* RNAi was able to suppress the increase in apoptosis (Figure 5.8C-D', G). Similarly, knockdown of the ETS-transcription, *yan,* also suppressed the adult wing phenotype and also suppressed apoptosis in the wing disc (Figure 5.8E-F', H).

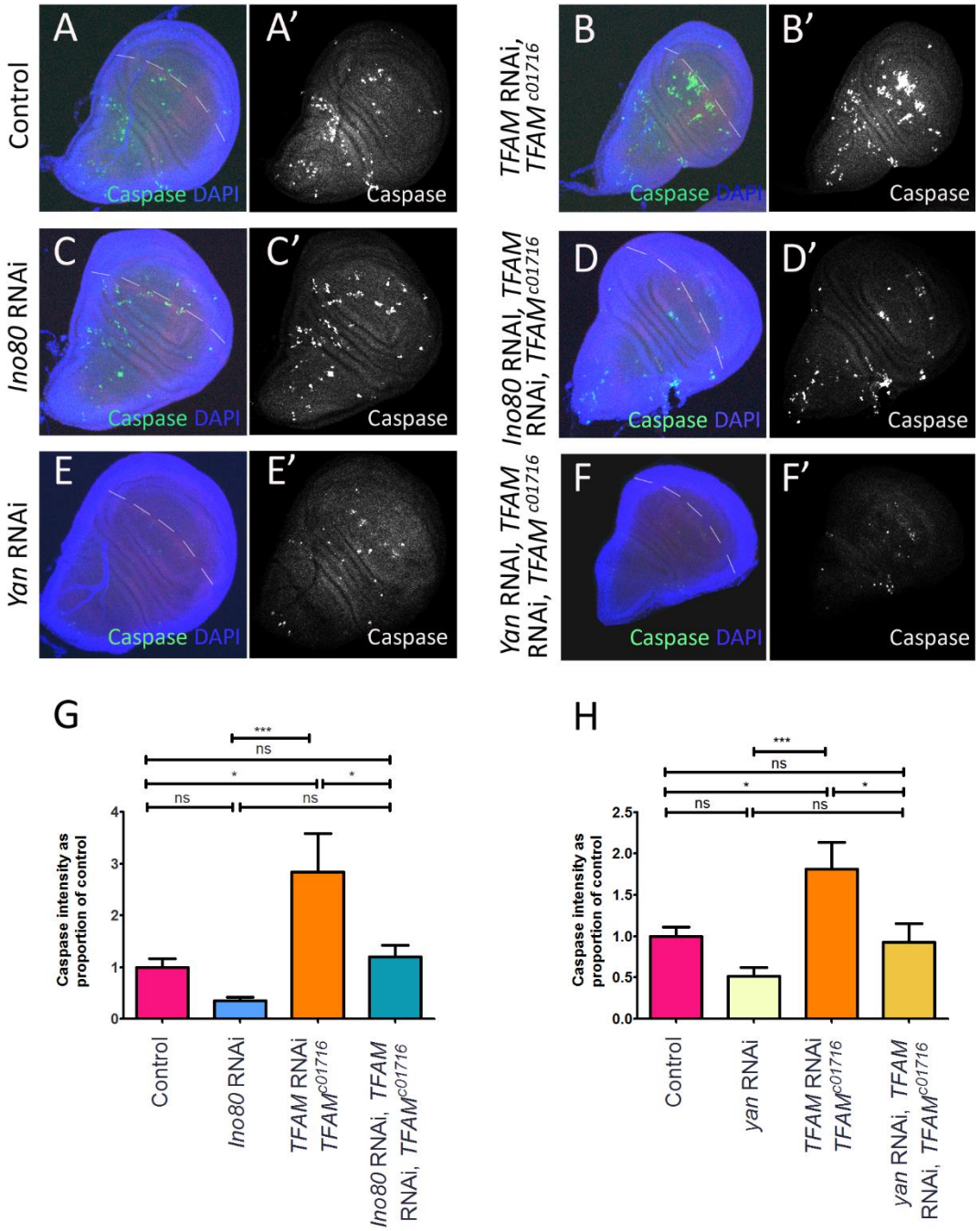

Figure 5.8 Screen suppressors, *Ino80* and *yan* RNAi, reduced mitochondrial dysfunction mediated cell death in the wing disc. Representative images of wing discs from third instar larvae. *MS1096-Gal4* driven **(A)** *w1118* (control), **(B)** *TFAM* RNAi, $TFAM^{c01716}$, **(C)** *Ino80* RNAi, **(D)** *Ino80* RNAi; *TFAM* RNAi, $TFAM^{c01716}$, **(E)** *yan* RNAi, **(F)** *yan* RNAi; *TFAM* RNAi, $TFAM^{c01716}$. In the merged images **(A-F)**, cleaved caspase antibody stains for apoptotic cells (green), and DAPI is used to visualise the wing discs (blue). The dashed line indicates the boundary between the dorsal and ventral wing pouch, identified by wingless staining. **(A'-F')** Caspase staining alone (white). **(G)** Quantification of wing discs in control (n = 19), *TFAM* RNAi, $TFAM^{c01716}$ (n = 19) *Ino80* RNAi (n = 19) and *Ino80* RNAi; *TFAM* RNAi, $TFAM^{c01716}$ (n = 19). **(H)** Quantification of wing discs in control (n = 26), *TFAM* RNAi, $TFAM^{c01716}$ (n = 23), *yan* RNAi (n = 29) and *yan* RNAi; *TFAM* RNAi, $TFAM^{c01716}$ (n = 25). Data were analysed with one-way ANOVA. Error bars represent SEM. ns not significant, * $p \leq 0.05$, *** $p \leq 0.001$.

5.3 Summary

In this chapter I aimed to develop and validate a genetic modifier screen, and then use this screen to investigate the cellular response to mitochondrial dysfunction. A modifier screen method was developed, in which mitochondrial dysfunction was induced in the wing by knockdown of *TFAM*. This produced a wing curve phenotype that could be quickly and easily scored. Transgenic lines could then be screened, in this background, for modification of this curve. The screen was validated with transgenic lines for disease linked mitochondrial proteins, PINK1, parkin, LRRK, DJ-1α and DJ-1β.

A total of 646 transgenic lines (579 genes) were screened. Of these lines, 295 were discounted as they gave a wing phenotype alone, 71 were found to enhance, and 9 to suppress the mitochondrial dysfunction phenotype. The genes identified had a wide range of functions, as expected for such a multifunctional organelle. There were also a large number of genes involved in regulation of transcription, which could play a part in the retrograde response.

Mitochondrial dysfunction in the wing disc resulted in an increase of apoptosis, which may be responsible for the curve phenotype observed in adult flies. Two of the identified genes were examined for their effect on apoptosis in the wing disc. The two suppressors, *Ino80* and *yan* RNAi, also suppressed apoptosis in the wing disc when mitochondrial dysfunction was induced. This suggests that the mitochondrial dysfunction phenotype can be manipulated by effects on apoptosis, however, apoptosis is not the only factor that can affect the adult wing curve phenotype (see Discussion 7.3.2).

6 INVESTIGATING THE ROLE OF GENES IDENTIFIED IN THE MODIFIER SCREEN, IN NEURONAL MITOCHONDRIAL DYSFUNCTION.

6.1 Introduction

I am particularly interested in investigating the cellular response to mitochondrial dysfunction in neurons, with the ultimate aim of further understanding neurodegenerative disease. Neurons have very high energy demand due to the production of action potentials and constant maintenance a resting membrane potential (Attwell and Laughlin 2001, Berndt and Holzhutter 2013). Neurons in the substantia nigra pars compacta, in the basal ganglia have been reported to be particularly susceptible to mitochondrial dysfunction as they have a particularly large surface area due to huge axonal arborisations (Pacelli, Giguere et al. 2015). This may explain why Parkinson's disease, in which these cells die, is strongly associated with mitochondrial dysfunction. The modifier screen described in the previous chapter was a useful tool to quickly identify genes that are involved in the cellular response to mitochondrial dysfunction. However, postmitotic neurons exert very different pressures and demands on mitochondria. It is therefore important to test the identified genes in a neuronal context to determine if they affect mitochondrial dysfunction here.

6.1.1 Chapter aims

The overall goal of this chapter is to investigate genes identified in the modifier screen to determine if they have the same impact on mitochondrial dysfunction in neurons. Genes that do affect neuronal mitochondrial dysfunction are then to be investigated further to improve our understanding of the cellular response to neuronal mitochondrial dysfunction.

To do this, I aim –

1. To investigate whether the RNAi lines identified in the modifier screen, modify phenotypes of mitochondrial dysfunction in motor neurons.
2. To test genes that do modify neuronal mitochondrial dysfunction in disease models.
3. To investigate the molecular pathways these genes are involved in and determine what influence these pathways have on mitochondrial dysfunction.

6.2 Results

6.2.1 Evaluation of genes identified in the modifier screen in neurons

To test genes identified in the modifier screen assay in neurons, mitochondrial dysfunction was induced with *D42-Gal4* and climbing ability and wing inflation were assessed. *TFAM* knockdown, with *TFAM* RNAi and *TFAM*^{c01716}, only induced a weak climbing phenotype, with motor neuron drivers, *D42-Gal4, OK371-Gal4, Ok6-Gal4* (Aberle, Haghighi et al. 2002) and *c380-Gal4* (Koh, Popova et al. 1999) and no wing inflation phenotype with *D42-Gal4* (Figure 6.1). However, overexpression of *TFAM* causes a robust phenotype with a 50% decrease in climbing and approximately 50% of flies with uninflated wings, when driven with *D42-Gal4* (see Results chapter 3, Figure 3.1 & 3.2). A phenotype at this level allows genes identified in the modifier screen to either enhance or suppress the dysfunction, in a manner that can be robustly measured. *TFAM* overexpression was therefore used to model neuronal mitochondrial dysfunction in neurons.

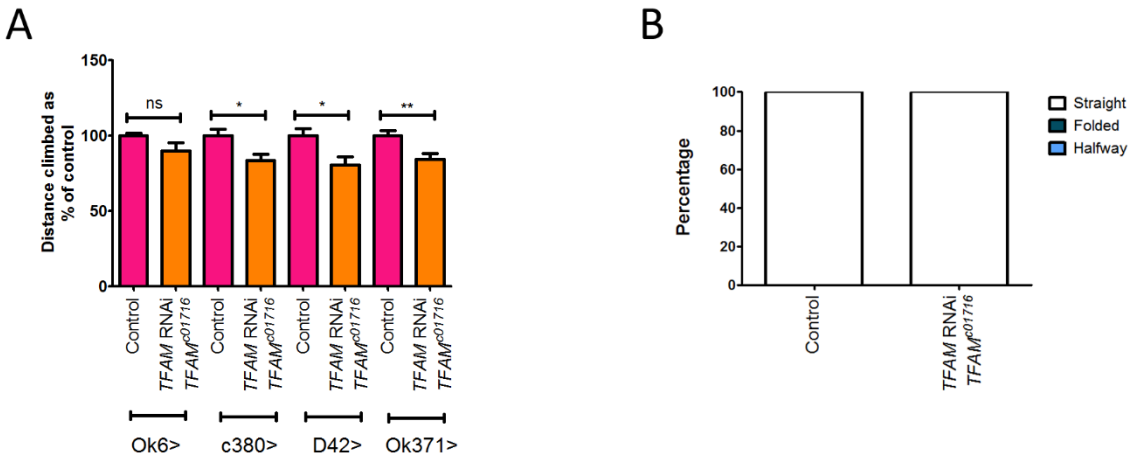

Figure 6.1 *TFAM* RNAi, *TFAM*^{c01716} knockdown in motor neurons causes a weak climbing phenotype and no wing inflation phenotype. (A) Quantification of climbing comparing *TFAM* RNAi, *TFAM*^{c01716} with controls for four motor neuron drivers, *OK6-Gal4* with *w1118* (control) (n = 10), *TFAM* RNAi, *TFAM*^{c01716} (n = 10). *c380-Gal4* with *w1118* (control) (n = 9), *TFAM* RNAi, *TFAM*^{c01716} (n = 9). *D42-Gal4* with *w1118* (control) (n = 11), *TFAM* RNAi, *TFAM*^{c01716} (n = 12). *OK371-Gal4* with *w1118* (control) (n = 18), *TFAM* RNAi, *TFAM*^{c01716} (n = 19). Data were analysed with student's t-tests. **(B)** *D42-Gal4* driven *TFAM* RNAi, *TFAM*^{c01716} (n = 47) does not result in any inflation phenotype compared to control (n = 121). Error bars represent SEM. ns not significant, * $p \leq 0.05$, ** $p \leq 0.01$.

Ideally, mitochondrial dysfunction in neurons would have been assessed in the same format as in the wing, with *TFAM* overexpression and the neuronal driver in the same fly crossed to each RNAi line. However, practical problems prevented the production of a stable stock containing both the neuronal driver and *TFAM* overexpression. A different approach therefore had to be taken, in which stocks containing the RNAi line and *TFAM* overexpression were created. This reduced the number of RNAi lines that it was practical to screen neuronally. The results of the modifier screen suggest that genes which enhance mitochondrial dysfunction are quite common. Any gene that plays a role in the normal mitochondrial function or metabolism may enhance mitochondrial dysfunction when knocked down. In the screen, genes that suppress mitochondrial dysfunction were much less common, suggesting that suppressing mitochondrial dysfunction is more difficult. Moreover, suppression genes may be of more interest therapeutically. Therefore, I focussed mainly on RNAi lines that suppressed the wing phenotype in the modifier screen. A few lines that caused enhanced mitochondrial dysfunction by knockdown of chromatin remodellers were also tested neuronally.

Seven out of the 11 lines tested, significantly altered the wing inflation phenotype in conjunction with *TFAM* overexpression, compared with *TFAM* overexpression alone (Table 18, Appendix 9.2.5). Five enhanced the inflation phenotype and 2 suppressed the phenotype (Table 18, Appendix 9.2.5). For all but one RNAi line, the significant changes to mitochondrial dysfunction in the neuronal assays were opposite to the changes observed in the modifier screen. Only one suppressor, *yan* RNAi, identified in the modifier screen also suppressed wing inflation.

The climbing phenotype was only significantly altered by RNAi for two of the genes tested, and did so robustly in at least two independent climbing assays (Table 18, Figure 6.2 & 6.3). These RNAi lines targeted *Hormone receptor-like in 39 (Hr39)* and *yan.*

Table 18. Results of neuronal assay for selected hits identified in the modifier screen. Any significant result was repeated at least once. ns not significant, * p≤0.05, ** p≤0.01, *** p≤0.001. *CG31125* RNAi climbing and wing expansion assays were carried out by Daniel Potter. Please refer to Appendix 9.2.1 for further information about the stocks.

CG #	Stock ID	Gene Name	Function	Screen result (score)	Climbing	Wing expansion
CG1966	3347	*Acf1*	Chromatin Remodelling	Enhancer (3)	ns	ns
CG8625	24505	*Iswi*	Chromatin Remodelling	Enhancer (4)	ns	ns
CG6363	110618	*MRG15*	Chromatin Remodelling	Enhancer (4)	ns	**Suppressed ** **
CG8676	NIG R3	*Hr39*	Nuclear Hormone Receptor	Suppressor	**Enhanced *** **	**Enhanced *** **
CG31212	106684	*Ino80*	Chromatin Remodelling	Suppressor	ns	**Enhanced ** **
CG6632	109799	*Ing3*	Chromatin Remodelling	Suppressor	ns	**Enhanced *** **
CG31301	104460		Nucleic Acid Binding	Suppressor	ns	**Enhanced *** **
CG31125	25700		Unknown	Suppressor	ns	ns
CG13399	31782	*Chrac-14*	Chromatin Remodelling	Suppressor	ns	ns
CG3166	NIG R3	*aop/ yan*	Transcription Factor	Suppressor	**Suppressed ** **	**Suppressed *** **
CG2244	110618	*MTA1-like*	Chromatin Remodelling	Suppressor	ns	**Enhanced *** **

6.2.2 Knockdown of *Hr39* enhances neuronal mitochondrial dysfunction

Hr39 RNAi was identified as a suppressor in the modifier screen, yet enhanced the *TFAM* overexpression wing inflation and climbing phenotype (Figure 6.2). Hr39 is a neurohormone known to inhibit normal axonal pruning in the mushroom body (Boulanger, Clouet-Redt et al. 2011). It also inhibits pruning in motor neurons through negative regulation of the ecdysone receptor (Boulanger, Farge et al. 2012). The fact that this gene gives the opposite result in the wing compared to neurons may be due to the difference in model, or the role of this gene in mitochondrial dysfunction may be tissue specific (see Discussion 7.4.1).

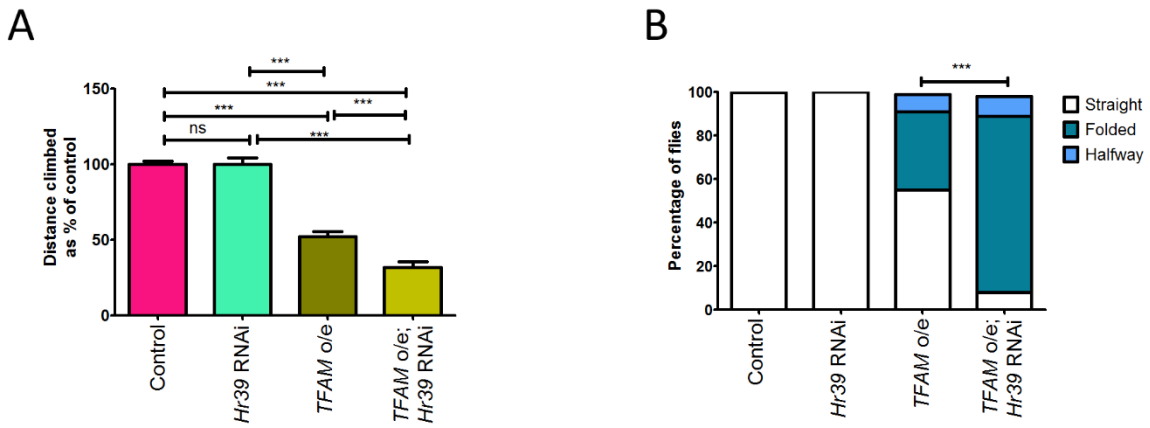

Figure 6.2 Enhanced neuronal mitochondrial dysfunction due to *Hr39* RNAi
(A) Climbing assay with *D42-Gal4* motor neuron driver of *w1118* (control) (n = 32) compared with *Hr39* RNAi (n = 11), *TFAM* overexpression (n = 32) and *TFAM* overexpression with *Hr39* RNAi (n = 32). Data were analysed with a one way ANOVA. **(B)** Wing inflation with *D42-Gal4* motor neuron driver of *w1118* (control) (n = 402) compared with *Hr39* RNAi (n = 224), *TFAM* overexpression (n = 246) and *TFAM* overexpression with *Hr39* RNAi (n = 153). Data were analysed with chi-squared. ns not significant, ** $p \leq 0.01$, *** $p \leq 0.001$.

6.2.3 Knockdown of *yan* suppresses neuronal mitochondrial dysfunction

The other RNAi line that altered both the *TFAM* overexpression inflation and climbing phenotype was *yan* RNAi (Figure 6.3). This RNAi was identified as a suppressor in the modifier screen and was shown to suppress apoptosis in the wing disc, which is normally induced by *TFAM* knockdown. In motor neurons, *yan* also suppresses the climbing phenotype caused by overexpression of *TFAM*. An independent RNAi for *yan* was used to verify that these results were not due to off target effects. The second *yan* RNAi suppresses mitochondrial dysfunction in the modifier screen assay, and in the neuronal wing inflation assay (Figure 6.4A, B, D). It does not suppress the climbing phenotype produced by *TFAM* overexpression but there is a trend towards suppression (Figure 6.4C).

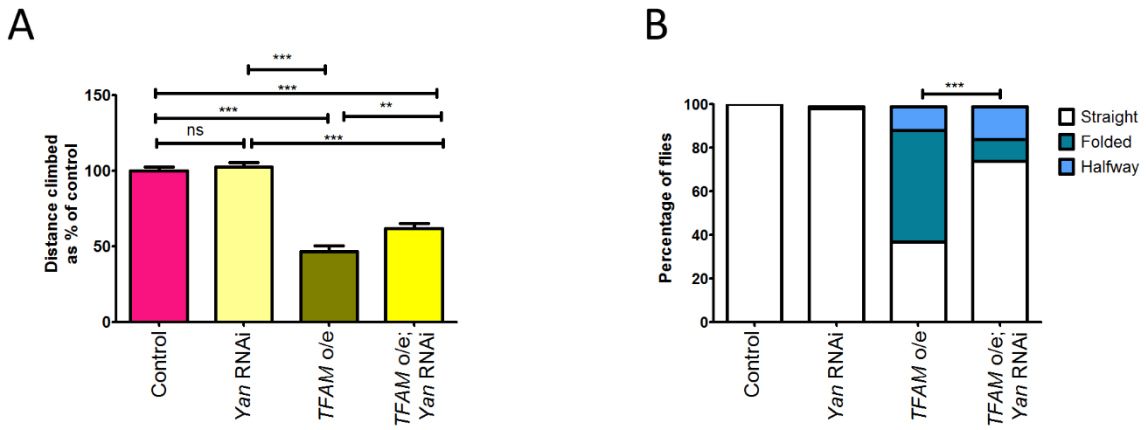

Figure 6.3 Suppressed neuronal mitochondrial dysfunction due to *yan* RNAi NIGR-1. (A) Climbing assay with *D42-Gal4* motor neuron driver of *w1118* (control) (n = 20) compared with *yan* RNAi (n = 20), *TFAM* overexpression (n = 20) and *TFAM* overexpression with *yan* RNAi (n = 20). Data were analysed with a one way ANOVA. **(B)** Wing inflation with *D42-Gal4* motor neuron driver of *w1118* (control) (n = 138) compared with *yan* RNAi (n = 73), *TFAM* overexpression (n = 81) and *TFAM* overexpression with *yan* RNAi (n = 93). Data were analysed with chi-squared. ns not significant, *** p≤0.001.

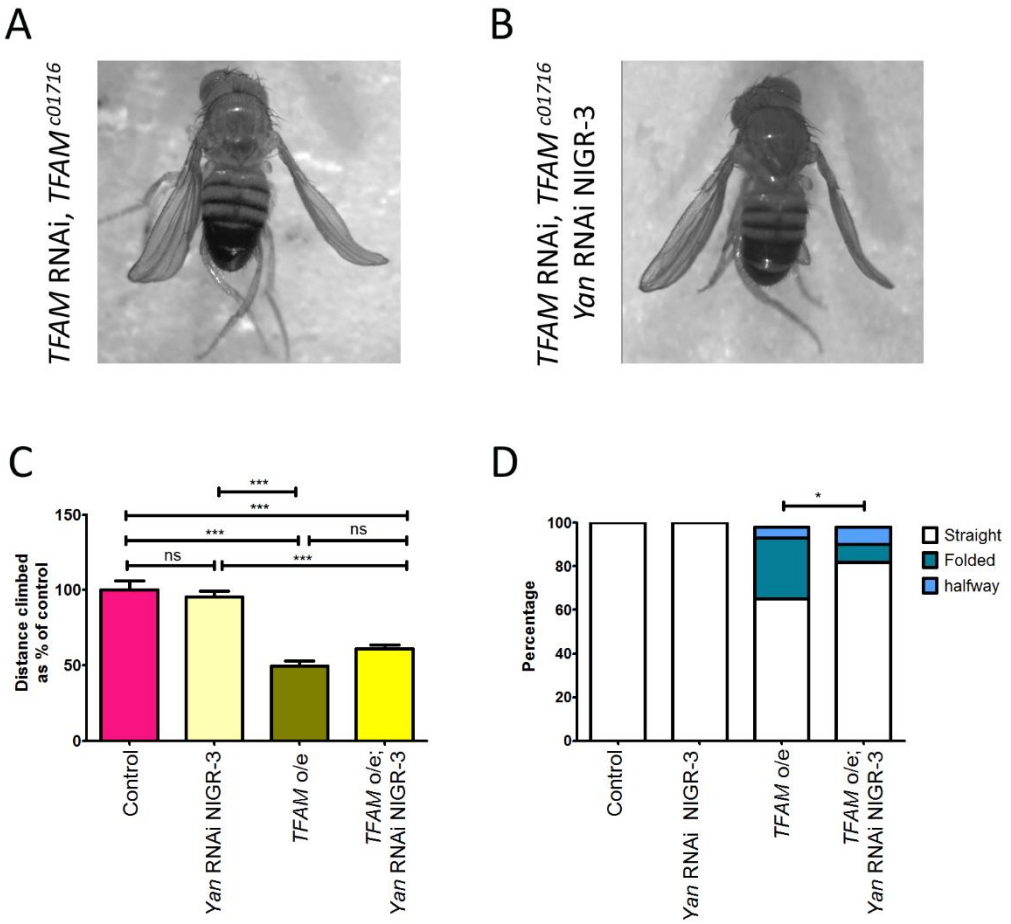

Figure 6.4 A non-overlapping *yan* RNAi also suppressed mitochondrial dysfunction. Representative images of *MS1096-Gal4* driven **(A)** *TFAM* RNAi, $TFAM^{c01716}$ and **(B)** *yan* NIGR-3, *TFAM* RNAi, $TFAM^{c01716}$. **(C)** Climbing assay with

D42-Gal4 motor neuron driver of control (n = 10) compared with *yan* RNAi NIGR-3 (n = 10), *TFAM* overexpression (n = 14) and *TFAM* overexpression with *yan* RNAi NIGR-3 (n = 13). Data were analysed with a one way ANOVA. **(D)** Wing inflation with *D42-Gal4* motor neuron driver of *w1118* (control) (n = 135) compared with *yan* RNAi NIGR-3 (n = 224), *TFAM* overexpression (n = 170) and *TFAM* overexpression with *yan* RNAi NIGR-3 (n = 35). Data were analysed with chi-squared. ns not significant, * $p \leq 0.05$, *** $p \leq 0.001$.

Yan is an ETS-transcription factor, which was first identified in the *Drosophila* eye as a repressor of differentiation (Lai and Rubin 1992). It is now known that Yan is a general repressor of both differentiation and proliferation (Rebay and Rubin 1995, Rogge, Green et al. 1995). Yan is regulated by cell surface tyrosine kinase receptors that activate the MAP kinase pathway (O'Neill, Rebay et al. 1994). Phosphorylation of Yan by this pathway results in Yan degradation and the activation of Pointed P2, Yan's antagonistic ETS-transcription factor partner (O'Neill, Rebay et al. 1994).

The two *yan* RNAis were validated by imaging *yan* expression in the eye disc of third instar larvae, a tissue which expresses high levels of *yan*. The *GMR-Gal4* driver expresses *Gal4* in all cells posterior to the morphogenetic furrow in the eye disc(Freeman 1996). Levels of Yan in the eye disc posterior to the morphogenetic furrow were reduced when both RNAis were driven by *GMR-Gal4*, compared to control (Figure 6.5).

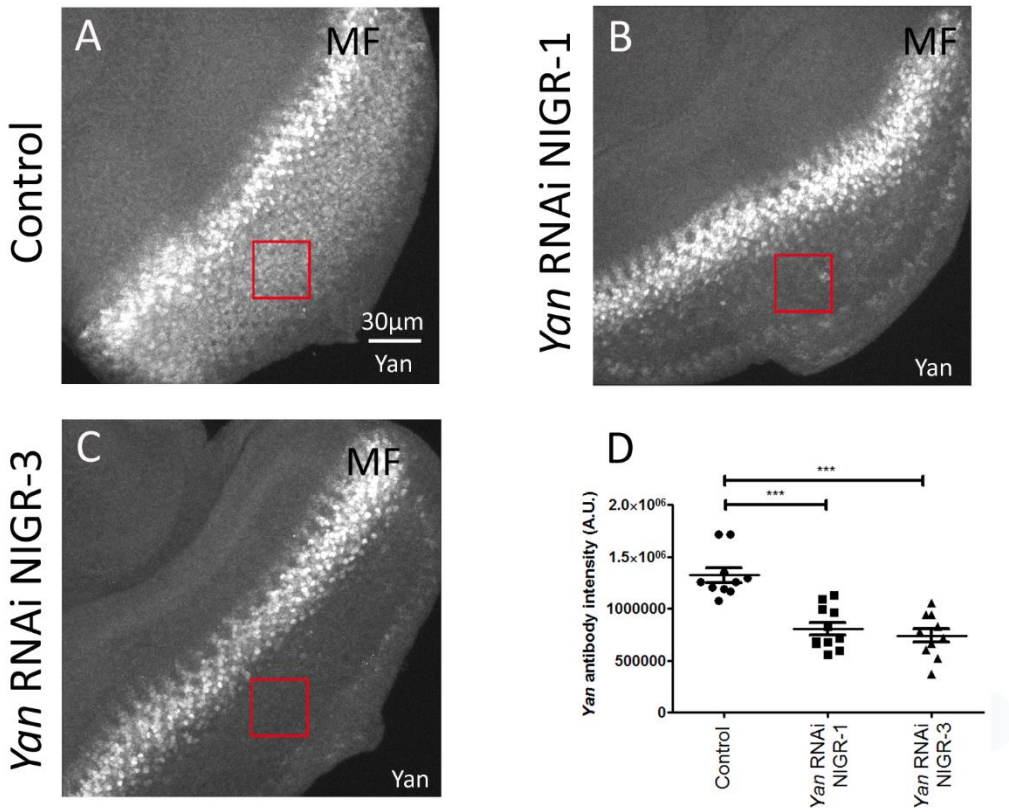

Figure 6.5 Validation of *yan* RNAi lines in the eye disc
Representative images of eye discs dissected from wandering third instar larvae with *GMR-Gal4* driver stained with a Yan antibody, the red boxes show where the antibody intensity was measured. MF indicates the morphogenetic furrow. Eye disc of **(A)** control, **(B)** *yan* RNAi NIGR-1 and **(C)** *yan* RNAi NIGR-3 had reduced staining posterior to the morphogenetic furrow. The eye disc is positioned anterior at the top left and posterior at the bottom right. **(D)** Quantification of control (*GMR-Gal4* crossed to *w1118)* (n = 10), *yan* RNAi NIGR-1 (n = 11) and *yan* RNAi NIGR-3 (n = 10) using a one way ANOVA. Error bars represent SEM. *** $p \leq 0.001$

As knockdown of *yan* suppresses the phenotypes caused by mitochondrial dysfunction in neurons, overexpression of *yan* was investigated to determine if it had the opposite effect. Climbing experiment and wing inflation assays with a *yan* overexpression line were carried out by Dr Vandana Singh. Overexpression of *yan* in motor neurons caused a climbing phenotype on its own as well as a folded wing phenotype and overexpression of *yan* in combination with *TFAM* overexpression was lethal (Figure 6.6). Although the lethality may be an additive effect of dysfunction due to *yan* overexpression and mitochondrial dysfunction, it does show that overexpression does indeed result in the opposite phenotype to *yan* knockdown.

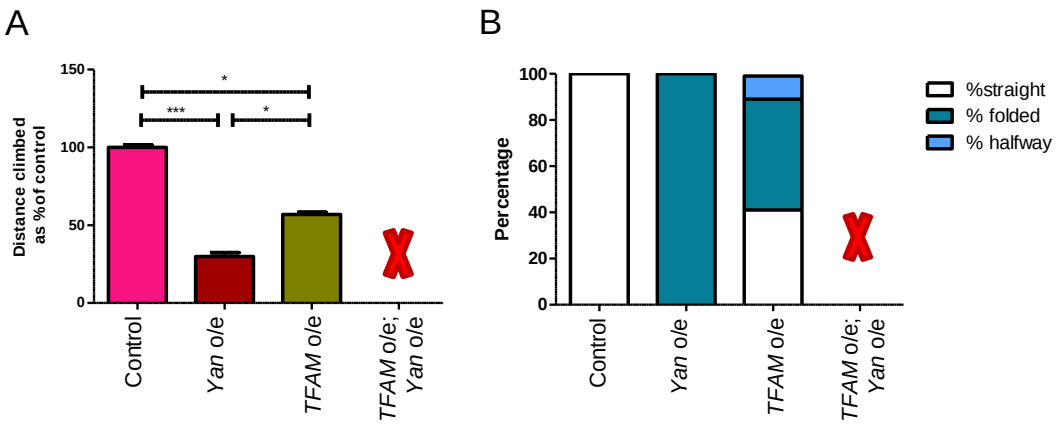

Figure 6.6 Motor neuron overexpression of *yan* is in lethal in the *TFAM* overexpression model of mitochondrial dysfunction. (A) Climbing assay with *D42-Gal4* motor neuron driver of *w1118* (control) (n = 10) compared with *yan* overexpression (n = 10) and *TFAM* overexpression (n = 10). Data were analysed with a one way ANOVA. **(A)** Wing inflation assay with *D42-Gal4* motor neuron driver of control (n = 10) compared with *yan* overexpression (n = 10) and *TFAM* overexpression (n = 10).These experiments were performed by Dr Vandana Singh. Error bars represent SEM, **X** indicates lethality. * $p \leq 0.05$, *** $p \leq 0.001$

6.2.4 Knockdown of *yan* suppresses mitochondrial dysfunction in a *Drosophila* model of Leigh syndrome, but not in a Parkinson's disease model.

Yan knockdown was tested in other models of mitochondrial dysfunction to determine whether it specifically suppressed mitochondrial dysfunction related to *TFAM* dysregulation. Two disease related *Drosophila* models were used, which model Leigh syndrome and Parkinson's disease. Previously, I have shown that climbing phenotypes caused by these two models of mitochondrial dysfunction can be rescued by knockdown of *sima* (Cagin, Duncan et al. 2015).

The most common single cause of Leigh Syndrome is mutations in the gene *Surf1*(Pequignot, Dey et al. 2001). Surf1 is an IMM protein that is required for the correct assembly of complex IV (Herrmann and Funes 2005). This syndrome can be modelled in the fly with knockdown of the *Drosophila* homologue of *Surf1*(Da-Re, von Stockum et al. 2014). *D42-Gal4* driven *Surf1* RNAi does not induce a strong climbing phenotype (data not shown), so the pan-neuronal driver *nSyb-Gal4* was used to knockdown *Surf1*. With *nSyb-Gal4* very few males were viable. Female flies were therefore used for the climbing assay and had a severely impaired climbing ability as well as a very penetrant wing inflation phenotype. *NSyb-Gal4* driven *yan* RNAi

significantly rescued the climbing deficit and wing inflation induced by *Surf1* RNAi (Figure 6.7).

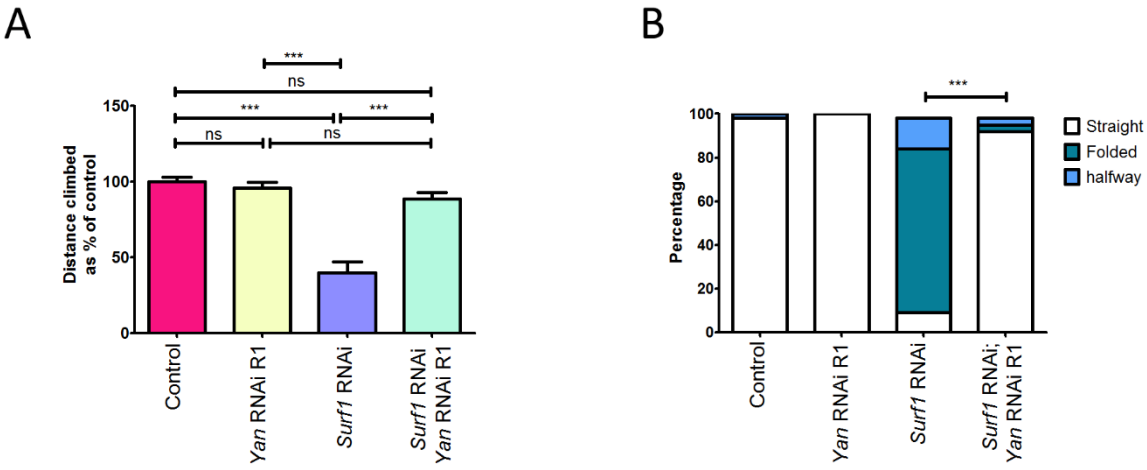

Figure 6.7 Knockdown of *yan* restores neuronal function in a *Drosophila* model of Leigh syndrome. (A) Climbing assay of female flies with pan neuronal *nSyb-Gal4* driver. Control (n = 10) (*nSyb-Gal4* crossed to *w1118)* compared with *yan* RNAi NIGR-1 (n = 9), *Surf1* RNAi (n = 10) and *Surf1* RNAi with *yan* RNAi NIGR-1 (n = 10). Data were analysed with a one way ANOVA. **(B)** Wing inflation with pan neuronal *nSyb-Gal4* driver of *w1118* (control) (n = 165) compared with *yan* RNAi (n = 153), *Surf1* RNAi (n = 162) and *Surf1* RNAi with *yan* RNAi (n = 154). Data were analysed with the chi-squared test. ns not significant, *** $p \leq 0.001$.

Parkinson's disease can be modelled in *Drosophila* with a null mutation in *parkin*, $park^{25}$ (Greene, Whitworth et al. 2005). Previously, the climbing deficit caused by $park^{25}$ has been rescued with ubiquitous *sima* knockdown, driven with the *daughterless* (*Da-Gal4*) driver. To test whether y*an* knockdown is capable of rescuing $park^{25}$ mutant flies, I therefore used the ubiquitous driver *Da-Gal4*. Ubiquitous *yan* knockdown did not significantly improve the climbing ability of $park^{25}$ flies (Figure 6.8).

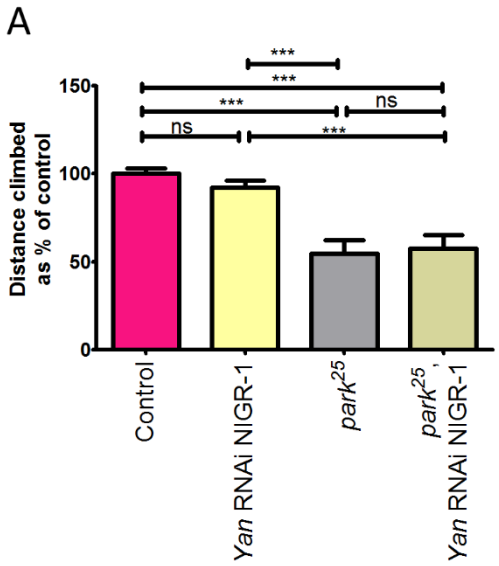

Figure 6.8 Knockdown of *yan* does not restore climbing ability in a *Drosophila* model of Parkinson's disease. (A) Climbing assays of *Da-Gal4; park*^{25} crossed to *w1118* as a control (n = 10), *yan* RNAi NIGR-1 (n = 10), *park*^{25} (n = 10) and *park*^{25}, *yan* RNAi NIGR-1 (n = 10). Heterozygous *park*^{25} mutants have no climbing phenotypes. Data was analysed with one way ANOVA. Error bars represent SEM. ns not significant, *** $p \leq 0.001$

6.2.5 Pointed mutant suppresses neuronal mitochondrial dysfunction.

Yan is thought to act antagonistically with another ETS-transcription factor, Pointed (Pnt) (O'Neill, Rebay et al. 1994), which acts as a positive regulator of gene expression, on the same genes repressed by Yan. There are two isoforms of Pnt, P1 and P2, due to two promoter regions separated by about 50kb (Klambt 1993). The two isoforms have a conserved 3' ETS DNA binding domain but, due to alternative 5' splicing, different activation domains (Klambt 1993). As a result, PntP1 is constitutively active, whereas PntP2 is regulated by the MAPK pathway (Gabay, Scholz et al. 1996).

A deletion mutation, which targets exons shared by both *pntP1* and *pntP2*, *pnt*$^{\Delta 88}$, was used to study the effect of *pnt* knockdown on neuronal mitochondrial dysfunction (Alvarez, Shi et al. 2003). Climbing ability was tested in the *TFAM* overexpression model of mitochondrial dysfunction and the *park*^{25} Parkinson's disease model. Heterozygous *pnt*$^{\Delta 88}$ suppressed the *TFAM* overexpression climbing and wing inflation phenotype (Figure 6.9A,B), and suppressed the climbing phenotype caused by *park*^{25} (Figure 6.9C).

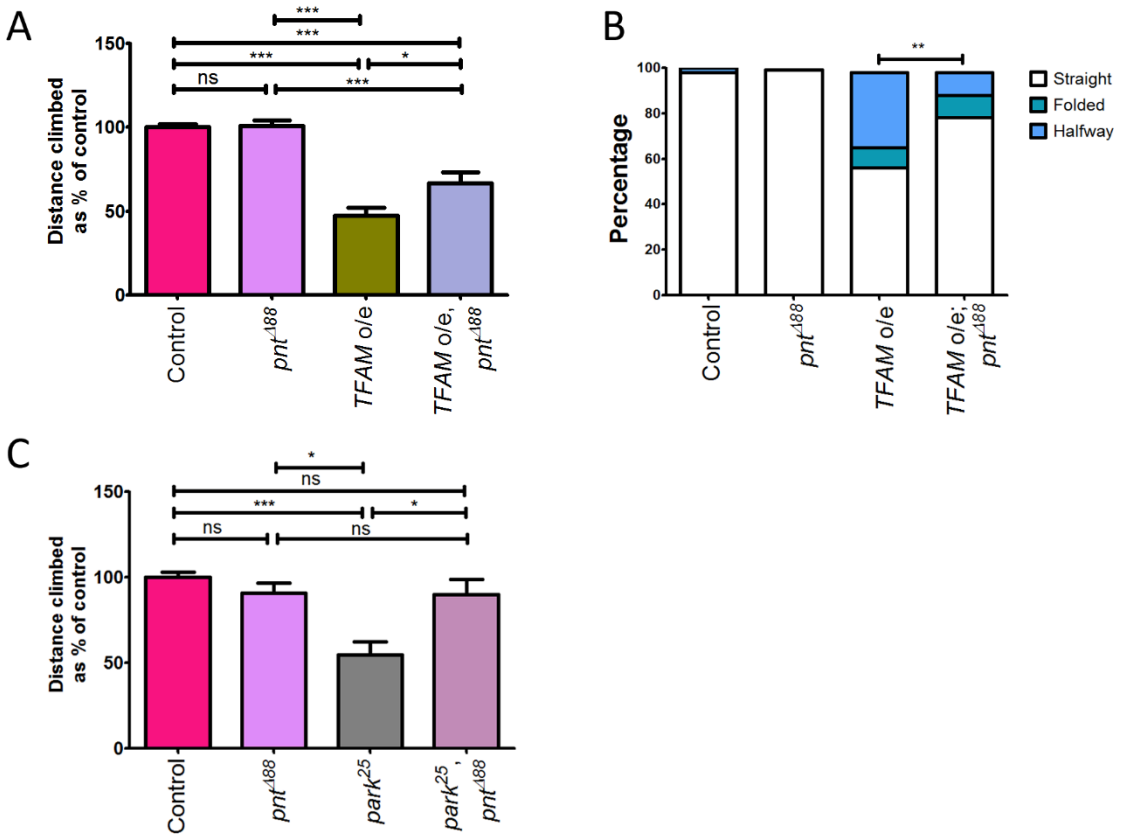

Figure 6.9 *Pointed* mutant restores neuronal function in *TFAM* overexpressing and *parkin* mutant flies. (A) Climbing assay of *D42-Gal4* driven *w1118* (control) (n = 10) $pnt^{\Delta 88}$ (n = 10), *TFAM* overexpression (n = 10) and $pnt^{\Delta 88}$ with *TFAM* overexpression (n = 10). **(B)** Wing inflation in *D42-Gal4* driven *w1118* (control) (n = 237) $pnt^{\Delta 88}$ (n = 259), *TFAM* overexpression (n = 173) and $pnt^{\Delta 88}$ with *TFAM* overexpression (n = 56). **(C)** Climbing assay of control (n = 10) $pnt^{\Delta 88}$ (n = 10), $park^{25}$ (n = 10) and $pnt^{\Delta 88}$ with $park^{25}$ (n = 10). Data were analysed with one way ANOVA or chi-squared. ns not significant, * p≤0.05, ** p≤0.01, *** p≤0.001.

6.2.6 MAP kinase signalling pathway activity is altered by mitochondrial dysfunction

Yan knockdown and $pnt^{\Delta 88}$ have been shown to robustly suppress mitochondrial dysfunction *in vivo*. I therefore investigated the MAPK pathway upstream of Yan and Pnt, to determine if MAPK signalling is altered by mitochondrial dysfunction. The homolog of Yan, Etv6 (previously known as Tel), is phosphorylated in mammals by the MAPK ERK1/2. The *Drosophila* homologue of ERK is Rolled. As a readout of the Ras/MAPK pathway activity, I used an antibody for double phosphorylated MAPK (pMAPK) to observe active MAPK in motor neuron cell bodies. Levels of pMAPK increased in VNC when *TFAM* was overexpressed (Figure 6.10).

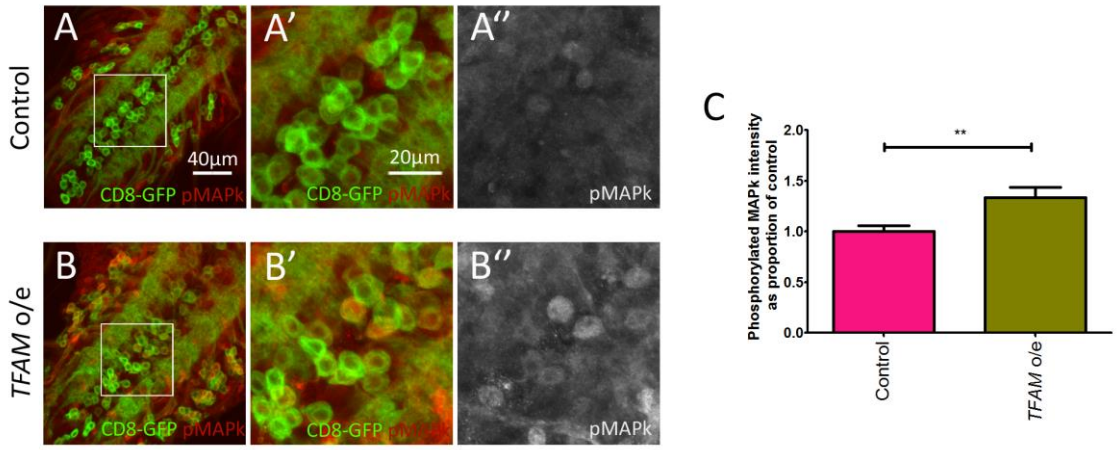

Figure 6.10 Increased activation of MAPK in neurons overexpressing *TFAM*
Representative images of the VNC from third instar larvae expressing *OK371-Gal4* driven CD8-GFP (green) and stained with an antibody for pMAPK (red in A,A',B,B' and white in A'' and B''). **(A-A'')** Control larvae. **(A')** Control VNC in the white box with mitoGFP and pMAPK, **(A'')** and with pMAPK staining alone. **(B-B'')** *TFAM* overexpression. **(B')** *TFAM* overexpression VNC in the white box with mitoGFP and pMAPK, and **(B'')** with pMAPK staining alone. **(A-B')** Merged images. **(A'',B'')** pMAPK alone. **(C)** Quantification of pMAPK measured in the cytosol of GFP expressing motor neuron cell bodies of control (n = 29) and *TFAM* overexpressing (n = 29) larvae. Data were analysed using a student's test with Welch's correction. Error bars represent SEM. ns not significant, ** $p \leq 0.01$.

6.3 Summary

In this chapter, I started with 11 genes identified in the modifier screen as modulators of mitochondrial dysfunction in the wing and investigated whether they also modified mitochondrial dysfunction in neurons. *TFAM* knockdown, the tool I used to induce mitochondrial dysfunction in the wing, was not strong enough to induce suitable phenotypes in motor neurons. I therefore used overexpression of *TFAM* rather than knockdown to induce neuronal mitochondrial dysfunction.

Seven of the genes tested significantly modified the wing inflation phenotype that results from neuronal mitochondrial dysfunction. This validates the modifier screen, indicating it is a useful way to identify genes that do have an effect on mitochondrial dysfunction in neurons. Not all of these genes modified mitochondrial dysfunction in neurons in the same way as they did in the wing screen e.g. in some cases a suppressor in the wing screen, enhanced mitochondrial dysfunction in motor neurons. This maybe because the model of mitochondrial dysfunction was changed from *TFAM* knockdown to *TFAM* overexpression or it may be due to tissue specific effects.

Only two of the genes investigated were able to modify the climbing phenotype caused by mitochondrial dysfunction, as well as the wing inflation phenotype. Knockdown of *Hr39*, a neurohormone that inhibits axonal pruning, enhanced the climbing phenotype and knockdown of the ETS transcription factor *yan*, which is regulated by the Ras/MAPK pathway, partially rescued the climbing phenotype. The ability of *yan* knockdown to suppress phenotypes caused by *TFAM* overexpression was confirmed with a second RNAi. *Yan* RNAi was also able to suppress phenotypes of neuronal mitochondrial dysfunction in a *Drosophila* model of Leigh syndrome, but not $park^{25}$ mutants.

A second ETS transcription factor, *pnt*, which is also regulated by the Ras/MAPK pathway was able to rescue neuronal mitochondrial dysfunction caused by *TFAM* overexpression and $park^{25}$ mutants.

I have identified downstream components of the Ras/MAPK pathway, so I looked at levels of activated MAPK to determine if it is altered by mitochondrial dysfunction.

Overexpression of *TFAM* induced an increase in active MAPK (pMAPK) in the soma of third instar larvae's motor neurons.

7 DISCUSSION

7.1 Characterising different mitochondrial insults in the *Drosophila* nervous system

I have characterised neuronal mitochondrial dysfunction in *Drosophila* using five different mitochondrial insults: knockdown of a single subunit of complex I, III, IV and V and reduced mtDNA encoded gene expression caused by *TFAM* overexpression. There are already numerous *in vivo* models of mitochondrial dysfunction (see Introduction 1.3.4 & Table 2). However, there has been little *in vivo* characterisation of mitochondrial dysfunction in neurons, and no comparison of dysfunction caused by loss of different OXPHOS subunits in neurons. As neurodegenerative diseases are associated with mitochondrial dysfunction, related particularly to deficits in specific complexes, this analysis is important for better understanding of these diseases.

I used a climbing assay to identify OXPHOS subunit RNAi lines that resulted in a functional impairment. This assay is a tool to broadly assess neuronal function. It has been particularly useful for evaluation of whether neuronal function has been rescued or impaired in genetic epistasis experiments. The exact cause of the climbing deficit has not been explored in this study but there are numerous putative mechanisms.

7.1.1 Functions of the OXPHOS subunits targeted by the selected RNAi lines

I focussed on one RNAi for a single subunit of complexes I, III, IV and V. The complex I subunit targeted was *ND-75,* which produces the NADH-ubiquinone oxidoreductase 75 kDa subunit, orthologue of the human NADH:ubiquinone oxidoreductase core subunit S1 (NDUFS1). This subunit is part of the iron-sulphur domain of complex I and has three putative sites for iron-sulphur cluster binding. It is thought to compose part of the active site where NADH is oxidised. Mutations in this subunit in humans results in impaired complex I assembly, neurological pathology and death in childhood (Hoefs, Skjeldal et al. 2010). Reduced levels of this subunit are also observed in brain tissue from AD and Down syndrome patients (Kim, Vlkolinsky et al. 2001). The 75kDa subunit is essential for progression of normal apoptotic processes. When apoptosis is

triggered, caspase enzymes are activated and are responsible for DNA fragmentation (Enari, Sakahira et al. 1998). Caspases are also required to cleave OXPHOS complexes I and II in order to disrupt IMM function and permanently depolarise mitochondria (Waterhouse, Goldstein et al. 2001, Ricci, Gottlieb et al. 2003). NDUFS1 contains an essential for site for caspase cleavage. Mutations in this site impairs apoptotic processes in HeLa cells that have been permeabilised and exposed to caspase-3 (Ricci, Muñoz-Pinedo et al. 2004). Unlike in control cells, the membrane potential and ATP production was maintained in these mutants (Ricci, Muñoz-Pinedo et al. 2004).

UQCR-14 RNAi targets the ubiquinol-cytochrome c reductase 14 kDa subunit of complex III, orthologue of the human ubiquinol-cytochrome c reductase binding protein (UQCRB). UQCRB is required for redox-linked proton pumping, as well as maintenance and assembly of complex III. Low complex III levels were observed in mitochondria isolated from a patient with a deletion in *UQCRB*, who suffers from episodes of hypoglycaemia and metabolic acidosis (Haut, Brivet et al. 2003). Studies in yeast also suggest are role for this subunit in complex III maintenance and assembly (Hemrika, Lobo-Hajdu et al. 1994).

The complex IV targeted *COX5B* RNAi knocks down cytochrome c oxidase subunit 5B. In yeast, COX5B is essential for assembly of complex IV: when *COX5B* is mutated other subunits are present but do not assemble into the stable complex (Dowhan, Bibus et al. 1985). COX5B levels are selectively downregulated in blood from patients with multiple sclerosis (compared to the COX2 subunit of complex IV) (Safavizadeh, Rahmani et al. 2013).

ATPsynCf6 RNAi targets knockdown of ATPsynthase coupling factor 6, orthologue of human ATP synthase, H+ transporting, mitochondrial F_o complex subunit F6 (ATP5J). ATPsynCf6 is a component of the rod domain, required for interactions between the catalytic F_1 domain and proton pore F_0 domain, essential for coupling proton translocation and ATP production. Mutations in *ATP5J* in patients causes Leigh syndrome, with loss of activity as well as impaired stability/assembly of complex V (Morava, Rodenburg et al. 2006).

7.1.2 Validation of OXPHOS subunit RNAi knockdown

qRT-PCR of third instar larvae ubiquitously expressing these RNAi showed a significant knockdown of *UCQR-14*, *COX5B* and *ATPsynCf6*, in respective lines, of between 85 and 95%. Complex I *ND-75* levels were not decreased in larvae ubiquitously expressing *ND-75* RNAi. ND-75 levels could be further investigated by western blot, to evaluate whether protein levels of ND-75 are altered in these larvae. It may be that the RNAi does not actually knockdown ND-75 and that the phenotypes it causes are due to off target effects. I believe this is unlikely, as this RNAi also causes synaptic mitochondrial loss, decreased ATP:ADP and increased ROS, all phenotypes that might be expected when complex I activity is reduced, yet unlikely to be caused by off-target effects. I also tested a non-overlapping RNAi for *ND-75*, which displayed the same level of lethality at 25^{o}C with *D42-Gal4* and *OK371-Gal4*, and a very similar climbing deficit at room temperature with *OK371-Gal4*.

As I am interested in the effect of mitochondrial dysfunction on neurons, I focussed my analysis of *ND-75* RNAi on neuronal tissue. I performed qRT-PCR on dissected brains of larvae expressing *ND-75* RNAi pan-neuronally and found that *ND-75* was knocked down in the CNS. The brain tissue also contains non-neuronal cells, which do not express the RNAi, so the 50% knockdown observed in the qRT-PCR is most likely an underestimate of the actual level of knockdown in neurons. Therefore, to have an understanding of the level of knockdown in this RNAi compared to the other RNAi lines, I also tested *UQCR-14* knockdown, which had given the strongest (95%) knockdown ubiquitously. In this assay *UQCR-14* was reduced by 75%, although this was not significant, due to a large variation in control tissues. This suggests that *ND-75* knockdown is to a reasonably similar level to the other RNAi lines in the CNS.

I hypothesise that mRNA levels of *ND-75* might not be decreased in the entire organism due to some feedback mechanism in some tissue types. Perhaps, when protein levels of this core subunit of complex I decreases, transcription of the subunit is increased or translation is decreased, resulting in an upregulation of *ND-75* mRNA observed in the qRT-PCR. In mice with heterozygous *TFAM* knockout, mtDNA levels were reduced in all tissues investigated (Larsson, Wang et al. 1998). In the heart and kidney there was a corresponding decrease in mitochondrial transcripts, but in liver and muscle there was no significant change in transcripts, attributed to modifications in mRNA stability and

reduced translation in these tissues (Larsson, Wang et al. 1998). Knockout of the muscle specific isoform of the adenine nucleotide translocator (ANT), which exchanges ADP from the cytosol for ATP from the matrix, results in proliferation of mitochondria (Graham, Waymire et al. 1997). These studies demonstrate that in some situations and tissues mitochondrial dysfunction can induce feedback loops to regulate mitochondrial proteins. It is also possible that ubiquitous *ND-75* RNAi induces such a strong phenotype that most larvae die before third instar, and the larvae collected for the qRT-PCR are somehow more resistant to the RNAi.

I have shown that mRNA of subunits *ND-75, UQCR-14*, *COX5B* and *ATPsynCf6* were reduced by the respective RNAi lines. However, it would be informative to determine what effect knockdown of these subunits have on the OXPHOS complexes as a whole, in terms of assembly and activity. Knockdown of individual subunits does not necessarily result in impaired assembly of the whole complex, as seen in *Drosophila* with OXPHOS subunit RNAi that caused increased longevity (Copeland, Cho et al. 2009). However, the extent of knockdown in these flies was less severe with these RNAis (6- 47% knockdown when ubiquitously expressed), which resulted in benefits to the organism, as opposed to the detrimental effects observed in my models (Copeland, Cho et al. 2009). As discussed above, the subunits I have knocked down have also all been associated with reduced levels of the targeted complex in human disease, and implicated in maintenance and assembly of each respective complex.

In vitro studies have shown, that due to the formation of supercomplexes, RNAi of one subunit may also effect the activity of other OXPHOS complexes. Knockout of the complex IV subunit, *COX10*, in a murine skin fibroblast cell line causes loss of other complex IV subunits and complex IV activity (Diaz, Fukui et al. 2006). It also results in loss of complex I subunits and complex I activity (Diaz, Fukui et al. 2006). The loss of complex I activity was not seen when cells were treated with potassium cyanide (KCN), a pharmacological inhibitor of complex IV (Diaz, Fukui et al. 2006). This suggests that the physical presence of the complex IV subunit is required for correct complex I maintenance/assembly, regardless of its activity. Similarly, mutant complex III catalytic subunit cytochrome b, in mouse and human cell lines, impairs complex III assembly and activity as well as complex I activity and assembly (Acin-Perez, Bayona-Bafaluy et al. 2004). Again pharmacological inhibition of complex III activity, with antimycin A, was not sufficient to impair complex I assembly (Acin-Perez, Bayona-Bafaluy et al. 2004).

A complex I subunit mutation in the murine cell line, impaired assembly of complex I, but had no effect on complex III assembly, suggesting that inter-complex stability is not necessarily a reciprocal process (Acin-Perez, Bayona-Bafaluy et al. 2004).

7.1.3 Reduced synaptic mitochondria caused by mitochondrial dysfunction

In the five models of neuronal mitochondrial dysfunction I characterised in Chapter 3, I found loss of synaptic mitochondria to be a common phenotype. Mitochondria were labelled genetically using a mitochondrial targeted GFP (mitoGFP). Import of proteins with MTS into mitochondria requires a negative membrane potential. I therefore cannot exclude the possibility that the synaptic loss of mitochondria observed actually corresponds to depolarised mitochondria at the synapse, which are unable to import mitoGFP. A better method to assess mitochondrial number irrespective of membrane potential might be to use an antibody for a OMM protein, such as porin or TOM. However, due to the position of the NMJ on top of muscle tissue, this method would also identify the copious numbers of muscle mitochondria and so identifying mitochondria in the neuron would be problematic. Transmission electron microscopy (TEM) of NMJs would be required to determine if the number of mitochondrial structures really decrease. Simultaneous expression of mitoGFP and the vital dye tetramethylrhodamine methyl ester (TMRM), which only stains polarized mitochondria, would help to determine whether mitoGFP is able to label mitochondria that have lost their membrane potential.

The mechanisms behind this synaptic loss of mitochondria are currently unclear. The most obvious explanations would be decreased biogenesis, increased mitophagy, altered axonal transport of mitochondria or combinations of these factors. Increased mitophagy causes decreased mitochondrial mass in patients with *OPA1* mutations that impair mitochondrial fusion (Dombi, Diot et al. 2016). In primary cultures of rat hippocampal neurons, PINK1 and Parkin have been shown to be necessary for local axonal mitophagy (Ashrafi, Schlehe et al. 2014). *In vivo* analysis of mitochondria in *Drosophila Parkin* mutants showed an unexpected loss of mitochondria in the NMJ, similar to the phenotype I observed (Sung, Tandarich et al. 2016). Mitophagy was then compared in *Drosophila* primary motor neuron cultures to the same neurons *in vivo*. Autophagic vacuoles colocalised with mitochondria were observed in axons and the cell body *in vitro*, but not *in vivo*. Colocalisation was decreased in *Parkin* mutants, showing

Parkin mediates mitophagy in axons and cell bodies *in vitro*, but may not *in vivo*. The *Parkin* mutant flies had more tubular mitochondria in the soma of the motor neurons, a morphology change that may be expected in cells with inhibited mitophagy (Sung, Tandarich et al. 2016). The authors suggest that *in vivo*, Parkin mediates quality control by regulating fission and fusion in the soma (Sung, Tandarich et al. 2016). They hypothesise that a barrier between the cell body and the axons only allows good quality mitochondria to pass into the axon (Sung, Tandarich et al. 2016). *Drosophila* overexpressing *TFAM* in motor neurons have decreased synaptic mitochondria, but increased mitochondrial fragmentation in the cell body (Cagin, Duncan et al. 2015). This putative quality control barrier may provide an explanation for this phenotype. Mitochondrial dysfunction causes increased fragmentation in the soma, perhaps Parkin mediated, and few mitochondria are of high enough quality to pass the quality control barrier. Those mitochondria that do pass may gradually become more dysfunctional overtime as they move anterogradely down the axon to the NMJ. This could potentially be occurring in all of the models of mitochondrial dysfunction I investigated. A complete characterisation of mitochondrial biogenesis, autophagy and transport in my models of mitochondrial dysfunction would address this hypothesis.

In cultured rat hippocampal neurons, PINK1 and Parkin have also been shown to inhibit transport of depolarised mitochondria by phosphorylation and degradation of Miro, which attaches mitochondria to motor proteins (Wang, Winter et al. 2011). However, *in vivo* analysis of mitochondria mobility in segmental nerves of *Drosophila Parkin* mutants showed a decrease in mitochondrial flux, due to the reduced quantity of mitochondria, with no change in velocity or percentage of moving mitochondria (Sung, Tandarich et al. 2016). *In vivo* evidence in mice sensory neurons shows that mitochondrial anterograde transport is increased with neuronal stimulation, leading to accumulation of mitochondria at peripheral terminals (Sajic, Mastrolia et al. 2014). It is therefore possible that fewer mitochondria accumulate at the synapse when mitochondria are dysfunctional because of reduced neuronal activity in the five models of mitochondrial dysfunction I have characterised.

The loss of synaptic mitochondria was accompanied by small changes in bouton number and diameter. The significant decrease in bouton diameter in each OXPHOS complex RNAi line was much smaller than the dramatic loss of mitochondrial volume and number, so is unlikely to explain this mitochondrial loss. *ATPsynCf6* RNAi (CV)

also results in a modest but significant decrease in bouton number, whereas, *ND-75* RNAi (CI) induces a significant increase in bouton number. Overgrowth of boutons, measured as increased bouton number, has previously been observed in three *Drosophila* mutants with increased levels of ROS: homozygous *spinster (spin), sod1* and *sod2* mutants (Milton, Jarrett et al. 2011). Overexpression of genes for antioxidant enzymes (*sod1, catalase and thioredoxin-reductase*), and dominant negative *jnk* and *fos*, reduces bouton number in *spin* mutant flies, indicating a causative role of increased ROS, mediated by c-Jun N-terminal kinase (JNK) signalling (Milton, Jarrett et al. 2011). *ND-75* RNAi (CI) was the only RNAi line that I investigated that caused an increase in roGFP-Grx oxidation. It therefore seems plausible that the increased bouton number in *ND-75* RNAi, is caused by increased ROS. This also adds weight to the finding that the other RNAi lines did not increase ROS, as there was no associated increase in bouton number. *Sod1* mutants also had reduced bouton diameter, similar to *ND-75* RNAi, however, this phenotype was not observed in the other mutants, so may not be a direct effect of increased ROS (Milton, Jarrett et al. 2011). I observed decreased bouton diameter in all RNAis, suggesting that this may be due to a general response to mitochondrial impairment, such as impaired Ca^{2+} sequestering.

7.1.4 Measuring reactive oxygen species in models of mitochondrial dysfunction

Measuring ROS levels using fluorescent probes, such as mito-roGFP-Grx, has the benefit of providing ROS readouts for the tissue and compartment of interest alone. Use of these probes has shown that there are distinct differences in ROS in different tissues (e.g. reduced E_{GSH} in muscle versus the fat body) and cellular compartments (cytosolic H_2O_2 increases in wandering larvae versus feeding larvae, but mitochondrial H_2O_2 does not) (Albrecht, Barata et al. 2011). Independent changes in the H_2O_2 probe (mito-roGFP-ORP) and the E_{GSH} probe (mito-roGFP-Grx) also indicates that all ROS are not equal, and so if one measurement shows no increase in ROS, that does not necessarily mean there are no other redox changes (Albrecht, Barata et al. 2011).

In this thesis, I used mitochondrially targeted roGFP-Grx to measure the redox state of the GSH/GSSG redox couple (Albrecht, Barata et al. 2011). This means I can only comment on the mitochondrial E_{GSH} in neurons with OXPHOS subunit knockdown. I found that the E_{GSH} was reduced in *COX5B* and *ATPsynCf6* RNAi (CIV and CV),

unchanged in *UQCR-14* RNAi (CIII) and oxidised in *ND-75* RNAi, thus demonstrating a major difference between the models of mitochondrial dysfunction.

ROS are produced as a by-product of mitochondrial dysfunction at complex I, complex II and complex III (see Introduction 1.2.4.1). The vast majority of mitochondrial ROS are formed at complex I (Andreyev, Kushnareva et al. 2005). This may explain why *ND-75* knockdown, results in E_{GSH} oxidation. Knockdown of the *Pdsw* subunit of complex I in the *Drosophila* eye disc also results in increased ROS production. In this tissue the ROS produced arrests the cell cycle in the G1 phase (Owusu-Ansah, Yavari et al. 2008). Knockdown of a complex IV subunit, *COX5A*, in the eye disc also arrests the cell cycle. However, this occurs via an alternative pathway (AMPK signalling) and ROS levels are found to drop by 20% in these cells (Owusu-Ansah, Yavari et al. 2008). Reduced protein and DNA oxidative damage has also been reported in neuron specific complex IV subunit, *COX10*, knockout mice (Fukui, Diaz et al. 2007). Conditional knockout of *TFAM* in murine skin cells results in decreased mtDNA encoded protein expression, decreased oxygen consumption and decreased ROS production, measured in primary cultures (Hamanaka, Glasauer et al. 2013). Taken together these data indicate that increased ROS production is not an inevitable consequence of mitochondrial dysfunction. To further investigate the role of ROS in these models, it would be informative to evaluate cysteine redox changes of neuronal proteins. This can be done using oxidative isotope-coded affinity tags (Menger, James et al. 2015).

To analyse the overall 'health' of neuronal mitochondria, a second *in vivo* ROS reporter, mitoTimer, was used. I found that *ND-75* RNAi induced a raised level of mitoTimer oxidation in motor neuron cell bodies and at the NMJ. The other models caused increased mitoTimer at the NMJ, apart from *UQCR-14* RNAi, which did not affect mitoTimer oxidation. Unlike the roGFP fused probes, which change fluorescence due to oxidation of inserted cysteine residues, fluorescence emitted by mitoTimer is irreversibly changed to red on oxidation due to oxidation of a tyrosine residue. This means that fluorescent changes in mitoTimer are more difficult to interpret. Increased levels of mitochondrial ROS would result in an augmented red signal, however, cytosolic ROS could potentially also have the same effect, due to the fact that mitoTimer is translated in the cytosol before translocating to the mitochondria (Laker, Xu et al. 2014). Mitochondrial proteins are only processed and folded once inside the matrix which might protect mitoTimer from oxidation in the cytosol that alters its

fluorescence, however, this has not yet been tested experimentally. Red fluorescence can also be an indicator of the age and turnover of mitochondrial proteins, as oxidation accumulates over time (Terskikh, Fradkov et al. 2000). Analysis of hippocampal neurons containing the construct shows young mitochondria in the soma and as the distance from the soma increases so does the ratio of red signal. Expression of a constitutively active version of *RHOT1*, a mitochondrial motor protein, increased the homogeneity of signal within the cells, indicating that increased red signal does correspond to increased age (Ferree, Trudeau et al. 2013). Pulsing expression of *mitoTimer* in HeLa cells reveals that *mitoTimer* can also be used to study biogenesis and mitophagy of mitochondria (Hernandez, Thornton et al. 2013).

The increased E_{GSH} observed in the NMJ of *ND-75* RNAi expressing larvae suggests that the changes in mitoTimer oxidation seen in this model are probably due to elevated ROS levels. This does not, however, exclude the possibility that there are also impairments in mitochondrial turnover contributing to the mitoTimer oxidation. *UQCR-14* RNAi did not affect the E_{GSH} or mitoTimer oxidation, so presumably in this model there is no ROS pathology or impairment of mitochondrial turnover. *COX5B* RNAi, *ATPsynCf6* RNAi and *TFAM* overexpression all had reduced mitochondrial E_{GSH}, but show greater oxidation of mitoTimer in NMJ mitochondria than control. The possibility of increased ROS in these flies, that affects other redox species without affecting GSH/GSSG cannot be formally ruled out, however, I think this result is more likely to indicate aged mitochondria either due to impaired biogenesis, reduced mitophagy or decreased transport of newly synthesised mitochondria to axonal terminals.

7.1.5 Analysis of ATP:ADP ratios

Finally, in order to characterise the mitochondrial dysfunction in the different models, I assessed the ATP:ADP ratio *in vivo* specifically in motor neurons, with the genetic construct Perceval. Almost all cellular work requires an input of energy, directly or indirectly, released from hydrolysis of the high energy bonds in ATP (Hardie and Hawley 2001). ATP is converted into ADP or AMP on hydrolysis, depending the number of phosphate groups removed. ATP:ADP levels are normally tightly controlled and maintained around 10:1, regardless of cellular activity. The normal ATP:AMP ratio is approximately 100:1 and therefore is a more sensitive measure of cellular energy (Hardie and Hawley 2001). Due to the greater sensitivity of the ATP:AMP ratio to

energetic changes, it was proposed that cellular sensors of energy may respond to this ratio. Indeed, the ATP:AMP ratio has been shown to regulate enzymatic activity, such as phosphofructokinase in yeast (Ramaiah, Hathaway et al. 1964) and to activate feedback mechanisms that increase production and decrease consumption of ATP, via AMP-activated kinase (AMPK) (Carling, Zammit et al. 1987). However, levels of AMP are usually lower than ATP and ADP by one to two orders of magnitude, so competitive binding of ADP to AMPK is a more probable event (Hardie, Carling et al. 2011). It is now known that AMPK also responds to ADP levels, which binds competitively with ATP and AMP at two sites within the kinase (Hardie 2011). Murine cells with *AMPK* knocked out are more sensitive to metabolic stress, such as treatment with mitochondrial toxin metformin, resulting in larger changes in AMP:ATP and ATP:ADP ratios than control (Foretz, Hebrard et al. 2010).

In order to measure ATP:ADP *in vivo*, the genetic construct Perceval has been developed (Berg, Hung et al. 2009). This construct has been used to measure ATP:ADP changes in primary cultures of mouse and human pancreatic cells (Li, Shuai et al. 2013). A version of the construct tuned to the expected ATP:ADP ratio in mammalian cells, PercevalHR, has also been used to measure ATP:ADP in murine primary neuronal, murine astrocyte cultures and primary neuronal cultures from rats (Tantama, Martinez-Francois et al. 2013, Rueda, Traba et al. 2015, Vaarmann, Mandel et al. 2016). This thesis is the first reported use of Perceval to measure ADP:ATP *in vivo*. I created flies containing this construct and used it to measure the ATP:ADP ratio in motor neuron cell bodies of *ATPsynCf6* RNAi, *ND-75* RNAi and *TFAM* overexpressing larvae. Due to time constraints I am yet to measure the ATP:ADP ratio in *UQCR-14* RNAi and *COX5B* RNAi larvae. Data from *ATPsynCf6* RNAi, *ND-75* RNAi and *TFAM* overexpression reveals another difference between complex I knockdown and the other models of mitochondrial dysfunction. ATP:ADP was unchanged in the cell bodies of motor neurons containing *ATPsynCf6* RNAi or *TFAM* overexpression. However, in larvae expressing *ND-75* RNAi, levels of ATP were decreased compared to ADP. ATP levels have been measured in many systems in which activity of individual complexes are impaired by chemicals inhibitor. For example, in cultured rat retinas, rotenone inhibition of complex I causes ATP depletion, in this model neuronal cells were found to be more susceptible to ATP loss than glial cells (Han, Casson et al. 2014). Inhibition of individual OXPHOS subunits does not always result in reduced ATP however. Specific inhibition of complex III activity in MEF cells, with a low dose (5ng/ml for 8

hours) of antimycin A, did not affect ATP levels (Ma, Jin et al. 2011). This dose was sufficient to inhibit autophagy in these cells, so it is unlikely that the dose was too low to affect complex III function. In fact, it appears that there is a threshold of activity required for ATP production and it is only when activity of a complex is below this threshold that ATP levels are decreased. In isolated mitochondria from *Drosophila,* with a large scale mtDNA deletion (5kb), complex I activity was reduced by 50% and complex III activity was reduced by 30%, however ATP synthesis was not impaired. Addition of rotenone, reducing complex I activity by a further 20% was required to reduce ATP synthesis (Farge, Touraille et al. 2002). The importance of glycolytic metabolism was highlighted in a study of hippocampal neurons isolated from embryos or postnatal rats. Oligomycin inhibition of complex V did not affect ATP in embryonic cultures, which rely mainly on glycolysis, but caused a sharp loss of ATP in postnatal cultures, which depend on OXPHOS (Surin, Khiroug et al. 2012). Loss of the ND-75 subunit may therefore have a more severe effect on the complex I OXPHOS activity than loss of the other subunits on complex III, IV and V, or these flies may be less able to use compensatory methods to produce ATP.

It would be preferable to measure ATP:ADP levels in the NMJ in my five models of mitochondrial dysfunction, as this is where the mitochondria are most dysfunctional. Limitations in the strength of the Perceval signal have meant I have been unable to carry out this experiment. In order to have a measurable signal in the cell body, I have had to express three copies of the Perceval construct. To increase the signal to allow measurement in the NMJ I may have to add a fourth copy of the transcript or perhaps a second *Gal-4* driver.

A second limitation of this construct, is its sensitivity to intracellular pH changes. Perceval fluorescence measured in HEK cells, in which the bathing solution was changed from 6.9 to 6.6, did change as a function of pH (Berg, Hung et al. 2009). As pH decreases, the ratio of 490/430nm emission also decreased, which would otherwise be interpreted as a loss of ATP:ADP ratio. This suggests that the lower ATP:ADP ratio observed in *ND-75* RNAi larvae could actually be a measurement of a lower pH. Glycolytic inhibition with 2-deoxyglucose (2-DG) has been shown to lower intracellular pH by 0.2 units, in cell culture (Pianet, Merle et al. 1991). Activity of neurons is also associated with pH changes, *in vivo* pH measurements in the cytosol of *Drosophila* motor neurons decreased by approximately 0.16 units on stimulation and by 0.3 units

when stimulated repeatedly (Rossano, Chouhan et al. 2013). Whether such large pH changes occur in the soma *in vivo* is not yet known, although similar changes have been observed *in vitro* in the soma of cultured frog motor neurons (Endres, Ballanyi et al. 1986). It is therefore possible that the lack of change observed in *ATPsynCf6* RNAi and *TFAM* overexpression is actually due to a reduced neuronal activity, leading to a higher pH, masking an ATP:ADP decrease. However, within the cellular range of pH, the dose response of Perceval to ATP levels was remarkably robust in HEK cells (Berg, Hung et al. 2009). Addition of 2-DG to these HEK cells did not alter intracellular pH measurements, although changes in Perceval signalling indicated a 20% in ATP:ADP ratio (Berg, Hung et al. 2009). Whether the Perceval changes I observed *in vivo* actually correspond to changes in ATP:ADP therefore depends on whether pH is changing in these neurons. ATP:ADP measurements in rat cortical neurons using PercevalHR (which is still sensitive to pH), showed an 23% increase in ATP:ADP when PGC1α was overexpressed (Vaarmann, Mandel et al. 2016). This data was not controlled to pH, and pH was not measured. However, the result was confirmed by ATP measurements via luciferase activity normalised by Renilla. This suggests that Perceval measurements may be accurate reflections of ATP:ADP in unstimulated neurons. To allow more accurate interpretation of the Perceval signal, pH should be measured simultaneously and Perceval normalised to pH changes. Measuring neuronal pH changes *in vivo* provides a challenge due to impermeability of the blood brain barrier, however, genetically encoded pH indicators have been developed in *Drosophila*, which would make this possible (Rossano, Chouhan et al. 2013).

7.1.6 Summary

At first appearance, mitochondrial dysfunction caused by all the models of mitochondrial dysfunction I used appeared to have a similar effect, loss of synaptic mitochondria and impaired climbing activity. Further characterisation revealed that there are actually differences in these models even though they have similar outcomes. Similarly, ubiquitous knockdown of five OXPHOS subunits in *Drosophila,* cause extended lifespan, but also have different effects on mitochondrial and cellular function (Copeland, Cho et al. 2009). Two of these lines target complex I subunits and the others target complex III, IV and V subunits. None of the RNAi lines caused a reduction in ATP levels, although one of the complex I RNAis actually increased ATP levels. Fertility was reduced in all of the lines, apart from the complex IV RNAi and although

three of the RNAi lines had increased resistance to ROS, the complex IV and V RNAi did not (Copeland, Cho et al. 2009). This demonstrates that different mitochondrial insults, may induce different changes even if the resultant phenotype is the same.

qRT-PCR evaluation of the RNAi lines indicated that the level of knockdown was similar in all RNAi models (see Discussion 7.1.2), so differences between the RNAi lines is unlikely to be due to different 'strengths' of knockdown. The effects of *UQCR-14* knockdown (CIII), were less severe than the other RNAi (the climbing deficit and synaptic mitochondrial loss was more modest and no ROS changes were detected). Complex III mutations are also rarely associated with human disease (Benit, Lebon et al. 2009). Conversely, the complex I *ND-75* knockdown induced the strongest deficit (in climbing, synaptic mitochondrial loss and ROS increase measured by mitoTimer). It also was the only model to have an oxidised mitochondrial E_{GSH} at the NMJ, evidence of oxidation in the VNC and a decreased ATP:ADP ratio. These differences may be due to the fact that complex I is the major site of ROS production in the mitochondria. *COX5B* RNAi (CIV), *ATPsynCf6* RNAi and *TFAM* overexpression had similar phenotypes in all assays (although ATP:ADP has not yet been measured for *COX5B* RNAi). Other features of these models that would be interesting to characterise include Ca^{2+} sequestering, metabolic changes and synaptic structure and activity.

7.2 Evaluating the transcriptional changes in different models of mitochondrial dysfunction.

Differential mito-nuclear signalling in individual tissue types has been demonstrated in the study of mitochondrial haplogroups. Mitochondrial haplotypes refer to mtDNA variants due to single nucleotide polymorphisms (SNPs) mostly in non-coding regions of D-loop. The human population can be divided into geographically distinct 'haplogroups', based on SNPs accumulated in a maternal lineage (Herrnstadt, Elson et al. 2002). Haplogroups confer a retrograde signal to the nucleus, as they alter the epigenetic status of nuclear DNA. One of the nine common European haplogroups, group J, has been shown to increase DNA methylation, in human blood tissue and *in vitro* in cybrids (Bellizzi, D'Aquila et al. 2012). These methylation changes are also accompanied by low ATP and ROS levels (Bellizzi, D'Aquila et al. 2012). This particular haplogroup has also been associated with increased longevity and decreased risk of PD in humans (De Benedictis, Rose et al. 1999, van der Walt, Nicodemus et al. 2003). Analysis of transgenic mice heteroplasmic for two haplotypes, showed that there was differential segregation of the two haplotypes in blood and spleen tissue versus kidney and liver tissue (Jenuth, Peterson et al. 1997). This data has been supported by evaluation of mtDNA haplotypes in four heteroplasmic mouse models, which show biased segregation of haplotypes in numerous tissues, including the brain (Burgstaller, Johnston et al. 2014). This suggests that the demands of different tissues effects segregation and proliferation of mtDNA haplotypes. As different haplotypes have different effects on nuclear epigenetics, differential segregation of mtDNA variants is likely to result in different epigenetic regulation of individual tissues. It also seems probable that these tissue specific demands would influence the cellular response to mitochondrial dysfunction, in that cell type. 'Conplastic' mice with genomic DNA from one strain and mtDNA from another (with a different haplotype), were very similar to control mice when young, however, with age a variety of differences were observed. Conplastic mice aged more healthily, with reduced tumour formation, telomere shortening and an increased median lifespan. Transcriptional changes were observed in these mice at 12 weeks, long before phenotypic differences were observed, including changes in genes required for free radical scavenging and carbohydrate and lipid metabolism (Latorre-Pellicer, Moreno-Loshuertos et al. 2016).

With the aim of understanding the retrograde responses occurring in the five models of neuronal mitochondrial dysfunction that I characterised in Chapter 3, I carried out microarray analysis to explore transcriptional changes occurring in these larvae. The RNAis and *TFAM* overexpression were driven with the pan-neuronal driver *nSyb-Gal4* and RNA was prepared from CNS tissue of third instar larvae. This allowed analysis of specifically neuronal changes, although the presence of other cell type in the CNS will have diluted the changes observed. Theoretically, transcriptional changes could also occur in glial cells in response to the mitochondrial dysfunction in neurons. It is also important to note, that the neuronal population is also made up of heterogeneous subtypes, which may respond differently to mitochondrial dysfunction. Never the less, robust transcriptional changes were observed in each mitochondrial dysfunction model (358- 840 genes were significantly altered). Approximately 50% of the genes in each model were only significantly changed in that model, demonstrating that the retrograde response depends on the mitochondrial insult. Roughly 50% of genes in each model were also altered in at least one other mitochondrial dysfunction model. Analysis of the common genes changed between each pair of models gave a significant positive correlation in each case. This indicates that there are also commonly regulated responses to mitochondrial dysfunction, which may be particularly important as therapeutic targets.

7.2.1 Pathways affected in all mitochondrial dysfunction models

Eleven genes were found to be significantly regulated in all conditions. *Impl3,* the *Drosophila* gene that encodes lactate dehydrogenase, was one of these genes, and was upregulated in all genotypes. Lactate dehydrogenase catalyses the reversible conversion of pyruvate to lactate, thus removing pyruvate to allow glycolytic reactions to proceed. Upregulation of this gene suggests increased glycolytic activity. Glycolytic processes also were identified in GO enrichment analysis of the mitochondrial dysfunction models. Compensatory upregulation of glycolysis is consistently identified in studies of the retrograde response to mitochondrial dysfunction. Changes in glycolytic genes were overrepresented in *Drosophila* S2 cells when the complex IV subunit *COX5A* was knocked down (including upregulation of *Impl3*) (Freije, Mandal et al. 2012). These transcriptional changes were accompanied by increased lactate in the media and an increased glycolytic capacity (Freije, Mandal et al. 2012). Mutations in the gene for mitochondrial ribosome protein S12, are associated with deafness in humans (Prezant,

Agapian et al. 1993). In a *Drosophila* model, in which the *tko* gene which encodes *Drosophila* mitochondrial ribosome protein S12 is mutated, *Impl3* is also upregulated. A cellular shift to alternative metabolism was also indicated in these flies by upregulation of genes involved in sugar transport, amino acid and fatty acid catabolism (Fernandez-Ayala, Chen et al. 2010). These pathways were also repeatedly identified in my five models of mitochondrial dysfunction. Additionally, a glucose transmembrane transporter (*CG10960*) was significantly upregulated in all five genotypes. *Pink1* mutant *Drosophila* also show metabolic shifts, with decreased TCA metabolites and increased levels of glutamate and glutamine (Tufi, Gandhi et al. 2014). In the CNS of *Parkin* mutant larvae, lactate levels increase (Vincent, Briggs et al. 2012). Moreover, metabolic reprogramming is observed in patients with mitochondrial diseases, most patients with mitochondrial oxidative defects have lactic acid build up (Robinson 2006). The search for a biomarker to aid diagnosis of Parkinson's disease has also revealed a significant increase in pyruvate levels in the blood of people with Parkinson's disease (Ahmed, Santosh et al. 2009).

In all conditions, expression of synapse protein 24 (Snap24) was strongly downregulated (-6.81 to -12.59 fold). Snap24 is a SNARE protein from the Snap25 subfamily (Niemeyer and Schwarz 2000). Originally, SNARE proteins were thought to mediate docking of vesicles to target membranes, however, now they are actually thought to be more important for membrane fusion. Exocytosis of docked vesicles is blocked in a *Drosophila* mutant that impairs SNARE formation (Littleton, Chapman et al. 1998). Snap25 protein is localised to synaptic regions and neuropil, whereas puncta of Snap24 are observed diffusely throughout neurons and predominantly in the soma (Niemeyer and Schwarz 2000). Despite its localisation, Snap24 has been shown to functionally replace *Snap25* knockout in *Drosophila*, maintaining neuronal transmission. However, this does not occur when *Snap25* is present but mutated, although overexpression of *Snap24* in this context does rescue neuronal activity. This indicates that Snap24 is unlikely to normally facilitate synaptic transmission (Niemeyer and Schwarz 2000). The precise role of Snap24 in vesicle trafficking is still unclear, however, its dramatic downregulation in all 5 models of neuronal mitochondrial dysfunction suggests that it is important in this context. Investigating the expression and requirement of Snap24 in these models will be of great interest.

The gene for Rieske iron-sulfur protein (RFeSP), a catalytic subunit of complex III (see Introduction 1.1.4), was also significantly altered in all five conditions. *RFeSP* was downregulated in every condition in which single OXPHOS subunits were knocked down, yet upregulated in *TFAM* overexpressing larvae, in which translation of all mitochondrial encoded proteins is likely to be reduced. Alongside its catalytic role in electron transfer, RFeSP is implicated in assembly of complex III into dimers: addition of RFeSP to immature yeast complex III results in a dramatic shift in its molecular weight (Zara, Conte et al. 2009). A role for RFeSP in assembly of supercomplexes has also been proposed, as supercomplex assembly was inhibited in yeast mutant for *RFeSP* (Zara, Conte et al. 2009). It would be particularly interesting to carry out blue native gels of the five models of mitochondrial dysfunction, to assess supercomplex assembly in the light of this finding. Perhaps in neurons with damage to a single complex, *RFeSP* is downregulated to inhibit supercomplexes forming with the damaged complex. In cases in which general mitochondrial protein translation is inhibited, *RFeSP* may be upregulated to promote supercomplex formation with any subunits that are present, in an attempt to boost OXPHOS. If this theory is correct, one might expect to see upregulation of *RFeSP* when mitochondrial translation is inhibited, such as *tko* mutants. However, *RFeSP* was strongly downregulated in whole fly homogenates of *tko* mutant *Drosophila* (Fernandez-Ayala, Chen et al. 2010). It would be interesting to see if this is the case in neuronal tissue alone.

These microarrays have given a glimpse into the pathways that are transcriptionally regulated in response to mitochondrial dysfunction. However, they are not without limitation. For example, genes expressed at very low levels that change stochastically can give high statistically significant result (Tarca, Romero et al. 2006). Analysis of hundreds of Affymetrix S98 yeast gene chips has shown that there can also be positional bias, in which the position of the probe on a chip can affect correlations between probes (Homouz, Chen et al. 2015). More rigorous processing and evaluation of the data can help to remove these limitations, however, I am using the microarray data as a starting point to identify genes and pathways involved in the retrograde response to mitochondrial dysfunction. It is therefore most important for me to test data and hypotheses from microarrays experimentally *in vivo*.

7.2.2 HIF signalling in neuronal mitochondrial dysfunction

HIF-1α is known to transcriptionally regulate a metabolic switch to glycolysis, by directly regulating genes such as *Impl3* (Bruick and McKnight 2001). In HeLa cells, HIF has also been shown to regulate the subunit composition of complex IV, to optimise the complex's activity in conditions of low oxygen (Fukuda, Zhang et al. 2007). HIF may also act to globally inhibit translation, while promoting transcription of stress related proteins (Liu and Simon 2004). Global translation inhibition has been identified as part of the UPR^{mt}, as a method of reducing demand on chaperone proteins (see Introduction 1.4.2.3), and may also be beneficial for energy conservation when mitochondria are dysfunctional. Previous analysis of neuronal *ATPsynCf6* RNAi and *TFAM* overexpression revealed an upregulation of *Thor*, the *Drosophila* homologue of 4E-BP (Cagin, Duncan et al. 2015). Sima, the *Drosophila* homologue of HIF-1α, was shown to regulate *Thor* expression *in vivo* in the third instar larval CNS (Cagin, Duncan et al. 2015). Hypophosphorylated 4E-BP acts to inhibit global translation by inhibiting cap dependant translation from the 5' end of mRNAs. *Thor* mutant flies have a reduced lifespan in starvation conditions compared to controls and burn fat supplies more quickly, leading to the hypothesis that 4E-BP acts as a metabolic brake in response to environmental stress (Teleman, Chen et al. 2005). HIF-1α has previously been suggested to regulate the mitochondrial retrograde response in *Drosophila* S2 cells with *COX5A* knockdown. Out of a stringent list of 22 genes altered in these cells, putative HIF-1α binding sites were identified within close proximity of the transcriptional start site of 19 genes. I therefore investigated the role of HIF-1α in mitochondrial retrograde signalling further, by knocking down the *Drosophila* orthologue, *sima*, in each model of mitochondrial dysfunction.

I evaluated the effect of *sima* knockdown in motor neurons on the climbing and wing inflation phenotypes (in models which cause inflation phenotypes) of the OXPHOS RNAi lines and *TFAM* overexpression. It is important to note that the exact mechanisms underlying these two phenotypes are unclear, but they can be used as a tool to assess neuronal function. Mitochondrial dysfunction is induced in neurons and phenotypes in processes that require neuronal input are disrupted. Genetic modifications that alter these phenotypes indicate a change in neuronal function, this may be due to changes in mitochondrial function or alterations in the neuronal response to mitochondrial dysfunction, without impact on the mitochondria themselves. I also assessed the effects

of *sima* knockdown on viability when mitochondrial dysfunction was induced pan-neuronally. Knockdown of *sima* was able to rescue the phenotypes caused by mitochondrial dysfunction in *UQCR-14* RNAi (CIII), *COX5B* RNAi (CIV), *ATPsynCf6* RNAi (CV) and *TFAM* overexpression models in at least one of these assays. Phenotypes caused by complex I *ND-75* RNAi were never rescued by *sima* knockdown. This raises two main questions: why does *blocking* retrograde signalling via *sima* rescue mitochondrial dysfunction phenotypes and why is complex I knockdown insensitive to this rescue?

7.2.3 Inhibition of retrograde signalling can provide salutatory effects

The counterintuitive finding that blocking the retrograde response rescues phenotypes caused by mitochondrial dysfunction has actually also been shown in a number of other studies. As previously mentioned (see Discussion 7.1.1), mutant complex IV subunit, *COX5B*, inhibits cell cycle progression in *Drosophila* eye discs through AMPK phosphorylation, which activates p53 (Mandal, Guptan et al. 2005). Whereas, complex I subunit, *Pdsw*, mutant inhibits cell cycle progression in *Drosophila* eye discs through redox signalling via JNK and FOXO (Owusu-Ansah, Yavari et al. 2008). Inhibition of these retrograde signals, by *p53* and *FOXO* mutations respectively, allows cells in the eye disc to re-enter the cell cycle (Owusu-Ansah, Yavari et al. 2008). Mutations in mitochondrial ribosome protein 12S, cause deafness in humans and mice due to ROS-dependant AMPK phosphorylation, which activates the proapoptotic transcription factor E2F1 (Raimundo, Song et al. 2012). Inhibition of this retrograde response, in a *E2F1* heterozygous mutant, restores hearing in mice (Raimundo, Song et al. 2012). Taken together, these data show that inhibition of retrograde responses can in some cases be beneficial.

This suggests that the retrograde response to mitochondrial dysfunction can itself have negative impacts on the cell. I think there may be three reasons for this. Firstly, some cellular adaptations to mitochondrial dysfunction induced by retrograde signalling, such as reduced protein translation, may confer benefits in the short term. This would allow cells to cope with transient dysfunction of mitochondria. However, in chronic mitochondrial dysfunction, in disease and *in vivo* models, these adaptations may contribute to cellular dysfunction. Activation of retrograde pathways due to mild mitochondrial dysfunction can result in salutary effects (Copeland, Cho et al. 2009).

Mild (50%) knockdown of *ND-75* in *Drosophila* muscles causes developmental delay and lethality before adulthood (Owusu-Ansah, Song et al. 2013). However, transient expression of this RNAi (24 hours) during development, using temperature sensitive *Gal-80* increased the longevity of flies compared to controls (Owusu-Ansah, Song et al. 2013). Expression of the antioxidant catalase abolishes the longevity benefits, and forced activation of the UPR^{mt} proteins, Hsp60 and Hsp60C, in muscle tissue was sufficient to increase lifespan (Owusu-Ansah, Song et al. 2013). These experiments demonstrate that transient mitochondrial dysfunction can be beneficial, due to retrograde signalling via ROS and the UPR^{mt}, whereas continuous mitochondrial dysfunction is detrimental. Secondly, retrograde responses that are advantageous in one cell type may have a negative impact on another tissue type that has different metabolic demands. Evidence from the modifier screen I carried out suggests that this might be the case (see Discussion 7.4.1). Neuronal tissue may be particularly sensitive to HIF-1α over-activity: genetic activation of HIF signalling in murine retinal pigment epithelium cells is sufficient to induce neurodegeneration (Kurihara, Westenskow et al. 2016). Finally, the effect of the retrograde response may be interrelated to the other cellular changes induced by mitochondrial dysfunction. HIF signalling may therefore only be beneficial in incidents of mitochondrial dysfunction when ROS levels increase. *Sima* knockdown improves phenotypes in mitochondrial dysfunction which does not increase ROS, e.g. *UQCR-14* RNAi, *COX5B* RNAi, *ATPsynCf6* RNAi and *TFAM* overexpression but not *ND-75* RNAi when ROS levels were seen to increase. *ND-75* RNAi also caused decreased ATP:ADP ratio and so it could be this difference which limits the beneficial effects of *sima* knockdown.

7.2.4 Mechanisms of HIF-1α regulation

HIF-1α is canonically regulated by decreased oxygen concentration, however it is also regulated by ROS, TCA metabolites, growth factors, cytokines and Ras/MAPK signalling (Masoud and Li 2015). In the five mitochondrial dysfunction models I investigated, increased ROS was evident in *ND-75* RNAi (which did not respond to *sima* knockdown), ROS was unchanged in *UQCR-14* RNAi and possibly decreased in the other three models (all of which were somewhat rescued by *sima* knockdown), this suggests that any changes in HIF in these models is unlikely to be mediated by ROS. Hypoxic regulation of HIF involves stabilisation of HIF-1α due to inhibition of the PHDs which target HIF-1α for degradation. Recent experiments in mice with *TFAM*

knockout in the skin demonstrate that in this tissue hypoxic stabilisation of HIF-1α requires functional ETC in the mitochondria (Hamanaka, Weinberg et al. 2016). Knockdown of *RFeSP*, which is a component of complex III (see Discussion 7.2.1) also reduced HIF-1α stabilisation in hypoxic conditions *in vitro* (Brunelle, Bell et al. 2005:Guzy, 2005 #1093). It is thought that hypoxia mediated HIF-1α stabilisation in these system requires ROS production, and destabilisation of HIF-1α is due to reduced ROS in these cells. This suggests that the mechanisms modulating HIF activity in hypoxic conditions may differ to mitochondrial dysfunction in normoxia.

There was no significant change in *sima* transcript levels in any of the microarrays I carried out, suggesting that regulation of Sima in these models of mitochondrial dysfunction is happening on the protein level rather than transcriptional level. Regulation of translation or stability of HIF-1α therefore may be altered in mitochondrial dysfunction. Western blots of HIF-1α protein levels would help determine if changes in these processes are causing an increase in HIF-1α protein levels. Alternatively, post-translational modifications that modify the activity of HIF-1α may also be responsible for the HIF mediated changes seen in mitochondrial dysfunction.

Impairments in TCA cycle components, succinate dehydrogenase (SDH, also complex II) and fumarate hydratase (FH), induces a 'pseudo-hypoxia' via inhibition of PHDs, that normally target HIF-1α for degradation, as TCA metabolites are required for PHD activity (MacKenzie, Selak et al. 2007). Stabilisation of HIF-1α in this manner is associated with tumour formation (Dahia, Ross et al. 2005, Pollard, Briere et al. 2005). Stabilisation of HIF-1α may also be promoted by binding with Hsp90. Two pharmacological agents, which disrupt Hsp90- HIF-1α interactions, have been shown to promote proteasomal degradation of HIF-1α (Osada, Imaoka et al. 2004, Han, Oh et al. 2005). Translation of HIF-1α is not yet well understood, however, numerous pathways have been identified which appear to promote HIF-1α protein synthesis, such as topoisomerases I and II, the mTOR pathway and tyrosine kinase receptor pathways (Masoud and Li 2015). Activity of HIF-1α is also inhibited in normoxia by factor inhibiting HIF-1 (FIH-1), which hydroxylates HIF-1α to inhibit its interaction with its coactivators, such as CBP/p300 (Lando, Peet et al. 2002). Further investigation is required to determine which of these pathways are involved in HIF-1α mediated neuronal retrograde signalling.

7.2.5 Interactions between complex I and HIF-1α

The interplay between complex I and HIF-1α has been mainly studied in the context of cancer. Six hundred mutations in complex I have been associated with different cancers, which have been reported to either increase growth and invasiveness of tumours or induce tumour arrest due to an inability to switch to Warburg metabolism (Garcia-Heredia and Carnero 2015). As described previously (see Discussion 7.2.4), knockout of *TFAM* in murine skin cells impairs ROS-dependent HIF-1α stabilisation. So the effect of complex I mutations on ROS levels is likely to affect HIF stabilisation, at least in some tissue types. In a human thyroid cell line with a truncation mutation in the mitochondrially encoded *MT-ND1* subunit of complex I, HIF-1α instability is independent of ROS signalling (Porcelli, Ghelli et al. 2010). Mutations in complex I have also been shown to alter HIF stabilisation via alterations in TCA cycle metabolites. A complex I null in a human bone cell line, with an *MT-ND1* subunit knocked out, was unable to stabilise HIF-1α, in cell culture (Calabrese, Iommarini et al. 2013). This was accompanied by an increase in α-ketoglutarate (α-KG) compared to succinate (SA) (Calabrese, Iommarini et al. 2013). This complex I deficiency caused an accumulation of NADH which inhibits the conversion of α-KG into SA in the TCA cycle (Porcelli, Ghelli et al. 2010). The levels of these metabolites then affects HIF-1α stabilisation as α-KG is the substrate of PHDs and so required for HIF-1α hydroxylation (Figure 7.1) (Porcelli, Ghelli et al. 2010). PHD inhibitors induced HIF-1α stabilisation in the human thyroid *MT-ND1* mutant cell line, and increased the tumourigenic potential of *MT-ND1* null human bone cell line (Porcelli, Ghelli et al. 2010, Calabrese, Iommarini et al. 2013). I speculate that in the *ND-75* RNAi neurons an increased α-KG:SA ratio may be inhibiting HIF-1α, which might explain why *sima* knockdown has no effect in these flies.

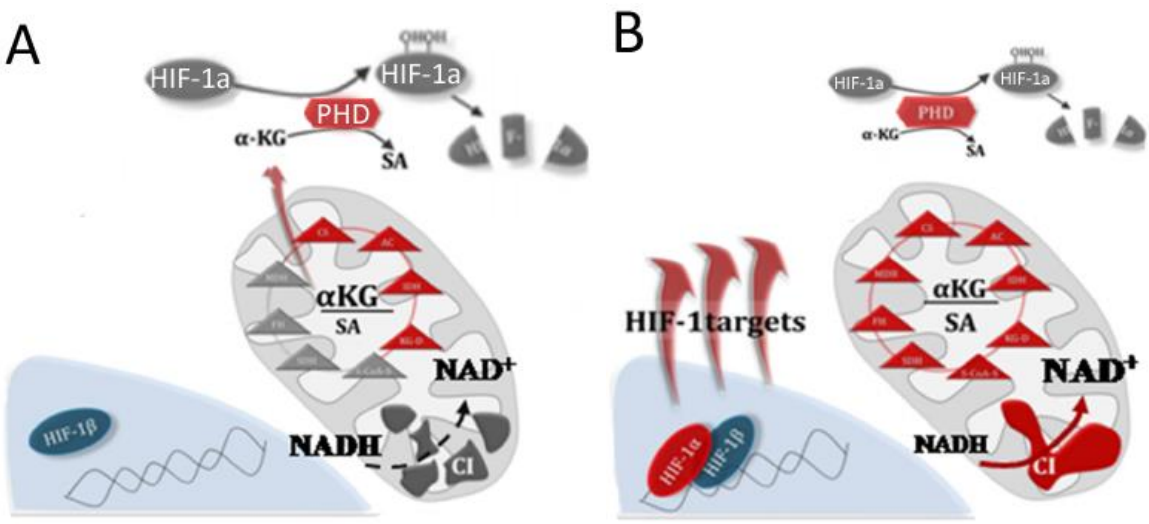

Figure 7.1 Complex I deficiency can inhibit HIF-1α stabilisation
(A) When complex I (CI) activity is impaired, NADH accumulates, which inhibits αKG conversion into SA. αKG is the substrate for PHDs, so PHD activity and therefore degradation of HIF-1α is enhanced. **(B)** If complex I is active, NADH is reduced to NAD^+. NAD^+ is required for αKG conversion to SA, so the αKG:SA ratio is rebalanced and the activity of PHDs reduced. Figure adapted from Calabrese et al., (Calabrese, Iommarini et al. 2013)

Phenotypes of a mouse model of Leigh syndrome, created by systemic knockout of complex I subunit *Ndufs4*, can be rescued by chronic exposure to hypoxic conditions of 11% oxygen (Jain, Zazzeron et al. 2016). This includes locomotor phenotypes and neuronal cell loss (Jain, Zazzeron et al. 2016). Whether the rescue is caused by increased activity of HIF-1α is yet to be shown. However, in the light of this evidence, it may be worth testing *sima* overexpression in neurons with *ND-75* RNAi, as perhaps mitochondrial dysfunction caused by complex I impairments can be improved by upregulation of HIF-1α retrograde signalling. If *ND-75* RNAi is impairing stabilisation of HIF-1α, it may also be necessary to use PHD inhibitors, to explore the possibility of HIF-1α rescuing *ND-75* RNAi phenotypes.

Analysis of transcriptional changes of genes known to be regulated by HIF signalling in hypoxia in *Drosophila* and in all five models of mitochondrial dysfunction showed that many of these genes were changed in a similar manner in all conditions. To understand what differences there might be in HIF signalling between complex I *ND-75* knockdown compared to the other models, I identified genes that were differentially regulated in this condition. HIF responsive genes involved in oxidation-reduction processes and metal binding properties were differentially regulated in complex I compared to the other mitochondrial dysfunction models. Further investigation of these

processes may therefore also help to understand the different response of *ND-75* RNAi flies to *sima* knockdown. Inducing changes in these genes in *ND-75* RNAi, comparable to the changes in other models would help elucidate if these genes are important for *sima* knockdown mediated rescue.

7.2.6 Summary

In Chapter 3, I characterised neuronal mitochondrial dysfunction when individual OXHPOS subunits were knocked down and *TFAM* was overexpressed. I found that complex III subunit knockdown induced relatively mild phenotypes, complex IV/V RNAi and *TFAM* overexpression resulted in similar phenotypes and complex I induced the most severe phenotype with obvious increases in ROS. In Chapter 4, I found further differences between complex I and the other models, as complex I knockdown was the only mitochondrial insult not to be rescued by *sima*. Further investigation is required to determine if benefits of reduced HIF signalling only occur in mitochondrial dysfunction that when ROS increase, as this could have important translational implications.

7.3 Identifying genes involved in the cellular response to mitochondrial dysfunction, in a modifier screen.

As well as comparing the neuronal response to mitochondrial dysfunction in different models, I also aimed to identify novel genes that are involved in the cellular response, by carrying out an *in vivo* genetic screen in the *Drosophila* wing. A library of 650 RNAi lines were screened and 80 genes were identified that modify the mitochondrial dysfunction phenotype.

7.3.1 *TFAM* knockdown and *TFAM* overexpression as models of mitochondrial dysfunction

In the modifier screen, I used *TFAM* knockdown as a model of mitochondrial dysfunction, as opposed to *TFAM* overexpression in results chapters 3 and 4, because *MS1096-Gal4* driven *TFAM* overexpression caused pupal lethality and so wing phenotypes could not be assessed. Western blot analysis of both *TFAM* knockdown and overexpression showed a decreased expression of mtDNA encoded COXI and no change in nuclear encoded ATPsynthase subunit α. The role of TFAM in packaging and stabilising mtDNA is most likely to explain why loss and accumulation both cause decreased mtDNA gene expression. Reducing levels of TFAM causes a corresponding drop in mtDNA, as non-specific binding of TFAM is required to stabilise mtDNA in HeLa cells (Kanki, Ohgaki et al. 2004). This was first shown *in vivo* in heterozygous knockout *TFAM* mice (Larsson, Wang et al. 1998). Studies of *TFAM* overexpression in HeLa cells and mice found mtDNA increased with *TFAM*, although there was decreased mitochondrial gene expression in mice (Kanki, Ohgaki et al. 2004, Ylikallio, Tyynismaa et al. 2010). A study in HEK cells showed that initially when TFAM levels are increased transcription increases, however when TFAM is double its normal level mitochondrial transcription is reduced (Maniura-Weber, Goffart et al. 2004). While small increases in TFAM increase mtDNA copy number and transcription, large concentrations of TFAM seem to saturate mtDNA. Analysis of the TFAM overexpression line used in this thesis showed that there was no change in mtDNA quantity in these flies (Cagin, Duncan et al. 2015), so loss of mtDNA expression is most likely due to enhanced TFAM binding decreasing transcription and translation. Both overexpression and knockdown of *TFAM* therefore reduce mtDNA encoded proteins,

however, the *TFAM* RNAi used in this work has a weaker phenotype than the overexpression line, as seen when driven in the wing and, in results chapter 5 when driven in motor neurons, on climbing phenotypes.

7.3.2 Mitochondrial dysfunction driven in the dorsal wing compartments causes a curved wing phenotype

The phenotype induced by *TFAM* knockdown in the wing was used for the screen because it is easy and quick to observe. Mitochondrial dysfunction was driven in the dorsal compartment of the wing with the driver *MS1096-Gal4.* This results in an approximately 45^{o} degree upward curve of the wing, presumably due to mismatched growth/cell death in the dorsal and ventral layers of the wing. Decreased growth and proliferation might be expected in the dorsal compartment if ATP production is reduced by mitochondrial dysfunction, and as mitochondria control apoptosis, there may also be an upregulation of apoptosis in this compartment. I investigated changes in apoptosis and found that apoptosis was upregulated in the dorsal compartment of the wing disc, in *TFAM* knockdown and *TFAM* overexpressing larvae. Interestingly there was no significant difference in the amount of apoptosis in the wing disc between the *TFAM* knockdown and *TFAM* overexpressing larvae even though *TFAM* overexpression causes pupal lethality. It may be that apoptosis continues to increase during pupariation in *TFAM* overexpressing flies, or the lethality may be due to some 'leakiness' of the driver. *MS1096-Gal4* driven expression of two suppressors identified in the wing screen suppressed the upregulated apoptosis caused by mitochondrial dysfunction. This suggests that apoptosis regulates the wing phenotype caused by mitochondrial dysfunction. However, this does not exclude the possibility of other factors, induced by mitochondrial dysfunction, contributing to this phenotype. Recent insight into the Curly wing phenotype, often used as a marker in fly husbandry, has revealed that this phenotype is due to a mutation in the *dual oxidase* (*duox*) gene (Hurd, Liang et al. 2015). Duox is best known in *Drosophila* for its role in defence against bacteria, which it does by ROS generation (Lee, Kim et al. 2015). It turns out that Duox generated ROS also plays a role in tyrosine crosslinking, creating covalent bonds between molecules (Hurd, Liang et al. 2015). On the final day of pupal development, this crosslinking is required for wing stabilisation, mediated by the heme peroxidase Curly Su (Hurd, Liang et al. 2015). TEM of the wing in *Curly* mutants revealed bunching of the surface of the wing possibly due to abnormal bonding of the two cutilces, which may be causing the

curved phenotype (Hurd, Liang et al. 2015). It is possible that mitochondrial ROS production may also contribute to the crosslinking process, in which case mitochondrial dysfunction that results in reduced OXPHOS activity and reduced ROS may also disrupt this process.

7.3.3 Genes that affect the mitochondrial dysfunction phenotype in the *Drosophila* wing

Through this modifier screen assay, 71 genes that when knocked down enhance the mitochondrial dysfunction phenotype were identified. The functions of these genes were varied, which reflects the multifunctional nature of the organelle. In the microarrays, altered transcription of genes involved in alternative metabolism were identified in each genotype. Similarly, GO analysis of screen enhancers revealed genes involved in glycolysis, glutamate/glutamine conversion and the pentose phosphate pathway. This demonstrates the importance of these metabolic pathways in the response to mitochondrial dysfunction and also establishes the validity of the screen assay.

Twelve of the enhancers were also significantly changed in at least one of the microarray conditions. Enhancers *neuroligin 2, breathless, dawdle, CG2124, dpr6* and *CG11347* were all also downregulated in the microarrays. Previously (see Discussion 7.2.3), I discussed retrograde signalling pathways that have a negative effect on cellular function, as blocking them improves mitochondrial dysfunction phenotypes. As knockdown of these genes enhances mitochondrial dysfunction in the wing screen I propose that blocking downregulation of these genes may be beneficial in mitochondrial dysfunction. Many of these genes are members of signalling pathways acting as receptors or ligands. GO analysis indicates that *CG2124* is a fibroblast growth factor (FGF) activated receptor, with protein tyrosine kinase receptor (RTK) activity. It is also predicted to localise to mitochondria. *Breathless* is also an FGF receptor, with protein tyrosine kinase activity. *Drosophila breathless* mutants have impaired tracheal development, as tracheal migration is not initiated, so tracheal branches do not form (Klambt, Glazer et al. 1992). A role for *breathless* has also been identified in adult axonal extension in the *Drosophila* brain, mediating axon retraction (Srahna, Leyssen et al. 2006). In *Drosophila* embryos, breathless tyrosine kinase activity is shown to activate the Ras/MAPK pathway leading to loss of the ETS transcription factor Yan (Ohshiro, Emori et al. 2002). This is particularly interesting as *yan* RNAi was found to

suppress mitochondrial dysfunction in the wing screen. Dawdle is a Transforming growth factor-β (TGFβ) ligand which acts via the type-I TGFβ receptor Baboon (Jensen, Zheng et al. 2009). TGF-β signalling regulates many processes, such as cell proliferation and differentiation. In *Drosophila*, activation of TGFβ via Dawdle is implicated in axonal guidance and remodelling (Parker, Ellis et al. 2006, Zhu, Boone et al. 2008). Thyroid hormone signalling has also been identified due to the *CG11347* gene. This is the *Drosophila* homologue of diabetes and obesity regulated gene (DOR). In HeLa cells and myocytes, DOR shuttles between the nucleus and cytoplasm in response to cellular stress and is shown to physically interact with autophagosomes (Mauvezin, Orpinell et al. 2010). This data was confirmed in third instar *Drosophila* larvae, which have a 40% decrease in autophagy when *CG11347* was knocked down (Mauvezin, Orpinell et al. 2010). RNAis for two cell adhesion molecules, *Neuroligin 2* and *dpr6*, also enhanced the wing phenotype and were downregulated in at least one microarray. Neuroligins, such as Neuroligin 2 bind to neurexins, such as dpr6, to create a physical junction between cells. Neuroligin 2 is particularly associated with inhibitory GABAergic synapses, its role in the wing disc is unknown (Varoqueaux, Jamain et al. 2004). Dpr6 has mainly been studied in the context of salt aversion, *Dpr* mutants have a defect in salt (but not sugar) responsiveness (Nakamura, Baldwin et al. 2002).

Conversely, *CG31436, CG17734, branchless* and *twin of eyeless* were upregulated in the microarrays, whereas knockdown enhanced mitochondrial dysfunction phenotypes. It is therefore possible that these genes take part in retrograde responses which are beneficial to the cell. This may be the case for *CG17734*, which encodes the *Drosophila* orthologue to the human *hypoxia-inducible gene 1 (HIG1)* family in humans. HIG1 proteins localise to mitochondria and protect murine pancreatic cells from apoptosis in glucose deprived or hypoxic conditions (Wang, Cao et al. 2006). Upregulation of *CG17734* was also seen in microarrays of *Drosophila tko* mutants described previously (see Discussion 7.2.1) (Fernandez-Ayala, Chen et al. 2010). A TGFβ family member, twin of eyeless, was also identified as an enhancer and upregulated in the microarray of *UQCR-14* RNAi expressing CNS tissue. Branchless, the ligand, for the RTK breathless, was identified as an enhancer in the screen and upregulated in the microarray of *ATPsynCf6* RNAi expressing brains. Further investigation of these pathways and their role in mitochondrial dysfunction could prove extremely interesting. Repeated identification of RTK and TGFβ family members suggests these pathways are of particular importance in the response to mitochondrial dysfunction.

I also identified 10 genes, which when knocked down suppressed the mitochondrial dysfunction phenotype in the wing. The proteins encoded by all of these genes have DNA binding properties, acting as transcription factors or chromatin remodellors (excluding CG31125 which has unknown function). This again reiterates the importance of retrograde signals from dysfunctional mitochondria to the nucleus, and demonstrates that targeting retrograde signalling may have therapeutic potential.

7.3.4 Advantages and limitations of the genetic wing screen

Previous screens have been carried out to identify genes required for mitochondrial function. Mutations in mitochondrial genes causes a 'glossy eye' phenotype in *Drosophila* due to inhibition of the cell cycle during eye development. Screening of this phenotype led to the identification of nuclear encoded mitochondrial genes (Liao, Call et al. 2006). Other approaches have also been taken to identify mitochondrial proteins. Mass spectrometry of genes localised to mitochondria has produced an inventory of mammalian mitochondrial genes, known as the MitoCarta (Calvo, Clauser et al. 2016).

The aim of the screen I performed, was not to identify genes required for mitochondrial function, but genes that could modify the cellular response to mitochondrial dysfunction. It was therefore imperative to use a modifier screen in which mitochondrial dysfunction is induced. This approach complements the data obtained in the microarrays in results chapter 4, however it differs as the microarrays will identify any transcriptional change that occurs following mitochondrial dysfunction, whereas the screen will only pick up genes that induce a functional change in the cell in conditions of mitochondrial dysfunction. These genes may be regulated by retrograde signalling, but the screen should also identify genes that are not normally altered in mitochondrial dysfunction, but can modify cellular function if they are.

In order to validate that this modifier screen would identify relevant genes, I tested genes that are associated with some aspect of mitochondria: *PINK1, Parkin, DJ-1α, DJ-1β* and *Lrrk*. Modification of all of these genes caused enhanced wing phenotypes with *TFAM* knockdown, validating the assay. However, not every line for each gene gave an enhancement, and some RNAis gave phenotypes by themselves. This demonstrates the limitations of RNAi libraries, different sequences may knockdown a gene more or less

efficiently and different insertion sites affects the expression of the RNA sequence. *PINK1, DJ-1α* and *DJ-1β* enhanced the mitochondrial dysfunction phenotype when both overexpressed and knocked down, which indicates that the level of these proteins are important in conditions of mitochondrial dysfunction. Other studies have also shown similar phenotypes due to *PINK1* knockdown and overexpression: a loss of function *PINK1* mutant induces mitochondrial clustering in *Drosophila* DA neurons, as does *PINK1* overexpression (Yang, Ouyang et al. 2008). Although the outcome is the same these phenotypes are actually functionally different, as *Parkin* overexpression can suppress this phenotype in *PINK1* mutants but not when *PINK1* is overexpressed (Yang, Ouyang et al. 2008).

There are of course several limitations of the modifier screen methodology. Analysing modifications of mitochondrial dysfunction in the wing was a trade-off between speed and an easily visualised phenotype and studying mitochondrial dysfunction in non-neuronal tissue. This means that genes identified may modify mitochondrial dysfunction in the wing, but there is no guarantee that they will do the same in neurons, and vice versa. The RNAi lines were selected because they are for genes that are strongly expressed in the brain relative to the rest of the body. This is beneficial for investigations of neurodegenerative processes, but may lead to false negatives, as if a gene is not expressed in the wing then the RNAi will not be able to knock it down. Genes that modify mitochondrial dysfunction may also be missed due to the control cross in which any gene that has an effect on the wing phenotype alone is excluded. This is however necessary, so that genes identified are known to be interacting with mitochondrial dysfunction. A relatively large number of genes had to be excluded this way. This may be because many processes can affect wing development, but it may also be due to the use of VDRC KK RNAi lines. These RNAi lines were produced by the targeted insertion of an RNAi hairpin vector into a specific landing site (position chromosome 2L: 22019296, cytological band 40D3). However, a second, unannotated landing site has been discovered into which the RNAi hairpin vector preferentially inserts (position chromosome 2L: 9437482, cytological band 30B3) (Green, Fedele et al. 2014). Out of 39 KK RNAi lines tested by Green et al., 38 had the insert in the unannotated site, 9 of those also contained a RNAi hairpin in the annotated site and 1 line contained no insert at all (Green, Fedele et al. 2014). Pan-neuronal expression of the nine RNAi lines with inserts in both landing sites resulted in a wing inflation phenotype and ubiquitous expression caused lethality (Green, Fedele et al. 2014). These

phenotypes are due to *UAS* driven overexpression of the Hippo pathway transcription factor *Tiptop* due to the RNAi vector insertion in the annotated site (Vissers, Manning et al. 2016). *MS1096-Gal4* expression of just a *UAS* inserted in the annotated site causes a wing phenotype (Vissers, Manning et al. 2016). Thus study suggests that in my modifier screen on average ≈ 25% of KK lines will give a wing phenotype when expressed with *MS1096-Gal4* due to *Tiptop* overexpression.

Another limitation of the modifier screen assay, is the variability in the wing curve throughout a population of flies of the same genotype. To try and reduce the effects of this variability, only wings of male flies were scored (female flies had a weaker phenotype, probably due to dosage compensation) and a semi-quantative scale was developed in which only flies that were scored 3 or above (see results chapter 5, Figure 5.3) were considered enhancers, to limit the number of false positives. The interaction of *TFAM* knockdown and RNAis that were deemed suppressors or enhancers in this screen were also checked twice to confirm the result. To further validate the screen hits, non-overlapping RNAi were assessed. 105 alternative RNAi were identified for 62 genes of the 80 genes identified in the screen. Of these 20 had to be excluded as they gave phenotypes on their own and 30 of the 62 genes were confirmed as hits with a non-overlapping RNAi. Lines that were not confirmed are not necessarily false positives as the alternative RNAis may have different levels of expression, however the 30 confirmed genes represent a list of modifiers that I can be particularly sure of. Two alternative RNAi gave the opposite phenotype to the initial RNAi tested. These genes have therefore not been included as suppressors or enhancers as further investigation will be required to find out why there is such disparity between the two RNAis. It could be due to off target effects, or the impact on the mitochondrial dysfunction phenotype may be a function of the level of knockdown or isoforms affected.

7.3.5 Summary

This genetic modifier screen has identified numerous genes and several pathways in particular which can modify the cellular response to mitochondrial dysfunction. Combined analysis of both the microarrays in chapter 4 and this modifier screen has been particularly helpful in identifying genes and pathways of interest. It is however, important to assess the genes identified in this screen in neurons, as the demands on mitochondria are very different in these postmitotic, electrically active cells.

7.4 Evaluating genes identified in the modifier screen, in neurons.

In order to evaluate whether hits from the screen also modify the outcome of mitochondrial dysfunction in neurons, mitochondrial dysfunction was induced in motor neurons and the effects of the RNAi lines were assessed on climbing and wing inflation phenotypes. *TFAM* RNAi and $TFAM^{c01716}$, only resulted in weak phenotypes when expressed in motor neurons and so *TFAM* overexpression was used as the model of mitochondrial dysfunction. As discussed previously, these two models both result in decreased expression of proteins encoded by mtDNA (see Discussion 7.3.1).

7.4.1 Tissue or model specific effects of RNAi lines on mitochondrial dysfunction phenotypes

Out of the wing screen hits that also modified neuronal mitochondrial dysfunction, 6 gave the opposite result than in the screen and only one line caused the same modification when driven in the wing and neurons (*yan* RNAi). Similarly, *sima* knockdown enhanced the wing phenotype but rescues mitochondrial dysfunction in neurons. There are two differences between the wing and neuronal experiments, which may explain these results. Firstly, the model of mitochondrial dysfunction is different. In the wing *TFAM* was knocked down as opposed to overexpression of *TFAM* in neurons, both of these manipulations lead to reduced mtDNA gene expression, but there may be intrinsic differences that effect the role of these genes. In mouse embryonic fibroblast cultures mtDNA escapes into the cytosol when *TFAM* is knocked down, which initiates an immune response (West, Khoury-Hanold et al. 2015). *TFAM* overexpression does not result in loss of mtDNA (Cagin, Duncan et al. 2015), so presumably this process does not happen in the *TFAM* overexpressing flies. Secondly, this may represent tissue specific effects. Heterozygous *TFAM* knockout mice display tissue specific responses to TFAM loss, with some tissues, such as skeletal muscle, able to maintain OXPHOS activity and mtDNA transcript levels, whereas heart tissue loses mtDNA transcripts and proteins as well as complex I, III, IV and V activity (Larsson, Wang et al. 1998). I would expect that a combination of these two factors results in many of the RNAi lines having different effects in the screen and neuronal assays.

7.4.2 Neuronal mitochondrial dysfunction phenotypes suppressed by *yan* RNAi

The only gene tested that had the same effect in both tissues was *yan*. *Yan* RNAi suppressed the wing phenotype in the modifier screen as well as suppressing both the wing inflation and climbing phenotypes in the nervous system. To further confirm *yan* RNAi as a suppressor, I also tested an independent RNAi and found that this line also rescued the wing curve and neuronal wing inflation. Knockdown of two upstream regulators of Yan, *branchless* and *breathless*, also enhanced in the wing screen. Further investigation of Yan's effect on mitochondrial dysfunction should include analysis of *yan* mutants and manipulation of upstream regulators such as MAPK (Rolled, homologue of ERK) and Ras.

Analysis of Yan-DNA binding in *Drosophila* embryos shows that Yan binds multikilobase regions of DNA. Maintenance of these long stretches requires the N-terminal sterile α-motif (Webber, Zhang et al. 2013). GO analysis of genes putatively regulated by the DNA bound regions identified a number of signalling pathways implicated in development, including TGFβ and p53 signalling (Webber, Zhang et al. 2013). These may be of particular interest in neuronal mitochondrial dysfunction as p53 is implicated in retrograde signalling in *COX5A* knockdown flies (Owusu-Ansah, Yavari et al. 2008) and TGFβ family members were identified in the modifier screen. Chromatin immunoprecipitation of adult flies with constitutively active Yan (Yan^{ACT}) revealed approximately 4000 bound regions close to 3000 genes in the gut and fat body (Alic, Giannakou et al. 2014). GO enrichment analysis found genes involved in the regulation of lipid metabolism most highly overrepresented (Alic, Giannakou et al. 2014). Microarray analysis of the fat body showed that Yan^{ACT} expression reduced genes involved in oxidation-reduction processes and the ETC (Alic, Giannakou et al. 2014). Yan may affect different targets in neurons, however roles in lipid storage, oxidation-reduction processes and the ETC may be mediating the rescue of mitochondrial dysfunction phenotypes observed in this thesis.

Yan^{ACT} expression in the gut and fat body of adult female flies is able to extend lifespan, although knockdown of *yan* in these tissues has no effect on longevity (Alic, Giannakou et al. 2014). Similarly, inhibition of Ras signalling, through ubiquitous expression of dominant negative *Ras* (Ras^{DN}) or *Ras* RNAi, in adult flies extends lifespan, in a Yan dependant manner (Slack, Alic et al. 2015). Administration of a pharmacological agent,

Trametinib, that inhibits Ras activation of Erk (a downstream MAPK) also increases *Drosophila* lifespan (Slack, Alic et al. 2015). The finding that *yan* RNAi suppresses mitochondrial dysfunction phenotypes may therefore seem surprising. However, if Yan activity reduces ETC genes in neurons as well as the gut and fat body, this could explain why *yan* knockdown is beneficial in situations of mitochondrial dysfunction. When the electron transport chain is impaired, further inhibition mediated by Yan may be detrimental to the cell. Mild mitochondrial dysfunction has been reported to have benefits, such as elongated longevity in *C. elegans* and *Drosophila* (Dillin, Hsu et al. 2002, Copeland, Cho et al. 2009). If mitochondria are functional, a reduction in mitochondrial activity may be beneficial, by either reducing ROS production or by activation of advantageous retrograde signals, as seen in mild mitochondrial dysfunction which also enhances longevity (Copeland, Cho et al. 2009).

7.4.3 The interplay between Yan and Pointed

Yan RNAi was also able to suppress neuronal phenotypes in a *Drosophila* model of Leigh syndrome, but not *Parkin* mutant flies. Interestingly, heterozygous expression of *pnt* mutant also suppressed mitochondrial dysfunction in the *TFAM* overexpressing and the *Parkin* mutant flies. This is surprising because canonically Pnt and Yan act antagonistically to each other, Pnt enhancing and Yan suppressing expression of the same genes. Phosphorylated ERK (pERK) phosphorylates both PntP2 and Yan, promoting cytosolic translocation, and degradation of Yan as well as promoting the activity of PntP2. In a feedforward mechanism, Pnt negatively regulates the expression of *yan* (Rohrbaugh, Ramos et al. 2002). A mathematical model of these dynamics describes two possible cellular states: gene repression with high Yan and low PntP2 activity versus promotion of gene expression due to low Yan and high PntP2 (Graham, Tabei et al. 2010). As this model predicts, expression of Yan and Pnt is mutually exclusive, with a short overlapping transition period, in most tissues affected by Ras/MAPK signalling when imaged throughout *Drosophila* development. However, this is not always the case and numerous tissues throughout development expressed both Yan and Pnt, such as cone cells during eye development (Boisclair Lachance, Pelaez et al. 2014). This suggests a greater level of complexity in the regulation of Yan and Pnt. Further regulation of Pnt and Yan is mediated by the protein Mae. Mae antagonises Yan activity by facilitating phosphorylation and nuclear export of Yan (Baker, Mille-Baker et al. 2001, Tootle, Lee et al. 2003), whereas Yan directly inhibits

Mae transcription and Pnt promote Mae transcription (Vivekanand, Tootle et al. 2004). This fits with the model of binary Yan activation corresponding to Ras/MAPK signalling. However, Mae also antagonises PntP2 activity *in vitro* and *in vivo* (Tootle, Lee et al. 2003, Vivekanand, Tootle et al. 2004). The role of Pnt in repression of Yan has also been questioned as clones of *pnt* null mutations in the eye induces loss of Yan (Pelaez, Gavalda-Miralles et al. 2015). Overexpression of PntP1 and constitutively active PntP2 in the eye did accelerate Yan degradation immediately, however later degradation of Yan was inhibited (Pelaez, Gavalda-Miralles et al. 2015). These data indicate that the dynamics between Yan and Pnt may be more complex than previously thought, and may be context dependant. The data in this thesis, showing repressed mitochondrial dysfunction due to *yan* knockdown and *pnt* knockdown, may indicate that Yan and Pnt do not act antagonistically in neuronal tissue, or may be due to complex inter-regulation of Yan and Pnt levels. Imaging Pnt and Yan levels in neurons in *yan* RNAi and the *pnt* mutants would help to determine what effect these manipulations are having on protein level. Development of antibodies for phosphorylated Yan and Pnt would also help to understand what is happening to activity of these proteins.

7.4.4 Ras/MAPK pathway activation in disease

Misregulation of the Ras/MAPK is strongly associated with cancer. Extracellular signal regulated protein (ERK), the homologue of *Drosophila* Rolled, promotes migration of cancerous cells. It also stimulates degradation of extracellular matrix proteins promoting tumour invasion, as well as regulating pro-apoptotic proteins such as BIM, enhancing apoptosis resistance (Kim and Choi 2010).

ERK activation is also implicated in neurodegenerative diseases, along with the other MAPK subfamilies, JNK and p38. Although levels of ERK do not change, activation of ERK via phosphorylation, is greater in post-mortem brain tissue of Alzheimer's (AD) patients relative to controls (Zhu, Castellani et al. 2001, Zhu, Lee et al. 2002). Amyloid β is implicated in ERK activation: in a mouse model of AD, transgenic for mutant human amyloid precursor protein, ERK activation is upregulated in neurons (Stein and Johnson 2002). ERK activation is also increased in the midbrain and substantia nigra of post-mortem tissue from patients with Lewy body diseases, such as Parkinson's (Zhu, Kulich et al. 2002). *In vitro*, the main component of Lewy bodies, α-synuclein, rapidly

stimulates ERK activation (Klegeris, Pelech et al. 2008). As ERK activation is found in diseases associated with mitochondrial dysfunction, and modifications of the pathway modifies mitochondrial dysfunction in the wing and neurons in my study, I looked at whether ERK activation was increased neuronally in the model of mitochondrial dysfunction I used. Activation of ERK was detected in motor neuron cell bodies of *TFAM* overexpressing larvae.

As well as increased activation, abnormal localisation of ERK in discrete cytoplasmic granules is reported in brain tissue from patients with Lewy body diseases and AD (Pei, Braak et al. 2002, Zhu, Kulich et al. 2002). Activated ERK in disease brains may therefore be unable to reach the nucleus to regulate transcription. I did not detect cytoplasmic granules in the soma of *TFAM* overexpressing third instar larvae. However, this does not exclude the possibility of cytosolic granules of pERK in the axon and NMJ or in adult flies. I measured pERK levels in the cytosol, because there was a greater level of staining there than in the nucleus in control and test larvae, it is therefore also unclear whether activation of ERK in these models is able to act on nuclear targets, such as Yan. *In vivo* quantification of Yan in mitochondrial dysfunction would help to elucidate whether this is the case or not.

There is some debate about whether activated ERK has a protective or detrimental effect on neurons in neurodegenerative diseases. Initially *in vitro* studies in rat cells differentiated into neurons illuminated a protective role of ERK activation against apoptosis (Xia, Dickens et al. 1995). In rat cortical cultures, ERK activation is necessary and sufficient to mediate BDNF apoptosis resistance, to toxins that induce DNA damage (Gozdz, Habas et al. 2003). ERK upregulation has also been shown to protect neuronally differentiated cells treated with 1-Methyl-4-phenylpyridinium (MPP^+), commonly used to model Parkinson's disease (Teng, Kou et al. 2014). Various other *in vitro* studies show the protective effects of ERK activation against oxidative stress, Ca^{2+} overload, hypoxia and neurotoxic viruses (Hetman and Gozdz 2004). However, numerous studies also show that *inhibition* of ERK activation is protective against many neuronal insults (Chu, Levinthal et al. 2004). *In vivo*, the presence of pERK correlates with neuronal degeneration starting in the transentorhinal region of the brain and spreading throughout the brain with the neurofibrillary neurodegeneration (Pei, Braak et al. 2002).

Two mechanisms may govern whether ERK activation is protective or damaging: the period of activation and the cellular localisation. Experiments in a murine hippocampal cell line reveals differential effects depending on transient or chronic ERK activation (Luo and DeFranco 2006). Addition of glutamate to neuronal cell cultures induces cell death, mediated by free radical production (Pereira and Oliveira 2000). Chronic ERK activation was shown to be necessary for cell death by glutamate-induced oxidative toxicity, as transfection a dominant negative MEK (the MAPKK that phosphorylates ERK), inhibited this process (Luo and DeFranco 2006). On the other hand, transient activation of ERK imminently following glutamate exposure was shown to promote survival (Luo and DeFranco 2006).

Localisation of pERK is important as it controls the substrates pERK acts upon. The cytosolic granules of pERK identified in patients with neurodegenerative diseases may lead to abnormal activity in the cytosol and a loss of normal activity in the nucleus. pERK is known to hyperphosphorylate tau in AD, and so its cytosolic activity may contribute to pathology by aberrant cytosolic phosphorylation (Harris, Brecht et al. 2004). Aggregation of pERK in the cytosol may inhibit activation of prosurvival pathways in the nucleus, such as regulation of BDNF (Chu, Levinthal et al. 2004). This may explain why *yan* knockdown is protective in neuronal mitochondrial dysfunction, if pERK translocation to the nucleus is impaired so it is unable to inhibit Yan itself.

7.4.5 Regulation of the Ras/MAPK pathway

Ras can be activated by cell surface RTKs including the epidermal growth factor receptor (EGFR), the insulin receptor and Sevenless. This allows the Ras/MAPK pathway to respond to extracellular signals. Ubiquitination of RTKs regulates the activity of this pathway, as ubiquitinated RTKs are endocytosed and targeted for degradation (Levkowitz, Waterman et al. 1999). Clones in the *Drosophila* eye disc, mutant for ubiquitin-activating enzyme E1 (E1), revealed an upregulation of pERK, and an overgrowth phenotype (Yan, Chin et al. 2009). Knockdown of *Egfr* did not affect the Ras/MAPK upregulation in the flies. Similarly, knockdown of *drk* and *sos*, which mediate Ras activation by RTKs, did not affect the Ras/MAPK activity. Removal of one copy of *ras*, however, did suppress MAPK activation (Yan, Chin et al. 2009). This suggests that direct ubiquitination of Ras can also regulate the activity of the pathway. Ras has also been shown to be activated by ROS mediated modification *in vitro*, by

stimulation of Ras's GTPase activity (Lander, Hajjar et al. 1997). Oxidative reactions also inactivate ERK inhibitors: In primary human ovarian cultures mitogen-activated protein kinase phosphatase 3 (MKP3) were degraded in a ROS dependant manner, and degradation was inhibited with antioxidant treatment (Chan, Liu et al. 2008). Calcium levels are also implicated in regulation of this pathway, as FCCP treatment, which causes cytosolic calcium accumulation in hippocampal rat cells activates ERK, whereas Oligomycin treatment, that does not result in mitochondrial Ca^{2+} release, did not activate ERK (Luo, Bond et al. 1997). High free Ca^{2+} increases the protein-protein binding activity of ERK *in vitro* and *in vivo*, which impairs translocation of ERK into the nucleus (Chuderland, Marmor et al. 2008). Determining which of these potential mechanisms leads to pERK activation in mitochondrial dysfunction requires further investigation.

7.5 Conclusions and future directions

In this thesis I hypothesised that greater knowledge of the neuronal response to mitochondrial dysfunction would allow modification of this response to improve neuronal function. Through transcriptional analysis of different mitochondrial dysfunction models and a genetic modifier screen I have identified two cellular responses, which when altered, improve neuronal function. Further research is required to elucidate the mechanisms of these pathways and to understand whether there is a relationship between them. I have also found that differences in mitochondrial insult affect the outcome of these manipulations, showing that complex I dysfunction is unresponsive to rescue by *sima* knockdown. This highlights the importance of considering the cause of mitochondrial dysfunction when developing treatments.

Both of the pathways identified in this thesis as potential therapeutic targets for mitochondrial dysfunction are also implicated as oncogenes, Ras/MAPK for its role in promoting growth and proliferation and HIF signalling for switching cellular metabolism to glycolysis, the Warburg effect. Mitochondrial dysfunction does not seem to normally cause cancer or help it spread (Ju, Alexandrov et al. 2014). Instead it appears that many cancer cells choose to switch to glycolytic processes and mitochondrial mutations accumulate in these cells because of enhanced proliferation of a single cell (Chinnery, Samuels et al. 2002, Fantin, St-Pierre et al. 2006). Enhanced ROS production in cancer cells is implicated in the activation of tumour promoting signals, such as Ras and HIF signalling (Liou and Storz 2010). Cancer cells adapt extremely well to mitochondrial damage and/or low mitochondrial activity, as can be seen by their highly proliferative nature. I therefore believe that a lot can be learnt from the adaptations cancer cells make (such as apoptosis resistance) when trying to deal with the impacts of mitochondrial dysfunction in neurodegeneration. It is of course extremely important to try and understand how to help cells adapt to mitochondrial dysfunction without triggering invasiveness and tumour formation. For this reason, I believe that most can be gained from exploring the downstream effects of the HIF and Ras/MAPK pathways. These pathways co-ordinate numerous outcomes and so it will be important to identify which of these downstream pathways can be manipulated beneficially and which should be left well alone. I speculate that some of the variability in the rescue of complex III, IV and V knockdowns with *sima* RNAi was due to the fact that some of the signalling mediated by Sima may be beneficial, whereas some may be

detrimental. Future work is required to determine what these downstream effects are and which should be targeted.

7.5.1 Future Experiments

The work in this thesis is a starting point from which we can uncover much more information about retrograde signalling in neurons and how we can manipulate those responses to salutatory effect. It has opened up many new questions, here I will outline what I believe to be the most important next steps for this research, although this is by no means an exhaustive list.

Blue native gels of each model of mitochondrial dysfunction would be beneficial as this assay would allow analysis of the level of each complex and the activities of these complexes, giving a greater understanding of the differences between the mitochondrial dysfunction models. Knockdown of one complex may affect assembly and activity of other complexes due to the formation of supercomplexes. Supercomplex formation could also be assessed with blue native gels. I would be particularly interested in whether there were global changes in supercomplex formation in the RNAi models (in which *RFeSP* was transcriptionally downregulated) and *TFAM* overexpression (in which *RFeSP* was transcriptionally upregulated) (see Discussion 7.2.1). Alternatively, analysis of oxygen consumption in relation to treatment with complex specific pharmacological inhibitors, could also be carried out to determine the activity of each OXPHOS complex in every model.

There are a number of other parameters that would be useful to measure in the mitochondrial dysfunction models I developed. Changes in metabolites would be interesting to evaluate. The KG:SA ratio would be particularly important, as it has been implicated in HIF-1α stabilisation, mediating the complex I mutant's inability to stabilise HIF-1α (see Discussion 7.2.5 & Figure 7.1). Recently a NADH oxidase from the bacteria *Lactobacillus brevis* (*Lb*NOX), has been used to increase the NAD^+:NADH ratio in individual compartments of human cells (Titov, Cracan et al. 2016). Mitochondrially targeted *Lb*NOX could address the hypothesis that the *ND-75* RNAi causes an increase of NADH, therefore increasing the KG:SA ratio and impairing HIF-1α stabilisation. Further analysis of ROS would also be beneficial in these models. I would hypothesise that complex I *ND-75* RNAi phenotypes are mediated by increased

ROS production, whereas the other models are not mediated by ROS. Genetic overexpression of antioxidant scavengers could test this hypothesis. Characterisation of Ca^{2+} dynamics in each mitochondrial dysfunction model would also be informative, particularly with regard to calcium regulation of MAPK activity and localisation (see Discussion 7.4.5).

In this thesis I have characterised several cellular changes that are induced by different mitochondrial insults. All of the models I have studied had functional impairments in climbing ability, however, I have not directly investigated the neuronal function in these models. The loss of mitochondria at the NMJ in these models suggests that synaptic transmission may be particularly impaired. It would be interesting to evaluate active zones in the models of mitochondrial dysfunction. *TFAM* overexpression in *Drosophila* motor neurons causes reduced active zones at the synapse, which is rescued by *sima* knockdown (Cagin, Duncan et al. 2015). I would like to measure active zones in the other models and to determine whether *sima* RNAi changes active zone number in these models too. Electrophysiology would be required to understand the functional effect of the mitochondrial dysfunction models on neuronal activity.

Having characterised five models of mitochondrial dysfunction, I have optimised and adapted tools to assess several features of neuronal mitochondrial dysfunction in *Drosophila* motor neurons. It would be beneficial to now use these assays to investigate the effect of modulating HIF and Ras/MAPK signalling on these features. *Sima* knockdown is known not to rescue the synaptic loss of mitochondria in *TFAM* overexpressing flies (Cagin, Duncan et al. 2015). Whether *sima* knockdown has an effect on other mitochondrial functions in this model is, however, unknown. Analysis of mitoTimer, roGFP-Grx and Perceval could help determine if *sima* knockdown alters mitochondrial phenotypes or if the functional rescue is purely due to retrograde signalling. In a mouse model of neurodegeneration, with IMM structural organisation impairments in forebrain neurons, neurodegeneration and neuroinflamation can be blocked by inhibition of mitochondrial fragmentation and mitophagy, without rescuing the mitochondrial dysfunction (Korwitz, Merkwirth et al. 2016).

Further investigation of the downstream effects of both Sima and Yan, will help elucidate targets for translational research and potential therapies for neurodegenerative diseases. I expect that both transcription factors mediate some downstream pathways in

neurons that have positive effects, possibly *CG17734* for example (see Discussion 7.3.3) and others that have negative effects on mitochondrial dysfunction. This could perhaps explain the variable efficacy of *sima* knockdown in different assays and different complex RNAi (CIII, CIV & CV). Microarray analysis of mitochondrial dysfunction models with *sima* and *yan* knockdown would reveal genes that are differentially altered when mitochondrial dysfunction is suppressed. Comparison of transcriptional changes in models that are rescued by *sima* knockdown and complex I RNAi, that was not rescued, may shed further light on transcriptional changes that are able to improve the cellular response to mitochondrial dysfunction. Chromatin immunoprecipitation and DamID of Sima and Yan in neuronal tissue would also be useful techniques to identify genes that are regulated by these transcription factors in this tissue.

Upstream mechanisms regulating HIF signalling and the Ras/MAPK pathway in neuronal mitochondrial dysfunction would also be interesting to investigate. I have discussed a number of regulator of these pathways (see Discussion 7.2.4 & 7.4.5). The MAPK pathway has also been shown to enhance the translation of HIF-1α and transcriptional activity of HIF, so there may be cross regulation between the two pathways. In hypoxic conditions, HIF-1α was phosphorylated in HeLa cell, in a pERK dependant fashion, resulting in enhanced transcriptional activity of HIF-1α (Richard, Berra et al. 1999). In human colon cancer cell line, insulin like growth factor 1 (IGF-1) stimulation increases HIF-1α protein levels, without reducing HIF-1α degradation, resulting in increased expression of HIF-1α target genes. Constitutively active MEK (the MAPKK that phosphorylates ERK) was sufficient to induce this process (Fukuda, Hirota et al. 2002). Currently an antibody for *Drosophila* HIF-1α, Sima, is being developed (Rachel Hunt), which will be used to determine if there are shifts in the molecular weight of Sima that may indicate posttranslational modifications. Epigenetic experiments could be carried out to determine if Yan and Sima activity interact. In the background of mitochondrial dysfunction, epigenetic experiments could also help determine if Yan and Sima act in parallel or synergistically in this context.

To further understand the role of the Ras/MAPK pathway plays in neuronal mitochondrial dysfunction, Yan and Pnt should be imaged in neurons in mitochondrial dysfunction models, *yan* RNAi, $pnt^{\Delta 88}$ mutants and combinations of these genotypes. Localisation and levels of Yan and Pnt will be equally informative. Increased activation

of ERK has been observed in motor neurons of the *TFAM* overexpression model. Phosphorylation of Yan is shown in the literature to induce nuclear export and degradation of Yan, so a loss of Yan and shift from the nucleus would be expected in these flies. I hypothesise that translocation of pERK to the nucleus is impaired in *TFAM* overexpressing flies and so Yan levels will not decrease. If this is the case *yan* knockdown may be beneficial as it causes the loss of Yan that the pERK was unable to achieve.

Finally, investigation of the effects of Sima and Yan on neuronal mitochondrial dysfunction phenotypes in mammalian systems will determine if these findings have translational potential. Testing of small molecules that inhibit or activate these pathways in *Drosophila*, cell culture and later in animal models of neurodegenerative disease would be a good starting point. The small molecule inhibitor of HIF-1α, PX-478, is already being investigated as a potential cancer treatment, and has successfully passed phase I clinical trials (Ban, Uto et al. 2011). Due to the fact that both *yan* RNAi and a *pnt* mutant suppress mitochondrial dysfunction in neurons, combined with potential nuclear translocation difficulties, it is unclear whether activation or inhibition of the Ras/MAPK pathway would be beneficial. To test the effect of inhibition of the Ras/MAPK pathway, MEK inhibitors such as Trametinib or PD98059 could be used.

Activators of this pathway are more difficult to come by, although chemotherapeutic drugs (taxol, etoposide and ceramide) have been reported to increase ERK activiation in two human cell lines, HeLa and A431 (Boldt, Weidle et al. 2002). I anticipate that drugs that improve nuclear transportation of pERK would be the most likely to ameliorate mitochondrial dysfunction. So perhaps targeting the protein binding affinity of pERK will be necessary. The effects of these drugs on neuronal mitochondrial dysfunction will aid our understanding of the roles of these pathways and the potential use of the drugs in the treatment of neurodegenerative diseases.

8 REFERENCES

A. Armstrong, R. (2013). "What causes alzheimer's disease?" Folia Neuropathologica **51**(3): 169-188.

Aberle, H., A. P. Haghighi, R. D. Fetter, B. D. McCabe, T. R. Magalhaes and C. S. Goodman (2002). "wishful thinking encodes a BMP type II receptor that regulates synaptic growth in Drosophila." Neuron **33**(4): 545-558.

Abrahams, J. P., A. G. Leslie, R. Lutter and J. E. Walker (1994). "Structure at 2.8 A resolution of F1-ATPase from bovine heart mitochondria." Nature **370**(6491): 621-628.

Acin-Perez, R., M. P. Bayona-Bafaluy, P. Fernandez-Silva, R. Moreno-Loshuertos, A. Perez-Martos, C. Bruno, C. T. Moraes and J. A. Enriquez (2004). "Respiratory complex III is required to maintain complex I in mammalian mitochondria." Mol Cell **13**(6): 805-815.

Acin-Perez, R., P. Fernandez-Silva, M. L. Peleato, A. Perez-Martos and J. A. Enriquez (2008). "Respiratory active mitochondrial supercomplexes." Mol Cell **32**(4): 529-539.

Ahmed, S. S., W. Santosh, S. Kumar and H. T. Christlet (2009). "Metabolic profiling of Parkinson's disease: evidence of biomarker from gene expression analysis and rapid neural network detection." J Biomed Sci **16**: 63.

Ahting, U., C. Thun, R. Hegerl, D. Typke, F. E. Nargang, W. Neupert and S. Nussberger (1999). "The TOM core complex: the general protein import pore of the outer membrane of mitochondria." J Cell Biol **147**(5): 959-968.

Akbari, M., P. Sykora and V. A. Bohr (2015). "Slow mitochondrial repair of 5'-AMP renders mtDNA susceptible to damage in APTX deficient cells." Sci Rep **5**: 12876.

Akram, M. (2014). "Citric Acid Cycle and Role of its Intermediates in Metabolism." Cell Biochemistry and Biophysics **68**(3): 475-478.

Albrecht, Simone C., Ana G. Barata, J. Großhans, Aurelio A. Teleman and Tobias P. Dick (2011). "In Vivo Mapping of Hydrogen Peroxide and Oxidized Glutathione Reveals Chemical and Regional Specificity of Redox Homeostasis." Cell Metabolism **14**(6): 819-829.

Albrecht, S. C., A. G. Barata, J. Grosshans, A. A. Teleman and T. P. Dick (2011). "In vivo mapping of hydrogen peroxide and oxidized glutathione reveals chemical and regional specificity of redox homeostasis." Cell Metab **14**(6): 819-829.

Alegre-Abarrategui, J., H. Christian, M. M. Lufino, R. Mutihac, L. L. Venda, O. Ansorge and R. Wade-Martins (2009). "LRRK2 regulates autophagic activity and localizes to specific membrane microdomains in a novel human genomic reporter cellular model." Hum Mol Genet **18**(21): 4022-4034.

Alic, N., M. E. Giannakou, I. Papatheodorou, M. P. Hoddinott, T. D. Andrews, E. Bolukbasi and L. Partridge (2014). "Interplay of dFOXO and two ETS-family transcription factors determines lifespan in Drosophila melanogaster." PLoS Genet **10**(9): e1004619.

Allen, G. F., R. Toth, J. James and I. G. Ganley (2013). "Loss of iron triggers PINK1/Parkin-independent mitophagy." EMBO Rep **14**(12): 1127-1135.

Allen, R. D., C. C. Schroeder and A. K. Fok (1989). "An investigation of mitochondrial inner membranes by rapid-freeze deep-etch techniques." J Cell Biol **108**(6): 2233-2240.

Alvarez, A. D., W. Shi, B. A. Wilson and J. B. Skeath (2003). "pannier and pointedP2 act sequentially to regulate Drosophila heart development." Development **130**(13): 3015-3026.

Amuthan, G., G. Biswas, H. K. Ananadatheerthavarada, C. Vijayasarathy, H. M. Shephard and N. G. Avadhani (2002). "Mitochondrial stress-induced calcium signaling,

phenotypic changes and invasive behavior in human lung carcinoma A549 cells." Oncogene **21**(51): 7839-7849.
Anderson, S., A. T. Bankier, B. G. Barrell, M. H. de Bruijn, A. R. Coulson, J. Drouin, I. C. Eperon, D. P. Nierlich, B. A. Roe, F. Sanger, P. H. Schreier, A. J. Smith, R. Staden and I. G. Young (1981). "Sequence and organization of the human mitochondrial genome." Nature **290**(5806): 457-465.
Andreyev, A. Y., Y. E. Kushnareva and A. A. Starkov (2005). "Mitochondrial metabolism of reactive oxygen species." Biochemistry (Mosc) **70**(2): 200-214.
Arnberg, A., E. F. van Bruggen and P. Borst (1971). "The presence of DNA molecules with a displacement loop in standard mitochondrial DNA preparations." Biochim Biophys Acta **246**(2): 353-357.
Ashrafi, G., J. S. Schlehe, M. J. LaVoie and T. L. Schwarz (2014). "Mitophagy of damaged mitochondria occurs locally in distal neuronal axons and requires PINK1 and Parkin." J Cell Biol **206**(5): 655-670.
Attwell, D. and S. B. Laughlin (2001). "An energy budget for signaling in the grey matter of the brain." J Cereb Blood Flow Metab **21**(10): 1133-1145.
Baird, G. S., D. A. Zacharias and R. Y. Tsien (1999). "Circular permutation and receptor insertion within green fluorescent proteins." Proc Natl Acad Sci U S A **96**(20): 11241-11246.
Baker, B. M., A. M. Nargund, T. Sun and C. M. Haynes (2012). "Protective coupling of mitochondrial function and protein synthesis via the eIF2alpha kinase GCN-2." PLoS Genet **8**(6): e1002760.
Baker, D. A., B. Mille-Baker, S. M. Wainwright, D. Ish-Horowicz and N. J. Dibb (2001). "Mae mediates MAP kinase phosphorylation of Ets transcription factors in Drosophila." Nature **411**(6835): 330-334.
Baker, S. K. and M. A. Tarnopolsky (2003). "Targeting cellular energy production in neurological disorders." Expert Opin Investig Drugs **12**(10): 1655-1679.
Baldelli, S., K. Aquilano and M. R. Ciriolo (2014). "PGC-1alpha buffers ROS-mediated removal of mitochondria during myogenesis." Cell Death Dis **5**: e1515.
Ballard, C., S. Gauthier, A. Corbett, C. Brayne, D. Aarsland and E. Jones (2011). "Alzheimer's disease." Lancet **377**(9770): 1019-1031.
Baloyannis, S. J. (2006). "Mitochondrial alterations in Alzheimer's disease." J Alzheimers Dis **9**(2): 119-126.
Baloyannis, S. J., V. Costa and D. Michmizos (2004). "Mitochondrial alterations in Alzheimer's disease." Am J Alzheimers Dis Other Demen **19**(2): 89-93.
Ban, H. S., Y. Uto and H. Nakamura (2011). "Hypoxia-inducible factor inhibitors: a survey of recent patented compounds (2004 - 2010)." Expert Opin Ther Pat **21**(2): 131-146.
Baum, D. A. and B. Baum (2014). "An inside-out origin for the eukaryotic cell." BMC Biol **12**: 76.
Bazan, S., E. Mileykovskaya, V. K. Mallampalli, P. Heacock, G. C. Sparagna and W. Dowhan (2013). "Cardiolipin-dependent reconstitution of respiratory supercomplexes from purified Saccharomyces cerevisiae complexes III and IV." J Biol Chem **288**(1): 401-411.
Beck, S. J., L. Guo, A. Phensy, J. Tian, L. Wang, N. Tandon, E. Gauba, L. Lu, J. M. Pascual, S. Kroener and H. Du (2016). "Deregulation of mitochondrial F1FO-ATP synthase via OSCP in Alzheimer/'s disease." Nat Commun **7**.
Behar, D. M., J. Blue-Smith, D. F. Soria-Hernanz, S. Tzur, Y. Hadid, C. Bormans, A. Moen, C. Tyler-Smith, L. Quintana-Murci, R. S. Wells and C. Genographic (2008). "A novel 154-bp deletion in the human mitochondrial DNA control region in healthy individuals." Hum Mutat **29**(12): 1387-1391.

Bellizzi, D., P. D'Aquila, M. Giordano, A. Montesanto and G. Passarino (2012). "Global DNA methylation levels are modulated by mitochondrial DNA variants." Epigenomics **4**(1): 17-27.
Benit, P., S. Lebon and P. Rustin (2009). "Respiratory-chain diseases related to complex III deficiency." Biochim Biophys Acta **1793**(1): 181-185.
Berg, J., Y. P. Hung and G. Yellen (2009). "A genetically encoded fluorescent reporter of ATP:ADP ratio." Nat Methods **6**(2): 161-166.
Berg JM, T. J., Stryer L. (2002). "Intermediates of the Citric Acid Cycle and Other Major Pathways." Biochemistry. **5th edition**.
Berndt, N. and H. G. Holzhutter (2013). "The high energy demand of neuronal cells caused by passive leak currents is not a waste of energy." Cell Biochem Biophys **67**(2): 527-535.
Bianchi, C., M. L. Genova, G. Parenti Castelli and G. Lenaz (2004). "The mitochondrial respiratory chain is partially organized in a supercomplex assembly: kinetic evidence using flux control analysis." J Biol Chem **279**(35): 36562-36569.
Biswas, G., O. A. Adebanjo, B. D. Freedman, H. K. Anandatheerthavarada, C. Vijayasarathy, M. Zaidi, M. Kotlikoff and N. G. Avadhani (1999). "Retrograde Ca2+ signaling in C2C12 skeletal myocytes in response to mitochondrial genetic and metabolic stress: a novel mode of inter-organelle crosstalk." EMBO J **18**(3): 522-533.
Biswas, G., H. K. Anandatheerthavarada, M. Zaidi and N. G. Avadhani (2003). "Mitochondria to nucleus stress signaling: a distinctive mechanism of NFκB/Rel activation through calcineurin-mediated inactivation of IκBβ." The Journal of Cell Biology **161**(3): 507-519.
Bogenhagen, D. F. (1996). "Interaction of mtTFB and mtRNA polymerase at core promoters for transcription of Xenopus laevis mtDNA." J Biol Chem **271**(20): 12036-12041.
Bohnert, M., N. Pfanner and M. van der Laan (2015). "Mitochondrial machineries for insertion of membrane proteins." Current Opinion in Structural Biology **33**: 92-102.
Boisclair Lachance, J. F., N. Pelaez, J. J. Cassidy, J. L. Webber, I. Rebay and R. W. Carthew (2014). "A comparative study of Pointed and Yan expression reveals new complexity to the transcriptional networks downstream of receptor tyrosine kinase signaling." Dev Biol **385**(2): 263-278.
Boldogh, I., N. Vojtov, S. Karmon and L. A. Pon (1998). "Interaction between mitochondria and the actin cytoskeleton in budding yeast requires two integral mitochondrial outer membrane proteins, Mmm1p and Mdm10p." J Cell Biol **141**(6): 1371-1381.
Boldt, S., U. H. Weidle and W. Kolch (2002). "The role of MAPK pathways in the action of chemotherapeutic drugs." Carcinogenesis **23**(11): 1831-1838.
Bonawitz, N. D., D. A. Clayton and G. S. Shadel (2006). "Initiation and beyond: multiple functions of the human mitochondrial transcription machinery." Mol Cell **24**(6): 813-825.
Bonawitz, N. D., M. S. Rodeheffer and G. S. Shadel (2006). "Defective mitochondrial gene expression results in reactive oxygen species-mediated inhibition of respiration and reduction of yeast life span." Mol Cell Biol **26**(13): 4818-4829.
Bonnefoy, N., H. L. Fiumera, G. Dujardin and T. D. Fox (2009). "Roles of Oxa1-related inner-membrane translocases in assembly of respiratory chain complexes." Biochim Biophys Acta **1793**(1): 60-70.
Booth, F. W. and J. O. Holloszy (1975). "Effect of thyroid hormone administration on synthesis and degradation of cytochrome c in rat liver." Arch Biochem Biophys **167**(2): 674-677.

Boulanger, A., C. Clouet-Redt, M. Farge, A. Flandre, T. Guignard, C. Fernando, F. Juge and J. M. Dura (2011). "ftz-f1 and Hr39 opposing roles on EcR expression during Drosophila mushroom body neuron remodeling." Nat Neurosci **14**(1): 37-44.
Boulanger, A., M. Farge, C. Ramanoudjame, K. Wharton and J. M. Dura (2012). "Drosophila motor neuron retraction during metamorphosis is mediated by inputs from TGF-beta/BMP signaling and orphan nuclear receptors." PLoS One **7**(7): e40255.
Bowmaker, M., M. Y. Yang, T. Yasukawa, A. Reyes, H. T. Jacobs, J. A. Huberman and I. J. Holt (2003). "Mammalian mitochondrial DNA replicates bidirectionally from an initiation zone." J Biol Chem **278**(51): 50961-50969.
Brown, D. T., D. C. Samuels, E. M. Michael, D. M. Turnbull and P. F. Chinnery (2001). "Random genetic drift determines the level of mutant mtDNA in human primary oocytes." Am J Hum Genet **68**(2): 533-536.
Brown, T. A., A. N. Tkachuk and D. A. Clayton (2008). "Native R-loops persist throughout the mouse mitochondrial DNA genome." J Biol Chem **283**(52): 36743-36751.
Browne, S. E., A. C. Bowling, U. MacGarvey, M. J. Baik, S. C. Berger, M. M. Muqit, E. D. Bird and M. F. Beal (1997). "Oxidative damage and metabolic dysfunction in Huntington's disease: selective vulnerability of the basal ganglia." Ann Neurol **41**(5): 646-653.
Bruick, R. K. and S. L. McKnight (2001). "A conserved family of prolyl-4-hydroxylases that modify HIF." Science **294**(5545): 1337-1340.
Brune, B. and J. Zhou (2003). "The role of nitric oxide (NO) in stability regulation of hypoxia inducible factor-1alpha (HIF-1alpha)." Curr Med Chem **10**(10): 845-855.
Brunelle, J. K., E. L. Bell, N. M. Quesada, K. Vercauteren, V. Tiranti, M. Zeviani, R. C. Scarpulla and N. S. Chandel (2005). "Oxygen sensing requires mitochondrial ROS but not oxidative phosphorylation." Cell Metab **1**(6): 409-414.
Bultema, J. B., H. P. Braun, E. J. Boekema and R. Kouril (2009). "Megacomplex organization of the oxidative phosphorylation system by structural analysis of respiratory supercomplexes from potato." Biochim Biophys Acta **1787**(1): 60-67.
Burgstaller, J. P., I. G. Johnston, N. S. Jones, J. Albrechtova, T. Kolbe, C. Vogl, A. Futschik, C. Mayrhofer, D. Klein, S. Sabitzer, M. Blattner, C. Gully, J. Poulton, T. Rulicke, J. Pialek, R. Steinborn and G. Brem (2014). "MtDNA segregation in heteroplasmic tissues is common in vivo and modulated by haplotype differences and developmental stage." Cell Rep **7**(6): 2031-2041.
Burns, N., B. Grimwade, P. B. Ross-Macdonald, E. Y. Choi, K. Finberg, G. S. Roeder and M. Snyder (1994). "Large-scale analysis of gene expression, protein localization, and gene disruption in Saccharomyces cerevisiae." Genes Dev **8**(9): 1087-1105.
Cagin, U. (2012). Investigating neuronal mitochondrial DNA loss in Drosophila. PhD, King's College London.
Cagin, U., O. F. Duncan, A. P. Gatt, M. S. Dionne, S. T. Sweeney and J. M. Bateman (2015). "Mitochondrial retrograde signaling regulates neuronal function." Proc Natl Acad Sci U S A **112**(44): E6000-6009.
Calabrese, C., L. Iommarini, I. Kurelac, M. A. Calvaruso, M. Capristo, P. L. Lollini, P. Nanni, C. Bergamini, G. Nicoletti, C. D. Giovanni, A. Ghelli, V. Giorgio, M. F. Caratozzolo, F. Marzano, C. Manzari, C. M. Betts, V. Carelli, C. Ceccarelli, M. Attimonelli, G. Romeo, R. Fato, M. Rugolo, A. Tullo, G. Gasparre and A. M. Porcelli (2013). "Respiratory complex I is essential to induce a Warburg profile in mitochondria-defective tumor cells." Cancer Metab **1**(1): 11.
Calvo, S. E., K. R. Clauser and V. K. Mootha (2016). "MitoCarta2.0: an updated inventory of mammalian mitochondrial proteins." Nucleic Acids Res **44**(D1): D1251-1257.

Cannon, B. and J. Nedergaard (2004). "Brown adipose tissue: function and physiological significance." Physiol Rev **84**(1): 277-359.
Cardoso, S. M., M. T. Proença, S. Santos, I. Santana and C. R. Oliveira (2004). "Cytochrome c oxidase is decreased in Alzheimer's disease platelets." Neurobiology of Aging **25**(1): 105-110.
Carling, D., V. A. Zammit and D. G. Hardie (1987). "A common bicyclic protein kinase cascade inactivates the regulatory enzymes of fatty acid and cholesterol biosynthesis." FEBS Lett **223**(2): 217-222.
Celotto, A. M., A. C. Frank, S. W. McGrath, T. Fergestad, W. A. Van Voorhies, K. F. Buttle, C. A. Mannella and M. J. Palladino (2006). "Mitochondrial encephalomyopathy in Drosophila." J Neurosci **26**(3): 810-820.
Centanin, L., P. J. Ratcliffe and P. Wappner (2005). "Reversion of lethality and growth defects in Fatiga oxygen-sensor mutant flies by loss of hypoxia-inducible factor-alpha/Sima." EMBO Rep **6**(11): 1070-1075.
Chacinska, A., C. M. Koehler, D. Milenkovic, T. Lithgow and N. Pfanner (2009). "Importing mitochondrial proteins: machineries and mechanisms." Cell **138**(4): 628-644.
Chae, S., B. Y. Ahn, K. Byun, Y. M. Cho, M. H. Yu, B. Lee, D. Hwang and K. S. Park (2013). "A systems approach for decoding mitochondrial retrograde signaling pathways." Sci Signal **6**(264): rs4.
Chan, D. W., V. W. Liu, G. S. Tsao, K. M. Yao, T. Furukawa, K. K. Chan and H. Y. Ngan (2008). "Loss of MKP3 mediated by oxidative stress enhances tumorigenicity and chemoresistance of ovarian cancer cells." Carcinogenesis **29**(9): 1742-1750.
Chang, D. T., A. S. Honick and I. J. Reynolds (2006). "Mitochondrial trafficking to synapses in cultured primary cortical neurons." J Neurosci **26**(26): 7035-7045.
Chen, H., M. Vermulst, Y. E. Wang, A. Chomyn, T. A. Prolla, J. M. McCaffery and D. C. Chan (2010). "Mitochondrial fusion is required for mtDNA stability in skeletal muscle and tolerance of mtDNA mutations." Cell **141**(2): 280-289.
Chen, J., X. Shi, R. Padmanabhan, Q. Wang, Z. Wu, S. C. Stevenson, M. Hild, D. Garza and H. Li (2008). "Identification of novel modulators of mitochondrial function by a genome-wide RNAi screen in Drosophila melanogaster." Genome Research **18**(1): 123-136.
Chen, X., R. Prosser, S. Simonetti, J. Sadlock, G. Jagiello and E. A. Schon (1995). "Rearranged mitochondrial genomes are present in human oocytes." Am J Hum Genet **57**(2): 239-247.
Chen, Y. C., E. B. Taylor, N. Dephoure, J. M. Heo, A. Tonhato, I. Papandreou, N. Nath, N. C. Denko, S. P. Gygi and J. Rutter (2012). "Identification of a protein mediating respiratory supercomplex stability." Cell Metab **15**(3): 348-360.
Chinnery, P. F., D. C. Samuels, J. Elson and D. M. Turnbull (2002). "Accumulation of mitochondrial DNA mutations in ageing, cancer, and mitochondrial disease: is there a common mechanism?" Lancet **360**(9342): 1323-1325.
Chintapalli, V. R., J. Wang and J. A. Dow (2007). "Using FlyAtlas to identify better Drosophila melanogaster models of human disease." Nat Genet **39**(6): 715-720.
Chu, C. T., D. J. Levinthal, S. M. Kulich, E. M. Chalovich and D. B. DeFranco (2004). "Oxidative neuronal injury. The dark side of ERK1/2." Eur J Biochem **271**(11): 2060-2066.
Chuderland, D., G. Marmor, A. Shainskaya and R. Seger (2008). "Calcium-mediated interactions regulate the subcellular localization of extracellular signal-regulated kinases." J Biol Chem **283**(17): 11176-11188.
Clapier, C. R. and B. R. Cairns (2009). "The biology of chromatin remodeling complexes." Annu Rev Biochem **78**: 273-304.

Clark, C. G. and A. J. Roger (1995). "Direct evidence for secondary loss of mitochondria in Entamoeba histolytica." Proc Natl Acad Sci U S A **92**(14): 6518-6521.
Cocheme, H. M., C. Quin, S. J. McQuaker, F. Cabreiro, A. Logan, T. A. Prime, I. Abakumova, J. V. Patel, I. M. Fearnley, A. M. James, C. M. Porteous, R. A. Smith, S. Saeed, J. E. Carre, M. Singer, D. Gems, R. C. Hartley, L. Partridge and M. P. Murphy (2011). "Measurement of H2O2 within living Drosophila during aging using a ratiometric mass spectrometry probe targeted to the mitochondrial matrix." Cell Metab **13**(3): 340-350.
Copeland, J. M., J. Cho, T. Lo, Jr., J. H. Hur, S. Bahadorani, T. Arabyan, J. Rabie, J. Soh and D. W. Walker (2009). "Extension of Drosophila life span by RNAi of the mitochondrial respiratory chain." Curr Biol **19**(19): 1591-1598.
Copeland, W. C. (2008). "Inherited mitochondrial diseases of DNA replication." Annu Rev Med **59**: 131-146.
Cotzias, G. C. (1968). "L-Dopa for Parkinsonism." N Engl J Med **278**(11): 630.
Crabtree, H. G. (1929). "Observations on the carbohydrate metabolism of tumours." Biochem J **23**(3): 536-545.
Cruciat, C. M., K. Hell, H. Folsch, W. Neupert and R. A. Stuart (1999). "Bcs1p, an AAA-family member, is a chaperone for the assembly of the cytochrome bc(1) complex." EMBO J **18**(19): 5226-5233.
Da-Re, C., S. von Stockum, A. Biscontin, C. Millino, P. Cisotto, M. A. Zordan, M. Zeviani, P. Bernardi, C. De Pitta and R. Costa (2014). "Leigh syndrome in Drosophila melanogaster: morphological and biochemical characterization of Surf1 post-transcriptional silencing." J Biol Chem **289**(42): 29235-29246.
Dahia, P. L., K. N. Ross, M. E. Wright, C. Y. Hayashida, S. Santagata, M. Barontini, A. L. Kung, G. Sanso, J. F. Powers, A. S. Tischler, R. Hodin, S. Heitritter, F. Moore, R. Dluhy, J. A. Sosa, I. T. Ocal, D. E. Benn, D. J. Marsh, B. G. Robinson, K. Schneider, J. Garber, S. M. Arum, M. Korbonits, A. Grossman, P. Pigny, S. P. Toledo, V. Nose, C. Li and C. D. Stiles (2005). "A HIF1alpha regulatory loop links hypoxia and mitochondrial signals in pheochromocytomas." PLoS Genet **1**(1): 72-80.
Dairaghi, D. J., G. S. Shadel and D. A. Clayton (1995). "Addition of a 29 residue carboxyl-terminal tail converts a simple HMG box-containing protein into a transcriptional activator." J Mol Biol **249**(1): 11-28.
De Benedictis, G., G. Rose, G. Carrieri, M. De Luca, E. Falcone, G. Passarino, M. Bonafe, D. Monti, G. Baggio, S. Bertolini, D. Mari, R. Mattace and C. Franceschi (1999). "Mitochondrial DNA inherited variants are associated with successful aging and longevity in humans." FASEB J **13**(12): 1532-1536.
Dell'agnello, C., S. Leo, A. Agostino, G. Szabadkai, C. Tiveron, A. Zulian, A. Prelle, P. Roubertoux, R. Rizzuto and M. Zeviani (2007). "Increased longevity and refractoriness to Ca(2+)-dependent neurodegeneration in Surf1 knockout mice." Hum Mol Genet **16**(4): 431-444.
Dennis, G., Jr., B. T. Sherman, D. A. Hosack, J. Yang, W. Gao, H. C. Lane and R. A. Lempicki (2003). "DAVID: Database for Annotation, Visualization, and Integrated Discovery." Genome Biol **4**(5): P3.
Denton, R. M. and J. G. McCormack (1985). "Ca2+ transport by mammalian mitochondria and its role in hormone action." Am J Physiol **249**(6 Pt 1): E543-554.
Dever, T. E., L. Feng, R. C. Wek, A. M. Cigan, T. F. Donahue and A. G. Hinnebusch (1992). "Phosphorylation of initiation factor 2 alpha by protein kinase GCN2 mediates gene-specific translational control of GCN4 in yeast." Cell **68**(3): 585-596.
Diaz, F., H. Fukui, S. Garcia and C. T. Moraes (2006). "Cytochrome c oxidase is required for the assembly/stability of respiratory complex I in mouse fibroblasts." Mol Cell Biol **26**(13): 4872-4881.

Dienhart, M. K. and R. A. Stuart (2008). "The yeast Aac2 protein exists in physical association with the cytochrome bc1-COX supercomplex and the TIM23 machinery." Mol Biol Cell **19**(9): 3934-3943.
Dietzl, G., D. Chen, F. Schnorrer, K.-C. Su, Y. Barinova, M. Fellner, B. Gasser, K. Kinsey, S. Oppel, S. Scheiblauer, A. Couto, V. Marra, K. Keleman and B. J. Dickson (2007). "A genome-wide transgenic RNAi library for conditional gene inactivation in Drosophila." Nature **448**(7150): 151-156.
Dillin, A., A. L. Hsu, N. Arantes-Oliveira, J. Lehrer-Graiwer, H. Hsin, A. G. Fraser, R. S. Kamath, J. Ahringer and C. Kenyon (2002). "Rates of behavior and aging specified by mitochondrial function during development." Science **298**(5602): 2398-2401.
Dombi, E., A. Diot, K. Morten, J. Carver, T. Lodge, C. Fratter, Y. S. Ng, C. Liao, R. Muir, E. L. Blakely, I. Hargreaves, M. Al-Dosary, G. Sarkar, S. J. Hickman, S. M. Downes, S. Jayawant, P. Yu-Wai-Man, R. W. Taylor and J. Poulton (2016). "The m.13051G>A mitochondrial DNA mutation results in variable neurology and activated mitophagy." Neurology **86**(20): 1921-1923.
Dowhan, W., C. R. Bibus and G. Schatz (1985). "The cytoplasmically-made subunit IV is necessary for assembly of cytochrome c oxidase in yeast." EMBO Journal **4**(1): 179-184.
Dudkina, N. V., H. Eubel, W. Keegstra, E. J. Boekema and H. P. Braun (2005). "Structure of a mitochondrial supercomplex formed by respiratory-chain complexes I and III." Proc Natl Acad Sci U S A **102**(9): 3225-3229.
Dudkina, N. V., R. Kouril, K. Peters, H. P. Braun and E. J. Boekema (2010). "Structure and function of mitochondrial supercomplexes." Biochim Biophys Acta **1797**(6-7): 664-670.
Dudkina, N. V., S. Sunderhaus, H. P. Braun and E. J. Boekema (2006). "Characterization of dimeric ATP synthase and cristae membrane ultrastructure from Saccharomyces and Polytomella mitochondria." FEBS Lett **580**(14): 3427-3432.
Durand, A. and M. Merrick (2006). "In vitro analysis of the Escherichia coli AmtB-GlnK complex reveals a stoichiometric interaction and sensitivity to ATP and 2-oxoglutarate." J Biol Chem **281**(40): 29558-29567.
Ekstrand, M. I., M. Terzioglu, D. Galter, S. Zhu, C. Hofstetter, E. Lindqvist, S. Thams, A. Bergstrand, F. S. Hansson, A. Trifunovic, B. Hoffer, S. Cullheim, A. H. Mohammed, L. Olson and N. G. Larsson (2007). "Progressive parkinsonism in mice with respiratory-chain-deficient dopamine neurons." Proc Natl Acad Sci U S A **104**(4): 1325-1330.
Enari, M., H. Sakahira, H. Yokoyama, K. Okawa, A. Iwamatsu and S. Nagata (1998). "A caspase-activated DNase that degrades DNA during apoptosis, and its inhibitor ICAD." Nature **391**(6662): 43-50.
Endres, W., K. Ballanyi, G. Serve and P. Grafe (1986). "Excitatory amino acids and intracellular pH in motoneurons of the isolated frog spinal cord." Neurosci Lett **72**(1): 54-58.
Ernster, L. and G. Schatz (1981). "Mitochondria: a historical review." J Cell Biol **91**(3 Pt 2): 227s-255s.
Eubel, H., J. Heinemeyer, S. Sunderhaus and H. P. Braun (2004). "Respiratory chain supercomplexes in plant mitochondria." Plant Physiol Biochem **42**(12): 937-942.
Fan, W., K. G. Waymire, N. Narula, P. Li, C. Rocher, P. E. Coskun, M. A. Vannan, J. Narula, G. R. Macgregor and D. C. Wallace (2008). "A mouse model of mitochondrial disease reveals germline selection against severe mtDNA mutations." Science **319**(5865): 958-962.
Fantin, V. R., J. St-Pierre and P. Leder (2006). "Attenuation of LDH-A expression uncovers a link between glycolysis, mitochondrial physiology, and tumor maintenance." Cancer Cell **9**(6): 425-434.

Farge, G., S. Touraille, R. Debise and S. Alziari (2002). "The respiratory chain complex thresholds in mitochondria of a Drosophila subobscura mutant strain." Biochimie **84**(12): 1189-1197.
Fernandez-Ayala, D. J., S. Chen, E. Kemppainen, K. M. O'Dell and H. T. Jacobs (2010). "Gene expression in a Drosophila model of mitochondrial disease." PLoS One **5**(1): e8549.
Fernandez-Vizarra, E., V. Tiranti and M. Zeviani (2009). "Assembly of the oxidative phosphorylation system in humans: what we have learned by studying its defects." Biochim Biophys Acta **1793**(1): 200-211.
Ferree, A. W., K. Trudeau, E. Zik, I. Y. Benador, G. Twig, R. A. Gottlieb and O. S. Shirihai (2013). "MitoTimer probe reveals the impact of autophagy, fusion, and motility on subcellular distribution of young and old mitochondrial protein and on relative mitochondrial protein age." Autophagy **9**(11): 1887-1896.
Finck, B. N. and D. P. Kelly (2007). "Peroxisome proliferator-activated receptor gamma coactivator-1 (PGC-1) regulatory cascade in cardiac physiology and disease." Circulation **115**(19): 2540-2548.
Firth, J. D., B. L. Ebert and P. J. Ratcliffe (1995). "Hypoxic regulation of lactate dehydrogenase A. Interaction between hypoxia-inducible factor 1 and cAMP response elements." J Biol Chem **270**(36): 21021-21027.
Fisher, R. P. and D. A. Clayton (1988). "Purification and characterization of human mitochondrial transcription factor 1." Mol Cell Biol **8**(8): 3496-3509.
Fisher, R. P., J. N. Topper and D. A. Clayton (1987). "Promoter selection in human mitochondria involves binding of a transcription factor to orientation-independent upstream regulatory elements." Cell **50**(2): 247-258.
Foretz, M., S. Hebrard, J. Leclerc, E. Zarrinpashneh, M. Soty, G. Mithieux, K. Sakamoto, F. Andreelli and B. Viollet (2010). "Metformin inhibits hepatic gluconeogenesis in mice independently of the LKB1/AMPK pathway via a decrease in hepatic energy state." J Clin Invest **120**(7): 2355-2369.
Forte, M., H. R. Guy and C. A. Mannella (1987). "Molecular genetics of the VDAC ion channel: structural model and sequence analysis." J Bioenerg Biomembr **19**(4): 341-350.
Fransson, A., A. Ruusala and P. Aspenstrom (2003). "Atypical Rho GTPases have roles in mitochondrial homeostasis and apoptosis." J Biol Chem **278**(8): 6495-6502.
Freeman, M. (1996). "Reiterative use of the EGF receptor triggers differentiation of all cell types in the Drosophila eye." Cell **87**(4): 651-660.
Freije, W. A., S. Mandal and U. Banerjee (2012). "Expression profiling of attenuated mitochondrial function identifies retrograde signals in Drosophila." G3 (Bethesda) **2**(8): 843-851.
Fukuda, R., K. Hirota, F. Fan, Y. D. Jung, L. M. Ellis and G. L. Semenza (2002). "Insulin-like growth factor 1 induces hypoxia-inducible factor 1-mediated vascular endothelial growth factor expression, which is dependent on MAP kinase and phosphatidylinositol 3-kinase signaling in colon cancer cells." J Biol Chem **277**(41): 38205-38211.
Fukuda, R., H. Zhang, J. W. Kim, L. Shimoda, C. V. Dang and G. L. Semenza (2007). "HIF-1 regulates cytochrome oxidase subunits to optimize efficiency of respiration in hypoxic cells." Cell **129**(1): 111-122.
Fukui, H., F. Diaz, S. Garcia and C. T. Moraes (2007). "Cytochrome c oxidase deficiency in neurons decreases both oxidative stress and amyloid formation in a mouse model of Alzheimer's disease." Proc Natl Acad Sci U S A **104**(35): 14163-14168.
Fukui, H. and C. T. Moraes (2009). "Mechanisms of formation and accumulation of mitochondrial DNA deletions in aging neurons." Hum Mol Genet **18**(6): 1028-1036.

Gabay, L., H. Scholz, M. Golembo, A. Klaes, B. Z. Shilo and C. Klambt (1996). "EGF receptor signaling induces pointed P1 transcription and inactivates Yan protein in the Drosophila embryonic ventral ectoderm." Development **122**(11): 3355-3362.
Garcia-Heredia, J. M. and A. Carnero (2015). "Decoding Warburg's hypothesis: tumor-related mutations in the mitochondrial respiratory chain." Oncotarget **6**(39): 41582-41599.
Garesse, R. and L. S. Kaguni (2005). "A Drosophila model of mitochondrial DNA replication: proteins, genes and regulation." IUBMB Life **57**(8): 555-561.
Gatenby, R. A. and R. J. Gillies (2004). "Why do cancers have high aerobic glycolysis?" Nat Rev Cancer **4**(11): 891-899.
Gatt, A. P., O. F. Duncan, J. Attems, P. T. Francis, C. G. Ballard and J. M. Bateman (2016). "Dementia in Parkinson's disease is associated with enhanced mitochondrial complex I deficiency." Mov Disord **31**(3): 352-359.
Gegg, M. E., J. M. Cooper, K. Y. Chau, M. Rojo, A. H. Schapira and J. W. Taanman (2010). "Mitofusin 1 and mitofusin 2 are ubiquitinated in a PINK1/parkin-dependent manner upon induction of mitophagy." Hum Mol Genet **19**(24): 4861-4870.
Gellerich, F. N., S. Trumbeckaite, J. R. Opalka, E. Seppet, H. N. Rasmussen, C. Neuhoff and S. Zierz (2000). "Function of the mitochondrial outer membrane as a diffusion barrier in health and diseases." Biochem Soc Trans **28**(2): 164-169.
Gillick, K. and M. Crompton (2008). "Evaluating cytochrome c diffusion in the intermembrane spaces of mitochondria during cytochrome c release." J Cell Sci **121**(Pt 5): 618-626.
Gollnick, P. D., R. B. Armstrong, C. W. t. Saubert, K. Piehl and B. Saltin (1972). "Enzyme activity and fiber composition in skeletal muscle of untrained and trained men." J Appl Physiol **33**(3): 312-319.
Goto, A., Y. Matsushima, T. Kadowaki and Y. Kitagawa (2001). "Drosophila mitochondrial transcription factor A (d-TFAM) is dispensable for the transcription of mitochondrial DNA in Kc167 cells." Biochem J **354**(Pt 2): 243-248.
Goto, Y., I. Nonaka and S. Horai (1990). "A mutation in the tRNA(Leu)(UUR) gene associated with the MELAS subgroup of mitochondrial encephalomyopathies." Nature **348**(6302): 651-653.
Gozdz, A., A. Habas, J. Jaworski, M. Zielinska, J. Albrecht, M. Chlystun, A. Jalili and M. Hetman (2003). "Role of N-methyl-D-aspartate receptors in the neuroprotective activation of extracellular signal-regulated kinase 1/2 by cisplatin." J Biol Chem **278**(44): 43663-43671.
Graham, B. H., K. G. Waymire, B. Cottrell, I. A. Trounce, G. R. MacGregor and D. C. Wallace (1997). "A mouse model for mitochondrial myopathy and cardiomyopathy resulting from a deficiency in the heart/muscle isoform of the adenine nucleotide translocator." Nat Genet **16**(3): 226-234.
Graham, T. G., S. M. Tabei, A. R. Dinner and I. Rebay (2010). "Modeling bistable cell-fate choices in the Drosophila eye: qualitative and quantitative perspectives." Development **137**(14): 2265-2278.
Green, E. W., G. Fedele, F. Giorgini and C. P. Kyriacou (2014). "A Drosophila RNAi collection is subject to dominant phenotypic effects." Nat Meth **11**(3): 222-223.
Greene, J. C., A. J. Whitworth, L. A. Andrews, T. J. Parker and L. J. Pallanck (2005). "Genetic and genomic studies of Drosophila parkin mutants implicate oxidative stress and innate immune responses in pathogenesis." Hum Mol Genet **14**(6): 799-811.
Greene, J. C., A. J. Whitworth, I. Kuo, L. A. Andrews, M. B. Feany and L. J. Pallanck (2003). "Mitochondrial pathology and apoptotic muscle degeneration in Drosophila parkin mutants." Proc Natl Acad Sci U S A **100**(7): 4078-4083.

Greenleaf, A. L., J. L. Kelly and I. R. Lehman (1986). "Yeast RPO41 gene product is required for transcription and maintenance of the mitochondrial genome." Proc Natl Acad Sci U S A **83**(10): 3391-3394.
Guo, X., G. T. Macleod, A. Wellington, F. Hu, S. Panchumarthi, M. Schoenfield, L. Marin, M. P. Charlton, H. L. Atwood and K. E. Zinsmaier (2005). "The GTPase dMiro is required for axonal transport of mitochondria to Drosophila synapses." Neuron **47**(3): 379-393.
Gutscher, M., A.-L. Pauleau, L. Marty, T. Brach, G. H. Wabnitz, Y. Samstag, A. J. Meyer and T. P. Dick (2008). "Real-time imaging of the intracellular glutathione redox potential." Nat Meth **5**(6): 553-559.
Hackenbrock, C. R., B. Chazotte and S. S. Gupte (1986). "The random collision model and a critical assessment of diffusion and collision in mitochondrial electron transport." J Bioenerg Biomembr **18**(5): 331-368.
Hales, K. G. and M. T. Fuller (1997). "Developmentally regulated mitochondrial fusion mediated by a conserved, novel, predicted GTPase." Cell **90**(1): 121-129.
Hallberg, B. M. and N. G. Larsson (2011). "TFAM forces mtDNA to make a U-turn." Nat Struct Mol Biol **18**(11): 1179-1181.
Hamanaka, R. B., A. Glasauer, P. Hoover, S. Yang, H. Blatt, A. R. Mullen, S. Getsios, C. J. Gottardi, R. J. DeBerardinis, R. M. Lavker and N. S. Chandel (2013). "Mitochondrial reactive oxygen species promote epidermal differentiation and hair follicle development." Sci Signal **6**(261): ra8.
Hamanaka, R. B., S. E. Weinberg, C. R. Reczek and N. S. Chandel (2016). "The mitochondrial respiratory chain is required for organismal adaptation to hypoxia." Cell reports **15**(3): 451-459.
Hampl, V., J. D. Silberman, A. Stechmann, S. Diaz-Trivino, P. J. Johnson and A. J. Roger (2008). "Genetic evidence for a mitochondriate ancestry in the 'amitochondriate' flagellate Trimastix pyriformis." PLoS One **3**(1): e1383.
Han, G., R. J. Casson, G. Chidlow and J. P. M. Wood (2014). "The Mitochondrial Complex I Inhibitor Rotenone Induces Endoplasmic Reticulum Stress and Activation of GSK-3β in Cultured Rat Retinal CellsRotenone Induces ER Stress and Activates GSK-3β." Investigative Ophthalmology & Visual Science **55**(9): 5616-5628.
Han, J. Y., S. H. Oh, F. Morgillo, J. N. Myers, E. Kim, W. K. Hong and H. Y. Lee (2005). "Hypoxia-inducible factor 1alpha and antiangiogenic activity of farnesyltransferase inhibitor SCH66336 in human aerodigestive tract cancer." J Natl Cancer Inst **97**(17): 1272-1286.
Hanson, G. T., R. Aggeler, D. Oglesbee, M. Cannon, R. A. Capaldi, R. Y. Tsien and S. J. Remington (2004). "Investigating mitochondrial redox potential with redox-sensitive green fluorescent protein indicators." J Biol Chem **279**(13): 13044-13053.
Hardie, D. G. (2011). "AMP-activated protein kinase—an energy sensor that regulates all aspects of cell function." Genes & Development **25**(18): 1895-1908.
Hardie, D. G., D. Carling and S. J. Gamblin (2011). "AMP-activated protein kinase: also regulated by ADP?" Trends in Biochemical Sciences **36**(9): 470-477.
Hardie, D. G. and S. A. Hawley (2001). "AMP-activated protein kinase: the energy charge hypothesis revisited." Bioessays **23**(12): 1112-1119.
Harding, H. P., Y. Zhang and D. Ron (1999). "Protein translation and folding are coupled by an endoplasmic-reticulum-resident kinase." Nature **397**(6716): 271-274.
Harman, D. (1956). "Aging: a theory based on free radical and radiation chemistry." J Gerontol **11**(3): 298-300.
Harris, F. M., W. J. Brecht, Q. Xu, R. W. Mahley and Y. Huang (2004). "Increased tau phosphorylation in apolipoprotein E4 transgenic mice is associated with activation of extracellular signal-regulated kinase: modulation by zinc." J Biol Chem **279**(43): 44795-44801.

Harris, Julia J., R. Jolivet and D. Attwell "Synaptic Energy Use and Supply." Neuron **75**(5): 762-777.
Hashimoto, Y., T. Niikura, H. Tajima, T. Yasukawa, H. Sudo, Y. Ito, Y. Kita, M. Kawasumi, K. Kouyama, M. Doyu, G. Sobue, T. Koide, S. Tsuji, J. Lang, K. Kurokawa and I. Nishimoto (2001). "A rescue factor abolishing neuronal cell death by a wide spectrum of familial Alzheimer's disease genes and Abeta." Proc Natl Acad Sci U S A **98**(11): 6336-6341.
Haut, S., M. Brivet, G. Touati, P. Rustin, S. Lebon, A. Garcia-Cazorla, J. M. Saudubray, A. Boutron, A. Legrand and A. Slama (2003). "A deletion in the human QP-C gene causes a complex III deficiency resulting in hypoglycaemia and lactic acidosis." Hum Genet **113**(2): 118-122.
Haynes, C. M., C. J. Fiorese and Y. F. Lin (2013). "Evaluating and responding to mitochondrial dysfunction: the mitochondrial unfolded-protein response and beyond." Trends Cell Biol **23**(7): 311-318.
Hemrika, W., G. Lobo-Hajdu, J. A. Berden and L. A. Grivell (1994). "The aromatic nature of residue 66 of the 11-kDa subunit of ubiquinol-cytochrome c oxidoreductase of the yeast Saccharomyces cerevisiae is important for the assembly of a functional enzyme." FEBS Lett **344**(1): 15-19.
Hernandez, G., C. Thornton, A. Stotland, D. Lui, J. Sin, J. Ramil, N. Magee, A. Andres, G. Quarato, R. S. Carreira, M. R. Sayen, R. Wolkowicz and R. A. Gottlieb (2013). "MitoTimer: a novel tool for monitoring mitochondrial turnover." Autophagy **9**(11): 1852-1861.
Herrmann, J. M. and S. Funes (2005). "Biogenesis of cytochrome oxidase-sophisticated assembly lines in the mitochondrial inner membrane." Gene **354**: 43-52.
Herrmann, J. M. and J. Riemer (2010). "The intermembrane space of mitochondria." Antioxid Redox Signal **13**(9): 1341-1358.
Herrnstadt, C., J. L. Elson, E. Fahy, G. Preston, D. M. Turnbull, C. Anderson, S. S. Ghosh, J. M. Olefsky, M. F. Beal, R. E. Davis and N. Howell (2002). "Reduced-median-network analysis of complete mitochondrial DNA coding-region sequences for the major African, Asian, and European haplogroups." Am J Hum Genet **70**(5): 1152-1171.
Hetman, M. and A. Gozdz (2004). "Role of extracellular signal regulated kinases 1 and 2 in neuronal survival." Eur J Biochem **271**(11): 2050-2055.
Hildenbeutel, M., E. L. Hegg, K. Stephan, S. Gruschke, B. Meunier and M. Ott (2014). "Assembly factors monitor sequential hemylation of cytochrome b to regulate mitochondrial translation." J Cell Biol **205**(4): 511-524.
Hill, J. H., Z. Chen and H. Xu (2014). "Selective propagation of functional mitochondrial DNA during oogenesis restricts the transmission of a deleterious mitochondrial variant." Nat Genet **46**(4): 389-392.
Hock, M. B. and A. Kralli (2009). "Transcriptional control of mitochondrial biogenesis and function." Annu Rev Physiol **71**: 177-203.
Hoefs, S. J., O. H. Skjeldal, R. J. Rodenburg, B. Nedregaard, E. P. van Kaauwen, U. Spiekerkotter, J. C. von Kleist-Retzow, J. A. Smeitink, L. G. Nijtmans and L. P. van den Heuvel (2010). "Novel mutations in the NDUFS1 gene cause low residual activities in human complex I deficiencies." Mol Genet Metab **100**(3): 251-256.
Holloszy, J. O. (1967). "Biochemical adaptations in muscle. Effects of exercise on mitochondrial oxygen uptake and respiratory enzyme activity in skeletal muscle." J Biol Chem **242**(9): 2278-2282.
Holt, I. J., A. E. Harding and J. A. Morgan-Hughes (1988). "Deletions of muscle mitochondrial DNA in patients with mitochondrial myopathies." Nature **331**(6158): 717-719.

Holt, I. J., H. E. Lorimer and H. T. Jacobs (2000). "Coupled leading- and lagging-strand synthesis of mammalian mitochondrial DNA." Cell **100**(5): 515-524.
Holt, I. J. and A. Reyes (2012). "Human mitochondrial DNA replication." Cold Spring Harb Perspect Biol **4**(12).
Homouz, D., G. Chen and A. S. Kudlicki (2015). "Correcting positional correlations in Affymetrix(R) genome chips." Sci Rep **5**: 9078.
Houten, S. M. and R. J. Wanders (2010). "A general introduction to the biochemistry of mitochondrial fatty acid beta-oxidation." J Inherit Metab Dis **33**(5): 469-477.
Houtkooper, R. H., L. Mouchiroud, D. Ryu, N. Moullan, E. Katsyuba, G. Knott, R. W. Williams and J. Auwerx (2013). "Mitonuclear protein imbalance as a conserved longevity mechanism." Nature **497**(7450): 451-457.
Huang, T. T., E. J. Carlson, A. M. Gillespie, Y. Shi and C. J. Epstein (2000). "Ubiquitous overexpression of CuZn superoxide dismutase does not extend life span in mice." J Gerontol A Biol Sci Med Sci **55**(1): B5-9.
Humphrey, D. M., R. B. Parsons, Z. N. Ludlow, T. Riemensperger, G. Esposito, P. Verstreken, H. T. Jacobs, S. Birman and F. Hirth (2012). "Alternative oxidase rescues mitochondria-mediated dopaminergic cell loss in Drosophila." Hum Mol Genet **21**(12): 2698-2712.
Hurd, T. R., F. X. Liang and R. Lehmann (2015). "Curly Encodes Dual Oxidase, Which Acts with Heme Peroxidase Curly Su to Shape the Adult Drosophila Wing." PLoS Genet **11**(11): e1005625.
Hyslop, L. A., P. Blakeley, L. Craven, J. Richardson, N. M. Fogarty, E. Fragouli, M. Lamb, S. E. Wamaitha, N. Prathalingam, Q. Zhang, H. O'Keefe, Y. Takeda, L. Arizzi, S. Alfarawati, H. A. Tuppen, L. Irving, D. Kalleas, M. Choudhary, D. Wells, A. P. Murdoch, D. M. Turnbull, K. K. Niakan and M. Herbert (2016). "Towards clinical application of pronuclear transfer to prevent mitochondrial DNA disease." Nature **534**(7607): 383-386.
Indo, H. P., H. C. Yen, I. Nakanishi, K. Matsumoto, M. Tamura, Y. Nagano, H. Matsui, O. Gusev, R. Cornette, T. Okuda, Y. Minamiyama, H. Ichikawa, S. Suenaga, M. Oki, T. Sato, T. Ozawa, D. K. Clair and H. J. Majima (2015). "A mitochondrial superoxide theory for oxidative stress diseases and aging." J Clin Biochem Nutr **56**(1): 1-7.
Inoue, K., K. Nakada, A. Ogura, K. Isobe, Y. Goto, I. Nonaka and J. I. Hayashi (2000). "Generation of mice with mitochondrial dysfunction by introducing mouse mtDNA carrying a deletion into zygotes." Nat Genet **26**(2): 176-181.
Isaacs, J. S., Y. J. Jung, D. R. Mole, S. Lee, C. Torres-Cabala, Y. L. Chung, M. Merino, J. Trepel, B. Zbar, J. Toro, P. J. Ratcliffe, W. M. Linehan and L. Neckers (2005). "HIF overexpression correlates with biallelic loss of fumarate hydratase in renal cancer: novel role of fumarate in regulation of HIF stability." Cancer Cell **8**(2): 143-153.
Ishihara, N., M. Nomura, A. Jofuku, H. Kato, S. O. Suzuki, K. Masuda, H. Otera, Y. Nakanishi, I. Nonaka, Y.-i. Goto, N. Taguchi, H. Morinaga, M. Maeda, R. Takayanagi, S. Yokota and K. Mihara (2009). "Mitochondrial fission factor Drp1 is essential for embryonic development and synapse formation in mice." Nat Cell Biol **11**(8): 958-966.
Iyengar, B., N. Luo, C. L. Farr, L. S. Kaguni and A. R. Campos (2002). "The accessory subunit of DNA polymerase gamma is essential for mitochondrial DNA maintenance and development in Drosophila melanogaster." Proc Natl Acad Sci U S A **99**(7): 4483-4488.
Jacobs, H. T. (1997). "Mitochondrial deafness." Ann Med **29**(6): 483-491.
Jahangir Tafrechi, R. S., P. J. Svensson, G. M. Janssen, K. Szuhai, J. A. Maassen and A. K. Raap (2005). "Distinct nuclear gene expression profiles in cells with mtDNA depletion and homoplasmic A3243G mutation." Mutat Res **578**(1-2): 43-52.
Jahangir Tafrechi, R. S., P. J. Svensson, G. M. C. Janssen, K. Szuhai, J. A. Maassen and A. K. Raap (2005). "Distinct nuclear gene expression profiles in cells with mtDNA

depletion and homoplasmic A3243G mutation." Mutation Research/Fundamental and Molecular Mechanisms of Mutagenesis **578**(1–2): 43-52.
Jain, I. H., L. Zazzeron, R. Goli, K. Alexa, S. Schatzman-Bone, H. Dhillon, O. Goldberger, J. Peng, O. Shalem, N. E. Sanjana, F. Zhang, W. Goessling, W. M. Zapol and V. K. Mootha (2016). "Hypoxia as a therapy for mitochondrial disease." Science **352**(6281): 54-61.
Jani-Acsadi, A., K. Krajewski and M. E. Shy (2008). "Charcot-Marie-Tooth neuropathies: diagnosis and management." Semin Neurol **28**(2): 185-194.
Jenkins, B. G., W. J. Koroshetz, M. F. Beal and B. R. Rosen (1993). "Evidence for impairment of energy metabolism in vivo in Huntington's disease using localized 1H NMR spectroscopy." Neurology **43**(12): 2689-2695.
Jensen, P. A., X. Zheng, T. Lee and M. B. O'Connor (2009). "The Drosophila Activin-like ligand Dawdle signals preferentially through one isoform of the Type-I receptor Baboon." Mechanisms of development **126**(11-12): 950-957.
Jenuth, J. P., A. C. Peterson and E. A. Shoubridge (1997). "Tissue-specific selection for different mtDNA genotypes in heteroplasmic mice." Nat Genet **16**(1): 93-95.
Jia, Y., B. Rothermel, J. Thornton and R. A. Butow (1997). "A basic helix-loop-helix-leucine zipper transcription complex in yeast functions in a signaling pathway from mitochondria to the nucleus." Mol Cell Biol **17**(3): 1110-1117.
Johnson, S. C., M. E. Yanos, E. B. Kayser, A. Quintana, M. Sangesland, A. Castanza, L. Uhde, J. Hui, V. Z. Wall, A. Gagnidze, K. Oh, B. M. Wasko, F. J. Ramos, R. D. Palmiter, P. S. Rabinovitch, P. G. Morgan, M. M. Sedensky and M. Kaeberlein (2013). "mTOR inhibition alleviates mitochondrial disease in a mouse model of Leigh syndrome." Science **342**(6165): 1524-1528.
Ju, Y. S., L. B. Alexandrov, M. Gerstung, I. Martincorena, S. Nik-Zainal, M. Ramakrishna, H. R. Davies, E. Papaemmanuil, G. Gundem, A. Shlien, N. Bolli, S. Behjati, P. S. Tarpey, J. Nangalia, C. E. Massie, A. P. Butler, J. W. Teague, G. S. Vassiliou, A. R. Green, M. Q. Du, A. Unnikrishnan, J. E. Pimanda, B. T. Teh, N. Munshi, M. Greaves, P. Vyas, A. K. El-Naggar, T. Santarius, V. P. Collins, R. Grundy, J. A. Taylor, D. N. Hayes, D. Malkin, I. B. C. Group, I. C. M. D. Group, I. P. C. Group, C. S. Foster, A. Y. Warren, H. C. Whitaker, D. Brewer, R. Eeles, C. Cooper, D. Neal, T. Visakorpi, W. B. Isaacs, G. S. Bova, A. M. Flanagan, P. A. Futreal, A. G. Lynch, P. F. Chinnery, U. McDermott, M. R. Stratton and P. J. Campbell (2014). "Origins and functional consequences of somatic mitochondrial DNA mutations in human cancer." Elife **3**.
Kalia, L. V. and A. E. Lang (2015). "Parkinson's disease." The Lancet **386**(9996): 896-912.
Kang, D., S. H. Kim and N. Hamasaki (2007). "Mitochondrial transcription factor A (TFAM): roles in maintenance of mtDNA and cellular functions." Mitochondrion **7**(1-2): 39-44.
Kanki, T., K. Ohgaki, M. Gaspari, C. M. Gustafsson, A. Fukuoh, N. Sasaki, N. Hamasaki and D. Kang (2004). "Architectural role of mitochondrial transcription factor A in maintenance of human mitochondrial DNA." Mol Cell Biol **24**(22): 9823-9834.
Karuppagounder, S. S., H. Xu, Q. Shi, L. H. Chen, S. Pedrini, D. Pechman, H. Baker, M. F. Beal, S. E. Gandy and G. E. Gibson (2009). "Thiamine deficiency induces oxidative stress and exacerbates the plaque pathology in Alzheimer's mouse model." Neurobiol Aging **30**(10): 1587-1600.
Kasamatsu, H., D. L. Robberson and J. Vinograd (1971). "A novel closed-circular mitochondrial DNA with properties of a replicating intermediate." Proc Natl Acad Sci U S A **68**(9): 2252-2257.
Kasamatsu, H. and J. Vinograd (1973). "Unidirectionality of replication in mouse mitochondrial DNA." Nat New Biol **241**(108): 103-105.

Kasiviswanathan, R., T. R. Collins and W. C. Copeland (2012). "The interface of transcription and DNA replication in the mitochondria." Biochim Biophys Acta **1819**(9-10): 970-978.
Kaufman, B. A., N. Durisic, J. M. Mativetsky, S. Costantino, M. A. Hancock, P. Grutter and E. A. Shoubridge (2007). "The mitochondrial transcription factor TFAM coordinates the assembly of multiple DNA molecules into nucleoid-like structures." Mol Biol Cell **18**(9): 3225-3236.
Kayalar, C., J. Rosing and P. D. Boyer (1977). "An alternating site sequence for oxidative phosphorylation suggested by measurement of substrate binding patterns and exchange reaction inhibitions." J Biol Chem **252**(8): 2486-2491.
Keeney, P. M., J. Xie, R. A. Capaldi and J. P. Bennett, Jr. (2006). "Parkinson's disease brain mitochondrial complex I has oxidatively damaged subunits and is functionally impaired and misassembled." J Neurosci **26**(19): 5256-5264.
Kemppainen, K. K., J. Rinne, A. Sriram, M. Lakanmaa, A. Zeb, T. Tuomela, A. Popplestone, S. Singh, A. Sanz, P. Rustin and H. T. Jacobs (2014). "Expression of alternative oxidase in Drosophila ameliorates diverse phenotypes due to cytochrome oxidase deficiency." Human Molecular Genetics **23**(8): 2078-2093.
Khakh, B. S. and G. Burnstock (2009). "The double life of ATP." Sci Am **301**(6): 84-90, 92.
Kim, E. K. and E. J. Choi (2010). "Pathological roles of MAPK signaling pathways in human diseases." Biochim Biophys Acta **1802**(4): 396-405.
Kim, K., Y. S. Lee, D. Harris, K. Nakahara and R. W. Carthew (2006). "The RNAi pathway initiated by Dicer-2 in Drosophila." Cold Spring Harb Symp Quant Biol **71**: 39-44.
Kim, S. H., R. Vlkolinsky, N. Cairns, M. Fountoulakis and G. Lubec (2001). "The reduction of NADH." Life Sciences **68**(24): 2741-2750.
Kim, Y., J. Park, S. Kim, S. Song, S. K. Kwon, S. H. Lee, T. Kitada, J. M. Kim and J. Chung (2008). "PINK1 controls mitochondrial localization of Parkin through direct phosphorylation." Biochem Biophys Res Commun **377**(3): 975-980.
Klambt, C. (1993). "The Drosophila gene pointed encodes two ETS-like proteins which are involved in the development of the midline glial cells." Development **117**(1): 163-176.
Klambt, C., L. Glazer and B. Z. Shilo (1992). "breathless, a Drosophila FGF receptor homolog, is essential for migration of tracheal and specific midline glial cells." Genes Dev **6**(9): 1668-1678.
Klegeris, A., S. Pelech, B. I. Giasson, J. Maguire, H. Zhang, E. G. McGeer and P. L. McGeer (2008). "α-Synuclein activates stress signaling protein kinases in THP-1 cells and microglia." Neurobiology of Aging **29**(5): 739-752.
Klein, C. and A. Westenberger (2012). "Genetics of Parkinson's disease." Cold Spring Harb Perspect Med **2**(1): a008888.
Knowles, H. J., R. R. Raval, A. L. Harris and P. J. Ratcliffe (2003). "Effect of ascorbate on the activity of hypoxia-inducible factor in cancer cells." Cancer Res **63**(8): 1764-1768.
Koh, Y. H., E. Popova, U. Thomas, L. C. Griffith and V. Budnik (1999). "Regulation of DLG Localization at Synapses by CaMKII-Dependent Phosphorylation." Cell **98**(3): 353-363.
Koopman, W. J., F. Distelmaier, J. A. Smeitink and P. H. Willems (2013). "OXPHOS mutations and neurodegeneration." EMBO J **32**(1): 9-29.
Korwitz, A., C. Merkwirth, R. Richter-Dennerlein, S. E. Troder, H. G. Sprenger, P. M. Quiros, C. Lopez-Otin, E. I. Rugarli and T. Langer (2016). "Loss of OMA1 delays neurodegeneration by preventing stress-induced OPA1 processing in mitochondria." J Cell Biol **212**(2): 157-166.

Krause, F., N. H. Reifschneider, S. Goto and N. A. Dencher (2005). "Active oligomeric ATP synthases in mammalian mitochondria." Biochem Biophys Res Commun **329**(2): 583-590.
Kruse, S. E., W. C. Watt, D. J. Marcinek, R. P. Kapur, K. A. Schenkman and R. D. Palmiter (2008). "Mice with mitochondrial complex I deficiency develop a fatal encephalomyopathy." Cell Metab **7**(4): 312-320.
Kukat, C. and N. G. Larsson (2013). "mtDNA makes a U-turn for the mitochondrial nucleoid." Trends Cell Biol **23**(9): 457-463.
Kunkele, K. P., S. Heins, M. Dembowski, F. E. Nargang, R. Benz, M. Thieffry, J. Walz, R. Lill, S. Nussberger and W. Neupert (1998). "The preprotein translocation channel of the outer membrane of mitochondria." Cell **93**(6): 1009-1019.
Kurihara, T., P. D. Westenskow, M. L. Gantner, Y. Usui, A. Schultz, S. Bravo, E. Aguilar, C. Wittgrove, M. Friedlander, L. P. Paris, E. Chew, G. Siuzdak and M. Friedlander (2016). "Hypoxia-induced metabolic stress in retinal pigment epithelial cells is sufficient to induce photoreceptor degeneration." Elife **5**.
Lai, Z. C. and G. M. Rubin (1992). "Negative control of photoreceptor development in Drosophila by the product of the yan gene, an ETS domain protein." Cell **70**(4): 609-620.
Laker, R. C., P. Xu, K. A. Ryall, A. Sujkowski, B. M. Kenwood, K. H. Chain, M. Zhang, M. A. Royal, K. L. Hoehn, M. Driscoll, P. N. Adler, R. J. Wessells, J. J. Saucerman and Z. Yan (2014). "A novel MitoTimer reporter gene for mitochondrial content, structure, stress, and damage in vivo." J Biol Chem **289**(17): 12005-12015.
Lander, H. M., D. P. Hajjar, B. L. Hempstead, U. A. Mirza, B. T. Chait, S. Campbell and L. A. Quilliam (1997). "A molecular redox switch on p21(ras). Structural basis for the nitric oxide-p21(ras) interaction." J Biol Chem **272**(7): 4323-4326.
Lando, D., D. J. Peet, J. J. Gorman, D. A. Whelan, M. L. Whitelaw and R. K. Bruick (2002). "FIH-1 is an asparaginyl hydroxylase enzyme that regulates the transcriptional activity of hypoxia-inducible factor." Genes & Development **16**(12): 1466-1471.
Lane, N. and W. Martin (2010). "The energetics of genome complexity." Nature **467**(7318): 929-934.
Langston, J. W., P. Ballard, J. W. Tetrud and I. Irwin (1983). "Chronic Parkinsonism in humans due to a product of meperidine-analog synthesis." Science **219**(4587): 979-980.
Lanning, Nathan J., Brendan D. Looyenga, Audra L. Kauffman, Natalie M. Niemi, J. Sudderth, Ralph J. DeBerardinis and Jeffrey P. MacKeigan "A Mitochondrial RNAi Screen Defines Cellular Bioenergetic Determinants and Identifies an Adenylate Kinase as a Key Regulator of ATP Levels." Cell Reports **7**(3): 907-917.
Larsson, N. G., J. Wang, H. Wilhelmsson, A. Oldfors, P. Rustin, M. Lewandoski, G. S. Barsh and D. A. Clayton (1998). "Mitochondrial transcription factor A is necessary for mtDNA maintenance and embryogenesis in mice." Nat Genet **18**(3): 231-236.
Latorre-Pellicer, A., R. Moreno-Loshuertos, A. V. Lechuga-Vieco, F. Sanchez-Cabo, C. Torroja, R. Acin-Perez, E. Calvo, E. Aix, A. Gonzalez-Guerra, A. Logan, M. L. Bernad-Miana, E. Romanos, R. Cruz, S. Cogliati, B. Sobrino, A. Carracedo, A. Perez-Martos, P. Fernandez-Silva, J. Ruiz-Cabello, M. P. Murphy, I. Flores, J. Vazquez and J. A. Enriquez (2016). "Mitochondrial and nuclear DNA matching shapes metabolism and healthy ageing." Nature.
Lavara-Culebras, E. and N. Paricio (2007). "Drosophila DJ-1 mutants are sensitive to oxidative stress and show reduced lifespan and motor deficits." Gene **400**(1–2): 158-165.
Lavista-Llanos, S., L. Centanin, M. Irisarri, D. M. Russo, J. M. Gleadle, S. N. Bocca, M. Muzzopappa, P. J. Ratcliffe and P. Wappner (2002). "Control of the hypoxic response in Drosophila melanogaster by the basic helix-loop-helix PAS protein similar." Mol Cell Biol **22**(19): 6842-6853.

Lee, H. J., S. Y. Shin, C. Choi, Y. H. Lee and S. J. Lee (2002). "Formation and removal of alpha-synuclein aggregates in cells exposed to mitochondrial inhibitors." J Biol Chem **277**(7): 5411-5417.
Lee, I. C., A. W. El-Hattab, J. Wang, F. Y. Li, S. W. Weng, W. J. Craigen and L. J. Wong (2012). "SURF1-associated Leigh syndrome: a case series and novel mutations." Hum Mutat **33**(8): 1192-1200.
Lee, K. A., B. Kim, H. You and W. J. Lee (2015). "Uracil-induced signaling pathways for DUOX-dependent gut immunity." Fly (Austin) **9**(3): 115-120.
Lee, T. and L. Luo (1999). "Mosaic Analysis with a Repressible Cell Marker for Studies of Gene Function in Neuronal Morphogenesis." Neuron **22**(3): 451-461.
Lefai, E., M. Calleja, I. Ruiz de Mena, A. T. Lagina, 3rd, L. S. Kaguni and R. Garesse (2000). "Overexpression of the catalytic subunit of DNA polymerase gamma results in depletion of mitochondrial DNA in Drosophila melanogaster." Mol Gen Genet **264**(1-2): 37-46.
Levkowitz, G., H. Waterman, S. A. Ettenberg, M. Katz, A. Y. Tsygankov, I. Alroy, S. Lavi, K. Iwai, Y. Reiss, A. Ciechanover, S. Lipkowitz and Y. Yarden (1999). "Ubiquitin ligase activity and tyrosine phosphorylation underlie suppression of growth factor signaling by c-Cbl/Sli-1." Mol Cell **4**(6): 1029-1040.
Lewis, S. C., L. F. Uchiyama and J. Nunnari (2016). "ER-mitochondria contacts couple mtDNA synthesis with mitochondrial division in human cells." Science **353**(6296): aaf5549.
Lezi, E. and R. H. Swerdlow (2012). "Mitochondria in neurodegeneration." Adv Exp Med Biol **942**: 269-286.
Li, J., H. Y. Shuai, E. Gylfe and A. Tengholm (2013). "Oscillations of sub-membrane ATP in glucose-stimulated beta cells depend on negative feedback from Ca(2+)." Diabetologia **56**(7): 1577-1586.
Li, X. B., J. D. Gu and Q. H. Zhou (2015). "Review of aerobic glycolysis and its key enzymes - new targets for lung cancer therapy." Thorac Cancer **6**(1): 17-24.
Li, Y., D. Padmanabha, L. B. Gentile, C. I. Dumur, R. B. Beckstead and K. D. Baker (2013). "HIF- and non-HIF-regulated hypoxic responses require the estrogen-related receptor in Drosophila melanogaster." PLoS Genet **9**(1): e1003230.
Liao, T. S., G. B. Call, P. Guptan, A. Cespedes, J. Marshall, K. Yackle, E. Owusu-Ansah, S. Mandal, Q. A. Fang, G. L. Goodstein, W. Kim and U. Banerjee (2006). "An efficient genetic screen in Drosophila to identify nuclear-encoded genes with mitochondrial function." Genetics **174**(1): 525-533.
Liao, X. S., W. C. Small, P. A. Srere and R. A. Butow (1991). "Intramitochondrial functions regulate nonmitochondrial citrate synthase (CIT2) expression in Saccharomyces cerevisiae." Mol Cell Biol **11**(1): 38-46.
Lill, R. (2009). "Function and biogenesis of iron-sulphur proteins." Nature **460**(7257): 831-838.
Lillig, C. H., C. Berndt and A. Holmgren (2008). "Glutaredoxin systems." Biochimica et Biophysica Acta (BBA) - General Subjects **1780**(11): 1304-1317.
Liou, G.-Y. and P. Storz (2010). "Reactive oxygen species in cancer." Free radical research **44**(5): 10.3109/10715761003667554.
Littleton, J. T., E. R. Chapman, R. Kreber, M. B. Garment, S. D. Carlson and B. Ganetzky (1998). "Temperature-sensitive paralytic mutations demonstrate that synaptic exocytosis requires SNARE complex assembly and disassembly." Neuron **21**(2): 401-413.
Liu, L. and M. C. Simon (2004). "Regulation of transcription and translation by hypoxia." Cancer Biol Ther **3**(6): 492-497.
Liu, S., T. Sawada, S. Lee, W. Yu, G. Silverio, P. Alapatt, I. Millan, A. Shen, W. Saxton, T. Kanao, R. Takahashi, N. Hattori, Y. Imai and B. Lu (2012). "Parkinson's

disease-associated kinase PINK1 regulates Miro protein level and axonal transport of mitochondria." PLoS Genet **8**(3): e1002537.
Liu, W., R. Gnanasambandam, J. Benjamin, G. Kaur, P. B. Getman, A. J. Siegel, R. D. Shortridge and S. Singh (2007). "Mutations in cytochrome c oxidase subunit VIa cause neurodegeneration and motor dysfunction in Drosophila." Genetics **176**(2): 937-946.
Liu, Z. and R. A. Butow (2006). "Mitochondrial retrograde signaling." Annu Rev Genet **40**: 159-185.
Logan, A., I. G. Shabalina, T. A. Prime, S. Rogatti, A. V. Kalinovich, R. C. Hartley, R. C. Budd, B. Cannon and M. P. Murphy (2014). "In vivo levels of mitochondrial hydrogen peroxide increase with age in mtDNA mutator mice." Aging Cell **13**(4): 765-768.
Luan, H., W. C. Lemon, N. C. Peabody, J. B. Pohl, P. K. Zelensky, D. Wang, M. N. Nitabach, T. C. Holmes and B. H. White (2006). "Functional dissection of a neuronal network required for cuticle tanning and wing expansion in Drosophila." J Neurosci **26**(2): 573-584.
Luo, Y., J. D. Bond and V. M. Ingram (1997). "Compromised mitochondrial function leads to increased cytosolic calcium and to activation of MAP kinases." Proc Natl Acad Sci U S A **94**(18): 9705-9710.
Luo, Y. and D. B. DeFranco (2006). "Opposing roles for ERK1/2 in neuronal oxidative toxicity: distinct mechanisms of ERK1/2 action at early versus late phases of oxidative stress." J Biol Chem **281**(24): 16436-16442.
Lynch, M. and G. K. Marinov (2016). "Reply to Lane and Martin: Mitochondria do not boost the bioenergetic capacity of eukaryotic cells." Proceedings of the National Academy of Sciences **113**(6): E667-E668.
Ma, H., H. Xu and P. H. O'Farrell (2014). "Transmission of mitochondrial mutations and action of purifying selection in Drosophila melanogaster." Nat Genet **46**(4): 393-397.
Ma, X., M. Jin, Y. Cai, H. Xia, K. Long, J. Liu, Q. Yu and J. Yuan (2011). "Mitochondrial Electron Transport Chain Complex III Is Required for Antimycin A to Inhibit Autophagy." Chemistry & biology **18**(11): 1474-1481.
MacAskill, A. F., J. E. Rinholm, A. E. Twelvetrees, I. L. Arancibia-Carcamo, J. Muir, A. Fransson, P. Aspenstrom, D. Attwell and J. T. Kittler (2009). "Miro1 Is a Calcium Sensor for Glutamate Receptor-Dependent Localization of Mitochondria at Synapses." Neuron **61**(4): 541-555.
MacKenzie, E. D., M. A. Selak, D. A. Tennant, L. J. Payne, S. Crosby, C. M. Frederiksen, D. G. Watson and E. Gottlieb (2007). "Cell-permeating alpha-ketoglutarate derivatives alleviate pseudohypoxia in succinate dehydrogenase-deficient cells." Mol Cell Biol **27**(9): 3282-3289.
Mahr, A. and H. Aberle (2006). "The expression pattern of the Drosophila vesicular glutamate transporter: a marker protein for motoneurons and glutamatergic centers in the brain." Gene Expr Patterns **6**(3): 299-309.
Majmundar, A. J., W. J. Wong and M. C. Simon (2010). "Hypoxia-inducible factors and the response to hypoxic stress." Mol Cell **40**(2): 294-309.
Malka, F., O. Guillery, C. Cifuentes-Diaz, E. Guillou, P. Belenguer, A. Lombes and M. Rojo (2005). "Separate fusion of outer and inner mitochondrial membranes." EMBO Rep **6**(9): 853-859.
Manczak, M., B. S. Park, Y. Jung and P. H. Reddy (2004). "Differential expression of oxidative phosphorylation genes in patients with Alzheimer's disease: implications for early mitochondrial dysfunction and oxidative damage." Neuromolecular Med **5**(2): 147-162.

Mandal, S., P. Guptan, E. Owusu-Ansah and U. Banerjee (2005). "Mitochondrial regulation of cell cycle progression during development as revealed by the tenured mutation in Drosophila." Dev Cell **9**(6): 843-854.
Maniura-Weber, K., S. Goffart, H. L. Garstka, J. Montoya and R. J. Wiesner (2004). "Transient overexpression of mitochondrial transcription factor A (TFAM) is sufficient to stimulate mitochondrial DNA transcription, but not sufficient to increase mtDNA copy number in cultured cells." Nucleic Acids Res **32**(20): 6015-6027.
Martin, H., C. Eckerskorn, F. Gartner, J. Rassow, F. Lottspeich and N. Pfanner (1998). "The yeast mitochondrial intermembrane space: purification and analysis of two distinct fractions." Anal Biochem **265**(1): 123-128.
Martin, J., K. Mahlke and N. Pfanner (1991). "Role of an energized inner membrane in mitochondrial protein import. Delta psi drives the movement of presequences." J Biol Chem **266**(27): 18051-18057.
Martin, W. and M. Muller (1998). "The hydrogen hypothesis for the first eukaryote." Nature **392**(6671): 37-41.
Masoud, G. N. and W. Li (2015). "HIF-1alpha pathway: role, regulation and intervention for cancer therapy." Acta Pharm Sin B **5**(5): 378-389.
Masoud, G. N. and W. Li (2015). "HIF-1α pathway: role, regulation and intervention for cancer therapy." Acta Pharmaceutica Sinica B **5**(5): 378-389.
Masters, B. S., L. L. Stohl and D. A. Clayton (1987). "Yeast mitochondrial RNA polymerase is homologous to those encoded by bacteriophages T3 and T7." Cell **51**(1): 89-99.
Maurer, I., S. Zierz and H. J. Moller (2000). "A selective defect of cytochrome c oxidase is present in brain of Alzheimer disease patients." Neurobiol Aging **21**(3): 455-462.
Mauvezin, C., M. Orpinell, V. A. Francis, F. Mansilla, J. Duran, V. Ribas, M. Palacin, P. Boya, A. A. Teleman and A. Zorzano (2010). "The nuclear cofactor DOR regulates autophagy in mammalian and Drosophila cells." EMBO Rep **11**(1): 37-44.
Maxwell, P. H., M. S. Wiesener, G. W. Chang, S. C. Clifford, E. C. Vaux, M. E. Cockman, C. C. Wykoff, C. W. Pugh, E. R. Maher and P. J. Ratcliffe (1999). "The tumour suppressor protein VHL targets hypoxia-inducible factors for oxygen-dependent proteolysis." Nature **399**(6733): 271-275.
McCammon, M. T., C. B. Epstein, B. Przybyla-Zawislak, L. McAlister-Henn and R. A. Butow (2003). "Global transcription analysis of Krebs tricarboxylic acid cycle mutants reveals an alternating pattern of gene expression and effects on hypoxic and oxidative genes." Mol Biol Cell **14**(3): 958-972.
McCulloch, V. and G. S. Shadel (2003). "Human mitochondrial transcription factor B1 interacts with the C-terminal activation region of h-mtTFA and stimulates transcription independently of its RNA methyltransferase activity." Mol Cell Biol **23**(16): 5816-5824.
McKenzie, M., M. Lazarou, D. R. Thorburn and M. T. Ryan (2006). "Mitochondrial respiratory chain supercomplexes are destabilized in Barth Syndrome patients." J Mol Biol **361**(3): 462-469.
Melser, S., Etienne H. Chatelain, J. Lavie, W. Mahfouf, C. Jose, E. Obre, S. Goorden, M. Priault, Y. Elgersma, Hamid R. Rezvani, R. Rossignol and G. Bénard (2013). "Rheb Regulates Mitophagy Induced by Mitochondrial Energetic Status." Cell Metabolism **17**(5): 719-730.
Menger, K. E., A. M. James, H. M. Cocheme, M. E. Harbour, E. T. Chouchani, S. Ding, I. M. Fearnley, L. Partridge and M. P. Murphy (2015). "Fasting, but Not Aging, Dramatically Alters the Redox Status of Cysteine Residues on Proteins in Drosophila melanogaster." Cell Rep **11**(12): 1856-1865.
Menzies, F. M., S. C. Yenisetti and K. T. Min (2005). "Roles of Drosophila DJ-1 in survival of dopaminergic neurons and oxidative stress." Curr Biol **15**(17): 1578-1582.

Mick, David U., S. Dennerlein, H. Wiese, R. Reinhold, D. Pacheu-Grau, I. Lorenzi, F. Sasarman, W. Weraarpachai, Eric A. Shoubridge, B. Warscheid and P. Rehling "MITRAC Links Mitochondrial Protein Translocation to Respiratory-Chain Assembly and Translational Regulation." Cell **151**(7): 1528-1541.
Milan, M., F. J. Diaz-Benjumea and S. M. Cohen (1998). "Beadex encodes an LMO protein that regulates Apterous LIM-homeodomain activity in Drosophila wing development: a model for LMO oncogene function." Genes Dev **12**(18): 2912-2920.
Miller, F. J., F. L. Rosenfeldt, C. Zhang, A. W. Linnane and P. Nagley (2003). "Precise determination of mitochondrial DNA copy number in human skeletal and cardiac muscle by a PCR-based assay: lack of change of copy number with age." Nucleic Acids Res **31**(11): e61.
Milton, V. J., H. E. Jarrett, K. Gowers, S. Chalak, L. Briggs, I. M. Robinson and S. T. Sweeney (2011). "Oxidative stress induces overgrowth of the Drosophila neuromuscular junction." Proc Natl Acad Sci U S A **108**(42): 17521-17526.
Mishra, P. and D. C. Chan (2016). "Metabolic regulation of mitochondrial dynamics." J Cell Biol **212**(4): 379-387.
Mitchell, P. (1961). "Coupling of phosphorylation to electron and hydrogen transfer by a chemi-osmotic type of mechanism." Nature **191**: 144-148.
Miyadera, H., H. Amino, A. Hiraishi, H. Taka, K. Murayama, H. Miyoshi, K. Sakamoto, N. Ishii, S. Hekimi and K. Kita (2001). "Altered quinone biosynthesis in the long-lived clk-1 mutants of Caenorhabditis elegans." J Biol Chem **276**(11): 7713-7716.
Miyako, K., T. Irie, T. Muta, S. Umeda, Y. Kai, T. Fujiwara, K. Takeshige and D. Kang (1999). "1-Methyl-4-phenylpyridinium ion (MPP+) selectively inhibits the replication of mitochondrial DNA." Eur J Biochem **259**(1-2): 412-418.
Mockett, R. J., B. H. Sohal and R. S. Sohal (2010). "Expression of multiple copies of mitochondrially targeted catalase or genomic Mn superoxide dismutase transgenes does not extend the life span of Drosophila melanogaster." Free Radical Biology and Medicine **49**(12): 2028-2031.
Moore, D. J., V. L. Dawson and T. M. Dawson (2006). "Lessons from Drosophila Models of DJ-1 Deficiency." Sci. Aging Knowl. Environ. **2006**(2): pe2-.
Morava, E., R. J. Rodenburg, F. Hol, M. de Vries, A. Janssen, L. van den Heuvel, L. Nijtmans and J. Smeitink (2006). "Clinical and biochemical characteristics in patients with a high mutant load of the mitochondrial T8993G/C mutations." Am J Med Genet A **140**(8): 863-868.
Murphy, M. P. (2009). "How mitochondria produce reactive oxygen species." Biochem J **417**(1): 1-13.
Murphy, M. P., M. J. Krueger, S. O. Sablin, R. R. Ramsay and T. P. Singer (1995). "Inhibition of complex I by hydrophobic analogues of N-methyl-4-phenylpyridinium (MPP+) and the use of an ion-selective electrode to measure their accumulation by mitochondria and electron-transport particles." Biochem J **306 (Pt 2)**: 359-365.
Nakamura, M., D. Baldwin, S. Hannaford, J. Palka and C. Montell (2002). "Defective proboscis extension response (DPR), a member of the Ig superfamily required for the gustatory response to salt." J Neurosci **22**(9): 3463-3472.
Narendra, D., A. Tanaka, D.-F. Suen and R. J. Youle (2008). "Parkin is recruited selectively to impaired mitochondria and promotes their autophagy." The Journal of Cell Biology **183**(5): 795-803.
Nargund, A. M., M. W. Pellegrino, C. J. Fiorese, B. M. Baker and C. M. Haynes (2012). "Mitochondrial import efficiency of ATFS-1 regulates mitochondrial UPR activation." Science **337**(6094): 587-590.
Nass, S. and M. M. Nass (1963). "Intramitochondrial Fibers with DNA Characteristics. Ii. Enzymatic and Other Hydrolytic Treatments." J Cell Biol **19**: 613-629.

Nemoto, S., M. M. Fergusson and T. Finkel (2005). "SIRT1 functionally interacts with the metabolic regulator and transcriptional coactivator PGC-1{alpha}." J Biol Chem **280**(16): 16456-16460.
Ngo, H. B., J. T. Kaiser and D. C. Chan (2011). "The mitochondrial transcription and packaging factor Tfam imposes a U-turn on mitochondrial DNA." Nat Struct Mol Biol **18**(11): 1290-1296.
Ni, J. Q., M. Markstein, R. Binari, B. Pfeiffer, L. P. Liu, C. Villalta, M. Booker, L. Perkins and N. Perrimon (2008). "Vector and parameters for targeted transgenic RNA interference in Drosophila melanogaster." Nat Methods **5**(1): 49-51.
Niemeyer, B. A. and T. L. Schwarz (2000). "SNAP-24, a Drosophila SNAP-25 homologue on granule membranes, is a putative mediator of secretion and granule-granule fusion in salivary glands." Journal of Cell Science **113**(22): 4055-4064.
Niikura, T., E. Sidahmed, C. Hirata-Fukae, P. S. Aisen and Y. Matsuoka (2011). "A humanin derivative reduces amyloid beta accumulation and ameliorates memory deficit in triple transgenic mice." PLoS One **6**(1): e16259.
Nusslein-Volhard, C. and E. Wieschaus (1980). "Mutations affecting segment number and polarity in Drosophila." Nature **287**(5785): 795-801.
O'Hagan, H. M., W. Wang, S. Sen, C. Destefano Shields, S. S. Lee, Y. W. Zhang, E. G. Clements, Y. Cai, L. Van Neste, H. Easwaran, R. A. Casero, C. L. Sears and S. B. Baylin (2011). "Oxidative damage targets complexes containing DNA methyltransferases, SIRT1, and polycomb members to promoter CpG Islands." Cancer Cell **20**(5): 606-619.
O'Neill, E. M., I. Rebay, R. Tjian and G. M. Rubin (1994). "The activities of two Ets-related transcription factors required for drosophila eye development are modulated by the Ras/MAPK pathway." Cell **78**(1): 137-147.
O'Neill, E. M., I. Rebay, R. Tjian and G. M. Rubin (1994). "The activities of two Ets-related transcription factors required for Drosophila eye development are modulated by the Ras/MAPK pathway." Cell **78**(1): 137-147.
Ohno, N., G. J. Kidd, D. Mahad, S. Kiryu-Seo, A. Avishai, H. Komuro and B. D. Trapp (2011). "Myelination and axonal electrical activity modulate the distribution and motility of mitochondria at CNS nodes of Ranvier." J Neurosci **31**(20): 7249-7258.
Ohshiro, T., Y. Emori and K. Saigo (2002). "Ligand-dependent activation of breathless FGF receptor gene in Drosophila developing trachea." Mech Dev **114**(1-2): 3-11.
Okado-Matsumoto, A. and I. Fridovich (2001). "Subcellular distribution of superoxide dismutases (SOD) in rat liver: Cu,Zn-SOD in mitochondria." J Biol Chem **276**(42): 38388-38393.
Orr, W. C. and R. S. Sohal (1994). "Extension of life-span by overexpression of superoxide dismutase and catalase in Drosophila melanogaster." Science **263**(5150): 1128-1130.
Osada, M., S. Imaoka and Y. Funae (2004). "Apigenin suppresses the expression of VEGF, an important factor for angiogenesis, in endothelial cells via degradation of HIF-1alpha protein." FEBS Lett **575**(1-3): 59-63.
Ostergaard, H., A. Henriksen, F. G. Hansen and J. R. Winther (2001). "Shedding light on disulfide bond formation: engineering a redox switch in green fluorescent protein." EMBO J **20**(21): 5853-5862.
Owusu-Ansah, E., W. Song and N. Perrimon (2013). "Muscle mitohormesis promotes longevity via systemic repression of insulin signaling." Cell **155**(3): 699-712.
Owusu-Ansah, E., A. Yavari, S. Mandal and U. Banerjee (2008). "Distinct mitochondrial retrograde signals control the G1-S cell cycle checkpoint." Nat Genet **40**(3): 356-361.

Pacelli, C., N. Giguere, M. J. Bourque, M. Levesque, R. S. Slack and L. E. Trudeau (2015). "Elevated Mitochondrial Bioenergetics and Axonal Arborization Size Are Key Contributors to the Vulnerability of Dopamine Neurons." Curr Biol **25**(18): 2349-2360.
Palade, G. E. (1953). "An electron microscope study of the mitochondrial structure." J Histochem Cytochem **1**(4): 188-211.
Parikh, V. S., M. M. Morgan, R. Scott, L. S. Clements and R. A. Butow (1987). "The mitochondrial genotype can influence nuclear gene expression in yeast." Science **235**(4788): 576-580.
Parisi, M. A., B. Xu and D. A. Clayton (1993). "A human mitochondrial transcriptional activator can functionally replace a yeast mitochondrial HMG-box protein both in vivo and in vitro." Mol Cell Biol **13**(3): 1951-1961.
Park, J., S. Y. Kim, G.-H. Cha, S. B. Lee, S. Kim and J. Chung (2005). "Drosophila DJ-1 mutants show oxidative stress-sensitive locomotive dysfunction." Gene **361**: 133-139.
Parker, L., J. E. Ellis, M. Q. Nguyen and K. Arora (2006). "The divergent TGF-beta ligand Dawdle utilizes an activin pathway to influence axon guidance in Drosophila." Development **133**(24): 4981-4991.
Parker, W. D., Jr., S. J. Boyson and J. K. Parks (1989). "Abnormalities of the electron transport chain in idiopathic Parkinson's disease." Ann Neurol **26**(6): 719-723.
Parsons, C. G., W. Danysz, A. Dekundy and I. Pulte (2013). "Memantine and cholinesterase inhibitors: complementary mechanisms in the treatment of Alzheimer's disease." Neurotox Res **24**(3): 358-369.
Pei, J. J., H. Braak, W. L. An, B. Winblad, R. F. Cowburn, K. Iqbal and I. Grundke-Iqbal (2002). "Up-regulation of mitogen-activated protein kinases ERK1/2 and MEK1/2 is associated with the progression of neurofibrillary degeneration in Alzheimer's disease." Brain Res Mol Brain Res **109**(1-2): 45-55.
Pelaez, N., A. Gavalda-Miralles, B. Wang, H. T. Navarro, H. Gudjonson, I. Rebay, A. R. Dinner, A. K. Katsaggelos, L. A. Amaral and R. W. Carthew (2015). "Dynamics and heterogeneity of a fate determinant during transition towards cell differentiation." Elife **4**.
Pequignot, M. O., R. Dey, M. Zeviani, V. Tiranti, C. Godinot, A. Poyau, C. Sue, S. Di Mauro, M. Abitbol and C. Marsac (2001). "Mutations in the SURF1 gene associated with Leigh syndrome and cytochrome C oxidase deficiency." Hum Mutat **17**(5): 374-381.
Pereira, C. F. and C. R. Oliveira (2000). "Oxidative glutamate toxicity involves mitochondrial dysfunction and perturbation of intracellular Ca2+ homeostasis." Neurosci Res **37**(3): 227-236.
Perrin, L., S. Bloyer, C. Ferraz, N. Agrawal, P. Sinha and J. M. Dura (2003). "The leucine zipper motif of the Drosophila AF10 homologue can inhibit PRE-mediated repression: implications for leukemogenic activity of human MLL-AF10 fusions." Mol Cell Biol **23**(1): 119-130.
Pfanner, N. and W. Neupert (1985). "Transport of proteins into mitochondria: a potassium diffusion potential is able to drive the import of ADP/ATP carrier." EMBO J **4**(11): 2819-2825.
Pianet, I., M. Merle, J. Labouesse and P. Canioni (1991). "Phosphorus-31 nuclear magnetic resonance of C6 glioma cells and rat astrocytes. Evidence for a modification of the longitudinal relaxation time of ATP and Pi during glucose starvation." Eur J Biochem **195**(1): 87-95.
Picard, M., J. Zhang, S. Hancock, O. Derbeneva, R. Golhar, P. Golik, S. O'Hearn, S. Levy, P. Potluri, M. Lvova, A. Davila, C. S. Lin, J. C. Perin, E. F. Rappaport, H. Hakonarson, I. A. Trounce, V. Procaccio and D. C. Wallace (2014). "Progressive increase in mtDNA 3243A>G heteroplasmy causes abrupt transcriptional reprogramming." Proc Natl Acad Sci U S A **111**(38): E4033-4042.

Pickrell, A. M., M. Pinto, A. Hida and C. T. Moraes (2011). "Striatal dysfunctions associated with mitochondrial DNA damage in dopaminergic neurons in a mouse model of Parkinson's disease." J Neurosci **31**(48): 17649-17658.
Pickrell, Alicia M. and Richard J. Youle "The Roles of PINK1, Parkin, and Mitochondrial Fidelity in Parkinson’s Disease." Neuron **85**(2): 257-273.
Pitkanen, S. and B. H. Robinson "Mitochondrial complex I deficiency leads to increased production of superoxide radicals and induction of superoxide dismutase." The Journal of Clinical Investigation **98**(2): 345-351.
Pohjoismaki, J. L., S. Wanrooij, A. K. Hyvarinen, S. Goffart, I. J. Holt, J. N. Spelbrink and H. T. Jacobs (2006). "Alterations to the expression level of mitochondrial transcription factor A, TFAM, modify the mode of mitochondrial DNA replication in cultured human cells." Nucleic Acids Res **34**(20): 5815-5828.
Pollard, P. J., J. J. Briere, N. A. Alam, J. Barwell, E. Barclay, N. C. Wortham, T. Hunt, M. Mitchell, S. Olpin, S. J. Moat, I. P. Hargreaves, S. J. Heales, Y. L. Chung, J. R. Griffiths, A. Dalgleish, J. A. McGrath, M. J. Gleeson, S. V. Hodgson, R. Poulsom, P. Rustin and I. P. Tomlinson (2005). "Accumulation of Krebs cycle intermediates and over-expression of HIF1alpha in tumours which result from germline FH and SDH mutations." Hum Mol Genet **14**(15): 2231-2239.
Pons, R., A. L. Andreu, N. Checcarelli, M. R. Vila, K. Engelstad, C. M. Sue, D. Shungu, R. Haggerty, D. C. de Vivo and S. DiMauro (2004). "Mitochondrial DNA abnormalities and autistic spectrum disorders." J Pediatr **144**(1): 81-85.
Porcelli, A. M., A. Ghelli, C. Ceccarelli, M. Lang, G. Cenacchi, M. Capristo, L. F. Pennisi, I. Morra, E. Ciccarelli, A. Melcarne, A. Bartoletti-Stella, N. Salfi, G. Tallini, A. Martinuzzi, V. Carelli, M. Attimonelli, M. Rugolo, G. Romeo and G. Gasparre (2010). "The genetic and metabolic signature of oncocytic transformation implicates HIF1alpha destabilization." Hum Mol Genet **19**(6): 1019-1032.
Prezant, T. R., J. V. Agapian, M. C. Bohlman, X. Bu, S. Oztas, W. Q. Qiu, K. S. Arnos, G. A. Cortopassi, L. Jaber, J. I. Rotter and et al. (1993). "Mitochondrial ribosomal RNA mutation associated with both antibiotic-induced and non-syndromic deafness." Nat Genet **4**(3): 289-294.
Puigserver, P., Z. Wu, C. W. Park, R. Graves, M. Wright and B. M. Spiegelman (1998). "A cold-inducible coactivator of nuclear receptors linked to adaptive thermogenesis." Cell **92**(6): 829-839.
Quinlan, C. L., A. L. Orr, I. V. Perevoshchikova, J. R. Treberg, B. A. Ackrell and M. D. Brand (2012). "Mitochondrial complex II can generate reactive oxygen species at high rates in both the forward and reverse reactions." J Biol Chem **287**(32): 27255-27264.
Quintana, A., S. E. Kruse, R. P. Kapur, E. Sanz and R. D. Palmiter (2010). "Complex I deficiency due to loss of Ndufs4 in the brain results in progressive encephalopathy resembling Leigh syndrome." Proc Natl Acad Sci U S A **107**(24): 10996-11001.
Quiros, P. M., A. Mottis and J. Auwerx (2016). "Mitonuclear communication in homeostasis and stress." Nat Rev Mol Cell Biol **17**(4): 213-226.
Raimundo, N., B. E. Baysal and G. S. Shadel "Revisiting the TCA cycle: signaling to tumor formation." Trends in Molecular Medicine **17**(11): 641-649.
Raimundo, N., L. Song, T. E. Shutt, S. E. McKay, J. Cotney, M. X. Guan, T. C. Gilliland, D. Hohuan, J. Santos-Sacchi and G. S. Shadel (2012). "Mitochondrial stress engages E2F1 apoptotic signaling to cause deafness." Cell **148**(4): 716-726.
Ramaiah, A., J. A. Hathaway and D. E. Atkinson (1964). "ADENYLATE AS A METABOLIC REGULATOR. EFFECT ON YEAST PHOSPHOFRUCTOKINASE KINETICS." J Biol Chem **239**: 3619-3622.
Ramanan, V. K. and A. J. Saykin (2013). "Pathways to neurodegeneration: mechanistic insights from GWAS in Alzheimer's disease, Parkinson's disease, and related disorders." Am J Neurodegener Dis **2**(3): 145-175.

Rebay, I. and G. M. Rubin (1995). "Yan functions as a general inhibitor of differentiation and is negatively regulated by activation of the Ras1/MAPK pathway." Cell **81**(6): 857-866.
Rehling, P., K. Brandner and N. Pfanner (2004). "Mitochondrial import and the twin-pore translocase." Nat Rev Mol Cell Biol **5**(7): 519-530.
Reinecke, F., J. A. Smeitink and F. H. van der Westhuizen (2009). "OXPHOS gene expression and control in mitochondrial disorders." Biochim Biophys Acta **1792**(12): 1113-1121.
Reiter, L. T., L. Potocki, S. Chien, M. Gribskov and E. Bier (2001). "A Systematic Analysis of Human Disease-Associated Gene Sequences In Drosophila melanogaster." Genome Research **11**(6): 1114-1125.
Ricci, J.-E., C. Muñoz-Pinedo, P. Fitzgerald, B. Bailly-Maitre, G. A. Perkins, N. Yadava, I. E. Scheffler, M. H. Ellisman and D. R. Green (2004). "Disruption of Mitochondrial Function during Apoptosis Is Mediated by Caspase Cleavage of the p75 Subunit of Complex I of the Electron Transport Chain." Cell **117**(6): 773-786.
Ricci, J. E., R. A. Gottlieb and D. R. Green (2003). "Caspase-mediated loss of mitochondrial function and generation of reactive oxygen species during apoptosis." J Cell Biol **160**(1): 65-75.
Richard, D. E., E. Berra, E. Gothie, D. Roux and J. Pouyssegur (1999). "p42/p44 mitogen-activated protein kinases phosphorylate hypoxia-inducible factor 1alpha (HIF-1alpha) and enhance the transcriptional activity of HIF-1." J Biol Chem **274**(46): 32631-32637.
Rivera, M. C. and J. A. Lake (1992). "Evidence that eukaryotes and eocyte prokaryotes are immediate relatives." Science **257**(5066): 74-76.
Rizzuto, R., D. De Stefani, A. Raffaello and C. Mammucari (2012). "Mitochondria as sensors and regulators of calcium signalling." Nat Rev Mol Cell Biol **13**(9): 566-578.
Robinson, B. H. (2006). "Lactic acidemia and mitochondrial disease." Mol Genet Metab **89**(1-2): 3-13.
Rogge, R., P. J. Green, J. Urano, S. Horn-Saban, M. Mlodzik, B. Z. Shilo, V. Hartenstein and U. Banerjee (1995). "The role of yan in mediating the choice between cell division and differentiation." Development **121**(12): 3947-3958.
Rohn, J. L., J. V. Patel, B. Neumann, J. Bulkescher, N. McHedlishvili, R. C. McMullan, O. A. Quintero, J. Ellenberg and B. Baum (2014). "Myo19 ensures symmetric partitioning of mitochondria and coupling of mitochondrial segregation to cell division." Curr Biol **24**(21): 2598-2605.
Rohrbaugh, M., E. Ramos, D. Nguyen, M. Price, Y. Wen and Z.-C. Lai (2002). "Notch Activation of yan Expression Is Antagonized by RTK/Pointed Signaling in the Drosophila Eye." Current Biology **12**(7): 576-581.
Rolland, S. G., E. Motori, N. Memar, J. Hench, S. Frank, K. F. Winklhofer and B. Conradt (2013). "Impaired complex IV activity in response to loss of LRPPRC function can be compensated by mitochondrial hyperfusion." Proc Natl Acad Sci U S A **110**(32): E2967-2976.
Rossano, A. J., A. K. Chouhan and G. T. Macleod (2013). "Genetically encoded pH-indicators reveal activity-dependent cytosolic acidification of Drosophila motor nerve termini in vivo." The Journal of Physiology **591**(Pt 7): 1691-1706.
Rouault, T. A. (2015). "Mammalian iron-sulphur proteins: novel insights into biogenesis and function." Nat Rev Mol Cell Biol **16**(1): 45-55.
Rubio-Cosials, A., J. F. Sidow, N. Jimenez-Menendez, P. Fernandez-Millan, J. Montoya, H. T. Jacobs, M. Coll, P. Bernado and M. Sola (2011). "Human mitochondrial transcription factor A induces a U-turn structure in the light strand promoter." Nat Struct Mol Biol **18**(11): 1281-1289.

Rueda, C. B., J. Traba, I. Amigo, I. Llorente-Folch, P. Gonzalez-Sanchez, B. Pardo, J. A. Esteban, A. del Arco and J. Satrustegui (2015). "Mitochondrial ATP-Mg/Pi carrier SCaMC-3/Slc25a23 counteracts PARP-1-dependent fall in mitochondrial ATP caused by excitotoxic insults in neurons." J Neurosci **35**(8): 3566-3581.
Runkel, E. D., S. Liu, R. Baumeister and E. Schulze (2013). "Surveillance-activated defenses block the ROS-induced mitochondrial unfolded protein response." PLoS Genet **9**(3): e1003346.
Rutter, J., D. R. Winge and J. D. Schiffman (2010). "Succinate dehydrogenase – Assembly, regulation and role in human disease." Mitochondrion **10**(4): 393-401.
Safavizadeh, N., S. A. Rahmani and M. Zaefizadeh (2013). "Investigation of cytocrom c oxidase gene subunits expression on the Multiple sclerosis." Indian J Hum Genet **19**(1): 18-25.
Saha, S., M. D. Guillily, A. Ferree, J. Lanceta, D. Chan, J. Ghosh, C. H. Hsu, L. Segal, K. Raghavan, K. Matsumoto, N. Hisamoto, T. Kuwahara, T. Iwatsubo, L. Moore, L. Goldstein, M. Cookson and B. Wolozin (2009). "LRRK2 modulates vulnerability to mitochondrial dysfunction in Caenorhabditis elegans." J Neurosci **29**(29): 9210-9218.
Sajic, M., V. Mastrolia, C. Y. Lee, D. Trigo, M. Sadeghian, A. J. Mosley, N. A. Gregson, M. R. Duchen and K. J. Smith (2014). "Impulse Conduction Increases Mitochondrial Transport in Adult Mammalian Peripheral Nerves <italic>In Vivo</italic>." PLoS Biol **11**(12): e1001754.
Sandra M Cardoso, A. R. E. (2015). "LRRK2 a pivotal player in mitochondrial dynamics and lysosomal clustering: highlights to sporadic Parkinson's disease." Therapeutic Targets for Neurological Diseases **2**.
Sasarman, F., H. Antonicka and E. A. Shoubridge (2008). "The A3243G tRNALeu(UUR) MELAS mutation causes amino acid misincorporation and a combined respiratory chain assembly defect partially suppressed by overexpression of EFTu and EFG2." Human Molecular Genetics **17**(23): 3697-3707.
Sato, M. and K. Sato (2013). "Maternal inheritance of mitochondrial DNA by diverse mechanisms to eliminate paternal mitochondrial DNA." Biochim Biophys Acta **1833**(8): 1979-1984.
Schagger, H. and K. Pfeiffer (2000). "Supercomplexes in the respiratory chains of yeast and mammalian mitochondria." EMBO J **19**(8): 1777-1783.
Schapira, A. H., J. M. Cooper, D. Dexter, P. Jenner, J. B. Clark and C. D. Marsden (1989). "Mitochondrial complex I deficiency in Parkinson's disease." Lancet **1**(8649): 1269.
Schapira, A. H. V. "Mitochondrial disease." The Lancet **368**(9529): 70-82.
Schatz, G., E. Haslbrunner and H. Tuppy (1964). "Deoxyribonucleic Acid Associated with Yeast Mitochondria." Biochem Biophys Res Commun **15**(2): 127-132.
Schieber, M. and N. S. Chandel (2014). "ROS function in redox signaling and oxidative stress." Curr Biol **24**(10): R453-462.
Schriner, S. E., N. J. Linford, G. M. Martin, P. Treuting, C. E. Ogburn, M. Emond, P. E. Coskun, W. Ladiges, N. Wolf, H. Van Remmen, D. C. Wallace and P. S. Rabinovitch (2005). "Extension of murine life span by overexpression of catalase targeted to mitochondria." Science **308**(5730): 1909-1911.
Schroeder, E. A., N. Raimundo and G. S. Shadel (2013). "Epigenetic silencing mediates mitochondria stress-induced longevity." Cell Metab **17**(6): 954-964.
Schwarz, T. L. (2013). "Mitochondrial trafficking in neurons." Cold Spring Harb Perspect Biol **5**(6).
Selak, M. A., S. M. Armour, E. D. MacKenzie, H. Boulahbel, D. G. Watson, K. D. Mansfield, Y. Pan, M. C. Simon, C. B. Thompson and E. Gottlieb (2005). "Succinate links TCA cycle dysfunction to oncogenesis by inhibiting HIF-alpha prolyl hydroxylase." Cancer Cell **7**(1): 77-85.

Semenza, G. L. (2010). "Oxygen homeostasis." Wiley Interdisciplinary Reviews: Systems Biology and Medicine **2**(3): 336-361.
Sesaki, H. and R. E. Jensen (2001). "UGO1 encodes an outer membrane protein required for mitochondrial fusion." J Cell Biol **152**(6): 1123-1134.
Sha, D., L. S. Chin and L. Li (2010). "Phosphorylation of parkin by Parkinson disease-linked kinase PINK1 activates parkin E3 ligase function and NF-kappaB signaling." Hum Mol Genet **19**(2): 352-363.
Shadel, G. S. (2004). "Coupling the mitochondrial transcription machinery to human disease." Trends Genet **20**(10): 513-519.
Shadel, G. S. and T. L. Horvath (2015). "Mitochondrial ROS signaling in organismal homeostasis." Cell **163**(3): 560-569.
Shahni, R., C. M. Cale, G. Anderson, L. D. Osellame, S. Hambleton, T. S. Jacques, Y. Wedatilake, J. W. Taanman, E. Chan, W. Qasim, V. Plagnol, A. Chalasani, M. R. Duchen, K. C. Gilmour and S. Rahman (2015). "Signal transducer and activator of transcription 2 deficiency is a novel disorder of mitochondrial fission." Brain **138**(Pt 10): 2834-2846.
Sheng, B., X. Wang, B. Su, H. G. Lee, G. Casadesus, G. Perry and X. Zhu (2012). "Impaired mitochondrial biogenesis contributes to mitochondrial dysfunction in Alzheimer's disease." J Neurochem **120**(3): 419-429.
Shi, S. Y., S. Y. Lu, T. Sivasubramaniyam, X. S. Revelo, E. P. Cai, C. T. Luk, S. A. Schroer, P. Patel, R. H. Kim, E. Bombardier, J. Quadrilatero, A. R. Tupling, T. W. Mak, D. A. Winer and M. Woo (2015). "DJ-1 links muscle ROS production with metabolic reprogramming and systemic energy homeostasis in mice." Nat Commun **6**: 7415.
Shoulson, I., D. Oakes, S. Fahn, A. Lang, J. W. Langston, P. LeWitt, C. W. Olanow, J. B. Penney, C. Tanner, K. Kieburtz and A. Rudolph (2002). "Impact of sustained deprenyl (selegiline) in levodopa-treated Parkinson's disease: a randomized placebo-controlled extension of the deprenyl and tocopherol antioxidative therapy of parkinsonism trial." Ann Neurol **51**(5): 604-612.
Simon, M. A., D. D. L. Bowtell, G. S. Dodson, T. R. Laverty and G. M. Rubin (1991). "Ras1 and a putative guanine nucleotide exchange factor perform crucial steps in signaling by the sevenless protein tyrosine kinase." Cell **67**(4): 701-716.
Slack, C., N. Alic, A. Foley, M. Cabecinha, M. P. Hoddinott and L. Partridge (2015). "The Ras-Erk-ETS-Signaling Pathway Is a Drug Target for Longevity." Cell **162**(1): 72-83.
Spang, A., J. H. Saw, S. L. Jorgensen, K. Zaremba-Niedzwiedzka, J. Martijn, A. E. Lind, R. van Eijk, C. Schleper, L. Guy and T. J. G. Ettema (2015). "Complex archaea that bridge the gap between prokaryotes and eukaryotes." Nature **521**(7551): 173-179.
Srahna, M., M. Leyssen, C. M. Choi, L. G. Fradkin, J. N. Noordermeer and B. A. Hassan (2006). "A signaling network for patterning of neuronal connectivity in the Drosophila brain." PLoS Biol **4**(11): e348.
St Johnston, D. (2002). "The art and design of genetic screens: Drosophila melanogaster." Nat Rev Genet **3**(3): 176-188.
Stehling, O., A. A. Vashisht, J. Mascarenhas, Z. O. Jonsson, T. Sharma, D. J. Netz, A. J. Pierik, J. A. Wohlschlegel and R. Lill (2012). "MMS19 assembles iron-sulfur proteins required for DNA metabolism and genomic integrity." Science **337**(6091): 195-199.
Stein, T. D. and J. A. Johnson (2002). "Lack of neurodegeneration in transgenic mice overexpressing mutant amyloid precursor protein is associated with increased levels of transthyretin and the activation of cell survival pathways." J Neurosci **22**(17): 7380-7388.
Stewart, J. B., C. Freyer, J. L. Elson, A. Wredenberg, Z. Cansu, A. Trifunovic and N. G. Larsson (2008). "Strong purifying selection in transmission of mammalian mitochondrial DNA." PLoS Biol **6**(1): e10.

Stiburek, L., K. Vesela, H. Hansikova, P. Pecina, M. Tesarova, L. Cerna, J. Houstek and J. Zeman (2005). "Tissue-specific cytochrome c oxidase assembly defects due to mutations in SCO2 and SURF1." Biochem J **392**(Pt 3): 625-632.
Storch, A., W. H. Jost, P. Vieregge, J. Spiegel, W. Greulich, J. Durner, T. Muller, A. Kupsch, H. Henningsen, W. H. Oertel, G. Fuchs, W. Kuhn, P. Niklowitz, R. Koch, B. Herting and H. Reichmann (2007). "Randomized, double-blind, placebo-controlled trial on symptomatic effects of coenzyme Q(10) in Parkinson disease." Arch Neurol **64**(7): 938-944.
Stowers, R. S., L. J. Megeath, J. Gorska-Andrzejak, I. A. Meinertzhagen and T. L. Schwarz (2002). "Axonal transport of mitochondria to synapses depends on milton, a novel Drosophila protein." Neuron **36**(6): 1063-1077.
Strogolova, V., A. Furness, M. Robb-McGrath, J. Garlich and R. A. Stuart (2012). "Rcf1 and Rcf2, members of the hypoxia-induced gene 1 protein family, are critical components of the mitochondrial cytochrome bc1-cytochrome c oxidase supercomplex." Mol Cell Biol **32**(8): 1363-1373.
Stros, M., D. Launholt and K. D. Grasser (2007). "The HMG-box: a versatile protein domain occurring in a wide variety of DNA-binding proteins." Cell Mol Life Sci **64**(19-20): 2590-2606.
Sung, H., L. C. Tandarich, K. Nguyen and P. J. Hollenbeck (2016). "Compartmentalized Regulation of Parkin-Mediated Mitochondrial Quality Control in the Drosophila Nervous System In Vivo." The Journal of Neuroscience **36**(28): 7375-7391.
Surin, A. M., S. Khiroug, L. R. Gorbacheva, B. I. Khodorov, V. G. Pinelis and L. Khiroug (2012). "Comparative analysis of cytosolic and mitochondrial ATP synthesis in embryonic and postnatal hippocampal neuronal cultures." Front Mol Neurosci **5**: 102.
Swerdlow, R. H., J. K. Parks, S. W. Miller, J. B. Tuttle, P. A. Trimmer, J. P. Sheehan, J. P. Bennett, Jr., R. E. Davis and W. D. Parker, Jr. (1996). "Origin and functional consequences of the complex I defect in Parkinson's disease." Ann Neurol **40**(4): 663-671.
Taanman, J. W. (1999). "The mitochondrial genome: structure, transcription, translation and replication." Biochim Biophys Acta **1410**(2): 103-123.
Tantama, M., J. R. Martinez-Francois, R. Mongeon and G. Yellen (2013). "Imaging energy status in live cells with a fluorescent biosensor of the intracellular ATP-to-ADP ratio." Nat Commun **4**: 2550.
Tantama, M., J. R. Martínez-François, R. Mongeon and G. Yellen (2013). "Imaging energy status in live cells with a fluorescent biosensor of the intracellular ATP-to-ADP ratio." Nat Commun **4**.
Tarca, A. L., R. Romero and S. Draghici (2006). "Analysis of microarray experiments of gene expression profiling." Am J Obstet Gynecol **195**(2): 373-388.
Taylor, R. W. and D. M. Turnbull (2005). "Mitochondrial DNA mutations in human disease." Nat Rev Genet **6**(5): 389-402.
Taylor, S. W., E. Fahy and S. S. Ghosh (2003). "Global organellar proteomics." Trends Biotechnol **21**(2): 82-88.
Taylor, S. W., E. Fahy, B. Zhang, G. M. Glenn, D. E. Warnock, S. Wiley, A. N. Murphy, S. P. Gaucher, R. A. Capaldi, B. W. Gibson and S. S. Ghosh (2003). "Characterization of the human heart mitochondrial proteome." Nat Biotechnol **21**(3): 281-286.
Teleman, A. A., Y. W. Chen and S. M. Cohen (2005). "4E-BP functions as a metabolic brake used under stress conditions but not during normal growth." Genes Dev **19**(16): 1844-1848.
Teng, L., C. Kou, C. Lu, J. Xu, J. Xie, J. Lu, Y. Liu, Z. Wang and D. Wang (2014). "Involvement of the ERK pathway in the protective effects of glycyrrhizic acid against

the MPP+-induced apoptosis of dopaminergic neuronal cells." Int J Mol Med **34**(3): 742-748.
Terskikh, A., A. Fradkov, G. Ermakova, A. Zaraisky, P. Tan, A. V. Kajava, X. Zhao, S. Lukyanov, M. Matz, S. Kim, I. Weissman and P. Siebert (2000). ""Fluorescent timer": protein that changes color with time." Science **290**(5496): 1585-1588.
Tieu, Q. and J. Nunnari (2000). "Mdv1p is a WD repeat protein that interacts with the dynamin-related GTPase, Dnm1p, to trigger mitochondrial division." J Cell Biol **151**(2): 353-366.
Tieu, Q., V. Okreglak, K. Naylor and J. Nunnari (2002). "The WD repeat protein, Mdv1p, functions as a molecular adaptor by interacting with Dnm1p and Fis1p during mitochondrial fission." J Cell Biol **158**(3): 445-452.
Tiranti, V., A. Savoia, F. Forti, M. F. D'Apolito, M. Centra, M. Rocchi and M. Zeviani (1997). "Identification of the gene encoding the human mitochondrial RNA polymerase (h-mtRPOL) by cyberscreening of the Expressed Sequence Tags database." Hum Mol Genet **6**(4): 615-625.
Titov, D. V., V. Cracan, R. P. Goodman, J. Peng, Z. Grabarek and V. K. Mootha (2016). "Complementation of mitochondrial electron transport chain by manipulation of the NAD+/NADH ratio." Science **352**(6282): 231-235.
Toivonen, J. M., K. M. O'Dell, N. Petit, S. C. Irvine, G. K. Knight, M. Lehtonen, M. Longmuir, K. Luoto, S. Touraille, Z. Wang, S. Alziari, Z. H. Shah and H. T. Jacobs (2001). "Technical knockout, a Drosophila model of mitochondrial deafness." Genetics **159**(1): 241-254.
Tootle, T. L., P. S. Lee and I. Rebay (2003). "CRM1-mediated nuclear export and regulated activity of the Receptor Tyrosine Kinase antagonist YAN require specific interactions with MAE." Development **130**(5): 845-857.
Tretter, L., I. Sipos and V. Adam-Vizi (2004). "Initiation of Neuronal Damage by Complex I Deficiency and Oxidative Stress in Parkinson's Disease." Neurochemical Research **29**(3): 569-577.
Trifunovic, A., A. Hansson, A. Wredenberg, A. T. Rovio, E. Dufour, I. Khvorostov, J. N. Spelbrink, R. Wibom, H. T. Jacobs and N. G. Larsson (2005). "Somatic mtDNA mutations cause aging phenotypes without affecting reactive oxygen species production." Proc Natl Acad Sci U S A **102**(50): 17993-17998.
Truscott, K. N., P. Kovermann, A. Geissler, A. Merlin, M. Meijer, A. J. Driessen, J. Rassow, N. Pfanner and R. Wagner (2001). "A presequence- and voltage-sensitive channel of the mitochondrial preprotein translocase formed by Tim23." Nat Struct Biol **8**(12): 1074-1082.
Tufi, R., S. Gandhi, I. P. de Castro, S. Lehmann, P. R. Angelova, D. Dinsdale, E. Deas, H. Plun-Favreau, P. Nicotera, A. Y. Abramov, A. E. Willis, G. R. Mallucci, S. H. Y. Loh and L. M. Martins (2014). "Enhancing nucleotide metabolism protects against mitochondrial dysfunction and neurodegeneration in a PINK1 model of Parkinson's disease." Nat Cell Biol **16**(2): 157-166.
Tuppen, H. A., E. L. Blakely, D. M. Turnbull and R. W. Taylor (2010). "Mitochondrial DNA mutations and human disease." Biochim Biophys Acta **1797**(2): 113-128.
Tyynismaa, H., K. P. Mjosund, S. Wanrooij, I. Lappalainen, E. Ylikallio, A. Jalanko, J. N. Spelbrink, A. Paetau and A. Suomalainen (2005). "Mutant mitochondrial helicase Twinkle causes multiple mtDNA deletions and a late-onset mitochondrial disease in mice." Proc Natl Acad Sci U S A **102**(49): 17687-17692.
Tyynismaa, H. and A. Suomalainen (2009). "Mouse models of mitochondrial DNA defects and their relevance for human disease." EMBO Reports **10**(2): 137-143.
Vaarmann, A., M. Mandel, A. Zeb, P. Wareski, J. Liiv, M. Kuum, E. Antsov, M. Liiv, M. Cagalinec, V. Choubey and A. Kaasik (2016). "Mitochondrial biogenesis is required for axonal growth." Development **143**(11): 1981-1992.

van den Ouweland, J. M. W., H. H. P. J. Lemkes, W. Ruitenbeek, L. A. Sandkuijl, M. F. de Vijlder, P. A. A. Struyvenberg, J. J. P. van de Kamp and J. A. Maassen (1992). "Mutation in mitochondrial tRNALeu(UUR) gene in a large pedigree with maternally transmitted type II diabetes mellitus and deafness." Nat Genet **1**(5): 368-371.
Van Raamsdonk, J. M. and S. Hekimi (2009). "Deletion of the mitochondrial superoxide dismutase sod-2 extends lifespan in Caenorhabditis elegans." PLoS Genet **5**(2): e1000361.
van der Walt, J. M., K. K. Nicodemus, E. R. Martin, W. K. Scott, M. A. Nance, R. L. Watts, J. P. Hubble, J. L. Haines, W. C. Koller, K. Lyons, R. Pahwa, M. B. Stern, A. Colcher, B. C. Hiner, J. Jankovic, W. G. Ondo, F. H. Allen Jr, C. G. Goetz, G. W. Small, F. Mastaglia, J. M. Stajich, A. C. McLaurin, L. T. Middleton, B. L. Scott, D. E. Schmechel, M. A. Pericak-Vance and J. M. Vance (2003). "Mitochondrial Polymorphisms Significantly Reduce the Risk of Parkinson Disease." American Journal of Human Genetics **72**(4): 804-811.
Vanden Broeck, L., M. Naval-Sánchez, Y. Adachi, D. Diaper, P. Dourlen, J. Chapuis, G. Kleinberger, M. Gistelinck, C. Van Broeckhoven, J.-C. Lambert, F. Hirth, S. Aerts, P. Callaerts and B. Dermaut (2013). "TDP-43 Loss-of-Function Causes Neuronal Loss Due to Defective Steroid Receptor-Mediated Gene Program Switching in Drosophila." Cell Reports **3**(1): 160-172.
Varoqueaux, F., S. Jamain and N. Brose (2004). "Neuroligin 2 is exclusively localized to inhibitory synapses." European Journal of Cell Biology **83**(9): 449-456.
Vartak, R., C. A. Porras and Y. Bai (2013). "Respiratory supercomplexes: structure, function and assembly." Protein Cell **4**(8): 582-590.
Vattem, K. M. and R. C. Wek (2004). "Reinitiation involving upstream ORFs regulates ATF4 mRNA translation in mammalian cells." Proc Natl Acad Sci U S A **101**(31): 11269-11274.
Veech, R. L., J. W. Lawson, N. W. Cornell and H. A. Krebs (1979). "Cytosolic phosphorylation potential." J Biol Chem **254**(14): 6538-6547.
Vermulst, M., J. H. Bielas, G. C. Kujoth, W. C. Ladiges, P. S. Rabinovitch, T. A. Prolla and L. A. Loeb (2007). "Mitochondrial point mutations do not limit the natural lifespan of mice." Nat Genet **39**(4): 540-543.
Vincent, A., L. Briggs, G. F. J. Chatwin, E. Emery, R. Tomlins, M. Oswald, C. A. Middleton, G. J. O. Evans, S. T. Sweeney and C. J. H. Elliott (2012). "parkin-induced defects in neurophysiology and locomotion are generated by metabolic dysfunction and not oxidative stress." Human Molecular Genetics **21**(8): 1760-1769.
Visch, H. J., G. A. Rutter, W. J. Koopman, J. B. Koenderink, S. Verkaart, T. de Groot, A. Varadi, K. J. Mitchell, L. P. van den Heuvel, J. A. Smeitink and P. H. Willems (2004). "Inhibition of mitochondrial Na+-Ca2+ exchange restores agonist-induced ATP production and Ca2+ handling in human complex I deficiency." J Biol Chem **279**(39): 40328-40336.
Vissers, J. H. A., S. A. Manning, A. Kulkarni and K. F. Harvey (2016). "A Drosophila RNAi library modulates Hippo pathway-dependent tissue growth." Nat Commun **7**.
Vivekanand, P., T. L. Tootle and I. Rebay (2004). "MAE, a dual regulator of the EGFR signaling pathway, is a target of the Ets transcription factors PNT and YAN." Mech Dev **121**(12): 1469-1479.
Vogel, R. O., R. J. Janssen, C. Ugalde, M. Grovenstein, R. J. Huijbens, H. J. Visch, L. P. van den Heuvel, P. H. Willems, M. Zeviani, J. A. Smeitink and L. G. Nijtmans (2005). "Human mitochondrial complex I assembly is mediated by NDUFAF1." FEBS J **272**(20): 5317-5326.
von Heijne, G. (1986). "Mitochondrial targeting sequences may form amphiphilic helices." EMBO J **5**(6): 1335-1342.

Wan, B., K. F. LaNoue, J. Y. Cheung and R. C. Scaduto, Jr. (1989). "Regulation of citric acid cycle by calcium." J Biol Chem **264**(23): 13430-13439.
Wang, C. and R. J. Youle (2009). "The role of mitochondria in apoptosis*." Annu Rev Genet **43**: 95-118.
Wang, H. and R. Morais (1997). "Up-regulation of nuclear genes in response to inhibition of mitochondrial DNA expression in chicken cells." Biochim Biophys Acta **1352**(3): 325-334.
Wang, J., Y. Cao, Y. Chen, Y. Chen, P. Gardner and D. F. Steiner (2006). "Pancreatic β cells lack a low glucose and O2-inducible mitochondrial protein that augments cell survival." Proceedings of the National Academy of Sciences **103**(28): 10636-10641.
Wang, J., S. Xiong, C. Xie, W. R. Markesbery and M. A. Lovell (2005). "Increased oxidative damage in nuclear and mitochondrial DNA in Alzheimer's disease." J Neurochem **93**(4): 953-962.
Wang, P., S. Saraswati, Z. Guan, C. J. Watkins, R. J. Wurtman and J. T. Littleton (2004). "A Drosophila temperature-sensitive seizure mutant in phosphoglycerate kinase disrupts ATP generation and alters synaptic function." J Neurosci **24**(19): 4518-4529.
Wang, X., B. Su, S. L. Siedlak, P. I. Moreira, H. Fujioka, Y. Wang, G. Casadesus and X. Zhu (2008). "Amyloid-beta overproduction causes abnormal mitochondrial dynamics via differential modulation of mitochondrial fission/fusion proteins." Proc Natl Acad Sci U S A **105**(49): 19318-19323.
Wang, X., D. Winter, G. Ashrafi, J. Schlehe, Y. L. Wong, D. Selkoe, S. Rice, J. Steen, M. J. LaVoie and T. L. Schwarz (2011). "PINK1 and Parkin target Miro for phosphorylation and degradation to arrest mitochondrial motility." Cell **147**(4): 893-906.
Waterham, H. R., J. Koster, C. W. van Roermund, P. A. Mooyer, R. J. Wanders and J. V. Leonard (2007). "A lethal defect of mitochondrial and peroxisomal fission." N Engl J Med **356**(17): 1736-1741.
Waterhouse, N. J., J. C. Goldstein, O. von Ahsen, M. Schuler, D. D. Newmeyer and D. R. Green (2001). "Cytochrome c maintains mitochondrial transmembrane potential and ATP generation after outer mitochondrial membrane permeabilization during the apoptotic process." J Cell Biol **153**(2): 319-328.
Webber, J. L., J. Zhang, L. Cote, P. Vivekanand, X. Ni, J. Zhou, N. Negre, R. W. Carthew, K. P. White and I. Rebay (2013). "The relationship between long-range chromatin occupancy and polymerization of the Drosophila ETS family transcriptional repressor Yan." Genetics **193**(2): 633-649.
West, A. P., W. Khoury-Hanold, M. Staron, M. C. Tal, C. M. Pineda, S. M. Lang, M. Bestwick, B. A. Duguay, N. Raimundo, D. A. MacDuff, S. M. Kaech, J. R. Smiley, R. E. Means, A. Iwasaki and G. S. Shadel (2015). "Mitochondrial DNA stress primes the antiviral innate immune response." Nature **520**(7548): 553-557.
Westermann, B. (2010). "Mitochondrial fusion and fission in cell life and death." Nat Rev Mol Cell Biol **11**(12): 872-884.
White, Jacqueline K., A.-K. Gerdin, Natasha A. Karp, E. Ryder, M. Buljan, James N. Bussell, J. Salisbury, S. Clare, Neil J. Ingham, C. Podrini, R. Houghton, J. Estabel, Joanna R. Bottomley, David G. Melvin, D. Sunter, Niels C. Adams, L. Baker, C. Barnes, R. Beveridge, E. Cambridge, D. Carragher, P. Chana, K. Clarke, Y. Hooks, N. Igosheva, O. Ismail, H. Jackson, L. Kane, R. Lacey, David T. Lafont, M. Lucas, S. Maguire, K. McGill, Rebecca E. McIntyre, S. Messager, L. Mottram, L. Mulderrig, S. Pearson, Hayley J. Protheroe, L.-A. Roberson, G. Salsbury, M. Sanderson, D. Sanger, C. Shannon, Paul C. Thompson, E. Tuck, Valerie E. Vancollie, L. Brackenbury, W. Bushell, R. Cook, P. Dalvi, D. Gleeson, B. Habib, M. Hardy, K. Liakath-Ali, E. Miklejewska, S. Price, D. Sethi, E. Trenchard, D. von Schiller, S. Vyas, Anthony P. West, J. Woodward, E. Wynn, A. Evans, D. Gannon, M. Griffiths, S. Holroyd, V. Iyer,

C. Kipp, M. Lewis, W. Li, D. Oakley, D. Richardson, D. Smedley, C. Agu, J. Bryant, L. Delaney, Nadia I. Gueorguieva, H. Tharagonnet, Anne J. Townsend, D. Biggs, E. Brown, A. Collinson, C.-E. Dumeau, E. Grau, S. Harrison, J. Harrison, Catherine E. Ingle, H. Kundi, A. Madich, D. Mayhew, T. Metcalf, S. Newman, J. Pass, L. Pearson, H. Reynolds, C. Sinclair, H. Wardle-Jones, M. Woods, L. Alexander, T. Brown, F. Flack, C. Frost, N. Griggs, S. Hrnciarova, A. Kirton, J. McDermott, C. Rogerson, G. White, P. Zielezinski, T. DiTommaso, A. Edwards, E. Heath, Mary A. Mahajan, B. Yalcin, D. Tannahill, D. W. Logan, D. G. MacArthur, J. Flint, V. B. Mahajan, S. H. Tsang, I. Smyth, F. M. Watt, W. C. Skarnes, G. Dougan, D. J. Adams, R. Ramirez-Solis, A. Bradley and K. P. Steel (2013). "Genome-wide Generation and Systematic Phenotyping of Knockout Mice Reveals New Roles for Many Genes." Cell **154**(2): 452-464.

Woodson, J. D. and J. Chory (2008). "Coordination of gene expression between organellar and nuclear genomes." Nat Rev Genet **9**(5): 383-395.

Xia, Z., M. Dickens, J. Raingeaud, R. J. Davis and M. E. Greenberg (1995). "Opposing effects of ERK and JNK-p38 MAP kinases on apoptosis." Science **270**(5240): 1326-1331.

Xiong, H., D. Wang, L. Chen, Y. S. Choo, H. Ma, C. Tang, K. Xia, W. Jiang, Z. Ronai, X. Zhuang and Z. Zhang (2009). "Parkin, PINK1, and DJ-1 form a ubiquitin E3 ligase complex promoting unfolded protein degradation." J Clin Invest **119**(3): 650-660.

Xu, B. and D. A. Clayton (1996). "RNA-DNA hybrid formation at the human mitochondrial heavy-strand origin ceases at replication start sites: an implication for RNA-DNA hybrids serving as primers." EMBO J **15**(12): 3135-3143.

Xu, H., S. Z. DeLuca and P. H. O'Farrell (2008). "Manipulating the metazoan mitochondrial genome with targeted restriction enzymes." Science **321**(5888): 575-577.

Yamamoto-Hino, M. and S. Goto (2013). "In Vivo RNAi-Based Screens: Studies in Model Organisms." Genes **4**(4): 646-665.

Yan, H., M. L. Chin, E. A. Horvath, E. A. Kane and C. M. Pfleger (2009). "Impairment of ubiquitylation by mutation in Drosophila E1 promotes both cell-autonomous and non-cell-autonomous Ras-ERK activation in vivo." J Cell Sci **122**(Pt 9): 1461-1470.

Yang, D., Y. Oyaizu, H. Oyaizu, G. J. Olsen and C. R. Woese (1985). "Mitochondrial origins." Proc Natl Acad Sci U S A **82**(13): 4443-4447.

Yang, M. Y., M. Bowmaker, A. Reyes, L. Vergani, P. Angeli, E. Gringeri, H. T. Jacobs and I. J. Holt (2002). "Biased incorporation of ribonucleotides on the mitochondrial L-strand accounts for apparent strand-asymmetric DNA replication." Cell **111**(4): 495-505.

Yang, W. and S. Hekimi (2010). "A mitochondrial superoxide signal triggers increased longevity in Caenorhabditis elegans." PLoS Biol **8**(12): e1000556.

Yang, Y., Y. Ouyang, L. Yang, M. F. Beal, A. McQuibban, H. Vogel and B. Lu (2008). "Pink1 regulates mitochondrial dynamics through interaction with the fission/fusion machinery." Proceedings of the National Academy of Sciences of the United States of America **105**(19): 7070-7075.

Yang, Z., Q. Zhang, J. Ge and Z. Tan (2008). "Protective effects of tetramethylpyrazine on rat retinal cell cultures." Neurochem Int **52**(6): 1176-1187.

Yasukawa, T., A. Reyes, T. J. Cluett, M. Y. Yang, M. Bowmaker, H. T. Jacobs and I. J. Holt (2006). "Replication of vertebrate mitochondrial DNA entails transient ribonucleotide incorporation throughout the lagging strand." EMBO J **25**(22): 5358-5371.

Yen, K., C. Lee, H. Mehta and P. Cohen (2013). "The emerging role of the mitochondrial-derived peptide humanin in stress resistance." J Mol Endocrinol **50**(1): R11-19.

Yildiz, O., C. Kalthoff, S. Raunser and W. Kuhlbrandt (2007). "Structure of GlnK1 with bound effectors indicates regulatory mechanism for ammonia uptake." EMBO J **26**(2): 589-599.
Ylikallio, E., H. Tyynismaa, H. Tsutsui, T. Ide and A. Suomalainen (2010). "High mitochondrial DNA copy number has detrimental effects in mice." Hum Mol Genet **19**(13): 2695-2705.
Zalman, L. S., H. Nikaido and Y. Kagawa (1980). "Mitochondrial outer membrane contains a protein producing nonspecific diffusion channels." J Biol Chem **255**(5): 1771-1774.
Zara, V., L. Conte and B. L. Trumpower (2009). "Evidence that the assembly of the yeast cytochrome bc1 complex involves the formation of a large core structure in the inner mitochondrial membrane." FEBS J **276**(7): 1900-1914.
Zhang, W., W. Zhang, Z. Li, J. Hao, Z. Zhang, L. Liu, N. Mao, J. Miao and L. Zhang (2012). "S14G-humanin improves cognitive deficits and reduces amyloid pathology in the middle-aged APPswe/PS1dE9 mice." Pharmacol Biochem Behav **100**(3): 361-369.
Zhu, C. C., J. Q. Boone, P. A. Jensen, S. Hanna, L. Podemski, J. Locke, C. Q. Doe and M. B. O'Connor (2008). "Drosophila Activin- and the Activin-like product Dawdle function redundantly to regulate proliferation in the larval brain." Development **135**(3): 513-521.
Zhu, J.-H., S. M. Kulich, T. D. Oury and C. T. Chu (2002). "Cytoplasmic Aggregates of Phosphorylated Extracellular Signal-Regulated Protein Kinases in Lewy Body Diseases." The American Journal of Pathology **161**(6): 2087-2098.
Zhu, J. H., S. M. Kulich, T. D. Oury and C. T. Chu (2002). "Cytoplasmic aggregates of phosphorylated extracellular signal-regulated protein kinases in Lewy body diseases." Am J Pathol **161**(6): 2087-2098.
Zhu, X., R. J. Castellani, A. Takeda, A. Nunomura, C. S. Atwood, G. Perry and M. A. Smith (2001). "Differential activation of neuronal ERK, JNK/SAPK and p38 in Alzheimer disease: the 'two hit' hypothesis." Mechanisms of Ageing and Development **123**(1): 39-46.
Zhu, X., H. G. Lee, A. K. Raina, G. Perry and M. A. Smith (2002). "The role of mitogen-activated protein kinase pathways in Alzheimer's disease." Neurosignals **11**(5): 270-281.
Ziello, J. E., I. S. Jovin and Y. Huang (2007). "Hypoxia-Inducible Factor (HIF)-1 regulatory pathway and its potential for therapeutic intervention in malignancy and ischemia." Yale J Biol Med **80**(2): 51-60.
Zordan, M. A., P. Cisotto, C. Benna, A. Agostino, G. Rizzo, A. Piccin, M. Pegoraro, F. Sandrelli, G. Perini, G. Tognon, R. De Caro, S. Peron, T. T. Kronnie, A. Megighian, C. Reggiani, M. Zeviani and R. Costa (2006). "Post-transcriptional silencing and functional characterization of the Drosophila melanogaster homolog of human Surf1." Genetics **172**(1): 229-241.

9 APPENDIX

9.1 Microarray appendices

9.1.1 The number of genes changed in each microarray condition, compared to control, p < 0.05 with fold change cut-offs of >1.5 and >2.

Genes with oppositely regulated probes were - fold change > 1.5 (CI) CG43102, mamo, mod(mdg4), (CIII) CG42594, CG42755, CG9650, (CIV) CG32369, Cyp18a1, (CV), Meltrin and - fold change > 2 (CI) CG43102, mamo, mod(mdg4), (CIII) CG42594, CG42755, (CIV) CG32369, Cyp18a1, (CV), Meltrin.

p < 0.05 fold change > 1.5

		Increased		Decreased		Only changed in this condition		Number of genes in common			
	Number of genes	**number of genes**	**%**	**number of genes**	**%**	**number of genes**	**%**	**C III**	**C IV**	**C V**	***TFAM***
CI	382	202	**53**	180	**47**	202	**53**	67	49	83	63
CIII	525	430	**82**	95	**18**	305	**58**		83	120	87
CIV	328	206	**63**	122	**37**	192	**59**			75	66
CV	539	438	**81**	101	**19**	268	**50**				154
TFAM	393	172	**44**	221	**56**	178	**45**				

p < 0.05 fold change > 2

		Increased		Decreased		Only changed in this condition		Number of genes in common			
	number of genes	**number of genes**	**%**	**number of genes**	**%**	**number of genes**	**%**	**CI II**	**CI V**	**CV**	***TFAM***
CI	275	145	**53**	130	**47**	173	**63**	48	37	44	45
CIII	418	299	**72**	119	**28**	253	**61**		64	92	65
CIV	274	89	**32**	185	**68**	172	**63**			62	51
CV	360	213	**59**	147	**41**	185	**51**				90
TFAM	276	118	**43**	158	**57**	136	**49**				

9.1.2 Correlation genes significantly changed in common *ND-75* RNAi and *UQCR-14* RNAi and *ND-75* RNAi and *COX5B* RNAi, without outlier removed.

R is Pearson's r, axis represent fold change.

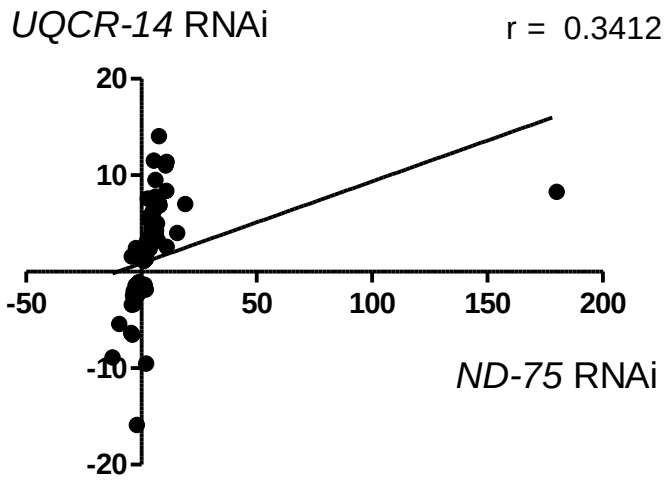

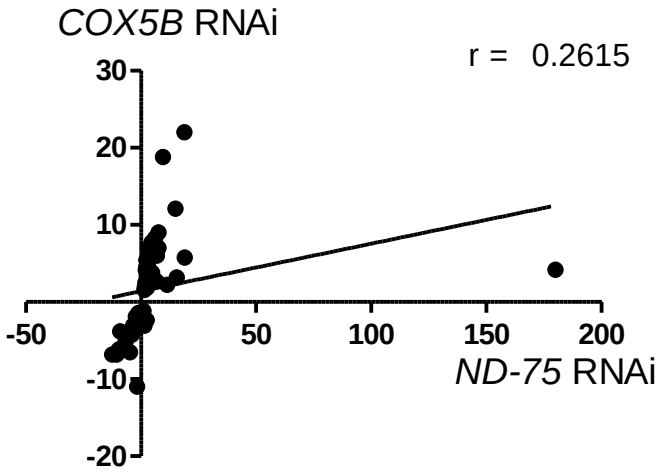

9.1.3 Enriched functional annotation clusters for genes significantly changed in *ND-75* RNAi, compared to control.

Showing the 15 most significant clusters

Enrichment Score: 1.623548522727936				
Term	Count	%	PValue	Fold Enrichment
GO:0004364~glutathione transferase activity	6	1.20	0.01	4.63
IPR010987:Glutathione S-transferase, C-terminal-like	6	1.20	0.01	4.29
IPR004045:Glutathione S-transferase, N-terminal	6	1.20	0.01	4.29
IPR004046:Glutathione S-transferase, C-terminal	6	1.20	0.01	4.29
IPR017933:Glutathione S-transferase/chloride channel, C-terminal	6	1.20	0.01	4.08
GO:0016765~transferase activity, transferring alkyl or aryl (other than methyl) groups	7	1.40	0.02	3.30
dme00980:Metabolism of xenobiotics by cytochrome P450	7	1.40	0.03	2.80
dme00982:Drug metabolism	7	1.40	0.04	2.72
dme00480:Glutathione metabolism	6	1.20	0.10	2.40
Posttranslational modification, protein turnover, chaperones	9	1.80	0.11	1.78
Enrichment Score: 1.2903890522275716				
Term	Count	%	PValue	Fold Enrichment
GO:0009074~aromatic amino acid family catabolic process	3	0.60	0.02	13.31
GO:0009063~cellular amino acid catabolic process	5	1.00	0.03	4.03
GO:0019439~aromatic compound catabolic process	3	0.60	0.03	9.98

GO:0009072~aromatic amino acid family metabolic process	4	0.80	0.04	5.32
GO:0009310~amine catabolic process	5	1.00	0.04	3.70
GO:0016054~organic acid catabolic process	5	1.00	0.09	2.96
GO:0046395~carboxylic acid catabolic process	5	1.00	0.09	2.96
GO:0046700~heterocycle catabolic process	3	0.60	0.18	3.80
Enrichment Score: 1.2825815160736065				
Term	Count	%	PValue	Fold Enrichment
GO:0007602~phototransduction	8	1.60	0.00	4.84
GO:0009583~detection of light stimulus	8	1.60	0.00	4.26
GO:0009582~detection of abiotic stimulus	8	1.60	0.00	3.87
GO:0009581~detection of external stimulus	8	1.60	0.01	3.55
GO:0051606~detection of stimulus	9	1.80	0.02	2.55
GO:0016027~inaD signalling complex	3	0.60	0.03	10.48
GO:0009628~response to abiotic stimulus	13	2.59	0.04	1.93
GO:0009416~response to light stimulus	8	1.60	0.04	2.51
GO:0016028~rhabdomere	4	0.80	0.04	5.03
GO:0009314~response to radiation	8	1.60	0.07	2.17
GO:0016056~rhodopsin mediated signalling pathway	3	0.60	0.13	4.70
GO:0044463~cell projection part	4	0.80	0.19	2.62
GO:0007601~visual perception	5	1.00	0.25	1.96
GO:0050953~sensory perception of light stimulus	5	1.00	0.26	1.93
GO:0042995~cell projection	6	1.20	0.27	1.70
GO:0019897~extrinsic to plasma membrane	3	0.60	0.30	2.70
vision	4	0.80	0.34	1.92
sensory transduction	5	1.00	0.76	0.98
Enrichment Score: 1.270008938219629				
Term	Count	%	PValue	Fold Enrichment
GO:0019898~extrinsic to membrane	12	2.40	0.01	2.47
GO:0055114~oxidation reduction	35	6.99	0.01	1.55

iron	14	2.79	0.01	2.14
GO:0005624~membrane fraction	9	1.80	0.02	2.70
GO:0005506~iron ion binding	17	3.39	0.02	1.86
GO:0005626~insoluble fraction	9	1.80	0.02	2.60
GO:0009055~electron carrier activity	14	2.79	0.02	1.99
GO:0000267~cell fraction	9	1.80	0.02	2.53
oxidoreductase	31	6.19	0.02	1.50
GO:0005783~endoplasmic reticulum	16	3.19	0.03	1.81
metal ion-binding site:Iron (heme axial ligand)	8	1.60	0.05	2.32
GO:0042598~vesicular fraction	7	1.40	0.06	2.50
GO:0005792~microsome	7	1.40	0.06	2.50
Monooxygenase	8	1.60	0.07	2.18
microsome	7	1.40	0.07	2.37
IPR001128:Cytochrome P450	7	1.40	0.09	2.24
IPR017973:Cytochrome P450, C-terminal region	7	1.40	0.09	2.24
Secondary metabolites biosynthesis, transport, and catabolism	7	1.40	0.11	2.07
IPR017972:Cytochrome P450, conserved site	7	1.40	0.11	2.14
dme00903:Limonene and pinene degradation	7	1.40	0.11	2.08
heme	8	1.60	0.11	1.96
GO:0020037~heme binding	9	1.80	0.12	1.83
GO:0046906~tetrapyrrole binding	9	1.80	0.12	1.83
IPR002401:Cytochrome P450, E-class, group I	6	1.20	0.15	2.15
endoplasmic reticulum	8	1.60	0.30	1.47
PIRSF000051:cytochrome P450 CYP3A5	3	0.60	0.40	2.16
Enrichment Score: 1.0610818389982286				
Term	Count	%	PValue	Fold Enrichment
GO:0046394~carboxylic acid biosynthetic process	8	1.60	0.01	3.13

GO:0016053~organic acid biosynthetic process	8	1.60	0.01	3.13
GO:0006633~fatty acid biosynthetic process	4	0.80	0.11	3.44
GO:0008652~cellular amino acid biosynthetic process	4	0.80	0.12	3.33
GO:0006631~fatty acid metabolic process	5	1.00	0.14	2.51
GO:0009309~amine biosynthetic process	4	0.80	0.29	2.13
GO:0008610~lipid biosynthetic process	6	1.20	0.45	1.37
Enrichment Score: 0.959667176407147				
Term	Count	%	PValue	Fold Enrichment
GO:0042802~identical protein binding	10	2.00	0.07	1.93
GO:0046983~protein dimerization activity	8	1.60	0.08	2.14
GO:0042803~protein homodimerization activity	4	0.80	0.23	2.42
Enrichment Score: 0.9301108663755913				
Term	Count	%	PValue	Fold Enrichment
IPR000719:Protein kinase, core	14	2.79	0.05	1.76
IPR001245:Tyrosine protein kinase	5	1.00	0.08	3.09
SM00219:TyrKc	5	1.00	0.09	2.95
GO:0004713~protein tyrosine kinase activity	5	1.00	0.17	2.32
IPR008266:Tyrosine protein kinase, active site	3	0.60	0.37	2.33
Enrichment Score: 0.8577947721427115				
Term	Count	%	PValue	Fold Enrichment
GO:0019748~secondary metabolic process	9	1.80	0.00	3.52
GO:0042440~pigment metabolic process	6	1.20	0.07	2.71
GO:0048066~pigmentation during development	5	1.00	0.13	2.56

GO:0008055~ocellus pigment biosynthetic process	3	0.60	0.14	4.44
GO:0033060~ocellus pigmentation	3	0.60	0.14	4.44
GO:0046152~ommochrome metabolic process	3	0.60	0.14	4.44
GO:0046158~ocellus pigment metabolic process	3	0.60	0.14	4.44
GO:0006727~ommochrome biosynthetic process	3	0.60	0.14	4.44
GO:0043473~pigmentation	5	1.00	0.15	2.42
GO:0046148~pigment biosynthetic process	4	0.80	0.28	2.17
GO:0006726~eye pigment biosynthetic process	3	0.60	0.28	2.85
GO:0042441~eye pigment metabolic process	3	0.60	0.30	2.75
GO:0048069~eye pigmentation	3	0.60	0.35	2.42
GO:0018130~heterocycle biosynthetic process	4	0.80	0.40	1.75
Enrichment Score: 0.8487844492402018				
Term	Count	%	PValue	Fold Enrichment
GO:0009628~response to abiotic stimulus	13	2.59	0.04	1.93
stress response	3	0.60	0.20	3.60
GO:0009408~response to heat	5	1.00	0.23	2.05
GO:0009266~response to temperature stimulus	5	1.00	0.25	1.96
Enrichment Score: 0.8424188853995306				
Term	Count	%	PValue	Fold Enrichment
GO:0016021~integral to membrane	52	10.38	0.06	1.23
GO:0031224~intrinsic to membrane	52	10.38	0.08	1.21
transmembrane	43	8.58	0.29	1.12
membrane	46	9.18	0.33	1.09
Enrichment Score: 0.8258888495662154				

Term	Count	%	PValue	Fold Enrichment
GO:0006817~phosphate transport	3	0.60	0.03	11.41
GO:0008509~anion transmembrane transporter activity	7	1.40	0.11	2.11
GO:0015698~inorganic anion transport	3	0.60	0.16	4.20
GO:0015114~phosphate transmembrane transporter activity	3	0.60	0.24	3.21
GO:0006820~anion transport	4	0.80	0.26	2.27
GO:0015103~inorganic anion transmembrane transporter activity	3	0.60	0.40	2.19
Enrichment Score: 0.749753045344896				
Term	Count	%	PValue	Fold Enrichment
GO:0046914~transition metal ion binding	58	11.58	0.08	1.20
GO:0043169~cation binding	73	14.57	0.09	1.17
GO:0043167~ion binding	73	14.57	0.10	1.16
GO:0046872~metal ion binding	70	13.97	0.12	1.15
metal-binding	36	7.19	0.17	1.22
GO:0008270~zinc ion binding	38	7.58	0.49	1.04
zinc	20	3.99	0.75	0.93
Enrichment Score: 0.7460443800081359				
Term	Count	%	PValue	Fold Enrichment
IPR001092:Basic helix-loop-helix dimerisation region bHLH	5	1.00	0.17	2.30
IPR011598:Helix-loop-helix DNA-binding	4	0.80	0.18	2.72
SM00353:HLH	5	1.00	0.19	2.20
Enrichment Score: 0.7183541899645033				
Term	Count	%	PValue	Fold Enrichment
binding site:ATP	10	2.00	0.01	2.72
active site:Proton acceptor	10	2.00	0.02	2.42

GO:0006468~protein amino acid phosphorylation	17	3.39	0.03	1.80
kinase	15	2.99	0.03	1.86
GO:0004674~protein serine/threonine kinase activity	13	2.59	0.05	1.82
IPR000719:Protein kinase, core	14	2.79	0.05	1.76
GO:0004672~protein kinase activity	16	3.19	0.07	1.62
domain:Protein kinase	7	1.40	0.08	2.32
serine/threonine-protein kinase	10	2.00	0.11	1.79
IPR002290:Serine/threonine protein kinase	8	1.60	0.12	1.94
IPR008271:Serine/threonine protein kinase, active site	10	2.00	0.12	1.74
GO:0016310~phosphorylation	21	4.19	0.12	1.38
IPR017441:Protein kinase, ATP binding site	11	2.20	0.13	1.64
SM00220:S_TKc	8	1.60	0.14	1.85
nucleotide phosphate-binding region:ATP	9	1.80	0.40	1.27
IPR017442:Serine/threonine protein kinase-related	8	1.60	0.42	1.29
GO:0006793~phosphorus metabolic process	22	4.39	0.42	1.11
GO:0006796~phosphate metabolic process	22	4.39	0.42	1.11
nucleotide-binding	29	5.79	0.51	1.04
GO:0000166~nucleotide binding	44	8.78	0.52	1.02
GO:0017076~purine nucleotide binding	36	7.19	0.54	1.02
GO:0032555~purine ribonucleotide binding	33	6.59	0.59	1.00
GO:0032553~ribonucleotide binding	33	6.59	0.59	1.00
GO:0030554~adenyl nucleotide binding	28	5.59	0.68	0.96
GO:0001883~purine nucleoside binding	28	5.59	0.69	0.96
atp-binding	21	4.19	0.70	0.95
GO:0001882~nucleoside binding	28	5.59	0.71	0.95
GO:0005524~ATP binding	25	4.99	0.74	0.94
GO:0032559~adenyl ribonucleotide binding	25	4.99	0.74	0.93
Enrichment Score: 0.7093783711719821				
Term	Count	%	PValue	Fold Enrichment

IPR015609:Molecular chaperone, heat shock protein, Hsp40, DnaJ	4	0.80	0.13	3.20
IPR001623:Heat shock protein DnaJ, N-terminal	4	0.80	0.19	2.65
SM00271:DnaJ	4	0.80	0.21	2.53
GO:0031072~heat shock protein binding	4	0.80	0.21	2.53
GO:0051082~unfolded protein binding	5	1.00	0.27	1.88
Enrichment Score: 0.6247087996073746				
Term	Count	%	PValue	Fold Enrichment
GO:0006457~protein folding	8	1.60	0.13	1.88
GO:0051082~unfolded protein binding	5	1.00	0.27	1.88
Chaperone	4	0.80	0.38	1.82

9.1.4 Enriched functional annotation clusters for genes significantly changed in *UQCR-14* RNAi, compared to control.

Showing the most significant 15 clusters

Enrichment Score: 1.623548522727936				
Term	Count	%	PValue	Fold Enrichment
GO:0004364~glutathione transferase activity	6	1.20	0.01	4.63
IPR010987:Glutathione S-transferase, C-terminal-like	6	1.20	0.01	4.29
IPR004045:Glutathione S-transferase, N-terminal	6	1.20	0.01	4.29
IPR004046:Glutathione S-transferase, C-terminal	6	1.20	0.01	4.29
IPR017933:Glutathione S-transferase/chloride channel, C-terminal	6	1.20	0.01	4.08
GO:0016765~transferase activity, transferring alkyl or aryl (other than methyl) groups	7	1.40	0.02	3.30
dme00980:Metabolism of xenobiotics by cytochrome P450	7	1.40	0.03	2.80
dme00982:Drug metabolism	7	1.40	0.04	2.72
dme00480:Glutathione metabolism	6	1.20	0.10	2.40
Posttranslational modification, protein turnover, chaperones	9	1.80	0.11	1.78
Enrichment Score: 1.2903890522275716				
Term	Count	%	PValue	Fold Enrichment
GO:0009074~aromatic amino acid family catabolic process	3	0.60	0.02	13.31
GO:0009063~cellular amino acid catabolic process	5	1.00	0.03	4.03
GO:0019439~aromatic compound catabolic process	3	0.60	0.03	9.98

GO:0009072~aromatic amino acid family metabolic process	4	0.80	0.04	5.32
GO:0009310~amine catabolic process	5	1.00	0.04	3.70
GO:0016054~organic acid catabolic process	5	1.00	0.09	2.96
GO:0046395~carboxylic acid catabolic process	5	1.00	0.09	2.96
GO:0046700~heterocycle catabolic process	3	0.60	0.18	3.80
Enrichment Score: 1.2825815160736065				
Term	Count	%	PValue	Fold Enrichment
GO:0007602~phototransduction	8	1.60	0.00	4.84
GO:0009583~detection of light stimulus	8	1.60	0.00	4.26
GO:0009582~detection of abiotic stimulus	8	1.60	0.00	3.87
GO:0009581~detection of external stimulus	8	1.60	0.01	3.55
GO:0051606~detection of stimulus	9	1.80	0.02	2.55
GO:0016027~inaD signalling complex	3	0.60	0.03	10.48
GO:0009628~response to abiotic stimulus	13	2.59	0.04	1.93
GO:0009416~response to light stimulus	8	1.60	0.04	2.51
GO:0016028~rhabdomere	4	0.80	0.04	5.03
GO:0009314~response to radiation	8	1.60	0.07	2.17
GO:0016056~rhodopsin mediated signalling pathway	3	0.60	0.13	4.70
GO:0044463~cell projection part	4	0.80	0.19	2.62
GO:0007601~visual perception	5	1.00	0.25	1.96
GO:0050953~sensory perception of light stimulus	5	1.00	0.26	1.93
GO:0042995~cell projection	6	1.20	0.27	1.70
GO:0019897~extrinsic to plasma membrane	3	0.60	0.30	2.70
vision	4	0.80	0.34	1.92
sensory transduction	5	1.00	0.76	0.98
Enrichment Score: 1.270008938219629				
Term	Count	%	PValue	Fold Enrichment
GO:0019898~extrinsic to membrane	12	2.40	0.01	2.47
GO:0055114~oxidation reduction	35	6.99	0.01	1.55

iron	14	2.79	0.01	2.14
GO:0005624~membrane fraction	9	1.80	0.02	2.70
GO:0005506~iron ion binding	17	3.39	0.02	1.86
GO:0005626~insoluble fraction	9	1.80	0.02	2.60
GO:0009055~electron carrier activity	14	2.79	0.02	1.99
GO:0000267~cell fraction	9	1.80	0.02	2.53
oxidoreductase	31	6.19	0.02	1.50
GO:0005783~endoplasmic reticulum	16	3.19	0.03	1.81
metal ion-binding site:Iron (heme axial ligand)	8	1.60	0.05	2.32
GO:0042598~vesicular fraction	7	1.40	0.06	2.50
GO:0005792~microsome	7	1.40	0.06	2.50
Monooxygenase	8	1.60	0.07	2.18
microsome	7	1.40	0.07	2.37
IPR001128:Cytochrome P450	7	1.40	0.09	2.24
IPR017973:Cytochrome P450, C-terminal region	7	1.40	0.09	2.24
Secondary metabolites biosynthesis, transport, and catabolism	7	1.40	0.11	2.07
IPR017972:Cytochrome P450, conserved site	7	1.40	0.11	2.14
dme00903:Limonene and pinene degradation	7	1.40	0.11	2.08
heme	8	1.60	0.11	1.96
GO:0020037~heme binding	9	1.80	0.12	1.83
GO:0046906~tetrapyrrole binding	9	1.80	0.12	1.83
IPR002401:Cytochrome P450, E-class, group I	6	1.20	0.15	2.15
endoplasmic reticulum	8	1.60	0.30	1.47
PIRSF000051:cytochrome P450 CYP3A5	3	0.60	0.40	2.16
Enrichment Score: 1.0610818389982286				
Term	Count	%	PValue	Fold Enrichment
GO:0046394~carboxylic acid biosynthetic process	8	1.60	0.01	3.13

GO:0016053~organic acid biosynthetic process	8	1.60	0.01	3.13
GO:0006633~fatty acid biosynthetic process	4	0.80	0.11	3.44
GO:0008652~cellular amino acid biosynthetic process	4	0.80	0.12	3.33
GO:0006631~fatty acid metabolic process	5	1.00	0.14	2.51
GO:0009309~amine biosynthetic process	4	0.80	0.29	2.13
GO:0008610~lipid biosynthetic process	6	1.20	0.45	1.37
Enrichment Score: 0.959667176407147				
Term	Count	%	PValue	Fold Enrichment
GO:0042802~identical protein binding	10	2.00	0.07	1.93
GO:0046983~protein dimerization activity	8	1.60	0.08	2.14
GO:0042803~protein homodimerization activity	4	0.80	0.23	2.42
Enrichment Score: 0.9301108663755913				
Term	Count	%	PValue	Fold Enrichment
IPR000719:Protein kinase, core	14	2.79	0.05	1.76
IPR001245:Tyrosine protein kinase	5	1.00	0.08	3.09
SM00219:TyrKc	5	1.00	0.09	2.95
GO:0004713~protein tyrosine kinase activity	5	1.00	0.17	2.32
IPR008266:Tyrosine protein kinase, active site	3	0.60	0.37	2.33
Enrichment Score: 0.8577947721427115				
Term	Count	%	PValue	Fold Enrichment
GO:0019748~secondary metabolic process	9	1.80	0.00	3.52
GO:0042440~pigment metabolic process	6	1.20	0.07	2.71
GO:0048066~pigmentation during development	5	1.00	0.13	2.56

GO:0008055~ocellus pigment biosynthetic process	3	0.60	0.14	4.44
GO:0033060~ocellus pigmentation	3	0.60	0.14	4.44
GO:0046152~ommochrome metabolic process	3	0.60	0.14	4.44
GO:0046158~ocellus pigment metabolic process	3	0.60	0.14	4.44
GO:0006727~ommochrome biosynthetic process	3	0.60	0.14	4.44
GO:0043473~pigmentation	5	1.00	0.15	2.42
GO:0046148~pigment biosynthetic process	4	0.80	0.28	2.17
GO:0006726~eye pigment biosynthetic process	3	0.60	0.28	2.85
GO:0042441~eye pigment metabolic process	3	0.60	0.30	2.75
GO:0048069~eye pigmentation	3	0.60	0.35	2.42
GO:0018130~heterocycle biosynthetic process	4	0.80	0.40	1.75
Enrichment Score: 0.8487844492402018				
Term	Count	%	PValue	Fold Enrichment
GO:0009628~response to abiotic stimulus	13	2.59	0.04	1.93
stress response	3	0.60	0.20	3.60
GO:0009408~response to heat	5	1.00	0.23	2.05
GO:0009266~response to temperature stimulus	5	1.00	0.25	1.96
Enrichment Score: 0.8424188853995306				
Term	Count	%	PValue	Fold Enrichment
GO:0016021~integral to membrane	52	10.38	0.06	1.23
GO:0031224~intrinsic to membrane	52	10.38	0.08	1.21
transmembrane	43	8.58	0.29	1.12
membrane	46	9.18	0.33	1.09
Enrichment Score: 0.8258888495662154				

Term	Count	%	PValue	Fold Enrichment
GO:0006817~phosphate transport	3	0.60	0.03	11.41
GO:0008509~anion transmembrane transporter activity	7	1.40	0.11	2.11
GO:0015698~inorganic anion transport	3	0.60	0.16	4.20
GO:0015114~phosphate transmembrane transporter activity	3	0.60	0.24	3.21
GO:0006820~anion transport	4	0.80	0.26	2.27
GO:0015103~inorganic anion transmembrane transporter activity	3	0.60	0.40	2.19
Enrichment Score: 0.749753045344896				
Term	Count	%	PValue	Fold Enrichment
GO:0046914~transition metal ion binding	58	11.58	0.08	1.20
GO:0043169~cation binding	73	14.57	0.09	1.17
GO:0043167~ion binding	73	14.57	0.10	1.16
GO:0046872~metal ion binding	70	13.97	0.12	1.15
metal-binding	36	7.19	0.17	1.22
GO:0008270~zinc ion binding	38	7.58	0.49	1.04
zinc	20	3.99	0.75	0.93
Enrichment Score: 0.7460443800081359				
Term	Count	%	PValue	Fold Enrichment
IPR001092:Basic helix-loop-helix dimerisation region bHLH	5	1.00	0.17	2.30
IPR011598:Helix-loop-helix DNA-binding	4	0.80	0.18	2.72
SM00353:HLH	5	1.00	0.19	2.20
Enrichment Score: 0.7183541899645033				
Term	Count	%	PValue	Fold Enrichment
binding site:ATP	10	2.00	0.01	2.72
active site:Proton acceptor	10	2.00	0.02	2.42

GO:0006468~protein amino acid phosphorylation	17	3.39	0.03	1.80
kinase	15	2.99	0.03	1.86
GO:0004674~protein serine/threonine kinase activity	13	2.59	0.05	1.82
IPR000719:Protein kinase, core	14	2.79	0.05	1.76
GO:0004672~protein kinase activity	16	3.19	0.07	1.62
domain:Protein kinase	7	1.40	0.08	2.32
serine/threonine-protein kinase	10	2.00	0.11	1.79
IPR002290:Serine/threonine protein kinase	8	1.60	0.12	1.94
IPR008271:Serine/threonine protein kinase, active site	10	2.00	0.12	1.74
GO:0016310~phosphorylation	21	4.19	0.12	1.38
IPR017441:Protein kinase, ATP binding site	11	2.20	0.13	1.64
SM00220:S_TKc	8	1.60	0.14	1.85
nucleotide phosphate-binding region:ATP	9	1.80	0.40	1.27
IPR017442:Serine/threonine protein kinase-related	8	1.60	0.42	1.29
GO:0006793~phosphorus metabolic process	22	4.39	0.42	1.11
GO:0006796~phosphate metabolic process	22	4.39	0.42	1.11
nucleotide-binding	29	5.79	0.51	1.04
GO:0000166~nucleotide binding	44	8.78	0.52	1.02
GO:0017076~purine nucleotide binding	36	7.19	0.54	1.02
GO:0032555~purine ribonucleotide binding	33	6.59	0.59	1.00
GO:0032553~ribonucleotide binding	33	6.59	0.59	1.00
GO:0030554~adenyl nucleotide binding	28	5.59	0.68	0.96
GO:0001883~purine nucleoside binding	28	5.59	0.69	0.96
atp-binding	21	4.19	0.70	0.95
GO:0001882~nucleoside binding	28	5.59	0.71	0.95
GO:0005524~ATP binding	25	4.99	0.74	0.94
GO:0032559~adenyl ribonucleotide binding	25	4.99	0.74	0.93
Enrichment Score: 0.7093783711719821				
Term	Count	%	PValue	Fold Enrichment

IPR015609:Molecular chaperone, heat shock protein, Hsp40, DnaJ	4	0.80	0.13	3.20
IPR001623:Heat shock protein DnaJ, N-terminal	4	0.80	0.19	2.65
SM00271:DnaJ	4	0.80	0.21	2.53
GO:0031072~heat shock protein binding	4	0.80	0.21	2.53
GO:0051082~unfolded protein binding	5	1.00	0.27	1.88
Enrichment Score: 0.6247087996073746				
Term	Count	%	PValue	Fold Enrichment
GO:0006457~protein folding	8	1.60	0.13	1.88
GO:0051082~unfolded protein binding	5	1.00	0.27	1.88
Chaperone	4	0.80	0.38	1.82
Enrichment Score: 0.5882269738765975				
Term	Count	%	PValue	Fold Enrichment
GO:0051327~M phase of meiotic cell cycle	8	1.60	0.15	1.82
GO:0007126~meiosis	8	1.60	0.15	1.82
GO:0007143~female meiosis	5	1.00	0.15	2.42
GO:0051321~meiotic cell cycle	8	1.60	0.17	1.76
GO:0045132~meiotic chromosome segregation	4	0.80	0.25	2.31
mutagenesis site	7	1.40	0.75	0.95
GO:0007059~chromosome segregation	4	0.80	0.76	1.01
Enrichment Score: 0.5575655031346909				
Term	Count	%	PValue	Fold Enrichment
compositionally biased region:Poly-Gln	8	1.60	0.05	2.37
compositionally biased region:Poly-Gly	5	1.00	0.24	1.99
compositionally biased region:Poly-Ala	4	0.80	0.71	1.09
compositionally biased region:Poly-Ser	4	0.80	0.72	1.08
Enrichment Score: 0.5224377598126936				

Term	Count	%	PValue	Fold Enrichment
GO:0010631~epithelial cell migration	4	0.80	0.08	3.94
GO:0007427~epithelial cell migration, open tracheal system	4	0.80	0.08	3.94
GO:0001667~ameboidal cell migration	4	0.80	0.10	3.55
GO:0008354~germ cell migration	4	0.80	0.14	3.04
GO:0016477~cell migration	9	1.80	0.21	1.57
GO:0048870~cell motility	9	1.80	0.28	1.45
GO:0051674~localization of cell	9	1.80	0.32	1.39
GO:0035295~tube development	5	1.00	0.47	1.42
GO:0001709~cell fate determination	6	1.20	0.53	1.25
GO:0006928~cell motion	11	2.20	0.59	1.06
GO:0035239~tube morphogenesis	3	0.60	0.80	1.01
GO:0060541~respiratory system development	4	0.80	0.92	0.71
GO:0007424~open tracheal system development	4	0.80	0.92	0.71
Enrichment Score: 0.5068778943816767				
Term	Count	%	PValue	Fold Enrichment
GO:0005578~proteinaceous extracellular matrix	4	0.80	0.20	2.57
GO:0031012~extracellular matrix	4	0.80	0.23	2.42
GO:0044421~extracellular region part	5	1.00	0.67	1.10
Enrichment Score: 0.4991250381248165				
Term	Count	%	PValue	Fold Enrichment
GO:0010259~multicellular organismal aging	6	1.20	0.25	1.77
GO:0008340~determination of adult life span	6	1.20	0.25	1.77
GO:0007568~aging	6	1.20	0.25	1.77
GO:0006979~response to oxidative stress	3	0.60	0.67	1.31

Enrichment Score: 0.4939274299252366				
Term	Count	%	PValue	Fold Enrichment
IPR000169:Peptidase, cysteine peptidase active site	3	0.60	0.18	3.88
GO:0004197~cysteine-type endopeptidase activity	3	0.60	0.29	2.78
GO:0008234~cysteine-type peptidase activity	3	0.60	0.63	1.41
Enrichment Score: 0.49100952349161914				
Term	Count	%	PValue	Fold Enrichment
GO:0045197~establishment or maintenance of epithelial cell apical/basal polarity	3	0.60	0.17	3.99
GO:0035088~establishment or maintenance of apical/basal cell polarity	3	0.60	0.25	3.07
GO:0007163~establishment or maintenance of cell polarity	4	0.80	0.78	0.99
Enrichment Score: 0.4820648145204265				
Term	Count	%	PValue	Fold Enrichment
IPR001680:WD40 repeat	10	2.00	0.22	1.50
SM00320:WD40	10	2.00	0.25	1.43
IPR015943:WD40/YVTN repeat-like	10	2.00	0.26	1.44
IPR019781:WD40 repeat, subgroup	8	1.60	0.30	1.47
IPR019782:WD40 repeat 2	7	1.40	0.40	1.38
wd repeat	8	1.60	0.40	1.32
IPR017986:WD40 repeat, region	6	1.20	0.61	1.13
Enrichment Score: 0.44828762374215625				
Term	Count	%	PValue	Fold Enrichment
GO:0007140~male meiosis	4	0.80	0.12	3.33
GO:0051327~M phase of meiotic cell cycle	8	1.60	0.15	1.82
GO:0007126~meiosis	8	1.60	0.15	1.82

GO:0051321~meiotic cell cycle	8	1.60	0.17	1.76
cell cycle	6	1.20	0.30	1.65
mitosis	4	0.80	0.30	2.07
GO:0000279~M phase	16	3.19	0.37	1.18
GO:0051301~cell division	9	1.80	0.40	1.28
cell division	4	0.80	0.42	1.70
GO:0022403~cell cycle phase	16	3.19	0.45	1.12
GO:0007067~mitosis	6	1.20	0.50	1.29
GO:0000087~M phase of mitotic cell cycle	6	1.20	0.51	1.27
GO:0000280~nuclear division	6	1.20	0.51	1.27
GO:0022402~cell cycle process	17	3.39	0.54	1.06
GO:0048285~organelle fission	6	1.20	0.55	1.22
GO:0007049~cell cycle	18	3.59	0.67	0.97
GO:0000278~mitotic cell cycle	10	2.00	0.88	0.80
Enrichment Score: 0.4474546457948761				
Term	Count	%	PValue	Fold Enrichment
IPR013087:Zinc finger, C2H2-type/integrase, DNA-binding	9	1.80	0.16	1.69
IPR007087:Zinc finger, C2H2-type	14	2.79	0.38	1.20
IPR015880:Zinc finger, C2H2-like	14	2.79	0.41	1.18
SM00355:ZnF_C2H2	14	2.79	0.47	1.13
GO:0008270~zinc ion binding	38	7.58	0.49	1.04
Enrichment Score: 0.43281586986952897				
Term	Count	%	PValue	Fold Enrichment
GO:0030528~transcription regulator activity	31	6.19	0.12	1.29
GO:0003704~specific RNA polymerase II transcription factor activity	6	1.20	0.14	2.17
GO:0003702~RNA polymerase II transcription factor activity	13	2.59	0.19	1.44
GO:0006357~regulation of transcription from RNA polymerase II promoter	10	2.00	0.28	1.41
GO:0003700~transcription factor activity	17	3.39	0.30	1.23

GO:0045449~regulation of transcription	31	6.19	0.31	1.13
GO:0006355~regulation of transcription, DNA-dependent	23	4.59	0.38	1.13
GO:0051252~regulation of RNA metabolic process	25	4.99	0.42	1.09
GO:0043565~sequence-specific DNA binding	10	2.00	0.44	1.21
transcription regulation	16	3.19	0.50	1.10
Transcription	16	3.19	0.52	1.08
GO:0006350~transcription	18	3.59	0.55	1.05
nucleus	31	6.19	0.70	0.96
GO:0003677~DNA binding	28	5.59	0.70	0.95
dna-binding	14	2.79	0.78	0.90
Enrichment Score: 0.42581162137465006				
Term	Count	%	PValue	Fold Enrichment
IPR003598:Immunoglobulin subtype 2	6	1.20	0.26	1.75
IPR003599:Immunoglobulin subtype	6	1.20	0.28	1.68
SM00408:IGc2	6	1.20	0.28	1.67
SM00409:IG	6	1.20	0.31	1.61
IPR013151:Immunoglobulin	5	1.00	0.35	1.68
IPR007110:Immunoglobulin-like	7	1.40	0.35	1.45
IPR013106:Immunoglobulin V-set	3	0.60	0.50	1.81
IPR013098:Immunoglobulin I-set	3	0.60	0.61	1.46
IPR013783:Immunoglobulin-like fold	5	1.00	0.62	1.17
Enrichment Score: 0.4159124467959462				
Term	Count	%	PValue	Fold Enrichment
domain:BTB	3	0.60	0.13	4.63
IPR011333:BTB/POZ fold	5	1.00	0.34	1.70
IPR013069:BTB/POZ	4	0.80	0.37	1.84
IPR000210:BTB/POZ-like	4	0.80	0.50	1.51
SM00225:BTB	4	0.80	0.53	1.44
GO:0006325~chromatin organization	6	1.20	0.74	0.97

Enrichment Score: 0.3996141036794812				
Term	Count	%	PValue	Fold Enrichment
GO:0007618~mating	5	1.00	0.19	2.18
GO:0007617~mating behavior	4	0.80	0.31	2.05
GO:0051705~behavioral interaction between organisms	4	0.80	0.32	2.01
GO:0019098~reproductive behavior	4	0.80	0.44	1.64
GO:0007619~courtship behavior	3	0.60	0.46	1.95
GO:0033057~reproductive behavior in a multicellular organism	3	0.60	0.55	1.63
GO:0007610~behavior	11	2.20	0.75	0.93
Enrichment Score: 0.3967914724357458				
Term	Count	%	PValue	Fold Enrichment
GO:0010941~regulation of cell death	9	1.80	0.04	2.26
GO:0043067~regulation of programmed cell death	9	1.80	0.04	2.26
GO:0060548~negative regulation of cell death	5	1.00	0.09	2.89
GO:0043069~negative regulation of programmed cell death	5	1.00	0.09	2.89
GO:0042981~regulation of apoptosis	7	1.40	0.13	2.03
GO:0006917~induction of apoptosis	3	0.60	0.25	3.07
Apoptosis	3	0.60	0.30	2.73
GO:0012502~induction of programmed cell death	3	0.60	0.37	2.35
GO:0043065~positive regulation of apoptosis	3	0.60	0.37	2.35
GO:0007435~salivary gland morphogenesis	6	1.20	0.42	1.41
GO:0022612~gland morphogenesis	6	1.20	0.42	1.41
GO:0043066~negative regulation of apoptosis	3	0.60	0.46	1.95
GO:0035071~salivary gland cell autophagic cell death	4	0.80	0.46	1.59
GO:0035070~salivary gland histolysis	4	0.80	0.46	1.59

GO:0048102~autophagic cell death	4	0.80	0.46	1.59
GO:0007559~histolysis	4	0.80	0.48	1.54
GO:0016271~tissue death	4	0.80	0.48	1.54
GO:0012501~programmed cell death	7	1.40	0.49	1.24
GO:0010942~positive regulation of cell death	3	0.60	0.49	1.82
GO:0043068~positive regulation of programmed cell death	3	0.60	0.49	1.82
GO:0009791~post-embryonic development	16	3.19	0.51	1.09
GO:0008219~cell death	7	1.40	0.53	1.19
GO:0016265~death	7	1.40	0.54	1.19
GO:0006915~apoptosis	4	0.80	0.55	1.40
GO:0035272~exocrine system development	6	1.20	0.58	1.17
GO:0007431~salivary gland development	6	1.20	0.58	1.17
GO:0009886~post-embryonic morphogenesis	12	2.40	0.63	1.02
GO:0048732~gland development	6	1.20	0.71	1.02
GO:0048707~instar larval or pupal morphogenesis	11	2.20	0.72	0.95
GO:0002165~instar larval or pupal development	13	2.59	0.76	0.92
GO:0048569~post-embryonic organ development	9	1.80	0.76	0.93
GO:0007552~metamorphosis	11	2.20	0.77	0.91
GO:0007444~imaginal disc development	11	2.20	0.86	0.83
GO:0048563~post-embryonic organ morphogenesis	7	1.40	0.90	0.76
GO:0007560~imaginal disc morphogenesis	7	1.40	0.90	0.76
Enrichment Score: 0.39215105638247444				
Term	Count	%	PValue	Fold Enrichment
GO:0006006~glucose metabolic process	5	1.00	0.19	2.22
glycolysis	3	0.60	0.21	3.45
dme00010:Glycolysis / Gluconeogenesis	4	0.80	0.31	2.02
GO:0006096~glycolysis	3	0.60	0.37	2.35

GO:0016052~carbohydrate catabolic process	5	1.00	0.37	1.62
GO:0019318~hexose metabolic process	5	1.00	0.39	1.58
GO:0006007~glucose catabolic process	3	0.60	0.47	1.90
GO:0019320~hexose catabolic process	3	0.60	0.47	1.90
GO:0005996~monosaccharide metabolic process	5	1.00	0.48	1.40
GO:0046365~monosaccharide catabolic process	3	0.60	0.48	1.86
GO:0044275~cellular carbohydrate catabolic process	3	0.60	0.56	1.60
GO:0046164~alcohol catabolic process	3	0.60	0.56	1.60
GO:0006091~generation of precursor metabolites and energy	7	1.40	0.77	0.93
Enrichment Score: 0.37139123397574175				
Term	Count	%	PValue	Fold Enrichment
GO:0050909~sensory perception of taste	5	1.00	0.21	2.11
IPR013604:7TM chemoreceptor	4	0.80	0.27	2.22
GO:0007186~G-protein coupled receptor protein signalling pathway	15	2.99	0.27	1.28
g-protein coupled receptor	11	2.20	0.30	1.35
GO:0008527~taste receptor activity	4	0.80	0.31	2.06
GO:0007600~sensory perception	12	2.40	0.42	1.19
GO:0050877~neurological system process	19	3.79	0.64	0.99
GO:0007606~sensory perception of chemical stimulus	7	1.40	0.72	0.98
GO:0050890~cognition	12	2.40	0.73	0.94
cell membrane	7	1.40	0.98	0.61
Enrichment Score: 0.37080382068197393				
Term	Count	%	PValue	Fold Enrichment
GO:0003704~specific RNA polymerase II transcription factor activity	6	1.20	0.14	2.17
differentiation	6	1.20	0.72	1.00

neurogenesis	3	0.60	0.75	1.12
Enrichment Score: 0.36922101599659796				
Term	Count	%	PValue	Fold Enrichment
iron-sulfur	3	0.60	0.26	3.05
GO:0051536~iron-sulfur cluster binding	3	0.60	0.55	1.63
GO:0051540~metal cluster binding	3	0.60	0.55	1.63
Enrichment Score: 0.3532372585825864				
Term	Count	%	PValue	Fold Enrichment
GO:0031968~organelle outer membrane	4	0.80	0.06	4.49
GO:0019867~outer membrane	4	0.80	0.06	4.34
GO:0005739~mitochondrion	22	4.39	0.14	1.33
GO:0005746~mitochondrial respiratory chain	4	0.80	0.38	1.80
GO:0042775~mitochondrial ATP synthesis coupled electron transport	4	0.80	0.39	1.77
GO:0031966~mitochondrial membrane	9	1.80	0.40	1.28
GO:0070469~respiratory chain	4	0.80	0.41	1.72
GO:0042773~ATP synthesis coupled electron transport	4	0.80	0.41	1.72
GO:0022904~respiratory electron transport chain	4	0.80	0.43	1.66
GO:0005740~mitochondrial envelope	9	1.80	0.49	1.18
GO:0022900~electron transport chain	4	0.80	0.56	1.37
GO:0044429~mitochondrial part	13	2.59	0.58	1.05
GO:0031967~organelle envelope	11	2.20	0.58	1.07
GO:0031975~envelope	11	2.20	0.58	1.06
GO:0019866~organelle inner membrane	7	1.40	0.60	1.11
GO:0005743~mitochondrial inner membrane	6	1.20	0.68	1.04
GO:0045333~cellular respiration	4	0.80	0.70	1.12
GO:0044455~mitochondrial membrane part	4	0.80	0.72	1.08
GO:0015980~energy derivation by oxidation of organic compounds	4	0.80	0.75	1.02

GO:0006091~generation of precursor metabolites and energy	7	1.40	0.77	0.93
GO:0031090~organelle membrane	12	2.40	0.78	0.91
GO:0006119~oxidative phosphorylation	4	0.80	0.83	0.89
dme00190:Oxidative phosphorylation	4	0.80	0.86	0.85
Enrichment Score: 0.35225911259062226				
Term	Count	%	PValue	Fold Enrichment
GO:0032561~guanyl ribonucleotide binding	9	1.80	0.30	1.41
GO:0019001~guanyl nucleotide binding	9	1.80	0.31	1.41
GO:0005525~GTP binding	8	1.60	0.43	1.28
GO:0003924~GTPase activity	6	1.20	0.47	1.32
gtp-binding	7	1.40	0.50	1.24
IPR005225:Small GTP-binding protein	3	0.60	0.82	0.97
Enrichment Score: 0.35030128533146093				
Term	Count	%	PValue	Fold Enrichment
IPR000215:Protease inhibitor I4, serpin	4	0.80	0.14	3.02
SM00093:SERPIN	4	0.80	0.16	2.88
GO:0004867~serine-type endopeptidase inhibitor activity	3	0.60	0.66	1.34
GO:0004866~endopeptidase inhibitor activity	3	0.60	0.76	1.10
GO:0030414~peptidase inhibitor activity	3	0.60	0.78	1.06
GO:0004857~enzyme inhibitor activity	3	0.60	0.89	0.82
Enrichment Score: 0.33461494273128717				
Term	Count	%	PValue	Fold Enrichment
GO:0016563~transcription activator activity	7	1.40	0.11	2.11
GO:0045941~positive regulation of transcription	6	1.20	0.41	1.43
GO:0010628~positive regulation of gene expression	6	1.20	0.42	1.41

GO:0045935~positive regulation of nucleobase, nucleoside, nucleotide and nucleic acid metabolic process	6	1.20	0.45	1.37
GO:0051173~positive regulation of nitrogen compound metabolic process	6	1.20	0.45	1.37
GO:0010557~positive regulation of macromolecule biosynthetic process	6	1.20	0.50	1.28
GO:0010604~positive regulation of macromolecule metabolic process	6	1.20	0.59	1.16
GO:0045893~positive regulation of transcription, DNA-dependent	4	0.80	0.65	1.21
GO:0031328~positive regulation of cellular biosynthetic process	6	1.20	0.66	1.08
GO:0009891~positive regulation of biosynthetic process	6	1.20	0.66	1.08
GO:0051254~positive regulation of RNA metabolic process	4	0.80	0.66	1.18
Enrichment Score: 0.3281931871064238				
Term	Count	%	PValue	Fold Enrichment
GO:0033554~cellular response to stress	10	2.00	0.18	1.58
GO:0006974~response to DNA damage stimulus	6	1.20	0.39	1.45
GO:0006281~DNA repair	4	0.80	0.71	1.10
GO:0006259~DNA metabolic process	5	1.00	0.96	0.64
Enrichment Score: 0.3252309916925633				
Term	Count	%	PValue	Fold Enrichment
GO:0016298~lipase activity	5	1.00	0.40	1.56
GO:0004091~carboxylesterase activity	5	1.00	0.52	1.34
GO:0004620~phospholipase activity	3	0.60	0.52	1.74
Enrichment Score: 0.3027954976726047				
Term	Count	%	PValue	Fold Enrichment

GO:0030534~adult behavior	5	1.00	0.34	1.68
GO:0008344~adult locomotory behavior	3	0.60	0.51	1.77
GO:0007626~locomotory behavior	5	1.00	0.71	1.04

9.1.5 Enriched functional annotation clusters for genes significantly changed in *COX5B* RNAi, compared to control.

Showing the most significant 15 clusters.

Enrichment Score: 1.6515985177115597				
Term	Count	%	PValue	Fold Enrichment
transmembrane region	23	6.80	0.00	2.15
GO:0016021~integral to membrane	44	13.02	0.00	1.55
GO:0031224~intrinsic to membrane	44	13.02	0.00	1.53
glycosylation site:N-linked (GlcNAc...)	18	5.33	0.00	2.25
topological domain:Cytoplasmic	17	5.03	0.00	2.28
transmembrane	39	11.54	0.01	1.55
GO:0050877~neurological system process	21	6.21	0.01	1.87
membrane	41	12.13	0.01	1.49
GO:0050909~sensory perception of taste	6	1.78	0.01	4.33
GO:0050890~cognition	15	4.44	0.02	2.01
IPR013604:7TM chemoreceptor	5	1.48	0.03	4.37
GO:0008527~taste receptor activity	5	1.48	0.04	3.90
glycoprotein	18	5.33	0.04	1.69
GO:0007166~cell surface receptor linked signal transduction	21	6.21	0.04	1.56
topological domain:Extracellular	11	3.25	0.06	1.88
GO:0007600~sensory perception	10	2.96	0.13	1.70
g-protein coupled receptor	9	2.66	0.16	1.70
GO:0005886~plasma membrane	21	6.21	0.17	1.29
transducer	9	2.66	0.22	1.57
GO:0007606~sensory perception of chemical stimulus	7	2.07	0.24	1.67
GO:0007186~G-protein coupled receptor protein signalling pathway	10	2.96	0.24	1.46
cell membrane	10	2.96	0.34	1.33
receptor	11	3.25	0.34	1.29
Enrichment Score: 1.3133509565378623				
Term	Count	%	PValue	Fold Enrichment

IPR005829:Sugar transporter, conserved site	5	1.48	0.02	4.46
GO:0051119~sugar transmembrane transporter activity	4	1.18	0.03	6.23
IPR005828:General substrate transporter	4	1.18	0.04	5.19
IPR003663:Sugar/inositol transporter	3	0.89	0.04	9.18
GO:0005355~glucose transmembrane transporter activity	3	0.89	0.05	7.89
GO:0015149~hexose transmembrane transporter activity	3	0.89	0.07	6.64
GO:0055085~transmembrane transport	6	1.78	0.08	2.57
GO:0015145~monosaccharide transmembrane transporter activity	3	0.89	0.09	5.74
Enrichment Score: 0.9698190913426162				
Term	Count	%	PValue	Fold Enrichment
IPR011333:BTB/POZ fold	6	1.78	0.04	3.21
domain:BTB	3	0.89	0.04	8.68
IPR000210:BTB/POZ-like	5	1.48	0.09	2.97
SM00225:BTB	5	1.48	0.09	2.93
IPR013069:BTB/POZ	4	1.18	0.16	2.90
mutagenesis site	4	1.18	0.75	1.02
Enrichment Score: 0.9607147547835124				
Term	Count	%	PValue	Fold Enrichment
GO:0035162~embryonic hemopoiesis	3	0.89	0.06	7.18
GO:0030097~hemopoiesis	4	1.18	0.07	4.23
GO:0048568~embryonic organ development	3	0.89	0.07	6.82
GO:0002520~immune system development	4	1.18	0.11	3.37
GO:0048534~hemopoietic or lymphoid organ development	4	1.18	0.11	3.37
GO:0048732~gland development	5	1.48	0.45	1.45
Enrichment Score: 0.9268694906194741				

Term	Count	%	PValue	Fold Enrichment
splice variant	20	5.92	0.01	1.75
alternative splicing	20	5.92	0.17	1.33
phosphoprotein	14	4.14	0.96	0.70
Enrichment Score: 0.9066632748734383				
Term	Count	%	PValue	Fold Enrichment
GO:0007611~learning or memory	6	1.78	0.02	3.69
GO:0007612~learning	5	1.48	0.03	4.37
GO:0007610~behavior	11	3.25	0.15	1.58
GO:0008355~olfactory learning	3	0.89	0.26	3.03
GO:0007635~chemosensory behavior	4	1.18	0.29	2.11
GO:0042048~olfactory behavior	3	0.89	0.54	1.66
Enrichment Score: 0.889157862484622				
Term	Count	%	PValue	Fold Enrichment
topological domain:Lumenal	5	1.48	0.03	4.20
Signal-anchor	4	1.18	0.12	3.31
GO:0005794~Golgi apparatus	7	2.07	0.13	2.02
golgi apparatus	5	1.48	0.16	2.35
GO:0044431~Golgi apparatus part	3	0.89	0.52	1.72
Enrichment Score: 0.7667288030337848				
Term	Count	%	PValue	Fold Enrichment
GO:0005624~membrane fraction	7	2.07	0.02	3.13
GO:0005626~insoluble fraction	7	2.07	0.03	3.02
GO:0000267~cell fraction	7	2.07	0.03	2.94
GO:0009055~electron carrier activity	9	2.66	0.09	1.93
metal ion-binding site:Iron (heme axial ligand)	5	1.48	0.11	2.71
GO:0042598~vesicular fraction	5	1.48	0.11	2.67
GO:0005792~microsome	5	1.48	0.11	2.67
microsome	5	1.48	0.13	2.60

GO:0005783~endoplasmic reticulum	10	2.96	0.13	1.69
IPR017973:Cytochrome P450, C-terminal region	5	1.48	0.14	2.52
IPR001128:Cytochrome P450	5	1.48	0.14	2.52
Secondary metabolites biosynthesis, transport, and catabolism	5	1.48	0.14	2.35
endoplasmic reticulum	7	2.07	0.14	1.97
IPR017972:Cytochrome P450, conserved site	5	1.48	0.15	2.41
Monooxygenase	5	1.48	0.22	2.09
heme	5	1.48	0.28	1.87
GO:0055114~oxidation reduction	16	4.73	0.34	1.21
oxidoreductase	16	4.73	0.37	1.19
GO:0019898~extrinsic to membrane	5	1.48	0.40	1.54
GO:0046906~tetrapyrrole binding	5	1.48	0.41	1.54
GO:0020037~heme binding	5	1.48	0.41	1.54
iron	6	1.78	0.42	1.40
IPR002401:Cytochrome P450, E-class, group I	3	0.89	0.53	1.69
dme00903:Limonene and pinene degradation	3	0.89	0.53	1.66
GO:0005506~iron ion binding	7	2.07	0.56	1.16
Enrichment Score: 0.7174069513716923				
Term	Count	%	PValue	Fold Enrichment
GO:0007126~meiosis	7	2.07	0.04	2.72
GO:0051327~M phase of meiotic cell cycle	7	2.07	0.04	2.72
GO:0051321~meiotic cell cycle	7	2.07	0.05	2.63
GO:0007131~reciprocal meiotic recombination	3	0.89	0.08	6.49
GO:0007140~male meiosis	3	0.89	0.15	4.26
GO:0006310~DNA recombination	3	0.89	0.20	3.59
GO:0007127~meiosis I	3	0.89	0.23	3.25
GO:0022402~cell cycle process	11	3.25	0.46	1.17
GO:0007049~cell cycle	12	3.55	0.51	1.11
GO:0000279~M phase	9	2.66	0.54	1.13

GO:0022403~cell cycle phase	9	2.66	0.59	1.08
GO:0006259~DNA metabolic process	5	1.48	0.68	1.09
Enrichment Score: 0.6914216518634427				
Term	Count	%	PValue	Fold Enrichment
GO:0031301~integral to organelle membrane	3	0.89	0.14	4.55
GO:0031300~intrinsic to organelle membrane	3	0.89	0.21	3.53
GO:0012505~endomembrane system	7	2.07	0.30	1.53
Enrichment Score: 0.6841102822995805				
Term	Count	%	PValue	Fold Enrichment
GO:0055082~cellular chemical homeostasis	4	1.18	0.09	3.79
GO:0048878~chemical homeostasis	4	1.18	0.16	2.89
GO:0019725~cellular homeostasis	5	1.48	0.20	2.16
GO:0006873~cellular ion homeostasis	3	0.89	0.23	3.25
GO:0050801~ion homeostasis	3	0.89	0.28	2.84
GO:0042592~homeostatic process	5	1.48	0.44	1.47
Enrichment Score: 0.6761817198959175				
Term	Count	%	PValue	Fold Enrichment
compositionally biased region:Gln-rich	8	2.37	0.03	2.64
GO:0030528~transcription regulator activity	22	6.51	0.11	1.38
GO:0003700~transcription factor activity	14	4.14	0.12	1.53
GO:0003702~RNA polymerase II transcription factor activity	10	2.96	0.14	1.68
GO:0007389~pattern specification process	13	3.85	0.15	1.51
GO:0051252~regulation of RNA metabolic process	18	5.33	0.17	1.35
GO:0003002~regionalization	12	3.55	0.18	1.49
GO:0006355~regulation of transcription, DNA-dependent	16	4.73	0.21	1.34

dna-binding	14	4.14	0.21	1.38
GO:0045449~regulation of transcription	20	5.92	0.24	1.25
GO:0006350~transcription	13	3.85	0.30	1.29
GO:0003677~DNA binding	21	6.21	0.46	1.08
transcription regulation	11	3.25	0.49	1.15
Transcription	11	3.25	0.51	1.14
nucleus	17	5.03	0.90	0.80
Enrichment Score: 0.6705400302801843				
Term	Count	%	PValue	Fold Enrichment
GO:0010941~regulation of cell death	7	2.07	0.03	3.00
GO:0043067~regulation of programmed cell death	7	2.07	0.03	3.00
compositionally biased region:Poly-Gln	6	1.78	0.03	3.33
GO:0042461~photoreceptor cell development	4	1.18	0.14	3.08
GO:0051252~regulation of RNA metabolic process	18	5.33	0.17	1.35
GO:0003002~regionalization	12	3.55	0.18	1.49
dna-binding	14	4.14	0.21	1.38
GO:0045165~cell fate commitment	8	2.37	0.23	1.59
GO:0046530~photoreceptor cell differentiation	5	1.48	0.25	1.94
GO:0007422~peripheral nervous system development	4	1.18	0.25	2.27
GO:0042051~compound eye photoreceptor development	3	0.89	0.29	2.78
GO:0042462~eye photoreceptor cell development	3	0.89	0.30	2.73
GO:0030182~neuron differentiation	11	3.25	0.31	1.33
developmental protein	16	4.73	0.35	1.21
GO:0001745~compound eye morphogenesis	6	1.78	0.36	1.51
GO:0048749~compound eye development	7	2.07	0.39	1.38
GO:0001751~compound eye photoreceptor cell differentiation	4	1.18	0.40	1.75

GO:0048592~eye morphogenesis	6	1.78	0.41	1.43
GO:0001754~eye photoreceptor cell differentiation	4	1.18	0.41	1.72
GO:0001654~eye development	7	2.07	0.44	1.31
GO:0007423~sensory organ development	7	2.07	0.68	1.02
Enrichment Score: 0.6605565711289421				
Term	Count	%	PValue	Fold Enrichment
IPR015880:Zinc finger, C2H2-like	12	3.55	0.13	1.59
SM00355:ZnF_C2H2	12	3.55	0.14	1.57
IPR007087:Zinc finger, C2H2-type	11	3.25	0.20	1.49
GO:0008270~zinc ion binding	24	7.10	0.62	0.99
Enrichment Score: 0.6471233172524414				
Term	Count	%	PValue	Fold Enrichment
IPR003591:Leucine-rich repeat, typical subtype	4	1.18	0.16	2.85
SM00369:LRR_TYP	4	1.18	0.17	2.81
leucine-rich repeat	4	1.18	0.29	2.10
IPR001611:Leucine-rich repeat	4	1.18	0.32	1.99

9.1.6 Enriched functional annotation clusters for genes significantly changed in *ATPsynCf6* RNAi, compared to control.

Showing the most significant 15 clusters.

Enrichment Score: 1.6670282151726432				
Term	Count	%	PValue	Fold Enrichment
IPR015421:Pyridoxal phosphate-dependent transferase, major region, subdomain 1	8	0.98	0.00	3.91
GO:0030170~pyridoxal phosphate binding	8	0.98	0.01	3.34
GO:0070279~vitamin B6 binding	8	0.98	0.01	3.34
IPR004839:Aminotransferase, class I and II	4	0.49	0.02	6.46
GO:0016769~transferase activity, transferring nitrogenous groups	5	0.61	0.03	4.07
GO:0019842~vitamin binding	12	1.47	0.04	2.00
pyridoxal phosphate	5	0.61	0.08	3.00
GO:0048037~cofactor binding	17	2.08	0.10	1.51
Enrichment Score: 1.5696306314705861				
Term	Count	%	PValue	Fold Enrichment
GO:0046365~monosaccharide catabolic process	9	1.10	0.00	3.52
GO:0005996~monosaccharide metabolic process	14	1.71	0.00	2.48
GO:0006006~glucose metabolic process	10	1.22	0.01	2.81
GO:0044275~cellular carbohydrate catabolic process	9	1.10	0.01	3.03
GO:0046164~alcohol catabolic process	9	1.10	0.01	3.03
dme00010:Glycolysis / Gluconeogenesis	9	1.10	0.01	2.88
GO:0019318~hexose metabolic process	12	1.47	0.01	2.40
GO:0006007~glucose catabolic process	8	0.98	0.01	3.21
GO:0019320~hexose catabolic process	8	0.98	0.01	3.21
binding site:Substrate	8	0.98	0.02	2.81
GO:0006096~glycolysis	6	0.73	0.05	2.97
dme00030:Pentose phosphate pathway	5	0.61	0.05	3.48
glycolysis	5	0.61	0.05	3.53

GO:0016052~carbohydrate catabolic process	10	1.22	0.05	2.05
dme00051:Fructose and mannose metabolism	5	0.61	0.11	2.67
GO:0006091~generation of precursor metabolites and energy	17	2.08	0.13	1.43
binding site:NAD	3	0.37	0.15	4.22
nucleotide phosphate-binding region:NAD	3	0.37	0.22	3.37
nad	5	0.61	0.26	1.93
Enrichment Score: 1.5047733950792477				
Term	Count	%	PValue	Fold Enrichment
GO:0034637~cellular carbohydrate biosynthetic process	6	0.73	0.01	4.21
GO:0016051~carbohydrate biosynthetic process	9	1.10	0.02	2.71
GO:0046165~alcohol biosynthetic process	3	0.37	0.16	4.21
Enrichment Score: 1.4482265659165616				
Term	Count	%	PValue	Fold Enrichment
IPR002293:Amino acid/polyamine transporter I	5	0.61	0.00	7.34
PIRSF006060:AA_transporter	5	0.61	0.00	6.98
GO:0006865~amino acid transport	7	0.86	0.03	2.95
GO:0015837~amine transport	7	0.86	0.04	2.81
GO:0015804~neutral amino acid transport	3	0.37	0.04	8.42
IPR004841:Amino acid permease-associated region	4	0.49	0.06	4.31
GO:0005275~amine transmembrane transporter activity	8	0.98	0.06	2.25
GO:0015849~organic acid transport	7	0.86	0.09	2.22
GO:0046942~carboxylic acid transport	7	0.86	0.09	2.22
GO:0015171~amino acid transmembrane transporter activity	6	0.73	0.17	2.04

Enrichment Score: 1.1169438747080616				
Term	Count	%	PValue	Fold Enrichment
SM00700:JHBP	5	0.61	0.07	3.20
IPR004272:Odorant binding protein	5	0.61	0.07	3.10
IPR013053:Hormone binding	5	0.61	0.09	2.88
Enrichment Score: 1.068391775877172				
Term	Count	%	PValue	Fold Enrichment
GO:0009309~amine biosynthetic process	8	0.98	0.03	2.69
GO:0008652~cellular amino acid biosynthetic process	6	0.73	0.04	3.16
GO:0046394~carboxylic acid biosynthetic process	8	0.98	0.11	1.98
GO:0016053~organic acid biosynthetic process	8	0.98	0.11	1.98
GO:0006790~sulfur metabolic process	4	0.49	0.39	1.77
Enrichment Score: 0.9781014441900322				
Term	Count	%	PValue	Fold Enrichment
GO:0016769~transferase activity, transferring nitrogenous groups	5	0.61	0.03	4.07
dme00250:Alanine, aspartate and glutamate metabolism	5	0.61	0.09	2.86
Aminotransferase	3	0.37	0.19	3.74
GO:0008483~transaminase activity	3	0.37	0.23	3.26
Enrichment Score: 0.9583958930900406				
Term	Count	%	PValue	Fold Enrichment
GO:0016765~transferase activity, transferring alkyl or aryl (other than methyl) groups	8	0.98	0.07	2.21
IPR004045:Glutathione S-transferase, N-terminal	6	0.73	0.08	2.55

IPR004046:Glutathione S-transferase, C-terminal	6	0.73	0.08	2.55
IPR010987:Glutathione S-transferase, C-terminal-like	6	0.73	0.08	2.55
dme00480:Glutathione metabolism	8	0.98	0.09	2.03
IPR017933:Glutathione S-transferase/chloride channel, C-terminal	6	0.73	0.10	2.42
Posttranslational modification, protein turnover, chaperones	12	1.47	0.11	1.60
GO:0004364~glutathione transferase activity	5	0.61	0.18	2.26
dme00980:Metabolism of xenobiotics by cytochrome P450	7	0.86	0.19	1.78
dme00982:Drug metabolism	7	0.86	0.21	1.73
Enrichment Score: 0.915447249219811				
Term	Count	%	PValue	Fold Enrichment
IPR004160:Translation elongation factor EFTu/EF1A, C-terminal	3	0.37	0.07	6.92
IPR004161:Translation elongation factor EFTu/EF1A, domain 2	4	0.49	0.08	3.80
IPR000795:Protein synthesis factor, GTP-binding	4	0.49	0.11	3.40
GO:0003924~GTPase activity	10	1.22	0.37	1.29
Enrichment Score: 0.8914180439102366				
Term	Count	%	PValue	Fold Enrichment
repeat:LRR 13	3	0.37	0.04	8.43
repeat:LRR 14	3	0.37	0.04	8.43
repeat:LRR 15	3	0.37	0.04	8.43
repeat:LRR 11	3	0.37	0.06	7.23
repeat:LRR 12	3	0.37	0.06	7.23
repeat:LRR 9	3	0.37	0.08	6.33
repeat:LRR 10	3	0.37	0.08	6.33
repeat:LRR 7	3	0.37	0.09	5.62

repeat:LRR 8	3	0.37	0.09	5.62
repeat:LRR 5	3	0.37	0.15	4.22
repeat:LRR 6	3	0.37	0.15	4.22
IPR001611:Leucine-rich repeat	9	1.10	0.16	1.69
repeat:LRR 4	3	0.37	0.22	3.37
repeat:LRR 3	3	0.37	0.29	2.81
SM00369:LRR_TYP	6	0.73	0.29	1.66
repeat:LRR 1	3	0.37	0.31	2.66
repeat:LRR 2	3	0.37	0.31	2.66
IPR003591:Leucine-rich repeat, typical subtype	6	0.73	0.31	1.61
leucine-rich repeat	7	0.86	0.34	1.47
Enrichment Score: 0.7464449797504061				
Term	Count	%	PValue	Fold Enrichment
transmembrane	74	9.06	0.09	1.18
GO:0031224~intrinsic to membrane	86	10.53	0.13	1.12
GO:0016021~integral to membrane	84	10.28	0.16	1.11
transmembrane region	37	4.53	0.29	1.12
membrane	73	8.94	0.35	1.06
Enrichment Score: 0.7055874960932808				
Term	Count	%	PValue	Fold Enrichment
GO:0009119~ribonucleoside metabolic process	4	0.49	0.14	3.06
GO:0042278~purine nucleoside metabolic process	3	0.37	0.18	3.88
GO:0046128~purine ribonucleoside metabolic process	3	0.37	0.18	3.88
GO:0009116~nucleoside metabolic process	4	0.49	0.34	1.92
Enrichment Score: 0.7040318208117982				
Term	Count	%	PValue	Fold Enrichment
IPR016040:NAD(P)-binding domain	15	1.84	0.06	1.67

IPR002347:Glucose/ribitol dehydrogenase	5	0.61	0.33	1.72
IPR002198:Short-chain dehydrogenase/reductase SDR	6	0.73	0.36	1.51
Enrichment Score: 0.6997494692070707				
Term	Count	%	PValue	Fold Enrichment
GO:0009063~cellular amino acid catabolic process	5	0.61	0.13	2.55
GO:0009310~amine catabolic process	5	0.61	0.16	2.34
GO:0046395~carboxylic acid catabolic process	5	0.61	0.28	1.87
GO:0016054~organic acid catabolic process	5	0.61	0.28	1.87
Enrichment Score: 0.6282781777575291				
Term	Count	%	PValue	Fold Enrichment
gtp-binding	14	1.71	0.13	1.52
GO:0005525~GTP binding	15	1.84	0.18	1.41
GO:0032561~guanyl ribonucleotide binding	15	1.84	0.20	1.38
GO:0019001~guanyl nucleotide binding	15	1.84	0.20	1.37
nucleotide phosphate-binding region:GTP	6	0.73	0.29	1.66
GO:0003924~GTPase activity	10	1.22	0.37	1.29
IPR005225:Small GTP-binding protein	7	0.86	0.42	1.35

9.1.7 Enriched functional annotation clusters for genes significantly changed in *TFAM* overexpression compared to control.

Showing the most significant 15 clusters.

Enrichment Score: 1.7198141162255618				
Term	Count	%	PValue	Fold Enrichment
GO:0005275~amine transmembrane transporter activity	9	1.47	0.00	3.47
GO:0015171~amino acid transmembrane transporter activity	8	1.31	0.00	3.73
IPR002293:Amino acid/polyamine transporter I	4	0.65	0.01	8.32
PIRSF006060:AA_transporter	4	0.65	0.01	7.55
IPR004841:Amino acid permease-associated region	4	0.65	0.03	6.10
GO:0006865~amino acid transport	6	0.98	0.03	3.49
GO:0015837~amine transport	6	0.98	0.03	3.33
GO:0015849~organic acid transport	6	0.98	0.07	2.64
GO:0046942~carboxylic acid transport	6	0.98	0.07	2.64
Enrichment Score: 1.3434307198420672				
Term	Count	%	PValue	Fold Enrichment
IPR016040:NAD(P)-binding domain	14	2.29	0.01	2.21
IPR002198:Short-chain dehydrogenase/reductase SDR	7	1.15	0.06	2.50
IPR002347:Glucose/ribitol dehydrogenase	5	0.82	0.15	2.43
Enrichment Score: 0.8318200087612984				
Term	Count	%	PValue	Fold Enrichment
GO:0015295~solute:hydrogen symporter activity	3	0.49	0.08	6.10
GO:0005416~cation:amino acid symporter activity	3	0.49	0.11	5.16

GO:0015294~solute:cation symporter activity	7	1.15	0.15	1.96
GO:0015293~symporter activity	7	1.15	0.17	1.86
GO:0015370~solute:sodium symporter activity	5	0.82	0.30	1.80
Enrichment Score: 0.8246448114776627				
Term	Count	%	PValue	Fold Enrichment
GO:0048563~post-embryonic organ morphogenesis	16	2.62	0.10	1.51
GO:0007560~imaginal disc morphogenesis	16	2.62	0.10	1.51
GO:0007424~open tracheal system development	11	1.80	0.11	1.72
GO:0060541~respiratory system development	11	1.80	0.11	1.72
GO:0035239~tube morphogenesis	6	0.98	0.25	1.77
GO:0035295~tube development	6	0.98	0.38	1.49
Enrichment Score: 0.8172480285450857				
Term	Count	%	PValue	Fold Enrichment
GO:0035114~imaginal disc-derived appendage morphogenesis	15	2.45	0.05	1.74
GO:0035107~appendage morphogenesis	15	2.45	0.05	1.72
GO:0048737~imaginal disc-derived appendage development	15	2.45	0.05	1.71
GO:0048736~appendage development	15	2.45	0.06	1.70
GO:0035120~post-embryonic appendage morphogenesis	14	2.29	0.07	1.70
GO:0007476~imaginal disc-derived wing morphogenesis	13	2.13	0.09	1.67
GO:0048569~post-embryonic organ development	17	2.78	0.09	1.53
GO:0007472~wing disc morphogenesis	13	2.13	0.09	1.65
GO:0048563~post-embryonic organ morphogenesis	16	2.62	0.10	1.51

GO:0007560~imaginal disc morphogenesis	16	2.62	0.10	1.51
GO:0007444~imaginal disc development	21	3.44	0.12	1.38
GO:0035220~wing disc development	15	2.45	0.14	1.47
GO:0003002~regionalization	21	3.44	0.15	1.34
GO:0007389~pattern specification process	22	3.60	0.16	1.31
GO:0009886~post-embryonic morphogenesis	18	2.95	0.19	1.33
GO:0007552~metamorphosis	18	2.95	0.22	1.30
developmental protein	29	4.75	0.23	1.19
GO:0009791~post-embryonic development	21	3.44	0.24	1.25
GO:0048707~instar larval or pupal morphogenesis	17	2.78	0.25	1.29
GO:0002165~instar larval or pupal development	19	3.11	0.34	1.18
GO:0007423~sensory organ development	16	2.62	0.36	1.19
GO:0001745~compound eye morphogenesis	10	1.64	0.37	1.29
GO:0048749~compound eye development	12	1.96	0.40	1.21
GO:0048592~eye morphogenesis	10	1.64	0.43	1.22
GO:0001654~eye development	12	1.96	0.47	1.15
Enrichment Score: 0.7904745828248017				
Term	Count	%	PValue	Fold Enrichment
GO:0007602~phototransduction	7	1.15	0.01	3.70
GO:0009583~detection of light stimulus	7	1.15	0.02	3.26
GO:0009582~detection of abiotic stimulus	7	1.15	0.03	2.96
GO:0009581~detection of external stimulus	7	1.15	0.04	2.72
GO:0009314~response to radiation	9	1.47	0.06	2.14
GO:0009416~response to light stimulus	8	1.31	0.07	2.19
GO:0051606~detection of stimulus	8	1.31	0.11	1.98
GO:0022400~regulation of rhodopsin mediated signalling pathway	3	0.49	0.12	4.99
GO:0016059~deactivation of rhodopsin mediated signalling	3	0.49	0.12	4.99
GO:0009628~response to abiotic stimulus	12	1.96	0.14	1.56

GO:0009586~rhodopsin mediated phototransduction	3	0.49	0.15	4.37
GO:0016056~rhodopsin mediated signalling pathway	3	0.49	0.16	4.11
GO:0007603~phototransduction, visible light	3	0.49	0.19	3.68
GO:0050908~detection of light stimulus involved in visual perception	3	0.49	0.23	3.33
GO:0050962~detection of light stimulus involved in sensory perception	3	0.49	0.24	3.17
GO:0008277~regulation of G-protein coupled receptor protein signalling pathway	3	0.49	0.24	3.17
GO:0009584~detection of visible light	3	0.49	0.29	2.79
GO:0007601~visual perception	5	0.82	0.33	1.71
GO:0050953~sensory perception of light stimulus	5	0.82	0.34	1.69
GO:0050906~detection of stimulus involved in sensory perception	3	0.49	0.64	1.40
vision	3	0.49	0.72	1.21
sensory transduction	6	0.98	0.74	0.98
GO:0050890~cognition	13	2.13	0.79	0.89
GO:0007600~sensory perception	9	1.47	0.89	0.78
Enrichment Score: 0.7746292167452069				
Term	Count	%	PValue	Fold Enrichment
GO:0004091~carboxylesterase activity	9	1.47	0.09	1.94
GO:0016298~lipase activity	8	1.31	0.10	2.01
GO:0004806~triacylglycerol lipase activity	3	0.49	0.51	1.77
Enrichment Score: 0.7287254533647473				
Term	Count	%	PValue	Fold Enrichment
GO:0035127~post-embryonic limb morphogenesis	4	0.65	0.13	3.21
GO:0007480~imaginal disc-derived leg morphogenesis	4	0.65	0.13	3.21

GO:0035109~imaginal disc-derived limb morphogenesis	4	0.65	0.14	3.10
GO:0007478~leg disc morphogenesis	4	0.65	0.15	3.00
GO:0007447~imaginal disc pattern formation	7	1.15	0.21	1.75
GO:0035110~leg morphogenesis	4	0.65	0.22	2.45
GO:0060173~limb development	4	0.65	0.23	2.39
GO:0035108~limb morphogenesis	4	0.65	0.23	2.39
GO:0035218~leg disc development	4	0.65	0.36	1.86
Enrichment Score: 0.7058090552956913				
Term	Count	%	PValue	Fold Enrichment
GO:0019320~hexose catabolic process	5	0.82	0.10	2.77
GO:0006007~glucose catabolic process	5	0.82	0.10	2.77
dme00620:Pyruvate metabolism	5	0.82	0.11	2.72
GO:0046365~monosaccharide catabolic process	5	0.82	0.11	2.71
dme00010:Glycolysis / Gluconeogenesis	5	0.82	0.12	2.56
GO:0044275~cellular carbohydrate catabolic process	5	0.82	0.16	2.33
GO:0046164~alcohol catabolic process	5	0.82	0.16	2.33
GO:0006096~glycolysis	4	0.65	0.18	2.74
GO:0006006~glucose metabolic process	5	0.82	0.25	1.94
GO:0016052~carbohydrate catabolic process	6	0.98	0.27	1.70
glycolysis	3	0.49	0.28	2.88
GO:0005996~monosaccharide metabolic process	6	0.98	0.38	1.47
GO:0019318~hexose metabolic process	5	0.82	0.49	1.39
GO:0006091~generation of precursor metabolites and energy	10	1.64	0.49	1.16
Enrichment Score: 0.6722522080814334				
Term	Count	%	PValue	Fold Enrichment
GO:0004091~carboxylesterase activity	9	1.47	0.09	1.94

IPR019819:Carboxylesterase type B, conserved site	3	0.49	0.15	4.29
IPR002018:Carboxylesterase, type B	4	0.65	0.19	2.62
Lipid metabolism	3	0.49	0.75	1.12
Enrichment Score: 0.638611044166274				
Term	Count	%	PValue	Fold Enrichment
GO:0048100~wing disc anterior/posterior pattern formation	3	0.49	0.10	5.37
GO:0035222~wing disc pattern formation	6	0.98	0.14	2.15
GO:0007447~imaginal disc pattern formation	7	1.15	0.21	1.75
GO:0045596~negative regulation of cell differentiation	6	0.98	0.21	1.89
GO:0007448~anterior/posterior pattern formation, imaginal disc	3	0.49	0.21	3.49
GO:0048190~wing disc dorsal/ventral pattern formation	4	0.65	0.33	1.98
GO:0007450~dorsal/ventral pattern formation, imaginal disc	4	0.65	0.41	1.72
GO:0009953~dorsal/ventral pattern formation	7	1.15	0.42	1.34
Enrichment Score: 0.6273746130923906				
Term	Count	%	PValue	Fold Enrichment
GO:0051119~sugar transmembrane transporter activity	4	0.65	0.12	3.31
IPR003663:Sugar/inositol transporter	3	0.49	0.12	4.90
GO:0005355~glucose transmembrane transporter activity	3	0.49	0.16	4.19
GO:0015149~hexose transmembrane transporter activity	3	0.49	0.21	3.53
GO:0015145~monosaccharide transmembrane transporter activity	3	0.49	0.26	3.05
GO:0055085~transmembrane transport	7	1.15	0.30	1.54

IPR005828:General substrate transporter	3	0.49	0.42	2.08
IPR005829:Sugar transporter, conserved site	3	0.49	0.63	1.43
Enrichment Score: 0.6242817651820919				
Term	Count	%	PValue	Fold Enrichment
GO:0006378~mRNA polyadenylation	3	0.49	0.12	4.99
GO:0043631~RNA polyadenylation	3	0.49	0.16	4.11
GO:0031124~mRNA 3'-end processing	3	0.49	0.26	3.04
GO:0031123~RNA 3'-end processing	3	0.49	0.32	2.59
GO:0006403~RNA localization	6	0.98	0.47	1.33
Enrichment Score: 0.619127763528576				
Term	Count	%	PValue	Fold Enrichment
GO:0006397~mRNA processing	12	1.96	0.09	1.70
GO:0016071~mRNA metabolic process	13	2.13	0.11	1.60
GO:0008380~RNA splicing	9	1.47	0.13	1.78
GO:0006396~RNA processing	17	2.78	0.14	1.41
GO:0000377~RNA splicing, via transesterification reactions with bulged adenosine as nucleophile	6	0.98	0.40	1.44
GO:0000398~nuclear mRNA splicing, via spliceosome	6	0.98	0.40	1.44
GO:0000375~RNA splicing, via transesterification reactions	6	0.98	0.41	1.43
dme03040:Spliceosome	6	0.98	0.42	1.39
GO:0005681~spliceosome	4	0.65	0.49	1.51
Enrichment Score: 0.5807036437396773				
Term	Count	%	PValue	Fold Enrichment
GO:0051247~positive regulation of protein metabolic process	3	0.49	0.18	3.88
GO:0032270~positive regulation of cellular protein metabolic process	3	0.49	0.18	3.88

GO:0010604~positive regulation of macromolecule metabolic process	9	1.47	0.24	1.52
GO:0032268~regulation of cellular protein metabolic process	6	0.98	0.63	1.12

9.1.8 Significant gene expression changes of the OXPHOS knockdown and *TFAM* overexpression models in HIF responsive genes, identified by Li et al., 2013.

	Fold Change				
Gene Symbol	**CI**	**CIII**	**CIV**	**CV**	***TFAM***
CG11652	-2.24				
CG4408		-2.03		-2.53	
lectin-28C	-2.67				
CG31274	2.73				
Gld	1.61				
CG17724		-1.31			
bnl				1.67	
CG34104					2.45
CG14957	-3.22	-2.71			
CG32694					-1.58
CG32369			-2.62		
ptr		5.53	6.4		2.81
CG18135				1.63	
Paip2	-1.34	-1.64			
CG7900					-1.48
CG43078	2.38				
fog					1.17
Syt7				-1.52	
MESK2	1.93				
RnrS	-1.31				
CG13117				-1.8	
comm2					-1.09
CG4783	-1.66	-1.61			-1.41
DsecGM11932			1.74	1.51	1.37
spir				1.37	1.42
dream					1.22
TBCB		-1.25	-1.46		
RhoGAP15B		2.91	3.23	2.28	2.67
scyl				1.21	1.27
CG10623	1.3				
th				-1.28	

	Fold Change				
Gene Symbol	**CI**	**CIII**	**CIV**	**CV**	***TFAM***
daw					-1.97
Rgk2				5.17	
RpL28		-3.04		-2.57	-2.46
pdgy				1.25	
lz			1.33	1.61	1.7
Glut1				-1.41	-1.57
Spt-I		-1.27		-1.23	-1.11
CG1542	-1.3				
CG10581				-2.3	-1.63
CG31809			-6.74		
CG12264	1.34			1.69	
CG13810		2.54			
nop5				1.22	
CG8326				1.35	
CG11318		3.17			
CG9630				1.3	
CG5789	1.35			1.7	
CG32053			-9.34		
Hsc70-5				1.39	
SdhB	-1.19				
CG7845				1.17	
CG8531		1.18		1.34	
CG8728				1.29	
obst-J				4.01	
escl				1.52	
Got2				1.31	
CG3803				1.27	
be			-1.7		
ns1				1.12	
CG14906	1.73			2.14	1.55
l(2)37Cg		-1.2			
JhI-21				1.94	1.39
Arc1	3.61	2.37		3.05	1.64
UGP	4.4				
EfTuM				1.15	

	Fold Change				
Gene Symbol	**CI**	**CIII**	**CIV**	**CV**	***TFAM***
CG2076	1.2	1.46		1.69	1.32
Fdxh		1.21		1.55	
CG11158	1.38				
CG4623				-2.51	
p24-2	-10.43				
Cyp6v1			2.89	3.7	2.58
AdSS				1.45	1.31
CG43739		-1.98			
Ast-C				2.42	
CG42684		3.81			
Amy-d				5.34	
mbl		-3.98			-2.59
PGRP-LF	3.18				
CG3608				2.18	1.64
Hmgs	1.27			1.43	1.34
Aatf	2.06				
CG6512	1.65			1.46	1.14
CG3476				1.99	
CG30022	1.39			1.34	
CG1894		-1.68			
Shawn				1.46	
Jafrac1				1.29	
CG10638		1.34			
mthl8	-2.62	-1.41		-1.97	-1.37
CG8066					-1.44
PMCA			3.17		
Alr				1.66	
CG31148		6.94			
CG1882				1.97	
Arc2	5.7	4.44		4.43	
CG3940	-1.19				
Mocs1	2.57				
CG10420				1.46	
CG30017		-18.27		-1.37	
Pdp1				2.04	1.8

	Fold Change				
Gene Symbol	**CI**	**CIII**	**CIV**	**CV**	***TFAM***
CG14237					-3.57
CG10182	2.9				
CG15093				1.33	
CG10918				-11.29	-9.18
Myo28B1			8.6	8.94	
CG2064	1.85	1.49		2.28	1.26
CG2065		1.56		2.36	1.58
l(2)03659		1.31		2.31	
bor				1.62	1.53
CG14906		1.43		1.41	1.49
Nop60B	1.3	-1.44		-1.11	-1.13
Hsp22	10.75	8.4		12.43	7.96
CG3706		2.76			
Arc1	19.02	7.02	5.78	9.2	5.68
CG15347		2.47			
CG6295					-4.6
CG32850	1.94				
LysX				-3.02	
CG31974		1.41			
SCAP	-3.48				
CG10910				-2.35	
pst			-2.12		1.69
Pepck			-3.5	3.34	
GstD2	4.4	4.41		4.23	2.09
Cyp9b2		2.82		2.93	
Cyp9b1		2.48	1.55		
spok				-6.69	
Est-Q					-5.33
NTPase				1.63	1.28
w		5.88		6.16	
CG13659					1.38
CG42335	-4.66				
CG33468	-3.97				
Cyp4p2		53.45			
Cyp28a5	-4.92				

	Fold Change				
Gene Symbol	**CI**	**CIII**	**CIV**	**CV**	***TFAM***
LysP		19.19			
y	28.12			1.92	
Cyp6a8	1.45				
CG2177	2.03	-9.51	2.21	2.05	-14.83
CG10559		-3.99	-2.29	-8.2	-5.76
CG5550		6.97			
CG15695					2.66
Rala				1.16	
CG8087				-3.22	-5.47
RFeSP	-9.63	-5.43	-6.16	-4.32	2.11
CG13658					6
Cyp6a17	179.91	8.29	4.19		
Jon66Cii		9.57		6.92	5.93
Mur29B		-1.31		-1.48	
Eip74EF	1.67				
CG10178	-13.51				
CG14945				1.25	
mnd				1.26	1.24
CG1773					-6.67
spz6	2.24	2.39			
CG1969					1.26
CG30083				-2.74	
Cpr65Ec				-1.94	-1.65
CG13488			-12.2		
RpS29					2.01
Pect	1.14			1.17	
Sp7	1.4				
CG7442				1.27	
WRNexo				-1.34	
CG5789					1.54
Jon66Ci		12.16			4.8
Art8				-1.1	
SpdS			1.36		
CG6961	1.07		-1.13		
Treh				1.74	

	Fold Change				
Gene Symbol	**CI**	**CIII**	**CIV**	**CV**	***TFAM***
CrzR				-1.92	
CG10527	-1.68			1.33	
CG15044			3.76		
CG14132	-1.95				
icln				1.09	
CG30375		2.67			
CG10903				1.17	
Gbp				-5.97	
CG11583					-1.1
Nop60B		-1.39			
CG9667		1.26		1.3	
Art3	-1.17				
CG17219				1.48	
pr				1.15	
CG42235		1.46		2.16	1.81
CG33099				-2.29	-2.18
CG9669			-1.17		
TBPH					1.5
CG13295					-1.38
RNaseX25			1.62	2.21	1.77
Gapdh2				1.72	
spict				-1.51	
Wbp2				1.36	
CG11367	1.1	1.11			
dm			1.67	1.4	
CG31635					1.65
CG30413					-5.03
dgo				2.4	1.83
kek1	-1.97			-2.2	
Acp24A4			3.82		
CG10274		1.2			
CG2812	-1.56				
ect					-1.54
CG7686				1.19	
Met			-13.06	-3.14	

	Fold Change				
Gene Symbol	**CI**	**CIII**	**CIV**	**CV**	***TFAM***
Acsl					1.27
Tsp42Eg	-6.36				
CG8399		-1.15		1.86	
Pi3K59F				-1.66	-1.71
CG10916	-1.58			-1.78	
Thor		6.89		9.88	3.77
CG14196		-3.97			
CG31810			7.29		
Rbp1				1.96	1.39
CG14608				2.15	
Bzd					-1.24
CG12081				-1.28	
Dgp-1	1.88	2.42	2.53	2.53	
Tsp42Er		2.96			
CG12576					1.18
yuri				2.13	1.78
CG17855			-4.75		
CG5639					-2.17
CG34376		-1.47			
Gadd45				5.38	
DOR					-1.58
CG10163		15.93		22.2	
CG43980		3.14			
Pkcdelta		7.53		8.24	
CG9449	-1.38				
c11.1	1.62			1.57	1.71
CG2217					1.27
Osi2			-6.2		
Timp				-1.24	
ImpL2					1.28
hebe				1.72	
Hex-A				3.25	1.82
CG5080		-1.19			
CG13868		1.97			
Cyp4p1		24.25			

	Fold Change				
Gene Symbol	**CI**	**CIII**	**CIV**	**CV**	***TFAM***
Wwox		-1.46		-1.47	-1.27
CG1113		3.52		3.48	
asparagine-synthetase				1.67	
CG3838					1.34
CG15784	15.54	4	3.19	7.34	3.16
CG8630	-1.38				
MFS3				1.8	

9.2 Modifier screen appendices

9.2.1 RNAi lines screened in the modifier wing screen.

The outcome of the screen is in the result column. Any lines that had a phenotype alone were excluded from the screen, so the result reads 'Excluded'. Any RNAi that in combination with *TFAM* knockdown scored a 3 or 4 is termed an 'Enhancer', if the wing curve was reduced the line is termed a 'Suppressor', if the score was lower than a 3 then the result is 'no effect'. The confirmed column refers to confirmation of the result with an independent RNAi for the same gene. If this is blank, then an alternative RNAi has not been tested.

Gene name	Gene symbol	Flybase ID	CG #	VDRC ID	NIG ID/ Trip ID	Result	Confirmed
-	*CG33170*	FBgn0053170	33170	102433		Enhancer	N
Enhancer of bithorax	*E(bx)*	FBgn0000541	32346	24740		Enhancer	N
breathless	*btl*	FBgn0005592	32134	27106		Enhancer	N
-	*CG31324*	FBgn0051324	31324	107220		Enhancer	N
scribbled	*scrib*	FBgn0263289	31082	102821		Enhancer	N
pyrexia	*pyx*	FBgn0035113	17142	110130		Enhancer	N
dawdle	*daw*	FBgn0031461	16987	105309		Enhancer	N
Inositol 1,4,5-triphosphate kinase 2		FBgn0266375	15745	102730		Enhancer	N
gamma-glutamyl carboxylase	*GC*	FBgn0035245	13927	109613		Enhancer	N
Neuroligin 2	*Nlg2*	FBgn0031866	13772	107166		Enhancer	N
-	*CG11658*	FBgn0036196	11658	108611		Enhancer	N
twin of eyeless	*toy*	FBgn0019650	11186	110353		Enhancer	N
Disabled	*Dab*	FBgn0000414	9695	109646		Enhancer	N
-	*CG9095*	FBgn0030617	9095	104608		Enhancer	N
Imitation SWI	*Iswi*	FBgn0011604	8625	24505		Enhancer	N
Sodium/solute co-transporter-like 5A11	*SLC5A11*	FBgn0031998	8451	104177		Enhancer	N
-	*Wdr62*	FBgn0031374	7337	110764		Enhancer	N

Gene name	Gene symbol	Flybase ID	CG #	VDRC ID	NIG ID/ Trip ID	Result	Confirmed
taranis	*tara*	FBgn0040071	6889	107508		Enhancer	N
-	*CG6847*	FBgn0030884	6847	22451		Enhancer	N
plum	*plum*	FBgn0039431	6490	101135		Enhancer	N
MORF-related gene 15	*MRG15*	FBgn0027378	6363	110618		Enhancer	N
arrow	*arr*	FBgn0000119	5912		HMC03571	Enhancer	N
-	*CG5466*	FBgn0038815	5466	104522		Enhancer	N
-	*CG5455*	FBgn0039430	5455	104118		Enhancer	N
-	*CG5059*	FBgn0037007	5059	107493		Enhancer	N
GATAd	*GATAd*	FBgn0032223	5034	100389		Enhancer	N
elbow B	*elB*	FBgn0004858	4220	104620		Enhancer	N
spoonbill	*spoon*	FBgn0263987	3249	105107		Enhancer	N
Integrator 6	*IntS6*	FBgn0261383	3125	110612		Enhancer	N
late bloomer	*lbm*	FBgn0016032	2374	102739		Enhancer	N
-	*CG2225*	FBgn0032957	2225	102815		Enhancer	N
ATP-dependent chromatin assembly factor large subunit	*Acf*	FBgn0027620	1966	33447		Enhancer	N
-	*CG8778*	FBgn0033761	8778	105442		Enhancer	Opposite
branchless	*bnl*	FBgn0014135	4608	5732		Enhancer	Y
Dual-specificity tyrosine phosphorylation-regulated kinase 2	*Dyrk2*	FBgn0016930	4551	101376		Enhancer	Y

Gene name	Gene symbol	Flybase ID	CG #	VDRC ID	NIG ID/ Trip ID	Result	Confirmed
Heat shock gene 67Bc	*Hsp67Bc*	FBgn0001229	4190	103974		Enhancer	Y
Reticulon-like1	*Rtnl1*	FBgn0053113	33113	110545		Enhancer	Y
X11Lbeta	*X11Lbeta*	FBgn0052677	32677	14872		Enhancer	Y
defective proboscis extension response 8	*dpr8*	FBgn0052600	32600	106791		Enhancer	Y
Keren	*Krn*	FBgn0052179	32179	6119		Enhancer	Y
-	*CG18549*	FBgn0038053	18549	107272		Enhancer	Y
Adenylate kinase 1	*Adk1*	FBgn0022709	17146	104475		Enhancer	Y
sloppy paired 1	*slp1*	FBgn0003430	16738	107562		Enhancer	Y
5-hydroxytryptamine (serotonin) receptor 1A	*5-HT1A*	FBgn0004168	16720		16720 R-1	Enhancer	Y
Capability receptor	*CapaR*	FBgn0037100	14575	13384		Enhancer	Y
distal antenna-related	*danr*	FBgn0039283	13651	11514		Enhancer	Y
Forkhead box K	*FoxK*	FBgn0036134	11799	110151		Enhancer	Y
Phosphoglucose isomerase	*Pgi*	FBgn0003074	8251	103616		Enhancer	Y
Wnt oncogene analog 5	*Wnt5*	FBgn0010194	6407	101621		Enhancer	Y
-	*CG6330*	FBgn0039464	6330	104776		Enhancer	Y
-	*CG5599*	FBgn0030612	5599	106456		Enhancer	Y
-	*CG4004*	FBgn0030418	4004	104537		Enhancer	Y
phtf	*phtf*	FBgn0028579	3268	103578		Enhancer	Y
Phosphoglycerate kinase	*Pgk*	FBgn0250906	3127	110081		Enhancer	Y
Amun	*Amun*	FBgn0030328	2446	104808		Enhancer	Y
lethal (1) G0289	*l(1)G0289*	FBgn0028331	2221	107283		Enhancer	Y

Gene name	Gene symbol	Flybase ID	CG #	VDRC ID	NIG ID/ Trip ID	Result	Confirmed
-	*CG2124*	FBgn0030217	2124	106235		Enhancer	Y
tropomodulin	*tmod*	FBgn0082582	1539	108389		Enhancer	Y
-	*CG18809*	FBgn0042132	18809	20702		Enhancer	
-	*ZAP3*	FBgn0052685	32685	22781		Enhancer	
-	*CG32521*	FBgn0052521	32521	110002		Enhancer	
stathmin	*stai*	FBgn0266521	31641	32370		Enhancer	
-	*CG31436*	FBgn0051436	31436	107606		Enhancer	
-	*CG17734*	FBgn0037890	17734	102605		Enhancer	
Lipase 2	*Lip2*	FBgn0024740	17116	102033		Enhancer	
roquin	*roq*	FBgn0036621	16807	23843		Enhancer	
defective proboscis extension response 6	*dpr6*	FBgn0040823	14162	103521		Enhancer	
caskin	*ckn*	FBgn0033987	12424	25222		Enhancer	
-	*DOR*	FBgn0035542	11347	105330		Enhancer	
Cytochrome P450-6a9	*Cyp6a9*	FBgn0013771	10246	100143		Enhancer	
-	*CG6154*	FBgn0039420	6154	23008		Enhancer	
-	*CG44774*	FBgn0266000	4068	103486		Enhancer	
encore	*enc*	FBgn0004875	10847	101500		Excluded	
-	*CG2970*	FBgn0034936	2970	110562		Excluded	
dead end	*dnd*	FBgn0038916	6560	104311		Excluded	
eIF5B	*eIF5B*	FBgn0026259	10840	109782		Excluded	
Heterogeneous nuclear ribonucleoprotein at 27C	*Hrb27C*	FBgn0004838	10377	101555		Excluded	
Zinc-finger protein	*Zif*	FBgn0037446	10267	100204		Excluded	
-	*CG6227*	FBgn0030631	6227	110778		Excluded	

Gene name	Gene symbol	Flybase ID	CG #	VDRC ID	NIG ID/ Trip ID	Result	Confirmed
Rab11	*Rab11*	FBgn0015790	5771	108382		Excluded	
bonus	*bon*	FBgn0023097	5206	101737		Excluded	
Rab5	*Rab5*	FBgn0014010	3664	103945		Excluded	
S-adenosylmethionine Synthetase	*Sam-S*	FBgn0005278	2674	103143		Excluded	
Vacuolar protein sorting 15	*Vps15*	FBgn0260935	9746	110706		Excluded	
mitochondrial ribosomal protein S11	*mRpS11*	FBgn0038474	5184	106653		Excluded	
grainy head	*grh*	FBgn0259211	42311	101428		Excluded	
grainy head	*grh*	FBgn0259211	42311	106879		Excluded	
Nipped-A	*Nipped-A*	FBgn0053554	33554	44781		Excluded	
Nipped-A	*Nipped-A*	FBgn0053554	33554	40789		Excluded	
Nipped-A	*Nipped-A*	FBgn0053554	33554	40790		Excluded	
Nipped-A	*Nipped-A*	FBgn0053554	33554	52436		Excluded	
Nipped-A	*Nipped-A*	FBgn0053554	33554	52487		Excluded	
nab	*nab*	FBgn0259986	33545	104811		Excluded	
Hormone receptor 3	*Hr3*	FBgn0000448	33183	106837		Excluded	
-	*CG33181*	FBgn0053181	33181	103142		Excluded	
-	*CG33129*	FBgn0053129	33129	107365		Excluded	
-	*CG32813*	FBgn0052813	32813	101839		Excluded	
-	*CG32767*	FBgn0052767	32767	42336		Excluded	
lethal (1) G0320	*l(1)G0320*	FBgn0028327	32701	110344		Excluded	
-	*CG32683*	FBgn0052683	32683	104029		Excluded	
Autophagy-related 8a	*Atg8a*	FBgn0052672	32672	109654		Excluded	
Death-associated	*Drak*	FBgn0052666	32666	107263		Excluded	

Gene name	Gene symbol	Flybase ID	CG #	VDRC ID	NIG ID/ Trip ID	Result	Confirmed
protein kinase related							
-	*CG32647*	FBgn0052647	32647	104082		Excluded	
lethal (1) G0007	*l(1)G0007*	FBgn0026713	32604	103940		Excluded	
-	*CG32549*	FBgn0052549	32549	103916		Excluded	
bves	*bves*	FBgn0031150	32513	104719		Excluded	
-	*CG32264*	FBgn0052264	32264	101503		Excluded	
Ecdysone-induced protein 74EF	*Eip74EF*	FBgn0000567	32180	105301		Excluded	
Formin-like	*Frl*	FBgn0267795	32138	110438		Excluded	
RNA-binding Fox protein 1	*Rbfox1*	FBgn0052062	32062	110518		Excluded	
Centaurin gamma 1A	*CenG1A*	FBgn0028509	31811	100123		Excluded	
virus-induced RNA 1	*vir-1*	FBgn0043841	31764	102534		Excluded	
Cnot 4 homologue	*Cnot4*	FBgn0051716	31716	110472		Excluded	
Trissin receptor	*TrissinR*	FBgn0085410	31645	42759		Excluded	
-	*Unc-115a*	FBgn0051352	31352	106405		Excluded	
curled	*cu*	FBgn0261808	31299	109759		Excluded	
couch potato	*cpo*	FBgn0263995	31243	14385		Excluded	
Lipophorin receptor 2	*LpR2*	FBgn0051092	31092	107597		Excluded	
hephaestus	*heph*	FBgn0011224	31000	110749		Excluded	
boca	*boca*	FBgn0004132	30498	108406		Excluded	
Prosap	*Prosap*	FBgn0040752	30483	103592		Excluded	
-	*CG30340*	FBgn0050340	30340	7387		Excluded	
Tetraspanin 42Ea	*Tsp42Ea*	FBgn0029508	18817	109172		Excluded	

Gene name	Gene symbol	Flybase ID	CG #	VDRC ID	NIG ID/ Trip ID	Result	Confirmed
moira	*mor*	FBgn0002783	18740	110712		Excluded	
Furin 2	*Fur2*	FBgn0004598	18734	101242		Excluded	
-	*CG18596*	FBgn0038953	18596	108183		Excluded	
Insulin-like receptor	*InR*	FBgn0283499	18402	991		Excluded	
Insulin-like receptor	*InR*	FBgn0283499	18402	992		Excluded	
TATA box binding protein-related factor 2	*Trf2*	FBgn0261793	18009	101318		Excluded	
Syncrip	*Syp*	FBgn0038826	17838	110542		Excluded	
-	*CG17816*	FBgn0037525	17816	103210		Excluded	
G protein alpha q subunit	*Galphaq*	FBgn0004435	17759	19088		Excluded	
frizzled	*fz*	FBgn0001085	17697	105493		Excluded	
Enolase	*Eno*	FBgn0000579	17654	110090		Excluded	
-	*CG17544*	FBgn0032775	17544	110169		Excluded	
derailed	*drl*	FBgn0015380	17348	100039		Excluded	
levy	*levy*	FBgn0034877	17280	101523		Excluded	
grapes	*grp*	FBgn0261278	17161	110076		Excluded	
homothorax	*hth*	FBgn0001235	17117		17117 R-2	Excluded	
homothorax	*hth*	FBgn0001235	17117	12763		Excluded	
homothorax	*hth*	FBgn0001235	17117	100630		Excluded	
-	*CG32295*	FBgn0260480	16757	105888		Excluded	
zipper	*zip*	FBgn0265434	15792	7819		Excluded	
-	*CG15771*	FBgn0029801	15771	106331		Excluded	
-	*CG15445*	FBgn0031161	15445	106271		Excluded	
Casein kinase II	*CkIIbeta*	FBgn0000259	15224	106845		Excluded	

Gene name	Gene symbol	Flybase ID	CG #	VDRC ID	NIG ID/ Trip ID	Result	Confirmed
beta subunit							
Pak3	*Pak3*	FBgn0044826	14895	107260		Excluded	
-	*CG14767*	FBgn0040777	14767	105373		Excluded	
Tachykinin	*Tk*	FBgn0037976	14734	103662		Excluded	
Cytochrome c oxidase subunit 5A	*COX5A*	FBgn0019624	14724	109070		Excluded	
-	*CG14722*	FBgn0037943	14722	105127		Excluded	
Bromodomain containing 8	*Brd8*	FBgn0039654	14514	104879		Excluded	
Glutamate receptor binding protein	*Grip*	FBgn0029830	14447	103551		Excluded	
-	*CG14438*	FBgn0029899	14438	100109		Excluded	
-	*CG14322*	FBgn0038532	14322	105876		Excluded	
-	*CG14291*	FBgn0038660	14291	107384		Excluded	
Cytochrome c oxidase subunit 6B	*COX6B*	FBgn0031066	14235	26848		Excluded	
domeless	*dome*	FBgn0043903	14226	19717		Excluded	
domeless	*dome*	FBgn0043903	14226	106071		Excluded	
-	*CG14215*	FBgn0031052	14215	103547		Excluded	
vrille	*vri*	FBgn0016076	14029	110751		Excluded	
-	*CG13917*	FBgn0035237	13917	32082		Excluded	
-	*CG13784*	FBgn0031897	13784	110080		Excluded	
MRG/MORF4L binding protein	*MrgBP*	FBgn0033341	13746	41402		Excluded	
MRG/MORF4L binding protein	*MrgBP*	FBgn0033341	13746	41403		Excluded	
pyramus	*pyr*	FBgn0033649	13194	36524		Excluded	

Gene name	Gene symbol	Flybase ID	CG #	VDRC ID	NIG ID/ Trip ID	Result	Confirmed
-	*CG12935*	FBgn0033547	12935	100154		Excluded	
Esa1-associated factor 6	*Eaf6*	FBgn0035624	12756	101457		Excluded	
olf413	*olf413*	FBgn0037153	12673	104097		Excluded	
Mothers against dpp	*Mad*	FBgn0011648	12399	12635		Excluded	
Lachesin	*Lac*	FBgn0010238	12369	107450		Excluded	
glial cells missing	*gcm*	FBgn0014179	12245	2961		Excluded	
glial cells missing	*gcm*	FBgn0014179	12245	2962		Excluded	
glial cells missing	*gcm*	FBgn0014179	12245	110539		Excluded	
licorne	*lic*	FBgn0261524	12244	106822		Excluded	
lethal (1) G0156	*l(1)G0156*	FBgn0027291	12233	106091		Excluded	
Dorsal switch protein 1	*Dsp1*	FBgn0278608	12223	101327		Excluded	
baiser	*bai*	FBgn0045866	11785	100612		Excluded	
Neural conserved at 73EF	*Nc73EF*	FBgn0010352	11661	107713		Excluded	
Ribosomal protein L6	*RpL6*	FBgn0039857	11522	107302		Excluded	
-	*CG11486*	FBgn0035397	11486	106497		Excluded	
-	*CG11241*	FBgn0037186	11241	110651		Excluded	
lethal (3) 04053	*l(3)04053*	FBgn0010830	11238	31465		Excluded	
DNA methyltransferase 1 associated protein 1	*DMAP1*	FBgn0034537	11132	103734		Excluded	
Mesoderm-expressed 2	*Mes2*	FBgn0037207	11100	109111		Excluded	
Activin-beta	*Actbeta*	FBgn0024913	11062		11062 R-1	Excluded	
-	*CG10949*	FBgn0032858	10949	107251		Excluded	
-	*CG10903*	FBgn0037543	10903	109610		Excluded	

Gene name	Gene symbol	Flybase ID	CG #	VDRC ID	NIG ID/ Trip ID	Result	Confirmed
-	*CG10898*	FBgn0037911	10898	103422		Excluded	
lethal (2) 37Cc	*l(2)37Cc*	FBgn0002031	10691	12360		Excluded	
vein	*vn*	FBgn0003984	10491	50358		Excluded	
-	*CG10479*	FBgn0035656	10479	106226		Excluded	
p21-activated kinase	*Pak*	FBgn0267698	10295	108937		Excluded	
Rm62	*Rm62*	FBgn0003261	10279	110102		Excluded	
Topoisomerase 2	*Top2*	FBgn0003732	10223	30625		Excluded	
Vacuolar protein sorting 8	*Vps8*	FBgn0035704	10144	105952		Excluded	
-	*CG10137*	FBgn0032800	10137	100007		Excluded	
Epidermal growth factor receptor	*Egfr*	FBgn0003731	10079	43267		Excluded	
Epidermal growth factor receptor	*Egfr*	FBgn0003731	10079	43268		Excluded	
Allatostatin A receptor 2	*AstA-R2*	FBgn0039595	10001	1326		Excluded	
Allatostatin A receptor 2	*AstA-R2*	FBgn0039595	10001	1327		Excluded	
Partner of paired	*Ppa*	FBgn0020257	9952	100298		Excluded	
transforming acidic coiled-coil protein	*tacc*	FBgn0026620	9765	101439		Excluded	
Neprilysin 2	*Nep2*	FBgn0027570	9761	102584		Excluded	
reptin	*rept*	FBgn0040075	9750		9750R-1	Excluded	
reptin	*rept*	FBgn0040075	9750		HMS00410	Excluded	
Tumor susceptibility gene 101	*TSG101*	FBgn0036666	9712	23944		Excluded	
domino	*dom*	FBgn0020306	9696	7787		Excluded	

Gene name	Gene symbol	Flybase ID	CG #	VDRC ID	NIG ID/ Trip ID	Result	Confirmed
-	*CG9674*	FBgn0036663	9674	100170		Excluded	
Sex comb on midleg	*Scm*	FBgn0003334	9495	109597		Excluded	
-	*CG9399*	FBgn0037715	9399	101455		Excluded	
Acetyl Coenzyme A synthase	*AcCoAS*	FBgn0012034	9390	100281		Excluded	
skywalker	*sky*	FBgn0032901	9339	108736		Excluded	
varicose	*vari*	FBgn0250785	9326	104548		Excluded	
-	*CG9257*	FBgn0032916	9257	103425		Excluded	
Lipid storage droplet-2	*Lsd-2*	FBgn0030608	9057	40734		Excluded	
tay bridge	*tay*	FBgn0260938	9056	107891		Excluded	
Glycerol 3 phosphate dehydrogenase	*Gpdh*	FBgn0001128	9042	105359		Excluded	
Ral guanine nucleotide dissociation stimulator-like ortholog (M. musculus)	*Rgl*	FBgn0026376	8865	106468		Excluded	
Sin3A	*Sin3A*	FBgn0022764	8815	105852		Excluded	
wallenda	*wnd*	FBgn0036896	8789	103410		Excluded	
-	*CG8728*	FBgn0033235	8728	110093		Excluded	
trithorax	*trx*	FBgn0003862	8651	108122		Excluded	
-	*CG8602*	FBgn0035763	8602	101575		Excluded	
scalloped	*sd*	FBgn0003345	8544	101497		Excluded	
combgap	*cg*	FBgn0000289	8367	102054		Excluded	
sulfateless	*sfl*	FBgn0020251	8339	5070		Excluded	

Gene name	Gene symbol	Flybase ID	CG #	VDRC ID	NIG ID/ Trip ID	Result	Confirmed
-	*CG8272*	FBgn0033337	8272	106686		Excluded	
Glycerophosphate oxidase-1	*Gpo-1*	FBgn0022160	8256	110608		Excluded	
PDGF- and VEGF-receptor related	*Pvr*	FBgn0032006	8222	105353		Excluded	
Methyl-CpG binding domain protein-like	*MBD-like*	FBgn0027950	8208	107151		Excluded	
Ecdysone-induced protein 75B	*Eip75B*	FBgn0000568	8127	108399		Excluded	
Mi-2	*Mi-2*	FBgn0262519	8103	107204		Excluded	
Vacuolar H[+] ATPase 44kD subunit	*Vha44*	FBgn0262511	8048	101527		Excluded	
-	*CG8034*	FBgn0031011	8034		HMS00331	Excluded	
Vacuolar H[+] ATPase AC45 accessory subunit	*VhaAC45*	FBgn0262515	8029	101726		Excluded	
-	*CG7991*	FBgn0035260	7991	109922		Excluded	
-	*CG7971*	FBgn0035253	7971	101384		Excluded	
-	*CG7966*	FBgn0038115	7966		7966R-1	Excluded	
similar	*sima*	FBgn0266411	7951	106187		Excluded	
Actin-related protein 5	*Arp5*	FBgn0038576	7940	110235		Excluded	
PNGase-like	*Pngl*	FBgn0033050	7865	103607		Excluded	
stripe	*sr*	FBgn0003499	7847	105282		Excluded	
Ribosomal protein S8	*RpS8*	FBgn0039713	7808	106835		Excluded	

Gene name	Gene symbol	Flybase ID	CG #	VDRC ID	NIG ID/ Trip ID	Result	Confirmed
Enhancer of Polycomb	*E(Pc)*	FBgn0000581	7776	35268		Excluded	
schnurri	*shn*	FBgn0003396	7734	105643		Excluded	
Mekk1	*Mekk1*	FBgn0024329	7717	110339		Excluded	
-	*CG7694*	FBgn0038627	7694	108995		Excluded	
charybde	*chrb*	FBgn0036165	7533	105757		Excluded	
-	*CG7488*	FBgn0038106	7488	106677		Excluded	
Histone deacetylase 1	*HDAC1*	FBgn0015805	7471	30599		Excluded	
Histone deacetylase 1	*HDAC1*	FBgn0015805	7471	30600		Excluded	
Histone deacetylase 1	*HDAC1*	FBgn0015805	7471	46929		Excluded	
Histone deacetylase 1	*HDAC1*	FBgn0015805	7471	46930		Excluded	
osa	*osa*	FBgn0261885	7467	7810		Excluded	
Ribosomal protein L22	*RpL22*	FBgn0015288	7434	104506		Excluded	
effete	*eff*	FBgn0011217	7425		7425R-2	Excluded	
Retinoblastoma-family protein	*Rbf*	FBgn0015799	7413	10696		Excluded	
Fatty acid (long chain) transport protein	*Fatp*	FBgn0267828	7400	100124		Excluded	
Lipase 1	*Lip1*	FBgn0023496	7279	18107		Excluded	
Glycogen phosphorylase	*GlyP*	FBgn0004507	7254	109596		Excluded	
-	*CG7222*	FBgn0033551	7222	34377		Excluded	
Cytochrome c oxidase subunit 8	*COX8*	FBgn0263911	7181	104047		Excluded	
scully	*scu*	FBgn0021765	7113	110802		Excluded	

Gene name	Gene symbol	Flybase ID	CG #	VDRC ID	NIG ID/ Trip ID	Result	Confirmed
happyhour	*hppy*	FBgn0263395	7097	103580		Excluded	
Brahma associated protein 111kD	*Bap111*	FBgn0030093	7055	104361		Excluded	
gilgamesh	*gish*	FBgn0250823	6963	106826		Excluded	
Oscillin	*Oscillin*	FBgn0031717	6957	106685		Excluded	
lethal (3) neo38	*l(3)neo38*	FBgn0265276	6930	107927		Excluded	
MYPT-75D	*MYPT-75D*	FBgn0036801	6896	109909		Excluded	
tolkin	*tok*	FBgn0004885	6863	110432		Excluded	
-	*CG6770*	FBgn0032400	6770	102402		Excluded	
Cysteine proteinase-1	*Cp1*	FBgn0013770	6692	110619		Excluded	
klingon	*klg*	FBgn0017590	6669	102502		Excluded	
klingon	*klg*	FBgn0017590	6669	108818		Excluded	
dorsal	*dl*	FBgn0260632	6667	10549		Excluded	
Fasciclin 1	*Fas1*	FBgn0262742	6588	101779		Excluded	
Brahma associated protein 55kD	*Bap55*	FBgn0025716	6546	24703		Excluded	
Brahma associated protein 55kD	*Bap55*	FBgn0025716	6546	24704		Excluded	
Ribosomal protein L18A	*RpL18A*	FBgn0010409	6510	107278		Excluded	
-	*CG6422*	FBgn0039261	6422	106251		Excluded	
UDP-N-acetyl-alpha-D-galactosamine:polypeptide N-acetylgalactosaminyltransferase	*GalNAc-T2*	FBgn0030930	6394	105160		Excluded	

Gene name	Gene symbol	Flybase ID	CG #	VDRC ID	NIG ID/ Trip ID	Result	Confirmed
2							
female lethal d	*fl(2)d*	FBgn0000662	6315	103361		Excluded	
twins	*tws*	FBgn0004889	6235	104167		Excluded	
Surfeit 4	*Surf4*	FBgn0019925	6202	108944		Excluded	
Tat interactive protein 60kDa	*Tip60*	FBgn0026080	6121	110617		Excluded	
Lipase 4	*Lip4*	FBgn0032264	6113	31021		Excluded	
sarah	*sra*	FBgn0086370	6072	107573		Excluded	
Aldolase	*Ald*	FBgn0000064	6058	101339		Excluded	
-	*CG6040*	FBgn0038679	6040	106606		Excluded	
Huntingtin-interacting protein 14	*Hip14*	FBgn0259824	6017	101736		Excluded	
brahma	*brm*	FBgn0000212	5942	37720		Excluded	
brahma	*brm*	FBgn0000212	5942	37721		Excluded	
Ribosomal protein S2	*RpS2*	FBgn0004867	5920	100308		Excluded	
ETHR	*ETHR*	FBgn0038874	5911	42716		Excluded	
Dichaete	*D*	FBgn0000411	5893	2940		Excluded	
Dichaete	*D*	FBgn0000411	5893	107194		Excluded	
-	*CG5694*	FBgn0032197	5694	102156		Excluded	
-	*CG5555*	FBgn0038686	5555	110162		Excluded	
scrawny	*scny*	FBgn0260936	5505	105989		Excluded	
Ribosomal protein L4	*RpL4*	FBgn0003279	5502	101346		Excluded	
Histone H2A variant	*His2Av*	FBgn0001197	5499	110598		Excluded	
Dodeca-satellite-binding protein 1	*Dp1*	FBgn0027835	5170	106047		Excluded	

Gene name	Gene symbol	Flybase ID	CG #	VDRC ID	NIG ID/ Trip ID	Result	Confirmed
-	*CG5003*	FBgn0039554	5003	26679		Excluded	
-	*CG5001*	FBgn0031322	5001	101532		Excluded	
mini spindles	*msps*	FBgn0027948	5000	21982		Excluded	
spalt-related	*salr*	FBgn0000287	4881	28387		Excluded	
hedgehog	*hh*	FBgn0004644	4637	1402		Excluded	
Nucleosome remodeling factor - 38kD	*Nurf-38*	FBgn0016687	4634	103776		Excluded	
YL-1	*YL-1*	FBgn0032321	4621	107951		Excluded	
-	*CG4612*	FBgn0035016	4612	52497		Excluded	
branchless	*bnl*	FBgn0014135	4608	5730		Excluded	
Phospholipase C at 21C	*Plc21C*	FBgn0004611	4574	108395		Excluded	
-	*CG4502*	FBgn0031896	4502	34858		Excluded	
no ocelli	*noc*	FBgn0005771	4491	108422		Excluded	
enhanced adult sensory threshold	*east*	FBgn0261954	4399	104091		Excluded	
Mitochondrial trifunctional protein alpha subunit	*Mtpalpha*	FBgn0028479	4389	100021		Excluded	
Star	*S*	FBgn0003310	4385	109838		Excluded	
Glutathione S transferase D3	*GstD3*	FBgn0010039	4381	106287		Excluded	
raptor	*raptor*	FBgn0029840	4320	13112		Excluded	
Multiple inositol polyphosphate phosphatase 2	*Mipp2*	FBgn0026060	4317	108018		Excluded	

Gene name	Gene symbol	Flybase ID	CG #	VDRC ID	NIG ID/ Trip ID	Result	Confirmed
Brahma associated protein 60kD	*Bap60*	FBgn0025463	4303	103634		Excluded	
Adaptor Protein complex 2, alpha subunit	*AP-2alpha*	FBgn0264855	4260	15565		Excluded	
Signal-transducer and activator of transcription protein at 92E	*Stat92E*	FBgn0016917	4257	43866		Excluded	
Chromatin assembly factor 1, p55 subunit	*Caf1-55*	FBgn0263979	4236	105838		Excluded	
Actin 5C	*Act5C*	FBgn0000042	4027	101438		Excluded	
pontin	*pont*	FBgn0040078	4003	105408		Excluded	
kraken	*kraken*	FBgn0020545	3943	105604		Excluded	
Chip	*Chi*	FBgn0013764	3924	107314		Excluded	
knockdown	*kdn*	FBgn0261955	3861	107642		Excluded	
Secreted decoy of InR	*Sdr*	FBgn0038279	3837	105549		Excluded	
-	*CG3812*	FBgn0030421	3812	109657		Excluded	
Ribosomal protein S24	*RpS24*	FBgn0261596	3751	104676		Excluded	
wings apart-like	*wapl*	FBgn0004655	3707	34686		Excluded	
bifid	*bi*	FBgn0000179	3578	100598		Excluded	
visceral mesodermal armadillo-repeats	*vimar*	FBgn0022960	3572	105618		Excluded	
cappuccino	*capu*	FBgn0000256	3399		HMS00712	Excluded	
Brahma associated	*Bap170*	FBgn0042085	3274	34582		Excluded	

Gene name	Gene symbol	Flybase ID	CG #	VDRC ID	NIG ID/ Trip ID	Result	Confirmed
protein 170kD							
-	*CG3104*	FBgn0031473	3104	101519		Excluded	
Hsc/Hsp70 -interacting protein related	*HIP-R*	FBgn0029676	2947	43724		Excluded	
Ras-like protein A	*Rala*	FBgn0015286	2849	105296		Excluded	
G protein alpha s subunit	*Galphas*	FBgn0001123	2835	24958		Excluded	
G protein alpha s subunit	*Galphas*	FBgn0001123	2835		2835R-1	Excluded	
u-shaped	*ush*	FBgn0003963	2762	104102		Excluded	
-	*CG2747*	FBgn0037541	2747	33566		Excluded	
Syntaxin 4	*Syx4*	FBgn0024980	2715	102466		Excluded	
shaggy	*sgg*	FBgn0003371	2621	101538		Excluded	
corto	*corto*	FBgn0010313	2530	3778		Excluded	
pipsqueak	*psq*	FBgn0263102	2368	106404		Excluded	
-	*CG2182*	FBgn0037360	2182	109653		Excluded	
-	*CG2162*	FBgn0035388	2162	33493		Excluded	
castor	*cas*	FBgn0004878	2102	100305		Excluded	
Ten-Eleven Translocation (TET) family protein	*Tet*	FBgn0263392	2083	110549		Excluded	
Ubiquitin conjugating enzyme 6	*Ubc6*	FBgn0004436	2013	23230		Excluded	
Protein C kinase 98E	*Pkc98E*	FBgn0003093	1954	108151		Excluded	
dre4	*dre4*	FBgn0002183	1828	106049		Excluded	
bifocal	*bif*	FBgn0014133	1822	109722		Excluded	
Protein tyrosine phosphatase 10D	*Ptp10D*	FBgn0004370	1817	110443		Excluded	

Gene name	Gene symbol	Flybase ID	CG #	VDRC ID	NIG ID/ Trip ID	Result	Confirmed
Cystathionine beta-synthase	*Cbs*	FBgn0031148	1753	107325		Excluded	
-	*CG1640*	FBgn0030478	1640	32681		Excluded	
eyeless	*ey*	FBgn0005558	1464	106628		Excluded	
Myocyte enhancer factor 2	*Mef2*	FBgn0011656	1429	15549		Excluded	
Cullin 5	*Cul5*	FBgn0039632	1401	108817		Excluded	
Heat shock protein 83	*Hsp83*	FBgn0001233	1242	7716		Excluded	
Alhambra	*Alh*	FBgn0261238	1070	102972		Excluded	
Snf5-related 1	*Snr1*	FBgn0011715	1064	108599		Excluded	
eyeless	*ey*	FBgn0005558	1464	42845		Excluded	
Chloride intracellular channel	*Clic*	FBgn0030529	10997		10997 R-3	No effect	
disconnected	*disco*	FBgn0000459	9908		JF03074	No effect	
Punch	*Pu*	FBgn0003162	9441	107296		No effect	
Lipid storage droplet-2	*Lsd-2*	FBgn0030608	9057		HMS01292	No effect	
Lipid storage droplet-2	*Lsd-2*	FBgn0030608	9057		HMS00629	No effect	
grainy head	*grh*	FBgn0259211	42311	33678		No effect	
grainy head	*grh*	FBgn0259211	42311	33680		No effect	
terribly reduced optic lobes	*trol*	FBgn0267911	33950	24549		No effect	
nab	*nab*	FBgn0259986	33545	39906		No effect	
Molecule interacting with CasL	*Mical*	FBgn0053208	33208	105837		No effect	
Heparan sulfate 3-O sulfotransferase-A	*Hs3st-A*	FBgn0053147	33147	4998		No effect	
Dpr-interacting	*DIP-alpha*	FBgn0052791	32791	104044		No effect	

Gene name	Gene symbol	Flybase ID	CG #	VDRC ID	NIG ID/ Trip ID	Result	Confirmed
protein alpha							
dunce	*dnc*	FBgn0000479	32498	107967		No effect	
-	*CG32195*	FBgn0052195	32195	108898		No effect	
Nuclear export factor 3	*Nxf3*	FBgn0263232	32135	104114		No effect	
-	*CG44838*	FBgn0266101	32043	49421		No effect	
-	*CG31690*	FBgn0051690	31690	43813		No effect	
Trissin receptor	*TrissinR*	FBgn0085410	31645	42758		No effect	
-	*CG31522*	FBgn0051522	31522	106652		No effect	
-	*CG31475*	FBgn0051475	31475	106664		No effect	
INO80 complex subunit	*Ino80*	FBgn0086613	31212	37473		No effect	
-	*CG31191*	FBgn0051191	31191	102425		No effect	
methuselah -like 11	*mthl11*	FBgn0045443	31147	5968		No effect	
-	*CG31098*	FBgn0051098	31098	21300		No effect	
Guanine nucleotide exchange factor in mesoderm	*GEFmeso*	FBgn0050115	30115	33858		No effect	
CCHamide -1 receptor	*CCHa1-R*	FBgn0050106	30106	1678		No effect	
-	*CG30022*	FBgn0050022	30022	30882		No effect	
Dopamine 1-like receptor 2	*Dop1R2*	FBgn0266137	18741	3392		No effect	
Ankyrin-repeat, SH3-domain, and Proline-rich-region containing Protein	*ASPP*	FBgn0034606	18375	25332		No effect	

Gene name	Gene symbol	Flybase ID	CG #	VDRC ID	NIG ID/ Trip ID	Result	Confirmed
midkine and pleiotrophin 2	*miple2*	FBgn0029002	18321	102644		No effect	
Rim2 ortholog (S. cerevisiae)	*Rim2*	FBgn0031359	18317	100807		No effect	
under-developed	*udd*	FBgn0033261	18316	25312		No effect	
Actin 87E	*Act87E*	FBgn0000046	18290	102480		No effect	
pleiohomeotic	*pho*	FBgn0002521	17743	110466		No effect	
-	*CG17646*	FBgn0264494	17646	100378		No effect	
-	*CG17600*	FBgn0031195	17600	102833		No effect	
scabrous	*sca*	FBgn0003326	17579	104703		No effect	
Lnk	*Lnk*	FBgn0028717	17367	103646		No effect	
pyrexia	*pyx*	FBgn0035113	17142	107870		No effect	
Lipase 2	*Lip2*	FBgn0024740	17116	31035		No effect	
methuselah-like 9	*mthl9*	FBgn0035131	17084	2769		No effect	
methuselah-like 9	*mthl9*	FBgn0035131	17084	2770		No effect	
pointed	*pnt*	FBgn0003118	17077	105390		No effect	
Dopamine 2-like receptor	*Dop2R*	FBgn0053517	17004	11470		No effect	
Dopamine 2-like receptor	*Dop2R*	FBgn0053517	17004	11471		No effect	
squid	*sqd*	FBgn0263396	16901	32395		No effect	
viking	*vkg*	FBgn0016075	16858	106812		No effect	
painless	*pain*	FBgn0060296	15860	39478		No effect	
Chromatin accessibility complex 16kD protein	*Chrac-16*	FBgn0043001	15736	104787		No effect	
ensconsin	*ens*	FBgn0264693	14998	106270		No effect	

Gene name	Gene symbol	Flybase ID	CG #	VDRC ID	NIG ID/ Trip ID	Result	Confirmed
-	*CG14971*	FBgn0035449	14971	108955		No effect	
ATPase 8B	*ATP8B*	FBgn0037989	14741	102648		No effect	
lost	*lost*	FBgn0263594	14648	110736		No effect	
Crustacean cardioactive peptide receptor	*CCAP-R*	FBgn0039396	14547	14767		No effect	
Ionotropic receptor 54a	*Ir54a*	FBgn0034272	14487	2720		No effect	
Ionotropic receptor 54a	*Ir54a*	FBgn0034272	14487	47091		No effect	
-	*CG14207*	FBgn0031037	14207	31802		No effect	
-	*CG13995*	FBgn0031770	13995	42525		No effect	
-	*CG13907*	FBgn0035173	13907	107339		No effect	
-	*CG13895*	FBgn0035158	13895	41511		No effect	
-	*CG13827*	FBgn0039068	13827	101466		No effect	
Myosuppressin receptor 2	*MsR2*	FBgn0264002	13803	49952		No effect	
Myosuppressin receptor 2	*MsR2*	FBgn0264002	13803	49953		No effect	
Pigment-dispersing factor receptor	*Pdfr*	FBgn0260753	13758	42724		No effect	
Repressed by TOR	*REPTOR*	FBgn0039209	13624	109612		No effect	
six-banded	*sba*	FBgn0016754	13598	101314		No effect	
Odorant-binding protein 57c	*Obp57c*	FBgn0034509	13421	44276		No effect	
Chromatin accessibility complex 14kD protein	*Chrac-14*	FBgn0043002	13399	39773		No effect	
Chromatin accessibility complex	*Chrac-14*	FBgn0043002	13399	50778		No effect	

Gene name	Gene symbol	Flybase ID	CG #	VDRC ID	NIG ID/ Trip ID	Result	Confirmed
14kD protein							
Chromatin accessibility complex 14kD protein	*Chrac-14*	FBgn0043002	13399	31781		No effect	
fuzzy	*fy*	FBgn0001084	13396	108550		No effect	
taiman	*tai*	FBgn0041092	13109	15709		No effect	
-	*CG12950*	FBgn0037736	12950	106353		No effect	
Esa1-associated factor 6	*Eaf6*	FBgn0035624	12756	31761		No effect	
forked end	*fend*	FBgn0030090	12664	110068		No effect	
thisbe	*ths*	FBgn0033652	12443	24538		No effect	
Diuretic hormone 44 receptor 2	*Dh44-R2*	FBgn0033744	12370	109558		No effect	
SP1029	*SP1029*	FBgn0263236	11956	105785		No effect	
Metazoan SpoT homolog-1	*Mesh1*	FBgn0039650	11900	108961		No effect	
-	*CG11873*	FBgn0039633	11873	108148		No effect	
seven up	*svp*	FBgn0003651	11502	37086		No effect	
seven up	*svp*	FBgn0003651	11502	37087		No effect	
cut	*ct*	FBgn0004198	11387	4138		No effect	
polybromo	*polybromo*	FBgn0039227	11375	108618		No effect	
-	*CG11367*	FBgn0037185	11367	103409		No effect	
Adipokinetic hormone receptor	*AkhR*	FBgn0025595	11325	9546		No effect	
Mesoderm-expressed 4	*Mes4*	FBgn0034726	11301	110192		No effect	
twin of eyeless	*toy*	FBgn0019650	11186	15919		No effect	
-	*CG11151*	FBgn0030519	11151	107530		No effect	
prickle	*pk*	FBgn0003090	11084	101480		No effect	

Gene name	Gene symbol	Flybase ID	CG #	VDRC ID	NIG ID/ Trip ID	Result	Confirmed
Retinoid- and fatty acid-binding glycoprotein	*Rfabg*	FBgn0087002	11064	6879		No effect	
Retinoid- and fatty acid-binding glycoprotein	*Rfabg*	FBgn0087002	11064		HM05157	No effect	
Autophagy-related 1	*Atg1*	FBgn0260945	10967	16133		No effect	
-	*CG10914*	FBgn0034307	10914	108735		No effect	
Corazonin receptor	*CrzR*	FBgn0036278	10698	44310		No effect	
-	*CG10639*	FBgn0032729	10639	103602		No effect	
Leucokinin receptor	*Lkr*	FBgn0035610	10626	22845		No effect	
tailup	*tup*	FBgn0003896	10619	103585		No effect	
-	*CG10600*	FBgn0032717	10600	31277		No effect	
crossbronx	*cbx*	FBgn0011241	10536	101755		No effect	
myoblast city	*mbc*	FBgn0015513	10379	16044		No effect	
-	*CG10365*	FBgn0039109	10365	108626		No effect	
spitz	*spi*	FBgn0005672	10334		10334 R-1	No effect	
-	*CG10209*	FBgn0033971	10209	106002		No effect	
Sprouty-related protein with EVH-1 domain	*Spred*	FBgn0020767	10155	18025		No effect	
M-spondin	*mspo*	FBgn0020269	10145	107608		No effect	
transformer 2	*tra2*	FBgn0003742	10128	101548		No effect	
traffic jam	*tj*	FBgn0000964	10034	30525		No effect	
-	*CG9932*	FBgn0262160	9932	107846		No effect	
-	*CG9921*	FBgn0030743	9921	110744		No effect	

Gene name	Gene symbol	Flybase ID	CG #	VDRC ID	NIG ID/ Trip ID	Result	Confirmed
Rad, Gem/Kir family member 1	*Rgk1*	FBgn0264753	9811	30104		No effect	
-	*CG9743*	FBgn0039756	9743	108185		No effect	
frizzled 2	*fz2*	FBgn0016797	9739	44391		No effect	
globin 1	*glob1*	FBgn0027657	9734	101830		No effect	
domino	*dom*	FBgn0020306	9696	7789		No effect	
real-time	*retm*	FBgn0031814	9528	44687		No effect	
Punch	*Pu*	FBgn0003162	9441	105761		No effect	
Calreticulin	*Calr*	FBgn0005585	9429	51271		No effect	
short gastrulation	*sog*	FBgn0003463	9224	105853		No effect	
vacuolar peduncle	*vap*	FBgn0003969	9209	107341		No effect	
Gas41	*Gas41*	FBgn0031873	9207	106922		No effect	
Pyrokinin 2 receptor 1	*PK2-R1*	FBgn0038140	8784	15988		No effect	
Pyrokinin 2 receptor 1	*PK2-R1*	FBgn0038140	8784	15989		No effect	
G protein beta-subunit 76C	*Gbeta76C*	FBgn0004623	8770	28869		No effect	
Imitation SWI	*Iswi*	FBgn0011604	8625	6208		No effect	
anachronism	*ana*	FBgn0011746	8084		JF02665	No effect	
Tachykinin-like receptor at 99D	*TkR99D*	FBgn0004622	7887	1374		No effect	
Actin-related protein 8	*Arp8*	FBgn0030877	7846	104425		No effect	
Enhancer of Polycomb	*E(Pc)*	FBgn0000581	7776	35271		No effect	
pumpless	*ppl*	FBgn0027945	7758	101751		No effect	
Octopamine-Tyramine receptor	*Oct-TyrR*	FBgn0004514	7485	26876		No effect	

Gene name	Gene symbol	Flybase ID	CG #	VDRC ID	NIG ID/ Trip ID	Result	Confirmed
heartless	*htl*	FBgn0010389	7223	6692		No effect	
heartless	*htl*	FBgn0010389	7223	27180		No effect	
-	*CG7149*	FBgn0031948	7149	102304		No effect	
four wheel drive	*fwd*	FBgn0004373	7004	110159		No effect	
Octopamine beta1 receptor	*Octbeta1R*	FBgn0038980	6919	47895		No effect	
Glycogen synthase	*GlyS*	FBgn0266064	6904	35136		No effect	
Leucine-rich-repeats and calponin homology domain protein	*Lrch*	FBgn0032633	6860	107047		No effect	
CTP synthase	*CTPsyn*	FBgn0266452	6854	12762		No effect	
dorsal	*dl*	FBgn0260632	6667	45998		No effect	
dorsal	*dl*	FBgn0260632	6667	45996		No effect	
-	*CG6420*	FBgn0039451	6420	110609		No effect	
Cysteine string protein	*Csp*	FBgn0004179	6395	103201		No effect	
-	*CG6329*	FBgn0033872	6329	104595		No effect	
-	*CG6325*	FBgn0037814	6325	35072		No effect	
-	*CG6123*	FBgn0030913	6123	22236		No effect	
Bicoid interacting protein 1	*Bin1*	FBgn0024491	6046	105352		No effect	
-	*CG6006*	FBgn0063649	6006	106513		No effect	
-	*CG33639*	FBgn0053639	5936	29644		No effect	
Dek	*Dek*	FBgn0026533	5935	100282		No effect	
Dichaete	*D*	FBgn0000411	5893	49549		No effect	
-	*CG5681*	FBgn0032658	5681	34139		No effect	

Gene name	Gene symbol	Flybase ID	CG #	VDRC ID	NIG ID/ Trip ID	Result	Confirmed
basket	*bsk*	FBgn0000229	5680	34138		No effect	
cylindromatosis ortholog (H. sapiens)	*CYLD*	FBgn0032210	5603	101414		No effect	
Phosphoethanolamine cytidylyltransferase	*Pect*	FBgn0032482	5547	109802		No effect	
Leucine-rich repeat kinase	*Lrrk*	FBgn0038816	5483	105630		No effect	
p38a MAP kinase	*p38a*	FBgn0015765	5475	34238		No effect	
Signal sequence receptor beta	*SsRbeta*	FBgn0011016	5474	12101		No effect	
SP2637	*SP2637*	FBgn0034371	5473	105482		No effect	
TBP-associated factor 4	*Taf4*	FBgn0010280	5444	109640		No effect	
Phosphodiesterase 8	*Pde8*	FBgn0266377	5411	101413		No effect	
Adiponectin receptor	*AdipoR*	FBgn0038984	5315		5315R-4	No effect	
locomotion defects	*loco*	FBgn0020278	5248	110275		No effect	
Glutathione S transferase E1	*GstE1*	FBgn0034335	5164	110529		No effect	
division abnormally delayed	*dally*	FBgn0263930	4974	14136		No effect	
Ror	*Ror*	FBgn0010407	4926	935		No effect	
Ror	*Ror*	FBgn0010407	4926	932		No effect	
wingless	*wg*	FBgn0004009	4889	13352		No effect	
boule	*bol*	FBgn0011206	4760	101435		No effect	
big brain	*bib*	FBgn0000180	4722	103327		No effect	
hedgehog	*hh*	FBgn0004644	4637	1403		No effect	

Gene name	Gene symbol	Flybase ID	CG #	VDRC ID	NIG ID/ Trip ID	Result	Confirmed
failed axon connections	*fax*	FBgn0014163	4609	103929		No effect	
branchless	*bnl*	FBgn0014135	4608	101377		No effect	
Innexin 2	*Inx2*	FBgn0027108	4590	102194		No effect	
Thiolase	*Thiolase*	FBgn0025352	4581	105500		No effect	
-	*CG4565*	FBgn0037841	4565	5665		No effect	
argos	*aos*	FBgn0004569	4531	47180		No effect	
methuselah-like 1	*mthl1*	FBgn0030766	4521	33136		No effect	
-	*CG4407*	FBgn0030431	4407	105541		No effect	
-	*CG4393*	FBgn0039075	4393	105381		No effect	
hemipterous	*hep*	FBgn0010303	4353	109277		No effect	
Major Facilitator Superfamily Transporter 10	*MFS10*	FBgn0030452	4330	108045		No effect	
moody	*moody*	FBgn0025631	4322	1800		No effect	
-	*CG4297*	FBgn0031258	4297	104552		No effect	
Signal-transducer and activator of transcription protein at 92E	*Stat92E*	FBgn0016917	4257	43867		No effect	
non-stop	*not*	FBgn0013717	4166	45776		No effect	
-	*CG4049*	FBgn0034976	4049	101670		No effect	
Abl tyrosine kinase	*Abl*	FBgn0000017	4032	110186		No effect	
jumeau	*jumu*	FBgn0015396	4029	12610		No effect	
Neurospecific receptor kinase	*Nrk*	FBgn0020391	4007	841		No effect	

Gene name	Gene symbol	Flybase ID	CG #	VDRC ID	NIG ID/ Trip ID	Result	Confirmed
Neurospecific receptor kinase	*Nrk*	FBgn0020391	4007	9653		No effect	
Neurospecific receptor kinase	*Nrk*	FBgn0020391	4007	36282		No effect	
Neurospecific receptor kinase	*Nrk*	FBgn0020391	4007	42442		No effect	
Neurospecific receptor kinase	*Nrk*	FBgn0020391	4007	103804		No effect	
pickled eggs	*pigs*	FBgn0029881	3973	34772		No effect	
-	*CG3967*	FBgn0035989	3967	106247		No effect	
-	*CG3860*	FBgn0034951	3860	109804		No effect	
-	*CG3838*	FBgn0032130	3838	106551		No effect	
Secreted decoy of InR	*Sdr*	FBgn0038279	3837	44576		No effect	
Secreted decoy of InR	*Sdr*	FBgn0038279	3837	44575		No effect	
cryptochrome	*cry*	FBgn0025680	3772	105172		No effect	
-	*CG3744*	FBgn0039240	3744	34695		No effect	
Chromodomain-helicase-DNA-binding protein 1	*Chd1*	FBgn0250786	3733	103640		No effect	
-	*Ggamma30A*	FBgn0267252	3694	26873		No effect	
-	*CG3625*	FBgn0031245	3625	106124		No effect	
-	*CG3409*	FBgn0033095	3409	37141		No effect	
earthbound 1	*ebd1*	FBgn0035153	3371	26180		No effect	
bigmax	*bigmax*	FBgn0039509	3350	110630		No effect	
Kruppel	*Kr*	FBgn0001325	3340	104150		No effect	
Brahma associated protein 170kD	*Bap170*	FBgn0042085	3274	34581		No effect	

Gene name	Gene symbol	Flybase ID	CG #	VDRC ID	NIG ID/ Trip ID	Result	Confirmed
-	*CG3168*	FBgn0029896	3168	48010		No effect	
Synaptotagmin 1	*Syt1*	FBgn0004242	3139	100608		No effect	
Allatostatin A receptor 1	*AstA-R1*	FBgn0266429	2872	48495		No effect	
-	*CG2211*	FBgn0035211	2211	100510		No effect	
FMRFamide Receptor	*FMRFaR*	FBgn0035385	2114	9594		No effect	
-	*CG2064*	FBgn0033205	2064	103276		No effect	
hikaru genki	*hig*	FBgn0010114	2040	109863		No effect	
Rho GTPase activating protein at 100F	*RhoGAP100F*	FBgn0039883	1976	106241		No effect	
ATP-dependent chromatin assembly factor large subunit	*Acf*	FBgn0027620	1966	33446		No effect	
sprouty	*sty*	FBgn0014388	1921	6948		No effect	
Rab40	*Rab40*	FBgn0030391	1900	110563		No effect	
Ady43A	*Ady43A*	FBgn0026602	1851	33133		No effect	
-	*Br140*	FBgn0033155	1845	101311		No effect	
Phosphorylase kinase gamma	*PhKgamma*	FBgn0011754	1830	110638		No effect	
BTB (POZ) domain containing 9 ortholog	*BTBD9*	FBgn0030228	1826	110685		No effect	
Histone deacetylase 4	*HDAC4*	FBgn0041210	1770	20522		No effect	
Ras oncogene at 64B	*Ras64B*	FBgn0003206	1167	6225		No effect	

Gene name	Gene symbol	Flybase ID	CG #	VDRC ID	NIG ID/ Trip ID	Result	Confirmed
Glucose transporter 1	*Glut1*	FBgn0264574	1086	13326		No effect	
KCNQ potassium channel	*KCNQ*	FBgn0033494	33135	106655		No effect	
LDL receptor protein 1	*LRP1*	FBgn0053087	33087	109605		No effect	
Secretory Pathway Calcium atpase	*SPoCk*	FBgn0052451	32451	110379		No effect	
-	*CG30389*	FBgn0050389	30389	101553		No effect	
sprite	*sprt*	FBgn0082585	30023	107873		No effect	
Lk6 kinase	*Lk6*	FBgn0017581	17342	109663		No effect	
Homeodomain interacting protein kinase	*Hipk*	FBgn0035142	17090	108254		No effect	
-	*CG17027*	FBgn0036553	17027	103270		No effect	
jim lovell	*lov*	FBgn0266129	16778	10739		No effect	
subdued	*subdued*	FBgn0038721	16718	108953		No effect	
Ceramide kinase	*Cerk*	FBgn0037315	16708	101550		No effect	
-	*CG16700*	FBgn0030816	16700	110058		No effect	
-	*CG15894*	FBgn0029864	15894	103818		No effect	
Juvenile hormone epoxide hydrolase 2	*Jheh2*	FBgn0034405	15102	30909		No effect	
Juvenile hormone epoxide hydrolase 1	*Jheh1*	FBgn0010053	15101	103249		No effect	
-	*CG15027*	FBgn0030611	15027	110436		No effect	
Glutamic acid decarboxylase 1	*Gad1*	FBgn0004516	14994	32344		No effect	
-	*CG14946*	FBgn0032405	14946	106023		No effect	

Gene name	Gene symbol	Flybase ID	CG #	VDRC ID	NIG ID/ Trip ID	Result	Confirmed
-	*CG13654*	FBgn0039290	13654	110349		No effect	
-	*CG12730*	FBgn0029771	12730	109016		No effect	
Shaker	*Sh*	FBgn0003380	12348	104474		No effect	
Mob2	*Mob2*	FBgn0259481	11711	107327		No effect	
-	*CG11593*	FBgn0035488	11593	108869		No effect	
-	*Lim1*	FBgn0026411	11354	104468		No effect	
fussel	*fuss*	FBgn0039932	11093	103367		No effect	
mirror	*mirr*	FBgn0014343	10601	50134		No effect	
chickadee	*chic*	FBgn0000308	9553	102759		No effect	
king tubby	*ktub*	FBgn0015721	9398	29110		No effect	
Sterol regulatory element binding protein	*SREBP*	FBgn0261283	8522	37641		No effect	
-	*CG8389*	FBgn0034063	8389	107639		No effect	
-	*CG7739*	FBgn0036509	7739	51521		No effect	
Src oncogene at 64B	*Src64B*	FBgn0262733	7524	35252		No effect	
-	*CG7341*	FBgn0036777	7341	109019		No effect	
Pyruvate kinase	*PyK*	FBgn0267385	7070	49533		No effect	
outspread	*osp*	FBgn0003016	3479	110701		No effect	
castor	*cas*	FBgn0004878	2102	2928		No effect	
Protein kinase N	*Pkn*	FBgn0020621	2049	108870		No effect	
-	*CG1882*	FBgn0033226	1882	41405		No effect	
Hormone receptor-like in 38	*Hr38*	FBgn0014859	1864	2971		No effect	
discs large 1	*dlg1*	FBgn0001624	1725	109274		No effect	

Gene name	Gene symbol	Flybase ID	CG #	VDRC ID	NIG ID/ Trip ID	Result	Confirmed
temperature-induced paralytic E	*tipE*	FBgn0003710	1232	4483		No effect	
-	*CG31301*	FBgn0051301	31301	104460		Suppressor	N
-	*CG31125*	FBgn0051125	31125	25700		Suppressor	N
Hormone receptor-like in 39	*Hr39*	FBgn0261239	8676		8676R-3	Suppressor	N
RYamide receptor	*RYa-R*	FBgn0004842	5811	1259		Suppressor	Opposite
INO80 complex subunit	*Ino80*	FBgn0086613	31212	106684		Suppressor	Y
Chromatin accessibility complex 14kD protein	*Chrac-14*	FBgn0043002	13399	31782		Suppressor	Y
Inhibitor of growth family, member 3	*Ing3*	FBgn0030945	6632	109799		Suppressor	Y
anterior open	*Aop/yan*	FBgn0000097	3166		3166R-1	Suppressor	Y
Metastasis associated 1-like	*MTA1-like*	FBgn0027951	2244	110632		Suppressor	Y
Daughters against dpp	*Dad*	FBgn0020493	5201	110644		Suppressor	

9.2.2 Enhancers classified as pathway components in Panther

Pathway	Gene name
5HT2 type receptor mediated signalling pathway (P04374)	*5-hydroxytryptamine (serotonin) receptor 1A*
ALP23B signalling pathway (P06209)	*dawdle*
Activin beta signalling pathway (P06210)	*dawdle*
Alzheimer disease-presenilin pathway (P00004)	*Wnt oncogene analog 5*
Angiogenesis (P00005)	*Heat shock protein 67Bc*
	Wnt oncogene analog 5
BMP/activin signalling pathway-drosophila (P06211)	*dawdle*
CCKR signalling map (P06959)	*Arrow*
	spoon
Cadherin signalling pathway (P00012)	*Wnt oncogene analog 5*
De novo purine biosynthesis (P02738)	*Adenylate kinase-1, isoform B*
Glycolysis (P00024)	*Phosphoglucose isomerase*
	Phosphoglycerate kinase
Heterotrimeric G-protein signalling pathway-Gi alpha and Gs alpha mediated pathway (P00026)	*5-hydroxytryptamine (serotonin) receptor 1A*
Pentose phosphate pathway (P02762)	*Phosphoglucose isomerase*
Salvage pyrimidine ribonucleotides (P02775)	*CG6330*
TGF-beta signalling pathway (P00052)	*dawdle*
VEGF signalling pathway (P00056)	*Heat shock protein 67Bc*
Wnt signalling pathway (P00057)	*Imitation SWI*
	Arrow
	Wnt oncogene analog 5

9.2.3 Suppressors classified as pathway components in Panther

Pathway	Gene name
Activin beta signalling pathway (P06210)	*Daughters against dpp*
BMP/activin signalling pathway-drosophila (P06211)	*Daughters against dpp*
DPP signalling pathway (P06213)	*Daughters against dpp*
TGF-beta signalling pathway (P00052)	*Daughters against dpp*
Wnt signalling pathway (P00057)	*Ino80*

9.2.4 Independent RNAi lines for screen enhancers

Gene name	Gene symbol	CG #	Bloomington ID	NIG ID/ Trip ID	Result
Forkhead box K	*FoxK*	*CG11799*	27994	JF02827	Enhancer
distal antenna-related	*danr*	*CG13651*	28378	JF03015	Enhancer
Capability receptor	*CapaR*	*CG14575*	27275	JF02577	Enhancer
tropomodulin	*tmod*	*CG1539*	31534	JF01094	Enhancer
5-hydroxytryptamine (serotonin) receptor 1A	*5-HT1A*	*CG16720*	33885	HMS00823	Enhancer
sloppy paired 1	*slp1*	*CG16738*	34633	HMS01107	Enhancer
Adenylate kinase 1	*Adk1*	*CG17146*	35582	GL00177	Enhancer
-	*CG18549*	*CG18549*	34391	HMS01385	Enhancer
-	*CG2124*	*CG2124*	55887	HMC04161	Enhancer
lethal (1) G0289	*l(1)G0289*	*CG2221*	32910	HMS00700	Enhancer
Amun	*Amun*	*CG2446*	43241	GLC01428	Enhancer
Phosphoglycerate kinase	*Pgk*	*CG3127*	33633	HMS00031	Enhancer
Phosphoglycerate kinase	*Pgk*	*CG3127*	35220	GL00101	Enhancer
Keren	*Krn*	*CG32179*		8056R-3	Enhancer
defective proboscis extension response 8	*dpr8*	*CG32600*	28744	JF03172	Enhancer
X11Lbeta	*X11Lbeta*	*CG32677*		32677R-2	Enhancer
phtf	*phtf*	*CG3268*	43631	GL01175	Enhancer
Reticulon-like1	*Rtnl1*	*CG33113*		18623R-4	Enhancer
-	*CG4004*	*CG4004*		4004R-2	Enhancer
Heat shock gene 67Bc	*Hsp67Bc*	*CG4190*	42607	HMS02440	Enhancer
Dual-specificity tyrosine phosphorylation-regulated kinase 2	*Dyrk2*	*CG4551*	35393	GL00313	Enhancer
branchless	*bnl*	*CG4608*	34572	HMS01046	Enhancer
-	*CG5599*	*CG5599*	32876	HMS00663	Enhancer
-	*CG6330*	*CG6330*	62240	HMC05247	Enhancer
Wnt oncogene analog 5	*Wnt5*	*CG6407*	34644	HMS01119	Enhancer
Wnt oncogene analog 5	*Wnt5*	*CG6407*	28534	HM05020	Enhancer
Phosphoglucose isomerase	*Pgi*	*CG8251*	51804	HMC03362	Enhancer
-	*CG11658*	*CG11658*	43298	HMS02671	Excluded
Neuroligin 2	*Nlg2*	*CG13772*	58128	HMJ22077	Excluded
dawdle	*daw*	*CG16987*	34974	HMS01110	Excluded
pyrexia	*pyx*	*CG17142*	51836	HMC03408	Excluded
Adenylate kinase 1	*Adk1*	*CG17146*	51799	HMC03355	Excluded
Integrator 6	*IntS6*	*CG3125*	52904	HMC03644	Excluded

Gene name	Gene symbol	CG #	Bloomington ID	NIG ID/ Trip ID	Result
Phosphoglycerate kinase	*Pgk*	*CG3127*	33632	HMS00030	Excluded
Enhancer of bithorax	*E(bx)*	*CG32346*	33658	HMS00065	Excluded
Enhancer of bithorax	*E(bx)*	*CG32346*	31193	JF01709	Excluded
scribbled	*scrib*	*CG43398*	39073	HMS01993	Excluded
scribbled	*scrib*	*CG43398*	38199	GL00638	Excluded
scribbled	*scrib*	*CG43398*	35748	HMS01490	Excluded
scribbled	*scrib*	*CG43398*	29552	JF03229	Excluded
-	*CG5466*	*CG5466*	35758	HMS01504	Excluded
arrow	*arr*	*CG5912*	31473	JF01261	Excluded
taranis	*tara*	*CG6889*	31634	JF01421	Excluded
Imitation SWI	*Iswi*	*CG8625*	32845	HMS00628	Excluded
-	*CG9095*	*CG9095*	61881	HMJ23371	Excluded
twin of eyeless	*toy*	*CG11186*	33679	HMS00544	No effect
twin of eyeless	*toy*	*CG11186*	29346	JF02508	No effect
-	*CG11658*	*CG11658*	31373	JF01340	No effect
Neuroligin 2	*Nlg2*	*CG13772*	28331	JF02966	No effect
gamma-glutamyl carboxylase	*GC*	*CG13927*	51897	HMC03471	No effect
tropomodulin	*tmod*	*CG1539*	41718	HMS02283	No effect
5-hydroxytryptamine (serotonin) receptor 1A	*5-HT1A*	*CG16720*	25834	JF01852	No effect
sloppy paired 1	*slp1*	*CG16738*	29354	JF02517	No effect
dawdle	*daw*	*CG16987*	50911	HMJ03135	No effect
pyrexia	*pyx*	*CG17142*	31297	JF01242	No effect
ATP-dependent chromatin assembly factor large subunit	*Acf*	*CG1966*	31340	JF01298	No effect
ATP-dependent chromatin assembly factor large subunit	*Acf*	*CG1966*	35575	GL00124	No effect
-	*CG2124*	*CG2124*	40868	HMS02035	No effect
lethal (1) G0289	*l(1)G0289*	*CG2221*	33690	HMS00558	No effect
-	*CG2225*	*CG2225*	29619	JF03298	No effect
late bloomer	*lbm*	*CG2374*	35459	GL00385	No effect
late bloomer	*lbm*	*CG2374*	27278	JF02589	No effect
Phosphoglycerate kinase	*Pgk*	*CG3127*	28053	JF02889	No effect
-	*CG31324*	*CG31324*	28774	JF03202	No effect
breathless	*btl*	*CG32134*	55870	HMC04140	No effect
breathless	*btl*	*CG32134*	43544	HMS02656	No effect
breathless	*btl*	*CG32134*	40871	HMS02038	No effect

Gene name	Gene symbol	CG #	Bloomington ID	NIG ID/ Trip ID	Result
Enhancer of bithorax	*E(bx)*	*CG32346*	35353	GL00265	No effect
spoonbill	*spoon*	*CG3249*	38205	GL00644	No effect
-	*CG33170*	*CG33170*	61856	HMJ23345	No effect
Inositol 1,4,5-triphosphate kinase 2	*IP3K2*	*CG34359*	55240	HMC02364	No effect
Heat shock gene 67Bc	*Hsp67Bc*	*CG4190*	35452	GL00377	No effect
elbow B	*elB*	*CG4220*	41960	HMS02357	No effect
scribbled	*scrib*	*CG43398*	58085	HMJ21977	No effect
Dual-specificity tyrosine phosphorylation-regulated kinase 2	*Dyrk2*	*CG4551*	41626	GL01208	No effect
GATAd	*GATAd*	*CG5034*	34625	HMS01300	No effect
GATAd	*GATAd*	*CG5034*	33747	HMS01086	No effect
GATAd	*GATAd*	*CG5034*	34640	HMS01115	No effect
-	*CG5059*	*CG5059*	42494	HMJ02058	No effect
-	*CG5455*	*CG5455*	43219	GL01564	No effect
arrow	*arr*	*CG5912*	31313	JF01260	No effect
MORF-related gene 15	*MRG15*	*CG6363*	35241	GL00128	No effect
plum	*plum*	*CG6490*	60062	HMC05055	No effect
-	*CG6847*	*CG6847*	42908	HMS02601	No effect
-	*Wdr62*	*CG7337*	53242	GLC01394	No effect
Sodium/solute co-transporter-like 5A11	*SLC5A11*	*CG8451*		8451R-4	No effect
Imitation SWI	*Iswi*	*CG8625*	31111	JF01582	No effect
Imitation SWI	*Iswi*	*CG8625*	51931	GLC01788	No effect
Reticulon-like1	*Rtnl1*	*CG8895*		8895R-1	No effect
Disabled	*Dab*	*CG9695*	42646	HMS02482	No effect
-	*CG8778*	*CG8778*	36793	GL00533	Suppressor

Appendix 1. Independent RNAi lines for screen suppressors

Gene name	Gene symbol	CG #	Bloomington ID	NIG ID/ Trip ID	Result
RYamide receptor	*RYa-R*	*CG5811*	25944	JF01964	Enhancer
-	*CG31125*	*CG31125*		31125R-2	Excluded
Metastasis associated 1-like	*MTA1-like*	*CG2244*	34905	HMS01251	Excluded
-	*CG31301*	*CG31301*	60121	HMC05115	No effect
Hormone receptor-like in 39	*Hr39*	*CG8676*	27086	JF02432	No effect
Hormone receptor-like in 39	*Hr39*	*CG8676*	33624	HMS00018	No effect

Gene name	Gene symbol	CG #	Bloomington ID	NIG ID/ Trip ID	Result
Chromatin accessibility complex 14kD protein	*Chrac-14*	*CG13399*	31052	35652	No effect
Metastasis associated 1-like	*MTA1-like*	*CG2244*	33745	HMS01084	No effect
Metastasis associated 1-like	*MTA1-like*	*CG2244*	34624	HMS01299	Suppressor
INO80 complex subunit	*Ino80*	*CG31212*	33708	HMS00586	Suppressor
INO80 complex subunit	*Ino80*	*CG31212*	37473	GL00616	Suppressor
Chromatin accessibility complex 14kD protein	*Chrac-14*	*CG13399*		13399R-6	Suppressor
Inhibitor of growth family, member 3	*Ing3*	*CG6632*		6632R-2	Suppressor
anterior open	*Aop/yan*	*CG3166*		3166R-3	Suppressor

9.2.5 Climbing and wing inflation assays of RNAi lines identified in screen.

Flies were grown at 25°C, RNAi is expressed in motor neurons with *D42-Gal4*. **(A-A')** *CG31301* RNAi **(B-B')** *CG13399* RNAi **(C-C')** *CG2244* RNAi **(D-D')** *CG1966* RNAi **(E-E')** *CG8625* RNAi **(F-F')** *CG6363* RNAi **(G-G')** *CG31212* RNAi **(H-H')** *CG6632* RNAi

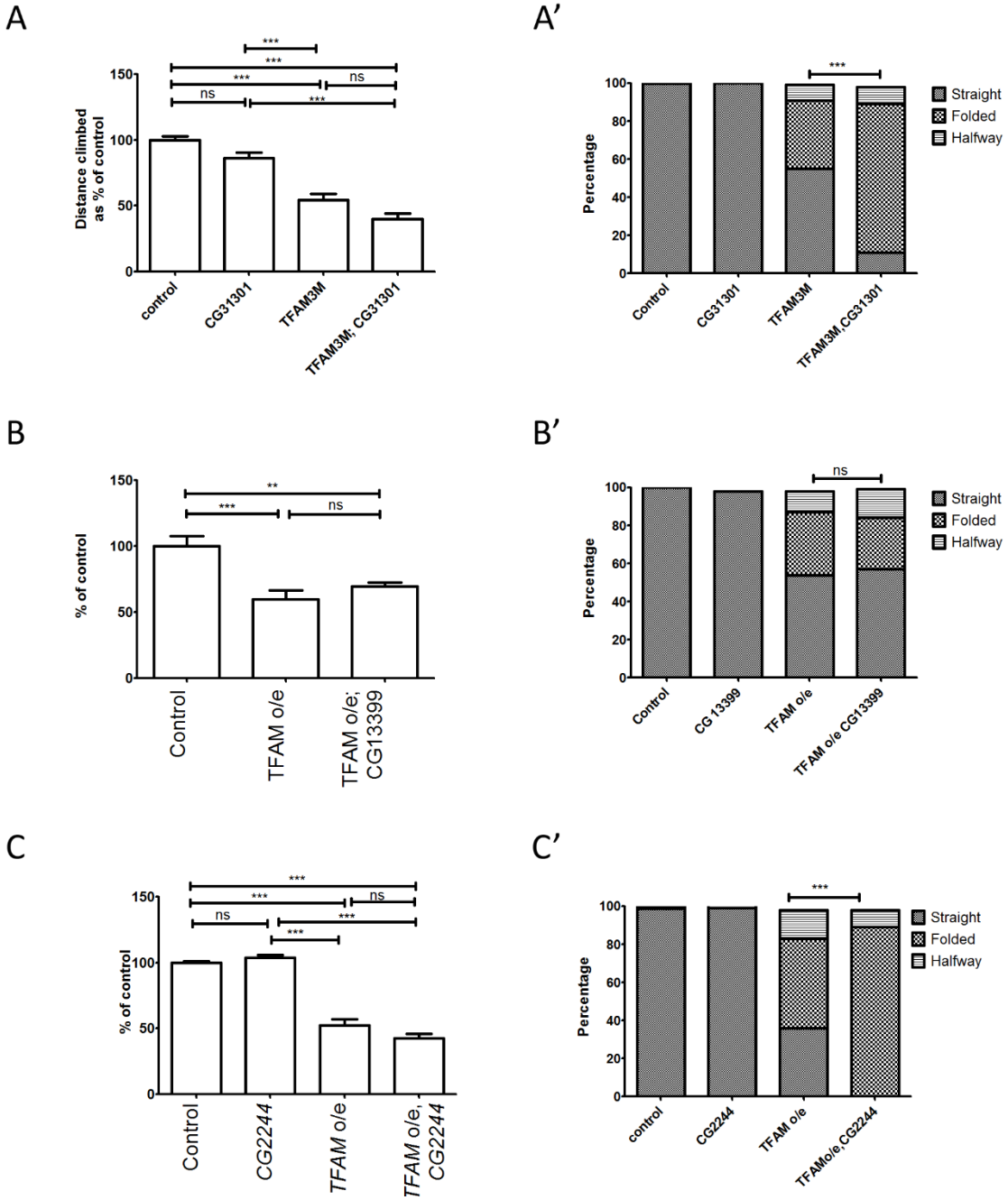

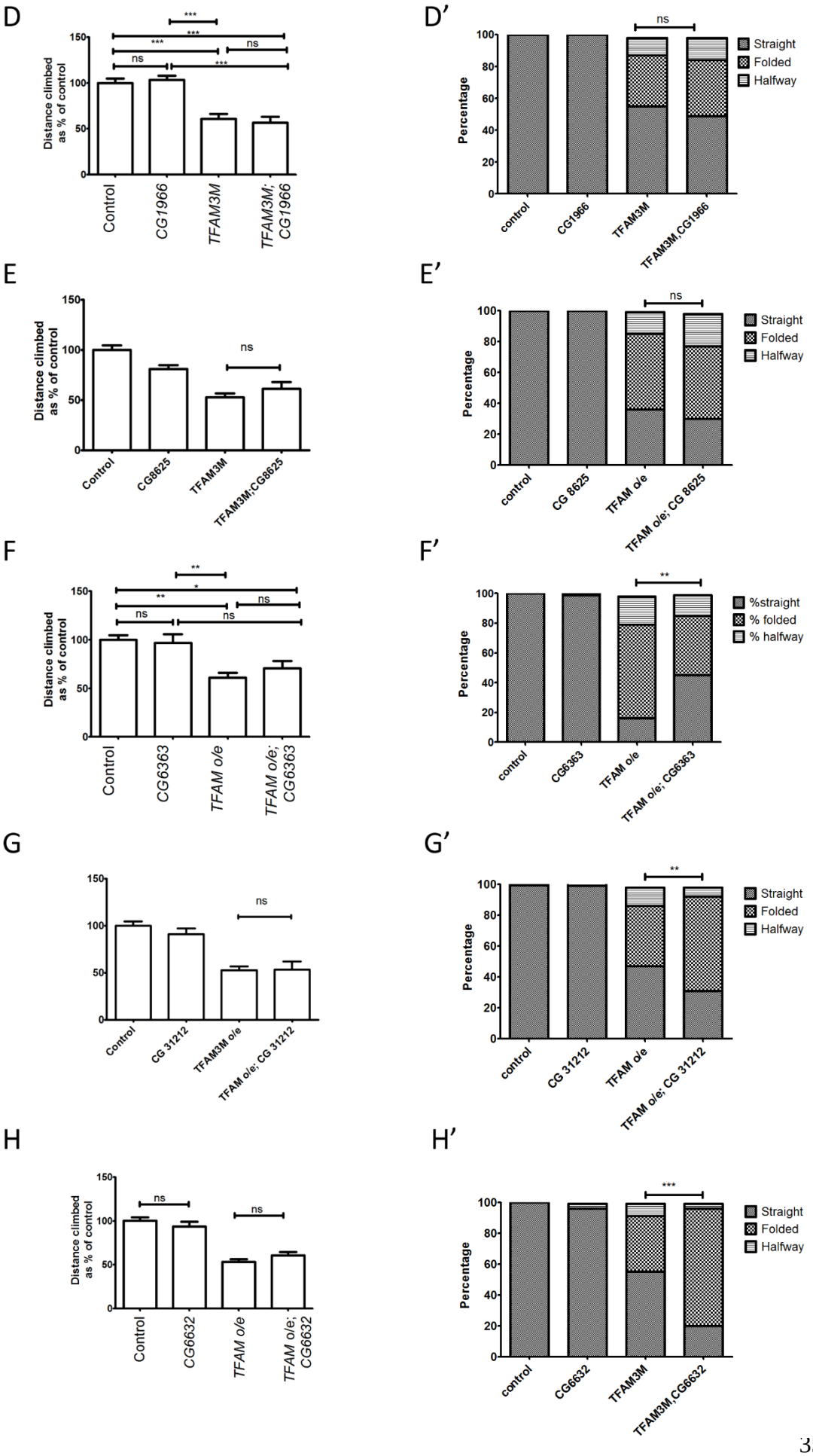
D
Distance climbed as % of control
Control
CG1966
TFAM3M
TFAM3M; CG1966
D'
Percentage
Straight
Folded
Halfway
control
CG1966
TFAM3M
TFAM3M,CG1966
E
Distance climbed as % of control
Control
CG8625
TFAM3M
TFAM3M;CG8625
E'
Percentage
Straight
Folded
Halfway
control
CG 8625
TFAM o/e
TFAM o/e; CG 8625
F
Distance climbed as % of control
Control
CG6363
TFAM o/e
TFAM o/e; CG6363
F'
Percentage
%straight
% folded
% halfway
control
CG6363
TFAM o/e
TFAM o/e; CG6363
G
Control
CG 31212
TFAM3M o/e
TFAM o/e; CG 31212
G'
Percentage
Straight
Folded
Halfway
control
CG 31212
TFAM o/e
TFAM o/e; CG 31212
H
Distance climbed as % of control
Control
CG6632
TFAM o/e
TFAM o/e; CG6632
H'
Percentage
Straight
Folded
Halfway
control
CG6632
TFAM3M
TFAM3M,CG6632